Proceedings of the 3rd Vienna Talk on Music Acoustics

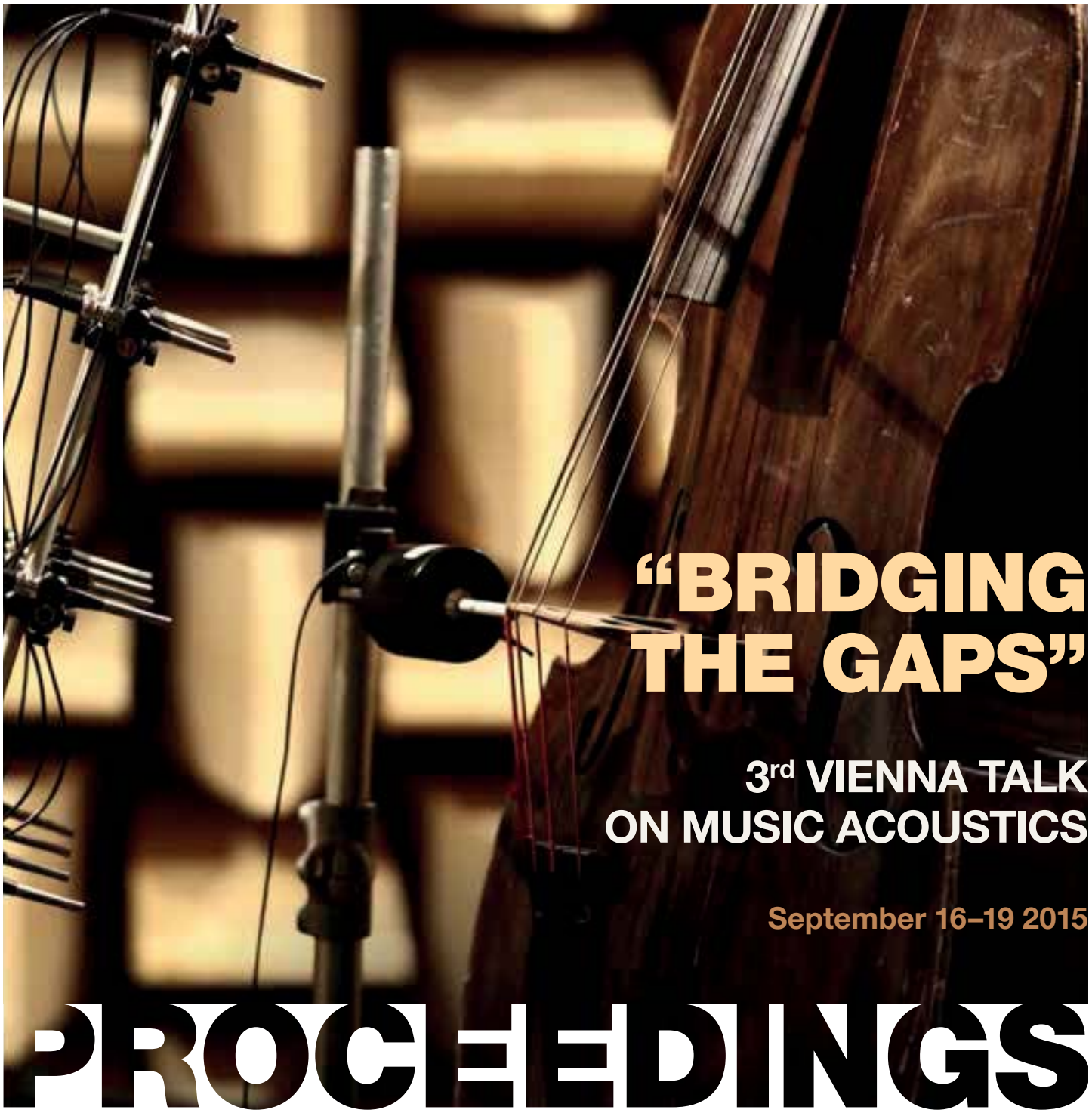

"BRIDGING THE GAPS"

3rd VIENNA TALK ON MUSIC ACOUSTICS

September 16–19 2015

PROCEEDINGS

ALEXANDER MAYER / VASILEIOS CHATZIIOANNOU / WERNER GOEBL (eds.)

mdw universität für musik und darstellende kunst wien

Proceedings of the Third Vienna Talk on Music Acoustics
edited by Alexander Mayer, Vasileios Chatziioannou, and Werner Goebl
Institute of Music Acoustics (Wiener Klangstil)
University of Music and Performing Arts Vienna
Anton-von-Webern-Platz 1, 1030 Vienna, Austria
Cover design, front and back matter typesetting: Saleh Siddiq
urn:nbn:at:at-ubmw-20151029154902813-1604213-2
http://viennatalk2015.mdw.ac.at

o.Univ.-Prof. Mag. Dr. Werner Hasitschka
Rector of the University of Music and Performing Arts Vienna

Preface

The Institute of Musical Acoustics („Wiener Klangstil“) celebrates its 35-year anniversary with Vienna Talk 2015, a three-day Symposium on Music Acoustics bringing together internationally renowned researchers, scholars, and instrument makers. The motto “Bridging the Gaps” again reflects a central concern of the Institute: to initiate a dialogue between artists, instrument makers and scientists, a dialogue that often does not take place because of existing fundamental differences in terminology, approaches, or simply ways of thinking.

Bridges between these disciplines can already be found among the members of the Institute. All of them have, in addition to their education as physicists, technicians, instrument makers, or musicologists, a strong musical background. Since its formation in 1980, the Institute has always been striving to bridge the gaps between music and physics and between artists and scientists. It was established as a competence center of Music Acoustics, a field that did not exist in Austria before. Many innovative ideas and products bear witness of the creative power of the team, such as the measuring systems and techniques for various musical instruments that have been developed to help instrument makers and musicians solve some of their specific problems.

Originally founded as a one-man concern to remedy the lack of knowledge about manufacturing original Viennese orchestral instruments, the Institute successfully developed into an internationally recognized research and education center that is considered to be leading in specific areas. We are proud of this Institute, because on the one hand it reflects the wide scientific range of our university, and on the other hand it is representative of the dialogue between arts and sciences. Congratulations for this anniversary and all the best for the future!

With best regards,
Werner Hasitschka

Scientific Committee

Table of contents

Conference Keynote

Brass wind instruments and their transient behaviour

Nonlinear wave propagation

Wall vibrations and air columns

Woodwinds

Early brass music and instruments

Preservation of historic instruments

Characterisation and documentation of instruments

Single note instruments

Numerical methods

Physiology

Experimental methods

Free reed instruments

Piano modelling

Gesture and communication in music performance

Timbre perception

Biomechanics workshop

Voice and auralization

Organ acoustics

Physical modeling tools for musical instruments

Audio signal processing

THROUGH THE LOOKING GLASS: FROM MUSICAL LISTENING TO ACOUSTICS

Michèle Castellengo

Institut Jean le Rond d'Alembert
Paris, France
michele.castellengo@upmc.fr

ABSTRACT

Psychoacoustics, which gives us keys to understanding how the auditory system analyzes sound, benefits today from an increasing number of studies using fMRI techniques to visualize high-level cognitive processes in the brain (such as music and speech). However, the formal nature of these studies whose aim is producing objective results, generalizable as valid for any listener, imposes the use of sound stimuli whose parameters are rigorously defined. The resulting stimuli fail to account for the diversity and complexity of listening by musicians when presented with the real music sounds. With the use of sound examples given throughout the presentation, we propose to reconsider the notions of pitch and intensity, classically considered parameters, as well as timbre with all its complexity, integrating them into a global approach of human perception. Grounded in both Gestalt theory and prototypic categorization, this approach makes use of musicians expertise and gives each individual the tools to interpret their listening, potentially explaining individual differences. In conjunction with temporo-spectral analysis and synthesis, this approach offers a new means for musicians to study the complex acoustics of instrumental and vocal sounds.

BRIDGING THE GAPS IN THE HARMONIC SERIES: VALVES, SLIDES AND FINGER HOLES IN BRASS INSTRUMENTS.

Murray Campbell

Univeristy of Edinburgh, United Kingdom of Great Britain and Northern Ireland
d.m.campbell@ed.ac.uk

ABSTRACT

On almost all lip-excited wind instruments it is possible for the player to sound a series of different pitches corresponding to the different acoustic resonances of the air column inside the instrument. The pitch intervals in this series depend on the bore profile of the instrument, which is usually designed so that the acoustic resonance frequencies of the basic tube are close to being members of a complete harmonic series. To obtain a chromatic scale over the compass of the instrument it is necessary to sound pitches which bridge the gaps between the harmonics, and several stratagems have been developed which allow this. The oldest method is to puncture the tube with side holes which can be opened or closed by the fingers. A fifteenth century innovation was a sliding section which allowed the tube length to be varied continuously. By the second decade of the nineteenth century valves had been designed which permitted discrete additional sections of tubing to be added to the basic bore. Some musical consequences of the science underlying these three approaches are explored in this review.

SIMULTANEOUS AND IN VIVO MEASUREMENTS OF CONTROL PARAMETERS USED IN TRUMPET PERFORMANCE

Lionel Velut, Christophe Vergez, Joël Gilbert, Patrick Sanchez

CNRS-LMA
MARSEILLE, France
velut@lma.cnrs-mrs.fr

ABSTRACT

Brass instrument players combine several parameters to control the sound emitted by their instrument. According to the statements of musicians, different ways to play the same note seems to exist, depending on the player's proficiency, formation and musical background. We would like to bring out these difference in a more measurable way. In order to measure different control parameters used by the musician while playing, and monitor the reactions of the instruments, a set of sensors have been installed on a trumpet. Our experimental device allows in vivo simultaneous measurements of the mouth pressure (continuous and acoustic part), the pressure at the input of the instrument (mouthpiece), the phase of the motion of the musician's lips, the position of the trumpet valves, the force applied to the lips by the mouthpiece rim, the airflow through the instrument, and the radiated sound. Experiments are carried out with different musicians : simple musical tasks are performed and the sensors output are recorded. Different analysis highlight links between control parameters and oscillating variables. While some trends are shared by the different trumpet players recorded, quantitative analysis reveal different strategies according to the player. Repetability for each player is also investigated, and confirm some abilities of experienced players.

TRANSIENTS OF TRUMPET TONE: BASIC LINKS BETWEEN PERCEPTION AND MEASUREMENTS OF LIPS OPENING SURFACE AND PRESSURE IN PLAYER'S MOUTH

Viktor Hruška, Martin Švejda, Milan Guštar

Musical Acoustics Research Centre
Music and Dance Faculty of the Academy of Performing Arts in Prague
hruska.viktor@hamu.cz

ABSTRACT

Selected transients of trumpet tone are documented using high-speed imaging and measuring of pressure in player's mouth. Key features are described including phenomena that couldn't be described without high sampling rate ("initial blow off" on soft tones, parameters of triple staccato, legato transients).

1. INTRODUCTION

The transient of a tone is known to be one of the key features in recognition of tone source and major characteristics of instrument's timbre. However, its observation is complicated due to the natural instability of the process.

Measurements of lips motion is a classical topic in acoustics of brass instruments [1, 2]. Although some methods based on optical means became available only few years ago thanks to the development in the field of a high-speed imaging.

Methods based on stroboscopy are well-suited for describing the stationary or quasi-stationary motion but the transient is unapproachable by these means.

We described the lips motion during the selected transients using a high-speed camera. As the information about lips opening area would be just "kinematic", we added the mouth pressure monitoring to describe a part of the dynamics as well.

The selection of transients was made according to the typical situations common in instrumentation of brasses. Presented results are product of pilot measurement only, they should not be overinterpreted, but they are valid as well-founded hypotheses for future research.

2. MEASURING PROCEDURES

Experimental procedures are close to Logie et al. [4]. In order to make the conditions for the mouth pressure as natural as possible, glass mouthpiece was used. Mentioned mouthpiece has a realistic rim, throat and direction of the main flow, a bigger cup and not perfectly conical backbore (Fig. 1).

Measuring experiment schematics is shown in Fig. 3. The high-speed camera (1)(Phantom SpeedSense v611) shoots player´s lips through special glass mouthpiece inserted to the trumpet. If the player is an experimenter concurrently, he can activate the camera via a footswitch (6) which triggers a differential pressure meter (2)(of our own construction). Camera synchronization signal is recorded together with microphone (5) signal using an external sound card. Player's lips were lit by a DC powered light source (Olympus Visera CLV-S45).

Camera sampling frequency was 12 000 frames per second (FPS), pressure meter sampling frequency was 2000 FPS. Common Bb trumpet (Joseph Monke, older model) was used playing F4 or Bb4 (349 and 466 Hz respectively), so the signals were enough sampled, though in the text we focus mainly on the shapes of envelopes.

The cooling of the devices was not turned off during these pilot experiments and an anechoic room was not used, so a noise occured in recorded sound and a weak reverberation should be counted in. Microphone was placed 0.5 m in front of the instrument.

A simple threshold filter is applied on the captured grayscale images to pick out just the pixels corresponding to the mouth opening. Then the count of these pixels is used. A "DC part" (always black pixels) is subtracted and the data are smoothed using Golay-Savitzki filter.

A conversion between black pixels and mm^2 was not made. However, the geometry of the experiment, lighting, data processing etc. was kept the same, so the data in units of black pixels can be used as relative.

Fig. 1 – Common trumpet mouthpiece and glass model used for measurement.

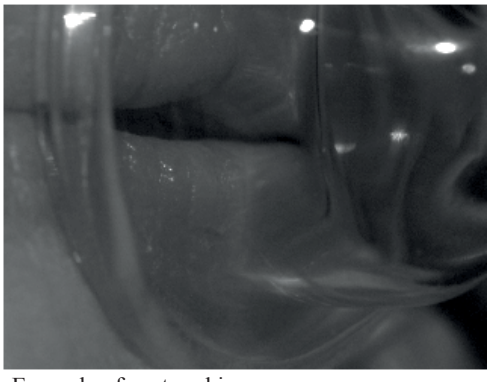

Fig. 2 – Example of captured image.

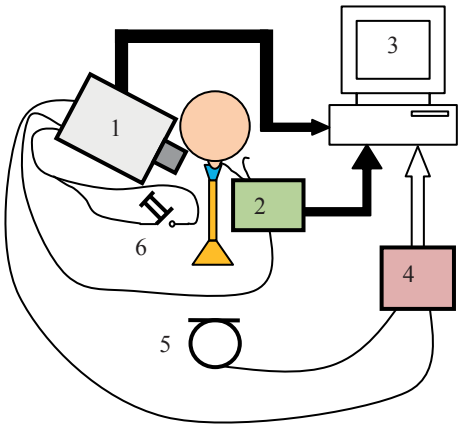

1 – High-speed camera
2 – Differential pressure meter
3 – Controlling PC
4 – External sound card
5 – Microphone
6 - Footswitch

Fig. 3 – Schematics of measuring system.

3. EXPERIMENTAL RESULTS

Description of selected transient follows. Triplets of plots are presented always in order *lips opening area* (black), *pressure in player's mouth* (blue), *recorded sound* (red).

a) *F4, mezzoforte, sharp beginning, loose ending*

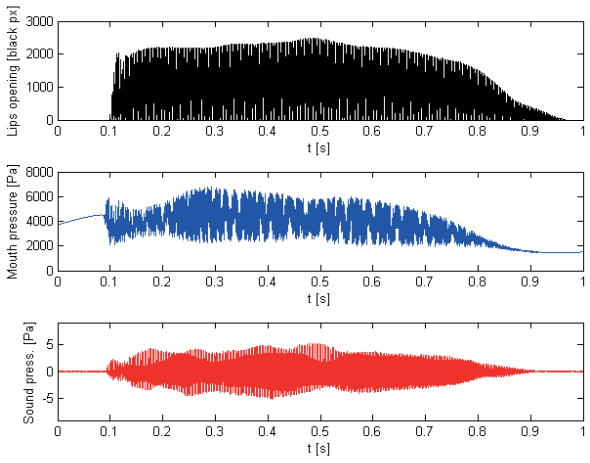

Fig. 4

Sharp beginning, typical for trumpet as a signal instrument. Initial leap of mouth pressure is almost 2 kPa (see Fig. 4), then a small attenuation and regular attack transient after brassy crack at the beginning comes.
Lips are opening and fully closing from the very beginning of the sound production. Amplitude of this opening almost does not vary except for "explosive opening" which could be seen at 0.1 s. Last but not least, the inertia of the lips is remarkable. At ca. 0.9 s, as the tone production is ended, the lips are still opening and closing.

b) *F4, piano, soft beginning, loose ending*

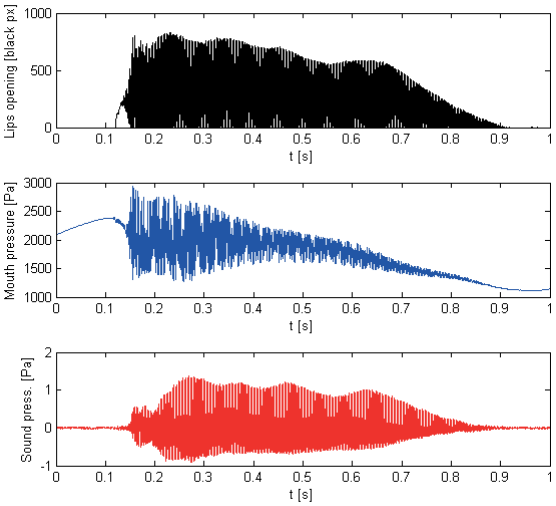

Fig. 5

Very soft, piano beginning, still clear and without noise or rustle.
Initial "blow off" of ca. 250 Pa is observed at 0.1s (see Fig. 5). Initial leap of mouth pressure is less than 1 kPa (so more or less a half of previous situation).
Soft beginning is easy to spot on the recorded sound, but the mouth pressure is a bit more monotonic.
The build up of the lips opening is remarkable:

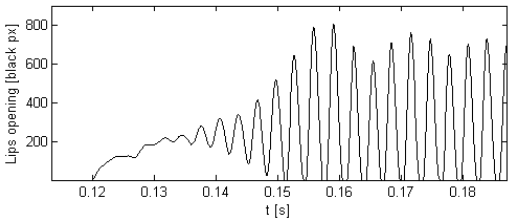

Fig. 6 – Detail of the first plot of Fig. 5 showing initial lips opening.

The oscillation actually started at the state of the opened mouth - hence the mentioned "initial blow off" removing the brassy crack.

c) *F4 to Bb4, legato, mezzoforte*

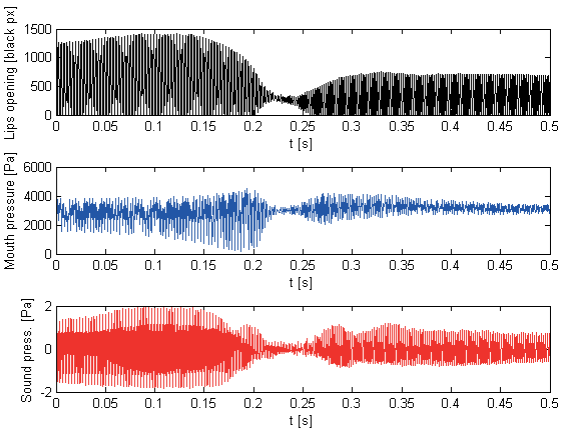

Fig. 7

As Logie et al. [4] showed, downward and upward legato (slur) is quite different in player's technique, therefore both cases are presented here.
An example of slow, sort of weary legato (with a bit more player's effort than is considered to be elegant) between two tones without action of valves (i.e. just change of the instrument's oscillation mode).
For a short time (0.2-0.25 s, see fig. 7) the player's lips are not fully closing. On a higher tone a lesser variation of the mouth opening is observed.
Small maximum (kind of "springing before the leap") in recorded sound at 0.2 s is created mainly by lower harmonics (see Fig. 8). The higher ones are attenuated before the mode change, which causes faulty but common tone without typical trumpet timbre.

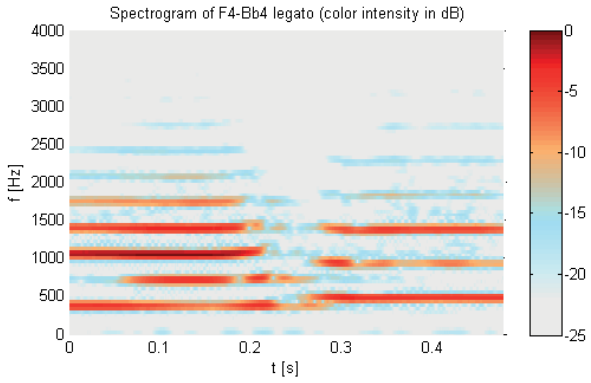

Fig. 8 – Spectrogram of sound in Fig. 7 (upward legato).

Simultaneously, mouth pressure is increasing its amplitude showing the player's preparation before the leap between the modes.
The same slur downwards (Bb4 to F4, see Fig. 9) exhibits less demands on player's embouchure. Less experienced players tend to loose their muscles too much causing audible attack on legato transient. Figure 9 depicting the downwards legato inclines to have signs of that at 0.15 s.

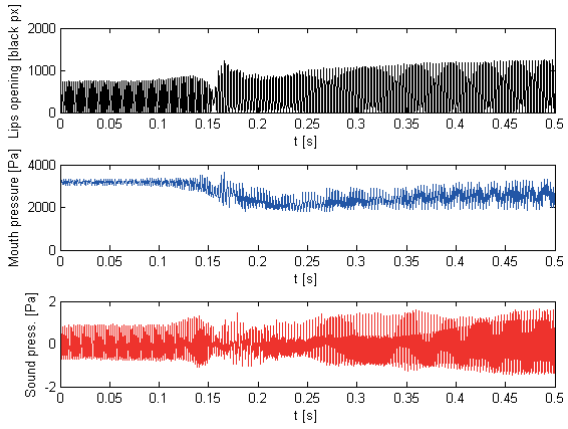

Fig. 9 – Legato downwards

d) *F4, triple staccato, mezzoforte*

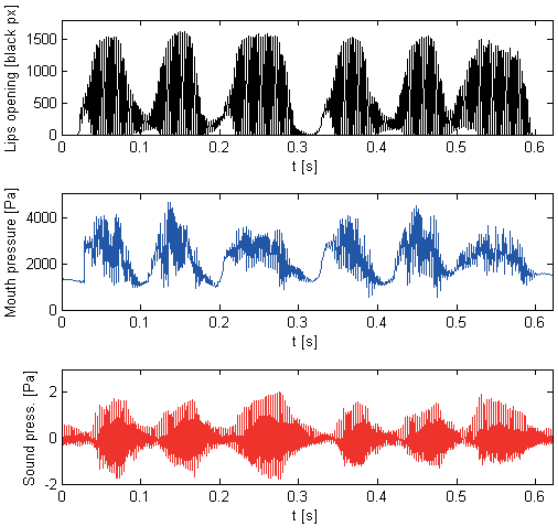

Fig. 10 – Triple staccato, depicted syllables in order ta-ta-ka-ta-ta-ka.

Soft triple staccato. The differences between toungue action ("ta" – 1st, 2nd, 4th, 5th wavelet) and throat action ("ka" – 3rd and 6th wavelet) are easily observable (see Fig. 10). Without tongue action there is no clear peak in the mouth pressure – it is a master technique to build the peak properly. "Ka-wavelets" are generally more flat, which could cause well-known loss on sharpness of the staccato while misusing this technique. Certainly, discussed quality strongly depends on player's mastery in double and triple staccato (see the discussion below).

4. DISCUSSION

The key features presented in the text are so far observed as systematic and repeatable, but only in a case of one particular player (semi-professional).
The main problem in applying this method to a wider group of players lies in a personal habit in inclining the direction of the blow relative to the plane of the mouthpiece rim. There are angles of inclination, in which the lips opening surface is not visible from the direction of instrument's leading pipe (and therefore not visible for the camera as well), but such a behavior is not to be generally condemned as a player's mistake.
Glass mouthpieces are comparable with real models only in a certain range of frequencies. The cup's acoustic compliance is much higher for a glass mouthpiece than for common ones. Hence, the input impedance looses on its maximal values so the higher tones demand more player's effort and are generally less accurate in pitch and less „brassy" in sound. To avoid this kind of data spoiling the measurements were made only in the middle (or lower) registers of the instruments.
Dynamics of tones (*p*, *mf*) was set subjectively in view of the player, so the connection between it and measured acoustic pressure might not be perfect. We have chosen this point of view for its link to the player's "self-adjustment".

5. CONCLUSIONS AND FUTURE GOALS

Some of the key features connected with the transients in trumpet sound were shown and commented. Especially the phenomena of "initial blow off" (see 3. b)), transients in legato or the "ka-wavelets" flattening couldn't be described without using the high-speed imaging.

The player's lips turned out to be a system with high inertia in the dynamics of the transient (see 3. a)). In correspondence with this statement no modulation or influence of subtle effects on them were observed so far.
Measured mouth pressures are corresponding to theoretical values proposed by Fletcher [3].
On the other hand, modulation on lower frequencies probably not connected with any simple geometrical proportions of the system were observed in player's mouth pressure. This topic as well as properties of the spectra of presented signals will be discussed in a future paper.
Without wider group of tested player's there cannot be any discussion of parallels between measured quantities and playability percieved by player [5]. This is one of the future goals as well.

6. ACKNOWLEDGMENTS

Supported by the Ministry of Education, Youth and Sports of the Czech Republic in the Long Term Conceptual Development of Research Institutes grant of the Academy of Performing Arts in Prague: The "Sound quality" project.

We would like to thank the technical glassworks of University of Chemistry and Technology in Prague, especially Mr. Josef Rotport, for accepting a peculiar challenge to make a glass mouthpiece.

7. REFERENCES

[1] Martin, D.W. "Lip Vibrations in a Cornet Mouthpiece," JASA 13(3), 1942.
[2] Yoshikawa, S. "Acoustical behavior of brass player's lips," JASA 97(3), 1997.
[3] Fletcher, N. "Mechanisms in Woodwind and Brass Instruments", Acustica 43, 1979.
[4] Logie, S., Chick, J., Stevenson, S., Campbell, M. "Upward and downward slurred transients on brass instruments: why is one not simply inverse of the other?", In: Proceedings of 10th Congres Francais d'Acoustique, Lyon, France, 2010.
[5] Logie, S., Bilbao, S., Chick, J., Campbell, M. "The Influence of Transients on the Perceived Playability of Brass Instruments", In: Proceedings of 20th International Symposium on Music Acoustics, Sydney and Katoomba 2010.

PLAYING ABOVE AND BELOW THE RESONANCE: THE CHANGING RELATIVE PHASES OF PRESSURE, FLOW AND TROMBONISTS' LIP MOTION

Henri Boutin, John Smith and Joe Wolfe

School of Physics, The University of New South Wales, United Kingdom
boutin@lam.jussieu.fr
john.smith@unsw.edu.au
j.wolfe@unsw.edu.au

ABSTRACT

We report the lip motion, upstream and downstream pressures, and flow components as trombonists play the compliant and inertive loads produced by lipping up and down from B♭2. The bore impedance is measured immediately after playing. The amplitudes of its impedance peaks monotonically decrease with playing an initially dry instrument; we attribute this to losses involving water phases. For playing durations less than 10 seconds, the resonance frequencies decrease, attributed to a dominant effect of CO2. Over longer times, increasing humidity and slowly increasing temperature overcome the CO2 effect and raise the resonance frequencies. Notwithstanding these effects, the bore impedance is usually compliant at normal playing frequencies, and its magnitude is more than 10 times larger than the upstream impedance measured in the mouth. Consequently, the mouthpiece acoustic pressure lags behind the flow and is much larger than that in the mouth. At these frequencies, a significant and early component of flow is due to the longitudinal sweeping motion of the lips. Lipping up and down from B♭2, players could readily play over more than three semitones, a range centred approximately on the bore resonance, with their lips auto-oscillating with a compliant or inertive load downstream. The vertical (z) component of the upper lip oscillation, in phase with the inter-lip aperture, lags behind the forwards (x) component by less than 90° and its amplitude is at least 50% larger. This phase difference is reduced while lipping up. The phase of the mouthpiece pressure is closer to z while lipping up and to x while lipping down, but always lies between them. The measured phase relations are consistent with a simple lip model with a bending or swinging x mode whose resonant frequency is always below the playing frequency f0, and a compressive z mode whose resonance lies always above f0.

EXPERIMENTAL INVESTIGATION OF DOPPLER SHIFT AND INFRASOUND GENERATION DURING WAVE PROPAGATION WITHIN THE BORE OF THE TROMBONE DURING SLIDE MOVEMENT

Jonathan Kemp[1], *Amaya López-Carromero*[2], *Alan Woolley*[2] *and Murray Campbell*[2]

[1]Department of Music
University of St Andrews, UK
jk50@st-andrews.ac.uk

[2]School of Physics and Astronomy
University of Edinburgh, UK

ABSTRACT

During glissando playing in the trombone the length of the approximately cylindrical slide section within the bore is altered while waves are propagating. Slide movements of 2 metres per second are not unusual. The simplest way to visualise the effect is in terms of the slide being represented by a moving reflector, resulting in a (small but measurable) Doppler shift in the wave coming from the mouthpiece before it arrives at the bell for instance. An additional effect is to be observed in terms of the volume of air within the instrument changing telescopically, leading to a localised change in DC pressure (and a resulting flow) which generates infrasound components within the bore and also impacts on the sound velocities for forward and backward going waves. Lastly there will be sections of bore with moving walls which could introduce additional mean flow effects and excitation of (mostly evanescent) transverse modes of vibration.

In this study experimental data is presented showing the pressures measured by microphones mounted in the mouthpiece, in the water key (in the slide section) and at the bell of a trombone while slide movements are performed. Some measurements were performed using a fixed excitation frequency provided by a loudspeaker mounted onto the mouthpiece. Moving the slide results in changes in both the amplitude and frequency of the signal being measured by microphones (in spite of the input signal being produced by the loudspeaker being fixed in frequency). Infrasound components were also detected inside the instrument bore. Frequency tracking of audio was combined with optical tracking of slide movement to provide evidence concerning the nature of the physics of wave propagation within the dynamically changing trombone bore and conclusions drawn concerning any implications for perception and synthesis.

1. INTRODUCTION

The slide of a trombone's primary function is to allow the player to change the length of the instrument in order to change the resonant frequencies available. Movements of the slide can be done in between sounding notes so that the bore has a static length during production of individual notes in many cases. A characteristic use of the instrument is to play during slide movement, however, and this facilitates powerful glissando and portamento techniques.

The mouthpiece (where the lips act as a valve to gate the pressure in the mouth to provide a source of acoustic excitation) and the bell are both stationary during such glissando playing, but the distance that acoustic waves must travel between these points changes due to the slide section increasing in length telescopically. From this point of view the forward going waves must undergo a change in frequency or Doppler shift due to the delay time for travel between the two points changing dynamically. Measurements of the motion of the slide in trombone playing suggest that speeds of around 2 m/s are sometimes exceeded [1] and peak velocities tend to be roughly proportion to the total distance travelled [2] and this results in measurable Doppler shifts.

Another consequence of slide motion is that the volume of the air column changes by a significant fraction, resulting in the production of significant quantities of low frequency (including infrasonic) pressure and flow within the bore.

Here differential pressure sensors are mounted in the mouthpiece and in the water key (in the slide section) of a trombone and a microphone is mounted in front of the bell. In some of the experiments the only source of acoustic energy was through the movement of the slide, while in other measurements a fixed excitation frequency was input using a loudspeaker mounted onto the mouthpiece end of the bore. Both infrasound components, generated by slide movement, and Doppler shifting of traveling waves were measured. These were compared to modelling based on optical tracking of slide movement in order to illuminate the nature of the physics of wave propagation within the dynamically changing trombone bore and draw conclusions concerning perception and synthesis.

2. APPARATUS

The experimental apparatus is shown in schematic form in figure 1. The trombone was a King Trombone with the bell partially cut off. Sensor Technics HCXM020D6V differential pressure transducers were used to measure the pressure inside the bore. Each transducer has two ports, one open to the outside air and one coupled to the air inside the instrument's bore via a 5cm long rubber pipe. The microphone located in front of the bell of the trombone was a Brüel & Kjær model 4192 microphone connected to a 2669 model signal conditioner and Nexus preamp. Data acquisition was achieved using a WaveBook/516E with WaveView 7.15.19 software. A JBL model 2446H, 8 Ohms, compression driver loudspeaker was used along with a Sherwood AX3030RA power amp. Slide position was measured using a Baumer OADM 20I4471 laser distance sensor. The position data required digital low pass filtering and time domain

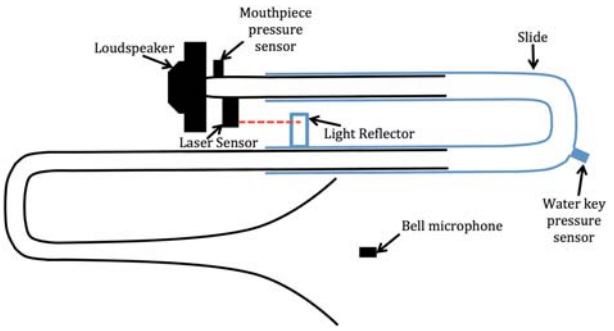

Figure 1: Schematic of the experimental apparatus including the trombone with a loudspeaker coupled in place of the mouthpiece. Blue is used to indicate the moving slide (and the light reflector and water key pressure sensor mounted on it).

interpolation to smooth high frequency noise and to upsample to an audio sample rate to act as an input for theoretical modelling. This was achieved by truncating and zero padding in the frequency domain. All calculations and plots were performed in MATLAB. Experiments were preformed in the anechoic chamber at the University of Edinburgh.

3. THEORY

3.1. Doppler shifting

The sound wave emitted by the loudspeaker must travel to the end of the slide and back again before reaching the bell section. In doing so it acts rather like a moving reflector. While the sound is not literally reflected to the source, it is redirected through 180 degrees as it propagated through the slide and thus arrives at the bell section with a time delay which depends on the time varying position of the slide. Making the approximation that the speed of sound is constant, it may be expected that the frequency of the wave received at the bell, f, is Doppler shifted according to the equation for active sonar[3]:

$$f = f_0 \left(\frac{c - 2v}{c} \right) \tag{1}$$

where f_0 is the frequency of the wave emitted by the source, v being the velocity of the slide (defining positive velocities for increasing bore length) and c is the speed of sound.

3.2. Pressure pumping

If we assume that the changes in air volume within the bore are so fast that no heat energy is exchanged with the walls and, for the moment, pretend that no energy escapes by propagation then, when the slide moves in the manner of a pump, an adiabatic change in pressure may be calculated. The initial absolute pressure and volume in the slide (P_0 and V_0) are related to the absolute pressure and volume in the slide after an approximately instantaneous change (P_1 and V_0) by:

$$P_1 = P_0 \left(\frac{V_0}{V_1} \right)^{\gamma}, \tag{2}$$

where γ is the adiabatic constant (equal to 1.4 for adiabatic gases). If the new volume is $V_1 = V_0 + dV$ and since we are considering a close to instantaneous change, the fractional change of volume in the slide will be small ($dV \ll V_0$) and we may use the binomial approximation to get

$$P_1 = P_0 \left(1 + \frac{dV}{V_0} \right)^{-\gamma} \approx P_0 \left(1 - \gamma \left(\frac{dV}{V_0} \right) \right). \tag{3}$$

Assuming that the change occurred in a time duration of t_s, we have a change of volume of $dV = 2vt_sS$ where again v is the velocity of the slide and S is the cross sectional area within the slide. The change in pressure is thus:

$$dP = P_1 - P_0 \approx -\gamma P_0 \left(\frac{2vt_sS}{V_0} \right). \tag{4}$$

So far we have ignored propagation in this analysis. In the time t_s, the pressure created will actually spread by propagation to a volume ct_sS (breaking the accuracy of the adiabatic assumption). To the first approximation, the pressure that will be generated in the volume V_0 will be given by dP multiplied by the ratio of pressure that remains $V_0/(ct_sS)$:

$$p_{gen} \approx dP \left(\frac{V_0}{ct_sS} \right) \approx -\gamma P_0 \left(\frac{2v}{c} \right) \tag{5}$$

The speed of sound itself is $c = \sqrt{P_0\gamma/\rho}$ where ρ is the equilibrium density of air so this is:

$$p_{gen} \approx -2v\rho c. \tag{6}$$

If a slide was able to achieve a velocity of 2 m/s close to instantaneously (after starting from atmospheric pressure at $P_0 \approx 10^5$), this indicates pressure changes of around -1.7 kPa. Typical fast slide movements, however, accelerate over the course of around 0.1 seconds and, since sound travels around 34 m in that time, reflection from the end of the trombone must be taken into account. In practice this significantly reduces the size of the observed pressure changes.

3.2.1. *Waveguide model*

Waveguide treatments of the trombone include the work of Smyth and Scott[4] while the use of varying delay times for modelling glissandos during slide motion is discussed in Vergez and Rodet[5]. These concentrate on the acoustic source from the lips and its interaction with the instrument, ignoring the effect of pump generated low frequency components. Since the pressure variations produced by the pumping action of the slide typically occur over the course of 0.1 seconds, we expect that signals of the order of 10 Hz will be produced. This is much lower than the first resonance of the trombone bore and thus the reflection at the bell is close to -1 for the generated pressures. We can therefore approximate the behaviour of the bore at this frequency in terms of a cylinder open at the bell and closed at the loudspeaker end. If we assume that the generated pressure is produced at the end of the slide such that the pressure sensor in the water key measures an initial forward going wave of amplitude $p_{gen}/2$ and that this, and an initial backward going wave of equal amplitude, will reverberate within the instrument then the pressure measured should be:

$$\begin{aligned} p_s(n) \quad = \quad & \frac{1}{2}\Big(p_{gen}(n) + l.p_{gen}(n - N_l) \\ & + r.p_{gen}(n - N_r) + l.r.p_{gen}(n - (N_l + N_r)\Big) \\ & + l.r.p_s\left(n - (N_l + N_r)\right), \end{aligned} \tag{7}$$

where p_s is the predicted acoustic pressure at the water key, n is the time domain sample number, l is the scalar reflection coefficient at the loudspeaker end (approximated as being $l = 1$),

r is the scalar reflection coefficient at the bell (approximated by $r = -0.95$), N_l is the (time varying) number of samples in the time domain for a round trip from the water key to the loudspeaker and back and N_r is the (time varying) number of samples for a round trip from the water key to the bell and back. This feedback equation can be run in the time domain by initialising p_s to zeros and calculating p_{gen} by putting the time varying slide velocity (calculated using the slide displacement data) into equation 5.

4. RESULTS

4.1. No source (other than slide movement)

Figure 2 shows the resulting bore pressure and movement data when the slide is moved from a large extension to low extension (as would be done during an upward glissando). A fairly large amplitude, low frequency pressure signal is produced (with the only source of energy being the compression of the air due to the pumping action of the slide movement). Also shown is the theoretical pressure signal at the water key using the simplified waveguide model given in equation 7. It may be noted that the main result of including reverberation within the bore of the instrument for the generated sound is to make any initial forward going wave (proportional to the negative of the slide velocity) followed after a time delay by its negative, meaning that the pressure buildup is loosely proportional to the negative of the acceleration of the slide (rather than its velocity).

Figure 3 shows the spectra of the pressure signals for the same experiment at the mouthpiece (blue) and water key (green). The spectra for the same microphones in the absence of slide movement are also shown to illustrate the noise floor. It should be noted that the low frequency pressure signal produced by the pumping action of the slide stands significantly clear of the noise floor below 100 Hz, giving over 115 dB re. 20μPa in the range between 0 and 3 Hz for this experiment. No clear pressure signal was observed above noise floor outside the bell (partly because the low frequency component is largely reflected by a close to negative one reflection coefficient as it approaches the bell).

Figure 4 shows the experimentally measured slide movement data and experimentally measured pressures in the bore along with the prediction from the cylindrical waveguide model for a slide movement corresponding to a downward then upward glissando (also with no source of acoustic energy other than the slide movement). Again the pressure build up is loosely proportional to the negative of the slide acceleration.

4.2. Constant frequency sine wave source

The experiment was repeated but with the addition of a constant, high frequency (nominally 10 kHz) sine wave source being played using the loudspeaker coupled to the mouthpiece side of the instrument. This high frequency was chosen because it is well above the cut-off frequency of the horn and so experiences minimal reflection in the bore, thus allowing the Doppler shift for a forward going wave to be measured without significant interference from reverberations within the bore. It is also below the cutoff frequency for higher mode propagation within the cylindrical sections of the bore.

Figure 5 shows the results when the slide movement (in the upper plot) is moving from small to large extension (as would occur for a downward glissando) with the resulting frequency tracking signal for the microphone in front of the bell shown in the lower plot in blue as a ratio to the initial frequency

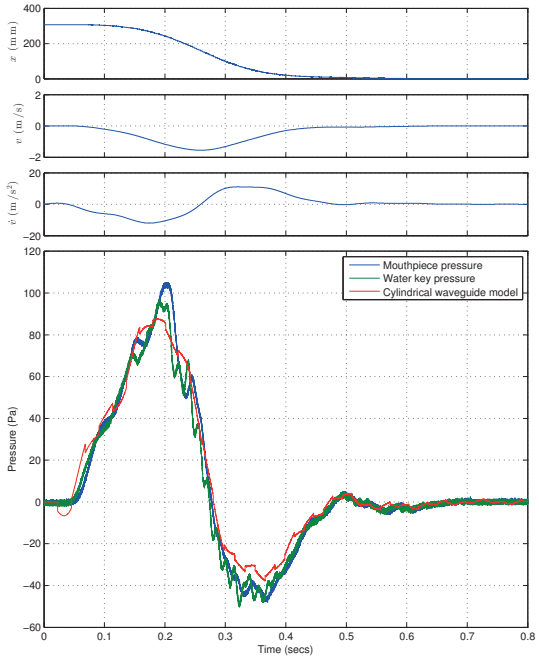

Figure 2: Slide displacement is shown in the top plot, slide velocity in the second highest plot, slide acceleration in the third plot and with the resulting bore pressure measured at the mouthpiece area and in the water key shown in the lower plot in blue and green respectively. The only energy input is provided by slide movement (in this case corresponding to an upward glissando). The red line shows the cylindrical waveguide model for the pressure build up as calculated entirely using the slide position data.

(which corresponds to the constant frequency emitted by the loudspeaker). Frequency tracking was performed by high pass filtering the bell microphone signal (Hanning filter with cut-off frequency 800 Hz), then calculating the frequency using zero crossings (using the same equations as in Kemp et al [6]) and finally averaging over 21 zero crossings in order to minimise the effects of noise. The theoretical Doppler shift for a moving reflector is shown in green as calculated directly from the slide displacement data and equation 1. It is clear that the frequency measured in front of the bell reduces during an outward slide movement and the slide acts as a moving reflector to the first approximation.

Figure 6 shows the spectra measured at the mouthpiece position (blue), water key (green) and outside the bell (red) during the same slide movement experiment as in figure 5, along with the corresponding spectra measured with the same source playing but without slide motion. The Doppler shifts observed at the water key position are roughly half of those measured outside the bell. This arrises because the water key is mounted in the moving slide section and is therefore acting as a moving receiver. No Doppler shift is observed at the mouthpiece as the Doppler shifted signal (chosen to be high in frequency) was almost all transmitted from the bore due to the cut-off frequency of the bell.

The corresponding plots for a downwards then upwards glis-

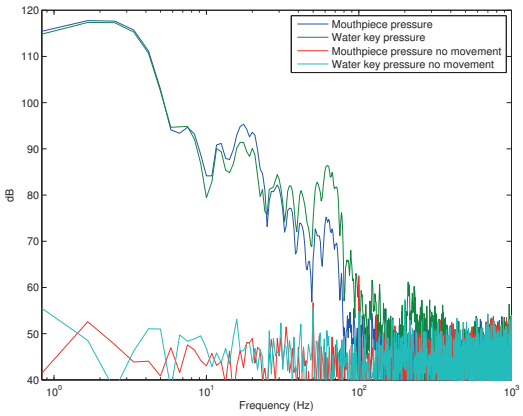

Figure 3: Spectra (with logarithmic frequency scale) for the bore pressure measured at the mouthpiece area (blue), in the water key (green) are shown during the same slide movement shown in figure 2. The only energy input is through moving the slide. Also shown are the spectra for the microphones during no slide movement (showing the noise floor).

sando are shown in figures 7 and 8. It is clear that both positive and negative Doppler shifts are present in this case.

5. DISCUSSION AND CONSEQUENCE FOR PLAYING AND SYNTHESIS

5.1. Pressure and lips

It is clear from figure 2 that during the initial stages of an upward glissando (when the slide is accelerating) the DC pressure in the mouthpiece will seem to increase (typically by the order of 100 Pa for a fast glissando) and this may be perceptible effect on the player, particularly if playing very quietly. The player will need to increase their mouth/supply pressure a little if they want to maintain the same overpressure (or pressure difference between the mouth and mouthpiece) while the slide is accelerating towards their lips. Correspondingly they may have to slightly reduce their mouth/supply pressure if they want to maintain the same overpressure during the deceleration at the end of an upward glissando. The reverse should be true for a downward glissando (with the initial acceleration requiring a slight drop in pressure etc.).

5.2. Doppler shift, glissando and slurs

When slurring to a new pitch in brass instruments without a slide, a new frequency must be instigated by the lips and the reverberant energy within the instrument will be sounding at the frequency of the previous note. The resulting forces can cause beating during the transient and split notes. In the trombone, on the other hand, the reverberant energy within the instrument is Doppler shifted, meaning that when the slide is moved, the lips can follow the frequency of the incoming pressure waves in order to play a glissando or slur to a new note with the same mode number. This is an easier task than on brass instruments without a slide.

The opposite extreme for the trombone is when a "cross grain slur" is required. This technique involves swapping mode number in order to make an upward pitch jump simultaneously with lengthening the instrument using the slide, or creating a downward pitch jump while shortening the instrument using the

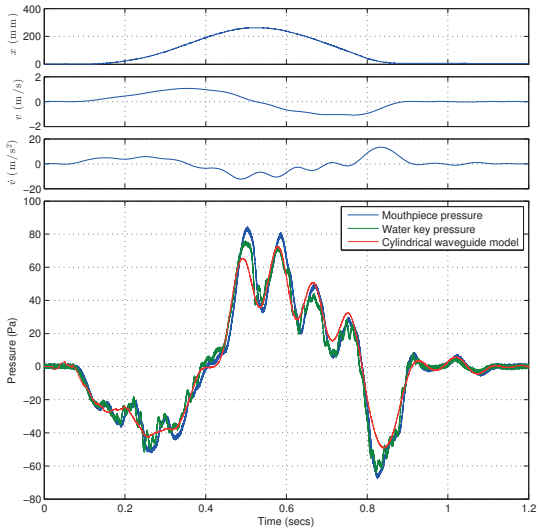

Figure 4: Slide displacement is shown in the top plot, slide velocity in the second highest plot, slide acceleration in the third plot and with the resulting bore pressure measured at the mouthpiece area and in the water key shown in the lower plot in blue and green respectively. The only energy input is provided by slide movement (in this case corresponding to a downward then upward glissando). The red line shows the cylindrical waveguide model for the pressure build up as calculated entirely using the slide position data.

slide. In these cases the task is especially difficult because not only does a new lip frequency have to be established on the instrument, but the reverberant energy which interferes with the lips is Doppler shifted in the wrong direction.

5.3. Acoustic velocity and mean flow

The pressure created by the motion of the slide will experience positive amplitude pressure reflection at the mouthpiece end, which is equivalent to a negative reflection for the acoustic velocity wave, leading to a cancellation of the velocity at the mouthpiece side of the slide. At the bell, on the other hand, the pressure travelling waves are reflected negatively, and this is equivalent to a positive velocity travelling wave reflection, meaning that the velocity wave is reinforced rather than cancelled.

This agrees with an intuitive visualisation of mean flow. In the case of a constant slide velocity, v, a steady mean flow of approximately $-2v$ is to be expected between the bell and slide necessary to prevent massive changes of DC pressure within the instrument during the large volume fraction changes. For the case of a $v \approx -2$ m/s slide motion, this implies that the peak mean flow to be expected would be approximately $-2v \approx 4$ m/s. Using the characteristic impedance of plane waves the difference between the pressures of the forward and backward going pressure waves would of the order of $2v\rho c \approx 1.7$ kPa. This is the value of the total generated pressure derived by a different route in equation 6, half of which is expected to propagate forward and half backward along the bore before the reflections occur. Given that the acoustic velocity in the pipe can be de-

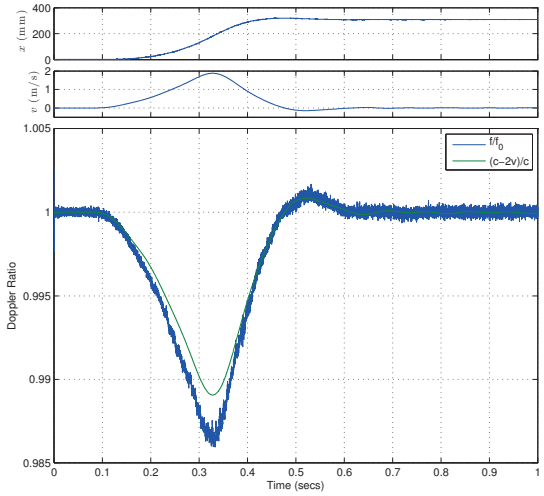

Figure 5: This experiment features a slide displacement, shown in the upper graph, that corresponds to a downward glissando with the slide velocity shown in the second graph. The measured Doppler shift ratio, f/f_0, shown in blue in the lower graph, is obtained by frequency tracking the signal measured in front of the bell and dividing by the source frequency. The theoretical Doppler shift for a moving reflector, $(c-2v)/c$, is given in green.

duced from the characteristic impedance:

$$p^+ - p^- = u\rho c \approx -2v\rho c \approx 1.7kPa, \qquad (8)$$

(in the case of a slide velocity of -2 m/s) where u is the acoustic particle velocity, p^+ and p^- are the forward and backward going acoustic pressure traveling waves respectively. It is clear that p^+ is therefore positive and peaks at just over 1.7/2 kPa = 850 Pa and p^-, being close to -1 times this value, reaches close to -850 Pa. When the slide is accelerating there is a significant imbalance between absolute values of the (velocity dependent) forward going and (delayed) backward going wave (hence the measured pressure signal of the order of $p^+ + p^- \approx 100$ Pa seen in figure 2).

5.4. Implications for synthesis

Doppler shifts are a natural consequence of having a varying delay time in the bore and these are already implicit in any waveguide model that incorporates a varying delay time when slide movement is modelled. More sophisticated treatments discussing the 3D wave equation under slide movement would be interesting although the experiments suggest that corrections involved would be slight. The low frequency sound generated by the acceleration of the slide may have an impact on the behaviour of lip models when playing at relatively quiet dynamics and fast glissandos and could be added into trombone models for completeness.

6. ACKNOWLEDGEMENTS

The research leading to these results has received funding from the People Programme (Marie Curie Actions) of the European Union's Seventh Framework Programme FP7/2007-2013/ under REA grant agreement No. 605867 supporting the BATWOMAN ITN Project.

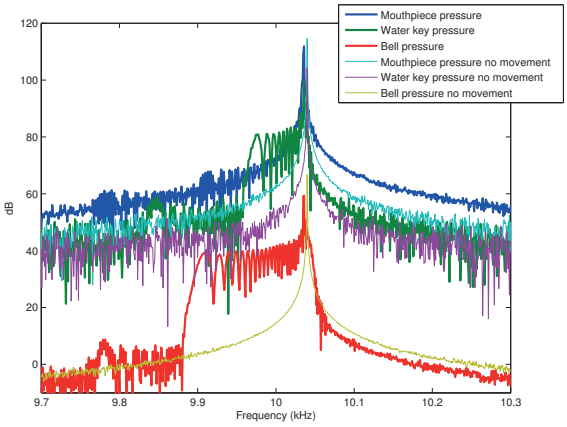

Figure 6: Spectra (around the frequency of the constant frequency input sine wave) for the bore pressure measured at the mouthpiece area (blue), in the water key (green) and outside the bell (red) during the same slide movement shown in figure 5. Also shown are the spectra for the microphones during no slide movement.

7. REFERENCES

[1] G. Ekdahl, "A simple model of the mechanics of trombone playing," Tech. Rep., Royal Institute of Technology, Department of Mechanics, SE-100 44 Stockholm, Sweden, 2001, http://www.mech.kth.se/thesis/2001/lic/lic_2001_gitte_ekdahl.pdf.

[2] W. J. Wadman, J. J. D. Van Der Gon, R. H. Geuze, and C. R. Mol, "Control of fast goal-directed arm movements," *Journal of Human Movement Studies*, vol. 5, no. 1, pp. 3–17, 1979, http://e.guigon.free.fr/rsc/article/WadmanEtAl79.pdf.

[3] L. E. Kinsler, A. R. Frey, A. B. Coppens, and J. V. Sanders, *Fundamentals of Acoustics*, p. 454, John Wiley & Sons, Inc, New York, 4th edition, 2000.

[4] T. Smyth and F. Scott, "Trombone synthesis by model and measurement," *EURASIP Journal on Advances in Signal Processing*, vol. 2011, pp. 1–13, 2011, doi:10.1155/2011/151436.

[5] C. Vergez and X. Rodet, "Comparison of real trumpet playing, latex model of lips and computer model," in *Proceedings of the 1997 International Computer Music Conference*, 1997, pp. 180–187, http://quod.lib.umich.edu/i/icmc/bbp2372.1997.050/.

[6] J. Kemp, "Sensing lip protrusion and vibratory motion in the mouthpiece during trumpet playing using a theremin," in *Proceedings of the International Symposium on Musical Acoustics (ISMA), July 7-12, 2014, Le Mans, France*, 2014, pp. 137–142, http://www.conforg.fr/isma2014/cdrom/data/articles/000114.pdf.

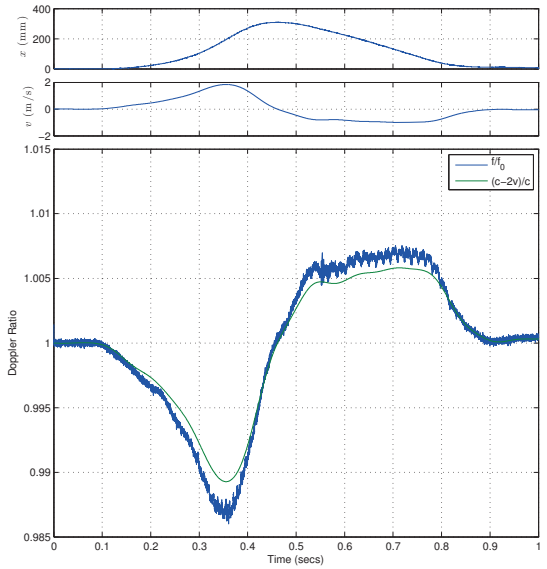

Figure 7: This experiment features a slide displacement, shown in the upper graph, that corresponds to a downward glissando then upward with the slide velocity shown in the second graph. The measured Doppler shift ratio, f/f_0 is shown in blue in the lower graph and the theoretical Doppler shift for a moving reflector, $(c-2v)/c$ is shown in green.

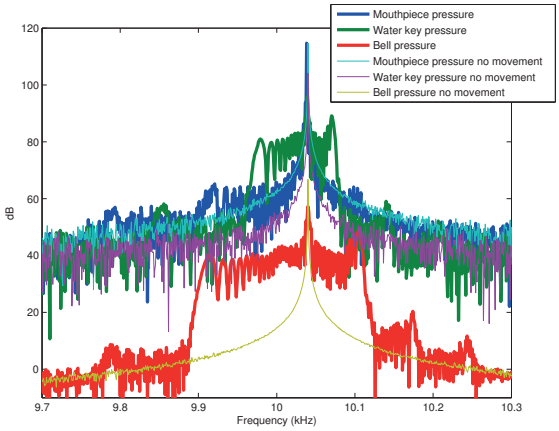

Figure 8: Spectra (around the frequency of the constant frequency input sine wave) for the bore pressure measured at the mouthpiece area (blue), in the water key (green) and outside the bell (red) during the same slide movement shown in figure 7. Also shown are the spectra for the microphones during no slide movement.

PITCH SHIFTS IN WIND INSTRUMENTS DUE TO CHANGES IN AIR COMPOSITION

Saranya Balasubramanian, Wilfried Kausel

Institute of Musical Acoustics
University of Music and Performing Arts Vienna, Austria
balasubramanian@mdw.ac.at

ABSTRACT

Our motivation is to understand the pitch deviation in a wind instrument that is caused by the introduction of orally expired air into a wind instrument. The effect of air composition, temperature, pressure and humidity on the speed of sound in air has been well studied for meterological purposes, and in this paper, we apply this robust model for calculating the speed of sound accounting for interaction between the gases involved and use it to calculate the acoustic impedance peaks and observe the shifts in the fundamental frequencies. In these simulations, the air composition and physical properties of air are chosen such that it closely mirrors playing conditions; and the pitch shifts are compared against experimental observations found in literature.

1. INTRODUCTION

Lip driven brass instruments or woodwinds that use reed or air-jet driven instruments like flute, recorder etc. all produce sound by means of oscillating air columns inside the instrument, regardless of the excitation mechanisms. As one just begins to play these instruments, the instrument response is different to a varying degree depending on the instrument. So as a preparation for a performance, musicians typically "warm up" the instruments [1]. Some even advise exhaling before playing [2] which shows the emphasis musicians place in the effect of the air they blow into the instrument on the sound produced.

This is quite logical because the pitch is the musical counterpart of the resonance frequencies of the air column, and the resonance frequencies of air are directly determined by the wavelength and the speed of sound in air in the instrument. And it is quite well-known to musicians, who in fact play different notes by altering the length of the air-column (using toneholes, sliding valves etc. depending on the instrument) thus altering the wavelength of the sound. The speed of sound however is not intentionally controlled by the player; it is simply a property of the medium through which sound propagates. The medium in this case, air, is a mixture of ambient air and the orally expired breath of the player or completely the expired breath of the player, depending on the playing technique, instrument length and shape and the interval between playing notes. The temperature and gaseous composition of expired breath are quite different from the atmospheric composition of air, and consequently alter the speed of sound; we will see in the following sections how these factors affect the speed of sound and hence the pitch.

We will consider the gases in the mixture as real and account for interaction between the gases and their effect on the specific heat capacity of the mixture and derive the speed of sound using the methods described in [3–7]. It is important to note that in this paper, we are assuming that we know the spatial distribution of the air composition, humidity and temperature along the instrument; and attempt to quantify the effect of various physical properties of the air in the instrument to the pitch. We will then compare the results obtained with measured observations of carbon dioxide content at the mouth of the instrumentalist and the calculated pitch deviation [8, 9].

2. EXHALED AIR AND AMBIENT AIR

Parameter	Ambient Air	Exhaled Air
Temperature	21 °C	31 °C
Oxygen	20 %	15.3%
Carbon dioxide	0.0395 %	2.5% - 6%
Water vapour	0.5%	1% - 6%
Nitrogen	78%	75%

Table 1: Comparison of Physical Composition and Properties of Ambient and Exhaled Air [10–14]

2.1. Breathing

The main function of the respiratory system is to absorb oxygen and expire carbon dioxide, and is typically done through the nose. Oral respiration bypasses the filtering that happens in the nasal passage however with respect to exhaled air composition, both these processes are nearly identical. While the physiological process of breathing is the same for all individuals, the gaseous composition of ones breath also varies from one person to another, for example - heavy smokers tend to have a higher carbon monoxide content in their breath [15], varying amounts of ethanol content depending on alcohol consumption and the individual's health and fitness[11]. Table 1 shows some commonly observed differences between exhaled air and ambient air.

2.2. Air Composition

As we noted before, the main gas exchange in respiration is between oxygen and carbon dioxide. The amount of CO_2 in one breath of exhaled air is around 4% [11]; and there are reported values between 2.5% and 6% [12]. The atmospheric level of CO_2 has been steadily rising, but it is still only at 0.0395% [13]. Carbon dioxide has a molecular mass of 44.00995 grams, and thus would become the heaviest constituent in the exhaled air mixture.

The air from lungs when exhaled, passes through moist surfaces and thus has a relative humidity of nearly a 100%[16, 17]. What this means is, apart from the oxygen absorbed and carbon dioxide released from the lungs, any gap in the air composition is filled with water-vapour. The actual water vapour content value of exhaled air depends on the humidity of inhaled air [10, pp. 941-942].

2.3. Temperature

Orally expired air is less sensitive to meteorological parameters such as ambient temperature and humidity [18], however exhaled air is usually warmer than the air initially present inside the instrument owing to human body temperature.

As the air travels inside the instrument it encounters various thermoviscous losses and consequently the temperature drops. This drop across the instrument has been found to be high as 12°C [19]. As one would expect, the extent of this effect depends on the instrument itself. For example, in a cornetto using the mean temperature of the air column as opposed to the temperature gradient along the bore doesn't appreciably alter the pitch [20] and on the other hand, in an experimental study of clarinets [21] a pitch difference of up to 8.5 cents was observed when the temperature gradient was replaced with an averaged temperature.

The heat diffusion is a much slower process than audio acoustic vibrations, hence the air compression and expansion resulting from oscillations behave less like an isothermal process and more like an isentropic process [22], i.e. the temperature changes will remain local, and hence it would be safer to assume a varying temperature gradient as opposed to an averaged temperature within the instrument.

3. SPEED OF SOUND

An ideal monatomic gas has only three degrees of freedom corresponding to translational motion in three dimensional space. Diatomic gases also have two rotational degrees of freedom. In ideal gases, we assume that the collisions between these molecules are completely elastic; and in atmospheric air, since Nitrogen and Oxygen are both diatomic and make up for more than 99% of its composition; it is often acceptable to ignore the interaction between these gases and treat air as an ideal diatomic gas, but in the case of exhaled air composition this would lead to inaccuracies.

Table 2 shows predicted values of speed of sound in air calculated using an approximate formula exists for speed of sound in air [23, pp. 17–18] with small amounts of additional gas, and another set of predictions using a more rigorous method (adapted from [4], described below) and the known reference values [6] for particular temperatures, and carbon dioxide and water vapour concentrations in air. The second method is described in greater detail below, which is more accurate will be used for all the simulations in this paper.

The ideal gas state equation, as one would expect applies only to an ideal gas, which is a theoretical construct. Real gases exhibit a more complex behaviour, owing to difference in the molecular properties of the constituent gases; and thus instead of the ideal gas state equation we will use the virial expansion upto the second virial coefficient (B). The virial coefficient is a temperature dependent quantity that accounts for the interaction between particles.

Speed of sound (c) in a mixture of real gases as derived in [4] is,

$$c = \sqrt{\gamma \frac{RT}{M}\left(1 + \frac{2pB}{RT}\right)}, \tag{1}$$

where, γ (specific heat ratio for real gases) is,

$$\gamma = \frac{C_{\mathrm{P}}^1}{C_{\mathrm{V}}^1}. \tag{2}$$

C_{P}^1 and C_{V}^1 (specific heats of real gases at constant pressure and constant volume respectively in kJ kg^{-1} K^{-1}) are defined [4] as,

$$C_{\mathrm{P}}^1 = C_{\mathrm{P}}^0 - \frac{R}{10^3 M}\frac{p}{RT}\left(T^2 \frac{\mathrm{d}^2 B}{\mathrm{d}T^2}\right), \tag{3a}$$

$$C_{\mathrm{V}}^1 = C_{\mathrm{P}}^0 - \frac{R}{10^3 M}\left(1 + \frac{2p}{RT}\left(\frac{T\,\mathrm{d}B}{\mathrm{d}T}\right)\right), \tag{3b}$$

where,

B	second virial coefficient (m^3 mol^{-1})
M	molar mass (kg mol^{-1})
R	universal gas constant (J K^{-1} mol^{-1})
T	thermodynamic temperature (K)
p	pressure (N m^{-2})

The specific heats at constant pressure (C_{P}^0) for ideal gases is calculated as the weighted sum of individual specific heats $C_{\mathrm{P}i}$, as shown below.

$$C_{\mathrm{P}}^0 = \sum_{i=1}^{n} C_{\mathrm{P}i}^0 x_i. \tag{4}$$

The individual specific heats of ideal gases are approximated as a polynomial function of temperature [24]

$$\bar{C_{\mathrm{P}i}} = a_i + b_i T + c_i T^2 + d_i T^3 \tag{5}$$

where,

$\bar{C_{\mathrm{P}i}}$	ideal gas specific heat (kJ kmol^{-1} K^{-1})
a_i, b_i, c_i	available for common gases in [24]
T	thermodynamic temperature (Kelvin)

The second virial coefficient (B in cm^3 mol^{-1}) for the constituent gases is computed using the square-well function [6]

$$B_i(T) = a_i - b_i e^{\frac{c_i}{T}}, \tag{6}$$

where the values for a, b, and c for the gases over applicable temperature range can be found here [25].

For a mixture of gases (excluding water vapour), we will use the following formula [4] to calculate the second virial coefficient :

$$B_{\mathrm{aa}} = \sum_{i=1}^{n} B_i x_i \frac{M_i}{M_{\mathrm{air}}}. \tag{7}$$

When humidity is present, the interaction virial coefficient between air and water vapour is too large to ignore, so we will use the mixing rule [6, vol. 3; p. 16] as follows

$$B = B_{\mathrm{aa}}(1 - x_h) + 2B_{\mathrm{ah}}x_{\mathrm{a}}x_{\mathrm{h}} + B_{\mathrm{hh}}x_h^2. \tag{8}$$

B_{hh} can be calculated either from equation (6) or using the following formula given in [5]

$$B_{\mathrm{hh}}(T) = 33.97 - \frac{55306}{T} 10^{\frac{T20000}{T^2}}. \tag{9}$$

B_{ah} is the interaction coefficient between dry air and water vapor, given by the following formula [5]

$$\begin{aligned} -B_{\mathrm{ah}} = \; & 36.98928 - 0.331705T_c + 0.13903510^{-2}T_c^2 \\ & - 0.57415410^{-5}T_c^3 + 0.32651310^{-7}T_c^4 \\ & - 0.14280510^{-9}T_c^5, \end{aligned} \tag{10}$$

where T_c is the temperature in Celsius. The formula holds good for -50°C $< T_c <$ 90°C.

Figures 1 and 2 show the trend in the speed of sound against water vapour and carbon dioxide content respectively, where all the other gases are kept at to standard atmospheric composition and proportionally decreased.

			Speed of Sound (m/s)		
Temperature (°C)	% CO_2	% H_2O	Method 1 [23]	Method 2 [4]	Actual [6]
0	0	0	331.43	331.596	331.43
0	0	1.21	332.032	332.065	332.06
0	0.0314	0	331.399	331.403	331.4
10	0	0	337.5	337.468	337.43
10	0	2.43	338.708	338.732	338.73
10	0.0314	0	337.469	337.433	337.4
20	0	0	343.57	343.397	343.31
20	0	4.62	344.917	345.867	345.84
20	0.0314	0	343.539	343.361	343.3
30	0	0	349.64	349.119	349.09
30	0	8.39	352.066	353.811	353.80
30	0.0314	0	349.649	349.082	349
51	100	0	262.959	279.151	280

Table 2: Comparison of predicted speed of sound with experimentally observed reference values. Humidity when not zero is the percentage of water molecules at a relative humidity of 100% at the given temperature.

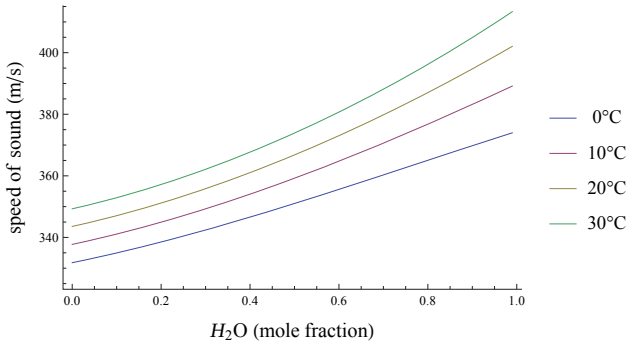

Figure 1: Predicted speed of sound for varying water vapour content at different temperatures

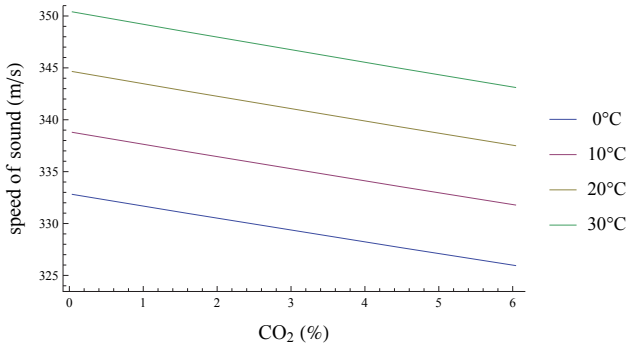

Figure 2: Predicted speed of sound for varying carbon dioxide up to 6% (exhaled air range) at different temperatures

4. PITCH SHIFTS

Pitch is a psychoacoustic property that is perceived by the brain, and cannot be explained in isolation by the fundamental frequency alone [26]. However, since we are only interested in the deviation from the initial pitch of the cold instrument, we will restrict ourselves to fundamental frequency to mean pitch. The deviation in cents is given by the difference between the frequencies of the first impedance peak. All the simulations have been done for a very simplified wind instrument model - a cylindrical tube 100 cm long and 1 cm in diameter.

Figures 3a, 3b show the simulated pitch deviations for varying carbon dioxide, water vapour content respectively. The initial conditions in both are were identical; standard dry and carbon dioxide free air at 21 °C. The expired air will be saturated with water vapour (100% relative humidity) and the corresponding specific humidity level is between 2.5% and 6% depending on other factors such as pressure and temperature. In this case, we can see that the effect on humidity alone is very slight - less than 0.5 cents increase for a 6% concentration of water vapour in the air mixture. Carbon dioxide on the other hand shows a much stronger effect, causing the pitch to drop by over 25 cents.

Figure 3c shows the pitch shift caused due to change in temperature. The initial reference pitch is calculated for standard dry and carbon dioxide free air at 0 °C and we can see that the pitch increases linearly up to nearly 30 cents for a temperature rise of 31 degrees.

When an instrument is being played, all these effects will act together and experimentally observed [9] pitch shifts while monitoring the CO_2 and O_2 and temperature levels cannot be inferred easily by studying the trends individually. The measurements from [9] are reproduced in figure 4.

Key observations from these measurements are,

1. right after the attack the pitch decreases and forms a plateau
2. when there's a new breath, the pitch increases to its former peak value and follows the same pattern as above
3. when circular breathing is performed (breathing without interruption of the sound), the pitch increases suddenly as observed in the above cases
4. when there is a break in sound, but no renewed breath, the pitch starts from its previous value (no sudden increase) and then follows the same pattern as above

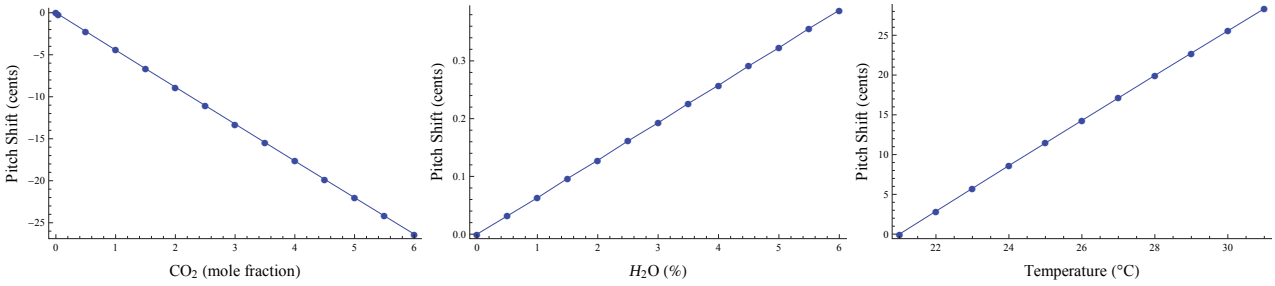

(a) Pitch shifts due to $C0_2$ content (b) Pitch shifts due to humidity in the air (c) Pitch shifts due to change in temperature

Figure 3: Simulated showing pitch shifts for varying temperature, carbon dioxide and water vapour content

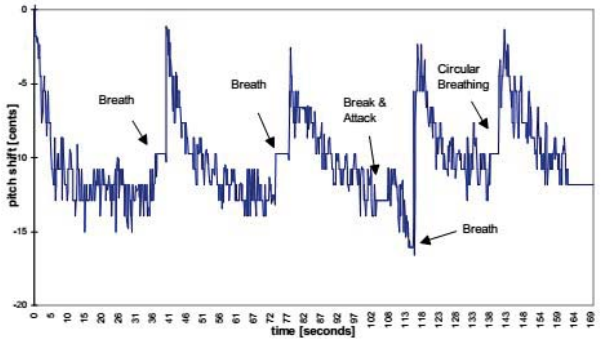

(a) Measured variation in pitch during continuous play

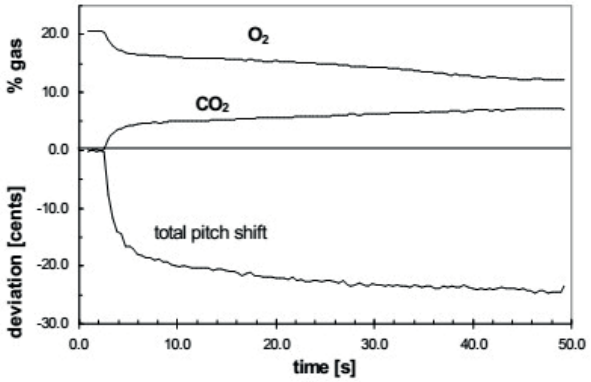

(b) Measured $C0_2$ and 0_2 contents (upper part of graph) and computed expected pitch shift (1ower part)

Figure 4: Relationship between carbon dioxide content and pitch shifts [9]

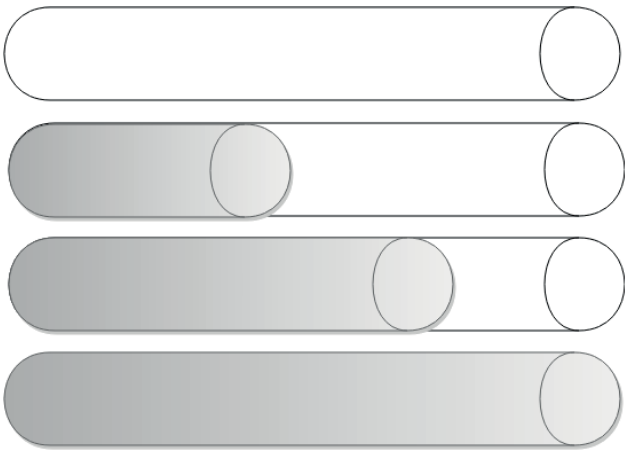

(a) Representation of air composition in the cylindrical tube. The shaded part represents exhaled air, and the unshaded part represents ambient air that was initially present in the instrument.

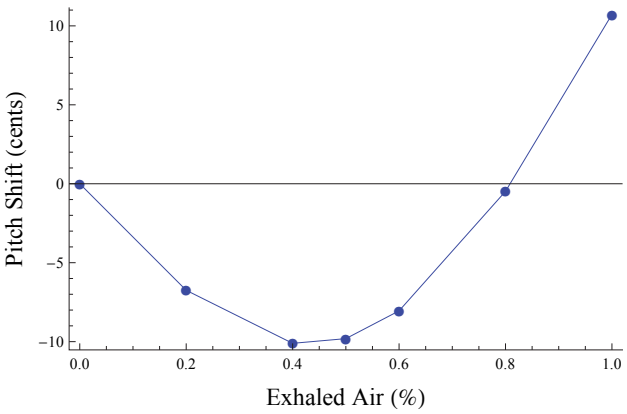

(b) Simulation of pitch shifts due to exhaled air

Figure 5: Pitch shifts simulated in a simplified instrument model - a cylindrical tube of length 100 cm, and diameter 1 cm

To simulate playing conditions, the reference pitch is calculated for the above-mentioned instrument, entirely filled with standard air at 21 °C. And then, we assume that the air inside the instrument is replaced with exhaled air as shown in figure 5a. In reality, the gases would diffuse in a complex manner and exhaled air and ambient air would not have a clear boundary as shown in figure 5a, nonetheless it is a useful means to visualise the pitch variation in terms of proportion of exhaled air content inside the instrument. In figure 5b the pitch decreases up to 10 cents when the exhaled air spreads up to nearly half the instrument. After that, the pitch starts to increase, nearly reaching the original pitch when exhaled air concentration is around 80% of the instrument, and increases still more by 10 cents when the instrument is completely filled with exhaled air. While we ignore the temperature losses along the instrument, the trend is quite similar to that observed in figure 4.

In [8], the carbon dioxide content was only measured in the player's mouth and gives no information about the spatial propagation of the gases; but considering the fact that the volume of air in a single breath cannot fill the instrument, and that the diffusion is not instantaneous, it seems dubious to assume that the gas distribution along the entire instrument would be identical to that measured in the player's mouth for calculating the resonant frequencies. Figure 5b does not show an increase in pitch at every attack though, the pitch is observed to increase only when the instrument is at least half filled with exhaled gas; which maybe the case from the second breath in the measurements in figure 4.

5. CONCLUSIONS

By establishing the spatial distribution of gases and their physical properties as an input parameter in calculating the pitch, we are excluding the modelling of propagation and diffusion of gases (which is a complex subject in its own right, theoretically modelled in [27]), localised temperature changes due to compression and rarefaction of the air during oscillations, thermoviscous losses near the wall and lossy boundaries from the scope of this exercise. It appears that along with varying air composition, the spatial distribution of gases too play a part in the pitch shifts observed; and needless to say, this needs to be verified experimentally.

6. ACKNOWLEDGEMENTS

This research work has been funded by the European Commission within the ITN Marie Sklodowska Curie Action project BATWOMAN under the 7th Framework Programme (EC grant agreement no. 605867). This work made use of Mathematica® 9 and ARTool [28] for calculations and simulations. The first author is extremely thankful to Vasileios Chatziioannou and Amaya López-Carromero for valuable pointers and literature suggestions.

7. REFERENCES

[1] M. Campbell, "Musical acoustics for musicians," in *Proceedings of the International Symposium on Music Acoustics, ISMA 2014*, Le Mans, France, 2014, French Acoustical Society (SFA), pp. 1–7.

[2] Joseph Robinson, "Oboists, exhale before playing," *Double Reed*, vol. 19, no. 3, pp. 93–96, 1996.

[3] George SK Wong, "Speed of sound in standard air," *The Journal of the Acoustical Society of America*, vol. 79, no. 5, pp. 1359–1366, 1986.

[4] Owen Cramer, "The variation of the specific heat ratio and the speed of sound in air with temperature, pressure, humidity, and CO_2 concentration," *Journal of the Acoustical Society of America (JASA)*, vol. 93, no. 5, pp. 2510–2516, 1993.

[5] RW Hyland, "A correlation for the second interaction virial coefficients and enhancement factors for moist air," *J. Res. Natl. Bur. Stand. A*, vol. 79, pp. 551–560, 1975.

[6] Allan J Zuckerwar, *Handbook of the speed of sound in real gases*, vol. 3, Academic Press, 2002.

[7] Howard C. Hardy, D. Telfair, and William J. Pielemeier, "The velocity of sound in air," *Journal of the Acoustical Society of America (JASA)*, vol. 13, pp. 226–233, 1942.

[8] Leonardo Fuks, "Prediction of pitch effects from measured CO_2 content variations in wind instrument playing," *KTH, TMH-QPSR*, vol. 4, no. 1996, pp. 37–43, 1996.

[9] Leonardo Fuks, "Prediction and measurements of exhaled air effects in the pitch of wind instruments," in *Proceedings of the International Symposium on Musical Acoustics, ISMA 1997*, St Alban (UK), 1997, Institute of Acoustics, vol. 2, pp. 373–378, MYERS, Arnold, Vol.19, Part 5, Book 2.

[10] John Denis Enderle and Joseph D Bronzino, *Introduction to biomedical engineering*, Academic Press, 2012.

[11] Boguslaw Buszewski, Martyna Kesy, Tomasz Ligor, and Anton Amann, "Human exhaled air analytics: biomarkers of diseases," *Biomedical Chromatography*, 2007.

[12] O.Yu. Nikiforova, Yu.N. Ponomarev, and A.I. Karapuzikov, "Accounting for humidity of exhaled air for retrieving gaseous biomarkers," *Atmospheric and Oceanic Optics*, vol. 26, no. 6, pp. 550–555, 2013.

[13] Pieter Tans and Ralph Keeling, "Trends in atmospheric carbon dioxide," 2014, [Online at `www.esrl.noaa.gov/gmd/ccgg/trends/`; accessed 2-December-2014].

[14] John W Coltman, "Resonance and sounding frequencies of the flute," *The Journal of the Acoustical Society of America*, vol. 40, no. 1, pp. 99–107, 1966.

[15] MJ Jarvis, MA Russell, and Y Saloojee, "Expired air carbon monoxide: a simple breath test of tobacco smoke intake.," *Bmj*, vol. 281, no. 6238, pp. 484–485, 1980.

[16] Elmer Berry, "Relative humidity of expired air," *American Physical Education Review*, vol. 19, no. 6, pp. 452–454, 1914.

[17] Nina Turner, John Parker, and Judy Hudnall, "The effect of dry and humid hot air inhalation on expired relative humidity during exercise," *American Industrial Hygiene Association Journal*, vol. 53, no. 4, pp. 256–260, 1992, PMID: 1529918.

[18] P Höppe, "Temperatures of expired air under varying climatic conditions," *International journal of biometeorology*, vol. 25, no. 2, pp. 127–132, 1981.

[19] AH Benade, "Thermal perturbations in woodwind bores," *The Journal of the Acoustical Society of America*, vol. 35, no. 11, pp. 1901–1901, 1963.

[20] MO Van Walstijn, JS Cullen, and DM Campbell, "Modeling viscothermal wave propagation in wind instrument air columns," *PROCEEDINGS-INSTITUTE OF ACOUSTICS*, vol. 19, pp. 413–418, 1997.

[21] D Noreland, "An experimental study of temperature variations inside a clarinet," in *Proceedings of the Stockholm Music Acoustics Conference*, 2013.

[22] Julius O. Smith, *Physical Audio Signal Processing*, Stanford University, 2010.

[23] Cornelis Johannes Nederveen, *Acoustical aspects of woodwind instruments*, Northern Illinois University Press DeKalb, 1998.

[24] Benjamin Gayle Kyle, "Chemical and process thermodynamics," 1984.

[25] D. Ambrose, M. B. Ewing, and M. L. McGlashan, "Critical constants and second virial coefficients of gases - tables of physical & chemical constants Kaye & Laby Online. version 1.0," 2005, [Online at `www.kayelaby.npl.co.uk/chemistry/3_5/3_5.html`; accessed 7-November-2014].

[26] Eric J Heller, *Why you hear what you hear: an experiential approach to sound, music, and psychoacoustics*, Princeton University Press, 2012.

[27] Giovanni Badino, "The legend of carbon dioxide heaviness," *Journal of Cave and Karst Studies*, vol. 71, no. 1, pp. 100–107, 2009.

[28] Alistair Braden, Delphine Chadefaux, Vasileios Chatzioannou, Sadjad Siddiq, Clemens Geyer, and Wilfried Kausel, "Acoustic research tool (ARTool)," 2013, [Online at `http://artool.sourceforge.net/`; accessed 7-February-2015].

INHARMONICITY OF A TRUMPET WITH A VARIABLE DEPTH MOUTHPIECE

Robin Tournemenne[1], Jean-François Petiot[1] and Joël Gilbert[2]

[1] Institut de Recherche en Communications et Cybernètique de Nantes, France
[2] Laboratoire d'Acoustique de l'Université du Maine, France
robin.tournemenne@irccyn.ec-nantes.fr
jean-francois.petiot@irccyn.ec-nantes.fr
joel.gilbert@univ-lemans.fr

ABSTRACT

This study focuses on the agreement between harmonicity criteria of the trumpet, calculated using either the resonance frequencies of the input impedances, or the playing frequencies of sounds produced by physical modeling (simulated sounds) or played by a musician (real sounds). In order to create different trumpets with different acoustical behavior, a variable depth mouthpiece was developed whose depth can be easily and continuously adjusted from "deep" to "shallow". After a measurement of the input impedance of the trumpet with different mouthpiece depths, simulations by physical modeling were produced on different notes with the harmonic balance technique and the impedance as input. A musician also played the trumpets on different notes. Four fingerings were considered in the study. The influence of the depth of the mouthpiece on the trumpet harmonicity was investigated using different estimators based on the Equivalent Fundamental Pitch (EFP). For a given reference frequency (resonance for the impedance, or tuning note for the sounds), and a given fingering, the EFP calculates the difference in cents between the multiples of this reference and the resonances of the impedance (or the playable notes). Different criteria are proposed to aggregate all these EFP over the regimes and/or fingerings in order to provide an estimator of the trumpet harmonicity. For different mouthpiece depths, a comparison of the harmonicity criteria obtained with the impedance, the simulations, or the played notes by a musician, is proposed. The results show that the simulations by physical modeling can be a relevant alternative to the input impedance measurements to predict certain qualities of the instrument, opening the door to virtual acoustics for instrument makers.

NON-LINEAR SOUND PROPAGATION AND SPECTRAL ENRICHMENT AS A KEY TO CHARACTERISING BRASS INSTRUMENT TYPES

Murray Campbell[1], Joël Gilbert[2], Arnold Myers[1], Romain Beauvais[2], Amaya Lopez-Carromero[1]

[1] Univeristy of Edinburgh, United Kingdom of Great Britain and Northern Ireland
[2] Laboratoire d'Acoustique de l'Université du Maine, France
d.m.campbell@ed.ac.uk
joel.gilbert@univ-lemans.fr
a.myers@ed.ac.uk
romain.beauvais.etu@univ-lemans.fr
a.lopez-carromero@sms.ed.ac.uk

ABSTRACT

Narrow-bore instruments are commonly perceived to be brighter than wide-bore models of the same kind of instrument. This effect is closely related to the effect of the bore profile of a brass instrument on the potential for non-linear propagation of sound within the tube. This paper reports on recent experimental work and numerical simulations aimed at deriving a quantitative prediction of the effect on timbre of nonlinear spectral enrichment in a brass instrument from measurements of its bore. An 'enrichment' parameter derived from bore shape and size is proposed which is can be used to characterise types of brass instrument.

A SIMULATION TOOL IN TIME DOMAIN FOR BRASSINESS STUDIES

Sylvain Maugeais[1], *Joël Gilbert*[2]

[1] Laboratoire Manceau de Mathématiques de l'Université du Maine, France
[2] Laboratoire d'Acoustique de l'Université du Maine, France
sylvain.maugeais@univ-lemans.fr
joel.gilbert@univ-lemans.fr

ABSTRACT

A time-domain numerical model of brass instrument sound production is proposed as a tool to predict their brassiness, defined as the rate of spectral enrichment with increasing dynamic level. It is based on generalized Burger's equations dedicated to weakly nonlinear wave propagation in nonuniform ducts. The relevance of the present tool is evaluated by carrying out simulations over distances longer than typical shock formation distances, and by doing preliminary simulations of periodic regimes in different brass bore geometries.

ANALYSIS OF THE ACOUSTIC INPUT IMPEDANCE OF A VIBRATING TROMBONE BELL

Mathieu Secail-Geraud[1], François Gautier[1], Joël Gilbert[1], Peter Hoekje[2]

[1] Laboratoire d'Acoustique de l'Université du Maine, France
[2] Baldwin Wallace University, United States of America
mathieu.secail-geraud@univ-lemans.fr
francois.gautier@univ-lemans.fr
joel.gilbert@univ-lemans.fr
phoekje@bw.edu

ABSTRACT

The acoustic oscillations of the internal air column of a wind instrument induce wall vibrations of the body. However, the importance of the influence of such vibrations on the produced sound is an open question. The case of the trombone bells is particular because of the small thickness of the wall and large diameter of the horn's extremity which favors the vibroacoustic coupling between the body's vibrations and the internal acoustical field.Experimental investigation of this vibroacoustic coupling is performed on a Courtois trombone. An experimental modal analysis of the bell is performed using a miniature impact hammer and a miniature triaxial accelerometer: bell modes are classified using their modal circumferencial index m. Most of the bell modeshapes are found to be non axisymetric. One of them (around 800Hz) is found to be axisymetric. The bell is placed inside a tank where the water level can be varied. Measurements of the acoustic input impedance of the duct and measurements of the mechanical mobility of the bell for different water levels show that the bell mechanical eigenfrequencies are significantly shifted by the fluid-loading. Small and repetable changes in the acoustic input impedance are also observed and show clearly the wall vibration effect.Modelling of such vibroacoustic coupling is performed using a plane wave representation of the internal acoustic field and a modal representation of the wall vibrations. This model allows us to compute the input acoustic impedance for different sets of bell eigenfrequencies and for different positions of the slide. The change of the input acoustic impedance by the wall vibrations is quantified when coincidence conditions between acoustical and structural modes are satisfied or not.

COUPLING BETWEEN WALL VIBRATIONS AND THE AIR COLUMN IN BRASS WIND INSTRUMENTS: A COMPARISON BETWEEN THEORETICAL PREDICTIONS AND EXPERIMENTAL RESULTS

Thomas Moore, Britta Gorman, and Michelle Rokni *Wilfried Kausel and Vasileios Chatziioannou*

Department of Physics
Rollins College, Winter Park, Florida, USA
tmoore@rollins.edu

University of Music and Performing Arts Vienna, Austria
kausel@mdw.ac.at

ABSTRACT

It has been shown that the bell vibrations of brass wind instruments can significantly affect the sound produced by the instrument, and over the past decade several theories have been proposed in attempts to explain how this is possible. All of the proposed theories can explain many of the observed effects, however, two aspects have been difficult to accurately predict: the broad-band response and the frequency dependence. Recently, Kausel, et al. [J. Acoust. Soc. Am. **137**, 3149 (2015)] have proposed a mechanism that may explain how the acoustic field inside the instrument can couple with the wall vibrations. We present the results of experimental investigations and compare them to predictions of this theory. The agreement between the predictions and the experimental results indicates that the proposed coupling mechanism can account for the observed phenomena.

1. INTRODUCTION

The question of whether the bell vibrations affect the sound of brass wind instruments has been a topic of discussion for at least a century. For most of that time musicians universally believed that bell vibrations affect the sound produced during play, but lacking experimental evidence scientists were not convinced. However, experiments performed a decade ago using artificial lips to play a trumpet conclusively determined that the sound produced by the instrument is affected by the vibrations of the bell, and this effect is significant enough to be perceived by the audience.[2] A thorough review of the subject can be found in Ref. 3.

It was proposed in the original work that showed the existence of such effects that the vibrations in the instrument feedback to the lips, changing lip motion and producing an altered sound.[2] While this may indeed happen, the characteristics of the effects attributable to bell vibrations indicate that there are other processes at work as well. Furthermore, these unidentified processes may be the dominant cause of the perceived differences in sound attributable to bell vibrations. Indeed, the effects of bell vibrations have been shown to be measurable when the air column is excited by a speaker attached to the mouthpiece, which eliminates any effects attributable to lip motion.[3]

Beyond the lack of the necessity of lip motion, two other important aspects of the effects of bell vibrations provide clues to the origin of the effects: the broad-band nature of the effects and the fact that the bell vibrations may enhance or decrease the sound level produced by the instrument depending upon the frequency of air column oscillations.[3] A successful theory must simultaneously explain the lack of necessity for lip motion, the broad-band nature of the effects, and the frequency dependence.

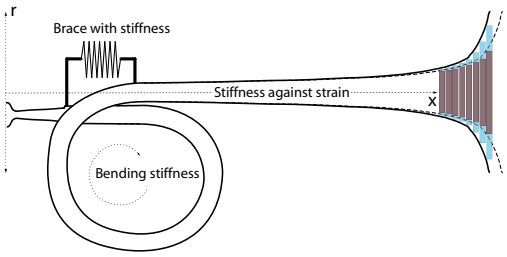

Figure 1: Diagram of a brass wind instrument and how axial vibrations can cause changes in the bore diameter. (After Ref. 1)

Recently, Kausel et al. have proposed an explanation for the origin of the effects of bell vibrations on the sound produced by brass wind instruments.[1] The theory posits that vibrations along the bell axis are responsible for these effects and it predicts both the broad-band nature of the effects and the fact that the sound power at some frequencies are enhanced while it is decreased at others. The work reported here was designed to test this theory.

2. PROPOSED THEORY

The proposed theory is presented in detail in Ref. 1, but for the present purposes it is sufficient to understand that the theory posits the existence of axial motion of the instrument. This axial motion, which can excite a series of axial resonances, results in changes in the cross sectional area of the of the bore within the bell region. The mechanism that translates axial motion to a change in bore area is illustrated in Fig. 1. As the bore oscillates in the axial direction, the motion causes the length of the instrument to change. Although the changes are small in comparison to the length of the instrument, and therefore the effect on the air column resonances will be minuscule, in the flaring region of the bell the axial motion translates into a change in the area of the bore. The theory posits that origin of the effects attributable to bell vibrations is this variation in the bore, which oscillates at the frequency of the resonating air column.

As presented in Ref. 1, the theory posits that the axial vibrations can be excited by the internal pressure in the mouthpiece, eliminating the need for considering lip vibrations. However, as noted above, for the theory to encompass the experimental evidence it must account for two other important observations: the broad-band nature and the changes in the sign of the effect as the frequency changes. Both of these characteristics are evident

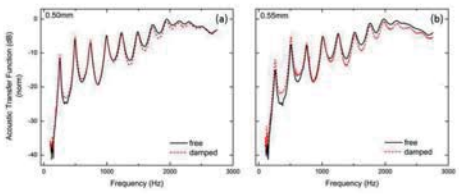

Figure 2: Acoustic transfer function of two straight bells with mouthpieces for the case of the bell freely vibrating (solid) and with the bell heavily damped with bags of sand (dashed).

when the acoustic transmission function (ATF) of a trumpet is measured under conditions where the bell is free to vibrate compared to when the bell vibrations are heavily damped by bags of sand. The results of this type of experiment were reported in Ref. 3 and they show a change in the ATF up to 3 dB over a bandwidth of approximately 2 kHz. Furthermore, the difference between the ATF measured for the two cases changes sign twice within this range, changing from the vibrations reducing the magnitude of the acoustic transfer function to increasing it and back to decreasing it. The frequency at which the sign of the effect changes is termed the *crossover frequency*. Similar effects are seen in measurements of the input impedance, and the theory developed in Ref. 1 predicts both of these effects.

Because the axial extension will be a maximum when the exciting frequency is near the frequency of an axial resonance, the bandwidth of the effects are predicted to be related to the bandwidth of the resonances. Since the effect on the radiated sound are typically broad-band, the theory demands that the axial resonances be similarly broad. Likewise, because the phase of the axial oscillations will experience a shift around the resonance frequency, the theory predicts that the effect on the air column will change sign at this frequency. Thus the theory can be tested by identifying the axial resonance frequencies, comparing the bandwidth of the resonances to the frequency range of the effects on the sound, and then identifying the crossover frequency as being the frequency of an axial resonance.

In what follows we describe experiments that measure the first axial resonance of two straight trumpet bells with an attached mouthpiece. The resonance frequencies and bandwidths are compared to the measured ATFs and it is found that the crossover frequency coincides with the axial resonance frequency. Similarly, the bandwidth of the resonance is shown to be broad enough to encompass the frequency range over which effects attributable to bell vibrations are observed.

3. EXPERIMENTS

3.1. Measurement of the acoustic transfer function

To test the predictions of the theory, two trumpet bells were manufactured by the Swiss instrument maker *Musik Spiri*. The bells were manufactured without bends and were both approximately 65 cm long. Both bells were manufactured identically, with the only difference being that the brass used in one bell had a thickness of 0.50 mm and the other was 0.55 mm thick. Each bell was fitted with a 7C trumpet mouthpiece and the acoustic transfer function was measured with the bell heavily damped with sandbags and again with it left free to vibrate.

To measure the ATF of the bells, a horn driver with a titanium diaphragm was attached to the mouthpiece. The adapter used to connect the speaker to the mouthpiece was modified to mount a microphone between the driver and the mouthpiece, and a matched microphone was placed approximately 1 m from the bell. The bell was braced with a 2.5 cm wide clamp centered approximately 37 cm from the driver. It is known that the bell of a trumpet radiates in all directions and that changes to the area near the rim can result in changes to the input impedance. Therefore, to ensure that the measurement was not affected by a change in the environment near the bell, a wooden baffle was placed around the bell with approximately 2 mm of clearance at the rim to ensure that the bell was free to vibrate. Measurements were made with sound absorbing foam surrounding the entire apparatus. These precautions ensured that any change in the input impedance was attributable to changes in the internal air column and not due to placing the bags of sand near the bell rim.

To ensure a precise measurement of the ATF, a sinusoidal signal lasting 1 s was used to drive the horn driver at each frequency of interest. The frequency of the signal was varied from 100 Hz - 3 kHz in increments of 1 Hz. A 1 s delay was inserted before changing the driving frequency to provide time for any bell vibrations to decay before driving the air column at the next frequency. The signals from the input and output microphones were recorded at each driving frequency and the power spectra were calculated in real time. The measured power in the driving frequency was then used to determine the transfer function before changing the frequency of the driving signal. The long sample time allowed for precise measurements as well as ensuring that the bell vibrations had adequate time to reach steady-state at each frequency. The results of these measurements for both bells are shown in Fig. 2. In Fig. 2 the solid line denotes the ATF measured when the bell is free to vibrate and the dashed line indicates that the bell vibrations were heavily damped. Note that the two bells behave similarly, with the magnitude of the ATF enhanced at low frequencies and depressed at higher frequencies. The difference between the two transfer functions for the thicker bell is shown in the top graph in Fig. 3, where it can be seen that the crossover frequency occurs at approximately 860 Hz.

The difference in the ATF calculated using the model described in Ref. 1 is shown in the middle graph in Fig. 3, which demonstrates that the predicted crossover frequency agrees with the experimental result. But while the agreement between the experimental determination of the crossover frequency and the prediction of the model is quite good, comparing the measured and calculated differences indicates that the overall form of the predicted change in the ATF is not similar to the measured change. This disagreement was found to be attributable to the 2 mm gap between the rim of the bell and the baffle. The gap between the baffle and the bell allowed the bell to freely vibrate while still ensuring that the presence of the sandbags used to damp the vibrations did not affect the acoustical arrangement. Unfortunately, the gap was sealed by the bags of sand when the bell vibrations were damped but open when it was left free to vibrate. It was found that the presence of this gap produced a small but measurable change in the ATF.

The bottom graph in Fig. 3 shows the calculated difference between the ATF of the bell with the gap and without it. In this case the wall vibrations were not included in the model, so one would predict that the measured ATF could be approximated by a weighted superposition of the two lower graphs in Fig. 3. The measurement, shown in the upper graph, does indeed have this

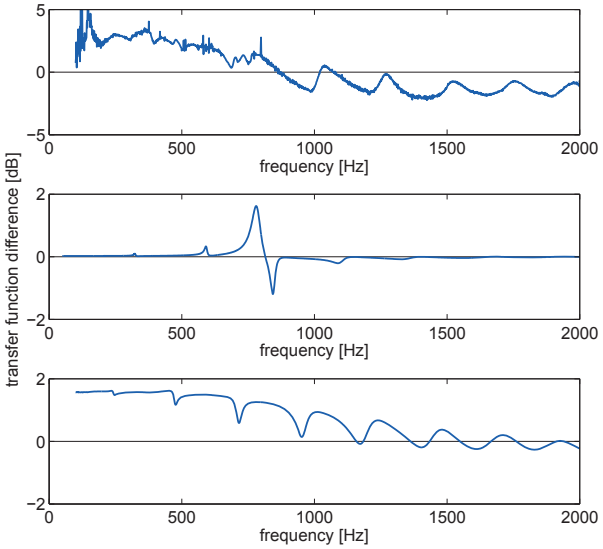

Figure 3: (Top) Difference in the acoustic transfer functions shown in Fig. 2b. The crossover frequency occurs at approximately 860 Hz. (Middle) Calculated difference in the ATF using the model described in Ref. [1]. (Bottom) Calculated difference in the ATF including the gap between the bell and baffle. Details are given in the text.

form.

The effects of the gap between the bell and the baffle complicate the interpretation of the measurement of the ATF, however, it does not appear to significantly affect the measurement of the crossover frequency. The crossover occurs at the frequency predicted by the model when the gap is not included, and as will be shown below, it also occurs at the frequency of an axial resonance.

3.2. Identification of axial mode frequencies

To compare the crossover frequencies with the axial resonance frequencies it is necessary to unambiguously identify the axial resonances. However, determining the frequencies of the axial resonances is more difficult than measuring the ATF. This difficulty stems primarily from the fact that there are numerous structural resonances of a trumpet bell, resulting in a variety of symmetric deflection shapes.[4] The majority of these resonances are attributable to elliptical mode shapes, which are characterized by radial vibrations that have one or more radial nodes and one or more nodal circles. These resonances typically have quality factors of 100 or more and only minimally affect the area of the bore because the contiguous antinodes are π out of phase.[3] Therefore, while it is highly unlikely that elliptical modes have a significant affect on the sound produced by an instrument, they make it difficult to determine which resonances can be attributed to purely axial motion.

Two methods were devised to distinguish between the axial modes and the elliptical modes so that the frequencies of the axial resonances could be unambiguously determined. Both methods involved measuring the mechanical transfer function (MTF) of axial vibrations from the mouthpiece to the end of the bell, averaged over the cross section of the bell. Although the measurements were made using two different experimental techniques, at two different laboratories, with two different bells, the results of the two experiments are similar.

In experiments conducted at Rollins College, Florida, USA

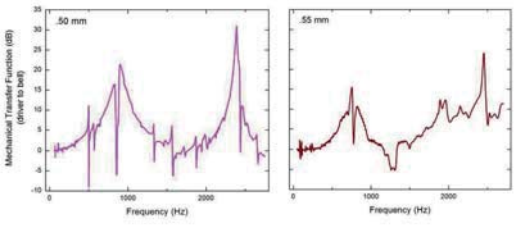

Figure 4: Axial MTF from mouthpiece to bell of the two trumpet bells. The transfer function for the 0.50 mm thick bell was measured using accelerometers and the measurements of the 0.55 mm thick bell were made using a laser Doppler vibrometer.

the vibrations of the straight bell with a nominal thickness of 0.55 mm were induced at the small end using a piezoelectric transducer that scanned the frequency spectrum from 100 Hz to 2.5 kHz. The frequency was scanned in a logarithmic sweep using BIAS software. The amplitude and phase of the motion of the driver were measured using a laser Doppler vibrometer (LDV), and similar measurements were made of the bell motion. To ensure that the whole-body motion was detected and the effects of the elliptical modes were diminished, measurements of the bell motion were made approximately 1 cm from the rim at 12 equally spaced radial locations. These measurements were then averaged in the complex plane so that the displacement attributable to symmetric antinodes canceled due to their complementary phases. This process ensured that only the displacement due to whole-body motion was recorded. Similar experiments were conducted with the 0.50 mm thick bell at the Institute of Music Acoustics (Wiener Klangstil) in Vienna, Austria, however, in these experiments eight accelerometers were attached to the bell and mouthpiece rather than using LDVs to measure the vibrations.

Results from both experiments are shown in Fig. 4, where the magnitude of the MTF is plotted as a function of driving frequency for both bells. The slight variations in the frequencies of the resonances can be attributed to the differing thicknesses of the metal and the added mass of the accelerometers in one case. The measurements of the 0.50 mm thick bell also show evidence of the elliptical modes, which are identifiable by their narrow-bandwidth. These can be explained by the fact that the placement of the accelerometers on the bell induced a slight asymmetry, which caused the amplitudes of the antinodes to not completely cancel during the averaging process. Laser Doppler vibrometry is a non-contact measurement, therefore the effects of these elliptical modes are greatly reduced in the measurements of the 0.55 mm thick bell.

The measurements shown in Fig. 4 reveal that there are two significant whole-body resonances that may be responsible for the observed acoustical effects. These resonances occur at approximately 835 Hz and 2.5 kHz in the 0.55 mm thick bell and at slightly lower frequencies in the thinner bell. Both resonances exhibit apparent mode splitting that can be attributed to asymmetries of the structure. The most significant asymmetry is probably the seam in the metal that extends along the length of the bell. This seam may have minimal effects on the local deflection shapes that characterize elliptical modes, but the whole-body resonance of the bell is attributable to the inte-

Figure 5: Decorrelated electronic speckle pattern interferograms of the bell with (a) no excitation, (b) oscillating at the first axial resonance frequency (883 Hz) and (c) oscillating at the second axial resonance freqeuncy (2451 Hz).

grated effects along the entire bell axis, resulting in a significant asymmetry in the axial direction.

To characterize the mode shapes of the two identified resonances and ensure that they do indeed represent whole-body motion, the thicker bell was driven at the two resonance frequencies using a piezoelectric transducer attached to the small end while the large end was imaged using decorrelated electronic speckle pattern interferometry.[5] To ensure that the interferograms were not biased by possible resonances of the driver, and to eliminate the effects attributable to common motion of the bell and driver, the reference beam of the interferometer was reflected from a mirror attached to the driving mechanism. In this way, only motion of the bell that differed in some manner from the driving motion was visible in the interferogram. The interferograms are shown in Fig. 5, where Fig. 5a is an image of the static bell, Fig. 5b is an image of the bell vibrating at the lower resonance frequency (883 Hz), and Fig. 5c is an image of the bell vibrating at the higher resonance frequency (2451 Hz). The slight shift in the frequencies of the resonances from those observed in the measurement of the transfer functions can be attributed to small changes in the mounting arrangement.

Nodes are represented as white in the interferograms and dark fringes indicate contours of equal displacement. The image in Fig. 5b shows no evidence of the normal ring structure associated with circular nodes because the entire bell was moving in phase. The dark image indicates whole body motion that is not in phase with the driver, with no evidence of a nodal line. This interferogram is consistent with whole-body motion with a slight asymmetry in the deflection, which results in a single diagonal fringe. The interferogram shown in Fig. 5c exhibits an obvious nodal line close to the rim. Both of these mode shapes agree with those predicted in Section II of Ref. 1.

4. CONCLUSIONS

As noted above, the model posited in Ref. 1 predicts that crossover frequencies occur whenever there is an axial resonance. As can be seen in Fig. 3, the crossover frequency for the 0.55 mm thick bell occurs at approximately 860 Hz. The MTF shown in Fig. 4 indicates that for this bell there is an axial resonance near that frequency. To determine the frequency of the resonance more precisely it is useful to plot the phase of the MTF, since the phase will experience a shift of $\pi/2$ as it passes through resonance. This is shown in Fig. 6, from which it can be determined that the axial resonance occurs within 3% of the crossover frequency. This small difference can be attributed to slight changes

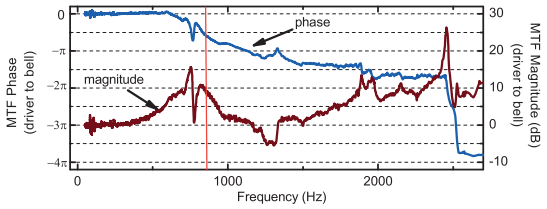

Figure 6: The phase and amplitude of the MTF of the 0.55 mm thick bell. The vertical line indicates the crossover frequency of the ATF seen in Fig. 3.

in the mounting between measurements.

The second experimental observation for which the theory of Ref. 1 must account is the broad-band nature of the affects of bell vibrations. As can be seen in Fig. 2, although the sign of the effect changes at the crossover frequency, the effects can be seen to span several hundred hertz. The MTF shown in Fig. 6 clearly indicates that the axial resonance has a bandwidth that extends over a similar range.

These measurements lend significant credence to the model presented in Ref. 1. Axial vibrations have been shown to exist in a trumpet bell and the difference in the ATF that is measured when the bell is free to vibrate compared to when the vibrations are damped is consistent with predictions. As predicted by the model, the bell vibrations can enhance or diminish the magnitude of the acoustic transfer function. Which manifestation of the effect is observed depends on the relative phase between the air column and the axial bell motion. Similarly, the broad-band nature of the effects of bell vibrations on the sound are explained by the fact that the axial resonances are similarly broad.

How important the mechanical vibrations of the lips are to the process has yet to be determined. There is no reason to expect that the vibrations of the lips transmitted to the mouthpiece will have a consistent phase relationship with the motion of the bell. Indeed, one may expect that the relative phase changes as a function of frequency and playing style. The role the lips play in the excitation of axial vibrations, the importance of vibratory feedback to the lips and the relationship between the phase of the lip motion and the phase of wall vibrations excited by the air column are suitable subjects for future research.

5. ACKNOWLEDGEMENTS

The portion of this work performed at Rollins College was supported by grant #PHY-1303251 from the National Science Foundation of the United States of America.

6. REFERENCES

[1] W. Kausel, V Chatziioannou, T. Moore, B. Gorman, and M. Rokni, "Structural vibrations of brass wind instruments and their acoustical effects Part I: Theory and simulations," *J. Acoust. Soc. Am.*, vol. 137, no. 6, pp. 3149–3162, 2015.

[2] Thomas R. Moore, Erin T. Shirley, Isaac E. Codrey, and Amy E. Daniels, "The effect of bell vibrations on the sound of the modern trumpet," *Acta Acustica united with Acustica*, vol. 91, no. 1, pp. 578–589, 2005.

[3] Wilfried Kausel, Daniel W. Zietlow, and Thomas R. Moore, "Influence of wall vibrations on the sound of brass wind instruments," *J. Acoust. Soc. Am.*, vol. 128, no. 5, pp. 3161–3174, 2010.

[4] T. Moore, J. Kaplon, G. McDowall, and K. Martin, "Vibrational modes of trumpet bells," *Journal of Sound and Vibration*, vol. 254, pp. 777–786, 2002.

[5] Thomas R. Moore and Jacob J. Skubal, "Time-averaged electronic speckle pattern interferometry in the presence of ambient motion. Part I. theory and experiments," *Appl. Opt.*, vol. 47, no. 25, pp. 4640–4648, 2008.

DOES AN EXPERIENCED RECORDER PLAYER START NOTES DIFFERENTLY THAN A NOVICE PLAYER?

Augustin Ernoult, Benoît Fabre
Institut Jean le Rond d'Alembert, Université Pierre et Marie Curie, France
ernoult@lam.jussieu.fr
benoit.fabre@umc.fr

ABSTRACT

The attack transients are very important in musical context. They influence the perception of the sound and they are a tool of musical interpretation. Despite that, there are only few studies on attack transients in flute-like instruments. The influence of the geometry and the control of the musician are not yet understand. By measuring simultaneously the pressure control and the sound of a recorder played by a musician, it is possible to characterize the attacks produced by a recorder player in musical context. A first study has allowed us to determine the global characteristics of an attack transient of recorder: its typical duration, its harmonic content, etc. Because a trained musician may control the attacks to keep a strong homogeneity between all the tones, it is not easy to identify the features of the attack transient related to the instrument from those related to the player's technique. For example all the attacks obtained show a weak contribution of high harmonics, whereas the studies on organ pipes show that a sharper attack leads to an attack richer in high harmonics. By asking a novice to play the same recorder, we analyze the differences between the characteristics of a ``controlled'' and an ``uncontrolled'' attack transient. It allows to identify which characteristics are controlled by the experienced player and to understand some techniques used to control the attack transients.

AN ACOUSTICAL ANALYSIS OF WAVE-LINE FLUTE TUBE JOINTS

Michael Lind, Alexander Mayer

Institute of Music Acoustics
University of Music and Performing Arts Vienna, Austria
michael_lind@gmx.at, mayer@mdw.ac.at

ABSTRACT

The object of this paper is the acoustical research of the Waveline flute. For an overall length reduction of this special children instrument, an omega-shaped joint instead of a straight tube is placed between the flute's head and the main tube. For this analysis the flute is alternately combined with four joint prototypes varying in bore. These different flute setups are compared using two measurement methods. The distinctions in intonation are determined by using an adapted Brass Instrument Analysis System (BIAS). For a sound comparison an artificial embouchure system has been developed. High-speed video recordings of the emerging jet supported the design. The results of the obtained data indicate distinctive differences in the acoustical behaviour in terms of intonation, sound and response.

1. INTRODUCTION

Learning musical instruments often starts in childhood. Some instruments are available in smaller sizes to fit to the proportions and make it easier to be played by children. To allow an early start learning the transverse flute, a reduction of the overall length would be necessary - but this would also change the tune. One solution provides a setup of the Waveline flute [1] (see Figure 1). Here an omega-shaped tube is inserted between the barrel and the head-joint (see Figure 2). The approach of this setting is, that the mouthpiece and flute body will still be arranged on the same axis. As this type of Instrument is already sold, the inventor still tries to optimize and improve the omega bow in terms of better acoustical characteristics, like intonation and response.

Figure 1: The ergonomic approach of the Waveline patent ([1] and [2]); comparison of spine bending while playing standard flute (left) and the Waveline flute (right).

The head-joint terminates with a different inner diameter as the bodyjoint starts. Therefore the Waveline joint represents a transition piece to fit to both dimensions. Three of the four prototypes tested vary in the arrangement of bore alteration (see Figure 3).

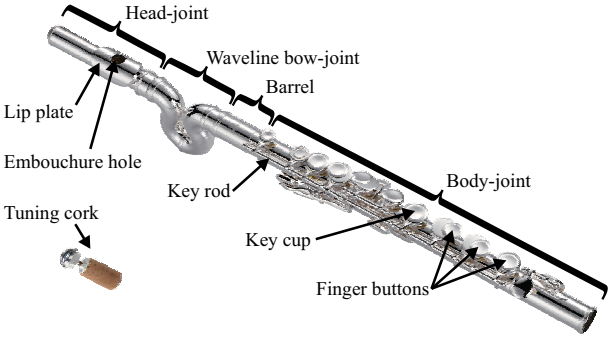

Figure 2: The Waveline flute and its components. As in all flutes the tuning cork is inserted into the head-joint.

2. THE PROTOTYPES

For a better intonation the bore of a standard flute is not shaped strictly cylindrical. Measured from the tuning cork inside the head-joint till the inner ending of the barrel, the head-joint diameter expands from about $17\,\mathrm{mm}$ to $19\,\mathrm{mm}$. If the resulting cone is transferred to the Waveline flute, the bore of the bow-joint will also have to increase. The production of step-less conical and bent tubes (especially for small radii) will turn into an expensive process. Because of this high effort the currently sold bow-joint is manufactured with a stepped expanding bore (Figure 3, Type I).

2.1. Prototype bore configuration

As prototyping is much easier using synthetic material the joints where made out of glued-together half-shell parts. The desired bore was milled out by an CNC-Mill. As reference and comparison an additional plastic prototype was milled out having the same bore as the original metal Waveline joint (Type I).

Type I (Figure 3, left): The transition from the diameter of the end of the head-joint ($17.8\,\mathrm{mm}$) to the diameter of the main tube ($19\,\mathrm{mm}$) takes place in two steps. The first step is positioned at the start of the bow-joint, where the head-joint ends with a diameter of $17.8\,\mathrm{mm}$ and the bow-joint starts with a diameter of $18.3\,\mathrm{mm}$. The position of the second step is on half way of the second bow: The diameter changes from $18.3\,\mathrm{mm}$ to the final diameter of $19\,\mathrm{mm}$.

Type II (Figure 3, middle): This prototype features one step of rising in diameter at the start of the bow-joint: from $17.8\,\mathrm{mm}$ mm to $18.3\,\mathrm{mm}$. The transition to the diameter of $19\,\mathrm{mm}$ at the position half way of the second bow happens continuously.

Type III (Figure 3, right): The rise of diameter from the end of the head-joint ($17.8\,\mathrm{mm}$) to the terminal diameter of $19\,\mathrm{mm}$ happens step-less. The diameter of $19\,\mathrm{mm}$ is reached at the position half way of the second bow.

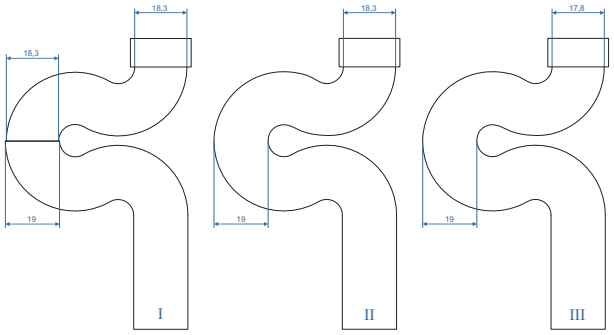

Figure 3: Bore of joint prototypes, from left to right: Type I, Type II and Type III

3. ARTIFICIAL MOUTH

Playing the flute a large variety of parameters have to be considered ([3] and [4]). These are:

- distance from the lip opening to the sharp edge
- embouchure angle
- vertical displacement to the sharp edge
- coverage of the embouchure hole
- shape and cross section lip opening
- air pressure inside the oral cavity and the resulting flow rate
- capacity of the oral cavity

While playing the flute, musicians tend to vary the embouchure parameters mostly unconsciously to match the flutes sound to their expectation. Differences of the acoustical behaviour of flutes can be equalized by most musicians in a wide range. As the influence of the analysed bow-joints on the acoustics of the flute is expected with only subtle distinctions, human playing tests have been taken out of consideration [5].

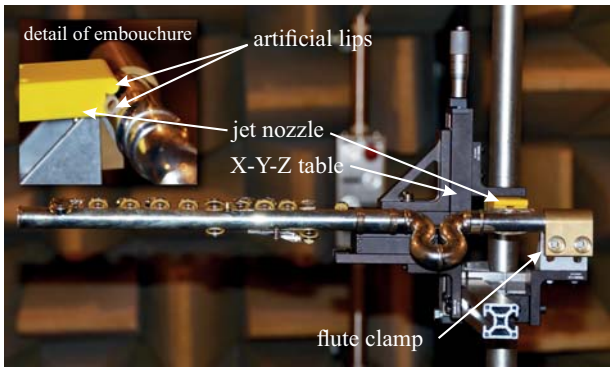

Figure 4: Setup of the artificial mouth system. The yellow plastic jet nozzle with its artificial lips presents the center piece of the artificial mouth.

To ensure an objective and reproducible analysis an artificial mouth was developed (Figure 4). The basic setup links the head-joint and jet nozzle to allow repeatable adjustments in the embouchure angle and the vertical and horizontal distance from the lip opening to the sharp edge. The head-joint is hold by a special flute clamp. An attached angle meter provides a readout of the current angle setting. The artificial mouth sits on a x-y-z table, micrometer screws allow fine adjustments on the desired distances. The air pressure needed to enforce a jet is generated by an air compressor. A digital air pressure sensor attached to the artificial mouth monitors the actual pressure setting.

3.1. Jet nozzle design

While a human player changes the lip gap depending on the desired note and loudness [6], the jet nozzle design should be as simple as possible. Still the artificial excitation should provide a wide range of possible notes including overblowed tones. First attempts were done by using a rectangular brass profile ($5.4\,\mathrm{mm}$ by $2.25\,\mathrm{mm}$). Although the excitation of the instrument was a success, the sound was poor in quality with a focus on the first harmonic. In general the response was insufficient for this analysis. Changing the nozzle cross section into an elliptical shape did not solve the problem. In the next step, high speed video recordings were done, to investigate jet formation.

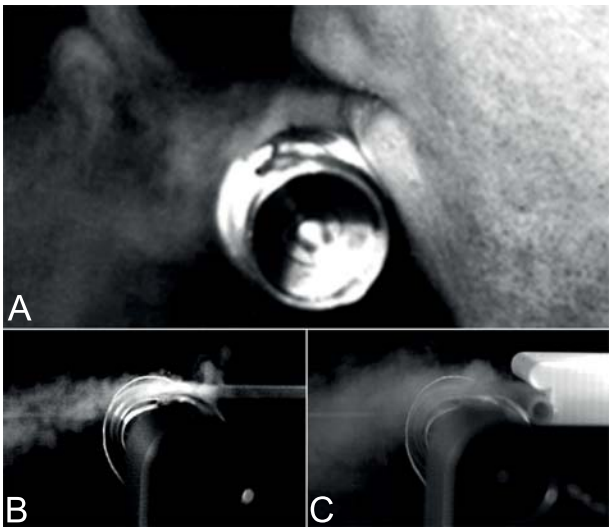

Figure 5: Three excitations in comparison: Jet formed by a human player (A), a rectangular brass profile (B)and by the final nozzle setup (C).

Smoke was used to ensure the visibility of the jet formed (see Figure 5). Although the examination of the recorded videos will show the differences very clear, the pictures shown, can indicate just a tendency. The slow-motion recordings of all constructions can be watched via the website `http://iwk.mdw.ac.at/am`. The jet formed by a human player (Figure 5/A) features a more diffused and swirled flow than the flow stimulated by the brass tube (Figure 5/B). The assumption that the musicians lips are causing a deflection, leads to the jet nozzle design drawn in Figure 6. As the bore of the construction is more complex, the final nozzle arrangement was created using rapid prototyping technology.

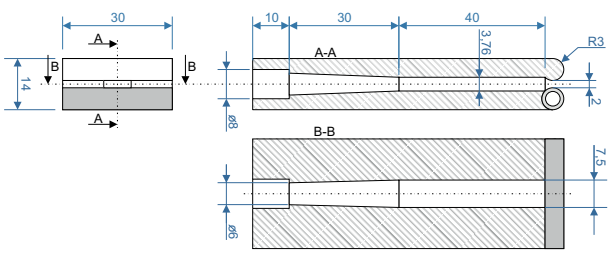

Figure 6: Technical drawing of the 3d plotted plastic jet nozzle (all measures in mm), for an airtight closure at the lip plate the lower artificial lip is made out of silicon tubing.

3.2. Final settings of the artificial mouth system

Following settings where chosen to excite the flute with the artificial mouth:

- angle between the center-axis of the jet nozzle and the upper side of the Embouchure hole: $50°$
- distance from the narrowest spot of the nozzle to the sharp edge of the embouchure hole: $8.73\,\mathrm{mm}$
- vertical offset of the center of the nozzle to the sharp edge of the embouchure hole: $1.07\,\mathrm{mm}$
- air pressure: from d4 to d#5: $350\,\mathrm{Pa}$; from e5 to g5: $1000\,\mathrm{Pa}$

4. ADAPTED BIAS

The Brass Instrument Analysis System (BIAS) [7] has been used to determine the resonance frequencies of the flute. This system consists of a measuring head and the BIAS 7 control and analysis software package. To allow a measuring of the impedance at the position of the stopper, the head-joint had to be prepared. To enable the attachment of the BIAS measuring head on the correct position the head-joint had to be shortened. A special silicon-ring ensures an airtight connection. While playing the instrument, a musician partly covers the embouchure hole with his/her lip (embouchure hole correction) [8]. For the measurement a fixed embouchure hole masking has to be applied to ensure a constant coverage (see also Figure 7).

Figure 7: Flute with trimmed head-joint connected to BIAS.

5. DISCUSSION OF THE MEASUREMENTS

The bow-joints had to be measured under the following aspects:

- Intonation of resonances
- Sounding intonation
- Maximum pressure for playing in the low register
- Normalized spectral centroid
- RMS of the amplitude

For each bow-joint connected and each measurement the flute was tuned at a4 with 440 Hz.

5.1. Intonation of the resonance frequencies:

At the low pitches of the first register (lowest note d4), the intonation proved to be lower than zero cents. At pitches above a4 in the first register (to the c#5) the intonation measures values above zero cents. This results in an overall stretch in intonation from d4 to c#5 (deepest possible to highest possible fingering in the first register). The highest stretch rate can be observed evaluating the measurements of the metal bow-joint (see Figure 8). Bow-joint II feature the lowest stretch of intonation. It is remarkable, that the differences between bow-joint I and the metal bow-joint are relatively high, though they are constructed having the same dimensions in bore.

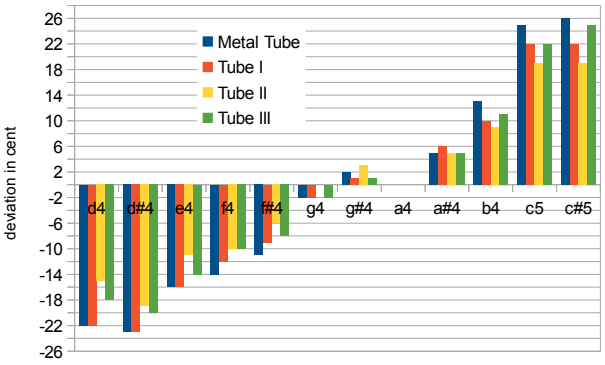

Figure 8: Resonance

5.2. Sounding intonation

Due to the edgetone-mechanism, the sounding intonation compared to the resonance gets lower with rising pitch [9]. The above mentioned stretch in intonation of the resonance frequencies counteracts this tendency. The lowering of intonation with higher pitch is even bigger than the counteracting rising intonation of the resonance-frequencies. The effect is an overall shrinkage of intonation from the deepest to the highest fingering in the first register (d4 to c#5).

As pictured in Figure 9 the original bow-joint (Metal Tube) features the lowest values of intonation shrinkage. Conversely bow-joint II shows the biggest amount of shrinkage. The differences between the metal bow-joint and bow-joint I are again significant despite their same construction-features.

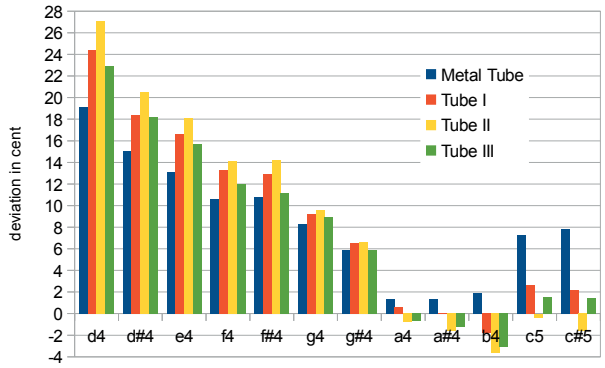

Figure 9: Sounding Intonation

5.3. Maximum pressure for playing in the low register

For musicians it is desirable, to have the possibility to play the flute with high blowing pressure without overblowing to the next register. In the bar-graph of Figure 10 the results of such measurements are presented. In general the maximum values are depending on the chosen fingerings corresponding to the excited note. Comparing the four bow-joint types no significant differences can be identified. In average bow-joint II indicates the widest pressure range. Therefore it can be played in most measured notes with the highest possible pressure, before changing to the second register.

5.4. Normalized spectral centroid

To discriminate the timbre of sounds, the difference of the normalized spectral centroid related to the fundamental frequency

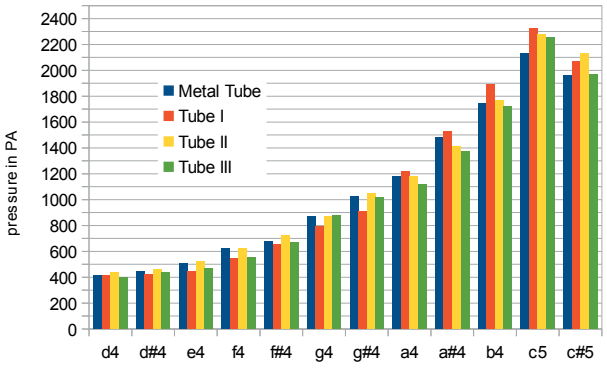

Figure 10: Maximum pressure for playing in the low register.

has to be at least at a value of 0.2 [10]. These differences are present at about one third of the measured fingerings: d4, d#4, c#5, d5, e5, f5, g5 in Figure 11. The values have been determined by using the soft-ware MQAN [11]. Referring to the calculated results, a continuous grading of the bow-joints is not discernible. At most fingerings bow-joint III features low to lowest values. This leads to the assumption, that the use of bow-joint III will result in the overall warmest and darkest sound.

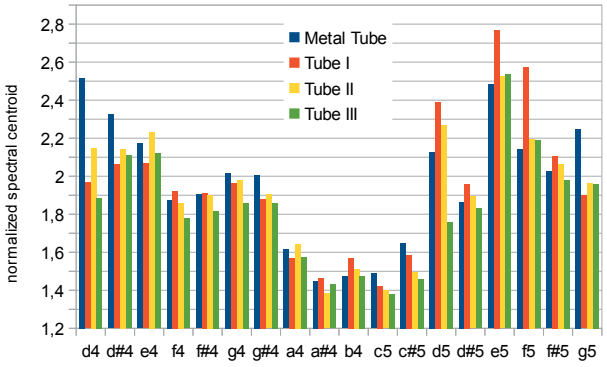

Figure 11: Normalized spectral centroid

5.5. RMS of the amplitude

As plotted in Figure 12 there is no bow-joint configuration, which RMS Amplitude measures the highest values over all fingerings. The y-axis of Figure 12 displays the unweighed values of the Amplitude in dB. The values have been related to the measured sound-level at 1000 Hz in dBA. The Microphone was placed at one meter in front of the center of the flute.

6. CONCLUSIONS

The setup of the artificial mouth proved to excite the flute reproducibly. The comparison of slow-motion videos of the jet exiting the human lips and different artificial nozzles lead to a special jet-nozzle design, which fits to the demanded specifications.

The results of the analysis of the different types of bow-joints clearly yield the high sensitivity of the instrument on small bore changes. A direct comparison of the values measured of the original metal- and type I bow-joint diverge more than expected. Tolerances in production or the influence of material can have caused this variations, and will be a main aspect in further analysis.

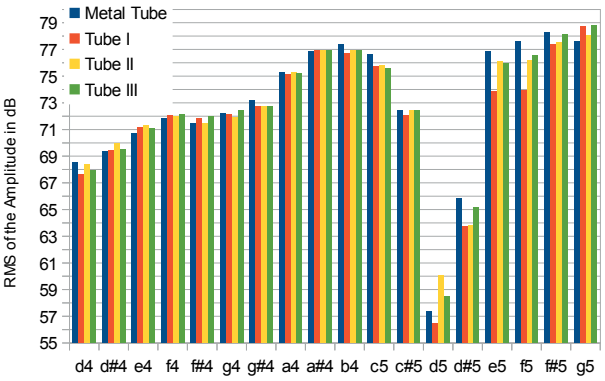

Figure 12: RMS of the amplitude

7. REFERENCES

[1] W. Tomasi and B. Gisler, "Transverse flute," Aug. 28 2013, EP Patent 2,237,265.

[2] Bärbel Thomasi, "Jupiter flute with wave line head joint," `http://de.slideshare.net/BrbelTomasi/english-enwurf` [25.10.2014].

[3] Nicolas Montgermont, Benoit Fabre, and Patricio de La Cuadra, "Flute control parameters: fundamental techniques overview," in *International Symposium on Musical Acoustics*, 2007.

[4] Patricio de la Cuadra, Benoît Fabre, Nicolas Montgermont, and Christopher Chafe, "Analysis of flute control parameters: A comparison between a novice and an experienced flautist," *Acta Acustica united with Acustica*, vol. 94, no. 5, pp. 740–749, 2008.

[5] Renate Linortner, "Silber, gold, platin... der materialaspekt bei querflöten: Spiel- und hörtests, umfragen und klanganalysen," 2001.

[6] Isabella Frenzl, "Messtechnische erfassung des ansatzes bei flötistinnen und flötisten," 2007.

[7] Werner Winkler and Gregor Widholm, "Bias - blas instrumenten analyse system," in *15 Jahre Institut für Wiener Klangstil (1980-1995)*, Eduard Melkus, Ed., pp. 95–106. Institut für Wiener Klangstil, Wien, 1996.

[8] Arthur H. Benade, *Fundamentals of Musical Acoustics*, vol. XII, New York, 1976.

[9] A. H. Benade and J. W. French, "Analysis of the flute head joint," *Journal of the Acoustical Society of America (JASA)*, vol. 37, no. 4, pp. 679–691, 1965.

[10] R. A. Kendall and E. C. Carterette, "Difference threshold for timbre related to spectral centroid," in *Proceedings of the 4th ICMPC*, Montreal, Canada, 1996, pp. 97–101, Proceedings of the 4th. International Conference on Music Perception and Cognition.

[11] R. Maher, J. Beauchamp, and Et Al, "Mqan: Analyse a sound using the mcaaulay-quatieri (mq) partial-tracking method.," API Guide, 2000, `http://dream.cs.bath.ac.uk/software/sndan/mqan.html` [4.12.2014].

LBM SIMULATION OF THE QUASI-STATIC FLOW IN A CLARINET

Yong Shi[1)], *Andrey R. da Silva*[2)], *Gary P. Scavone*[1)]

[1)] Computational Acoustic Modeling Laboratory,
Centre for Interdisciplinary Research in Music Media and Technology,
Schulich School of Music, McGill University,
Montreal, Quebec, Canada.
yong.shi2@mail.mcgill.ca, gary.scavone@mcgill.ca

[2)] Laboratory of Vibrations and Acoustics, Department of Mechanical Engineering,
Federal University of Santa Catarina, Florianpolis - SC - Brazil.
andrey.rs@ufsc.br

ABSTRACT

This paper investigates the nonlinear characteristics of the mouthpiece-reed system of a clarinet using the lattice Boltzmann method (LBM) in a two dimensional domain. The mouthpiece has been investigated for cases of both a fixed reed and a moving reed, with the outlet of the mouthpiece being replaced by an absorbing boundary to thwart possible acoustic oscillations. The influence of the geometry of reed channel has been investigated. Numerical results are compared to the quasi-stationary model based on a simplified memoryless reed and the Bernoulli flow.

1. INTRODUCTION

A clarinet can be roughly divided into a non-linear active component (the mouthpiece-reed system) and a linear passive component (the instrument's resonant bore). The sound production of a clarinet depends on flow-induced vibrations, with the reed modulating the air flow entering into the instrument by opening and closing a narrow channel defined between the reed tip and the lay of the mouthpiece.

Previous studies on the resonator components have produced many useful discoveries and satisfactory models. On the other hand, studies on the non-linear mouthpiece-reed system have been relatively less reported. The characteristic of the mouthpiece-reed system is defined as the non-linear relationship of the volume flow and the pressure difference across the reed channel. Since the pioneering work of Backus [1], the non-linear function of single-reed woodwind instruments has been investigated experimentally and theoretically by a number of authors ([2], [3], [4], [5], [6], [7], [8], [9], [10]).

Besides traditional experimental and theoretical approaches, computational simulations have become popular in the field of musical acoustics thanks to the development of new numerical algorithms and inexpensive computers. Numerical simulations have advantages related to precise parametric control, as well as in certain situations where experimental measurements and theoretical modeling are either very difficult or impossible.

The present paper provides a numerical investigation of the nonlinear element and the physical phenomena involved using a relatively new computational fluid dynamic (CFD) tool called the lattice Boltzmann method (LBM). Compared to other traditional CFD techniques, the main advantage of LBM is represented by its simplicity in simulating the interactions of the moving reed, the air flow and the acoustic field directly and simultaneously. Also, LBM is well suited for parallel computation, which is advantageous for problems involving complicated geometries and long simulation times.

To obtain the complete characteristics of the reed, the volume flow must be measured in a quasi-static condition, i.e., the air flow is free to pass through the reed channel and the transfer of momentum between the fluid and the reed is neglected. For a fixed reed, it is easy to obtain a quasi-static condition in the simulations. But for the case of a freely moving reed, a tiny initial disturbance of the reed might be reinforced by the acoustic feedback from the mouthpiece chamber as well as the resonator. Dalmont used an orifice as a non-linear acoustic absorber to thwart possible acoustic oscillations in the experimental measurement [9]. In this study, the open end of the resonator is replaced by an absorbing boundary condition (ABC) that is used as a pressure-reducing element and a nonlinear absorber that suppresses possible standing waves in the mouthpiece. On the other hand, the inside boundaries of the mouth cavity are also equipped with an ABC prescribed with non-zero pressure and velocity, functioning as both the flow source and an acoustical absorber.

The objectives of this paper are to obtain the complete nonlinear characteristic curve including both the increasing and decreasing stage of mouth pressure to compare the flow behavior for cases corresponding to both fixed reed and moving reed and to verify the validity of the quasi-stationary model.

2. PREVIOUS WORK

The first result of experimentally measured characteristics of a single-reed instrument under steady flow conditions was given by Backus [1]. He fit his experimental results by a non-linear expression relating the volume flow U and the pressure difference Δp and the opening h, given as $U = 37\Delta p^{2/3}h^{4/3}$. However, Backus' empirical formula has not been verified by other researchers.

Assuming no pressure recovery from the reed channel to the air column input, most flow models describe the relationship between the volume flow and the pressure difference across the reed channel by means of the stationary Bernoulli equation ([2], [4], [3]), given as:

$$U = S_j \sqrt{\frac{2\Delta p}{\rho}}, \tag{1}$$

where ρ is the density of the air, $S_j = wh$ is the effective cross section of the jet, w is the effective width of the reed channel and h is the reed opening.

Then assuming the reed opening is linearly related to the pressure difference by its stiffness, the volume flow U can be described by the elementary model:

$$U = \begin{cases} wh\left(1 - \frac{\Delta p}{P_M}\right)\sqrt{\frac{2\Delta p}{\rho}}, & \text{if } \Delta p \le P_M \\ 0, & \text{if } \Delta p > P_M \end{cases} \tag{2}$$

where P_M is the closing pressure of the reed channel. Since the Bernoulli equation is only valid for inviscid flow, the elementary model only holds for the case of relatively high Reynolds number ($Re = U/w\nu$), where w is the width of the reed used as the characteristic length, and ν is the kinematic viscosity of the fluid.

Hirschberg et al. [11] proposed a more complex flow model using numerical simulations which takes the effect of flow separation and friction into account. This model is improved and verified based on experimental results by Van Zon et al. ([12]). Depending on the geometry of the flow channel, which is characterized by L/h, where L and h are the length and the height of the flow channel respectively, there are two types of flows.

For short channels ($L/h \le 1$), the flow is estimated by a contracted uniform flow

$$U = \alpha w h \sqrt{\frac{2\Delta p}{\rho}} \mathrm{sgn}(\Delta p), \tag{3}$$

where α is the dimensionless contraction parameter, typically found in the range of $[0.5, 0.611]$ in Van Zon's measurement.

For long channels ($l/h \ge 4$), the flow is given by

$$\begin{aligned} U &= \Omega\left[1 - \sqrt{1 - \tfrac{h^4(24c-1)\Delta p}{72\rho\nu^2(L-l_r)^2(1-\delta^*)^2}}\right] \\ \Omega &= \tfrac{12\nu\, w(L-l_r)(1-\delta^*)^2}{h(24c-1)} \end{aligned} \tag{4}$$

where ρ is the undisturbed density of the fluid, $\delta^* = 0.2688$ is a generalization of the boundary layer thickness for an arbitrary h, and $c = 0.0159$.

Dalmont et al. [9] measured the flow behavior using an artificial mouth-lip system and a real clarinet mouthpiece and found a flow behavior similar to that described by the quasi-stationary flow model. Interestingly, Almeida et al. [10] measured double-reed woodwind instruments and found that the normalized pressure flow characteristics of a bassoon and an oboe are similar to that of a clarinet and can be well described by the quasi-stationary model.

Da Silva [13] simulated the flow into a clarinet mouthpiece of different geometries using the lattice Boltzmann method for cases of both static and free oscillating reed. Da Silva's results agree well with Van Zon's model for both short and long reed channels in terms of vena contracta factor as a function of reduced Reynolds number as well as the volume flow as a function of pressure difference. However, the characteristic given in [13] is not complete because only a discrete number of values of mouth pressure were tested. Also, the simulation was less realistic because the flow was generated by a negative pressure source at the left end of the mouthpiece.

To obtain the complete curve of flow characteristics, the mouth pressure should continuously increases from zero to a maximum value until the reed reaches the lay such that the reed channel is changing from fully opened to fully closed. Also, due to the viscoelasticity of the reed and the inertia and damping effects of the fluid, it is possible to observe a hysteresis effect due to the change of the rest position of the reed when closing versus when opening. This requires the measurement of the flow for both an increasing mouth pressure and a decreasing mouth pressure.

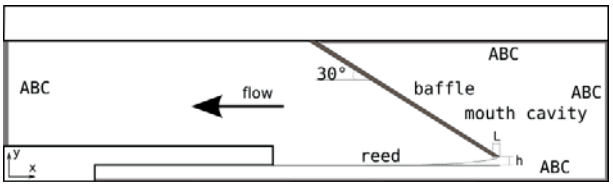

Figure 1: The LBM scheme of the mouthpiece and the mouth cavity.

3. NUMERICAL PROCEDURE

In this study, we carried out the simulation of a mouthpiece-reed system of a clarinet using the two-dimensional LBM. On one hand, the relatively simple implementation of boundary conditions of the LBM allows us to easily explore different geometrical boundaries of a clarinet. On the other hand, the efficiency of our computation is greatly improved by using a parallel computing technique based on a low-cost Nvidia GPU graphic card installed on a personal computer. We used the multiple relaxation time (MRT) scheme [14] [15] and a relatively high numerical viscosity to maintain the numerical stability.

The LBM scheme, as depicted by Fig. 1, is described by thin walls resembling the cross section of a mouthpiece-reed system of a clarinet immersed in a fluid domain. The fluid domain is represented by a rectangular D2Q9 structure [16]. The domain boundaries along the solid walls of the mouthpiece are treated by a simple bounce-back scheme [17], which creates a no-slip condition at the wall and simulates a viscous boundary layer. The remaining boundaries have an absorbing boundary conditions prescribed with a zero velocity, as proposed by Kam et al. [18].

The size of the LB model representing the clarinet is given by $nX = 1240$ and $nY = 589$, which are the number of lattice cells along the x- and y-axes, respectively. The space resolution $dx = 8.5{\cdot}10^{-5}\ m$ representing the unit length of one lattice cell is determined by both the available computing resources and the smallest geometrical length of the boundary, which is the maximum value of the opening h of the reed channel. The number of lattice cells representing the height h is 14, which is sufficient in consideration of both stability and accuracy, according to our previous experiences. The time step is $dt = 1.44 \cdot 10^{-7}\ s$. To improve the numerical stability in the dynamic reed configuration, the lattice relaxation time is chosen as 0.532 and used in both static reed and dynamic reed cases, corresponding to a relatively high physical kinematic viscosity of $5.33 \cdot 10^{-4}\ m^2/s$.

The LB model is implemented by a custom parallel computing code written in Pycuda [19], and runs on a desktop PC equipped with a Nvidia GeForce GTX 670 graphics card. The speed-up factor is about 20 compared to the same model running on the CPU in serial mode.

The reed is based on the one-dimensional distributed model of a clamped-free bar with varying cross section and resolved with an implicit finite difference scheme, as proposed by Avanzini and Van Walstijn [20]. The length and width of the reed are specified as 34 mm and 13 mm, respectively. The

equilibrium tip opening is 1.2 mm. The external force component applied on the reed's surface is calculated from the pressure field around the reed in each iteration, where the torsional and longitudinal modes are neglected. The interaction between the reed and the mouthpiece lay is considered to be inelastic, as discussed and justified in [20].

The problem of a moving curved boundary associated with the moving reed is solved by using an extrapolation scheme proposed by Guo et al [21]. This technique represents the no-slip condition and the transfer of momentum from the reed to the flow with an accuracy of second order. The displacement and the velocity of the reed is updated by the reed model based on the aerodynamic force upon the reed's surface in each iteration, and the curved boundary is updated accordingly.

To eliminate the acoustic oscillation of the reed caused by the acoustic coupling of the chamber in the mouthpiece, an absorbing boundary scheme prescribed with a zero velocity, as proposed by Kam et al. [18], is placed along the cross-section at the left open end.

The source flow in the mouth is implemented using a variation of the absorbing boundary scheme, where the pressure of a non-zero target flow is prescribed with a customized profile. The pressure in the mouth cavity (pm) and in the mouthpiece chamber (pa), as well as the volume flow in the mouthpiece chamber (U) are measured, averaged and saved during the simulation. The pressure difference dp is calculated as $dp = pm - pa$. A typical duration of such a simulation is about 68 ms, or 500,000 iterations.

Two geometries of reed channel have been used in the simulation, namely the short channel (L/h=1) and the long channel (L/h=4), as depicted in Fig. 2.

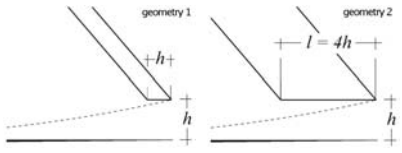

(a) (b)

Figure 2: Two geometries of the reed channels: (a) short channel (L/h=1), (b) long channel (L/h=4).

Also, we conducted the simulation for both a static reed (stationary simulation) and a moving reed (dynamic simulation), respectively. There are two main differences between the present study and the previous work [13]. For the case of a static reed, the complete characteristic is measured continually for both increasing mouth pressure and decreasing mouth pressure. For the case of a moving reed, the disturbance of acoustic oscillations is minimized by using two approaches. One approach is to use a relatively slow change rate of the mouth pressure. Another approach is to use a higher fluid damping coefficient in Avanzini and Van Walstijn's reed model, keeping key mechanical parameters such as Young's modulus of elasticity and visco-elastic constant unchanged such that the mechanical characteristic of the reed is not affected.

4. RESULTS

4.1. Static Reed

The results of the stationary simulations for the cases of short channel and long channel (depicted in Fig. 2) are shown in Figs. 3 and 4, respectively.

Figures 3(a) and 4(a) depict the time history of the target pressure pmt prescribed on the absorbing boundary in the mouth cavity, the measured mouth pressure pm, the average pressure in the mouthpiece chamber pa and the pressure difference across the reed channel $dp = pm - pa$. In a typical simulation, the target pressure pmt increases linearly from zero to the highest value 9.5 kPa in a duration of about 28.87 ms (200,000 iterations, marked as Stage I) and holds for about 7.22 ms (50,000 iterations), then decreases linearly to zero in the duration of about 28.87 ms (marked as Stage II), and holds there for about 7.22 ms until the simulation is finished. The mouth pressure follows the pattern of pmt though at a reduced level. Since the reed is fixed, the reed channel is fully open during the course of the simulation and the mouth pressure never reaches the prescribed pressure due to the non-zero flow passing through the mouthpiece.

The measured flow U is compared to the Bernoulli flow Ub and the theoretical flow Uz calculated from Van Zon's model for both short channel and long channel, as shown in Fig. 3(b) and 4(b), respectively. Since the opening and the width of the reed is fixed, the Bernoulli flow is only related to the measured pressure difference dp. Figures 3(c) and 4(c) represent the same flow data as a function of pressure difference, where $U(1)$ and $Uz(1)$ are the flows associated with Stage I, and $U(2)$, $Uz(2)$ are the flows associated with Stage II. The contraction parameter of Van Zon's model for short channel is 0.7. In general, the measured flow is lower than the Bernoulli flow due to the flow separation occurring at the entrance of the reed channel. For the short channel, the measured flow is in good agreement with Van Zon's model for most of the duration. However, for the long channel, the measured flow is significantly lower than the theoretical flow, which is only a little bit lower than the Bernoulli flow.

The phenomena of flow contraction, caused by the boundary layer effects on the walls of the lay and the reed and the flow separation at the entrance, can be quantitatively described by the vena contracta factors $vcf = U/Ub$, as depicted in Figs. 3(d) and 4(d), where $vcf(1)$ is associated to Stage I and $vcf(2)$ is associated to Stage II. The vena contracta factors of Van Zon's model, noted as $vcf_z(1)$ and $vcf_z(2)$, corresponding to Stage I and Stage II respectively, are depicted in parallel.

In the case of the short channel, the measured vcf is in good agreement with theoretical vcf_z for most of the duration. In the case of the long channel, the measured vcf is significantly lower than the theoretical vcf_z. Also, the vcf corresponding to the long channel is lower than that of the short channel, which might be explained by the relatively higher damping in the long channel that is caused by friction from the flow and the walls.

A slight hysteresis effect can be observed in the region of low pressure difference for both geometries, i.e., $dp < 0.5$ for short channel and $dp < 1$ for long channel. Since the reed is fixed, the hysteresis phenomena cannot be caused by the viscoelasticity of the reed, rather, it is more likely due to the inertia of the air flow. We notice the variation of vcf is very small in about 80% of the duration of the simulation for both geometries, which suggests that a constant vcf used in the quasi-static model is a reasonable approximation for the case of a fixed reed.

4.2. Dynamic Reed

Throughout the dynamic simulations, the reed is moving as the pressure difference across the reed changes. The results corresponding to the short channel and the long channel are depicted in Figs. 5 and 6, respectively.

Figures 5(a) and 6(a) depict the time history of the tar-

get pressure pmt prescribed on the absorbing boundary in the mouth cavity, the measured mouth pressure pm, the average pressure in the mouthpiece chamber pa and the pressure difference across the reed channel $dp = pm - pa$. The target pressure is prescribed in the same way as in the simulations of the fixed reed, i.e., pmt increases linearly from zero to the highest value of 9.5 kPa, holds, and then decreases linearly and holds at zero until the simulation is finished.

Before the reed closes in Stage I, the mouth pressure increase along with pmt, though at a reduced level. The pressure in the mouthpiece pa increases and reaches a peak value in about 9 (short channel) to 12 ms (long channel), then decreases because the amount of flow entering into the mouthpiece chamber is reduced due to a smaller opening of the reed channel. When the reed is completely closed at the closing pressure, which is about 8783 Pa for the short channel and 8939 Pa for the long channel, there is almost no flow entering into the mouthpiece chamber, and pa drops to zero. In Stage II, pa starts to increase when the decreasing mouth pressure is lower than the closing threshold. The threshold of the closing pressure in Stage II is lower than that in Stage I. This phenomenon is explained by the bifurcation delay, which is discussed in [22].

Figures 5(b) and 6(b) depict the reed channel opening as a function of dp for the case of short channel and long channel, respectively. For the most part, the opening is almost linearly related to dp. A hysteresis effect is found in the region of dp that is higher than about 7 kPa. There is a sudden drop and increase of opening when the mouth pressure reaches the closing pressure in Stage I and Stage II, respectively.

Figures 5(c) and 6(c) depict the Bernoulli flow Ub, the measured flow U and the theoretical flow Uz calculated from Van Zon's model as a function of time. Figures 5(c) and 6(c) represent the same flow data as a function of pressure difference, where $U(1)$, $Uz(1)$ and $U(2)$, $Uz(2)$ are the flow associated with Stage I and Stage II, respectively. The contraction parameter of Van Zon's model for short channel is 0.7.

The measured flow in the case of the moving reed shows some differences to the quasi-stationary model. The measured flow shows hysteresis for cases of both short channel and long channel. The quasi-stationary model, on the other hand, only shows hysteresis for the long channel because the displacement of reed is taken into account. For the short channel, the measured flow U is higher than the Bernoulli flow Ub and theoretical flow Uz of the quasi-stationary model in the region where dp is more than about 3 kPa. Similarly, for the long channel, U is higher than Ub and Uz in the region where dp is more than about 4 kPa. It can also be observed in Figures 5(e) and 6(e) that the vena contracta factor shows a value larger than unity in the region of higher dp. This phenomenon might be explained by the discussion in [9], where the quasi-stationary models assumes the reed channel with a fixed separation point and a uniform height, which is questionable in the case of a more realistic clarinet mouthpiece. The discrepancies might also be related to the flows of low Reynolds number that cannot be described by the Bernoulli's equation. The measured vcf associated with the region of $dp > 6.5$ kPa is questionable and is discarded due to the dramatical change of both U and Ub, as depicted in the region around about 43 ms in Figures 5(c) and 6(c).

5. DISCUSSIONS AND CONCLUSIONS

The staircase-like ripples found in the measured flow and opening for the cases of moving reed (Figs. 5 and 6) might be studied from two aspects. The first influence comes from the mechanical oscillation of the reed initiated by the relatively quick changing rate of the mouth pressure, especially in the decreasing stage of the pm curve. A slower changing rate can reduce the likelihood of acoustic oscillations at the cost of a prolonged simulation time. The measurements times reported in [9] are between 50 to 100 seconds, but this time scale is not practical in the current model even using parallel GPU computation. Another factor is related to the low spatial resolution. When the reed channel is nearly closed, the cells can be very few and insufficient to represent the flow crossing the reed channel and the boundary layer effect. This problem cannot be immediately solved by simply using an extremely large lattice because of the limited computation and memory resources allowed by the GPU device. An adaptive grid refinement technique [23] might be helpful but is not implemented in the current model yet. Nevertheless, a low-discretized lattice can still capture reasonable well global parameters such as the averaged volume flow.

Due to the relatively higher numerical viscosity, the Reynolds number in the numerical simulation is lower than the realistic one. In the situation of static reed, the highest Reynolds number is 140, which is much lower than the realistic Reynolds number 4762 (assuming the same volume velocity). Consequently, the measured flow is not exactly the same as the Bernoulli flow and the quasi-stationary model, which is based on the assumption of inviscid flow. A low numerical viscosity is not practical for the dynamic reed case because, apart from the issue of numerical stability, there is the difficulty of eliminating the noise caused by acoustic oscillations when the viscosity is very low. Nevertheless, useful results can still be obtained from the current model.

As already noted in Fig. 4(b), the predicted volume flow rate deviates largely from Van Zon's model for the long channel case. We attempted to investigate this discrepancy by estimating the boundary layer thickness from the spatial distribution and evolution of the jet. Figures 7(a) and 8(a) visualize the velocity field ($u = \sqrt{u_x^2 + u_y^2}$) for the cases of static short and long reed channels respectively, from which we can observe that the flow is passing through the reed channel and is dissipated in the mouthpiece chamber. Figures 7(b) and 8(b) depict the velocity profile of the jet passing through the short and long reed channel, respectively. In the short channel, a flow separation can be observed at the entrance and the total critical thickness of the boundary layers on both top and bottom walls is about 7 cells, corresponding to an averaged dimensionless thickness of 0.2333 for one wall, which is slightly lower than the thickness of 0.2688 used in Van Zon's model. For the case of long channel, a reattachment of the flow occurs after a distance on the order of the reed channel height, and a Poiseuille flow is developed after a transition zone. The averaged dimensionless thickness of the boundary layer is about 0.3 (9 cells in total). The lower volume flow for the long channel case might be caused by the boundary layer thickness which is slightly higher than that used in Van Zon's model, But it could also be influenced by the flow pattern characterized by a low Reynolds number, because the boundary layer thickness estimated from the velocity profile is not very accurate due to the low-discretization. In a dynamic situation, though, the flow profile would certainly not match Van Zon's assumption. The flow detachments at the reed tip can be better observed in Fig. 7(c) and 8(c), where the velocity profiles in the neighboring area of reed tip are depicted in a larger scale. The magnitude of the counter-flow at the reed wall is much lower than that of the maximum flow velocity but still can be observed.

The current LBM scheme is limited by its 2D nature, which is not fully capable of representing the 3D behavior of the real flow. Further, the flow measured from the mouthpiece-reed sys-

tem with a fully coupled acoustic resonator will be more realistic. This will be investigated in our next research project.

Acknowledgments

The authors wish to acknowledge funding from the Fonds québécois de la recherche sur la nature et les technologies (FQRNT), the Natural Sciences and Engineering Research Council of Canada (NSERC), and the Centre for Interdisciplinary Research in Music Media and Technology.

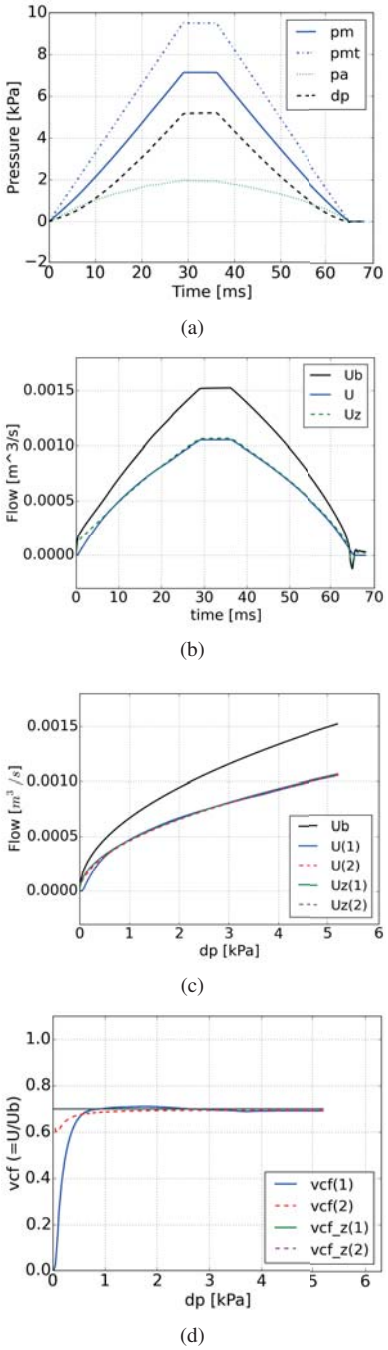

Figure 3: Static reed, short channel (L/h = 1): (a) pressure profile, (b) flow as function of time, (c) flow as function of pressure difference, and (d) vcf as function of pressure difference.

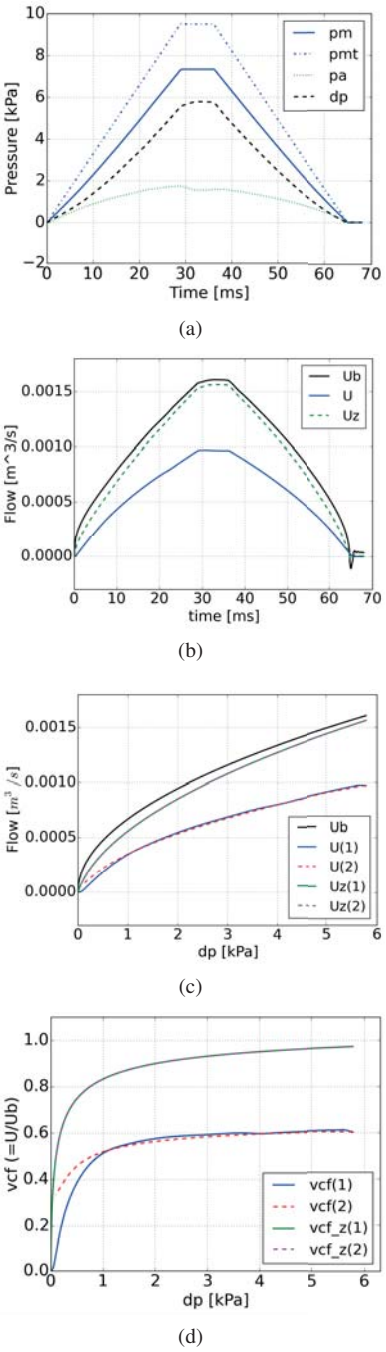

Figure 4: Static reed, long channel (L/h = 4): (a) pressure profile, (b) flow as function of time, (c) flow as function of pressure difference, and (d) vcf as function of pressure difference.

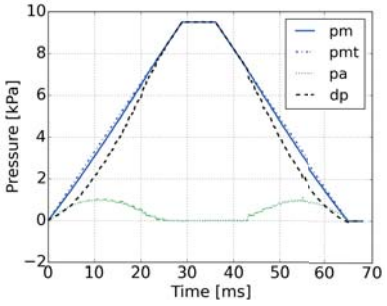

(a)

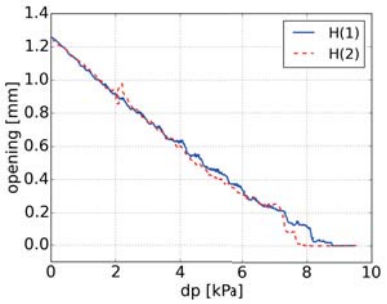

(b)

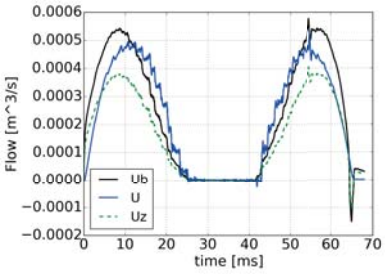

(c)

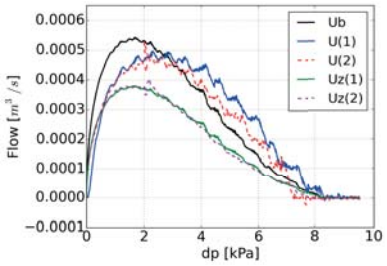

(d)

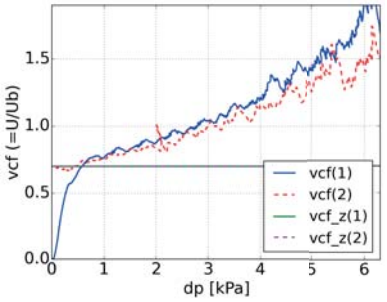

(e)

Figure 5: Moving reed, short channel (L/h = 1): (a) pressure profile, (b) opening as function of pressure difference, (c) flow as function of time, (d) flow as function of pressure difference, and (e) vcf.

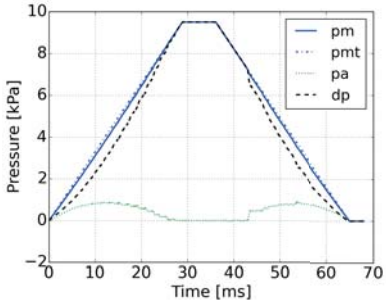

(a)

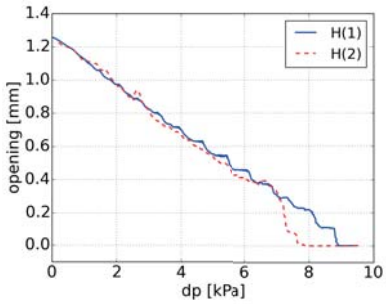

(b)

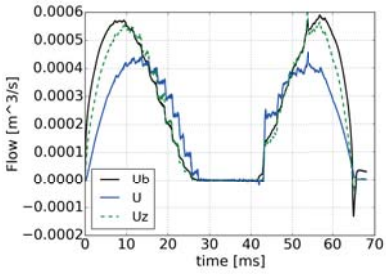

(c)

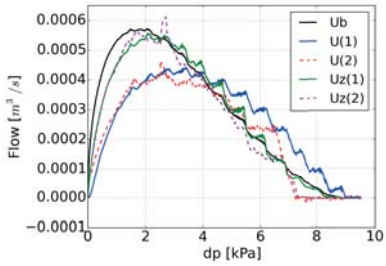

(d)

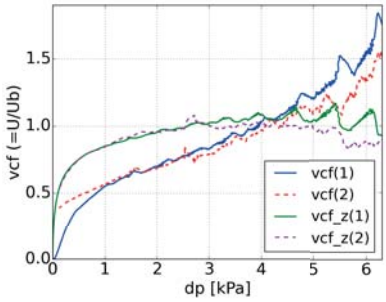

(e)

Figure 6: Moving reed, long channel (L/h = 4): (a) pressure profile, (b) opening as function of pressure difference, (c) flow as function of time, (d) flow as function of pressure difference, and (e) vcf.

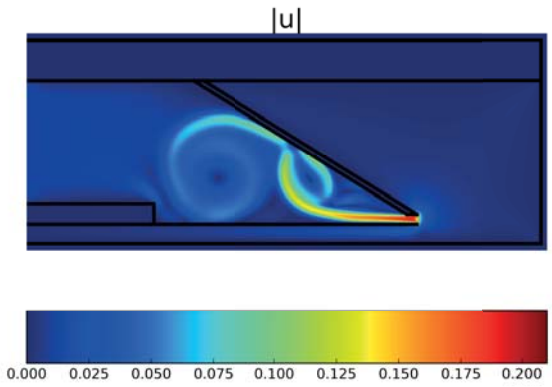

(a)

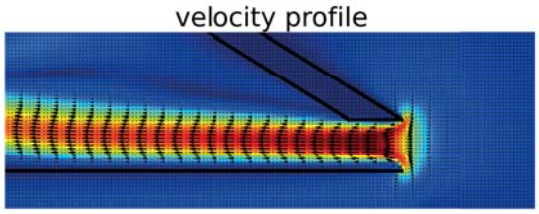

(b)

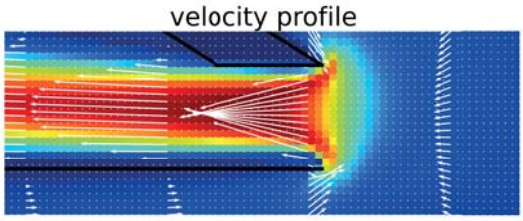

(c)

Figure 7: Velocity field, static short reed channel: (a) absolute velocity, (b) velocity profile of the jet passing through the reed channel, (c) velocity profile depicted in a larger scale.

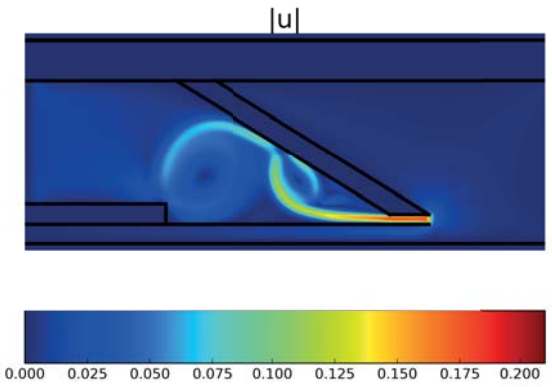

(a)

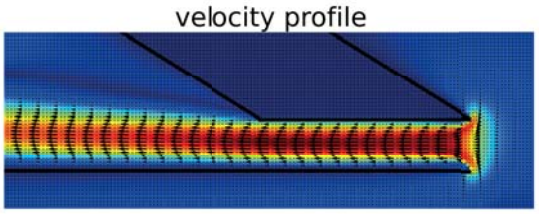

(b)

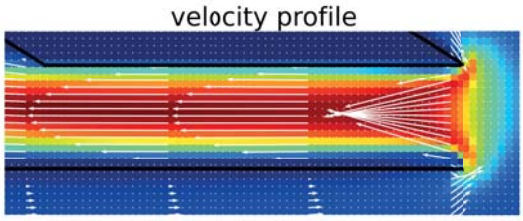

(c)

Figure 8: Velocity field, static long reed channel: (a) absolute velocity, (b) velocity profile of the jet passing through the reed channel, (c) velocity profile depicted in a larger scale.

6. REFERENCES

[1] John Backus, "Small-vibration theory of the clarinet," *The Journal of the Acoustical Society of America*, vol. 35, no. 3, pp. 305–313, 1963.

[2] Theodore A Wilson and Gordon S Beavers, "Operating modes of the clarinet," *The Journal of the Acoustical Society of America*, vol. 56, no. 2, pp. 653–658, 1974.

[3] Junich Saneyoshi, H Teramura, and S Yoshikawa, "Feedback oscillations in reed woodwind and brasswind instruments," *Acta Acustica united with Acustica*, vol. 62, no. 3, pp. 194–210, 1987.

[4] Neville H Fletcher, "Autonomous vibration of simple pressure-controlled valves in gas flows," *The Journal of the Acoustical Society of America*, vol. 93, no. 4, pp. 2172–2180, 1993.

[5] Jean Kergomard, "Elementary considerations on reed-instrument oscillations," *Courses and lectures-international centre for mechanical sciences*, pp. 229–290, 1995.

[6] Jean Kergomard, Sébastien Ollivier, and Joel Gilbert, "Calculation of the spectrum of self-sustained oscillators using a variable truncation method: Application to cylindrical reed instruments," *Acta Acustica united with Acustica*, vol. 86, no. 4, pp. 685–703, 2000.

[7] S Ollivier, J-P Dalmont, and J Kergomard, "Idealized models of reed woodwinds. part i: Analogy with the bowed string," *Acta acustica united with acustica*, vol. 90, no. 6, pp. 1192–1203, 2004.

[8] S Ollivier, Jean Kergomard, and Jean-Pierre Dalmont, "Idealized models of reed woodwinds. part ii: On the stability of," *Acta acustica united with acustica*, vol. 91, no. 1, pp. 166–179, 2005.

[9] Jean-Pierre Dalmont, Joël Gilbert, and Sébastien Ollivier, "Nonlinear characteristics of single-reed instruments: Quasistatic volume flow and reed opening measurements," *The Journal of the Acoustical Society of America*, vol. 114, no. 4, pp. 2253–2262, 2003.

[10] André Almeida, Christophe Vergez, and René Caussé, "Quasistatic nonlinear characteristics of double-reed instruments," *The Journal of the Acoustical Society of America*, vol. 121, no. 1, pp. 536–546, 2007.

[11] A. Hirschberg, R. W. A. van de Laar, J. P. Marrou-Mauriere, A. P. J. Wijnands, H. J. Dane, S. G. Kruijswijk, and A. J. M Houtsma, "A quasi-stationary model of air flow in the reed channel of single-reed wind instruments," *Acustica*, vol. 70, 1990.

[12] J. Van Zon, A. Hirschberg, J. Gilbert, and A. P. J. Wijnands, "Flow through the reed channel of a single reed instrument," in *J. Phys., Paris, Colloq. 54, C2 821824*, 1990.

[13] A. R. da Silva, *Numerical Studies of Aeroacoustic Aspects of Wind Instruments*, Ph.D. thesis, McGill University, Montreal, Canada, 2008.

[14] Dominique d'Humieres, "Generalized lattice-boltzmann equations," *Rarefied gas dynamics- Theory and simulations*, pp. 450–458, 1994.

[15] Zhaoli Guo and Chang Shu, *Lattice Boltzmann Method and Its Applications in Engineering*, World Scientific Publishing, 2013.

[16] Y.H. Qian, D. d'Humieres, and P. Lallemand, "Lattice BGK models for Navier-Stokes equation," *Europhysics Letters*, vol. 17, no. 6, pp. 479–484, 1992.

[17] S. Succi, *The lattice Boltzmann equation for fluid dynamics and beyond*, Oxford University Press, 2001.

[18] E.W.S. Kam, R.M.C. So, and R.C.K. Leung, "Non-reflecting boundary conditions for one-step LBM simulation of aeroacoustics," in *27th AIAA Aeroacoustics Conference, 8-10 May 2006, Cambridge, Massachusetts*, 2006.

[19] Andreas Klöckner, Nicolas Pinto, Yunsup Lee, Bryan Catanzaro, Paul Ivanov, Ahmed Fasih, AD Sarma, D Nanongkai, G Pandurangan, P Tetali, et al., "Pycuda: Gpu run-time code generation for high-performance computing," *Arxiv preprint arXiv*, vol. 911, 2009.

[20] Federico Avanzini and Maarten van Walstijn, "Modelling the mechanical response of the reed-mouthpiece-lip system of a clarinet. part i. a one-dimensional distributed model," *Acta Acustica united with Acustica*, vol. 90, no. 3, pp. 537–547, 2004.

[21] Zhaoli Guo, Chuguang Zheng, and Baochang Shi, "An extrapolation method for boundary conditions in lattice boltzmann method," *Physics of Fluids (1994-present)*, vol. 14, no. 6, pp. 2007–2010, 2002.

[22] Baptiste Bergeot, André Almeida, Bruno Gazengel, Christophe Vergez, and Didier Ferrand, "Response of an artificially blown clarinet to different blowing pressure profiles," *The Journal of the Acoustical Society of America*, vol. 135, no. 1, pp. 479–490, 2014.

[23] M. Rohde, D. Kandhai, J. J. Derksen, and H. E. A. van den Akker, "A generic, mass conservative local grid refinement technique for lattice-boltzmann schemes," *International Journal for Numerical Methods in Fluids*, vol. 51, no. 4, pp. 439–468, 2006.

ANALYTICAL MODEL OF THE TRANSITION BETWEEN CYLINDER AND CONICAL TUBES

Jean Kergomard[1], Antoine Lefebvre[2], Gary Scavone[2]

[1] Laboratoire de Mécanique et d'Acoustique, France
[2] McGill University, Canada
kergomard@lma.cnrs-mrs.fr
antoine.lefebvre2@mail.mcgill.ca
gary@music.mcgill.ca

ABSTRACT

For musical wind instruments, the problem of the transition between a cylindrical tube and a conical one occurs in many situations. In a sufficiently long cylinder, only planar waves can propagate, while in a sufficiently long cone, only spherical waves can propagate. Modelling the matching between the two tubes requires the consideration of higher-order modes, which are evanescent, i.e., close to the matching volume. A mode-matching method yields complicated computation, thus a numerical discretization method (such as the Finite Element Method, FEM), or experiment are more suitable. However the general shape of the model is known, under the condition that only one mode propagates in each tube, i.e., that the frequency is low enough. The model includes the effect of compressibility of the matching volume, and three acoustic masses. The major result is that the latter are linked together by the geometrical parameters, therefore only one mass has to be determined numerically or experimentally. It is proportional to the so-called length correction. Its knowledge allows the determination of an analytical model valid up to the first cutoff frequency. The results of the analytical formulas are compared with those of the FEM method, and the agreement is very good. The literature on this subject is rare, except the papers by Chester (J. Sound Vib. 1987) and Martin (J. Eng. Math., 2011). Comparison with formulas found in these papers is carried out, and it is found that the present study improves their results. Furthermore, for the particular case of a cylindrical tube radiating with an infinite flange, the analytical formula compares very well with the exact result (Norris and Sheng, J. Sound Vib. 1989), up to the first cutoff frequency.

PERIODIC AND QUASI-PERIODIC REGIMES OF AN ALTO SAXOPHONE ACCORDING TO THE CONTROL PARAMETERS AND THE BORE INHARMONICITY

Jean-Baptiste Doc, Christophe Vergez

Laboratoire de Mécanique et d'Acoustique, France
jbdoc@lma.cnrs-mrs.fr
vergez@lma.cnrs-mrs.fr

ABSTRACT

The aim of this work is to highlight experimentally how inharmonicity of the bore res- onance frequencies of an alto saxophone influence the nature of the oscillation regimes. A variable volume branching from the neck of an alto sax at an appropriate position allows to change the frequency of the first resonance independently from the second. A blowing machine with artificial lips is used to make the saxophone play while controlling independently the control parameters: the blowing pressure and an embouchure parameter. Values of these parameters are estimated experimentally through the measurement of the nonlinear characteristics linking the mean air flow blown into the instrument to the static pressure difference across the reed. Experiments with different values of the control parameters as well as of the inharmonicity produce different kinds of oscillation regimes. These regimes are categorized through the analysis of the pressure signal inside the mouthpiece. The resulting maps demonstrate that the emergence of quasi-periodic regimes, and their extent, depend on the level of inharmonicity, but also on the values of the control parameters. Periodic regimes playable by choosing appropriate values of the control parameters also differ according to the level of inharmonicity, a higher inharmonicity facilitating the emergence of the third register. Trends highlighted experimentally in this article are in agreement with numerical results obtained in a previous work. This numerical study was based on the use of a minimal model of wind instruments, so it is possible to deduce that features neglected in this model are not determining in the production of quasi-periodic regimes (inertia and damping of the reed, resonance modes higher than the third one)

COMPARISON BETWEEN THE MEASURED AND PLAYED INTONATION ON FOUR E-FLAT CLARINETS IN THE ALTISSIMO REGISTER

Manuel Gangl and Alex Hofmann***

*Institute of Music Acoustics
University of Music and Performing Arts Vienna, Austria
manuel.gangl@students.mdw.ac.at
**The Austrian Research Institute for Artificial Intelligence (OFAI), Austria

ABSTRACT

In this paper, two experiments were conducted to compare the intonation in the altissimo register (C#6–C7) on four german Eb-clarinets. In order to perform the experiments a fingering chart was created including twelve main fingerings with up to eight alternative fingerings (68 fingerings in total). As a first method, a professional clarinetist recorded the 68 fingerings in an anechoic chamber under controlled performance conditions. As a second method, input impedance measurements (BIAS) were done to gain objective data of the instrument's build quality, independent of a player. From the results of the first experiment, the tones of the altissimo register were subdivided into three groups of tones: In the first group (C#6–F#6) the main fingerings resulted in a correct intonation. In the second group (G6–G#6), alternative fingerings were proposed which helped to correct the intonation. In the third group (A6–C7), it was impossible for the professional performer to play the targeted pitches. A comparison of the intonation curves from the audio recordings and from the input impedance measurements indicated contrary trends. It remains an open question, which factors are actually limiting the playing range of the instruments. It is hypothesized that both, the low input impedance peaks for the altissimo notes and the reed's natural frequency may limit the playing range of the instrument.

1. INTRODUCTION

The Eb-clarinet belongs to the family of the high clarinets and does sound a minor third higher than written [1, 2]. The instrument often carries the top line in unison with the piccolo, first violins or solo alone and adds strength and brilliance to the notoriously weak upper register of every orchestra [3]. Many instrumentation and orchestration books [5, 6, 7] give a smaller tonal range for Eb-clarinets (E3–G6), in comparison to Bb-/Ab-clarinets (E3–C7, [8]). Composers frequently use the Eb-clarinet in the altissimo register [1, 9], but tend to ignore the range limit of G6 [10]. Playing on the Eb-clarinet is more difficult than on Bb-clarinets and many players [2, 3, 4, 8, 11, 12] reported intonation problems (being too flat in pitch) in the altissimo register. In such a case, audio recordings might help to better understand which tones are too flat.

The intonation in the altissimo register is mainly influenced by three factors.

First, the player can correct the pitch with his embouchure (lip pressure, blowing pressure or vocal tract configuration, [13, 14]). Larger deviations form a correct pitch can only be compensated by using alternative fingerings instead of main fingerings. An advantage of using alternative fingerings is that the player can maintain a constant embouchure which is not determined to one specific instrument. This allows an easier switch between different clarinets. Nevertheless, the player has to learn different fingerings which are sometimes difficult to apply in fast musical sequences. Numerous fingering charts exist in clarinet schools [15, 16, 17] and in the internet[1] which facilitate to correct the intonation in the altissimo register for the german clarinet system. Unfortunately, these fingering charts propose other main and alternative fingerings, especially in the altissimo register. It is planned to design a new fingering chart with main and alternative fingerings based on their frequency.

The second factor is the quality of the instrument (geometry, mouthpiece characteristic, reed characteristic). Thirdly, the environment (temperature, humidity) has to be taken into account [18]. However, this paper focusses on the player and the quality of the instrument.

Input impedance measurements on wind instruments have been shown to be a reliable method to characterize the objective quality of an instrument, independent of the player. Since now, Bb-clarinets were measured with the mouthpiece, using an adaptor for the input impedance measuring head [19]. Alternatively, mouthpiece and instrument body can be measured together or measured independently and combined later [20]. Input impedance measurements on Eb-clarinets could detect possible problem tones.

The clarinet [18] vibrates with modes that are odd multiples of the fundamental frequency (see figure 1) and tones are excited at high input impedance peaks. The 2^{nd} mode of oscillation has a frequency three times that of the fundamental, musically an octave and a fifth. The modes [18] of an input impedance curve of a clarinet can be subdivided into three registers. Depending on the fingering, the first mode excites tones between E3–A#4 (chalumeau register), the second mode tones between B4–C6 (clarion register) and the third and higher modes tones between C#6–C7 (altissimo register). Table 1 shows the subdivisions of the modes into three registers.

Mode	**Tonal range**	**Register**
Mode 1	E3–A#4	chalumeau register
Mode 2	B4–C6	clarion register
Mode 3 and higher	C#6–C7	altissimo register

Table 1: The modes of the input impedance curve of a clarinet can be subdivided into three registers.

However, nobody has so far assigned the main fingerings of the altissimo register to the respective modes.

[1] www.hueyng.de; timeforclarinets.de; klarinette-lernen.de; klarinette24.de

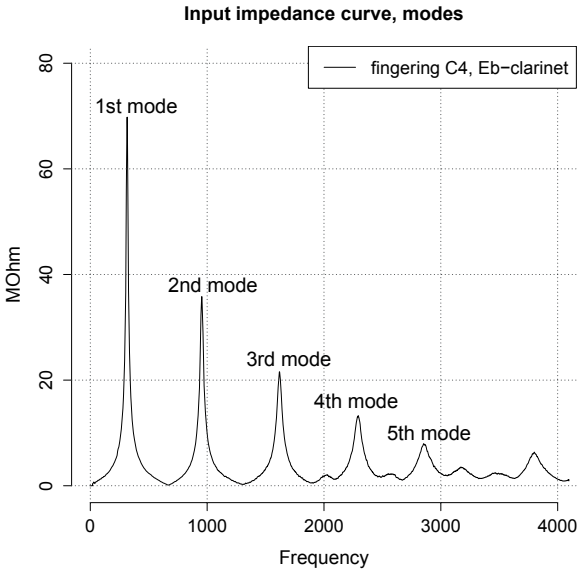

Figure 1: An input impedance curve can be subdivided into several modes.

2. AIMS

The author aims to design a new fingering chart with main and alternative fingerings, based on their frequency. In order to compare the played and measured intonation on four Eb-clarinets, audio recordings and input impedance measurements are foreseen. Better fingerings will be proposed for problem tones. Furthermore, the main fingerings of the altissimo register will be assigned to modes.

3. METHODS

First, a new fingering chart was designed to perform two different experiments on four Eb-clarinets (see table 2). In the first experiment the author recorded the pitch of 68 fingerings. In the second experiment main and alternative fingerings were measured through input impedance measurements.

Name	Instrument maker	Type
FH	F. Hammerschmidt	FH 11
OH	O. Hammerschmidt	16F
UE	A. Uebel	Eb
WH	H. Wurlitzer	120S

Table 2: Names, instrument makers and types of the four different Eb-clarinets which were used in the experiments.

3.1. Fingering chart

3.1.1. Procedure

A new fingering chart with 12 main and 56 alternative fingerings (4–8 alternative fingerings per main fingering) was created based on their frequency, which is a collection of a master thesis [19], different clarinet schools [15, 16, 17] and online charts[2]. The fingering chart was designed using Inkscape [21].

[2]www.hueyng.de; timeforclarinets.de; klarinette-lernen.de; klarinette24.de

3.2. Audio recording

In this experiment a professional clarinetist (17 years experience, author) played the tones of the altissimo register (12 main fingerings, 56 alternative fingerings) on four Eb-clarinets in the anechoic chamber.

3.2.1. Equipment/Setup

The experimental setup consisted of a measuring microphone (RG-50, by Roger), a metronome (KDM-1, by Korg Inc.), headphones and a professional hard disk recording device (by RME, 44 kHz, 32 Bit). The same Bb-clarinet reed was used for all recordings (White Master: German Cut, Reed Strength: 3 1/2, cut at the end to fit on the smaller mouthpiece lay) with a mouthpiece by MAXTON (material: PMMA).

3.2.2. Procedure

For each instrument, 12 tones were recorded with up to 8 alternative fingerings (68 fingerings in total). Each tone was played for three seconds with a break of one second. A metronome click (60 bpm) on open headphones (by AKG) was used for tempo orientation. The author played all tones with the same embouchure configuration (high lip pressure, high blowing pressure, high tongue position, miming "ee") and used an embouchure aid (paper over the lower teeth) to avoid lip pain. The audio recordings were loaded into Sonic Visualizer and the performed pitch was analyzed using the "Aubio Pitch Detector" plugin (Version.1.9; Pitch Detection Function Type: Spectral Comb). The raw data (fundamental frequencies) was imported into R-statistics to calculate the pitch for each note to the equal tempered scale and for further analysis.

3.2.3. Results

In the first analysis the pitch of the main fingerings were investigated. Figure 2 shows that the pitch of the main fingerings can be subdivided into three groups.

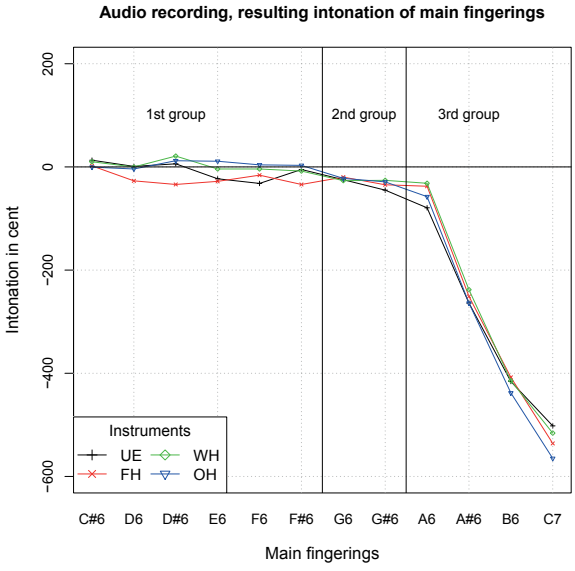

Figure 2: The pitch analysis of the altissimo tones showed that the main fingerings can be subdivided into three groups.

In the first group the tones C#6–F#6 were close to a correct pitch. In the second group the tones G6 and G#6 caused too flat tones on all Eb-clarinets and in the third group (A6–C7) the main fingerings produced tones, which were more than a halftone too flat. Consequently, in a second analysis the alternative fingerings of G6 and G#6 (second group) were observed to find fingerings towards best intonation. Figure 3 shows that an alternative fingering (G6Fing2, red) was able to correct the pitch offset for G6.

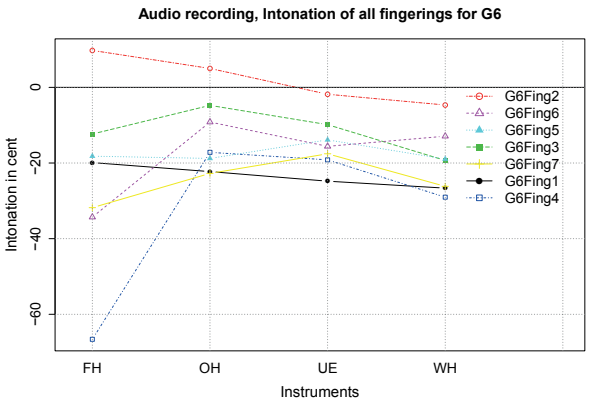

Figure 3: The pitch analysis of G6 showed that an alternative fingering (G6Fing2, red) helped to correct the pitch.

The same was the case for the tone G#6 (see figure 4), where the alternative fingering (G#6Fing5, cyan) helped to correct the pitch. The fingering G#6Fing5 was chosen as the best fingering, because the ”UE” Eb-clarinet was close to a correct pitch. On the remaining three instruments (FH, OH, WH) the player can easily lip down a too sharp pitch with his embouchure. Input impedance measurements might help to understand the influence of these alternative fingerings.

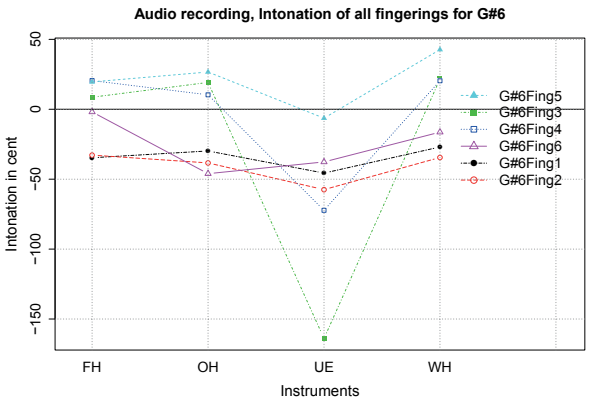

Figure 4: An alternative fingering (G#6Fing5, cyan) helped to correct the pitch for G#6.

However, further analysis of alternative fingerings of the tones A6–C7 showed that the pitch could not be corrected by using alternative fingerings.

3.3. Input impedance measurement

3.3.1. Equipment/Setup

The technical set up for the input impedance measurement (BIAS[3] Version 7.1, by ARTIM) consisted of the measuring head (Nr. 206S) held by a spring attached to a microphone stand, triggered by a foot switch (see figure 5).

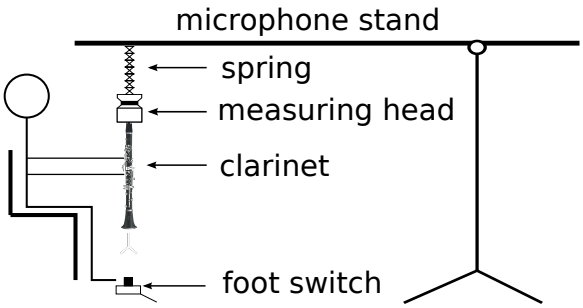

Figure 5: Measuring method using a microphone stand with a spring to reduce the weight of the measuring head and the instrument for the player.

This method reduces the weight of the instrument and the measuring head for the player and allows to measure the four Eb-clarinets with a natural posture. A foot switch helps to trigger the measurement after positioning the fingerings. The mouthpiece was replaced by a tube (14 mm inner bore, 58 mm length) to allow an easy exchange of the instruments and to calibrate the inner volume. The inner volume was calibrated with inlays of 6 x 1 mm to be equal to that of an Eb-clarinet mouthpiece. Figure 6 shows the cross section of the BIAS measuring head.

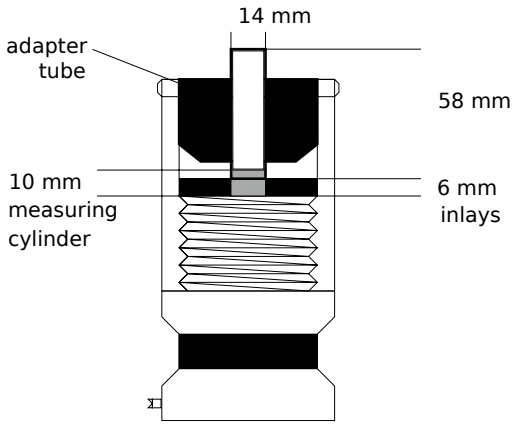

Figure 6: Cross section of the BIAS measuring head with new customized adapter tube, replacing the Eb-clarinet mouthpiece.

[3]Brass Instrument Analysis System

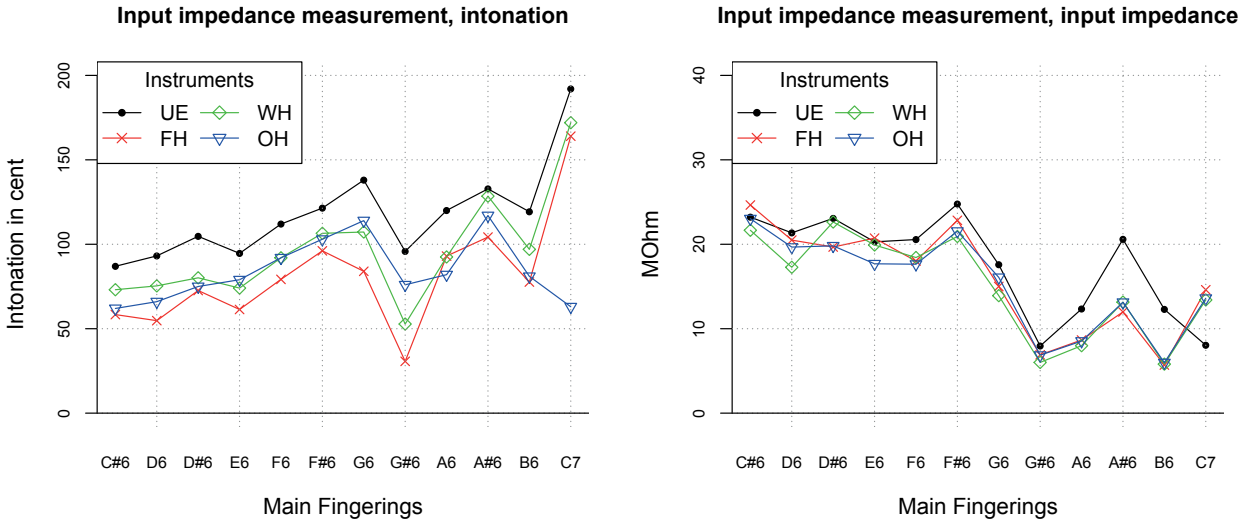

Figure 7: The intonation curves of the input impedance measurements (left) show two kinks at G#6 and B6. These tones are problem tones. The same can be seen at the input impedance curves (right).

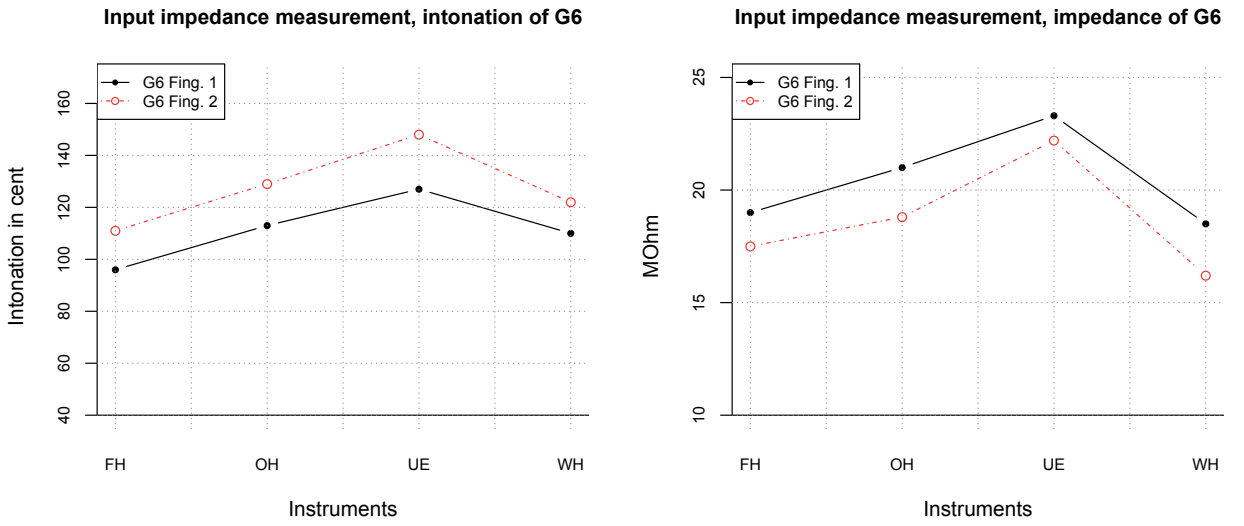

Figure 8: An alternative fingering (G6 Fing. 2, red) resulted in a sharper pitch, but with a lower input impedance (right), in comparison to the main fingering (G6 Fing. 1, black) on all Eb-clarinets.

3.3.2. Procedure

The 12 main fingerings (C#6–C7) and two alternative fingerings (G6Fing2, G#6Fing5) were measured separately on four Eb-clarinets (14 fingerings X 4 Eb-clarinets).
From these 56 input impedance curves the coordinates of the input impedance peaks (input impedance and frequency), which were close to the targeted frequency, were manually extracted with the curser in BIAS. Furthermore, the author counted the mode (Input impedance peak) of the extracted coordinates. The raw data (Fingerings, Frequency, Input impedance, Mode) was exported from a excel table into R-statistics. In R-statistics the pitch for each fingering was calculated to the equal tempered scale for further analysis.

3.3.3. Results

In the first analysis the 12 main fingerings were investigated. The analysis shows that the measured pitch is much sharper (>50 cent) than the expected pitch on all main fingerings (see figure 7, left). Normally, the measured pitch is close to the targeted pitch. The increasing intonation curves (see figure 7, left) show two kinks at G#6 and B6. The intonation of these both tones indicate possible problem tones. The same can be seen taking a look at the input impedances (see figure 7, right). On all instruments G#6 and higher tones resulted in a very low input impedance. This low input impedances could be a second indicator for problem tones.
In the second analysis the main fingerings of G6 and G#6 were compared with the alternative fingerings (G6 Fing. 2, G#6 Fing. 5). Figure 8 shows the input impedance measurement of the

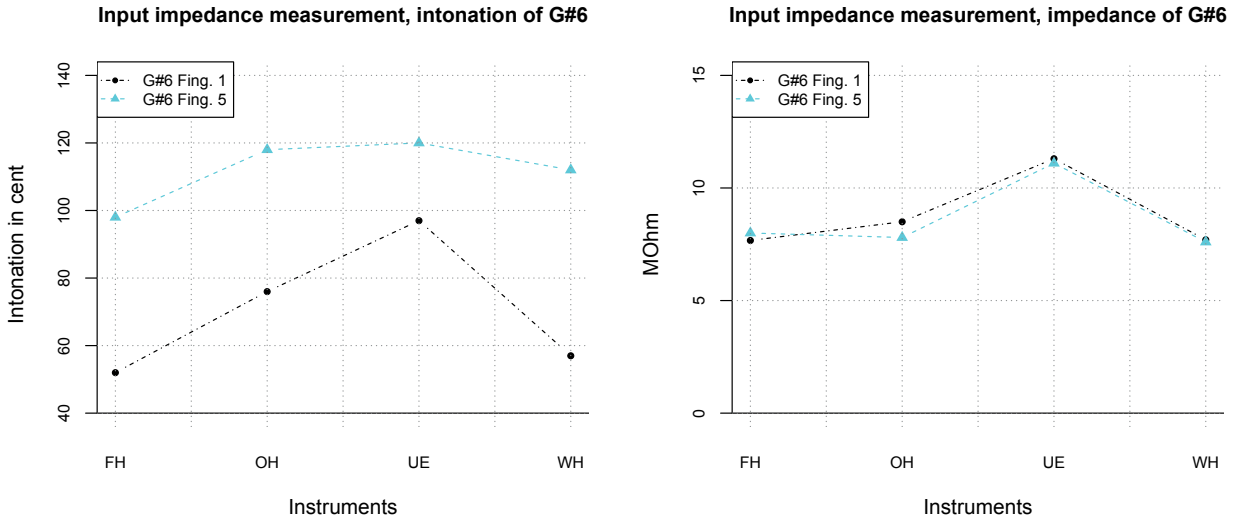

Figure 9: An alternative fingering (G#6Fing. 5, cyan) resulted in a sharper pitch and had nearly the same input impedance (right) in comparison to the main fingering (G#6 Fing. 1, back).

main fingering (G6 Fing. 1, black) and alternative fingering (G6 Fing. 2, red) for G6. The alternative fingering G6 Fing. 2 (red) resulted in a sharper pitch, but with a lower input impedance on all Eb-clairnets. The input impedance measurement confirms the influence of a sharper pitch in the audio recording. The same can be seen in figure 9 of the main fingering (G#6 Fing. 1, black) and alternative fingering (G#6 Fing. 5, cyan) for G#6. The alternative fingering G#6 Fing. 5 (cyan) resulted in a sharper pitch and had nearly the same input impedance on all Eb-clarinets.

In the third analysis the main fingerings were assigned to the respective modes. The analysis (see table 3) shows that the modes of the main fingerings, which were chromatically arranged, did not ascend with higher tones. The order of the modes changed from G#6 upwards.

Tone	**Mode**	**Frequency**	**Register**
E3–A#4	Mode 1	197.3–558.1 Hz	chalumeau
B4–C6	Mode 2	591.3–1253 Hz	clarion
C#6–E6	Mode 3	1327.5–1578.7 Hz	altissimo
F6–G6	Mode 4	1672.5–1877.4 Hz	”
G#6	Mode 3	1989 Hz	”
A6	Mode 5	2107.3 Hz	”
A#6/B6	Mode 7	2232.6–2365.3 Hz	”
C7	Mode 6	2506 Hz	”

Table 3: The altissimo register tones are played on the 3^{rd} mode or higher. The arrangement of the modes changes from G#6 upwards.

4. DISCUSSION

This study investigated the altissimo register on four Eb-clarinets in two different experiments.

In the first experiment the author recorded twelve main fingerings with up to 8 alternative fingerings on four Eb-clarinets in an anechoic chamber. The results showed that the pitch of the altissimo tones can be subdivided into 3 groups (see figure 2). In the first group (C#6–F#6) the pitch resulted in a correct intonation, in the second group (G6 and G#6) the tones were too flat and in the third group (A6–C7) tones were produced which were more than a halftone too flat. Alternative fingerings corrected the intonation in the second group (G6 and G#6), but no other fingerings helped to correct the pitch on higher tones than G#6.

In the second experiment the twelve main fingerings and two alternative fingerings were measured through input impedance measurements on four Eb-clarinets. The results of the main fingerings indicated two problem tones (G#6 and B6, see figure 7). The main fingering for G#6 showed a flat intonation and a low input impedance. The same was the case for the tone B6.

Two alternative fingerings (G6 Fing. 2 and G#6 Fing. 5) helped to correct the pitch offset in the audio recording. This can be confirmed by the input impedance measurements (see figures 8, 9). Additionally, the modes changed from G#6 upwards (see table 3). A comparison between the played intonation of the audio recordings (red) and the calculated intonation of the input impedance measurements (blue) shows that both intonation curves drift apart (see figure 11).

It is hypothesized that the reed characteristic (mass, stiffness) and the vocal tract configuration may be the reason for the problem tones of the second and third group of tones (G6–C7, see figure 11).

The resonance frequency [22, 23] of the reed (f),

$$f = 1/2\pi * \sqrt{(Stiffness/Mass)} \quad (1)$$

is proportional to the root of the stiffness (higher stiffness = higher resonance frequency) of the reed, vice versa to the mass. When the playing frequency is below f, the stiffness and the mass of the reed do not influence the playability [22, 23]. The higher the played notes, the more important becomes the mass and the stiffness of the reed. Some clarinetists use Bb-clarinet reeds on Eb-clarinets. They cut the reeds at the end to fit them to the shorter lay of the Eb-mouthpiece. The reed's natural frequency is in the range of 2000–4000 Hz [18, 24], which overlaps with the tones G#6 (1989 Hz)–C7 (2506 Hz) on Eb-clarinets (Table 4).

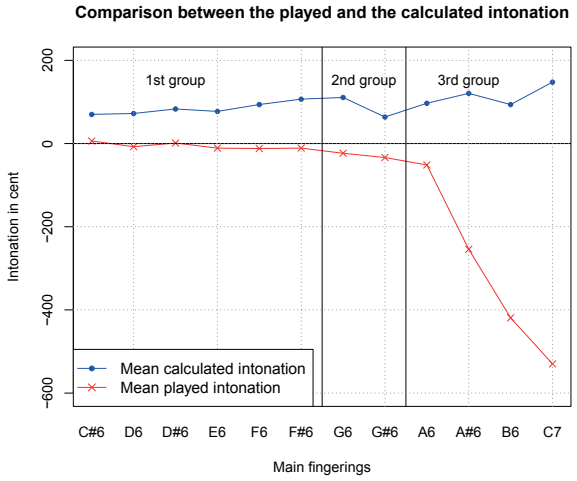

Figure 10: The intonation curves of the audio recordings (red) and the input impedance measurements (blue) drift apart for the main fingerings.

Playing range	E3		G6	C7
Eb-clarinet	**197.3 Hz**	–	**1877.4 Hz**	(2506 Hz)
Bb-clarinet	**147.8 Hz**		–	**1877.4 Hz**

Table 4: Eb-clarinets and Bb-clarinets have the same frequency limit. The note G6 on the Eb-clarinet corresponds to a C7 on the Bb-clarinet. The frequency of the note C7 on the Eb-clarinet has a frequency of 2506 Hz, which is close to the reed's natural frequency.

It is recommended to use harder reeds in the altissimo register [3, 25, 26], which can be explained by their characteristic to have a high resonance frequency f.
Chen et al. [27] have shown the influence of the vocal tract resonances on the pitch in the altissimo register. This is caused by the overlapping between the vocal tract resonances and the bore resonances. Under the condition of low impedance peaks inside the instrument, the impedance of the players vocal tract has to be considered. Additionally, in the altissimo register the reed's natural frequency is close to the playing frequencies on Eb-clarinets. It was observed that the end of the playing range of the instruments was A6. Harder reeds, which have higher resonance frequencies, might help to improve the intonation of altissimo tones and increase the playing range.
In summary, it is assumed that from a certain point on, when the input impedance peaks decrease, other factors (e.g.: reed characteristics, embouchure settings) have a strong influence on the resulting pitch. To better understand the behavior of the Eb-clarinets in the altissimo register, measurements including vocal tract resonance, reed resonance, blowing pressure, and lip pressure measurements are foreseen. From such enhanced measurements the significance of these factors can be determined.

5. AUTHOR CONTRIBUTIONS

Conceived and designed the experiments: MG. Performed the experiments: MG AH. Input impedance measurements: MG. Analysis of the recordings: AH MG. Wrote the paper: MG

6. ACKNOWLEDGMENTS

This research was supported by the Austrian Science Fund (FWF: P23248, P24546)

7. APPENDIX

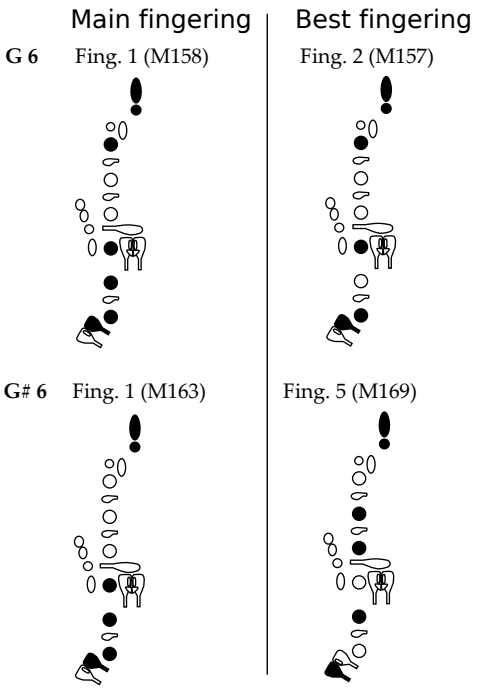

Figure 11: Alternative fingerings (best fingerings) helped to correct the pitch for the tones G6 and G#6. For the tone G6, a slightly change (opening the middle finger of the right hand) of the main fingering sharpened the pitch. For the tone G#6, a completely different fingering compared to the main fingering resulted in a sharper pitch.

8. REFERENCES

[1] Hans Kunitz, *Die Instrumentation: ein Hand-und Lehrbuch*, Ardent Media, 1956.

[2] Basil Tschaikov, *The Cambridge companion to the clarinet*, chapter The high clarinets, pp. 43–55, Cambridge University Press, Lawson, Colin James, 1995.

[3] Don McCathren, "Playing in tune–the e-flat soprano clarinet," *Woodwind Anthology 1992*, vol. Vol. 2, pp. 63–64, 1958.

[4] James McCoy, "Playing the e-flat clarinet: An optimistic approach," *Woodwind Anthology 1992*, pp. 527–529, 1967.

[5] Jindřich Praveček, Karel Mikuláštík, Adolf Langer, and Wieland Ziegenrücker, *Instrumentationslehre für Blasorchester*, chapter Das Instrumentarium des Blasorchesters, p. 11, Dt. Verlag f. Musik, 1981.

[6] Oskar Kroll and Diethard Riehm, *Die Klarinette*, Kassel [u.a.] : Bärenreiter, 1965.

[7] Richard Strauss, *Instrumentationslehre von Hector Berlioz*, vol. 1, chapter Die Klarinetten, pp. 214–236, Edition Peters, 1904.

[8] Jack Brymer, *The clarinet*, Halstan, Co Ltd., Amersham, Bucks, 1978.

[9] Walter Piston, *Orchestration*, WW Norton New York, 1955.

[10] Kathleen M. Gardiner, *An annotated bibliography of twenieth-century solo and chamber literature for the e-flat clarinet*, Ph.D. thesis, Ohio State University, 2002.

[11] Gerorge E. Waln, "Playing differences in clarinets: The e-flat soprano clarinet," *Woodwind Anthology 1992*, vol. Vol. 2, pp. 18–19, 1951.

[12] Larry Guy, *Intonation Training for Clarinetists*, Rivernote Press, 1996.

[13] Andre Almeida, David George, John Smith, and Joe Wolfe, "The clarinet: How blowing pressure, lip force, lip position and reed "hardness" affect pitch, sound level, and spectrum," *The Journal of the Acoustical Society of America*, vol. 134, no. 3, pp. 2247–2255, 2013.

[14] Jer-Ming Chen, John Smith, and Joe Wolfe, "How players use their vocal tracts in advanced clarinet and saxophone performance," in *Proc. Int. Symp. Music Acoustics*, 2010.

[15] Carl Baermann and Oskar Schubert, *Klarinetten Schule*, vol. Erster Teil, op. 63, Johann André, 502a edition, 1917.

[16] Carl J. Wimmer, *Grundschule für Klarinette 1*, Preissler, 1983.

[17] Willy Schneider, *Erstes Klarinettenspiel: Lieder, Tänze und Kanons für 1-3 Klarinetten*, Schott, 1966.

[18] John Backus and Richard Baskerville, *The acoustical foundations of music*, vol. 8, Norton New York, 1977.

[19] Alexander Pilgerstorfer, "Umfassende Grifftabelle für die deutsche Klarinette sowie Impedanzanalyse aller Töne," M.S. thesis, Institut for Music Acoustics/Vienna, 1995.

[20] Wilfried Kausel and Helmut Kuehnelt, "A practical way to measure intonation quality of woodwind instruments using standard equipment without custom made adapters," *IEEE Transactions on Instrumentation and Measurement*, vol. 53, no. 4, pp. 1097–1105, 2004.

[21] Tavmjong Bah, *Inkscape: Guide to a Vector Drawing Program (Digital Short Cut)*, Pearson Education, 2009.

[22] Cornelis Johannes Nederveen, *Acoustical aspects of woodwind instruments*, Northern Illinois University Press DeKalb, 1998.

[23] John Backus, "Small-vibration theory of the clarinet," *The Journal of the Acoustical Society of America*, vol. 35, no. 3, pp. 305–313, 1963.

[24] Jürgen Meyer, *Zur Akustik der Klairnette*, pp. 177–184, Restle, Conny/Fricke, Heike (Hg.): Faszination Klarinette. München ua, 2004.

[25] Walther Krüger, "Zur Funktion von Mundstück und Rohrblatt bei Klarinetten," *rohrblatt, Magazin f. Oboe, Klarinette, Fagott und Saxophon*, vol. 16, pp. 21–27, 2001.

[26] Gary P Scavone, Antoine Lefebvre, and Andrey R da Silva, "Measurement of vocal-tract influence during saxophone performance," *The Journal of the Acoustical Society of America*, vol. 123, no. 4, pp. 2391–2400, 2008.

[27] Jer-Ming Chen, John Smith, and Joe Wolfe, "Pitch bending and glissandi on the clarinet: roles of the vocal tract and partial tone hole closure," *The Journal of the Acoustical Society of America*, vol. 126, no. 3, pp. 1511–1520, 2009.

IMPROVING A G-HIGH CLARINET USING MEASUREMENT DATA AND AN ELECTRONIC CIRCUIT ANALYSIS PROGRAM

Fritz Schueller, Carl Poldy

Private Researchers
Vienna, Austria

fritz.schueller@aon.at
carl.poldy@nativeprogramming.at

ABSTRACT

Electromechanical and electroacoustical analogies are widely used in mechanics and acoustics. Highly developed theories for electric networks, including sources, inductive, capacitive and resistive elements, as well as resonating circuits, electrical lines, etc. can thus be directly used to simulate the behaviour of musical instruments [1].

There exist special Circuit Analysis Programs, such as Micro Cap [2], that are useful for simulating complex electrical networks. Applying the above mentioned analogies, these tools can be used in different ways to simulate characteristics of wind instruments, such as input impedance, transient behaviour, spectra, etc.

The authors have developed special so called “macros” that allow a convenient application of the software tool for mechanical and acoustical systems.

A method was developed to simulate a complete clarinet body (without reed and mouthpiece). This method was then used successfully to develop a new G-high clarinet, a special Viennese instrument, called Picksuesses Hoelzl and used in Schrammelmusik. How this was done, also with the help of BIAS [3] will be described in detail in the article.

The purpose of this paper is to show the possibilities that exist, using software-based models of wind instruments, especially of clarinets. It is not meant to be a recipe for instrument manufacturers. Intensive training would be needed to use the described method in practice.

1. INTRODUCTION

1.1 The software model

The model of the clarinet comprises a combination of electrical elements. Some of these elements are part of the original software package of the Electronic Circuit Analysis Program, others are specially developed macros (electric circuits with inputs and outputs that are building blocks for the software model). Examples for the originally available elements are electric wires, current sensors (ampere meters), current and voltage sources and measuring points (nodes).

The specially developed macros include tubes, holes radiators, etc.. The macros have special shapes, so that the structure of the model can be understood intuitively.

An example of a macro is a lossy cylindrical tube of freely definable length, diameter and number in parallel (Fig. 1). All physical dimensions used are in SI-units and not explicitly given in the schematics. Therefore 11.2m in Fig. 1 means 11.2mm, 11 alone would stand for 11 meter. Several tubes of the same length and diameter could be connected in parallel. For a single tube N has to be set to 1 (the only case needed for a wind instrument). These physical dimensions are the numerical input to the macros.

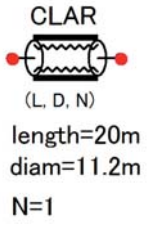

Fig. 1, Representation of a tube macro

Inside the macro there are several electrical elements and formulae to describe its detailed function (Fig. 2). The physics of the needed elements can be found in the literature, see [4] as an example.

The complete circuit of the G-high clarinet, including impedance sensor and radiator is shown in Fig. 3. This is meant to show the overall view of the model and to demonstrate its structure. The macros for sideholes can be seen, including the values for diameter, depth, diameter of the pad and pad-opening. Additionally the macro for lossy conical tube and cylindrical tubes is shown together with the lengths and diameters. The fingering for this clarinet is the same as for all German-type instruments.

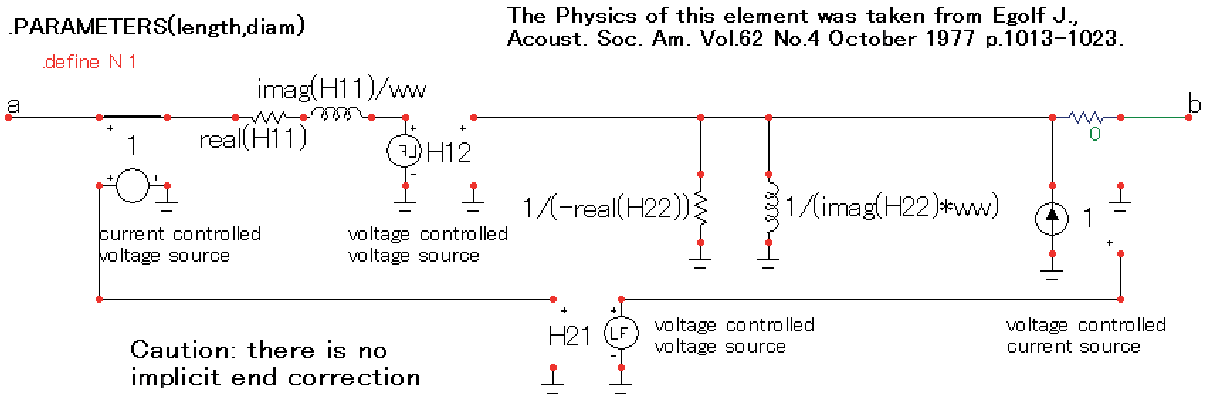

Fig. 2, Circuit inside a macro

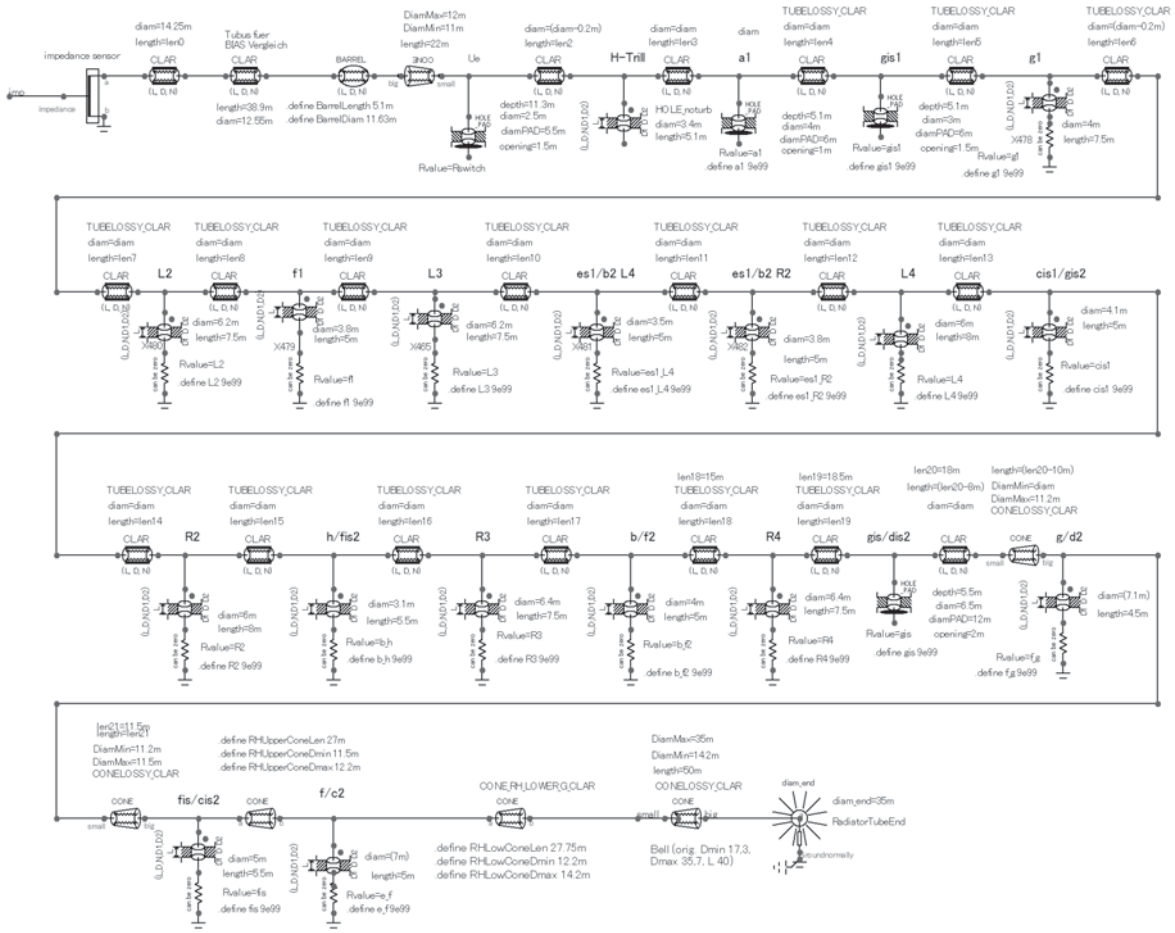

Fig. 3, Circuit diagram of a complete clarinet

Fig. 4 shows the result of the simulation for the impedances from B5 to C6 (fingered tones). Similar graphs also exist for the other playing registers of the clarinet. While the analysis is running, a so called stepping procedure is operational. That means that the opening or closing of side-holes is simulated, according to the correct fingering of each tone.

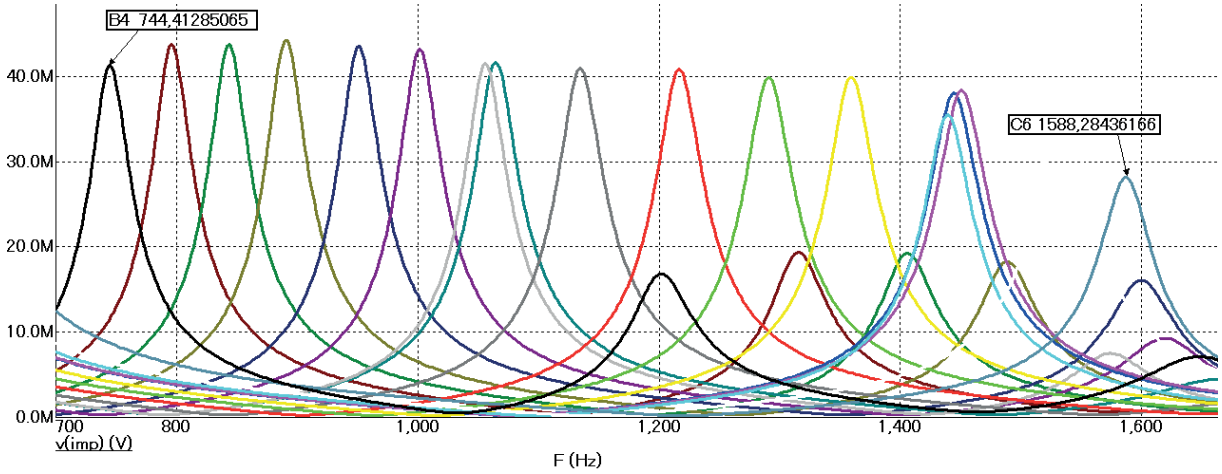

Fig. 4, Simulated frequency response of the impedance, stepped for various fingerings

1.2 Limitations of the model

There are several simplifications that limit the accuracy of the model. We neglect nonlinear effects and the inner and outer open-hole interactions. The sum effect of the tube losses is combined in an empirical factor that effectively increases the shear viscosity. This factor is in the range of 2 to 4 to give optimum results. Further down it is shown how these inaccuracies are compensated using BIAS and a music tuner.

2. FROM A PROTOTYPE TO AN IMPROVED DEFINITIVE INSTRUMENT

2.1 Main idea

The primary quality criterion for a musical instrument is good intonation. The player should be in a position to produce correct pitches fitting to either pure intonation or equal temperament. That means that the tones offered by the instrument are in a range of +/- 5 cent compared to the values for the tempered scale. The player is then able to adjust the pitch to the musically correct value by adapting the embouchure.

The aim of the software simulation is to develop a list of geometrical parameters suitable for producing a good clarinet. These parameters are diameter of the bore, conical elements in the bore, tone hole positions, diameters, depth, pad diameters and pad openings dimensions of the barrel and the bell. The simulation is not suited for developing a clarinet from scratch. A working prototype is needed first.

Fig. 5 shows the simple prototype that was used as a starting point. It has only two rings, no correction holes at all and no F#3/C#5 fork mechanics (special extension of the German-type clarinet, included in every modern clarinet).

2.2 Geometrical dimensions of the prototype

First of all the geometrical dimensions of the prototype are measured and documented. The bore and its profile along the axis is measured using a bore gauge. The other dimensions are measured using slide calipers.

2.3 Simulating the prototype

The mechanical dimensions are now fed into the circuit diagram of the model. This is time consuming and has to be done very carefully. After that a so-called AC (alternating current) analysis is started. The analysis for all common fingerings runs automatically. A diagram of resonances as shown in Fig. 4 is the result. For practical reasons the registers of the clarinet are simulated separately. These are the low (chalumeau) register from E2 to E3, the “throat-tones” F3 to Bb3, and B3 to C5 (clarin register). In this article the tones are always to be understood in written notation (if not otherwise mentioned).

The impedance sensor needs to be connected to the clarinet model via a special adapter-tube, as such a tube is also needed for the BIAS-measurement. In the simulation its dimensions must correspond to the adapter used for the BIAS-measurement (see below).

It is practical to use a spread sheet to collect and compare the intonation data. The results of the simulation, namely the frequency of the peaks and the magnitude (in acoustic Ohms S.I.) are entered into the third column of the spread-sheet. In the first column are the names of the tones (E2 to C5) including lines for alternative fingerings (e.g. fork fingerings). In the second column are the respective frequencies of the tones for equal temperament based on the concert pitch (in our case 443Hz). The cent deviations between second and third column are shown in the fourth column. There are several reasons for the deviations: The simulation is not perfect due to the limits of the model, the tube does not act like the mouthpiece-reed combination and there might be some measuring errors in the mechanical dimensions of the clarinet. But the main reason of course is, that the instrument is not yet optimised.

Fig. 5, Prototype used as a starting point

Fig. 6, BIAS measuring setup

2.4 Measuring the prototype using BIAS

The clarinet (the barrel) is connected to the BIAS measuring head not directly, but via a cylindrical tube (adapter). Its volume is chosen to be approximately equal to the volume of the mouthpiece. The diameter of this adapter has to fulfil two requirements: It should be similar to the bore-diameter of the clarinet and it has to be big enough to slip over the measuring cylinder of the BIAS head (diameter 14mm). Therefore in practice the adapter has two parts. One part of diameter 14mm and a length of about 10mm. This part slips over the BIAS-cylinder. The longer part of the tube has a diameter of 11mm (depending on the bore of the clarinet). And its length is chosen such that the mouthpiece volume is equal to the volume of the whole adapter. The values are not critical.

The clarinet is mounted together with the BIAS head on a special setup, including a spring and a tripod. (see Fig. 6, showing a Bb-clarinet). The same fingerings as used in the simulation are measured and the results are entered into the spreadsheet. Now a comparison of the BIAS measurement and the simulation in cent-difference is available. This comparison is also done for the height of each peak.

The differences between the frequencies of the resonance peaks are used for detecting measuring errors of the mechanical dimensions and incorrect values in the circuit diagram. Care must be taken that the room temperature in the simulation is the same as when making the BIAS measurements.

The basic model needs to be corrected by a loss factor. This is done by multiplying the shear-viscosity eta = 1.86 x 10-5 kg/(ms) by this factor. It is determined in such a way that the impedance of the peaks is approximately the same in BIAS and in the simulation. A value between 2 and 4 is the result.

After resolving obvious errors and finding a suitable loss factor this part of the procedure is completed (see Fig. 7). As can be seen, it was not possible to bring the difference down to an acceptable level for the C6 (fork fingering at the German clarinet). The reason remains unclear for the moment. Only the values of the simulation are used for the next steps. BIAS will later be used again to check the performance of the final model after its realisation.

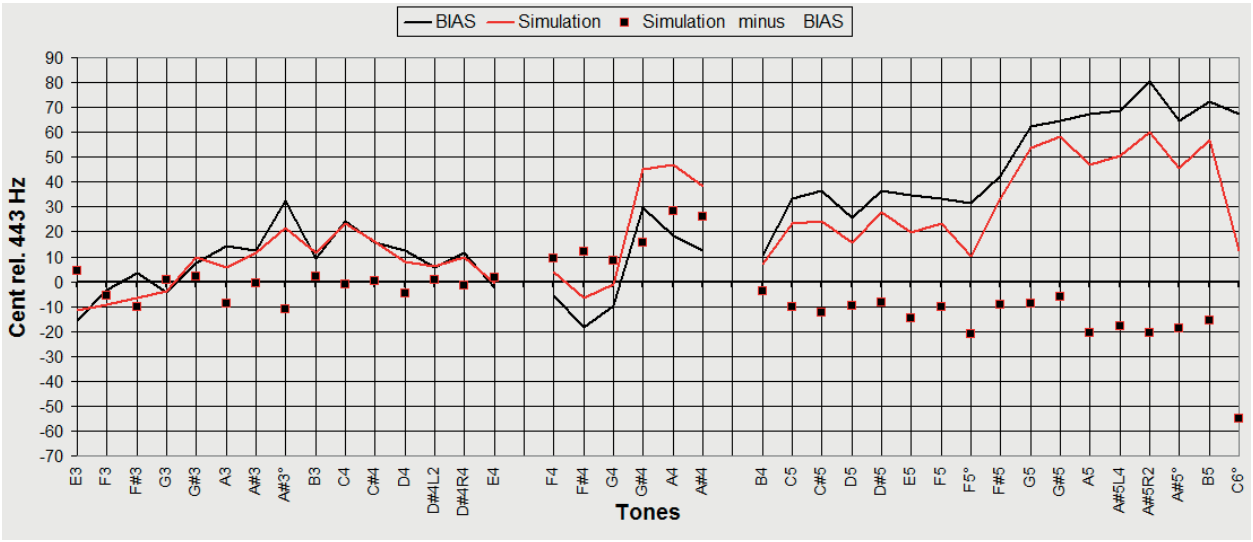

Fig. 7, Comparison BIAS versus simulation for all three registers up to C6

2.5 Pitch determination by blowing the prototype

So far the actual performance of the clarinet has not been considered. The mouthpiece-reed combination has a great influence on the intonation of the instrument. The aim of the whole procedure is to get an instrument which is suitable for playing each note in the desired intonation. This means that every tone should be adjustable (by the embouchure) in a range of about minus 15 to plus 15 cent referred to the equal tempered scale. This presumes that the intonation ”offered” by the instrument does not deviate too much from the tempered scale. If this is fulfilled it is possible to play also with pure intonation.

Thus the existing prototype needs to be blown with a medium mouthpiece-reed combination. “Medium” in this sense means firstly that the reed is not too soft and not too hard. Secondly the mouthpiece should be similar to one intended for the final instrument. Ideally there should be several mouthpieces available, from which one with average or best performance can be chosen.

After warming up the instrument, the whole chromatic scale is played, including any alternative fingerings. For each tone three intonation values are measured with a tuner and recorded in the spread-sheet. One is the minimum frequency that can be achieved with normal tone quality, one the highest, and one the frequency that is achieved with a medium, comfortable embouchure (optimum). Additionally an average value is computed for the maximum and minimum value to detect possible errors in reading the tuner.

If the prototype is not yet good enough, there will be some tones that do not fulfil the requirement of the playing range as mentioned above. This situation is shown in Fig. 8, taken from the prototype that was to be improved.

There are several imperfections to be seen in Fig. 8. For example it is impossible to play A#3° (fork fingering) and C4 in tune. Both are too sharp. A#5L4 (special fingering on the German clarinet with the ring finger of the left hand) is too low. Another problem is that there is a jump of more than 20 cent between the A#3 and the A#3° (fork). But the corresponding two tones (twelfths) in the clarin register (F5 and F5°) are not far apart. So any change in the tone holes that would improve the relation A#3 to A#3° would worsen the situation for F5 and F5°. This is because the prototype is a simple instrument lacking a special correction hole needed to bring all the four pitches A#3, A#3°, F5, F5° close to the zero-line. Using the simulation it was possible to place this correction hole at the right place with the right diameter and length.

It should be mentioned that also a correction of the bore was necessary to compensate for the above mentioned imperfections of the prototype. An article by Krueger [5] and a spread-sheet trial-and-error method was used to determine the conical parts of the bore. How this was done in detail is outside of the scope of this publication.

2.6 Calculation of correction factors

Now there exist two pitch values for each tone on the clarinet. One value comes from the simulation and one from actually playing the original prototype (optimum, as described above). The idea is that any correction of the tuning should bring the optimum (in the sense of blowing) value to zero cent (as compared to the tempered scale). Thus if y is a certain tone of the chromatic scale, we call the pitch of the played tone opt_proto(y) and the pitch of the simulation sim_proto(y). Then, expressing everything in cent:

opt_proto(y)-sim_proto(y)=k(y)

It is assumed that k stays roughly the same when simulating and blowing the instrument to be developed, so that

k(y)=opt_new(y)-sim_new(y)

As opt_new should be zero, the result is simply

sim_new(y) = -k(y)

The reason for the pitch differences between the simulation and of playing the clarinet are mainly:

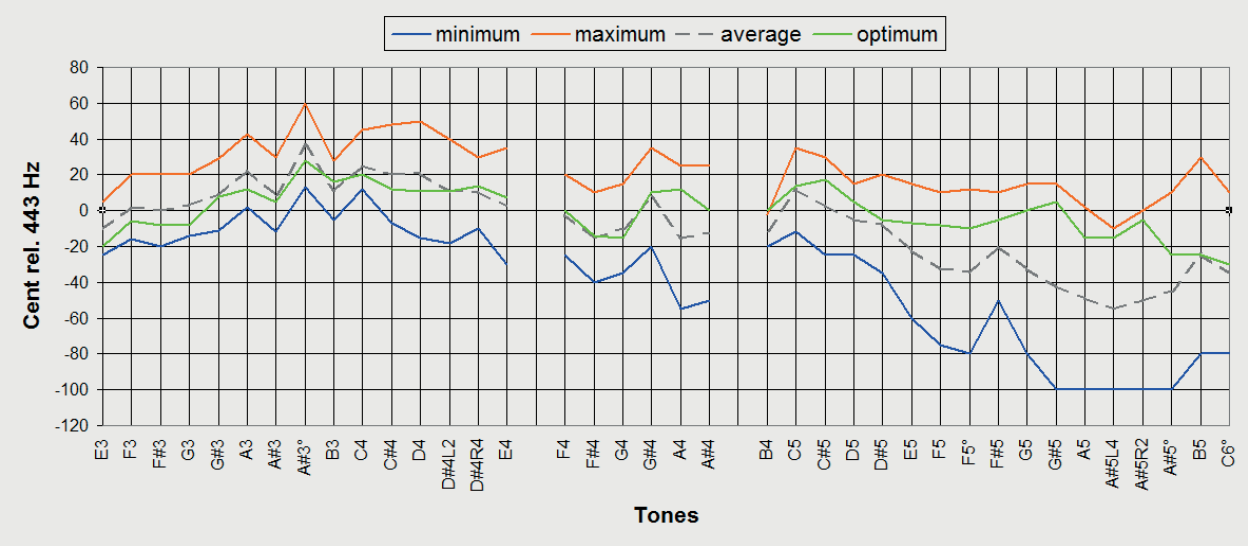

Fig. 8, Result of the tuner reading

At present the SW-model is not yet sufficiently developed for simulating the influence of the mouthpiece, reed and player on the intonation. This is because: first, the clarinet is simulated with a short cylindrical tube, whereas in reality a mouthpiece-reed combination is used. Second, the model does not fully take into account nonlinear effects (turbulence) and does not distinguish between the different kinds of losses, but uses a single factor (see above) to approximate reality.

At the connections of the side holes to the main tube, the flow lines have a complicated form that cannot be simulated perfectly by a simple T-connection as done in the model. Information about such effects can be found in the literature [6].

2.7 Adapting the simulation model to improve intonation

From the correction factors (see above) the necessary improvements can be deduced. Much creativity is needed to find the new dimensions. But - as the simulation takes only some minutes on an average computer - the trial and error procedure soon leads to a usable result.

Several experiments with the simulation model showed that it is not possible to obtain satisfactory intonation for the normal and fork-fingerings of A#3 and F5 (see above) by just altering the positions, diameters and depths of the corresponding tone holes or the bore diameter. Therefore an additional correction hole was introduced (see also 2.5). This kind of correction hole is a standard device in good German-type clarinets. The prototype, being a very simple model, also lacked the hole and mechanics for F#3 and C#5 fork fingering. The first choice of dimensions and positions of the two new holes was found by studying an ordinary Bb-clarinet. After several attempts suitable values for the new holes could be found. Of course the dimensions of neighbouring holes had to be modified too. Again this was a trial and error procedure. The following simple rules were applied: To increase the frequency of a certain tone the corresponding hole (namely the one which mainly influences the pitch) needs to be shifted towards the barrel. It can also be widened or reduced in depth. This takes several attempts: one run of the simulation of a complete register (E3 to E4, F4 to A#4, and B4 to C6) takes a few minutes.

2.8 Building the final model based on the simulation

The dimensions found to be optimal with the help of the simulation were sent to a professional instrument maker (Foag). This maker operates a CNC (Computer Numeric Controlled) milling machine and is able to reproduce the required dimensions with an accuracy in the order of 10 microns. Fig. 9 shows the final result. The newly introduced two holes turned out to have the correct dimensions, giving a satisfactory result (see Fig. 10).

3. FUTURE WORK

The main focus of the method described was to find mechanical dimensions that allow the clarinet to be played perfectly in tune. There are many solutions to achieve this goal. A different combination of hole distances, diameters and depths, as well as different bore characteristics could also lead to a good instrument. In the work done no special focus was laid on other factors, such as sound quality, balance of tones or attack characteristics. Presumably the software model would have to be refined if such characteristics should be taken into account.

For standard A- and Bb-Clarinets there exist so many good models that it is usually sufficient for instrument makers to copy an existing instrument. Nevertheless even such instruments could be improved using simulation software. For example it is not possible nowadays to play a fork-fingered F4 on the German-style clarinet with good intonation (it is much too sharp). The simulation could be used for finding an additional correction hole. This hole

Fig. 9, G-high clarinet, new model

Fig. 10, Detail of the right hand side, showing the two additional holes

would be open for the C6 (normally a fork fingering on the German clarinet), but closed for the F4. This could be achieved by introducing a lever that is combined with the speaker vent mechanism. Before building an actual instrument, the dimensions and position of such a hole could be found with the help of the model.

4. CONCLUSION

The aim of the project, namely to develop a new clarinet based on a working prototype and using software simulation was fulfilled. This method is especially advantageous for rare types of instruments, such as the G-high clarinet. Instead of building several prototypes and each time hoping for the best, one needs only to change the dimensions of an existing software model. This efficient approach saves time and material. It also motivates to explore new ground in clarinet development.

5. REFERENCES

[1] Philippow, Eugen, Taschenbuch Elektrotechnik, Band 3, Nachrichtentechnik, VEB Verlag Technik Berlin, 1969

[2] Micro-Cap, Electronic Circuit Analysis Program, Spectrum Software 1021 South Wolfe Road, Sunnyvale, CA 94086

[3] Widholm, Gregor, 2008 - BIAS 6 Handbuch, Acoustic Research Team

[4] Egolf, David et al., Experimental scheme for analyzing the dynamic behavior of elektroacoustic transducers, J. Acoust. Soc. Am. Vol. 62 No.4 October 1977

[5] Krueger, Walther: Methode zur Stimmungskorrektur von Blasinstrumenten, HF-Technik und Elektroakustik 80 (1971)

[6] Nederveen, C.J. et al.: Corrections for Woodwind Tone-Hole Calculations, ACUSTICA - Acta Acustica Vol. 84 (1998)

INFLUENCE OF THE TRUNCATION LENGTH OF THE OBOE CONE ON THE REED CLOSING TIME

Sandra Carral and Vasileios Chatziioannou

Institute of Music Acoustics
University of Music and Performing Arts Vienna, Austria
s.carral.rl@gmail.com

ABSTRACT

Proponents of the Pulse Forming Theory (see for instance [1] and [2]) claim that the reed closing time of wind instruments remains approximately constant over their playing range. The theory presented in [3] might provide an explanation for this phenomenon in terms of the geometry of the resonator. This paper aims to test the hypothesis that, for a conical instrument, the closing time of the reed is proportional to the truncation length of the cone. This is done by simulating (through physical modelling) and recording an oboe with a normal staple and with a short staple, assuming that the staple at the top of the instrument is part of the resonator. While the simulations confirm the hypothesis, the recordings show interesting results that invite us to postulate other possibilities.

1. INTRODUCTION

Wind instruments are often shortened or lengthened in order to change the pitch. This results in a different resonance curve for every note. It would be logical to deduce that every note has therefore its own unique sound colour. Nevertheless, the perceived sound colour of wind instruments seems to remain constant across much of its playing range [4]. The reason for this seems to lie both in the sound production mechanism and in the resonance and radiation characteristics of the resonator itself.

Proponents of the Pulse Forming Theory including [1], [2], [5] and [6], found that the spectra of wind instruments have constant spectral gaps and constant formant areas in between these gaps. Fransson [7] used an ionophon instead of a reed to excite the resonator, and changed the pulse length per period until the radiated sound was as close as possible to that of the instrument played with the reed. Voigt [1] used a high speed camera to record the movement of a bassoon reed. Both concluded that the reason why there are gaps in the spectrum is that the closing time τ of the reed remains approximately constant independently of the playing frequency. The ratio between the reed closing time τ and the signal period T determines the position of the spectral minima: When the reed is closed e.g. 1/10 of the complete period, the spectrum will show minima on the 10^{th}, 20^{th}, 30^{th}, etc. harmonic, in other words, the spectral minima lie on the $\frac{T}{\tau}{}^{\text{th}}$ harmonic and its integer multiples. With his ionophon experiment, Fransson found a closing time of 0.4 ms for the oboe. Likewise, Heptner [8] quotes a closing time of 0.45 ms.

It is well known (see for instance [9], [10]) that the spectrum of a bowed or plucked string strongly depends on the position at which the string is excited. Plucking or bowing near an antinode for a particular mode will excite it, whereas plucking or bowing near a node for a particular node will suppress it. Thus, if the string is excited at 1/2 of its length, the spectrum will have missing harmonics: 2^{nd}, 4^{th}, 6^{th}, etc. If it is excited at 1/5 of its length, the missing harmonics will be the 5^{th}, 10^{th}, 15^{th}, etc, and so on. According to Ollivier et al. [3], changing the position of the string excitation is equivalent to changing the length of the truncation for conical woodwinds, such as the oboe. A crucial difference between string and woodwind players though, is that woodwind players cannot control this parameter, since the length of the truncation is fixed. Let $T = t_o + t_c$ be the signal period, t_o and t_c the opening and closing times respectively, L_b the length of the truncated cone, and L_a the length of the truncation. If $\frac{t_o}{t_c}$ or $\frac{t_c}{t_o} = \frac{L_b}{L_a}$, the oscillation is called "Helmholz motion", in which case the ratio of the durations of the two parts of the signal is determined by the resonator [11].

The constant closing time (and therefore the missing harmonics) found in the Pulse Forming Theory can be explained by this analogy as follows: Since at every note the length of the resonator changes, the ratio $\frac{L_b}{L_a}$ changes as well, however, the length L_a remains constant independently of the playing frequency. Assuming a Helmholz motion scenario, the ratio $N = \frac{L_b}{L_a}$ is equal to the ratio $N = \frac{t_o}{t_c}$, and since the signal period $T = t_c + t_o$ is directly proportional to the total length of the cone $L = L_a + L_b$, then it follows that t_c remains constant independently of playing frequency (as does L_a) and is directly dependent on the length of the truncation L_a (see Appendix). From this theory, the closing time t_c depends only on the geometry of the cone, specifically on the length of the truncation L_a.

The aim of this paper is to test the hypothesis that the closing time of the oboe is directly proportional to the truncation length. This is done as follows:

- increase the truncation length of a normal oboe by cutting the staple in half, and compare its closing time to that of a normal oboe with a normal staple: Is the closing time with the modified staple longer, as expected?
- simulate the above with a physical model with a simplified version of a real oboe: one straight cone for the main body of the instrument, another straight cone for the staple.

This paper is organised as follows: Section 2 describes a method to measure the closing time from the mouthpiece pressure waveform. Section 3 describes the physical model used for the simulations, the geometry of the instruments that were simulated with two different truncation lengths, and the experimental setup to obtain the recorded signals from an oboe with a normal staple and with a short staple. Section 4 presents the results obtained from the simulation and recordings presented in Section 3, and Section 5 presents a general discussion and the conclusions drawn from the results obtained in Section 3.3.

2. MEASURING THE CLOSING TIME

According to [3], the reed opening and the mouthpiece pressure have the same phase, so one can measure the reed closing time by looking at the mouthpiece pressure, which can be measured with a microphone. Since the oboe reed is so small, the place at which the microphone is placed becomes problematic. A compromise has been found between the proximity to the reed and the practicality of placing a microphone: The first hole of the oboe body from the top is opened, which corresponds to the second octave key hole, located approximately 2 cm below the bottom end of the staple, where a 1/8" microphone can be inserted. Placing a microphone closer to the tip of the reed would involve either drilling a hole in the instrument or in the staple, however the staple has a bottom diameter of 4.8mm, and in the oboe used, the bottom 1 cm of it is inserted in the instrument. Trying to insert a microphone in the middle of the staple would mean making a hole on a 3 mm diameter tube, adapting the microphone with a tiny probe, and disturbing the flow of air into the instrument, should the probe minimally protruded inside the air channel. Special consideration has to be made on the choice of microphone due to the high sound pressure levels inside the oboe while being played.

2.1. Signal Analysis

From the mouthpiece pressure signal it is possible to find out the opening and closing times of the reed. This is done as follows: The mean value of the pressure over a period must be zero [3]. The pressure $P_{ref} = P_{max} + P_{min}$ is calculated. The time in which the pressure is below P_{ref} is then the closing time [12].

Each period of the steady state of the time domain signal is found by looking at the pressure maxima. Then P_{ref} is calculated, and the number of samples that fall above and below P_{ref} are counted and saved as opening N_o and closing N_c samples respectively. The opening t_o and closing t_c times are calculated from the number of samples as follows: $t_o = \frac{N_o}{f_s}$ and $t_c = \frac{N_c}{f_s}$, where f_s is the sampling frequency.

The mean and standard deviation of t_o and t_c throughout the duration of the steady state of the recorded note is then calculated. Figure 1 shows an example of how the mouthpiece pressure would look like (taken from a recording with the microphone at the top of the instrument), and where P_{ref} would be in that case.

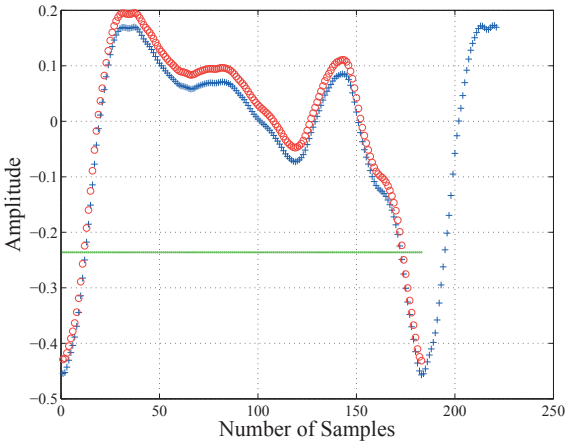

Figure 1: Method to extract t_o and t_c from the time domain signal: The blue crosses show the time domain samples of a segment of the signal, the red circles show the time domain samples of one period with mean pressure value of zero taken from maximum to maximum amplitude, and the green dots show the threshold pressure $P_{ref} = P_{max} + P_{min}$. Samples that are above P_{ref} are counted to calculate t_o, samples below P_{ref} are counted to calculate t_c. The data shown in this plot comes from a recorded signal.

3. SIMULATION AND EXPERIMENT

This Section describes the physical model used to obtain the simulated mouthpiece pressure, as well as the experimental setup to record the pressure inside the oboe as close as possible to the mouthpiece.

The oboe is usually played with the aid of a mouthpiece that consists of a conical brass tube called staple, to which two cane reed blades are bound. If we consider the staple as being part of the geometry of the resonator, we could shorten the staple so as to make the length of the truncation longer. By doing this the hypothesis is that the closing time will increase, since according to the theory, it is proportional to the truncation length.

3.1. Physical Model

The details of the model used to make the simulation is described in [13]: It is a time domain lumped reed model that incorporates mass, damping and stiffness. Since the reed displacement of the double reed is symmetrical [14], the double reed is modelled as a single mass-spring system, where the reed-lay interaction is modelled with a conditional contact force based on a power-law:

$$m\frac{d^2y}{dt^2} + mg\frac{dy}{dt} + ky + k_c(\lfloor y - y_c \rfloor^{\alpha}) = \Delta p, \qquad (1)$$

where m is the effective reed mass, g is the damping per unit area, k is the effective reed stiffness per unit area, Δp is the pressure difference $p_m - p$, p_m is the mouth pressure, p is the mouthpiece pressure, k_c and α are power-law constants, and y_c represents the displacement value above which the contact force becomes active, i.e.:

$$\lfloor y - y_c \rfloor = \begin{cases} y - y_c & \text{if } y > y_c \\ 0 & \text{otherwise.} \end{cases} \qquad (2)$$

The flow into the mouthpiece consists of two components: the flow through reed channel u_f, which is assumed to be governed by Bernoulli's law, and the volume flux u_r induced by the reed motion [15]:

$$u_f = \lambda h \sqrt{\frac{2\Delta p}{\rho}} \qquad (3)$$

where λ is the effective width of the reed, $h = y_m - y$ is the reed opening, y_m is the reed opening at rest, y is the reed displacement, and ρ is the air density, and

$$u_r = S\frac{dy}{dt} \qquad (4)$$

where S is the effective reed surface.

The response of the resonator can be calculated via convolution of the forward-travelling pressure wave p^+ at the mouthpiece entry with the bore reflection function (see Appendix of [13]):

$$p^- = r_f * p^+, \qquad (5)$$

where p^- is the returning wave. The relationship with the mouthpiece flow is:

$$Z_0 u = p^+ - p^-, \tag{6}$$

where Z_0 is the characteristic impedance at the mouthpiece entry [10].

In all the simulations shown below, the input impedance Z_{in} is calculated with the program VIAS[1] using the bore geometry, and the reflection function r_f is then calculated from it according to [16].

3.2. Instruments

The geometry of the instruments used to do this simulation is based on measurements on a real oboe: First it is assumed that the staple is a straight cone with a top diameter of 2.38mm (when round), a bottom diameter of 4.8mm and a length of 47mm. These measurements were taken from a standard Guercio D12/47 staple. Likewise, the body of the oboe is assumed to be a straight cone, where its angle can be calculated taking the top diameter, the bottom diameter at the bottom of the bottom joint, and the length. The oboe used for these measurements is a full Conservatory professional automatic oboe (Stencil oboe marked Reisser Musik, made by Hans Kreul in Tübingen, Germany in the early 1980's, model 9111VA), for which the (half) angle is approximately 0.7°.

The instruments are built as follows: The top of the original instrument has the same dimensions as a standard oboe staple (Guercio D12/47). The main cone continues from the staple with a (half) angle of 0.7° to a length L_M which, together with the staple, give a first impedance peak close to the frequencies that correspond to the notes C_4, E_4, G_4 and B_4. Since the impedance peaks of cones are inherently inharmonic, the volume of the missing part of the cone has to be replaced [17], [18] in order to regain harmonicity. In order to do that, an equivalent angle θ_E for each cone was calculated, taking the top diameter of the staple and the bottom diameter of the main cone and the total length L_T. Then the truncation length L_a is calculated using that equivalent angle and the top diameter of the staple. A cylinder of length $L_c = \frac{L_a}{3}$ is added to the top of the instrument, which replaces the volume of the missing part of the cone of length L_a and diameter D_T.

The modified instruments should have a longer truncation. To achieve this, the staple is cut to half its length L_s, and its top diameter is measured. The staple section of the original instrument is then replaced with the dimensions of the short staple to make the modified instruments. The main cone of the modified instruments has the same dimensions as those of the original instruments. The top cylinder has a length $L_c = \frac{L_a}{3}$, and the diameter is the same as the top diameter of the short staple.

Table 1 shows the dimensions of the top of the two instruments, and Table 2 shows the dimensions of the main cones, giving 8 instruments in total. Figure 2 shows the configuration of staple plus main cone corresponding to note B_4 of both instruments. The reed parameters were the same for all instruments, and are presented in Table 3.

3.3. Recordings

In order to confirm the simulation results, an experiment is made with an oboe played with a normal staple and with a short staple. In order to measure the sound pressure inside the oboe, a 1/8" G.R.A.S. pressure microphone model 40DP was inserted tightly inside the second octave key hole of the instrument. The microphone was connected to a G.R.A.S. preamplifier model 26AS, then to a BSWA microphone conditioning unit model MC702. The output of the latter was connected via a coaxial cable to the input of a sound card of a modern computer (Intel Core 2 Duo CPU E7400, 2.8 GHz, 4GB RAM, 64 bit). The recording was made with the program Audacity. The sampling rate was set as $f_s = 44.1$kHz.

[1] www.bias.at

Parameter	Oboe	Modified Oboe
D_T [mm]	2.38	3.5
D_B Staple [mm]	4.8	4.8
L_s [mm]	47	23.5
θ_E [°]	0.8	0.75
L_c [mm]	29	46

Table 1: Geometrical parameters corresponding to the top of the instruments.

Parameter	C_4	E_4	G_4	B_4
L_M [mm]	470	330	270	190
D_B [mm]	16.3	12.9	11.4	9.44

Table 2: Geometrical parameters corresponding to the main cones, which are the same for both Oboe and Modified Oboe.

The cylindrical section L_c used in the simulations above should account for the whole truncation volume, since the reed does not have a volume in the model. In real life, a reed is attached to the staple. If we assume that the standard oboe reed plus standard oboe staple account for the volume of the truncated cone, once the staple is cut in half, the extra missing volume has to be replaced. In order to do this, the cane is shaped in such a way that reed dimensions are somewhat bigger than those of a standard reed. The fact that this new reed plus short staple assembly plays at approximately the same pitch as the standard reed on the same oboe is an indication that both assemblies have approximately the same volume.

An amateur oboist played the oboe referred to in Section 3.2, first with a standard staple and reed assembly and then with a short staple and bigger reed. She played a diatonic C major scale from C_4 to G_5 at a mezzoforte dynamic level.

Reed Parameter	
k [Pa/m]	30×10^{6}
S [m^2]	90×10^{-6}
y_m [m]	350×10^{-6}
p_m [Pa]	4.5×10^{3}
λ [m]	7×10^{-3}
m [kg/m^2]	150×10^{-3}
g [1/s]	15×10^{3}
k_c [Pa/m^2]	85×10^{12}
y_c [m]	200×10^{-6}
α	2.5

Table 3: Reed parameters used to simulate the cones.

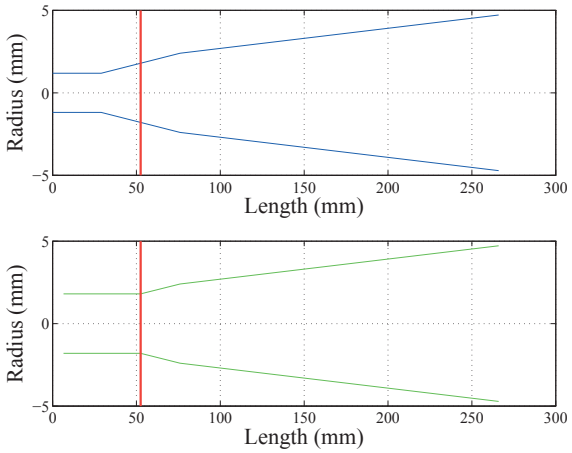

Figure 2: Configuration of staple plus main cone corresponding to note B_4 of the Oboe (top) and Modified Oboe (bottom). The red vertical line shows the point at which the normal staple was cut short.

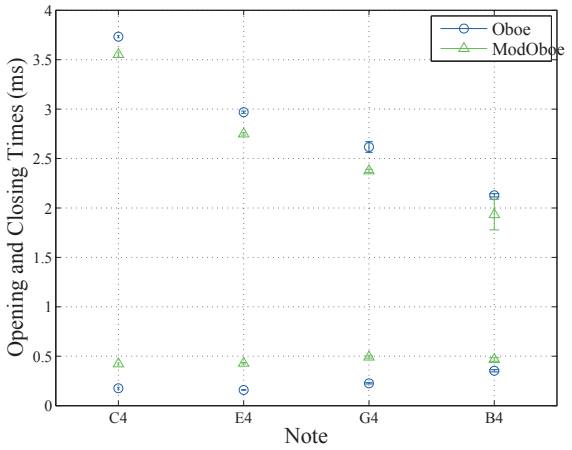

Figure 3: Opening and closing times of a simulated Oboe (short truncation) and a Modified Oboe (long truncation).

4. RESULTS

4.1. *Simulation*

Figure 3 shows the opening and closing times of the two instruments and four notes. The closing time remains approximately constant for both instruments, and in all cases it is shorter for the Oboe case than for the Modified Oboe case, which confirms the hypothesis that by increasing the truncation length the closing time increases.

4.2. *Recording*

Figure 4 shows the opening and closing times of the Oboe with standard staple and reed assembly and of the Modified Oboe with the short staple and bigger reed. The closing time of the Modified Oboe is shorter than that of the Oboe for notes C_4, D_4, E_4, F_4, and A_4, and about the same as that of the Oboe for the note G_4. By note B_4 the opening and closing times are about the same and above that, the closing time is longer than the opening time. This same recording was repeated with a professional oboist, and similar results were obtained.

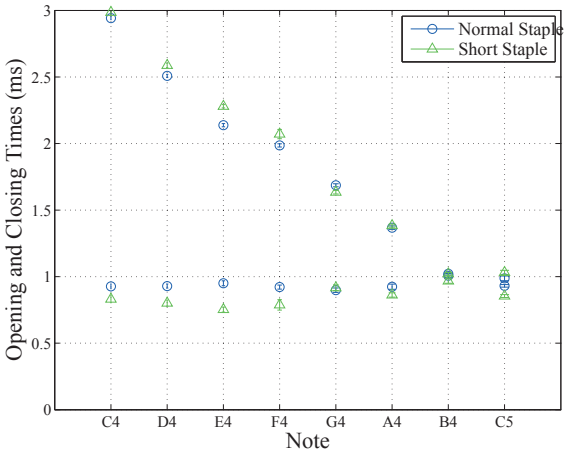

Figure 4: Opening and closing times of an oboe played with a standard staple and reed assembly and with a short staple and bigger reed.

5. DISCUSSION

The hypothesis to be tested in this paper is whether increasing the truncation of a conical woodwind instrument increases the reed closing time. While the simulations confirm this hypothesis, the recording shows the opposite for most notes. A reason why this is the case could be that the theory from Ollivier et al. [3] assumes perfect conicity. For the simulation we assumed that the bore of a real oboe is perfectly conical (straight with one taper), which might not be the case. And even if it were the case, the oboe has tone holes, which when closed, present an extra volume which would not be there in the case of a perfect cone. Also, the staple and the main cone have different tapers, that is, the simulated instruments presented here are also not one perfect cone. Furthermore, the theory from Ollivier et al. [3] is based on a lossless Raman-type model, which gives "two-step" solutions of the reed movement, that is, the reed is either completely open or completely closed. Figure 1 shows that the mouthpiece pressure is not a square waveform. Similar mouthpiece pressure waveforms were obtained in the recordings.

The discrepancies found between the simulations and the recordings lead us to believe that, while the geometry of the cone surely plays a role in the closing time, there must be other mechanisms that influence it. One possibility is the detailed geometry of the reed and the fluid dynamics of the air jet inside it. It is interesting to note that the closing time in the simulations is always shorter than that of the recordings. The reason for the discrepancies discussed here is unclear, and remains to be investigated.

A further reason for the discrepancies discussed here could be the placement of the microphone inside the oboe, which does not directly measure the mouthpiece pressure that applies on the reed, rather the pressure some distance below the mouthpiece.

6. APPENDIX

According to [3] and [11], the ratio N of the cone and its truncation is the same as the ratio of the two signal episodes:

$$N = \frac{L_b}{L_a} = \frac{t_o}{t_c} \tag{7}$$

$$t_o = N t_c \tag{8}$$

$$L_b = N L_a \tag{9}$$

$$\tag{10}$$

The signal period T is related to the total length of the cone (including truncation) by:

$$L_a + L_b = \frac{\lambda}{2} = \frac{c}{2}(t_o + t_c) \tag{11}$$

Combining equations (7) and (11) leads to

$$t_c = \frac{2}{c} \cdot La \tag{12}$$

Therefore, t_c is directly proportional to L_a, and given that L_a is constant, so is t_c.

7. ACKNOWLEDGEMENTS

We would like to thank Jonathan Kemp for providing the code to convert the input impedance to the time domain reflection function used for the simulations, as well as for the fruitful discussions that we had about this matter.

8. REFERENCES

[1] Wolfgang Voigt, *Kölner Beiträge zur Musikforschung, Band 5: Untersuchungen zur Formantbildung in Klängen von Fagott und Dulzianen*, Gustav Bosse, 1975.

[2] J. Fricke, "Formantbildende Impulsfolgen bei Blasinstrumenten," in *Proceedings of the DAGA 1975, 13. Jahrestagung für Akustik*, 1975, pp. 407–411.

[3] S. Ollivier, J.-P. Dalmont, and J. Kergomard, "Idealized models of reed woodwinds. part I: Analogy with the bowed string," *Acta Acustica united with Acustica*, vol. 90, pp. 1192–1203, 2004.

[4] Christoph Reuter, *Klangfarbe und Instrumentation*, Lang, Frankfurt, 2002.

[5] F. Fransson, "The source spectrum of double-reed woodwind instruments I," Tech. Rep., Department for Speech, Music and Hearing, KTH Computer Science and Communication, 1966.

[6] F. Fransson, "The source spectrum of double-reed woodwind instruments II," Tech. Rep., Department for Speech, Music and Hearing, KTH Computer Science and Communication, 1967.

[7] F. Fransson, "The STL ionophone sound source," Tech. Rep., Department for Speech, Music and Hearing, KTH Computer Science and Communication, 1965.

[8] Thomas Heptner, "Zur Akustik der Oboe: Theoretische Erörterungen und experimentelle Ergebnisse," *TIBIA*, vol. 12, no. 1, pp. 325–339, 1987.

[9] Murray Campbell and Clive Greated, *The musician's guide to acoustics*, Schimer Books, 1987.

[10] Neville H. Fletcher and Thomas D. Rossing, *The physics of musical instruments*, Springer, second edition, 1998.

[11] Jean-Pierre Dalmont, Joël Gilbert, and Jean Kergomard, "Reed instruments, from small to large amplitude periodic oscillations and the Helmholtz motion analogy," *Acta Acustica united with Acustica*, vol. 86, pp. 671–685, 2000.

[12] Jean-Pierre Dalmont and Jean Kergomard, "Elementary model and experiments for the Helmholz motion of single reed wind instruments," in *Proceedings of the International Symposium on Musical Acoustics*, Dourdan, France, 1995, pp. 115–120, Société Française d'Acoustique.

[13] V. Chatziioannou and M. van Walstijn, "Estimation of clarinet reed parameters by inverse modelling," *Acta Acustica united with Acustica*, vol. 98, no. 4, pp. 629–639, 2012.

[14] André Almeida, Christophe Vergez, and René Caussé, "Experimental investigation of reed instrument functioning through image analysis of reed opening," *Acta Acustica united with Acustica*, vol. 93, pp. 645–658, 2007.

[15] J. Kergomard, "Elementary considerations on reed-instrument oscillations," in *Mechanics of musical instruments*, A. Hirschberg, J. Kergomard, and G. Weinreich, Eds., Lecture notes CISM, chapter 6, pp. 229–290. Springer, Vienna, 1996.

[16] B. Gazengel, J. Gilbert, and N. Amir, "Time domain simulation of single reed wind instrument. from the measured input impedance to the synthesis signal. where are the traps?," *Acta Acustica*, vol. 3, pp. 445–472, 1995.

[17] A. H. Benade, "Oboe normal mode adjustment via reed and staple proportioning," *Journal of the Acoustical Society of America*, vol. 76, no. 5, pp. 1794–1803, 1983.

[18] C. J. Nederveen, *Acoustical aspects of woodwind instruments*, Northern Illinois University Press, 1998.

PARAMETER RANGES FOR ARTIFICIAL BASSOON PLAYING

Timo Grothe

Erich-Thienhaus-Institut, Hochschule für Musik Detmold, Detmold, Germany
grothe@hfm-detmold.de

ABSTRACT

This contribution presents bassoon blowing experiments with an artificial mouth. Given the precise adjustability of lip position and blowing pressure, the challenge in the presented experiment is to find those parameter combinations, that produce "reasonable" sustained sounds. In a large set of blowing experiments, artifical mouth adjustment parameters are identified, for which sounding pitch is within af few Cents deviation from the nominal pitch expected for that fingering. For those musically relevant regimes, an overview on the steady-state parameters of bassoon playing is given. The overview comprises artificial mouth parameters (lip force, blowing pressure, time-averaged flow-rate, RMS reed pressure, and reed pressure shape parameters) and sound related parameters (harmonic spectral centroid, formant frequencies, and loudness). The experiments were carried out with one and the same synthetic bassoon reed on five modern german bassoons and cover the complete playing range in frequency (notes) and dynamics (loudness). The observed variability between the five instruments is relatively small. Yet the comparison of the steady-state parameters with acoustic impedance curves provides some insight into the resonator-reed interaction in the bassoon.

1. INTRODUCTION

When a reed wind instrument produces a sound, the periodic closing of the reed valve is triggered by reflections of pressure waves from the air column. The range of possible oscillatory states is very broad; depending on the player's interaction with the reed, many different sounds can be produced for one and the same air column.

Here, the aim is to investigate sustained notes in the usual playing range of the bassoon. While it is relatively intuitive even for a completely untrained person to start and maintain single notes on a bassoon, it is problematic to imitate this process with an artificial mouth: Even if such a device provides control over the relevant parameters, it is still demanding to determine ranges of these parameters, for which the blowing machine produces a musical sound at the expected pitch on the instrument.

One systematic approach to study the operating regimes is to keep one playing parameter constant, while varying others. Scanning through the parameters in this way, the broad range of oscillatory and non-oscillatory states are explored, and the limits of the working range of the reed can be found [1]. The parameter, that was kept constant here was not an adjustment parameter, but the fundamental frequency f_0 of the produced sound. Parameter pairs of lip force and blowing pressure were indentified, to play sustained notes in tune. Similar to the requirements that musicians must meet, the tolerated pitch deviation was only ± 5 Cent. The fact that the blowing machine could be operated successfully at reasonable levels with the required pitch accuracy suggests, that the parameters obtained from "artifical" bassoon playing are also meaningful for the real musical performance.

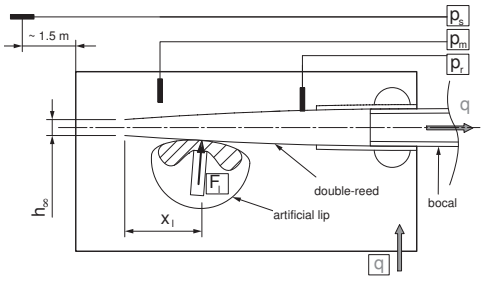

Figure 1: Sketch of the experimental setup. Measured quantities in boxes (p_m, p_r, F_{lip}, q, p_s) are recorded instantaneously during the experiment.

2. MATERIAL AND METHODS

2.1. Experimental setup

To measure the performance characteristics of the bassoon, a self-built artificial mouth has been used that facilitates precise lip adjustment (Figure 1). The main component of the device is a synthetic bassoon double-reed (270M, Conn-Selmer Inc., Elkhart, Indiana, U.S.A.) which is rigidly mounted at its rear end in the mouth pressure cavity. An artificial lip can be moved towards the reed. The lip assembly consists of a rigid rib, imitating the teeth, which is sheathed by a piece of cellular rubber. On top of this, a glycerin filled air balloon is overlayed imitating the dynamic properties of human lips. The lip is mounted onto a precision load cell that can be positioned by two micrometer screws parallel and normal to the longitudinal axis of the reed. The pressure inside the reed is measured 30 mm downstream of the reed tip. The mouth cavity is air-tight and the flow-rate into the box is measured with a thermal mass-flow meter. The external microphone was placed about 1.5 m from the large end of the bassoon perpendicular to the longitudinal axis. Details of the setup are given in [2].

The experimental procedure was as follows: After initiating the tone, the blowing pressure p_m in the mouth and the lip force F_{lip} were carefully balanced to play the note in tune at the softest possible dynamic level. Having adjusted the correct pitch, the blowing pressure was increased, followed by a readjustment of the lip force to maintain the tuning. This procedure was repeated to explore the complete parameter range for blowing pressure p_m and lip force F_{lip} for which this note on the instrument could be sounded in tune. The blowing pressures were in normal range reported for bassoon playing 1 kPa $< p_m <$ 9 kPa [3], and standard fingerings [4]. The study was restricted to sounds at the expected pitches for the respective fingerings, multiphonics and other unusual sounds were excluded.

In this way, the complete musically relevant dynamical range of a note, available for the specific fingering at a fixed lip position, has been obtained experimentally.

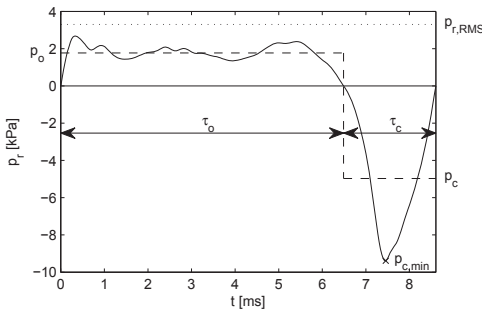

Figure 2: Reed pressure (solid) and the corresponding simplified Helmholtz-pattern (dashed), and integral mean reed pressure $\bar{p_r} > 0$, for the note B2 ($f_0 = 116$ Hz).

2.2. Directly measured quantities

During the experiments, several quantities are directly measured (see Fig. 1). Considering the instrument as a black box, the measured quantities can be divided into input and output parameters.

Artificial mouth adjustment parameters

x_l the position of the lip along the reed

F_l the force of the lip

p_m the blowing pressure in the "mouth" cavity.

Together with these adjustment parameters, the resulting output data characterize the

Working point of the reed

p_r the unsteady reed pressure in the reed,

p_s the sound pressure in the surrounding of the setup

q the mean volume flow-rate through the reed

At a fixed position of the lip, for a given resonator, the experimental situation is completely defined with these five measures. The setup is rugged enough to swap the resonator parts (i.e. bassoon and bocal) without changing the embouchure.

2.3. Derived parameters

Additional features have been extracted from the raw data recordings in the time and frequency domain. Time averaged values of lip force F_{lip} and blowing pressure p_m have been used to link the experimental situations to an analytical two-parameter model for the reed.

Reed pressure waveform parameters

In the normal playing regimes on the bassoon, the reed fully closes once per period and performs a two-step motion. During one part of the period (duration τ_o), the reed remains open, $p_r > 0$; in the subsequent part (duration τ_c) the reed is closed $p_r < 0$. The subscripts $(.)_o$ and $(.)_c$ mark the open and closed period during one cycle. For a typical bassoon reed configuration, the measured reed pressure waveform (p_r) is shown in Fig. 2. Within the two episodes of the pressure waveform p_r which are determined by the zero crossing of the reed pressure signal, the integral mean pressures are p_o and p_c, respectively.
Another measure that can be read from the pressure waveform is the RMS values of the reed pressure. This excitation sound level is related to the dynamic playing level of the instrument. As an additional parameter the maximum underpressure during the closed episode of the reed p_c, min is given.
In summary, the following six time-domain parameters are used to describe the operation point of the bassoon reed:

$\tau_{o,c}$ the duration of reed opening and closure during one cycle,

$p_{o,c}$ the integral mean pressure in the reed during the opened and closed episode,

$p_{c,min}$ the minimum pressure during the closed episode,

$p_{r,RMS}$ the RMS value of the reed pressure

Timbral spectral parameters

Characteristics of the spectrum of a sound are correlated with the perception of timbre. Many acoustical parameters and "features" of sounds have been suggested as descriptors of timbre. Only very few, purely spectral parameters will be used here, based on the widely accepted algorithms from the ISO Standard ISO/IEC 15938 (MPEG-7) [5], the phonetics software `praat` [10], and the German standard DIN 45631.
The MPEG-7 description standard defines among many others, three purely spectral parameters for timbre characterization. The three parameters are called the *harmonic spectral centroid* (hsc) in Hertz, *the harmonic spectral spread* (hss) and the *harmonic spectral deviation* (hsd). They are defined as the amplitude-weighted mean of the harmonic peaks of the spectrum (hsc), and the amplitude-weighted standard deviation of the harmonic peaks divided by the harmonic spectral centroid hsc (hss). The harmonic spectral deviation (hsd) is a measure for the deviation of the amplitudes of the partials from a global (smoothed) spectral envelope [5].
The parameters have been calculated with freely available code `TimbreToolbox` [5] from the developers of the standard.
A similar timbre characterisation method in the frequency domain is the formant analysis. Formants are broad peaks in the spectral envelope of a sound [6]. Although "formant" is a term from voice analysis, formants are not only found in sounds of singers, but also in the sound of conical wind instruments [7, 8]. In contrast to the spectral centroid it based on analyzing a number of local maxima in the spectrum. Their relative positions on the frequency axis are relevant for the impression of timbre. Each formant is characterized by a center frequency F_i and a bandwidth B_{Fi}, where i is the ordinal number of the formant. Formant analysis is attractive here, because the formant frequencies detected in bassoon sounds were largely insensitive to the sound recording position in non-ideal room acoustics [9]. In this study the Burg-Algorithm in `praat` [10] has been used to detect four formants for frequencies up to 5 kHz with the Burg-Algorithm from the recorded time-domain data of one second duration. These spectral timbral descriptors are calculated for both the pressure inside the reed and the sound pressure in the surrounding of the instrument. In psychoacoustics a number of approaches are suggested to assign a metric to a sound that describes its perceived loudness. These loudness models take spectral and temporal characteristics of the sound pressure into account, with respect to the capabilities of the human auditory system. Here, the first standardized loudness model of Zwicker (DIN 45631) has been used to assign a scalar loudness value N in the dimension Sone to the sound recorded in approximately 1.5 m distance from the instrument.
In summary, the following ten frequency-domain parameters are used to describe the operation point of the bassoon reed and the sound radiated from the instrument. The subscripts $(.)_r$ and $(.)_s$ indicate whether the property was derived from the sound spectrum measured inside (reed pressure) or outside

(sound pressure) of the instrument.

$hsc_{r,s}$ the harmonic spectral centroid

hss_s the harmonic spectral spread,

hsd_s the harmonic spectral deviation,

$F_{i\,r,s}$ ($i = 1..4$), the center frequencies of the first four formants

$B_{Fi\,s}$ ($i = i..4$), the band widths of the first four formants

N_s the psychoacoustical loudness

Quasistatic reed model parameters

The quasistatic reed model [11] predicts the flow-rate through the pressure dependent reed slit opening as

$$q = q_A \left(1 - \frac{\Delta p}{p_M}\right) \sqrt{\frac{\Delta p}{p_M}} \tag{1}$$

where $\Delta p = p_r - p_m$ is the pressure difference between the pressure p_r inside the reed and the pressure p_m in the mouth cavity; q_A and p_M are model parameters in dimensions of volume-flow rate and pressure. The function given by Eq. 1 has a maximum $q_{\max}$ at the so called saturation pressure $p_{m,s}$. Reading these two values from measured curves, the model parameters can be determined as

$$q_A = \frac{3}{2}\sqrt{3}\, q_{\max}, \quad p_M = 3\, p_{m,s} \tag{2}$$

For details see [11, 12] Especially p_M and q_A are important, as they can be used to characterize the working point with respect to an analytic model [11, 13]. The non-dimensional blowing pressure γ and non-dimensional embouchure parameter ζ are defined as

$$\gamma = \frac{p_m}{p_M}, \quad \zeta = Z_c \frac{q_A}{p_M}, \tag{3}$$

where Z_c is the characteristic impedance of the air in the cross section at the bocal tip, where the reed is attached to the resonator.

The applicability of this analytic single-reed model to the case of the double-reed has been proven [12]. From p_M and q_A a reed equivalent stiffness K_s per unit area can be deduced as

$$K_s = \frac{p_M}{q_A} \sqrt{\frac{2\, p_M}{\rho}}, \tag{4}$$

where ρ is the air density.

These parameters depend upon the initial slit height of the reed, which is closely related to the lip force applied to the reed blade. Measuring lip force during performance allows to link any quasistatic working point of the reed to these model parameters [14, 2].

In summary, the five parameters that were derived from the artificial mouth adjustment parameters and the describing the embouchure under playing conditions are the following:

p_M pressure parameter,

q_A volume-flow parameter,

K_s reed stiffness per unit area,

γ non-dimensional blowing pressure

ζ embouchure parameter

2.4. Bassoons and bocals used in the experiment

The tested bassoons were modern German Bassoons from the manufacturers Adler, Hüller, and Heckel. From the latter manufacturer, a student model and a professional model have been used. The bocal were type CD0 and CC1 of Fa. Heckel (Wiesbaden, Germany) and type N6 of Fa. Wolf (Kronach, Germany). The N6 bocal used here has the same length as Heckels CC1; CD0 is about 5 mm shorter. One of the bassoons has been measured with both N6 and CD0.

3. RESULTS

3.1. Parameter ranges

For the parameters described above, characteristical values are given in Table 1. These values have been obtained from blowing experiments with an artificial mouth, obtained with one and the same synthetic bassoon reed on five different bassoon-bocal combinations. For all instruments and notes played, the lip was in the same intermediate position $x_l = 10.75$ mm from the reed tip.

Table 1: Typical values for parameters in artificial mouth blowing experiments on a modern German bassoon. The values are given as a range $(\cdot)_{min} \ldots (\cdot)_{max}$ or as a mean value $\bar{(\cdot)} \pm \sigma$ (σ: standard deviation).

		Symbol	Unit	Range
artificial mouth adjustment parameters	directly measured	p_m	[kPa]	$1.1 \ldots 12$
		F_{lip}	[N]	$0 \ldots 7$
		x_l	[mm]	$0 \ldots 15$
working point of the reed		q	[l/s]	$0.02 \ldots 0.42$
		$p_r(t)$	[kPa]	$-24 \cdots + 8$
		$p_s(t)$	[Pa]	arbitrary
	derived parameters	f_0	[Hz]	$58 \ldots 592$
		$p_{r,RMS}$	[kPa]	$1 \ldots 9$
		$p_{s,RMS}$	[dB SPL]	$72 \ldots 95$
		hsc_r	[Hz]	$380 \ldots 1000$
reed pressure waveform parameters		τ_c	[ms]	$2.8 \ldots 0.75$
		τ_c/τ	[-]	$0.1 \ldots 0.45$
		p_o	[kPa]	$0.2 \ldots 8$
		p_c	[kPa]	$-12 \cdots - 2$
		$p_{c,min}$	[kPa]	$-24 \cdots - 5$
		$\lvert p_c/p_o \rvert$	[-]	$1 \ldots 7$
timbral spectral parameters		hsc_s	[Hz]	$580 \ldots 1500$
		hss_s	[-]	$0.2 \ldots 0.7$
		hsd_s	[-]	$0.1 \ldots 0.3$
		F_1	[Hz]	540 ± 110
		F_2	[kHz]	1.2 ± 0.18
		F_3	[kHz]	1.9 ± 0.2
		F_4	[kHz]	3.1 ± 0.6
		B_{F1}	[Hz]	220 ± 160
		B_{F2}	[Hz]	470 ± 280
		B_{F3}	[Hz]	730 ± 450
		B_{F4}	[Hz]	890 ± 470
		N_s	[Sone]	44 ± 12
quasistatic reed model parameters		p_M	[kPa]	7.4 ± 1.8
		q_A	[m^3/s]	$(0.6 \pm 0.3)\, 10^{-3}$
		K_s	[Pa/m^2]	$(1.6 \pm 0.35)\, 10^9$
		γ	[-]	$0.16 \ldots 1.4$
		ζ	[-]	$0.6 \ldots 2.7$

3.2. Comparison of five instruments

The mouth pressures p_m range from 1.5 kPa to more than 10 kPa (Fig. 3(a)). Blowing pressures larger than 10 kPa are unrealistically high [3]. Therefore, the vertical axis in Fig. 3(a) is cropped

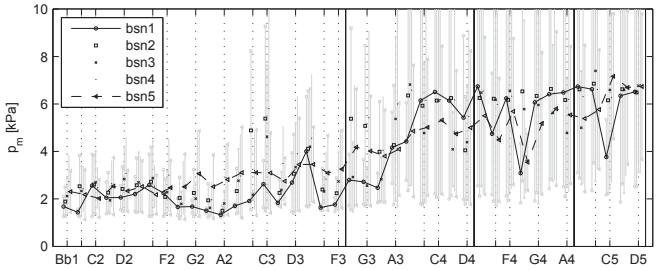

(a) Mouth pressure

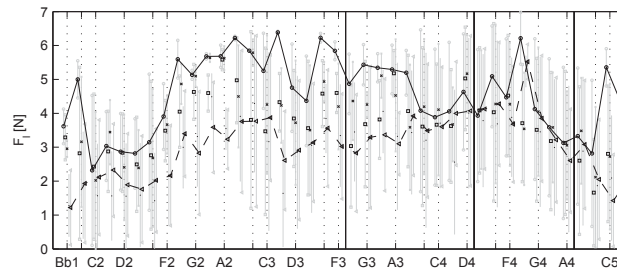

(b) Lip force

Figure 3: Input parameters p_m and F_{lip}

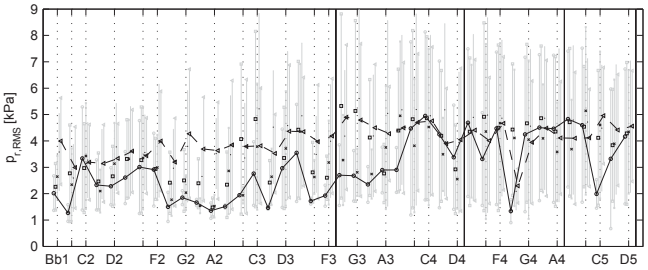

(a) Root-Mean-Square of the reed pressure

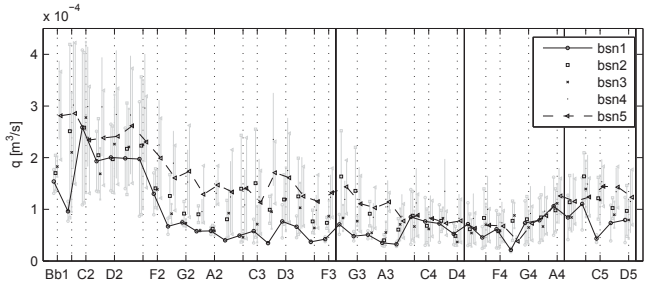

(b) Time averaged flow-rate

Figure 4: Output parameters $p_{r,RMS}$ and q

at this value, although notes could be played for even higher mouth pressures.

Ascending the scale, the minimum mouth pressure to sound a note in tune increases approximately linear with log-frequency: Lower notes require less blowing pressure than higher notes.

In general, two regions can be identified in Fig. 3(a): The lower notes (from B♭1 to A3) offer a smaller blowing pressure range (1 kPa< Δp_m <5.5 kPa) and are played at lower mean value of $\bar{p_m} \approx 2.5$ kPa; the higher notes (A3-D5) have a larger blowing pressure range (4.5 kPa< Δp_m <9 kPa) and a higher blowing pressure offset. Compared to the mouth pressure, the lip force characteristics to sound the notes in tune is irregular, no simple dependence on the log-frequency scale can be observed (Fig. 3(b)). Very generally speaking, the mean values $\bar{F_l}$ are smaller at the lower and upper limit of the tonal range, and larger in between. Adjacent notes may require a very different F_{lip} offset. For each single note, the lip force range ΔF_{lip} indicates the adjustments needed to compensate for tuning when changing the dynamic level. This value reaches up to several Newtons and largely depends on the tuning properties of each instrument, and, naturally, on the position x_l of the lip on the reed, which was constant in all measurements presented here. Apparently the bassoon-bocal combination *bsn1* (open circles in the graphs) was tuned too low and required globally a higher lip force, whereas for the combination *bsn5* (triangles in the graphs) the opposite trend is observed in Fig. 3(b).

For each note, the oscillatory regime established for a combination of p_m and F_{lip} is characterized by the output parameters RMS-value of the reed pressure $p_{r,RMS}$ and the time-averaged volume flow-rate q. These may be called primary output parameters, because they are distinct measures at the operating reed, directly measurable without further analysis.

The RMS reed pressure $p_{r,RMS}$ for musically relevant regimes ranges from 1 to 9 kPa, equivalent to 154 to 173 dB SPL (Fig. 4(a)). The minimum value for the softest regimes is $\bar{p}_{m,min} = 2 \pm 0.5$ kPa, the differences on one note comparing between instruments exceed 1 kPa. This observation is largely influenced by the tuning of the instrument. Ascending the scale, the mean RMS reed pressure $p_{r,RMS}$ tends to increase slightly. The notes of the lower register have a large fluctuation in $\bar{p}_{r,RMS}$ across the log-frequency axis. This fluctuation is decreased for higher notes; apart from some outliers, $\bar{p}_{r,RMS}$ is here around 4.2 kPa. The time-averaged volume flow-rate q ranges from up to 4.5×10^{-4} m^3/s for C2 at the lower end of the tonal range, to less than a tenth of this value at F4 in the medium high register (0.25×10^{-4} m^3/s). The notes B♭1 to E2 require the most volume flow ($\bar{q}$ = 2×10^{-4} m^3/s). From F2 to G4, the mean flow $\bar{q}$ decreases from 2 to 1×10^{-4} m^3/s. From A4 upwards in the note scale $\bar{q}$ tends to increase again (Fig. 4(b)). These general trends in the flow-characteristics resemble the inverted lip force characteristics (Fig. 3(b)). The flow-rate tends to be increased for notes which are played at lower lip forces.

3.3. Relation with resonator acoustics

To experimentally determine the number of relevant air-column modes n_{modes} for a real bassoon and to show its change with the fingering, a rescaling of the magnitude of the input impedance curve is helpful. When the reed is beating, it is locked as a nonlinear exciter to a linear resonator. For a qualitative description of this mode-locking phenomenon, Fletcher gave several qualitative criteria for both system components [15]. He postulated that i) air column modes must be strong and ii) nearly harmonically related to participate in a mode-locked regime of oscillation. In the present study, measured input impedance curves of the bassoon have been analyzed with respect to these criteria. For each fingering, a selection of modes has been made in order to meet Fletchers criteria. To meet criterion i), the impedance peaks -6 dB lower than the maximum peak were neglected. To meet criterion ii) all modes which are more than 100 Cent (one semitone) off the nearby harmonic frequency were excluded. Summing up the remaining modes yielded the number of *supporting* air column modes n_{modes}. The comparison of $|p_c/p_o|$ from blowing experiments and n_{modes} obtained from the above

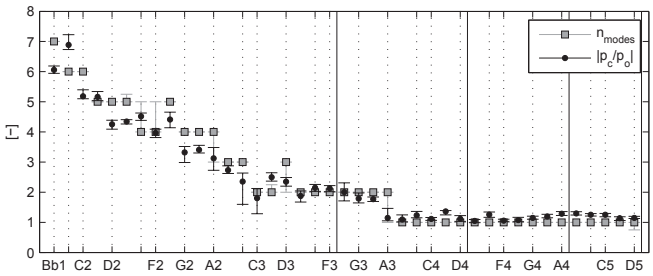

Figure 5: Relation between the mouthpiece pressure waveform ($|p_c/p_o|$) and the number of supporting resonator modes (n_{modes}).

analysis, shows their close relationship (Fig. 5). This very good agreement with the theoretical predictions [16, 17] indicates the proper choice of the thresholds $\pm$ 100 Cent for the harmonicity and -6 dB for the impedance magnitude, to determine the number of relevant air-column modes.

4. DISCUSSION

With an experimental apparatus it is possible to "artificially" play the bassoon and to investigate its acoustical behaviour under realistic playing conditions. The possibility to precisely adjust the artificial lip is very important to being able to carry out blowing experiments covering the full tonal and dynamical range of this instrument. A large set of benchmarking data describing the bassoon under quasi-stationary operation conditions is presented, including the time-averaged volume flow during playing. In particular, the measurements include the time-averaged volume flow and lip force during playing. The measured lip forces and blowing pressures for each note allow insights into the intonation corrections, that musicians have to do in fine-tuning the pitch.

The mean lip force during a sustained note can be used to link the steady-state operating parameters of the reed with the classical model of quasi-static flow through a reed channel. A reasonable applicability of this model for the case of the bassoon has been shown elsewhere [2]. This makes it possible to "translate" artificial mouth adjustment parameters characterizing realistic embouchure configurations into reed model parameters in relevant playing regimes.

Furthermore, attempts have been made to relate aspects of the bassoon performance to the resonance properties of the air column. The presented experimental data confirms for the practical case of the bassoon that the reed pressure waveform is largely determined by the number of supporting air column modes of the resonator which ranges up to seven for the lowest notes.

5. ACKNOWLEDGEMENT

The author wishes to thank Roger Grundmann, Johannes Baumgart, Mico Hirschberg and Kees Nederveen for support and helpful suggestions. This paper is based on results obtained in the author's thesis.

6. REFERENCES

[1] Andre Almeida, David George, John Smith, and Joe Wolfe, "The clarinet: How blowing pressure, lip force, lip position and reed hardness affect pitch, sound level, and spectrum," *The Journal of the Acoustical Society of America*, vol. 134, no. 3, pp. 2247–2255, 2013.

[2] Timo Grothe, *Experimental Investigation of Bassoon Acoustics*, Ph.D. thesis, Technische Universität Dresden, 2014.

[3] Leonardo Fuks and Johan Sundberg, "Blowing pressures in bassoon, clarinet, oboe and saxophone," *Acta Acustica united with Acustica*, vol. 85, pp. 267–277(11), March/April 1999.

[4] Terry Ewell and Lisa Hoyt, "The bassoon-family fingering companion" http://www.idrs.org/resources/BSNFING/BsnFingerings.pdf, last viewed 2015/07/01, 1999.

[5] Geoffroy Peeters, Bruno L. Giordano, Patrick Susini, Nicolas Misdariis, and Stephen McAdams, "The timbre toolbox: Extracting audio descriptors from musical signals," *The Journal of the Acoustical Society of America*, vol. 130, no. 5, pp. 2902–2916, 2011.

[6] Ingo R. Titze, Ronald J. Baken, Kenneth W. Bozeman, Svante Granqvist, Nathalie Henrich, Christian T. Herbst, David M. Howard, Eric J. Hunter, Dean Kaelin, Raymond D. Kent, Jody Kreiman, Malte Kob, Anders Löfqvist, Scott McCoy, Donald G. Miller, Hubert Noé, Ronald C. Scherer, John R. Smith, Brad H. Story, Jan G. Švec, Sten Ternström, and Joe Wolfe, "Toward a consensus on symbolic notation of harmonics, resonances, and formants in vocalization," *The Journal of the Acoustical Society of America*, vol. 137, no. 5, pp. 3005–3007, 2015.

[7] Jürgen Meyer, *Acoustics and the Performance of Music – Manual for Acousticians, Audio Engineers, Musicians, Architects and Musical Instruments Makers*, Springer, 2009.

[8] Wolfgang Voigt, *Untersuchungen zur Formantbildung in Klängen von Fagott und Dulzianen*, Gustav Bosse Verlag, 1975.

[9] Timo Grothe and Peter Wolf, "A study of sound characteristics of a new bassoon as compared to a modern german bassoon," in *Proceedings of the Stockholm Music Acoustics Conference 2013, SMAC 2013, Stockholm, Sweden*, 2013.

[10] Paul Boersma and David Weenink, "Praat: doing phonetics by computer [computer program]. version 5.1.34" retrieved 22 April 2012 from http://www.praat.org/, 2012.

[11] Jean Kergomard, *Elementary Considerations on Reed-Instrument Oscillations*, chapter 6, pp. 230–290, Springer Verlag Wien - New York, 1995.

[12] Andre Almeida, Christophe Vergez, and Rene Causse, "Quasistatic nonlinear characteristics of double-reed instruments," *Journal of the Acoustical Society of America*, vol. 121, no. 1, pp. 536–546, 2007.

[13] Fabrice Silva, Jean Kergomard, Christophe Vergez, and Joël Gilbert, "Interaction of reed and acoustic resonator in clarinetlike systems," *The Journal of the Acoustical Society of America*, vol. 124, no. 5, pp. 3284–3295, 2008.

[14] Timo Grothe, "Investigation of bassoon embouchures with an artificial mouth," in *Program of the 11th Congrès Français d'Acoustique and 2012 IOA annual meeting, Acoustics2012, Nantes*, 2012.

[15] N. H. Fletcher, "Mode locking in nonlinearly excited inharmonic musical oscillators," *The Journal of the Acoustical Society of America*, vol. 64, no. 6, pp. 1566–1569, 1978.

[16] Jean-Pierre Dalmont, Joël Gilbert, and Jean Kergomard, "Reed instruments, from small to large amplitude periodic oscillations and the helmholtz motion analogy," *Acta Acustica united with Acustica*, vol. 86, pp. 671–684(14), July/August 2000.

[17] S. Ollivier, J.-P. Dalmont, and J. Kergomard, "Idealized models of reed woodwinds. part i: Analogy with the bowed string," *Acta Acustica united with Acustica*, vol. 90, no. 6, pp. 1192–1203, 2004.

QUESTIONNAIRE: SATISFACTION ON THE E-FLAT CLARINET

Gangl Manuel

Institute of Music Acoustics
University of Music and Performing Arts Vienna, Austria
manuel.gangl@students.mdw.ac.at

ABSTRACT

This paper investigates the satisfaction of the intonation on the Eb-clarinet. The participants (N = 39, male = 27, women = 12) had to judge the intonation[1] in different registers on their Eb-clarinets. The tones (E3 – C7) were subdivided into the chalumeau register, the throat tone register[2], the clarion register and the altissimo register.

Register	**Tones**
chalumeau	E3 – F4
throat tones	F# 4 – A#4
clarion	B4 – C6
altissimo	C#6 – C7

Furthermore, I calculated the mean values for the satisfaction of the intonation of all participants. Overall, four groups joined this survey: professional players, advanced students, beginning students and sideline musicians (Fig. 1). The questionnaire showed that all groups reported having problems in the throat tone register and the altissimo register (Fig. 2). Furthermore, the satisfaction with the intonation of the professional group (48%), which is able to judge the quality of instruments more accurate than other groups, was observed. Figure 3 shows the satisfaction of the intonation of the professional group. They reported having problems only in the altissimo register.

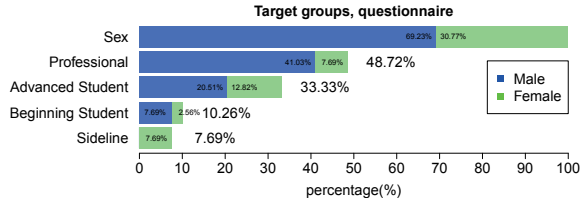

Figure 1: Four different groups joined this survey: professional players, advanced students, beginning students and sideline musicians.

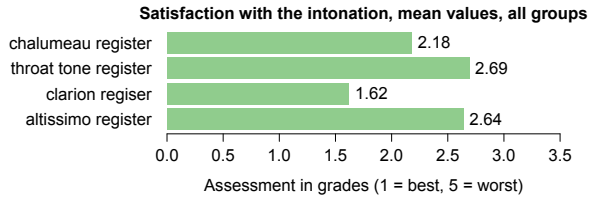

Figure 2: All groups reported having problems in the throat tone register (mean = 2.69) and in the altissimo register (mean = 2.64).

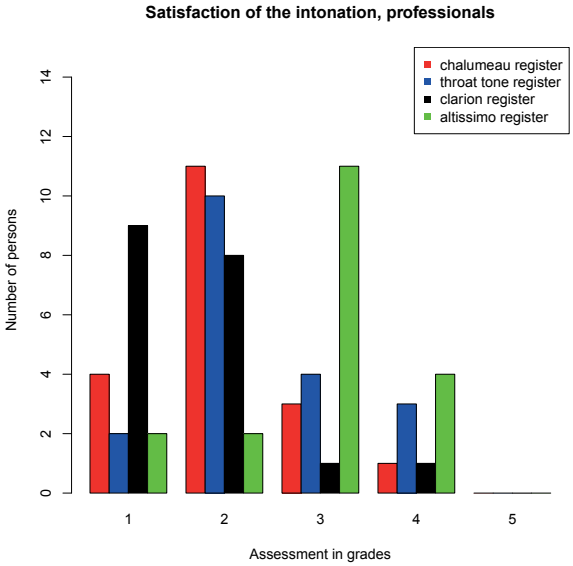

Figure 3: The professional group reported having problems in the altissimo register (green).

[1] assessment of the intonation in grades between 1 = best and 5 = worst

[2] normally the chalumeau register includes the throat tones, for the questionnaire we subdivided these tones!

INFLUENCE OF MOUTHPIECE GEOMETRY ON SAXOPHONE PLAYING

Sandra Carral[a], Valerio Lorenzoni[b] and Jouke Verlinden[c]

[a]Institute of Music Acoustics
University of Music and Performing Arts Vienna, Austria
s.carral.rl@gmail.com

[b]Delft University of Technology
The Netherlands
valeriolorenzoni@gmail.com

[c]Delft University of Technology
The Netherlands
J.C.Verlinden@tudelft.nl

ABSTRACT

The hypothesis to be tested in this paper is whether there is a measurable difference in radiated sound (in terms of spectral centroid and sound pressure level) and in playability, when playing mouthpieces with different internal geometries. In-vivo radiated sound and blowing pressure measurements were carried out on a panel of five different mouthpieces while playing the same note sequence. The results revealed a scarce influence of the mouthpiece geometry on the radiated sound in terms of pressure root mean square amplitude and spectral centroid. Larger differences were found in the measured mouth pressure for several mouthpiece pairs. Playability (also called ease of playing) was quantified through an effort ratio, corresponding to the ratio of blowing pressure over radiated sound *rms*. This showed non-negligible difference among some of the models in good agreement with the perception of the player. In particular differences between the original reference mouthpiece (commercial mouthpiece) and the modified (3D printed) mouthpieces were observed at the attack and end of the note for several notes. Only for specific notes, differences were detected for a longer time interval. In general the reference mouthpiece showed a lower effort ratio (higher ease of playing) with respect to the modified mouthpieces. The effort ratio seems to be a valid quantitative parameter for the characterization of a mouthpiece.

1. INTRODUCTION

It is generally agreed upon among saxophone players and instrument makers that the mouthpiece of the saxophone strongly influences the sound quality and the experience of the player, in terms ease of playing and the ability to modify the sound characteristics

Several researchers have attempted to identify the connection between the internal geometry of the mouthpieces and the sound quality of the coupled mouthpiece-instrument system. Among these, Benade [1] presented the effect of cavity dimensions on the brightness of the produced sound. Wynman [2] performed acoustic measurements on five different geometrical-types of alto saxophone mouthpiece models and found connections between baffle shape and tone color. An interesting overview of mouthpiece investigations can be found in the PhD thesis of Scavone [3], which describes the modeling of single-reed wind instruments in waveguides domain.

Recently, a team of researchers at Delft University of Technology has started using 3D printing techniques for the manufacturing of saxophone mouthpieces [4]. These techniques offer advantages compared to standard manufacturing techniques in terms of reducing production costs and achievable geometrical complexity [5].

The first application focused on modifications of the mouthpiece baffle according to aerodynamic findings [6] and musician considerations. The aim was to improve the acoustic properties of a mouthpiece according to specific sound requirements by exploiting the capabilities of 3D printing. This paper presents an analysis of sound and pressure measurements, carried out at the Institute of Musical Acoustics of the University of Music and performing Arts, Vienna on a panel of mouthpieces produced at TU Delft. Modifications in this case were made to both the baffle geometry and the size of the cavity. The aim of the tests is to identify the differences in radiated sound and mouth pressure among mouthpieces with different baffle and cavity geometries.

2. METHODOLOGY

Measurements were performed on a panel of five mouthpieces: one original commercial mouthpiece and five 3D printed copies of it, with modified baffle and chamber geometries. In particular: One original Vandoren v16, aperture 6, small chamber, modified by hand by Lebayle (the length of the table under the mouthpiece was decreased,

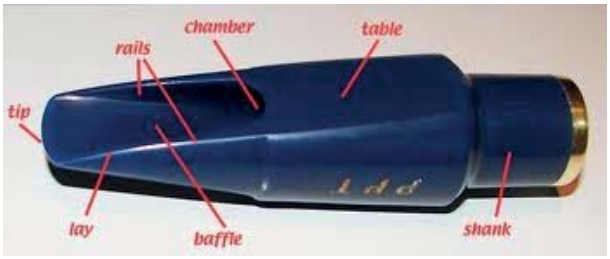

Figure 1: Different parts of a saxophone mouthpiece

increasing the projection of the mouthpiece) used as reference mouthpiece, a 3D printed copy of the latter one (description of the production are described in subsection 2.1), one with a narrower cylindrical chamber, one with a conical chamber, and one with a baffle ramp. Figure 2 shows the internal profile of the latter four mouthpieces.

2.1. Mouthpiece production

The Vandoren v16 was chosen as reference mouthpiece for the geometrical modifications and a 3D scan of it was made at TU Delft using a Phoenix Nanotom S CT scanner (http://www.ge-mcs.com /en /radiography-x-ray /ct-computed-tomography /nanotom-s.html). The scanned model was reconstructed in SolidWorks and modifications have then been made to the baffle and chamber of the original mouthpiece shape as shown in Figure 2. For producing these mouthpieces an Objet Eden 260 machine was used. The machine is able to produce objects up to the size of 600 x 252 x 200 mm at a resolution of 600dpi and layer thickness of 16 micrometer. The material used was a biocompatible resin marketed by Objet as MED610. It is a rigid transparent material developed and approved for prolonged contact with human tissue (http://objet.com /3d-printing-materials /bio-compatible).

The printed mouthpieces were polished using fine sand paper to remove support material without altering the geometry of the mouthpiece. The final surface roughness of the printed models is slightly higher than the original mouthpiece. This factor is considered to have minor influence on the radiated sound. The geometry of the reconstructed mouthpiece differed in the order of a fraction of a millimeter with respect to the scanned original mouthpiece by visual inspection in CAD environment. No geometrical measurements have been made after the printing.

2.2. Measurement setup

The tests consisted of in-vivo (with a player) far-field acoustic measurements and blowing pressure measurements. A professional player played his saxophone (Yamaha Custom YAS-855) with these mouthpieces, using a Légère plastic reed, StudioCut, strength 2.5. He played a written C major scale from C_4 to C_6 (on alto saxophone key, i.e. $F\#$ first octave corresponds to concert A_4 (440 Hz) note) with a metronome set at 120 bpm. Figure 3 shows how the scale was played. The scale was played five consecutive times on each mouthpiece, each time is called trial. It was noticed that the strength of the plastic reed was not affected by consecutive playing. The player carefully positioned the reed in the same position with respect to the mouthpiece for all the different tested mouthpieces.

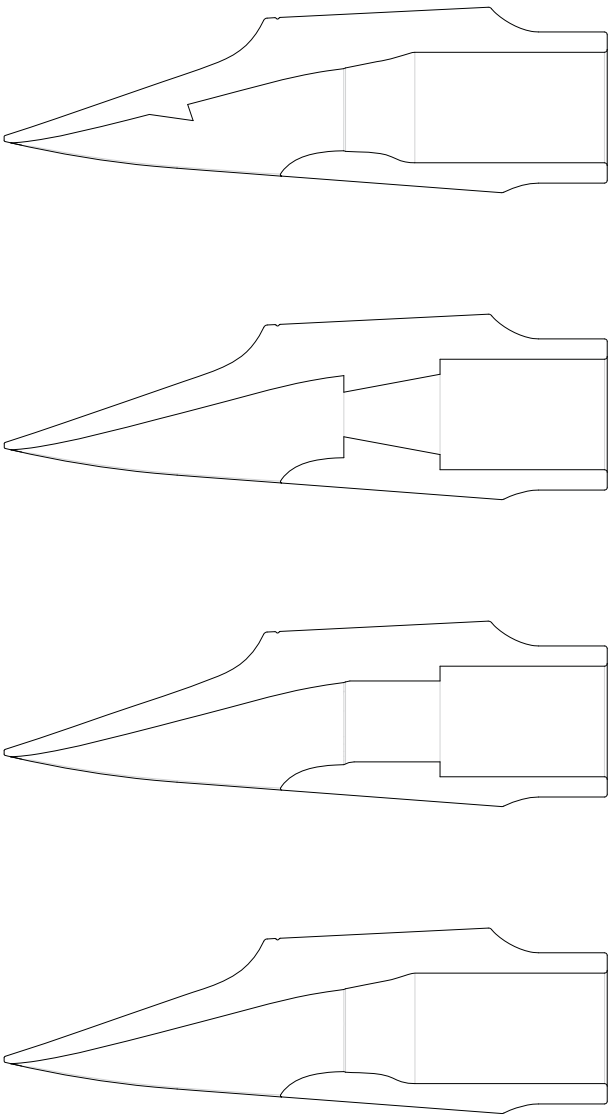

Figure 2: Internal profiles of the four mouthpieces that were 3D printed. From top to bottom: ramp baffle , conical chamber, cylindrical chamber, copy.

The following signals were recorded:

- the radiated sound was recorded with a ROGA microphone model RG-50 placed in the far field at an angle of 45° and a distance of 1.5 m above the player.
- the mouth pressure was measured with an ENDEVCO pressure transducer model 8507C-2. This was placed inside the mouth of the player beside the mouthpiece (details of the set-up are described in Ref. [7]).
- the metronome signal.

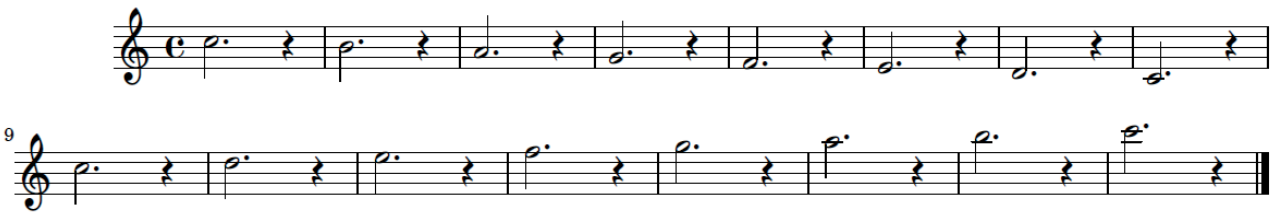

Figure 3: Order and duration of notes of the C major scale played during the recordings (alto saxophone key, i.e. $F\#$ first octave corresponds to concert A_4 (440 Hz) note)

The signals from the microphone and metronome were connected to a Phantom preamplifier model MPA 2017. The level of the microphone signal from the preamplifier was adjusted to be as high as possible without saturating (when playing forte). This adjustment was done once at the beginning of the measurement. The signals from the ENDEVCO sensor were connected to an ENDEVCO DC differential voltage amplifier model 136. The outputs from the preamplifiers were then connected to an ADAT HD24 digital recorder, which converted the signals from analog to digital, and into an optical interface, before being connected to an RME computer sound card model DIGI96/8 PST. The computer to which all signals were fed was running a LabView script which recorded all signals in a multitrack wave file with a sampling frequency f_s =48 kHz.

The recordings were separated into five trials, where each trial was one played instance of the full scale, and was approximately 32 seconds long.

2.3. Signal Analysis

The segments recorded from the microphone placed on the far field were analyses using the MQ analysis method [8] [9] coded in Matlab. This analysis delivers an analysis file with information about the amplitudes $A_k[n]$ and frequencies $f_k[n]$ of the k peaks that are present at every time frame n. In this case, the time difference between two frames was approximately 5.3 ms, giving a total of just under 6000 frames per segment.

With the information delivered by the analysis file, the following parameters were calculated for each time frame:

- P_{rad} radiated pressure root-mean-square:

$$P_{rad}[n] = 20 \cdot log_{10}\left(\sqrt{\sum_{k=1}^{K} A_k^2[n]}\right) \quad [\text{dB}] \tag{1}$$

- Normalized spectral centroid:

$$NSC[n] = \frac{\sum_{k=1}^{K} k \cdot A_k[n]}{\sum_{k=1}^{K} A_k[n]} \tag{2}$$

Calculations of P_{rad} amplitude and normalized spectral centroid vs time for all segments were saved in a file. The *rms* of the mouth pressure measured by the ENDEVCO sensor was also calculated as described above.

Depending on the amplitude of P_{rad}, each frame was labeled as belonging to the transient (amplitude increasing at the beginning of the note), the steady state (remaining more or less steady oscillating around a constant value) or the end of the note (decreasing at the end of the note), respectively [10].

3. RESULTS AND DISCUSSION

The calculations were divided into five groups, according to which mouthpiece (1. conical, 2. copy, 3. cylindrical, 4. ramp and 5. original), which of the fifteen notes, and which of the five trials was played. All the frames of the steady state of same note for all the trials were taken and a one way ANOVA test was performed along the five mouthpieces.

3.1. Radiated sound

The p-value from the statistical analysis was used to indicate when statistical differences were found with respect to the original mouthpiece. A value $p > 0.05$ indicates that there is no significant difference between the actual measurement and the reference measurement. The comparison of the five trials, for all the mouthpieces, gave a p-value > 0.05 which confirmed that there was no statistical difference between the trials played for the same mouthpiece.

Figure 4 and Figure 5 show the plots of the NSC over time for the mouthpiece pairs: conical mouthpiece (in blue) vs original mouthpiece (in red) (Figure 4) and cylindrical (in blue) vs original mouthpiece is (in red) (Figure 5).

The x-axis of the following figures corresponds to the time in seconds in which the note sequence, shown in Figure 3, was played. Whenever the values are different from zero there is a note playing; the zero intervals are pauses between one note and the next.

The black bars are the confidence interval of the difference within the mouthpiece pair, when $p < 0.05$. The error bars are shown only in the steady state of the notes.

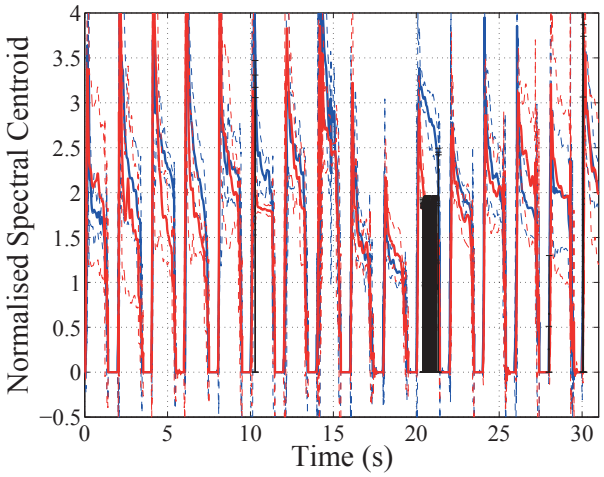

Figure 4: Normalized spectral centroid for mouthpieces conical (in blue) and original (in red)

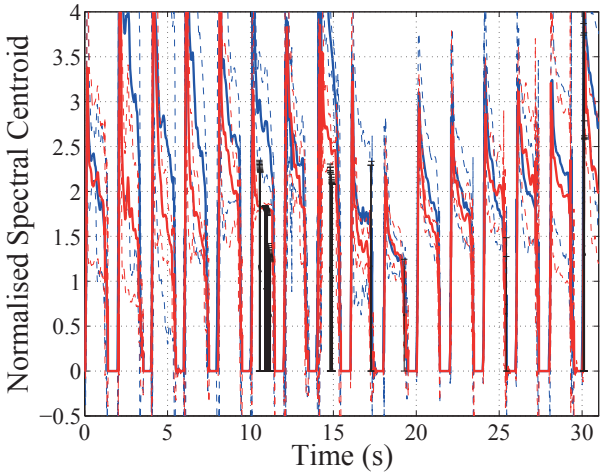

Figure 5: Normalized spectral centroid for mouthpieces cylindrical (in blue) and original (in red)

Differences in NSC were limited to notes: E_4, for the pair cylindrical-original and note E_5, for pair conical-original.

Other mouthpiece pairs gave no statistical differences in NSC and are therefore not presented.

These plots give an indication that while the ease of playing experienced by the player was different for the different mouthpieces, P_{rad} and spectral centroid remained mostly constant independently of the mouthpiece.

3.2. Mouth pressure

An ANOVA analysis was made also on the mouth pressure measured by the transducer in the mouth of the player. The results are shown for the pairs: copy-original, copy-cylindrical and copy-ramp. These pairs are the ones producing the highest differences in the analysis. No mouth pressure data are available for the conical mouthpiece due to a problem during acquisition.

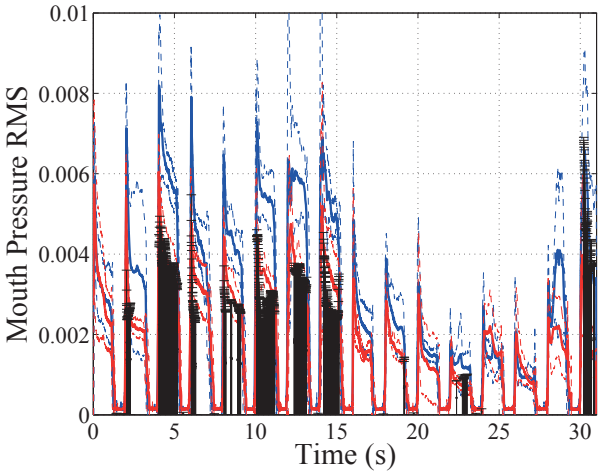

Figure 6: Mouth pressure rms for the copy mouthpiece (blue) and original (red)

Differences in the mouth pressure for the pair copy-original extend over most of notes A_4,E_4,D_4 and C_4. The copy mouthpiece requires higher blowing pressure, especially in the first part of the sequence (lower pitch notes).
Since the copy mouthpiece is meant to be an exact copy of the original mouthpiece and no noticeable differences were observed between the reconstructed and scanned mouthpieces, it is hypothesized that the differences are caused by slight geometrical distortion during the printing process or surface refining.

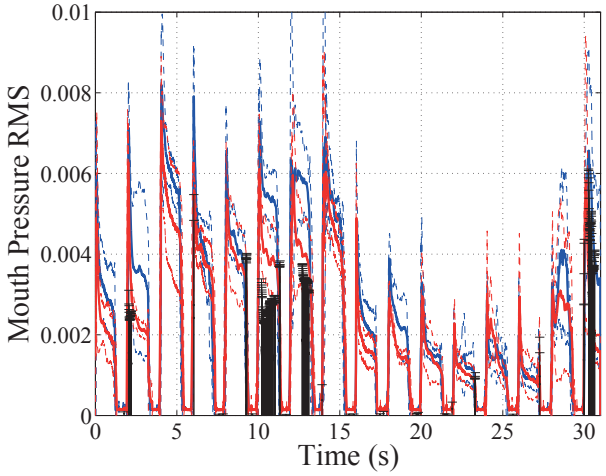

Figure 7: Mouth pressure rms for the copy mouthpiece (blue) and cylindrical (red)

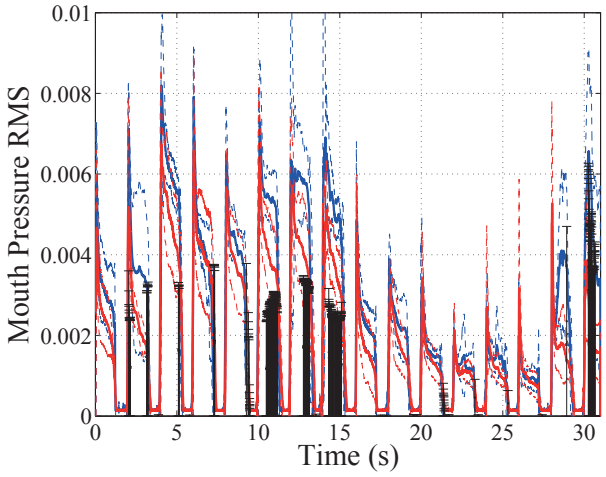

Figure 8: Mouth pressure rms for the copy mouthpiece (blue) and ramp (red)

The largest differences for the ramp-copy pair are found in the notes E_4, D_4 and C_4, in particular towards the end of the note.

3.3. Ease of playing

In order to investigate the playability of the mouthpieces an "effort" ratio was calculated:

$$E = \frac{P_m}{P_{rad}} \tag{3}$$

where E is the effort ratio, P_m is the *rms* of the mouth pressure or blowing pressure, and P_{rad} is the *rms* of the radiated sound measured by the ROGA microphone in the far field. A smaller ratio (less effort) would mean that less blowing pressure is needed to obtain the same P_{rad} output. Conversely, a smaller effort ratio would be obtained if, using the same blowing pressure, one mouthpiece gave a higher P_{rad} value than the other.

The effort ratio E was calculated for the whole duration of each note and an ANOVA test was performed in the steady state for the various mouthpieces with respect to the reference mouthpiece and across the trials for the same mouthpiece.

Plots of the effort ratio, for only the mouthpieces giving a p-value < 0.05 with respect to the reference mouthpiece, are shown in Figure 9 and Figure 10. As already mentioned, no pressure data are available for the conical mouthpiece, therefore this mouthpiece is excluded by the following analysis. The showed data are averages of the five played instances (trials).

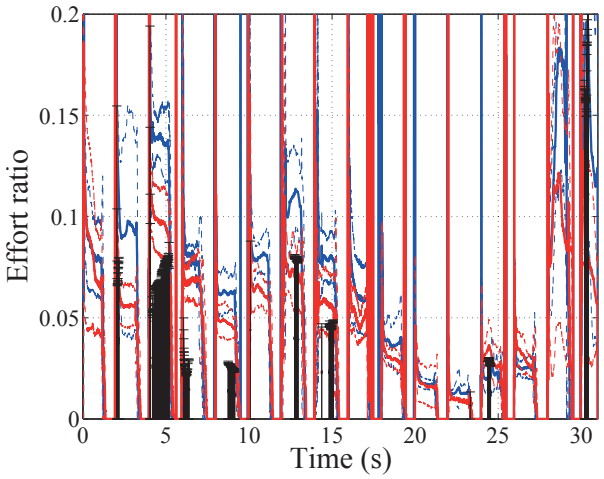

Figure 9: Effort ratio for the pair: copy (blue) vs original (red)

In Figure 9 the effort ratio (thick line) plus minus standard deviation (dashed line) are shown for the mouthpiece original (red) and the copy mouthpiece (blue).

Looking at the error bars the main differences are found for notes: A4 (during most of the note), G4 (at the beginning), F4 , D4 and C4 (at the end), G5 (in the middle). The highest values of the effort ratio are found at the beginning of the note, during the attack, when the mouth pressure value is relatively high compared to the radiated sound.

From the comparison between the effort ratio in Figure 9 and the mouth pressure in Figure 6 for the copy-original pair, it can be noticed that the effort ratio futures smaller differences than the mouth pressure. This might be due to a different response of the two mouthpieces. The copy mouhtpiece requires higher blowing pressure

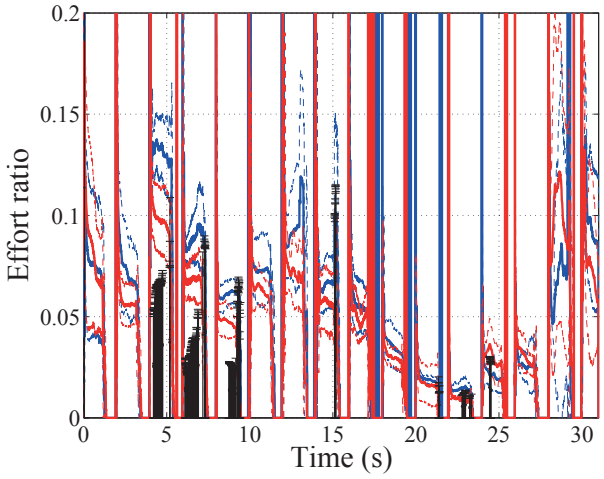

Figure 10: Effort ratio for the pair: ramp (blue) vs original (red)

for some notes but this also produces a higher radiated sound rms. Measurement of the air flux entering the mouthpiece might help explaining the differences.

Figure 10 shows the differences in effort ratio between the baffle ramp mouthpiece and the original. In this case differences are found for notes A4 (during the first half), G4 (during most of the note), and F4 (at the end).

No relevant statistical differences in effort ratio were found for the other mouthpiece pairs.

The player experienced that the copy mouthpiece was the hardest to play. This can be explained by the fact that the overall level of the differences with respect to the original mouthpiece is higher and more extended for the copy mouthpiece compared to the other mouthpieces.

4. CONCLUSIONS

It is hypothesized that different mouthpiece internal shapes determine differences in radiated sound and ease of playing.

A panel of five mouthpieces with modified baffle and chamber geometries was measured through in-vivo measurements with one player. Radiated sound (P_{rad}) and mouth pressure (P_m) were acquired while the player was playing on a fixed note sequence and compared with an ANOVA test.

The radiated sound and normalized spectral centroid remained almost the same for all mouthpieces, despite their obvious geometrical differences.

However non-negligible differences were observed for the mouth pressure in particular at the lower register.

Since the player reported a significant difference in the playability of the mouthpieces, especially between mouthpieces "Original" and "Copy", an effort ratio E was defined, as the ratio of blowing pressure over radiated sound *rms*, and compared with the aid of an ANOVA test.

A higher difference in the effort between these two mouthpieces was found compared to the other pairs, while the difference among trials on the same mouthpiece was not significant. We found that the effort ratio is therefore correlated with the playability of the mouthpiece and seems to be a useful parameter in classifying different mouthpieces.

In order to generalize these results, further investigations are required with more players in order to assess the response of different players to the different mouthpiece geometries.
Also geometric measurements on the printed mouthpieces will be made and compared with the scanned mouthpiece to check the effect of printing on the final shape.
Furthermore a more thorough analysis is required lo link the differences in effort ratio of specific notes to geometric differences of the mouthpieces from an acoustic and aerodynamic point of view.

Acknowledgments

The authors would like to thank Alex Hofmann for playing the saxophone during the recordings and the valuable feedbacks and Vasileios Chatziioannou for all the fruitful discussions about the project. Zjenja Doubrovski is also gratefully acknowledged for the design and manufacturing of the 3D printed mouthpieces.

5. REFERENCES

[1] Arthur H. Benade, *Fundamentals of musical acoustics*, Oxford Univesity Press, 1976.

[2] Frederick S. Wynman, *An acoustical study of alto saxophone mouthpiece chamber design*, Ph.D. thesis, Eastman School of Music, 1972.

[3] Gary P. Scavone, *An acoustic analysis of single reed woodwind instruments with an emphasis on design and performance issues and digital waveguide modeling techniques*, Ph.D. thesis, Stanford University, 1997.

[4] Zjenja Doubrovski, Jouke C. Verlinden, and Jo M. P. Geraedts, "Optimal design for additive manufacturing: Opportunities and challenges," in *ASME 2011 International Design Engineering Technical Conferences and Computers and Information in Engineering Conference*, Washington D.C, USA, 2001, The American Society of Mechanical Engineers.

[5] Valerio Lorenzoni, Zjenja Doubrovski, and Jouke C. Verinden, "Embracing the digital in instrument making: Towards a musician-tailored mouthpiece by 3D printing," in *Proceedings of the Stockholm Musical Acoustics Conference 2013*, Stockholm, Sweeden, 2013, KTH Speech, Music and Hearing.

[6] Valerio Lorenzoni and Daniele Ragni, "Experimental investigation of the flow inside a saxophone mouthpiece by particle image velocimetry," *Journal of the*

Acoustical Society of America, vol. 131, no. 1, pp. 715–721, 2012.

[7] Vasileios Chatziioannou and Alex Hofmann, "Physics-Based Analysis of Articulatory Player Actions in Single-Reed Woodwind Instruments," in *Acta Acustica*, Vol. 101, 2015, pp. 292 – 299.

[8] Robert J. McAulay and Thomas F. Quatieri, "Speech analysis/synthesis based on a sinusoidal representation," *IEEE Transactions on Acoustics, Speech, and Signal Processing*, vol. ASSP-34, no. 4, pp. 744–754, 1986.

[9] James W. Beauchamp, "Analysis and synthesis of musical instrument sounds," in *Analysis, synthesis and perception of musical sounds: The sound of music*, James W. Beauchamp, Ed., pp. 1–89. Springer, 2007.

[10] John M. Hajda, "The effect of dynamic acoustical features on musical timbre," in *Analysis, synthesis, and perception of musical sounds*, James W. Beauchamp, Ed., pp. 250–268. Springer Science+Business Media, LLC, 2007.

SOFTWARE SIMULATION OF THE TONE-HOLE LATTICE IN CLARINET-LIKE SYSTEMS

Fritz Schueller, Carl Poldy

Private Researchers
Vienna, Austria

fritz.schueller@aon.at
carl.poldy@nativeprogramming.at

ABSTRACT

Arthur Benade introduced the notion of a tone-hole lattice in the early 1960s. He found that there exists a so-called "cutoff frequency" that is determined by the structural dimensions of the tube and its side-holes. Since then several other researchers have studied the properties of the tone-hole lattice, especially dealing with the row of open tone-holes. When simulating mechanical and acoustical systems it is convenient to use electromechanical and electro-acoustical analogies. Highly developed theories for electric networks can thus be directly used to simulate the behaviour of musical instruments.
Special software applications, such as Micro-CAP by Spectrum Software of California, an electrical Circuit Analysis Program, can be used for this purpose. To build a bridge from the electrical to the mechanical and acoustical world there exist so called "macros" that were developed mainly by the second author, with mechanical input parameters, so the user need not necessarily think in electrical terms. Examples of such macros are two-ports representing lossy cylindrical and conical tubes, two-poles for short holes etc. all of which occur in wind instruments. Other useful two-ports are ideal transformers for coupling mechanical and acoustical parts of the model.
The impedance-versus-frequency diagrams that are easily derived with the aid of Micro-CAP can help to detect influences of the several dimensions of the tone hole system. It is also possible to show pressure and flow profiles along the axis of the tube with opened and closed side-holes. Such work can lead to a further understanding of the properties of real woodwind instruments.

1. INTRODUCTION

The applicability of the simulation tool for the tone-hole lattice was tested using the work of Benade as an entry point. In his book Fundamentals of Musical Acoustics [2], Benade gives an example of a tube 61 cm long extended by a tube with side holes. The impedance curve is shown in Fig. 21.3 of the book. No more details about the tube are given there. Using the simulation tool, the authors were able to reconstruct approximately the dimensions of the tube Benade used for his measurement. The influence of the cutoff frequency can be seen clearly.

Throughout this article geometrical parameters are used with the symbols Benade introduced in [1]. The diameter of the cylindrical bore is *2a*, the radius of a tone hole is *2b* and the distance between the holes is *2s*. For the depth of the hole (thickness of the wall) the symbol *t* is used.

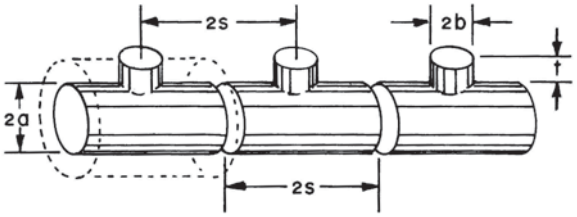

Fig. 1, Arthur H. Benade's tone-hole lattice

Three T-shaped elements of the tone-hole lattice are shown in Fig.1 (copy of the upper part of Fig. 21.8 on page 448 of [2]). Here we deal only with the lattice of open tone holes. Thus the air in the holes can move freely and an inner and outer end-correction needs to be taken into account. Benade uses the definition $t_e = t+1.5b$ for the effective length of the side holes.

Section 2 is an attempt to reconstruct the tone-hole lattice that Benade measured to get Fig. 21.3 (page 435 of [2]). In section 3 the impedance curves for the non-lossy case, based on an article of Moers and Kergomard [4] are shown. And finally section 4 shows a simulation of the lossy case, using the macro for lossy tubes with circular cross section.

The main purpose of the present article is to check the simulation against the measurement results and theoretical formulations. The whole article is about the regular tone-hole lattice. But different values of *a, b, s,* and t_e are used in the three following sections. For all simulations the speed of sound is taken to be 346.2 m/s, the viscosity coefficient 1.86×10^{-5} kg/(ms) and the density 1.186 kg/m^3 (air at *23°C*).

2. BENADE'S TONE-HOLE LATTICE

Beginning on page 434 of [2] Benade gives an incomplete description of the geometrical setup for the curves of Fig. 21.3 [2]. For the upper curve (pipe alone) he quotes a length of 61 cm and a first peak of the input impedance at 140 Hz.

The simulation in Fig. 2 corresponds to the lower half of Fig. 21.3 [2]. The dimensions are given in the figure directly. The first part of Benade's tube (containing no holes) had to be shortened to 542 mm to keep the first resonance at 140 Hz.

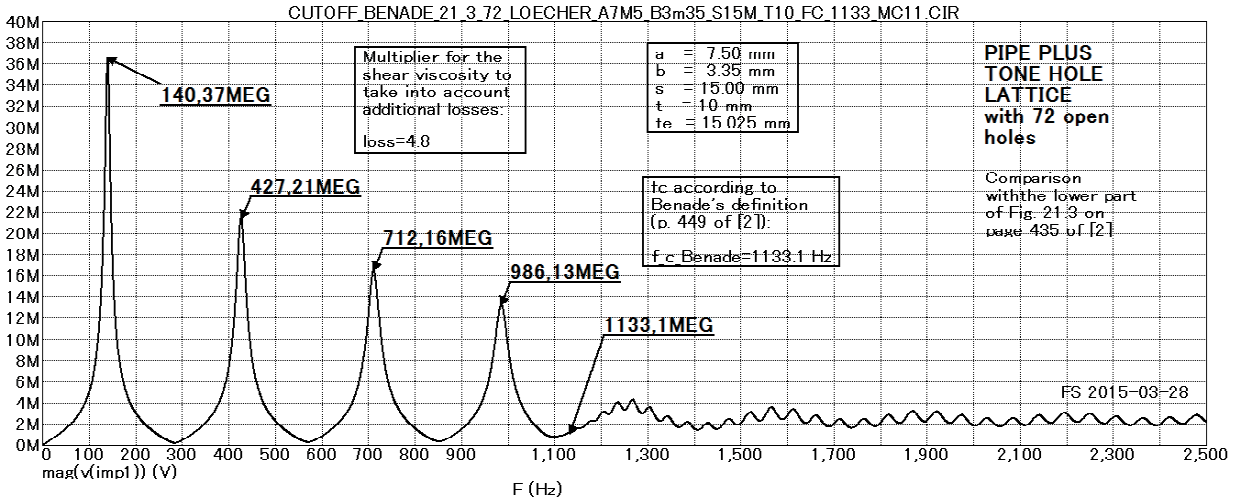

Fig. 2, Reconstruction of Benade's experiment

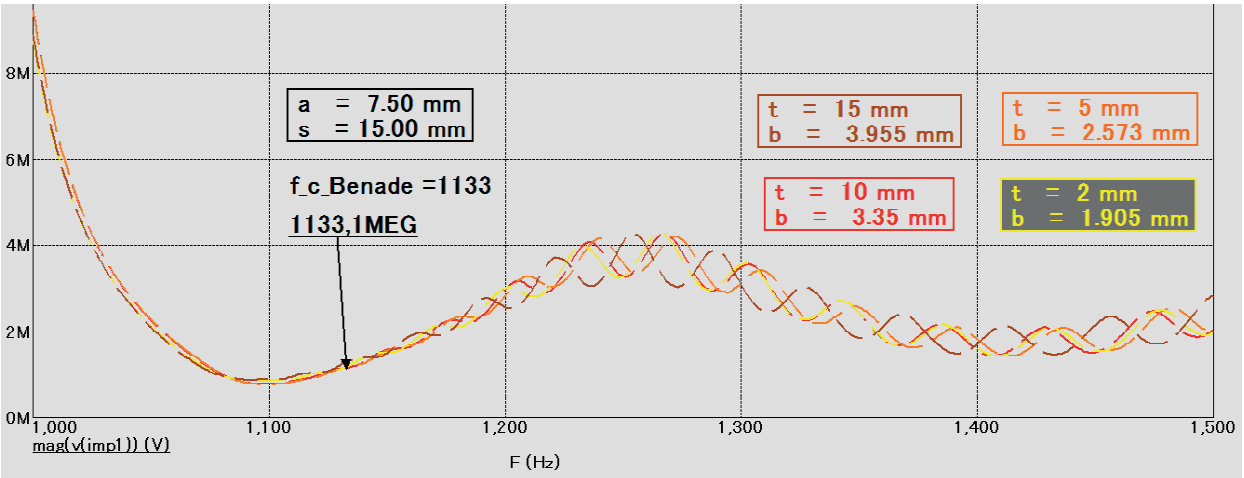

Fig. 3, f_c constant, *t* and *b* variable

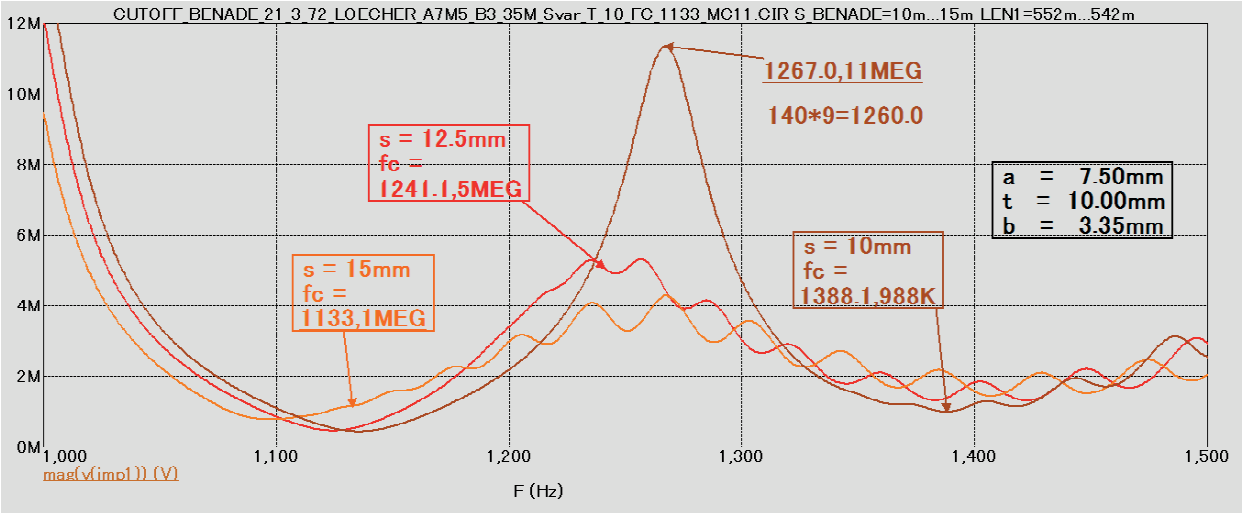

Fig. 4, *s* variable, leading to different values of f_c

The simulation is based on an increased value for the shear viscosity ($4.8 \times 1.86 \times 10^{-5}$ kg/m/s). The factor 4.8 was found experimentally, in order to achieve a similar height of the impedance peak at 140 Hz as Benade measured. A minimal number of 72 open holes is needed to bring the peaks to the right of the cutoff frequency down to less than 4 MOhm (corresponding to Fig. 21.3 of [2]). It is important to stress that the cutoff frequency as indicated in the figure is calculated for the non-lossy case, as stated in [1] in the text (damping is neglected) above equ. (8). The simulation however - as in Benade's experiment - involves lossy tube- and lossy hole-elements.

Some interesting experiments can now be done with the model. Using the same sizes for *a* and *s* as before, but changing *b* and *t* in such a way that f_c stays at 1133 Hz, one obtains the result of Fig. 3. Here the *x*- and *y*-ranges have been reduced compared to Fig. 2. We see here that there is not much difference in the overall picture. Only the peaks of the wiggling part above cutoff occur at different frequencies. The envelope curve does not change at all.

In the next experiment all geometrical parameters except *s* are kept constant. This leads to different cutoff frequencies, as can be seen in Fig. 4. For the smallest *s* (10 mm) the fifth resonance peak of that part of the tube without holes (approx. 9 times 140 Hz) falls below cutoff, thus not affecting the peak very much. The tube without holes had to be lengthened for the smaller values of *s*, to keep the basic resonance at 140 Hz (552mm for *s*=10mm, 547mm for *s*=12.5mm).

3. TWO TREATMENTS OF THE NON-LOSSY CASE

Benade gives a formula for f_c in [2] on page 449:

$$f_c = 0.110\,(b/a)\,c\,[1/(s\,t_e)]^{1/2} \qquad (1)$$

This formula was used for calculating f_c in the preceding section although it contains a small rounding error. Setting the denominator to zero in the original formula (8) of [1] gives the correctly rounded value of *0.109* as the first factor. In this section the more accurate value is used to calculate Benade's cutoff frequency.

The original formula (8) of [1] is shown here (2):

$$Z_0 = \left(\frac{\rho\,c}{\pi a^2}\right)\left(\frac{1+\frac{1}{2}(b/a)^2\,cot(\omega t_e/c)\,tan(\omega s/c)}{1-\frac{1}{2}(b/a)^2\,cot(\omega t_e/c)\,cot(\omega s/c)}\right)^{1/2} \qquad (2)$$

Solving for zero in the denominator was done with MicroCAP by searching the pole of the reciprocal value of the denominator on the frequency scale. Since the circuit analysis program has numerical limitations a very big but finite value is the result for the peak height.

Using the parameters of Fig. 2, the cutoff frequency now becomes 1123 Hz (=1133 x 0.109/0.110).

But there is also another value of the cutoff frequency, that can be derived from the article of Moers and Kergomard [4]. On page 986 of [4] we see the elements of the transfer matrix of a single T-shaped element for the non-lossy case. Z_c (corresponding to Benade's Z_o, "o" probably standing for "open") is not given explicitly in [4]. But it can be easily calculated by substituting the matrix elements *B* and *C* into the equation for Y_c^2 (given below equation (2) on page 986).

By eliminating all the abbreviations used in *B* and *C* and using Benade's symbols one obtains for Z_c:

$$Z_c = \left(\frac{\rho\,c}{\pi a^2}\right)\left(\frac{1+\frac{1}{2}\,(b/a)^2\,(c/(\omega t_e))\,tan(\omega s/c)}{1-\frac{1}{2}\,(b/a)^2\,(c/(\omega t_e))\,cot(\omega s/c)}\right)^{1/2} \qquad (3)$$

A detailed derivation and a comparison with equation (8) of [1] can be found in the appendix 1.

Moers and Kergomard [4] give a good approximation of f_c in (6) on page 987. It is very close to the frequency where the denominator of Z_c becomes zero. Rounded to one Hz f_c is 1140Hz in both cases, either using (6) or looking for the pole of Z_c calculated from the matrix elements *B* and *C*.

Next we see a simulation using a number of simple T-shaped elements (100 elements all in one dimension). Fig. 5 shows the beginning of the tone-hole lattice. Included are the impedance sensor at the input and one of the T-shaped elements. Grounding means that an aperture is open because a current (volume flow) can flow into zero voltage (zero pressure).

The two components of the T-shaped element are a non-lossy tube (transmission line) and a non-lossy inductor. The tube elements are simply delay lines, giving a delay corresponding to the speed of sound *c* and the length *s* of the element. The inductor represents the acoustic mass of the air in the hole (including inner and outer end-corrections). The inductance becomes $L = \rho t_e/(\pi b^2)$, taking into account that the acoustic part is linked to the electrical part by a factor of $1/area^2$ $(area=\pi b^2)$. The density of air at *23°C* is $\rho = 1.186 kg/m^2$ in these simulations.

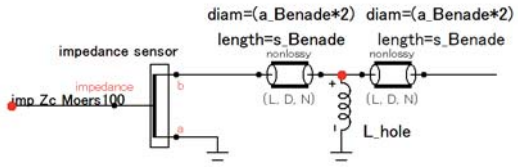

Fig. 5, Impedance sensor and one T-shaped element

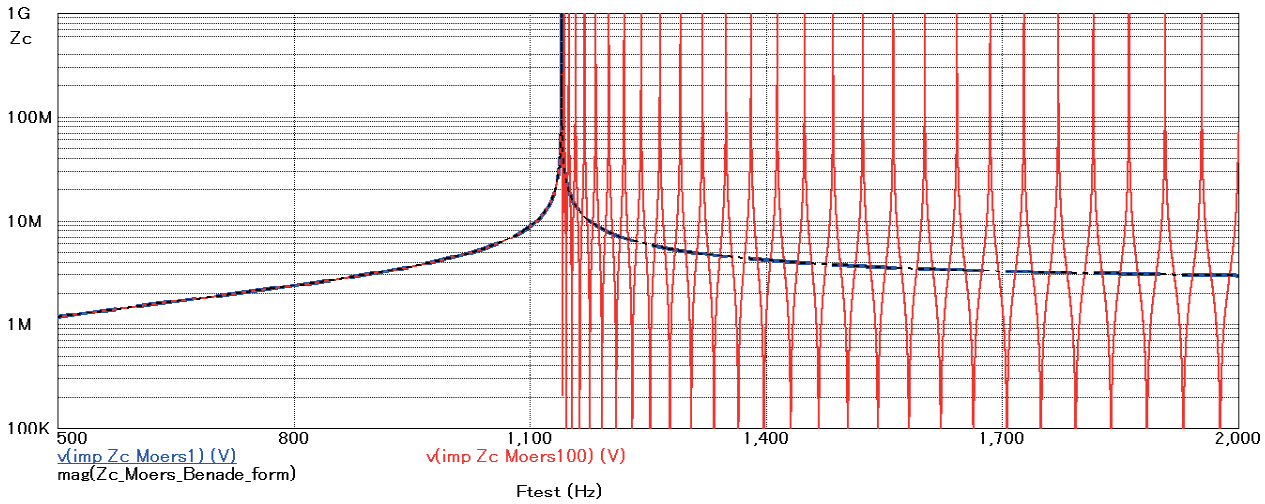

Fig. 6, Input impedance of tone-hole lattice with 100 open holes and Z_c

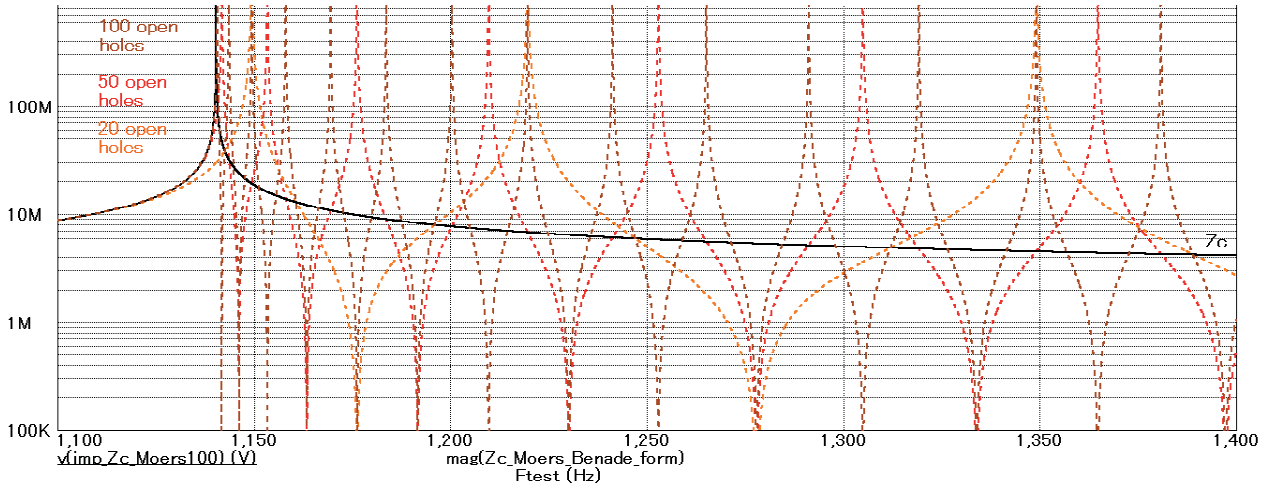

Fig. 7, Input impedance of tone-hole lattices with, 100, 50 and 20 open holes and Z_c

Now the simulation is used to show the agreement of the formula for Z_c with the model. The magnitude of the input impedance for a tone-hole lattice with one hundred open holes is shown (Fig. 6). Unlike the preceding section, there is no part of the tube without side holes. As there are no losses, the peaks theoretically go to infinity and the minima are zero. It is interesting to see that the peaks come closer together, when approaching f_c from higher frequencies. Reducing the number of open holes leads to fewer peaks and fewer minima and the lowest peak moves further away from f_c. Fig. 7 shows the situation for 100, 50 and 20 open holes in a smaller frequency range than before (again no damping). Fig. 7 shows the same for 100, 50 and 20 open holes in a smaller frequency range than before (again no damping).

4. PRESSURE AND FLOW ALONG THE TUBE, LOSSY CASE

We return now to the model with losses. Again there is an artificial increase of the shear viscosity used, as described in section 2 (4.8 x 1.86 x 10^{-5} kg/m/s). The T-shaped element now consists of tube elements (macros) only (see Fig. 8). A detailed description of the tube model is given in appendix 2. The tube elements themselves do not contain any end correction. Therefore the length of the side hole (tube) has to be set to t_e (Benade's fomula $t_e = t + 1.5b$ is used). The measuring points *Px* and *Fx* will be described later in this section. There are 68 open side holes used in the following experiments. At the end of the complete lattice a radiator is placed, as shown in Fig. 9.

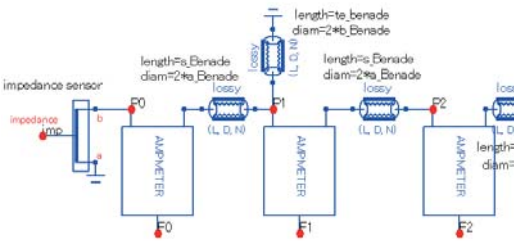

Fig. 8, Setup for impedance measurement; impedance sensor, ampere meter, measuring points

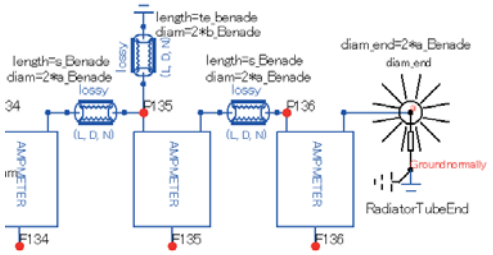

Fig . 9, End of the tone-hole lattice, with radiator

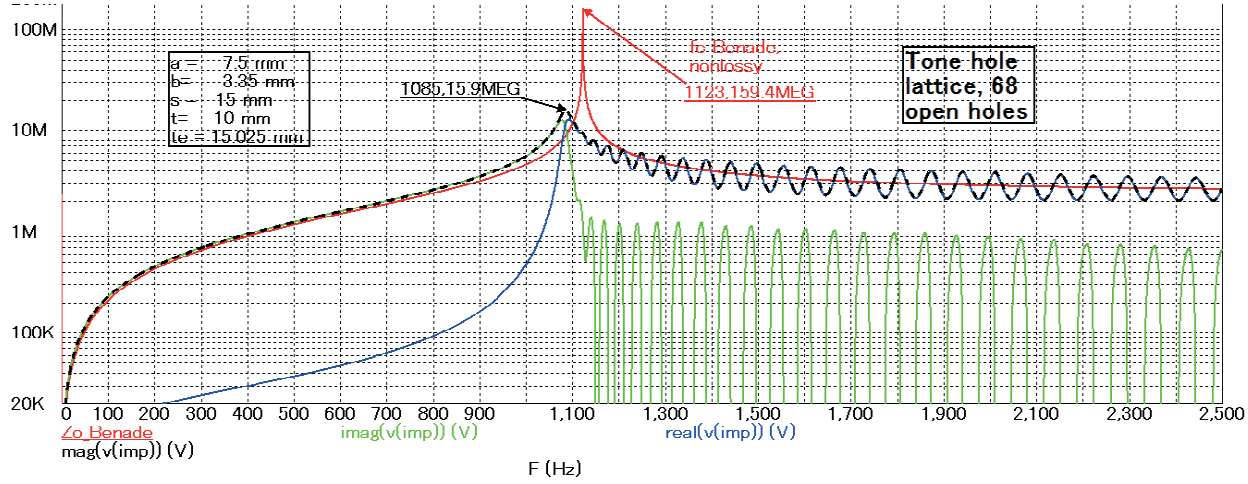

Fig. 10, impedance chart for 68 open holes

The input impedance is computed and shown in Fig. 10. As there are losses, according to the theory there is also a small real part below cutoff (blue) and a small imaginary part above cutoff (green). Benade's f_c (non-lossy case) is indicated for comparison (red). There are more resonances in the range above 5 kHz, also including a negative imaginary part. This is not considered further here.

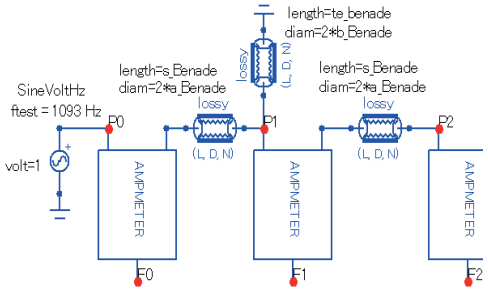

Fig. 11, Setup for pressure and flow measurement

Now to get an idea of the pressure and flow in the tube, the impedance sensor is replaced by a sine voltage source (Fig. 11). The frequency of the peak (1093 Hz) is chosen for the experiment and the voltage is set to 1V (1Pa). The result (Fig. 12 and Fig. 13) is not a simple standing wave, but a combination of a standing wave and a travelling wave. For a pure standing wave, the imaginary part of the pressure would be zero along the whole tube.

Voltages at points *Px* (*x*=0 ... 136) correspond to pressure values (Pa), voltages at points *Fx* (*x*=0 ... 136) to volume flow (m^3/s). Point *P0* (*F0*) would be the mouthpiece tip of a woodwind instrument, *P136* (*F136*) the end of the bell. The open holes are at the positions *Px* with *x* being an odd number (1 to 135).

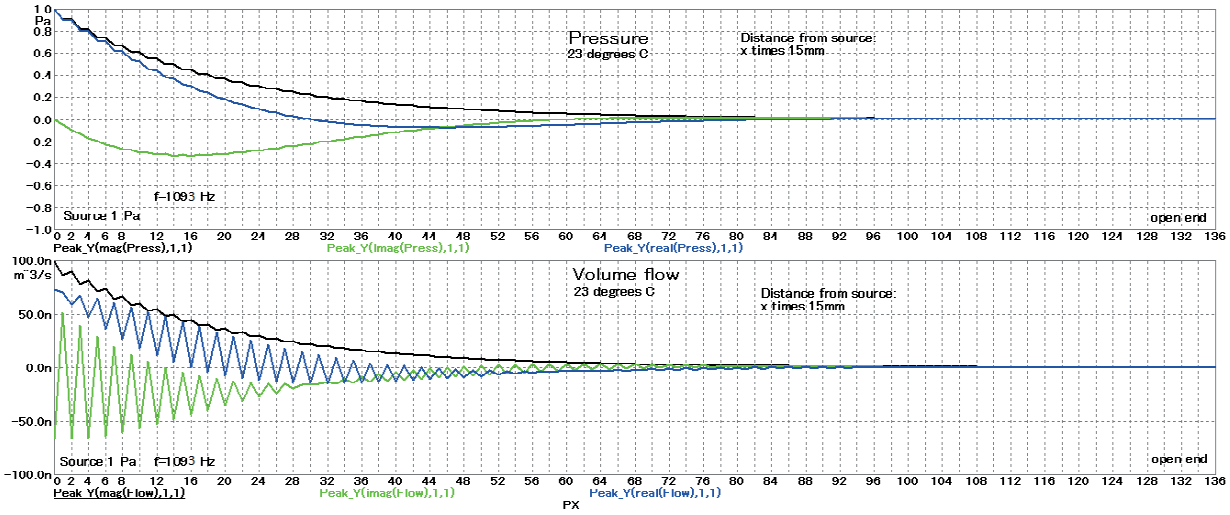

Fig. 12, Pressure and volume flow along the tube with 68 open holes

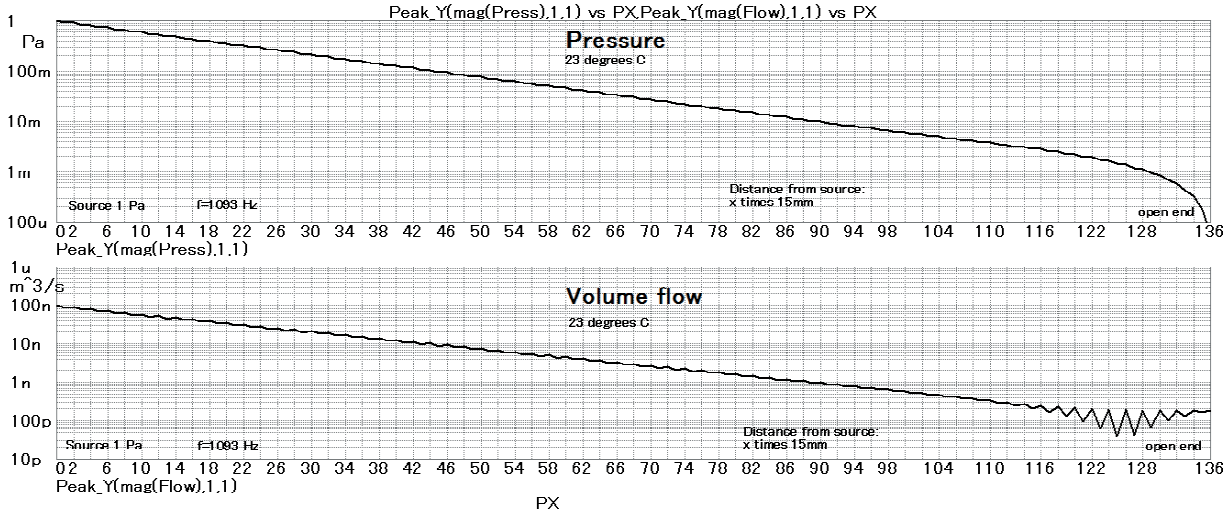

Fig. 13, Magnitude of pressure and flow along the tube with 68 open side holes, logarithmic scale

5. CONCLUSION

In this article some simple structures of tone-hole lattices were analysed showing the suitability of an electronic circuit analysis program to study acoustical questions concerning musical wind instruments. It can be seen that there is good agreement with theory and experiments in the relevant literature. This opens the way to study many other questions. This could be the impedance, pressure and flow properties of wind instruments with irregularly placed tone-holes (which is the normal case). There also exist macros for conical tubes, tubes with rectangular cross section, etc., developed by the second author. Thus also conical instruments, such as oboes, bassoons and saxophones could be studied.

The user interface and the circuit diagrams are very intuitive, so the use of this kind of software simulation is also valuable for teaching and studying. There exists more literature treating the cutoff frequency and the side hole, e.g. [5], [6], [7] and [8] that could be used for a cross check. But most important is the fact that real instruments could be analysed, based on the geometrical dimensions of the bore and the holes.

The method of raising the shear viscosity to cope for losses that are not known in detail could be improved by looking into the cause of the losses (turbulence, porosity, friction, radiation, etc.) and trying to model these parameters effectively.

A very ambitious aim would be to try to include nonlinear effects and/or two-dimensional simulations. This would mean developing new, probably rather complicated macros.

6. APPENDIX 1

Here it is described how to express the characteristic impedance Z_c from Moers and Kergomard [4] in a form similar to that which Benade used in [1].

First the matrix elements *B* and *C* [4] are divided by j. Then the variables *Y*, Z_c, *k* are replaced by ω *(=2πf)*, ρ (density of air), *c* (speed of sound), *a* (tube radius), *b* (hole radius) and t_e (effective hole depth). For the length of the tube elements *s* is used, as Benade did in [1]. All necessary formulae for these replacements can be found on page 986 and 987 of [4].

This gives *B/j* and *C/j* in the form of

$$B/j = \frac{\rho c}{\pi a^2}\left[2\sin(\omega s/c)\cos(\omega s/c) + (b/a)^2\,(c/(\omega t_e))\cos^2(\omega s/c)\right] \quad (4)$$

$$C/j = \frac{\pi a^2}{\rho c}\left[2\sin(\omega s/c)\cos(\omega s/c) - (b/a)^2\,(c/(\omega t_e))\cos^2(\omega s/c)\right] \quad (5)$$

Therefore *Zc =1/Yc* becomes

$$Z_c = \sqrt{\frac{B}{C}} = \frac{\rho c}{\pi a^2}\left[\frac{2\sin(\omega s/c)\cos(\omega s/c) + (b/a)^2\,(c/(\omega t_e))\cos^2(\omega s/c)}{2\sin(\omega s/c)\cos(\omega s/c) - (b/a)^2\,(c/(\omega t_e))\cos^2(\omega s/c)}\right] \quad (6)$$

Now reducing the fraction by

$$2\sin(\omega s/c)\cos(\omega s/c) \quad (7)$$

gives Z_c in a similar form as the Z_o in (8) of [1].

$$Z_c = \left(\frac{\rho c}{\pi a^2}\right)\left(\frac{1 + \frac{1}{2}(b/a)^2\,(c/(\omega t_e))\tan(\omega s/c)}{1 - \frac{1}{2}(b/a)^2\,(c/(\omega t_e))\cot(\omega s/c)}\right)^{1/2} \quad (8)$$

Comparing the two equations for Z_c and Z_o (8), one finds that only the term $cot(\omega t_e/c)$ in (8) is replaced by $c/(\omega t_e)$.

Remark: Benade uses Z_c for "Z for tubes with *closed* holes" and Z_o for "Z for tubes with *open* holes", whereas in [4] Z_c stands for "characteristic impedance".

These two functions are very similar for frequencies where $\lambda/4$ is much bigger than t_e. This is valid for the cutoff frequency of 1140 Hz and t_e being about *15mm*. Benade evidently treated the side-hole as a tube, whereas Moers simplified the model to a rigid mass in the side hole. The latter method is sufficient for many applications and runs faster on a computer. Fig. 14 shows the curve shapes of the two different equations for Z_c, Z_o and the real and imaginary parts thereof.

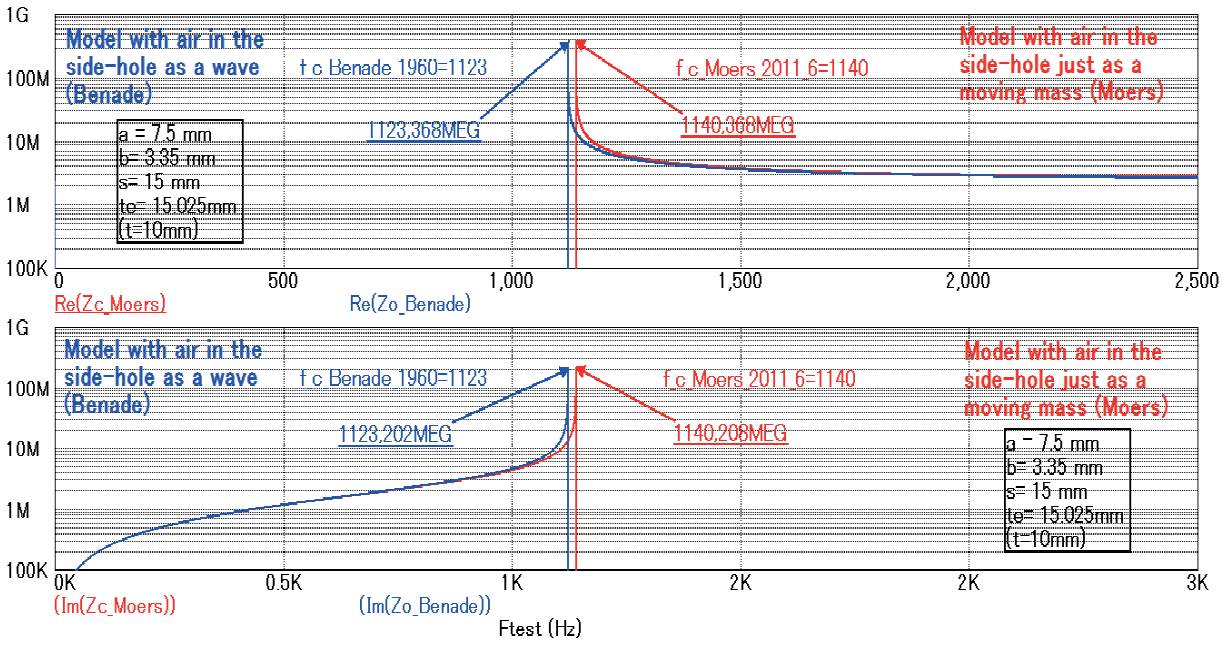

Fig. 14, comparison of f_c, side hole as a tube and only mass

7. APPENDIX 2

Here we describe the model (macro) for the lossy tube. There are two versions of the macro. One simple, for almost plane waves in tubes where Bessel functions are not needed. This is only valid for frequencies very much higher than fo=64*visc/(pi*rho*diam^2, cylindrical tube). The second model is also applicable for low frequencies (small diameters). It is based on Bessel functions and takes into account the friction on the walls of the tube. Simulation with the latter can be time consuming. The diameters used in the simulation (a_Benade = 15 mm, b_Benade = 3.35mm require only the simple model, so this is described here in detail.

The physical quantities used for the simulations are:

Standard temperature:	Celsius_standard = 23 °C
Speed of sound:	speed = 346.217 m/s
Standard pressure:	P_{atmos} = 101.325 Pa
Density of air (1% argon):	rho = 1.186 kg/m^3
Shear viscosity:	visc = 18.6*10^-6 kg/m/s
Dimensionless loss factor:	loss = 4.8
Specific heat ratio (c_p/c_v):	kappa = 1.40267
Prandtl number:	prandtl = 0.719551

The diameter of the cylindrical tube with circular cross section is “diam” and its length is named “length”. The frequency in Hz is called “F”. The circuit diagram of the macro is shown in Fig. 15. It includes the elements of the hybrid matrix shown in Fig. 16, together with the transmission matrix elements that are calculated from the propagation constant gamma and the characteristic impedance zwl1.

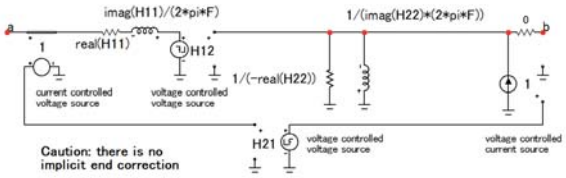

Fig. 15, circuit diagram of the lossy tube macro

Chain matrix lossy	
.define A11 (cosh(gamma*length))	.define A12 (zwl1*(sinh(gamma*length)))
.define A21 ((1/zwl1)*(sinh(gamma*length)))	.define A22 (cosh(gamma*length))
H matrix lossy	
.define H11 (A12/A22)	.define H12 (1/A22)
.define H21 (1/A22)	.define H22 (-A21/A22)

Fig. 16, Definition of the matrix elements

8. REFERENCES

[1] Benade, Arthur H.: On the mathematical theory of woodwind finger holes. J. Acoust. Soc. Am. 32 (1960) 1591–1608.

[2] Benade, Arthur H.: Fundamentals of Musical Acoustics. University Press, London, 1976. Reprinted and corrected in 1990 by Dover Publications, Mineola, N.Y.

[3] Micro Cap, Electronic Circuit Analysis Program, Spectrum Software, 1021 South Wolfe Road, Sunnyvale, CA 94086, programmed by Andy Thompson, Tim O'Brian, Bill Steele.

In Fig. 17 and Fig. 18 the definitions for gamma and zwl1 are shown in the form as they are used in the Circuit Analysis Program.

```
.define gamma

j*2*pi*F/speed*
(
   (1-2*j*(kappa-1)/
      (
         (-j*2*pi*F*rho*prandtl/
            (loss*visc)
         )^0.5*diam/2
      )
   )/
 (1+2*j/
   (
      (
         (-j*2*pi*F*rho/
            (loss*visc)
         )^0.5
      )*diam/2
   )
)
)^0.5
```

Fig. 17, Definition of gamma

```
.define zwl1

rho*speed/(pi*(diam/2)^2)*
(1-2*j*(kappa-1)/
      (
         (-j*2*pi*F*rho*prandtl/
            (loss*visc)
         )^0.5
      )*diam/2
/
      (1+2*j/
         (
            (-j*2*pi*F*rho/
               (loss*visc)
            )^0.5
         )*diam/2
      )
)^0.5
```

Fig. 18, Definition of zwl1

[4] E. Moers, J. Kergomard: On the Cutoff Frequency of Clarinet-Like Instruments. Geometrical versus Acoustical Regularity, Acta Acustica united with Acustica, Vol. 97 (2011) 984 – 996

[5] Keefe, Douglas: Woodwind air column models, Journal of the Acoustical Society of America, 88 (1990), 35 -51

[6] Nederveen, C.J. et. al.: Corrections for Woodwind Tone-Hole Calculations, ACUSTICA - Acta Acustica Vol. 84 (1998) 957 – 966

[7] Dalmont, Jean-Pierre et al.: Experimental Determination of the Equivalent Circuit of an Open Side Hole: Linear and Non Linear Behaviour. Acta Acustica united with Acustica, Vol. 88 (2002) 567 – 575

[8] Noreland, Kergomard, Laloë, Vergez, Guillemain, Guilloteau: The Logical Clarinet: Numerical Optimization of the Geometry of Woodwind Instruments. Acta Acustica united with Acustica, Vol. 99 (2013) 615 – 628

COMPARISON OF MOUTHPIECE PRESSURE SIGNAL AND REED BENDING SIGNAL ON CLARINET AND SAXOPHONE

Alex Hofmann[1], *Christoph Reuter*[2]
[1] Institute of Music Acoustics,University of Music and Performing Arts Vienna, Austria
[2] Musicological Institute of the University of Vienna, Austria
hofmann-alex@mdw.ac.at
christoph.reuter@univie.ac.at

ABSTRACT

The clarinet and the saxophone have a similar sound excitation principle. For both instruments, a single reed is mounted to a beak shaped mouthpiece and becomes excited by the player's blowing. Caused by the different shapes of the resonators, the sound of the cylindrical clarinet contains only the odd numbered harmonics, whereas the sound of the conical saxophone contains all members of the harmonic series. Measurements on double reed instruments by Voigt (1975) showed that the closing time of the double reed was constant across all pitches played on the instrument. Consequently, only the offset period was modulated. Characteristic frequency gaps in the spectrum (formants) of an instrument's sound were explained by this specific motion pattern of the oscillator (pulse forming theory, Fricke 1975). Can this theory also be applied to single reed instruments, like the saxophone and the clarinet? For our measurements on a Bb-clarinet and an alto-saxophone, synthetic single-reeds were equipped with strain gauge sensors, to capture the bending of the reed during sound production. A pressure transducer inside the chamber of the mouthpiece tracked the inner mouthpiece pressure. Two professional players performed a chromatic scale over the whole range of the instrument, either on the clarinet or the saxophone. From the reed bending measurements, we calculated the ratio between the opening time and the closing time for each played tone. On the clarinet, this ratio was almost constant for all played tones (M = 0.71, SD = 0.09), whereas on the saxophone these ratios showed larger deviations, but no clear pattern in relation to the played pitch (M = 0.64, SD = 0.44). Closing times for the tones eb', ab' and b' on the saxophone were much shorter than the neighboring pitches. Spectrograms of the reed signal and the mouthpiece pressure signal were calculated for the steady state part of the tones. For the saxophone, both the spectrograms were almost identical, depicting all members of the harmonic series in a decreasing fashion. Against our expectations, we also observed all harmonics in the reed signal of the clarinet, whereas only in the mouthpiece pressure signal merely the odd harmonics appeared. However, these reed bending measurements indicate that the pulse forming theory, which is valid for double reed instruments, can not be transferred to single reed instruments like the clarinet or the saxophone, where the closing time varies with the pitch.

FROM MERSENNE TO ROBARTES: THE TRUMPET, THE TRUMPET MARINE, AND THE DISCOVERY OF THE HARMONIC SERIES

Stewart. Carter
Wake Forest University, United States of America
carter@wfu.edu

ABSTRACT

Because they rely on the harmonic series for all their tones, the trumpet and the trumpet marine were frequently invoked as case studies in early attempts to explain overtones. Marin Mersenne, was the first scholar to describe overtones in any detail, mentioning them initially in Quaestiones celeberrimae in Genesim (1623) and continuing to refine his thoughts on the subject in correspondence he carried on with other scientists. Mersenne convinced his colleagues that he could hear "little delicate sounds" (petits sons delicats) above the fundamental tone (son propre), but he could not explain how they were produced. In his Harmonie universelle (1636) Mersenne described overtones up to the sixth harmonic. He understood the similarities between "trumpet notes" and the tones produced by the trumpet marine, but he failed to recognize a relationship between these notes and overtones. Moreover, he ignored trumpet notes that did not conform to his theory of consonance. My paper reveals how later authors expanded on Mersenne's work. John Wallis' demonstration of nodes in vibrating strings (1677) strongly influenced Francis Robartes' "Discourse on the Musical Notes of the Trumpet and the Trumpet Marine" (1692). Robartes (Roberts) did not set out to elucidate the harmonic series; his modest objective was to explain why the seventh, eleventh, thirteenth, and fourteenth notes of the trumpet are not in tune. He compared the "flageolet tones" of the trumpet marine with the notes of the trumpet and demonstrated mathematically that the four out-of-tune notes cannot be accommodated to just intonation. Without realizing the importance of his discovery, Robartes offered the most cogent demonstration of the harmonic series prior to that of Joseph Sauveur (1701).

TRUMPET MUTE PITCH: AN ANALYSIS OF THREE HISTORIC MUTES

Sabine K. Klaus

Joe R. and Joella F. Utley Curator of Brass Instruments
National Music Museum, The University of South Dakota
Vermillion, SD 57069 USA
sabinekklaus@gmail.com

Robert W. Pyle

11 Holworthy Place
Cambridge, MA 02138 USA
rpyle@post.harvard.edu

ABSTRACT

Musical scores and historic writings from Claudio Monteverdis *Orpheo* to Ernst Johann Altenburgs treatise on trumpet playing mention that mutes of the baroque era raised the pitch of the trumpet by a whole tone. On the other hand, playing experiments with surviving trumpet mutes generally show a rise in pitch of only approximately a semitone. This conundrum remains unsolved.

In this paper we use data from acoustical measurements of three late eighteenth-century historic trumpet mutes, formerly associated with trumpets by the Viennese maker Anton Kerner (1726-1806), now in the Utley Collection at the National Music Museum. These mutes have been measured with trumpets by Johann Leonhard Ehe II and III (ca. 1710 and 1730) and a reproduction of a trumpet by Hanns Hainlein from 1632 in the same collection. In addition we will discuss the acoustical behavior of a differently-shaped mute developed by the late Ralph Bryant for copies of the 1632 Hainlein trumpet.

1. INTRODUCTION

In an earlier paper [1], one of the authors (Pyle) used a computational model to calculate the pitch rise produced by a mute in a baroque trumpet. The hypothesis tested was that the shape of earlier conical Renaissance trumpet bells with a wider throat allowed the same mute to be inserted further into the bell, hence shortening the air-column length more than in later baroque trumpets with narrower throat and wider final flare. The computation was based on measurements of trumpets by Hanns Hainlein from 1632 and Johann Leonhard Ehe III from 1746. The conclusion was that the mute raised the pitch by approximately a semitone in the Ehe trumpet, and more than a semitone but much less than a whole tone in the Hainlein. The computation left the question unresolved and therefore experimental measurements were desirable.

There was a considerable variation in bell contours between earlier and later trumpets. Rarely does a natural trumpet survive with its unambiguously matching mute, but only this kind of match would definitely indicate by how much a specific mute raises the pitch of a particular trumpet. The spectrum of trumpet-bell shapes during the seventeenth and eighteenth century falls into two extremes. The bell type of the renaissance and early baroque trumpet, as exemplified by the Hainlein, has a wide throat and almost conical bell with very little flare. Later baroque trumpets, such as those by the Ehe family, have a much narrower bell throat and much wider final flare. See Figure 1.

Surviving mutes, such as those shown in Figure 2, show an even greater variety of shapes [2]. The leftmost mute appears built so that either end can be inserted into the bell. The two ends have somewhat different tapers, indicating that it might have been made to fit two slightly different bell contours.

Figure 1: The three trumpets tested. From left to right, Johann Leonhard Ehe II (ca. 1710), Johann Leonhard Ehe III (ca. 1725-30), and Hanns Hainlein (1632, copy by Joe Utley).

This paper focuses on three mutes, formerly in the possession of Dr. Gerhard Stradner in Vienna, that are now part of the Utley Collection at the National Museum Museum in Vermillion.

The three historic mutes were formerly associated with a trumpet by Anton Kerner (1726-1806) in Vienna; however, their actual date is difficult to determine. Expertly turned from fruitwood (likely plum), they show the skills of an experienced turner. All three are basically identical in shape, although they vary slightly in workmanship. The external shape is more sophisticated than that of any of the Prague or Nuremberg mutes. The pear-shaped curvature allows a snug fit with the flare of a specific trumpets.

CT scans, such as that in Figure 4, show that BA-102 is the crispest, because it was turned from the hardest wood section the turner had at his disposal; therefore this exemplar was used for the testing described below. BA-101 has extensive woodworm damage and therefore leaks, while BA-097 is made of a wood section of slightly lesser density and therefore the turning is not as regular as that of BA-102. The backbore is carefully shaped and flaring, changing from hyperbolic to slightly flaring. BA-097 is interesting for its remains of a tied-on brass wire.

A comparison of the bell profiles of these instruments with the external shape of the mute (Figure 5) shows how it fits into these trumpets: the mute BA-102 is a near-perfect match for the Ehe II trumpet, NMM 7250. It also fits quite well into the trumpet by his nephew Ehe III, NMM 7160. BA-102 fits rather less well into the bell of the Hainlein trumpet copy, and at the same time it can be inserted much further into this instrument.

Figure 2: Baroque trumpet mutes in the National Museum of Prague [2].

Figure 3: Three mutes formerly associated with a trumpet by Anton Kerner (1726-1806). Date unknown. From left to right, BA-102, BA-101, and BA-097.

Perhaps this was the reason why one of the three mutes has a brass wire tied to it. The wire might have served to anchor a leather strap, by which the mute could be pulled out of a trumpet into which it disappeared.

The best mute among the three historic ones in the Utley Collection, BA-102, was selected to be tested with the three trumpets shown in Figure 1.

2. EXPERIMENTAL METHODS

The BIAS apparatus developed at the Institut für Wiener Klangstil was used to measure the input impedance and impulse response of the trumpets with bell open and with the mute inserted. The mutes alone (BA-102 and the Bryant mute) were also measured.

After some three centuries, it is not surprising that the cross sections of the bells on the Ehe trumpets were no longer exactly circular. The mute did not fit snugly into the bells, and consequently there was considerable air leakage between mute and bell. The outside of the mute was therefore wrapped with a cloth to form a reasonably airtight seal between the mute and the bell. This also meant that the mute could not be inserted quite as far into the bell as originally intended.

Although the bell cross section of the Hainlein copy was more accurately circular, mute BA-102, even with the cloth,

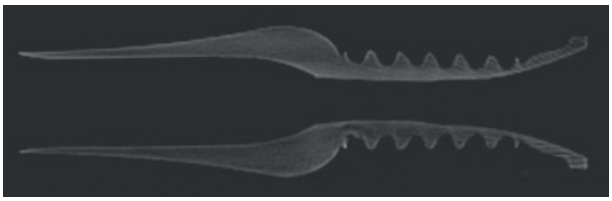

Figure 4: Computer tomography scan of mute BA-102.

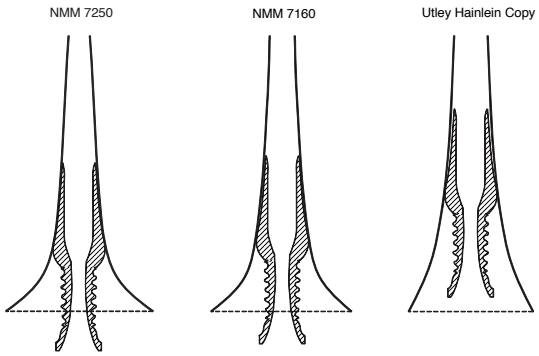

Figure 5: Profiles of mute BA-102 inserted into three trumpet bells. From left to right, the trumpets are in the same order as in Figure 1. Note the wider bell throat and the smaller flare of the earlier Hainlein trumpet compared with the later Ehe trumpets.

could not be made to seal adequately. A close examination of Figure 5 shows that only the shoulder of the mute touches the bell. Measurement of this trumpet-mute combination was thus abandoned. Instead, a different Hainlein copy, made by one the authors (Klaus), was measured with the Bryant mute that was made especially to fit it.

The acoustic measurements on the Ehe II and Ehe III trumpets were so similar that results will be shown only for the Ehe II.

2.1. Finding the frequency of the pedal tone

In a professional-grade modern valve trumpet, the frequencies of the second and higher impedance peaks closely follow integer multiples of the instrument's pedal tone. (The lowest peak is much flatter than the pedal tone.) The frequency spacing between consecutive peaks can then be used to estimate the fre-

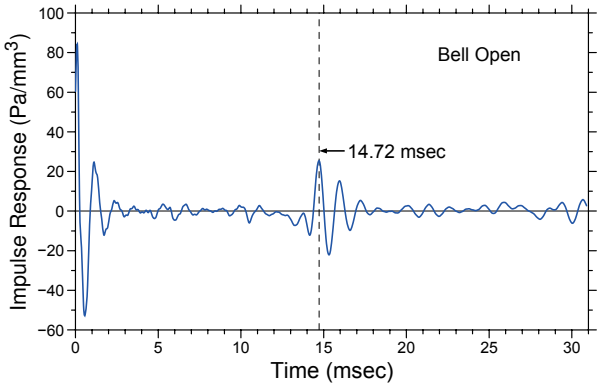

Figure 6: Impulse response of the Ehe II trumpet (NMM 7250).

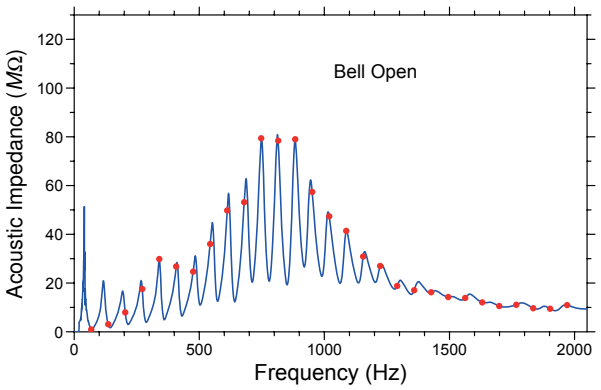

Figure 7: Input impedance of the Ehe II trumpet with the bell open.

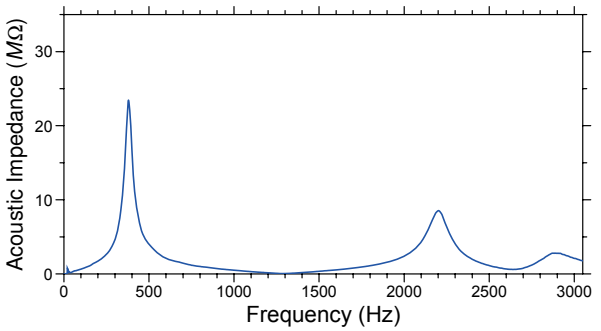

Figure 8: Input impedance of the BA-102 mute.

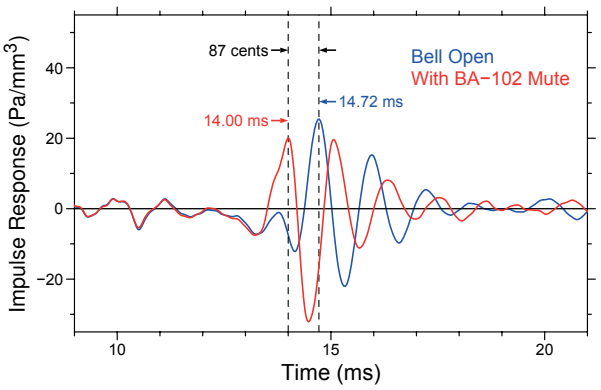

Figure 9: Expanded view of the principal reflection in the impulse response of the Ehe II trumpet, with bell open and with the BA-102 mute.

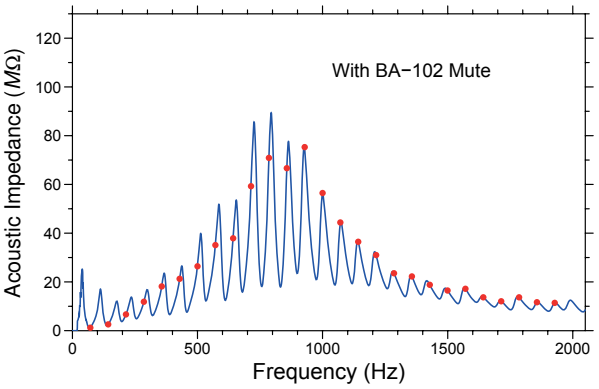

Figure 10: Input impedance of the Ehe II trumpet with BA-102 mute inserted (with cloth wrapping).

quency of the pedal tone. This was not the case with the baroque trumpets examined here. The spacing between peaks was much less uniform than on the modern trumpet. Therefore, the impulse response was used to calculate the pedal-tone frequency.

Figure 6 shows the impulse response of the Ehe II trumpet. The time of the largest positive response following the initial ringing of the mouthpiece is taken to be the period of the pedal-tone frequency. In this case, the period of 14.72 msec corresponds to a pedal-tone frequency of close to 68 Hz, or a tuning frequency of A4 = 408 Hz for a trumpet in D.

Figure 7 shows the input impedance of the Ehe II trumpet with dots placed on the impedance curve at harmonics of the pedal tone. The dots lie reasonably close to the impedance peaks except for the lowest three peaks and those above about 1200 Hz (the sixteenth harmonic is 1088 Hz). Note that the height of the impedance peaks diminishes rapidly above 1200 Hz, due to the loss of energy through radiation from the bell.

2.2. Acoustical relatives of the muted baroque trumpet

There are two more-recent forms of muted brass instruments that bear some acoustical similarity to the muted baroque trumpet: the echo cornet and the fully-stopped horn. These have been studied and offer some insight into what might be expected in the present case [3][4][5].

The mute, or echo bell, or the hand, seen from the upstream side within the instrument, looks like a Helmholtz resonator. That is, within the frequency range of interest, it has but a single mass-spring resonance determined by the compliance of the cup volume (the "spring") and the inertance of the narrow neck (the "mass"). Below the frequency of this resonance, the mute presents a mass-like load to the instrument and lowers its resonance frequencies. Above, the mute looks spring-like, and raises the resonance frequencies. Near the mute resonance, the mute appears to split the nearest unmuted resonance into two, one above and one below the original.

For the mute to raise the pitch consistently throughout the playing range of the instrument, it is then desirable that the mute resonance frequency lie below, or at least in the lower part of, the playing range.

3. EXPERIMENTAL RESULTS

3.1. The Ehe II trumpet with the BA-102 mute

The impedance of the BA-102 mute is shown in Figure 8. As expected, it has only one resonance below 2000 Hz, but that one is just below 400 Hz. This is close to the sixth harmonic of the pedal tone, that is, it is *not* below the playing range. The lesser peaks seen at 2200 and 2900 Hz arise from standing waves in the narrow neck.

Figure 9 shows the effect of the mute on the impulse response of the Ehe II. There are two reflections of nearly equal amplitude, neither as tall as the principal peak for the open bell. The earlier peak is the larger. Taking its time as the period of the muted pedal tone, the pedal tone frequency moves from 67.9 Hz to 71.4 Hz, a pitch rise of 87 cents.

The impedance of the muted trumpet, Figure 10, shows that

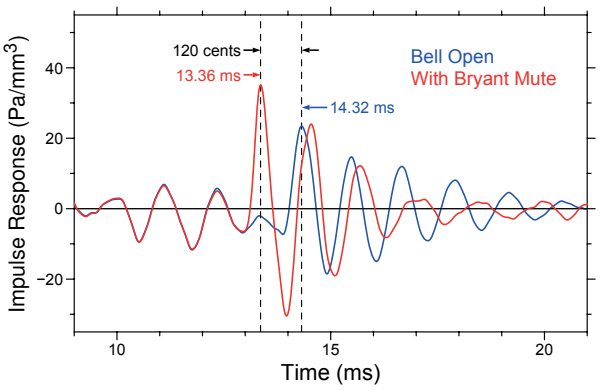

Figure 11: Expanded view of the principal reflection in the impulse response of the Hainlein trumpet copy, with bell open and with the Bryant mute.

below about 900 Hz, the impedance peaks do not lie as close to harmonics of the pedal tone as for the unmuted trumpet. Above 900 Hz, they agree almost exactly. With radiation losses reduced by the mute, the impedance shows small but quite distinct peaks well beyond the 1200 Hz "cutoff" of the open bell.

3.2. The Hainlein trumpet copy with the Bryant mute

The interior contour of the Bryant mute differs greatly from that of BA-102. The cup volume is a little smaller, but this is outweighed by the much narrower and longer throat through the neck. The result is that the Bryant's Helmholtz resonance frequency is 200 Hz, nearly an octave below that of BA-102. The mute was custom-made to fit the Hainlein bell, and has a cork ring that makes a fully airtight seal with the bell.

Figure 11 (corresponding to Figure 9 for the Ehe II trumpet) shows the principal reflection in the impulse response. The reflection with the mute inserted has nearly the same shape as the reflection with the bell open, but it is larger and, of course, occurs at an earlier time. The calculated pitch rise in this case is 120 cents, substantially greater than for the Ehe II trumpet, but still well short of a whole tone.

Figures 12 and 13 show the input impedance with the bell open and muted, respectively. For the muted trumpet, the lower harmonics of the pedal tone lie much closer to the impedance peaks than was the case for the Ehe II.

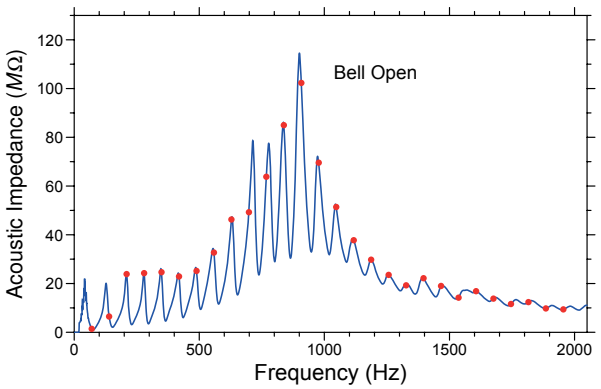

Figure 12: Input impedance of the Hainlein trumpet copy with the bell open.

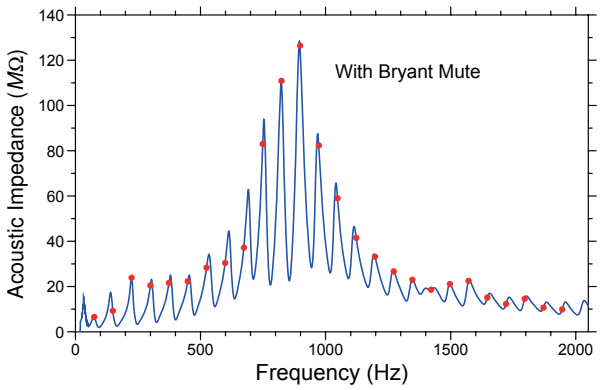

Figure 13: Input impedance of the Hainlein trumpet copy with the Bryant mute.

4. DISCUSSION

The present experiment seems only to have confirmed the computational model of Reference [1]. No combination of trumpet and mute that was tested came close to a pitch rise of a whole tone. Why did the historic mute BA-102 combined with the Ehe II trumpet yield a calculated pitch rise of less than a semitone? The cloth that was necessary to seal the mute to the bell flattened the pitch by reducing the distance that the mute could be inserted into the bell, but probably not enough to account for the shortfall of 12 or 13 cents. The three historic mutes are so close to each other dimensionally that their design must have met the needs of their day, presumably raising the pitch a semitone on the trumpet for which they were designed.

BIAS measurements made on the Ehe II trumpet without the cloth wrapping around the mute were clearly suspect. It was difficult to obtain consistent results, and both impedance and impulse response looked implausible. It is clear that the mute should fit tightly into the bell, minimizing or eliminating any leakage of air past the outside of the mute. Thus the exterior contour of the mute should match the interior contour of the bell as closely as possible.

In another paper at Vienna Talk 2015, Dr. Gerhard Stradner presented a new hypothesis to expain the absence of historic whole-tone mutes.

References

[1] R. Pyle, "A Computational Model of the Baroque Trumpet and Mute", *Historic Brass Society Journal*, vol. 3, pp. 79-97, 1991.

[2] J. Keller, "Antique Trumpet Mutes", *Historic Brass Society Journal*, vol. 2, pp. 97-103, 1990.

[3] Robert W. Pyle and Sabine K. Klaus, "The acoustics of the echo cornet," *J. Acoust. Soc. Am.*, vol. 112, p. 2211, 2002.

[4] Robert W. Pyle, "Pitch Change of the Stopped French Horn," *J. Acoust. Soc. Am.*, vol. 36, p. 1025, 1964.

[5] Robert Pyle, "Factitious Tones and Hand-Stopping," *The Horn Call*, Vol. XXI no. 1, pp. 36-43, October 1990

[6] Gerhard Stradner, "Transposing Mutes for Trumpets", in *Proceedings of Vienna Talk 2015*, Vienna, Austria, 2015.

TRANSPOSING MUTES FOR TRUMPETS

Gerhard Stradner
(Translation: Edward H. Tarr)

Vienna, Austria
gerhard.stradner@gmail.com

ABSTRACT

The main question with regard to early trumpet mutes concerns their transposing interval: Do they raise the pitch by a half-step or a whole step? Modern reference books offer the unsatisfactory answer that both transpositions are possible. Surviving mutes raise the pitch by a half-step, but theoretical and musical sources from the seventeenth and eighteenth centuries specify a whole step.

I began my research by comparing surviving mutes, many of which were tested acoustically by Hannes Vereecke with original trumpets, using the *Brass Instrument Analyzing System* (*BIAS*). No mute could be found that raised the instrument's pitch by a whole step, so the research was abandoned.

In an effort to solve this problem I read the relevant treatises again, comparing them with music for muted trumpets and evaluating this information in light of performance-practices of the time. The most important consideration here is the necessity for trumpeters to move from *Chorton* to *Cammerton* by exchanging bows of different sizes, and also to adjust the mutes when they are used with different bows in order to play in tune in several different keys. It can be shown that upward transposition of a whole tone is the best solution for all situations. All surviving mutes can be used for transposing up a whole step by removing a half-tone-bow (mute minus halftone-bow = two half-steps = whole step up). The variable difference between *Chorton* and *Cammerton* of a half-step to a minor third always accommodates this procedure.

Many of the remarks on mutes on Altenburg's *Versuch* (1795) are incorrect; perhaps he simply copied his information from earlier books. In any case, it appears that a mute for upward transposition by a whole step did not exist during the heyday of the natural trumpet.

1. DISCUSSION

"Do old trumpet mutes transpose the pitch a half or a whole tone higher?" This is the central question which many musicians pose in connection with this issue. In music lexica we read answers such as: "The wooden mutes of olden times raised the pitch by one or two half tones."[1] How did it come to this unsatisfactory statement?

1. Written and printed sources[2] and music[3] all speak of whole-tone transposition. However, no whole-tone transposing mute has ever been found.
2. All surviving transposing mutes raise the pitch by approximately half a tone.[4] No written or published source, however, mentions half-tone transposition. Nevertheless, the music shows the possibility of using existing mutes for half-tone transposition.[5]

Up until now these absurdities and contradictions could not be explained or solved,[6] and one article even speaks of a mystery.[7] A recent attempt at a solution has appeared in the form of a particularly long mute which in fact does transpose a whole step upwards.[8] The question arises, however, as to whether such mutes ever existed.

The present article dealing with the solution of the above-mentioned problems will consider pitch ratios as well as tuning practice, leading to a hypothesis which will be verified – i.e. confirmed or investigated as to its accuracy – towards the end.

"All transposing trumpet mutes raise the pitch by half a tone. With them, when playing together with other instruments, a whole-tone transposition upwards could be effectuated by simultaneously removing a half-tone crook. There were no special whole-tone transposing mutes."

When a trumpet is playing alone or in a trumpet ensemble, the extent of the pitch rise caused by the mute is irrelevant, because all performers are equally affected. The pitch rise consists of half a step, a fact which is later confirmed and, additionally to

[1] Riemann Musik Lexikon, Sachteil (Mainz 1976), "Dämpfer", 194.

[2] Daniel Speer, Grundrichtiger Unterricht … (Ulm 1697), 219; Johann Mattheson, Das Neu-Eröffnete Orchestre (Hamburg 1713), 266; Johann Mattheson, Exemplarische Organisten-Probe (Hamburg 1719), 63; Johann Mattheson, Critica Musica (Hamburg 1722); Johann Mattheson, Der vollkommene Capellmeister (Hamburg 1739), 461; Johann Heinrich Zedler, Grosses Universal Lexikon … (Leipzig 1731-1754), Bd. 38 (1743), 524, Bd. 39 (1744), 478, 524; Joseph Majer, Museum Musicum (Schwäbisch Hall 1732), 40; Johann Philipp Eisel, Musicus autodidaktos … (Erfurt 1738), 92; Johann Gottfried Walther, Musikalisches Lexikon … (Leipzig 1732), 571, 610; Johann Ernst Altenburg, Versuch einer Anleitung zur heroisch-musikalischen Trompeter- und Pauker-Kunst … (Halle 1795), 75, 85, 86, 109, 110, 111; Heinrich Christoph Koch, Musikalisches Lexikon (Frankfurt am Main 1802), 1605, 1606; Edward Tarr, Johann Ernst Altenburg, Essay on an Introduction to the Heroic and Musical Trumpeters' and Kettledrummers' Art (1795), Engl. transl. with preface (Nashville 1974). If these treatises mention a "Thon" or "Ton", a whole step is always meant.

[3] They will be presented during the course of this article.

[4] We will comment on this later.

[5] This issue, too, will be commented on later.

[6] Christian Friedrich Daniel Schubart, Ideen zu einer Ästhetik der Tonkunst (Vienna 1806), 310; Gustav Schilling, Enzyklopädie der gesammten musikalischen Wissenschaften.… 2 (Stuttgart 1845), 356, "Dämpfer"; Hermann Eichborn, Das alte Clarinblasen auf Trompeten (Leipzig 1891), 96; Wolfgang Osthoff, "Trombe Sordine", Archiv für Musikwissenschaft 13 (1956), 77-95; Andrew McCredie, Instrumentarium und Instrumentation in the North German Baroque Opera (Hamburg 1964), 78; Don Smithers, The Music & History of the Baroque Trumpet before 1721 (London 1973); Detlef Altenburg, Untersuchungen zur Geschichte der Trompete im Zeitalter der Clarinblaskunst, 3 vols. (Regensburg 1973); Robert Pyle Jr., "A Computational Model of the Baroque Trumpet and Mute", HBSJ 3 (1991), 79-97; Tom Crown, "Antique Trumpet Mutes", HBSJ 3 (1991), 263-264; Peter Downey, "More on Mutes", HBSJ 3 (1991), 264-268; Jeffrey Nussbaum, "Baroque Trumpet Mutes", HBSJ 3 (1991), 260; Don Smithers, "Antique Trumpet Mutes: A retrospective Commentary", HBSJ 10 (1998), 103-111.

[7] Tom Crown, loc. cit. – see footnote 6.

[8] Developed by Ralph Bryant and Friedemann Immer. See also FN 37.

the muting effect, results in playing in a tonality felt to be strange.[9] This characteristic distinguishes trumpet mutes from those used by bowed instruments.[10]

During the course of our acoustical survey of surviving trumpet mutes, one particular specimen stood out, because the accompanying instrument also survives.[11] The pitch rise amounts to exactly half a tone. Other late Baroque mutes in private and public Austrian collections,[12] when combined with surviving original instruments from the same time period,[13] all yield a pitch rise of approximately half a tone.[14] Similar dimensions of further existing mutes[15] allow the conclusion that all surviving mutes from the seventeenth and eighteenth centuries raised the pitch by half a tone. Mutes from the early Baroque period have not yet been discussed; we will deal with them later.

In general, trumpets were tuned to choir pitch.[16] During the course of time this pitch was subject to only the slightest of fluctuations. Stringed and woodwind instruments, on the other hand, were tuned to low chamber pitch. During the seventeenth century this was approximately a minor third lower than choir pitch, but with time it gradually became higher, so that at the end of the eighteenth century it was only about half a tone lower. Therefore, when performing together with other instruments, trumpeters had to adapt to the prevailing chamber pitch by lengthening their instruments, adding crooks or tuning bits. The use of crooks is described in many sources, often close to data about mutes.[17] Even though the subtraction of crooks as a contrary measure to their application is hardly ever mentioned, it is a matter of course in connection with tuning.[18]

Whenever trumpet mutes were required, trumpeters were compelled to re-tune. At least theoretically, muted trumpets could be tuned to any desired higher or lower interval by manipulation of its crooks and bits. It was thus necessary to find a connecting note from the scale of the instruments sounding in chamber pitch, a note that would make sense both for these instruments and for the trumpets. Tuning down would bring the following disadvantages:

1. The typical rise in pitch due to the mutes would be abolished.
2. Extra crooks normally did not exist.
3. Adding further crooks would make the trumpet's response less stable than before, because the instrument with many crooks would tend to wiggle.
4. The longer air passage would result proportionally in a narrower bore.

These arguments also applied to re-tuning to chamber pitch by adding a half-tone crook.[19] A higher pitch therefore presented itself by the removal of a crook. An obvious solution would seem to be an adaptation to the higher fourth or fifth of the chamber pitch. Such transpositions, however, could not be carried out for the following two reasons:

1. The trumpets would dispose of too few crooks to be removed.
2. For the other instruments many notes would become unplayable, since they would go beyond their pitch range.

For these reasons, a whole-tone upward transposition was the only option. A half-tone crook was thereby removed from the trumpets. Because of the insertion of the mute, the instrument's pitch had already been raised by half a tone, so that with the removal of such a crook a whole-tone upward transposition was finally effectuated. Hence the resulting formula: trumpet + mute – half-tone crook = two half-tones higher = one whole tone higher. Such a reduction of crooks was always possible, since

[9] Today the half-tone step is not unusual. In the Baroque period we find only the whole-tone step.

[10] Gustav Johann Petri, Anleitung zur praktischen Musik (Leipzig 1782), 383.

[11] Both the trumpet and the mute come from the period around 1800; they were found in the church of Dietmanns near Gmünd, northern Waldviertel, Lower Austria. They are now in the Kunsthistorisches Museum Vienna, inv. no. SAM 825 and 824; see Gerhard Stradner, Die Klangwelt Mozarts (Vienna 1991), no. 212, ill. 19 and 53.

[12] Seven of these mutes come from Austria and one from south Germany: National Music Museum BA 0097, 0101 and 0102; from the collection of Nikolaus Harnoncourt, four mutes; Musikinstrumenten-Museum Schloss Kremsegg, inv. no. PIZ 041. See G. Stradner, op. cit., nos. 21 -215 and ill. 46; Sabine Klaus, "Historical Instrument Window", International Trumpet Guild Journal 36/2 (January 2012), 65.

[13] The trumpets combined with mutes come from Germany and Austria: Friedrich Ehe (Nuremberg 1750), Johann Wilhelm Haas (Nuremberg), Wolf Magnus Ehe (Nuremberg), Leonhard Ehe (Nuremberg) (all from the collection of N. Harnoncourt); Carl Starzer (Vienna c. 1770) and Joseph Huschauer (Vienna 1806) (both from the Museum Schloss Kremsegg). See G. Stradner, op. cit., nos. 209-211 and ill. 53.

[14] Since the trumpets belonging to them are not known, various bell profiles yield different pitches. All objects were tested acoustically by Hannes Vereecke with using the Brass Instrument Analyzing System (BIAS).

[15] Trumpet mutes not mentioned up to now are found in the following collections, among others: Nationalmusuem Prague (18); Kunsthistorisches Museum Vienna, Sammlung alter Musikinstrumente (5); Germanisches Nationalmuseum Nuremberg (2); Musikmuseum Basel (1); Reichsstadt Museum Rothenburg ob der Tauber (1). See Jindrich Keller, "Alte Trompetendämpfer", Glareana 18/1 (1969), 2-9 (Keller is mistaken, when he indicates that all Prague mutes raise the pitch a whole step); see G. Stradner, op. cit., no. 213 and ill. 8; Konrad Ruhland, Musikinstrumente aus Oberbayern vom 17. bis 19. Jahrhundert, Stadtmuseum Deggendorf (Deggendorf 1993), 151; Dieter Krickeberg & Klaus Martius, "Two trumpet mutes recently acquired by the Germanisches Nationalmuseum Nuremberg", HBSJ 6 (1994), 394-354; Jindrich Keller, "Antique Trumpet Mutes", HBSJ 6 (1998), 97-103.

[16] If we use today's pitch as a point of departure, then choir pitch was approximately a half step higher. Concerning the various pitches, see J. E. Altenburg, op.cit., 84; Gerhard Stradner, "Zur Stimmtonhöhe der Blasinstrumente zur Zeit Joseph Haydns", in: Joseph Haydn (Munich 1986), 81-86; Gerhard Stradner, "The Evolution of Pitch of Cornetts and Trombones at the Time of Schein and Buxtehude", in: Dietrich Buxtehude and Hermann Schein (Saskatchewan 1987), 106-110; Gerhard Stradner, "Stimmtonhöhe, Tonarten und Klangcharakter", in: G. Stradner, op. cit. in FN 11, 109-120; Bruce Haynes, A History of Performing Pitch (Lanham, Maryland, and Oxford 2002).

[17] Michael Praetorius, Theatrum Instrumentorum (Wolfenbüttel 1620), VIII (four illustrations of lengthening pieces); Daniel Speer, Grundrichtiger Unterricht … (Ulm 1697), 219; Joseph Majer, Museum Musicum (Schwäbisch Hall 1732), 40f.; Johann Gottfried Walther, Musikalisches Lexikon … (Leipzig 1732), 572, 619; Johann Heinrich Zedler, Grosses Universal Lexikon …, Bd. 38 (Leipzig 1743), 524; Johann Philipp Eisel, Musicus autodidaktos … (Erfurt 1738), 92; Johann Ernst Altenburg, Versuch einer Anleitung zur heroisch-musikalischen Trompeter- und Pauker-Kunst … (Halle 1795), 84 f.; Heinrich Christoph Koch, Musikalisches Lexikon (Frankfurt am Main 1802), 884, 1602 f., 1605 f. Koch, to be sure, was aware of J. E. Altenburg's book, but did not take over his opinion about whole-tone mutes.

[18] Because of the variances in pitch, the tuning possibilities during the Baroque period were more complicated than today, where only a small pitch correction is required.

[19] John Henry van der Meer supposes that the simultanous use of a mute plus a half-step crook results in echo effects. See John Henry van der Meer, Johannn Josef Fux als Opernkomponist (Bilhoven 1961), vol. 3, 183; Dagmar Glüxam, Instrumentarium und Instrumentalstil in der Wiener Hofoper zwischen 1705 und 1740 (Tutzing 2006), 558, FN 2576.

the trumpeters had previously adapted to chamber pitch and thus had at least one half-step crook at their disposal.[20]

The trumpet was thus raised in pitch by a whole step when a mute was inserted and simultaneously a half-step crook was removed. The removal of a crook belonged to the process of tuning, was thus regarded as self-evident, and was therefore not mentioned in treatises. Trumpeters became especially conscious of the rise in pitch with the insertion of a mute when they were to perform in chamber pitch and this fact compelled them to tune anew.[21] Because of this the mute was attributed the capability of raising the pitch by a whole tone. Mutes therefore are qualified for transposition a whole tone higher, as we can read in many treatises[22] and pieces of music.[23]

If trumpets already tuned to chamber pitch were in use during the eighteenth century, muting could be accomplished in a similar way: one took a trumpet pitched a whole step higher,[24] added simultaneously a mute and a half-step crook,[25] thus accomplishing both the transposition and the muting.

If mutes were inserted into a trumpet without any further tuning, a half-tone upward transposition resulted. Although this fact is not mentioned in any source, it could be utilized in practice, for example in the *Sonata Mortuorum à 5* by Johann Georg Linike.[26] Here we assume a chamber pitch lying a whole step below choir pitch. Trumpets in choir pitch are in C will be in D in chamber pitch. If that work is to be performed in E-flat (chamber pitch), it would suffice to insert a mute into the trumpets when asked for.[27]

The previous conclusions were drawn from surviving late Baroque mutes. Early Baroque trumpets had a wider bell throat and correspondingly thicker mutes, as can be seen from the earliest pictorial representation of trumpet and mute by Marin Mersenne.[28] Early Baroque pieces of music, such as *L'Orfeo* (1607) by Claudio Monteverdi,[29] allow us to conclude that mutes from that period displayed the same transposing properties as surviving later ones. They raised the pitch by half a tone, and by removing a half-tone crook a whole-step upward transposition was effectuated.

Johann Ernst Altenburg was in 1795 the first to write an extremely detailed treatise about trumpet-playing.[30] His models were books by Johann Joachim Quantz,[31] Carl Philipp Emanuel Bach,[32] and Leopold Mozart.[33] He succeeded in presenting a logical sequence of ideas, whereby, as far as mutes are concerned, his starting point was a false assumption.[34] Apparently he was not familiar with existing mutes and their use, deriving his information simply from statements printed in other books. He interpreted them literally and came to the conclusion that a mute raised the pitch of a trumpet by a whole step. He wrote: "when it is inserted underneath into the trumpet, it not only gives the trumpet a completely different, almost oboe-like tone, but it also raises it [in pitch] by a whole tone …"[35] Altenburg was the first to write clearly about whole-tone mutes. Because of his false assumption he prepared the erroneous way that many later authors followed, searching in vain for a single example of this kind of mute.[35/36]

In this connection, the following attempt seems to guarantee success. We insert one of the surviving late Baroque mutes into the wide bell of an early Baroque trumpet. Because of its slim diameter it fits very far into the instrument. Because of the considerable shortening of the windway, the transposition interval was more than half a tone. This situation shows the way to make a mute that fits far enough into the trumpet to result in a whole-tone transposition. Such whole-tone mutes are offered by Annegret Schaub.[37] The question remains, however, as to whether such mutes ever existed. The following arguments speak against the existence of a historical whole-tone mute and also show why there never was any demand for the production of such a mute. They furthermore support the hypothesis established at the beginning about mutes and their incapability for whole-tone transposition:

1. With normal mutes the pitch could be preserved by the addition of a half-tone crook. This was not mentioned by

[20] As explained above, to lower trumpets from choir to chamber pitch, into the instruments crooks had been inserted that lowered the pitch between a minor third and a half step, dependent on the chamber pitch.

[21] If mutes were used in the trumpet ensemble or for solo playing, this process did not apply.

[22] For example, Daniel Speer wrote: "so gebrauche man sich eines Sertins, … so lautet es um einen Thon höher …" ("if one uses a mute, … then it sounds a whole step higher"). See D. Speer, Grundrichtiger Unterricht … (Ulm 1697), 219.

[23] For example, Pavel Josef Vejvanovský (1633-1693), Sonata Sancti Mauritii à 7. This work begins for the unmuted trumpets in C Major. After twelve bars pause mutes are called for, and then the trumpets sound in D Major. After further 24 bars the mutes are removed for playing again in C Major. Thus there is enough time for changing mutes and crooks. See also Maurizio Cazzati, Sonata La Cappara à 5, Op. 35/10; Dietrich Buxtehude (1637-1707), Ihr Christen, freut euch nun; Buxtehude, Auf! Stimmet die Saiten; Georg Philipp Telemann (1681-1767), Trauerkantate auf das Ableben Friedrich August II. von Sachsen und Pohlen (1737).

[24] J. E. Altenburg refers to trumpets in various pitches. See Altenburg, op. cit., 85.

[25] Mutes and half-step crooks used together cancelled the transposition effect.

[26] Johann Georg Linike, Sonata Mortuorum à 5 (1737).

[27] This procedure also functions when a different chamber pitch is involved.

[28] Marin Mersenne, Harmonie universelle (Paris 1636), XX, fig. 56. The representation also shows that the thick mute inserted into the wide bell throat is located more or less in the same place as with thinner mutes in later trumpets.

[29] Claudio Monteverdi (1567-1643), L´Orfeo, 1607. His instruction for the performance of the introductory toccata reads: "Toccata / che si suona avanti il levar de la tela tre volte con tutti li stromenti / & si fa un tuono più alto volendo sonar le trombe con le sordine." (English translation: "Toccata which is sounded beofre the raising of the curtain three times with all the instruments, and it is performed a whole step higher if one wishes the trumpets to be played with mutes.")

[30] Both earlier trumpet treatises, by Cesare Bendinelli (1614) and Girolamo Fantini (1638), were methods that went into much less detail. See J. E. Altenburg, op. cit.

[31] Johann Joachim Quantz, Versuch einer Anweisung die Flöte traversiere zu spielen (Berlin 1752).

[32] Carl Philipp Emanuel Bach, Versuch über die wahre Art das Clavier zu spielen (Berlin 1753).

[33] Leopold Mozart, Gründliche Violinschule … (Augsburg 1756).

[34] J. E. Altenburg, op. cit., 86-87. Lars Laubhold has investigated Altenburg's treatise critically, thereby pointing out several absurdities, also in connection with trumpet mutes: Lars Laubhold, Magie der Macht (Würzburg 2009), 53; see Edward Tarr's review thereof in HBSJ 21 (2009), 115-118.

[35] Original text: " … wenn es … unten in die Trompete gesteckt wird, so giebt es ihr nicht nur einen ganz andern, fast einer Oboe ähnlichen Klang, sondern erhöhet ihn … auch um einen ganzen Thon." J. E. Altenburg, op. cit., 86. See also: „Aus meines Herzensgrunde" 110, 111.

[36] See the numerous articles mentioned in FN 6, and especially FN 22 with a quote from Daniel Speer. Actually Altenburg quoted on p. 87 from the first edition of Johann Mattheson's [Exemplarische] Organisten-Probe (Hamburg 1719), 63, where the change of pitch through muting goes from C to D, or from D to E, although the exact relationship of these keys to each other differed slightly because a kind of unequal temperament was in use.

[37] These mutes were developed together with Ralph Bryant after a suggestion made by Friedemann Immer. See FN 8.

the theorists. The surviving mutes transposed half a step upwards, a fact they also did not mention. On the other hand, they often spoke of transposition a whole step upwards. As we have shown, this was effectuated through crook reduction. Mutes, then, were a universal tool, by means of which – together with suitable crook manipulation – it was possible to transpose various intervals upwards or even downwards.

2. One needed no special whole-tone mute, since it was already possible to tune a whole step higher with existing mutes.[38]
3. It is not comprehensible that the surviving mutes could be said to be used only for half-step transposition.
4. Most musical instruments have the possibility of pitch correction. Why should this not have applied as well to muted trumpets, since for them via crook reduction whole-tone transposition is possible?
5. Throughout historical developments we cannot recognize any occasion that would have called for an alteration of the mute type.[39]
6. Why are hints about whole-tone mutes missing before J. E. Altenburg's treatise?
7. Numerous mutes survive, but among them there is not a single whole-tone mute. It is highly unlikely that they existed but that all of them were lost.
8. We can expect a normal mute to produce a better sound than a whole-tone mute, because when the half-tone crook is removed, the trumpet's bore comes closer to its standard size.

When we take all these arguments into account, it appears unlikely that a whole-tone transposing mute had ever existed. Therefore the hypothesis offered at the beginning will be sufficiently confirmed, and the solution reads:

There existed only one kind of transposing mute with which it was possible to tune a whole step upwards. It was actually a half-tone mute, but because of the accompanying crook reduction it achieved the function of whole-tone transposition.

The mystery of trumpet mutes has finally disappeared.

[38] This applies to any tool, which is only then requested and used when it is needed.

[39] With this we mean the presence of both kinds of mute, either at different times or simultaneously.

I would like to thank Edward Tarr for his helpful advice.

REFINING THE NARRATIVE OF ANTON WEIDINGER'S PROTOTYPE KEYED TRUMPET

Bryan Proksch
Lamar University, United States of America
bproksch@lamar.edu

ABSTRACT

Viennese trumpeter Anton Weidinger (1766–1852) was the first to develop a fully chromatic trumpet in the guise of his revolutionary keyed instrument, and as such stands as a pivotal figure bridging the gap between the natural trumpet and the modern valve trumpet. The narrative of his connections with his "close friend" Joseph Haydn before the composition of the 1796 Trumpet Concerto (based purely on a family anecdote dating to 1907) and of the invention itself (especially that a functional prototype existed in 1796) do not, however, stand up to close scrutiny. The curious delay between Haydn's composition and its 1800 premiere combined with the chronological inconsistencies between Weidinger's arrival in Vienna in 1792 and Haydn's absences during his two London journeys (in 1792–93 and 1794–96) are significant irregularities that have been overlooked in the scholarly literature. My paper will use surviving works for Weidinger's keyed trumpet by Leopold Koželuch (1798) and Joseph Weigl, Jr. (1799) together with concert reviews and other surviving biographical details to refine the chronology of events that transpired as the chromatic trumpet finally emerged. Replacing the oft-repeated "close friend" narrative, I will make the case that Weigl, Haydn's godson and a composer closely associated with the same Viennese theatres as Weidinger, was potentially the figure who convinced Haydn to undertake the composition. I will argue that when Haydn wrote his Trumpet Concerto in 1796 he had little direct knowledge of Weidinger's invention and that the instrument itself was not developed to the point of being capable of playing the work publicly until ca. 1800. This indicates that Haydn composed a work for an idealized chromatic trumpet not yet in existence and that the work was not tailor-made to be idiomatic to Weidinger's invention.

THE LATE KEYED TRUMPET

Adrian V. Steiger
Bern University of the Arts, Switzerland
adrian.vonsteiger@hkb.bfh.ch

ABSTRACT

The keyed trumpet is the instrument type from the trumpet's transitional era (1750–1850) that has hitherto been best explored (for examples see [1]–[4]). The reason for this wealth of research is the popularity of the trumpet concertos of Haydn and Hummel, both originally composed for Anton Weidinger's keyed trumpet. Statistically, the extant sources draw a contrary picture, however. Weidinger rarely played these concertos and did not pass them on to other players. In fact, we have fewer extant sources for the keyed trumpet (methods, compositions and instruments) than for the other trumpet types such as the invention, stopped and slide trumpets, or for the keyed bugle or ophicleide. Two sources have hitherto remained unknown to scholars, however. They date from the end of the keyed trumpet's use in musical practice (before its 1970s revival) and are the focus of this paper: a nine-keyed trumpet and a 123-page method. The nine-keyed trumpet is signed "Carl Gottl[ob]. Schuster in Neukirchen" and is today held by the Burri Collection in Berne. No other extant trumpet has nine or more keys. Its key touchpieces are organized in two levels, after the manner of a keyboard. The 123-page "Metodo e Studio" for the keyed trumpet was written by the Italian brass player Giuseppe Pignieri. It addresses an unknown type of four-keyed trumpet and includes a large number of studies in all keys. Copies are held by the Biblioteca del Conservatorio di Musica at Milan. They are handwritten by a "copisteria" in Naples. These sources on the one hand serve to underline the basic imperfection of the keyed trumpet, but on the other hand they demonstrate that as late as up to ca. 1840 some musicians and instrument makers believed that innovation might still help to realize the potential of the keyed trumpet.
[1] Dahlqvist, R., The Keyed Trumpet and Its Greatest Virtuoso, Anton Weidinger, The Brass Press, Nashville, 1975. [2] Anzenberger, F., "Method Books for Keyed Trumpet in the 19th Century: An Annotated Bibliography", Historic Brass Society Journal 6, 1994, pp. 1–10. [3] Klaus, S.K., "The Keyed Trumpet", Trumpets and other High Brass, vol. 2, Vermillion, 2013, pp. 158–191. [4] Bacciagaluppi, C., Skamletz, M., editors, Romantic Brass Symposium 1, Proceedings, Bern, 2015 (in press). Papers concerning the keyed trumpet by Dahlqvist, Klaus, Tarr, Egger, Kováts, Rouček, Callmar and v. Steiger.

SCHEDIPHONE: CASE STUDY ON A RARE BRASS INSTRUMENT

Viktor Hruška[1], *Tereza Berdychová-Žůrková*[2]

[1]Musical Acoustics Research Centre, Academy of Perfoming Arts in Prague, Czech Republic
[2]National Museum – Czech Museum of Music, Czech Republic
hruska.viktor@hamu.cz

ABSTRACT

Josef Šediva (Schediwa), a czech instrument maker, invented a family of brass instruments with a distinctive construction that allows a player to switch between waveguides to achieve trombone-like (brighter) or euphonium-like (softer) sound. The case study presents the instrument housed in the Czech Museum of Music as a part of unique collection. In order to document this, feature spectra and radiation characteristics are presented, as well as other general characteristics of brass instruments (profiles of the both horns, input impedance, etc.). The acoustic documentation is supplemented by historical background. The case study presents theses of a future wider study.

1. INTRODUCTION

1.1 The Maker

Josef Šediva (1853-1915, also Schediwa) was born in Semily (north-east Bohemia) as a son of a brass instrument maker. After his apprenticeship Šediva worked for various master craftsmen, probably including well-known Václav František Červený in Hradec Králové (Königgratz). Following the death of his father Šediva's place of residence become Odessa (Russian Empire, now Ukraine). He started an independent enterprise at the latest by 1882. Šediva's business in Odessa evidently prospered because already in the 1880s he opened a branch of his company in Samarkand (now Uzbekistan). His company mostly supplied its instruments to brass bands from the Russian military. It seems to have been dissolved during the October Revolution of 1917, two years after its founder's death. [1, 2]

Figure 1: Josef Šediva (1853–1915), an undated photograph. (© National Museum – Czech Museum of Music)

1.2 The Instrument

Šediva, the instrument maker, was an inventor of many brass instruments prototypes or their parts and additional devices (quarter-tone cornet, pocket cornet or echo playing device among others). His experimenting with duplex instruments began with creating the duetton, in which he combined a cornet in C or in B-flat with a tenor trombone pitched an octave lower. However, this instrument was not very succesful due to natural complications of instrument possesing features of two different playing ranges, different required mouthpieces etc. The schediphone (patented in 1901, czech: šedifon) consists of the combination of two instruments tuned to the same pitch but with varying bores (cylindrical and conical). The waveguides could be switched using so called distribution valve. Šediva bulit the instruments in four variants (alto, tenor, bariton and bass), Shediphones became a popular part of Russian military bands, as they could replace both euphoniums and trombones in smaller-staffed ensembles. [1, 2]

For this study alto schediphone (alto Eb euphonium combined with alto Eb trombone) was used ans original Šediva's mouthpiece was attached. Its parameters correspond more to the fluegelhorn family of mouthpieces causing a bit worse playability of higher notes with the trombone waveguide.

Figure 2 a,b: the alto Eb schediphone used for measurements. The distribution valve is the fourth on the bottom picture and its lever could be seen above the valves on the upper picture.

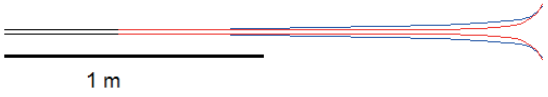

Figure 3: Waveguides proportions (euphonium – blue, trombone – red, conjoint part – black).

Length of the euphonium waveguide cylindrical section is ca. 730 mm (including ca. 450 mm of the conjoint part). Broadening part ends with the bell with diameter of 190 mm. Conversely, length of the trombone waveguide cylindrical section is ca. 1090 mm and the bell have diameter of 200 mm. Total length of the instrument is for the both waveguides ca. 2100 mm (see Fig. 3).

Figure 4: 8th Don Cossack Regiment military band with Šediva's instruments and with Josef Šediva in the middle in 1905. (© National Museum – Czech Museum of Music)

Figure 5: Josef Šediva's Musical Instruments in the Exposition of National Museum – Czech Museum of Music. (© National Museum – Czech Museum of Music)

2. ACOUSTICAL PARAMETERS

2.1 Sound spectra

Overtones of the fundamental (Eb2) were recorded and adjusted to the same psychological loudness before the processing. See the FFT spectra and differences of harmonic spectra in Fig. 13-17.

Main formant of both waveguides at ca. 500 Hz for the euphonium and ca. 800 Hz for the trombone waveguide are apparent. The eufonium waveguide (blue) formant is broader in low frequencies and its maximum is lower than the spectral peak of the trombone waveguide (red). Hence the dominance of fundamental in higher euphonium waveguide registers, which never occurs on the trombone waveguide. On the other hand, the trombone waveguide formant is broader in higher frequencies causing more harmonics to be recognized. The euphonium fundamental is always stronger than the trombone fundamental.

2.2 Efficiency of the distribution valve

Šediva's system allows player to change waveguides immediately, even during the sound production (see spectrogram on Fig. 6). It shows his mastery in brass instrument making: small mistake in any of waveguides shape is enough to make smooth switch complicated. Good correspondence in input impedance peaks (on playable tones) assures that no major impedance changes occur when the distribution valve is used (see Fig. 7, measured by BIAS system).

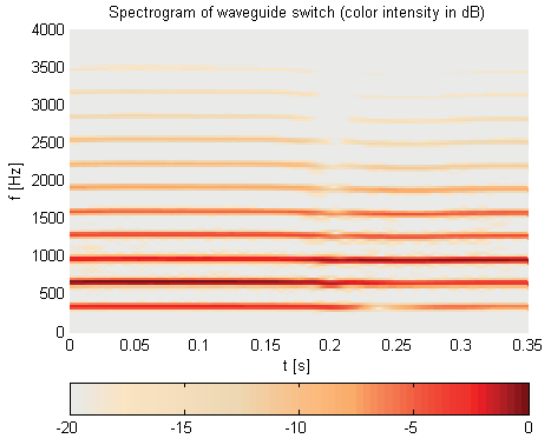

Figure 6: recorded sound spectrogram, waveguide switch at ca. 0.2 s.

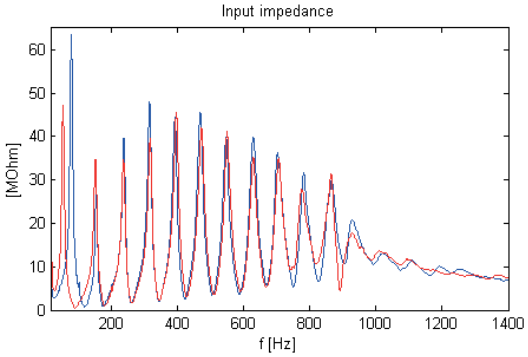

Figure 7: acoustical input impedance of the euphonium (blue) and the trombone (red) waveguides (unweighted, without any valve pressed).

2.3 Directivity

Radiation patterns measurement was conducted in an anechoic room, 12 microphones were used in one plane. The data in figures 8-12 are splined, 0 dB corresponds to the radiation maximum (recomputed for every waveguide and every frequency band), 0° corresponds to the player's line of sight.

Since the both bells are placed above player's head there is no expressive radiation shadow caused by his body. Radiation patterns in the horizontal bells including plane are presented (see Fig. 8-12). More pronounced directivity of higher frequencies is observable as well as effect of small diversion between euphonium (blue) and trombone (red) waveguide caused by different bell angle. It is apparent (see e.g. Fig. 12) that the trombone-like bell is better suited for higher frequency radiation.

3. CONCLUSIONS AND FUTURE GOALS

Features and efficiency of alto schediphon were presented and documented. Acoustic spectra show expected behavior: the trombone waveguide formant is placed higher than the euphonium waveguide formant, the euphonium waveguide has generally stronger fundamental frequency. Input impedance

peaks of both waveguides agree well. It can be concluded, that Šediva's mechanism works as planned.
Collection of Šediva's instruments in the Czech Museum of Music provides an opportunity to realize similar measurements with the other members of the schediphone family and related instruments to make this study complete in the future.

4. REFERENCES

[1] Keller, J.: "Čeští hudební nástrojaři v Rusku" [Czech Instrument Makers in Russia], In: Sborník Národního muzea v Praze XXXIII (1979), pp. 17–29.

[2] Žůrková, T.: "Josef Šediva (1853-1915) a jeho sbírka hudebních nástrojů v Národním muzeu - Českém muzeu hudby v Praze" [Josef Šediva (1853–1915) and His Collection of Musical Instruments at the National Museum – Czech Museum of Music in Prague], (Forthcoming, 2016).

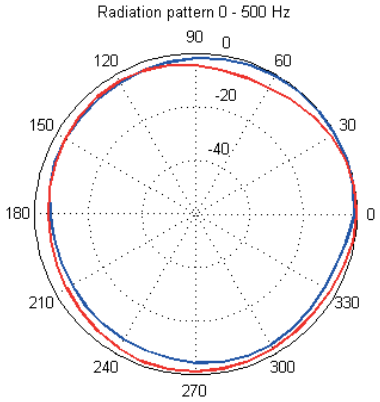

Figure 8: radiation pattern at 0-500 Hz, euphonium (blue), trombone (red), radial axis in dB

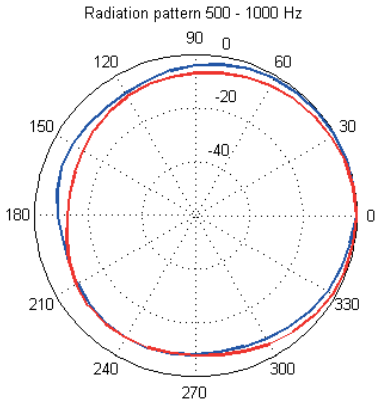

Figure 9: radiation pattern at 500 Hz-1000 Hz, euphonium (blue), trombone (red), radial axis in dB

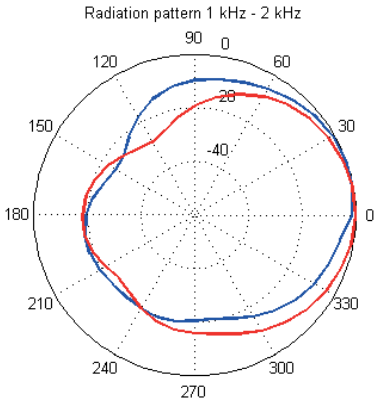

Figure 10: radiation pattern at 1 kHz-2 kHz, euphonium (blue), trombone (red), radial axis in dB

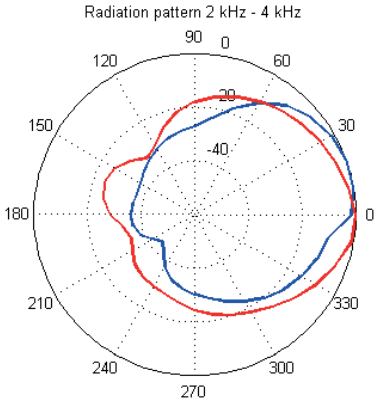

Figure 11: radiation pattern at 2 kHz-4 kHz, euphonium (blue), trombone (red), radial axis in dB

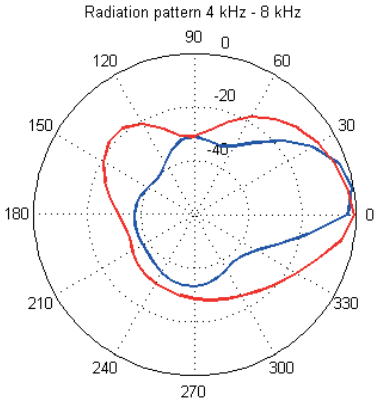

Figure 12: radiation pattern at 4 kHz-8 kHz, euphonium (blue), trombone (red), radial axis in dB

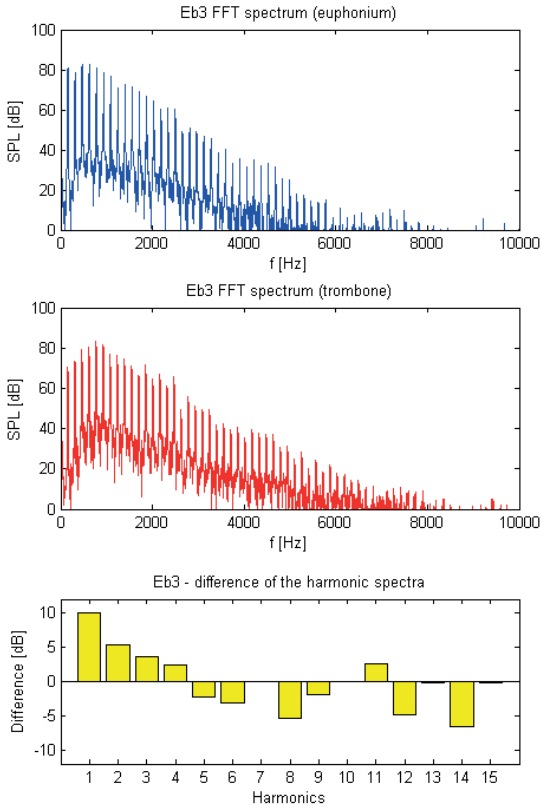

Figure 13: FFT spectra and difference of harmonic spectra on Eb3.

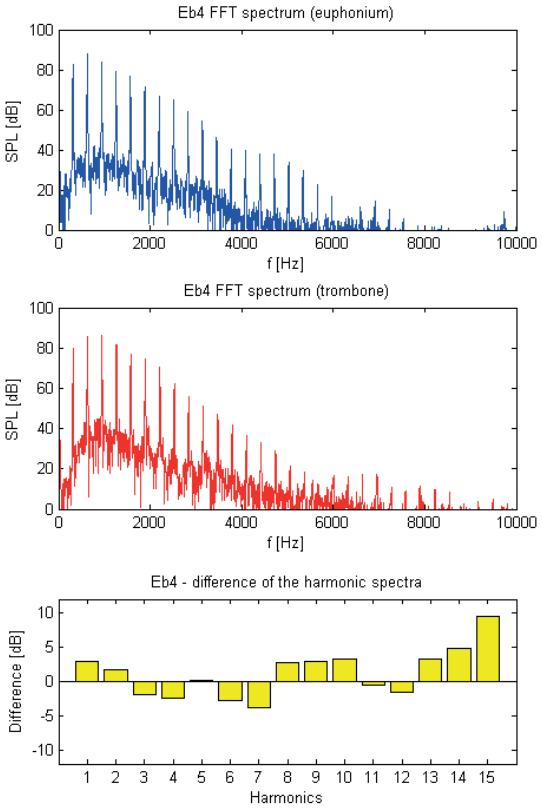

Figure 15: FFT spectra and difference of harmonic spectra on Eb4.

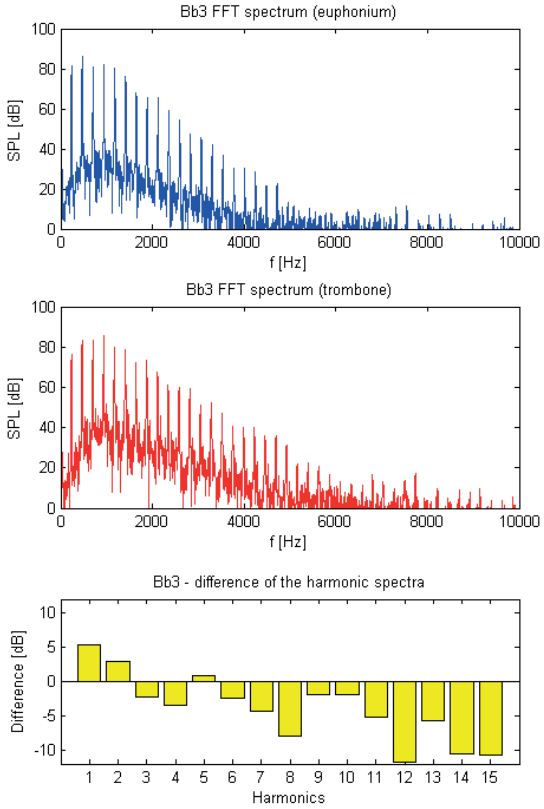

Figure 14: FFT spectra and difference of harmonic spectra on Bb3.

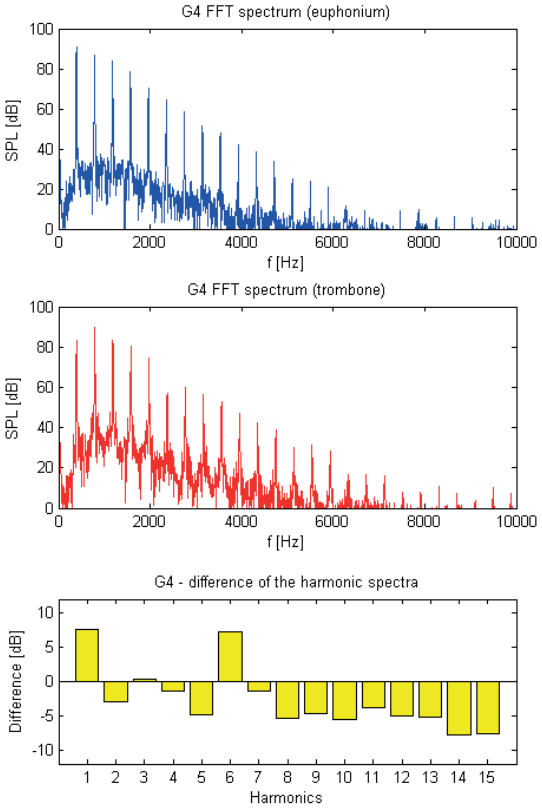

Figure 16: FFT spectra and difference of harmonic spectra on G4.

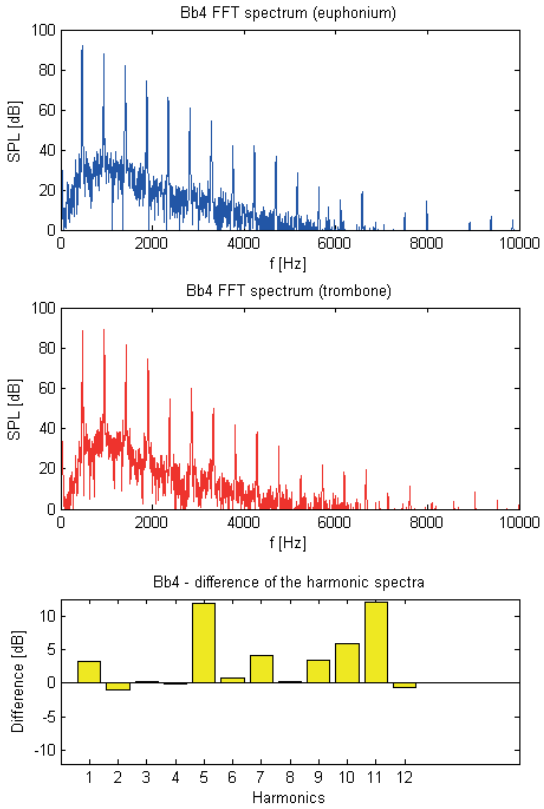

Figure 17: FFT spectra and difference of harmonic spectra on Bb4.

HUMIDITY IN BRASS INSTRUMENTS AND THE PREVENTION OF CORROSION

Martin Ledergerber, Marion Alter, Emilie Cornet, Erwin Hildbrand

Swiss National Museum, Collection Centre, Affoltern am Albis, Switzerland
martin.ledergerber@snm.admin.ch

ABSTRACT

The moisture generated in historical wind instruments during musical performances poses a serious threat to their long-term preservation. The potential damage impact varies greatly depending on the material. While the effects of humidity fluctuations caused by playing had previously been analysed in woodwind instruments [1], similar research on brass instruments had not yet been conducted. This study aims to gauge the processes and consequences occurring inside regularly played historic brass instruments as well as to provide suggestions for suitable preventive measures in order to minimise possible damage. The study took place within the frame of the interdisciplinary research project "Brass instruments of the 19th and early 20th centuries between long-term conservation and use in historically informed performance practice" by the Swiss Nationalfonds. The project is a collaboration between the Bern University of Arts, the Swiss National Museum, the ETH Zurich and the Paul Scherrer Institute Villigen.

Approximately 100-years-old brass instruments, later used in historically informed performances of Stravinsky's *Le sacre du printemps* [2], were deeply investigated. Based on temperature and humidity measurements, the climatic conditions were assessed before, during and after playing of different historical brass instruments, ranging in scale length from the trumpet to the tuba. It could be established that the instruments' internal relative humidity reached very high levels after just a few minutes playing and that these values decreased only very slowly afterwards, despite emptying the tuning slides, which is common practice for musicians. Regularly played brass instruments have therefore a very high, permanent level of internal relative humidity which consequently increases the risk of metal corrosion.
Amongst other things, the concept of preventive conservation included tests on various greases and oils in order to access their suitability for conservation. But the main task aimed at devising a simple drying method easy to apply daily by musicians. Climatic measurements showed that the moisture levels inside the instruments can be reduced within short time using simple fans (figure 1). The efficiency of this preventive conservation protocol is tested by a long-term survey during which 16 brass instruments, divided into two groups, are played daily by musicians. The first group is played according to specific preventive conservation guidelines while the second one is played following common practice. All instruments are analysed by non-destructive methods at different times in order to evaluate the progression of their corrosion state [3]. Comparison between the conditions of the two groups, will allow an assessment of the efficiency.

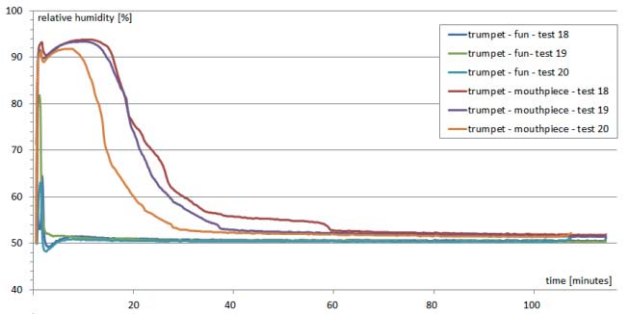

Figure 1: Decrease of relative humidity over time observed inside a trumpet at different places, using a fan as drying device.

REFERENCES

[1] Ilona Stein: "Blasfeuchte in Holzblasinstrumenten", Friedemann Hellwig, ed.: Studien zur Erhaltung von Musikinstrumenten. Kölner Beiträge zur Restaurierung und Konservierung von Kunst- und Kulturgut, vol. 16. München 2004, pp.9–121.

[2] T. Lombardo, M. Alter, E. Cornet, M. Ledergerber, F. Kergourlay, M. Wörle, B. Elsener, F. Cocco, M. Fantauzzi, A. Rossi, E. Lehmann, D. Mannes, D. Allenbach, M. Mürner, A. von Steiger, and M. Skamletz, Brass instruments of the 19th and early 20th centuries between long-term conservation and use in historically informed performance practice, presented at Int. Conference "Non-destructive and microanalytical techniques in art and cultural heritage" TECHNART 2015, Catania 27-30, 2015. For further information and links see http://www.hkb-interpretation.ch/index.php?id=87 as well as http://www.hkb.bfh.ch/en/research/forschungsschwerpunkte/fspinterpretation/korrosion/

[3] B. Elsener, M. Alter, T. Lombardo, M. Ledergerber, M. Wörle, F. Cocco, M. Fantauzzi, A. Rossi, A non-destructive in-situ approach to monitor corrosion inside historical brass instruments, presented at Int. Conference "Non-destructive and microanalytical techniques in art and cultural heritage" TECHNART 2015, Catania 27-30, 2015

TO KNOW, TO REMEMBER, TO PRESERVE: DOCUMENTING OBJECTS AND SITES RELATED TO SOUND PRODUCTION

Patricia Lopes Bastos
ANIMUSIC, Portugal
plopesbastos@gmail.com

ABSTRACT

An increasing interest is being given to the implementation of art and science documenting strategies, essential to the safe-guarding and memory keeping of a human patrimony which history and even recent occurrences have proved to be very fragile and vulnerable. Consistency, uniformity, and objectivity, are necessary factors for the construction of a reliable documenting system. For an effective communication, a clear methodology used in the description of an object or of a landscape consequently helps the reader to immediately recognize the item or geographic features, and in most cases facilitates their reproduction. The easily accessible and non-electrical techniques and equipment used to identify a given object or natural sites, related or unrelated, combined or disperse, are associated with technological evolution on both universal and specific schemes, here brought to discussion. These may be used in both cataloguing a limited collection and in the construction of a general database of musical instruments, iconography, and natural locations with a relevant human sound-making role. To use the universal measurement procedure is especially effective in the case of objects with irregular contours, such as percussion instruments made with seeds, odd shaped ocarinas, or large sized rocks, as examples. The specific measurements are valuable for those seeking further details and expert information on features particular to each item. In this paper we shall present the methodologies used in our work, in our efforts to better understand the sound patrimony and to record the obtained information in a clear uniform system, seeking to contribute to the share of knowledge and preservation of a significant part of our cultural and scientific heritage.

IN SEARCH OF THE REMAINING ELEMENTS OF SÉBASTIEN ÉRARD AND GABRIEL JOSEPH GRENIÉ'S ORGANS, FIRST EXPRESSIVE ORGANS BUILT IN FRANCE

Thierry Maniguet
Musée de la musique Philharmonie de Paris, France
tmaniguet@cite-musique.fr

ABSTRACT

Well known for his piano and harp actions, Sébastien Érard (1752-1831) also worked more than thirty years on the development of a new pipe organ on which it was possible to express musical dynamics. Achieved shortly before Érard's death, this ingenious mechanism never really had the chance to be used. The most important instrument of the kind was built in Paris in 1829 for the King's chapel but was badly damaged during the revolutionary events of July 1830. Rebuilt in 1854 in the Castel of Tuileries, it was destroyed when the building was set on fire in May 1871. Apart this organ, it was commonly believed that two other instruments were built during Érard's life but their becoming was not clearly established until today. The orgue expressif of Gabriel Joseph Grenié (1756-1837) is also mainly known from literature. Pioneer in the use of free reed, Grenié patented in 1810 an expressive instrument in which reeds were laid out in resonators. His system would be developed by his apprentice Théodore Achille Müller (1801-1871) until the 1860's, supplanted by Debain's and Alexandre's harmoniums in the mid-19th century. As well as Érard's organs, none instrument from Grenié seemed to have survived. This paper will examine Erard and Grenié's systems, very different in their approach of the same purpose. The story of the built organs by these makers will be retraced up to the present day.

VICTOR-CHARLES MAHILLON AND HIS ANTI-CORNET STRATEGY

Géry Dumoulin
Musée des instruments de musique (MIM), Brussels, Belgium
g.dumoulin@mim.be

ABSTRACT

The irruption of the valve cornet in the music world of the first half of the nineteenth century has been a milestone in the brass instruments history and is considered by modern scholars to have influenced the technical evolution of the trumpet. But its etymology, its social connotations, and its tone were hardly compatible with the noble character of the trumpet. While finding a place in many orchestras thanks to its playing capabilities, the cornet became the target of some authors who complained about its use as a substitute to the trumpet. In the third quarter of the 19th century, the Belgian maker, acoustician, organologist and museum curator, Victor-Charles Mahillon also feared the imminent extinction of the trumpet in symphony orchestras. That's why he took "strong measures" – as he said in his famous Éléments d'acoustique musicale & instrumentale (1874) – to depart from the cornet timbre and to reinstate the trumpet as an important brass orchestral and solo instrument. This paper will detail the strategies used by Mahillon to reach his goal, and the process that led him to develop – like other brass makers of his time – new forms of trumpets, from hybrids between cornet and trumpet to still higher-pitched instruments.

MODAL ANALYSIS OF VIOLONCELLO TAILPIECES - COPIES DERIVED FROM 3 TAILPIECES ASCRIBED TO STRADIVARI (MUSEE DE LA MUSIQUE PARIS)

Anne Houssay (1) & Eric Fouilhé (2)

(1) Musée de la musique's Laboratory, Paris
(2) LMGC Montpellier 2 University, CNRS UMR 5508
ahoussay@cite-musique.fr

ABSTRACT

In previous publications, we identified the vibrating modes of a cello tailpiece free and under string tension on a dead-rig (2009-2010), using hammer and accelerometer with George Stoppani's software, and then its behaviour on a cello. We compared different measurement methods and measured the variability of wood choices on vibration modes and frequencies (2011 - 2012). The adjusted position of the tailpiece has also been explored, by varying the "after-length", i.e. the distance of the tailpiece to the bridge which leaves a small length of vibrating string (2013). We showed that, even if less mentioned by luthiers and musicians, the distance of the attachment at the bottom of the instruments has more influence on the modes and on the sound than the "afterlength". Our study took a more historical path to identify the trends and theories on the "afterlength" significance (2014). We showed that the "afterlength", often discussed as an adjusting parameter of the sound, became an issue especially when the industrialization process in Markneukirchen enhanced the standardization of tailpiece length, with the consequence of a loss of experience on the violin makers' part, which stopped altogether making the tailpieces themselves.

Different historical types of tailpieces of the 17th and 18th century assigned to Stradivari which show different stages in historical set up at a time of transformation of the lower register instruments in the violin family are studied. Made on the same outline, their modal analysis free-free as well under the string tension on a dead-rig helps us to compare their behaviour.

1. INTRODUCTION

The most important change for string musical instruments in the 17th century is a change in paradigm concerning the understanding of vibrating strings.

Figure 1: Parameters of vibrating strings until the 17th century.

The mathematics explaining the tuning of string were ascribed to Pythagorus since ancient Greece, linking tunig to the length, the tension, and the "fatness" of the string, which lead to a theory of proportions described by the monochord. The tensions were measured by weights hanged to the nut of the monochord [1]. Different materials, mostly metals (copper, silver, gold, etc.) symbolised by different planets gave different notes, associated with different lengths. Musical treatees of meadieval times, latin as well as arabic, took the same theory for the complete story [2]. These ratios were used for musical intervals also and for designing purposes, in architecture as well as for the making of musical instruments well into the Renaissance. The questioning of musical scales preoccupied greatly music theorists during the italian Renaissance, as they tried to define consonances and dissonances. [3]
The discovery came from Vincenzo Galilei, a great luthenist and theorician, and his son Galileo. They spent a part of the summer 1592 measuring strings and weighing them, and were the first to calculate the influence of the density of the material of a musical string, or more precisely the mass per unit length, or linear mass **μ**. [4] which came to the mathematical expression :

$$\mathbf{f = (1/(2L))*\sqrt{(T/\mu)}}$$

This discovery was a threat to the authority of the Catholic Church, then strongly involved with *Counter Reformation.* God's creation of a coherent and beautyfull world was explained with theories of the Celestial Spheres and of Universal Harmony, with the beauty of the ratios of whole numbers. This paradigm coud'nt safely be contradicted at the time, thus leading Galileo to well known difficulties. In consequence, this musical discovery was to be published more than fourty years later, four years before Galileo's death in 1638. The book was published in Leyden, were the main University of the Reformed Netherland Republic had its site. The text was immediately translated in French by father Mersenne, who had published his "Harmonie Universelle" only two years earlier [5].

So heavier strings could lower the sound dramatically, and instruments could be made shorter for the same tessiture. A harpsichord's tuning could be lowered by an octave with golden strings instead of normal iron and copper strings, experiment which was tempted at the Medici court [6] [7]. By 1664, wound strings were for sale at Playford's shop in London, and shortly elsewere.
In consequence, lower instruments could me made shorter. The violoncello replaced the Bass violin, and the lower contrabass appeared in Paris around 1700, as musical answers to the technical wounded strings [8]. Cellos tuned likee Bass violins had much more manageable string lengths and Bass violins were often recut to satisfy the new demand [4].

In this context, Antonio Stradivari came at the right time to redesign not only the solo violin but also the new violoncellos, as well as their fittings. Historical tailpieces are kept in the Musée de

la musique's collections and give evidence to his experiments. Changes Stradivari was bringing for the second age of the baroque are technically very informed [9]. As Tony Faber states: "After a reconstruction of the design of violins between 1685 and 1709, Stradivari also started to apply the new features that were such a succes for "big" sounding violins to cellos: flatter archings, adapted length (29 inches), to meet the challenge of tone projection and a balance between trebble played in higher positions, and the bass strings. After a six-year gap in the making of cellos, he started again with new designs; These models became "a template for generations of cello –makers up to our days. "

2. DESCRIPTION OF TAILPIECES ASCRIBED TO STRADIVARI AND CHOICE OF MODELS FOR TESTS

2.1 Differences between the original tailpieces

In the Musée de la musique's collection, violin tailpieces and four larger tailpieces are ascribed to Stradivari. They have most probably be taken off instruments of the master brought to Paris after the Napoleonic Italian wars. J.-B. Vuillaume himself made trips to Italy to buy instruments, as other musicians and dealers as well. Three of these tailpieces (**E.487, E.486.1 and E.486.2)** were given to the *Musée Instrumental du Conservatoire de Paris* by violin maker and dealer Jean-Baptiste Vuillaume [11]. The inlayed maple tailpiece **E.619** was given by the violin maker and dealer Eugène Gand in 1874. [11].

Research in the iconography has showed us a probable chronological order (see some examples in our historical study [14]).

Figure 2: **E.487, C.161** [1]**:** A. Stradivari. Curved and carved walnut wood (?) for a middle size 'contralto' or 'tenor' violin. Being of 210 mm, it is quite a lot shorter than the others and will not be part of this study on cello tailpieces, but it is worth noting that Stradivari probably made this type of tailpiece also for larger basses at the beginning of his career.

Figure 3: **E.619,** C.193: Violoncello tailpiece**,** c. 1700**,** A. Stradivari. Plain maple with purfling inlays. Carved in inlayed solid maple, with original attach in gut passing through holes drilled in the top surface

Figure 4: **E.486.1** C.114. Violoncello tailpiece**,** A. Stradivari around 1710. Maple with an inlayed ebony veneer (a thin plate wood glued on the lowered surface) surrounded by a white purfling leaving the maple at the edge.

Figure 5: **E.486.2**, C.114. Violoncello tailpiece**,** A. Stradivari, 18th c**.** In plain maple with complete thick ebony veneer in one piece all over the surface.

2.2 Types of attachment

Different attachments were used by Strradivari from simple holes, which are in use for many baroque violins of all sizes and often seen on iconography, but also attachments which are not visible from the top, where guts or metal wires are inserted in longitudinal holes.

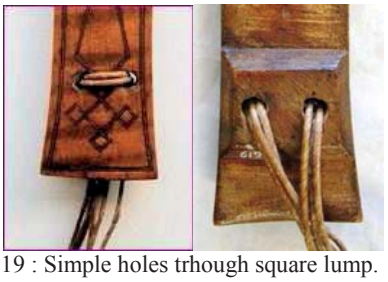

Figure 6: E. 619 : Simple holes trhough square lump.

Figure 7: E. 486.1 : square lump with longitudinal holes for thick gut; E. 486.2 : Square lump with longitunal holes for through attachments in brass

2.3 Choices of models for the tests

In this transition period when the violoncello is changing status from a part of the violin "concert" to a continuo and soloist instrument, these changes participate to the innovations from Bass violin to violoncello. Let us study their differences in dimensions and decide the size, weights, materials and structure of our models made for the tests.

Measures in mm			**Tested models**	
	E619	**E486.1**	**Tailpieces made for analysis**	**E486.2**
Total length	235.5	238	238	243
Width mini	30	31	32.5	30.2
Width at bottom	36.6	40.3	40.3	39.9

Figure 8: main measurements.

Here, if we assume that the plane maple tailpiece is the oldest, it is nevertheless the shortest. and the three are not exactly proportional in dimensions.:

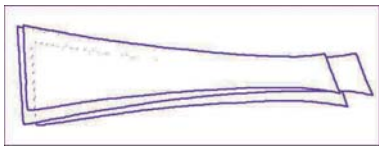

Figure 9: These three Stravivari's tailpieces : **E619, E486.1, and E486.2** are made of different lengths and proportions.

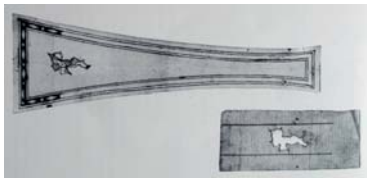

Figure 10: Design of a contralto tailpiece Stradivari 1690 (Sacconi). *Museo del Violono, Cremona* Notice that there is no attachment hole visible on the top at the smaller end. Sacconi explains that Stradivari made the tailpieces made proportionally to the instruments [9].

2.4 Weights and thicknesses

If we are right with the chronological order, there is a deliberate increase in the weight and thicknesses from one to the next. The use of first a thin ebony veneer, and then a thicker one, makes the piece even stronger, stiffer and heavier.

Strad made the tailpieces with increasing weights (the last piece contains remains of a brass wire which makes it even heavier). The first two have comparable thicknesses, the last piece is deliberatly thicker all over by more than a mm, and heavier at the bottom with the lump of attachment 3 mm thicker.

Measures in g and mm			**Tested models**	
	E619	**E486.1**	**Tailpieces made**	**E486.2**
Weight	48g	64.6g	Different weights, similar	79.9g – (without bass plate and wire)
Thickness center of head	11.2	10.3	10.3	12.4 at top holes 10.3 at top edge
Thickness in the middle	8.9	8.2	8.2	9.9
Thickness at the minim. width	7.7	7.8	7.8	9.2
Total max. thickness at lump	11.5	11.6	11.8	16.5

Figure 11: Main dimensions of the orginal tailpieces and choices for tested models..

We haven't done the much heavier lump at the end of the piece because of the way the copies were produced, i.e. with the same geometry. It would be worth trying another time, though.

3. MAKING THE TAILPIECES FOR TESTING

3.1 Shape and materials for the tests

To compare the behaviour of the materials and carving of the three Stradivari violoncello tailpieces, we decided to make three different copies reduced to the same dimensions using different materials and thicknesses thus obtaining several weights and behaviours. Eight tailpieces were produced on the same design;
Maple and African Blackwood were used to make tailpieces from a unique outline drawn numerically and cut with a numerically controlled machine (CNC).
African blackwood has a specific modulus three times higher than maple and these woods have been compared in a preceeding article [14].

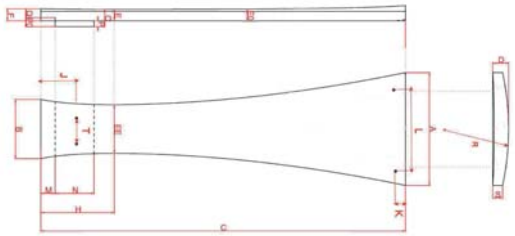

Figure 12: Same design for the eight test tailpieces produced

Eight tailpieces were made: two in plain maple with two types of attachment, Two with thin blackwood A. Blackwood adjusted shell glued on maple, two with thick A. Blackwood adjusted shell glued on maple. We will compare 2A, 5C, 7A, one with a plain African Blackwood tailpiece with two different types of attachment: 8A and 8B and a modern tailpiece made in Dyospiros spp. in H35A.

Figure 13: View from upper surface of the eight tailpieces made on the same outline. , two are in plain maple, two covered by thin 1.8 mm of A. Blackwood adjusted shell, two with thick 1.8 mm of A. Blackwood adjusted shell. One is in plain blackwood, and N°1 is in hardwood (Massaranduba) weighing 70g.

Figure 14bis: View from underneath surface of the eight tailpieces made on the same outline.

Figure 15: 2, 8A with simple attachment holes, identical square lumps with longitudinal attachment 5C, 7A and 8B.

N°	Materials	Length	Top width	Bottom width	Weight wood	Common points with tailpieces by Stradivari
N°1	Massaranduba	238	40.3	32.5	70 g	tests outline. Simple attachment
2A	Plain maple with inlays	238	40.3	32.5	49 g	E.619 material + Simple attachment
5C	Maple + fine 1.8 mm A. Blackwood adjusted shell	238	40.3	32.5	64 g	E.486.1 material + Square lump with longitudinal attachment
7A	Maple + thicker 2.8 mm A. Blackwood adjusted shell	238	40.3	32.5	78 g	E.486.2 material + Square lump with longitudinal attachment
8 A	Plain Black-wood	238	40.3	32.5	88.5 g	Same as 8B simple holes and chord
8 B	Plain Black-wood	238	40.3	32.5	88.5 g	Same square lump with longitudinal holes, metal wire
MT H35A	Dyospiros spp.	235	<<<	<<<	64 g	**Modern tailpiece**

Figure 16: Characteristics of the tested tailpieces.

The set ups of the after-length on the dead-rig are not very different from each other.
Attachments also differ, as the originals : tailpieces 2, 8A with simple attachment holes going through. Square lump with longitudinal attachment 5C, 7A and 8B.

4. METHODOLOGY

We use Stoppani's different software:
"Acquisition" is for capturing frequency response functions, using a mini impulse hammer and an accelerometer.
"ModeFit" is for estimating mode parameters and other data manipulations from the measurements.
"ModeShape" allows imposing the measured movements on the outline of the drawing, for plotting mode shapes and viewing animations and other operations on plots.
"FRFOverlay" is for comparing Frequency response functions FRFs or complex Fast Fourrier Transform FFT data and can do all sorts of averaging. [14], [15], [16], [17], [18], [19].

Eighteen points are marked on each tailpiece to place accelerometer and hammering points. For the free-free measurements, the tailpieces rest on elastic bands.

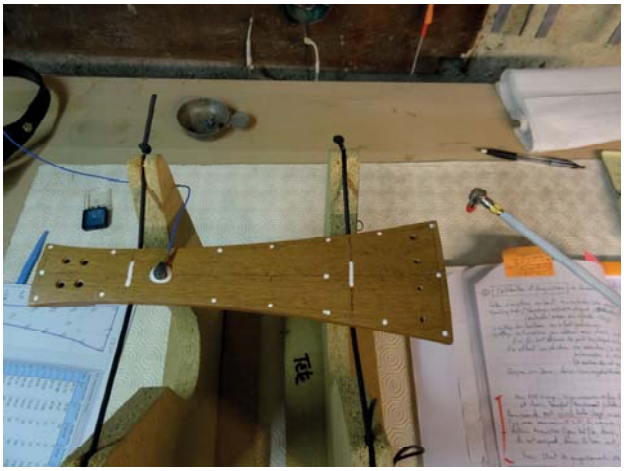

Figure 17: Free-free measurements of n°1.

For the measurements under string tension, a dead-rig is used, constructed on an IPN rail used for our preceding experiences, of standard lengths for a cello, with a solid wooden bridge, and with always the same set of modern strings, in order to keep as much as possible the same parameters each time in order to make easier comparisons on the behavior of tailpieces. The rig was tested for its inert behavior at the considered frequencies [14].

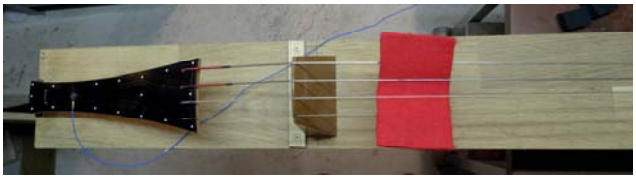

Figure 18: Tailpiece set on dead-rig for modal analysis measurements under tension of the same set of cello strings C G D A, Savarez (Middle) in bare gut for D and A and Aluminum and Silver covering on gut for G and C.

5. RESULTS

5.1 Free-free modal analysis

The reference tailpiece n°1 we show here show the modal shapes of a hardwood (Massaranduba) tailpiece of the same size, weighing 70g. A split flexion mode F1 & F2 shows similar figures at two different frequencies, but on opposite directions, as if the mechanical properties of the two sides of the piece were not symmetrical from a vibrational point of view.
We do not find this feature in the three test pieces which have a strong and unique first flexion mode F1. If our chronological conjecture is right, Strad was tuning these tailpieces higher and higher : the fundamental first Flexion mode of the thin 1.8 mm A. Blackwood adjusted shell glued on maple tailpiece 5C is one semi-tone higher than the plain maple with purfling inlays 2A, while the thick 2.8 mm A. Blackwood adjusted shell glued on maple 7A is a fourth higher the plain maple with purfling inlays 2A, being a third higher the thin 1.8 mm A. Blackwood adjusted shell glued on maple 5C. The order stays the same in higher frequencies.

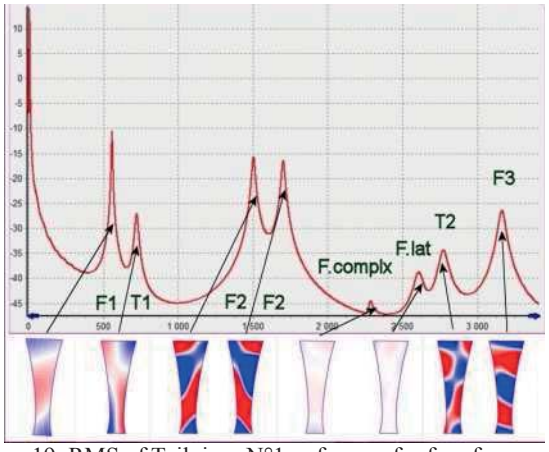

Figure 19: RMS of Tailpiece N°1, reference for free-free modes.

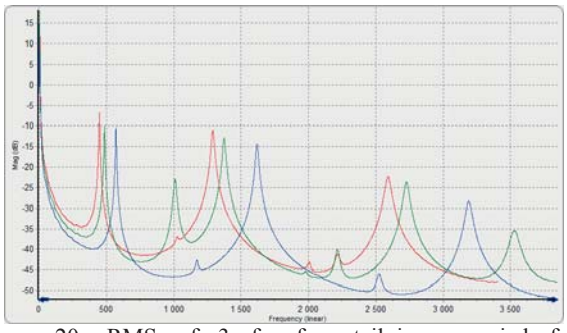
Figure 20: RMS of 3 free-free tailpieces copied from Stradivari's chosen characteristics: 2A red , 5C green, 7A blue.

This gives quite a drastic change to the main sound of the piece. If we chose a'=450 Hz, which could exist at the time (as tunings were not as fixed as today) the tailpiece 2A is tuned a', 5C is tuned b' and 7A is tuned at d". Of course, the original tailpieces are probably not exactly at these frequencies, but these measurements allow us to have an order of magnitude of these pieces made by the same maker within around some 15 years or 20 years of drastic changes of the violoncello.
Another important feature of the thin 1.8 mm A. Blackwood adjusted shell glued on maple 5C's free motion is a strong torsion mode around 1010 Hz (between b" and c3) while plain maple tailpiece 2A and thick 2.8 mm A. Blackwood adjusted shell glued on 7A, considered as the oldest and the more recent, are not a all mobile at the first torsion mode, which was not necessarely to be expected.
The second flexion mode F2 is strong in amplitude and in the same frequency order as F1 : 2A, 5C and 7A. E3, f3 and a3 : a semi-tone and a third again.
The torsion modes are negligible, and the two first flexion modes are strong.

N°	**Mode 1 F1**	Mode 2 T1	**Mode 3 F2**	Mode 4	Mode 5	**Mode 6 F3**	Mode 7
2A	**450 Hz**	1030 mini	**1290 high**	2010 mini	2220 mini	**2590 high**	
5C	**480 Hz**	**1010 medium**	**1380 high**	1980 mini	2210 mini	**2730 high**	3530
7A	**570 Hz**	1170 mini	**1610 high**		2520	**3190 high**	
H35A plain Dyospiros spp. Modern tailpiece	**475**	-	**1300**	1818 mini	-	**2340**	mini

Figure 21: Free-free frequency modes of 2A 5C and 7A test-tailpieces, compared with a modern plain Blackwood tailpiece.

The modern taipice doesn't seem to show the first torsion mode T1 between the two first flexion modes F1 and F2 : the torsion seems to have been eliminated from the lower frequencies, thus saving energy of a motion that is not useful to the bridge rotation, i.e. for the transmission of energy to the body of the instrument.

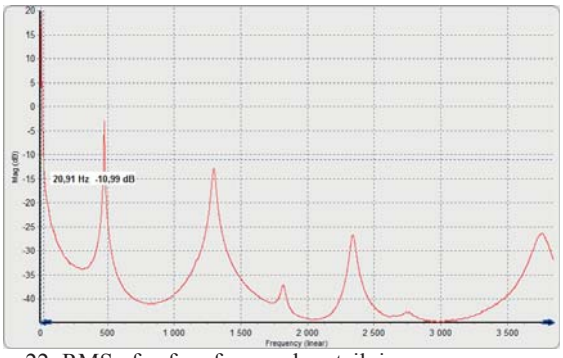

Figure 22: RMS of a free-free modern tailpiece.

This could be an element in enhancing the power of the instrument. The modes F1 and F2 are much lower on the modern tailpiece, thus enhancing the motion of the bridge in the lower notes, but may be not so efficiently if this motion is not really transmitted efficiently to the bridge itself. But the very tense steel strings probably help to do that, compare to the old gut strings used in baroque times.
To put it in fewer words, in the free-free modes, the modern tailpiece behaves more like a beam, which allowed the 1st and second flexion modes to be lowered a little in frequency, while the baroque tailpieces behave like thick plates and have twisting modes in lower frequencies.

5.2 Modal analysis of tailpieces under tension

Once under tension, obviously, the modal analysis changes dramatically from the free-free behaviour and presents a different frequency distribution, which can be interpreted in terms of mobility and energy. It is somewhat comparable to the condition under which the tailpiece will behave on an instrument, except that the acoustics of the box of the instrument itself and the action of

bow, bridge, and strings are eliminated. We had checked that the main frequencies are much higher than the ones we study here.
Under string tension on a dead-rig with a solid bridge, we showed [22] that the two first modes are solid body modes: the first one is the bridge jumping up and down. It has very strong amplitude on our RMS because we are tapping the tailpiece from the top, and it depends a lot from the length of the attachment. On a playing cello, this mode won't be as much driven by the lateral action of the bow. The second mode is the windscreen movement of the tailpiece rotating from left to right also affected by the attachment. Higher from these, we look at the flexion and torsion modes which are characteristics of the tailpieces themselves.
The third mode is the First flexion mode for all tailpieces studied here. The main differences we can see between Strad's three models of tailpieces under tension (plain maple, thin 1.8 A. Blackwood adjusted shell glued on and thick 2.8 mm A. Blackwood adjusted shell glued on maple) is to be noticed on the 7A tailpiece with thick 2.8 mm A. Blackwood adjusted shell glued on maple which manages to be higher in Frequency for F1, F2 than the same modes of the two other tailpieces (2A in plain maple and 5C with fine 1.8 mm A. Blackwood adjusted shell glued on).

N° F (Hz)	**Mode 1 CS**	Mode 2 CS	**Mode 3 F1**	Mode 4	Mode 5	**Mode 6 F2**	Mode 7
2A	65 Hz	178 high	490 middle	816 mini	909 mini	1304 small	1420 high
5C	**63-65 split high**	**184 high**	**522 middle**	603 mini	995 mini	1237 mini	**1400 high**
7A	**60- 97 Split high/small**	30 …370 Split High/middle	**699 middle**		2520	**1696 high**	
8A plain black wood	**56**	149	**332 /384**	703	989	**1029**	1154
8 B plain black wood	**57**	223	**535**	722 / 795	961	**1050**	1180
H35A plain Dyospiros spp. Modern tailpiece	**65**	253	**506-575 small**	676	-	**1080 – 1110 high**	**1168 high**

Figure 23: Frequency modes of test-tailpieces under tension on dead-rig.

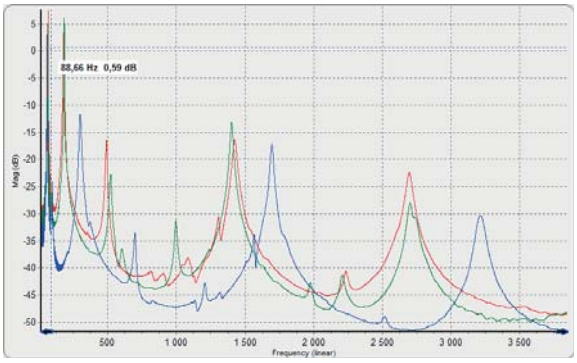

Figure 24: RMS averages of 3 tailpieces under tension on dead-rig : 2A in red, 5C in green; 7A in blue.

The two plain Blackwood tailpieces 8A and 8B differ by their attachment; the first has a chord trough to simple holes, the other longitunial holes through the lump and metal wire. We confirm the imporance of this for the Solid Body modes, and can see that it doesn't impact much the frequency of the flexion modes. Nevertheless, we can see an impact of the rigidity of the metal wire in the splitting of the modes.

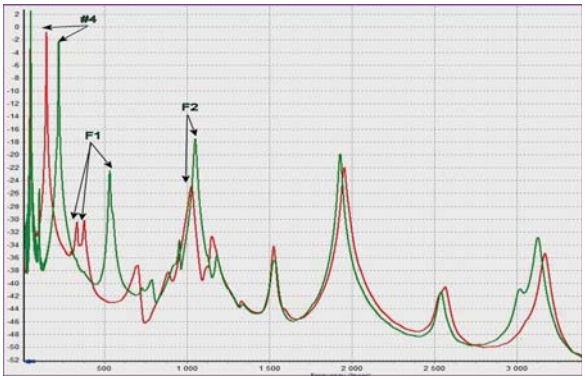

Figure 25 : RMS averages of two blackwood tailpieces with different attachments: 8A (red) simple holes and chord and 8B (green) longitudinal holes, metal wire on a dead-rig.

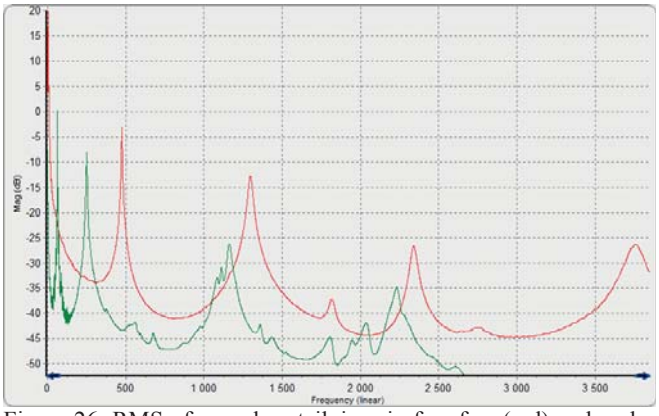

Figure 26: RMS of a modern tailpiece in free-free (red) and under tension on a dead rig (green).

The vibrations of modern tailpiece in free-free under tension on the dead-rig do'nt really have a torsion mode before the first flexion mode, feature that we have seen already on the free-free modal analysis. It shows lower amplitudes and a split of the first Flexion mode at low amplitude. It looks like there is less energy going into the tailpiece, and the pics are less clear and splitted, which indicate less define frequencies. This probalbly avoids to enhance one frequency in particular, which would create wolf notes and absorb energy when the corresponding note is played.

6. CONCLUSIONS

Stradivari has designed stronger and stronger, stiffer and stiffer, heavier an heavier tailpieces as the cello was becoming more of a solo instrument and being played more in the higher positions. Also, the attachment became stiffer as virtuosity and tessiture increased. The mobility was thus diminished, even without fixing the tailpiece like the anchorage on a viol, which could dampen the vibration of the bridge, and he instead used a metal wire allowing left to right movements. He must have been concious of the energy loss that the older very mobile tailpieces could cause to the sound of the cello, and this show how the famous maker experimented with and payed attention to each piece of the instrument in order to

transfomr the cello from a concert group instrument into a powerful solo tool.

Next orientations for this research will be to measure models of tailpieces form the second half of the 18th c. and of the 19th c. to establish a chronology of behaviour, using appropriate stringing. Another approach will be to do a link between acoustical properties and musical perception: powerfulness, playability, musicality, and harmonic complexity.

7. REFERENCES

[1] Frederick V. Hunt, *Origin in Acoustics*, Acoustical Society of America, 1992 (Reprint), p.1.

[2] Gioseffo Zarlino, *Le istitutioni harmoniche del reverendo M. Gioseffo Zarlino […]*, Venise, s.n., 1562, part. 2, chap. 24, p. 93-96, 126.

[3] Houssay A., "Cordes filées et violons en Italie au XVIIe siècle ; quelques cas d'instruments crémonais recoupés" in "L'orchestre à cordes sous Louis XIV - Instruments, répertoires, singularités" Jean Duron & Florence Gétreau Dir., Vrin, Paris, to be published in 2015.

[4] Marin Mersenne, *Novarum observationum physico-mathematicarum*, Paris, Antoine Berthier, 1647, vol. 3, p. 165; see Barbieri, ≪ Gold and Silver ≫, p. 123.

[5] Patrizio Barbieri, ≪ Gold and Silver-Stringed Musical Instruments : Modern Physics vs Aristotelianism in the Scientific Revolution ≫, *Journal of the American Musical Instrument Society*, 36, 2010, p. 11-154.

[6] Piero Gargiulio, ≪ Strumenti musicali alla corte medicea : nuovi documenti e acognosciuti inventari (1553-1609) ≫, *Note d'archivio per la storia musicale,* 3, 1985, p. 70 ; see Barbieri, ≪ Gold and Silver ≫,p. 120.

[7] Stephen Bonta, ≪ From Violone to Violoncello: a Question of Strings ? ≫, *Journal of American Musical Instruments Society*, 3, 1977, p. 64-99.

[8] Sacconi S., Les "secrets" de Stradivari, Castlli & Bour'his, Nantes, 1989.

[9] Faber, Tony, Stradivarius: Five violins, one cello and a genius, Pan Macmillan, 2011, p.55-56.

[10] Chouquet, G., "Le Musée du Conservatoire national de musique – Catalogue raisonné des instruments de cette collection", Paris, 1875.

[11] Houssay Anne, Fouilhé Eric, "The string "after length" and the cello tailpiece: History, acoustics and perception", International symposium of Musical acoustics: ISMA'2014, Le Mans, July 7-12 2014.

[12] Fouilhe E., Houssay A., Brémeaud I.,"Dense and hard woods in Musical instrument making: comparison of mechanical properties and perceptual quality grading", Proceedings of ISMA'2014, Nantes 2012, p. 2689-94.

[13] Houssay A., Fouilhé E., "The string "after length" and the cello tailpiece: History, acoustics and perception", - Fouilhé Eric, Houssay Anne, "String "after-length" and the cello tailpiece: acoustics and perception", Stockholm Music Acoustics Conference SMAC 2013.

[14] Hutchins, C. M., "The effect of relating the tailpiece frequency to that of other violin modes", Catgut Acoustical Society Journal, Vol.2 N°3, (Series II), 5-8, 1993.

[15] Stough, Bruce, "The Lower Violin Tailpiece Resonances", Catgut Acoustical Society Journal, Vol. 3 (Series II) May1996, p. 17-24.

[16] Woodhouse, J., "Body vibration of the violin- What can a maker expect to control ?", CAS 10. J Catgut acoustical society journal, vol 4 N°5 serie I, 2002.

[17] Fouilhe Eric, Goli Giacomo, Houssay Anne, Stoppani George, "Preliminary study on the vibrational behaviour of tailpieces in stringed instruments", COST IE0601, STSM results, Hambourg, 2009.

[18] E. Fouilhe, G. Goli, A. Houssay, G. Stoppani, "The Cello tailpiece: how it affects the sound of the instrument", Viennatalk 2010.

[19] "Vibration modes of the cello tailpiece", in *Archives of Acoustics*, 36, 4, 2011, pp. 713-726. http://acoustics.ippt.gov.pl/ DOI: 10.2478/v10168-011-0048-2.

VIOLIN PROJECTION: PERCEPTUAL AND SEMANTIC ANALYSES

Claudia Fritz, Danièle Dubois
Institut Jean le Rond d'Alambert, Université Pierre et Marie Curie, France
claudia.fritz@upmc.fr
daniele.dubois@upmc.fr

ABSTRACT

Projection is often cited as a criterion contributing the the quality of a "good" violin, especially by soloists. However, it is one of the most intriguing criteria: soloists seem (at least some of them) to be able to evaluate the projecton of their instrument at the back of the room while hearing it under their ear; players claim that some instruments can be loud under the ear but without projecting well; projection may be one of the criteria that distinguish great Old Italian violins from their newer counterparts. A series of listening experiments have therefore being conducted to investigate this property and understand better the concept of projection. These experiments consisted in comparing pairs of violins, either live or through recordings, either solo or with orchestral accompaniment. Pairs of violins were usually constituted by one Old Italian and one new violin. Listeners had to evaluate the relative projection as well as some other properties like richness, loudness and brigthness to search for correlations between projection and other properties. A compilation of the results of these different experiments will be presented at the conference. In addition, listeners from one of the main live experiments had to answer the question "What is your definition of projection , i.e. the one you used to evaluate the different violins?". A linguistic analysis was conducted on the 37 answers collected and revealed a large diversity (lexical variation) in the linguisitc expression of projection which contrasts with the large consensus on the different semantic properties which characterise the concept, namely "the capacity of an instrument to produce a powerful, clear, rich in harmonics sound, which carries across the room, not only in solo but above the orchestra too".

MEASUREMENTS ON HISTORIC PIANOS

Antoine Chaigne[1], Gert Hecher[2]
[1] Institute of Music Acoustics, University of Music and Performing Arts Vienna, Austria
[2] Das KlavierAtelier, Vienna, Austria
antchaigne@gmail.com
gerthecher@gmx.at

ABSTRACT

Measurements were conducted on three historic pianos by Johann Baptist Streicher: one from 1836, and two from 1851 (with two different piano actions). Another series of measurements was performed on a copy of a typical 1800/05 piano by Nanette Streicher, made by Gert Hecher. These measurements were focused on the vibrations of strings and soundboard, and on the sound pressure, for isolated notes with different striking forces. Other data were collected, relative to the geometry and design of the soundboard, and on the string scaling, for each piano. The ultimate objective of this campaign is to establish links between physical parameters of the pianos and their tone quality. To achieve this, the method consists first to derive the appropriate parameters from time and spectral analysis of the various measured signals, in conjuction with the geometrical and material data. In some case, these last data are not available and some realistic assumptions must be made. In a second step, simulations of some piano tones relative to the four instruments are conducted and compared to the original ones. These simulations are made with the help of a numerical model previously developed by Juliette Chabassier. The presentation will start with a short history of the measured pianos. In a second part, preliminary results of measurements and comparisons with simulations will be discussed.

PERIOD INSTRUMENTS REVIVAL WITH PIANOTEQ KIVIR PROJECT

Juliette Chabassier, Philippe Guillaume, Julien Pommier
Modartt, France
juliette.chabassier@pianoteq.com
philippe.guillaume@pianoteq.com
julien.pommier@pianoteq.com

ABSTRACT

Modartt supports the KIViR (Keyboard Instruments Virtual Restoration) cultural project which we believe ``bridges a gap'' between physics based synthesis, reconstruction of period instruments and musical practice on a controller. The usual way of bringing historical keyboard instruments back to life consists in restoring them properly, by repairing structure components like soundboard, pinblock, frame, or by replacing worn parts like strings, hammers or other fragile elements made of felt or skin, which fall into disrepair along time. However safeguarding great historical valued instruments' manufacturing can be a priority. Besides, it may be risky to put ancient instruments under playing condition. Sometimes only some of the notes are restored. In both situations, it impossible to play music on such instruments. Digital restoration is a new experimental and innovating technology which attempts to solve the above mentioned problem. By the use of the mathematical and physical model Pianoteq, a virtual copy of the period instrument is reconstructed and calibrated from a detailed physical description and from the existing notes which sound correctly, after what the missing notes are reconstructed by the model. These virtual copies can then be numerically tuned and voiced in order to correct some defects issued from recording, tuning or regulation difficulties. It is therefore now possible to bring an historical instrument back to life, while keeping the major part untouched at its original state. The collection does not only serve as a maintainable testimony of the past, with playable devices in museums available to the public, but also brings ancient sounds into the Pianoteq equipped computer of any musician or composer worldwide. In this talk we will present and play a selection of instruments hosted by the museums Schloss Kremsegg, Kremsmünster, Austria and Handelhaus, Halle, Germany, among piano predecessors (clavichord, cimbalom, harpsichord…), fortepianos and historical pianos.

BRASSWIND ENGINEERING: SOME PRACTICAL OBSERVATIONS

Vereecke Hannes
Institute of Music Acoustics, University of Music and Performing Arts Vienna, Austria
vereecke@mdw.ac.at

ABSTRACT

Well known for his piano and harp actions, Sébastien Érard (1752-1831) also worked more than thirty years on the development of a new pipe organ on which it was possible to express musical dynamics. Achieved shortly before Érard's death, this ingenious mechanism never really had the chance to be used. The most important instrument of the kind was built in Paris in 1829 for the King's chapel but was badly damaged during the revolutionary events of July 1830. Rebuilt in 1854 in the Castel of Tuileries, it was destroyed when the building was set on fire in May 1871. Apart this organ, it was commonly believed that two other instruments were built during Érard's life but their becoming was not clearly established until today. The orgue expressif of Gabriel Joseph Grenié (1756-1837) is also mainly known from literature. Pioneer in the use of free reed, Grenié patented in 1810 an expressive instrument in which reeds were laid out in resonators. His system would be developed by his apprentice Théodore Achille Müller (1801-1871) until the 1860's, supplanted by Debain's and Alexandre's harmoniums in the mid-19th century. As well as Érard's organs, none instrument from Grenié seemed to have survived. This paper will examine Erard and Grenié's systems, very different in their approach of the same purpose. The story of the built organs by these makers will be retraced up to the present day.

SINGLE NOTE INSTRUMENTS – FROM SPECTRA TO PERFORMANCE

Noam Amir
Tel Aviv University, Ramat Aviv, Israel
noama@post.tau.ac.il

ABSTRACT

A small number of ethnic instruments from different parts of the world produce a single fundamental frequency in their traditional use. Most notable are the didgeridoo, the mouth-harp, and the overtone singing technique. Constraining a musical instrument to play a single frequency sounds like a contradiction in terms, however these instruments resort to a variety of means to nevertheless make their sound rich and musically interesting. In this talk we will discuss the characteristic spectra of these instruments, how this influences their playing styles, and how they rely on the perception of the listeners to create music that is pleasing to traditional as well as contemporary audiences.

METHODS FOR EXCITING WINE GLASSES BY COUPLING TO PLUCKED STRINGS - THEORY AND EXPERIMENT

Lior Arbel[1], Yoav Schechne[2], Noam Amir[3]
[1] Industrial Design, Technion – Israel Institute of Technology, Israel
[2] Dept. of Electrical Engineering, Technion - Israel Institute of Technology, Haifa, Israel
[3] Department of Communication Disorders, Sackler Faculty of Medicine, Tel Aviv University, Israel
lior51@yahoo.com
yoav@ee.technion.ac.il
noama@post.tau.ac.il

ABSTRACT

Wine glasses can be used to produce musical sounds, either as standalone makeshift instruments or as components of carefully tuned instruments such as the Glass Harp. Typically, wine glasses are played either by rubbing a moistened finger around the rim, or by using a mallet or a bow. The glasses are tuned to specific pitches and each glass is used for producing a single note. The current study proposes a new method for exciting wine glasses, using a concept similar to that of sympathetic strings, found in such instruments as the Sitar. While the Sitar uses sympathetic resonance between sets of coupled strings, this research explores the idea of using sympathetic resonance between strings and wine glasses, where the vibration of the string produces vibration in the glass. Two methods for creating string-glass coupling were explored: 1) by direct contact; 2) by using an intermediate component similar to a string instrument's bridge. The coupling component was developed by a process of topology optimization using FEM simulations, resulting in a small cane-shaped design. Experiments tested the responses of three wine glasses having different frequency responses to excitation by pitched strings using both methods.The findings show that both methods produce audible responses from the glasses, with the direct string-glass contact method having the loudest responses. Each glass responded to several different pitches, with each response having a different spectrum. The methods developed in this research offer a new approach to the design of wine glass based instruments. Instruments designed with this approach can have a small number of glasses, each producing different notes without being directly excited by the player. The use of the coupling component allows for greater flexibility in the placement of both glasses and strings.

THE ETIOLOGY OF CHATTER IN THE HIMALAYAN SINGING BOWL

Samantha R. Collin, Chloe L. Keefer, Thomas R. Moore

Rollins College
Florida, USA
tmoore@rollins.edu

ABSTRACT

The Himalayan singing bowl is a nearly symmetric metal bowl that produces a musical sound by rotating a wooden stick around the outside rim. The wooden stick, referred to as a *puja*, excites vibrations through a stick-slip mechanism. The amplitude of vibration is related to the applied force and velocity of the puja as it moves around the bowl. Typically the (2,0) mode dominates the motion, resulting in narrow-band oscillation at a frequency determined by the size of the bowl. However, as the angular velocity of the puja increases and/or the force of the puja on the bowl decreases, an audible chatter will often occur. The goal of the work reported here is to determine the origin of this chatter. Initial results indicate that the puja does not lie directly on a node of the radiating deflection shape. Therefore, it appears that as the amplitude of the radiating mode is increased the puja can lose contact with the bowl resulting in a chattering sound.

1. INTRODUCTION

The Himalayan singing bowl is an idiophone that originated around 500 B.C.E. in the Tibetan mountain region. This instrument was classically used for meditation and religious purposes, but today it is also used for contemporary music making and personal enjoyment. The nearly symmetric bowls can range from approximately 10 to 30 centimeters in diameter and are traditionally made of several metals, including: tin, mercury, copper, gold, silver, lead, and iron. The instrument is played by rotating the *puja*, typically a wooden stick covered with felt or leather, around the outer rim of the bowl.[1]

This instrument is known to produce its signature ringing sound from a complex stick-slip mechanism, which is assumed to be similar to the process of using ones finger to make a wine glass sing.[2] While this stick-slip motion has been extensively studied in other instruments, to our knowledge, there have been few attempts to model the singing bowl and even fewer attempts to experimentally investigate the instrument. In the work reported here, we experimentally investigate a well known characteristic of the singing bowl, which we refer to as chatter. This phenomenon can be described as the rapid ”knocking” of the puja on the bowl as it rotates around the bowl.

2. THEORY

To our knowledge the work reported by Inacio et al. represents the only attempt to model the singing bowl. In this work, the rim motion of the singing bowl was modeled as a ring.[3] The results of this modeling effort predicted many of the notable characteristics of the singing bowl, including the ratio of the frequencies of the bowl resonances. Furthermore, acoustic measurements indicated that the radiating deflection shape is dominated by the (2,0) mode and that the deflection shape rotates around the bowl with the puja. The model proposed by Inacio et al. also predicted that as the angular velocity of the puja increases and/or the force of the puja on the bowl decreases chatter will occur.

While these investigations provided insight into the physics involved in the motion of the singing bowl and confirmed some of the predictions from the model, many questions remain unanswered. It was proposed that the puja always lies near the node of the rotating deflection shape, but the exact location was not determined and it is not clear why the puja does not lie directly on the node. Additionally, the model used a simplified representation of stick-slip motion that has yet to be experimentally examined. In the work reported here, we experimentally confirm that the deflection shape primarily consists of the (2,0) modal structure that rotates with the puja. We also investigate the stick-slip motion of the puja and confirm that the puja does not lie at a point of minimum displacement on the bowl.

3. EXPERIMENTS

The singing bowl under investigation has a diameter of approximately 123 mm, a height of approximately 72.5 mm, and a thickness of approximately 3.72 mm. The first resonant frequency occurs at 620.7 ± 0.3 Hz.

To confirm that the deflection shape does indeed rotate around the bowl with a (2,0) modal structure, the vibrations of the bowl during play were studied optically using high-speed electronic speckle pattern interferometry (HSESPI).[4] The bowl was mounted on a stationary platform and the puja was rotated around the bowl by hand. The frame rate of the camera was 9.9 kHz. To view the relative displacement of the bowl as the puja rotated around it, each frame was subtracted from a frame captured at a point of minimum deflection. These images resemble a contour map where black lines represent contours of equal displacement. The interferrograms shown in Fig. 1 verify that the deflection shape resembles the (2,0) mode shape of a ring and that the position of the node travels around the bowl in near proximity to the puja.

The resonance frequencies of the bowl were determined by striking the stationary bowl with the puja and recording the audio signal with a microphone. We identified the frequency components with significant power from a power spectrum similar to the one shown in Fig. 2.

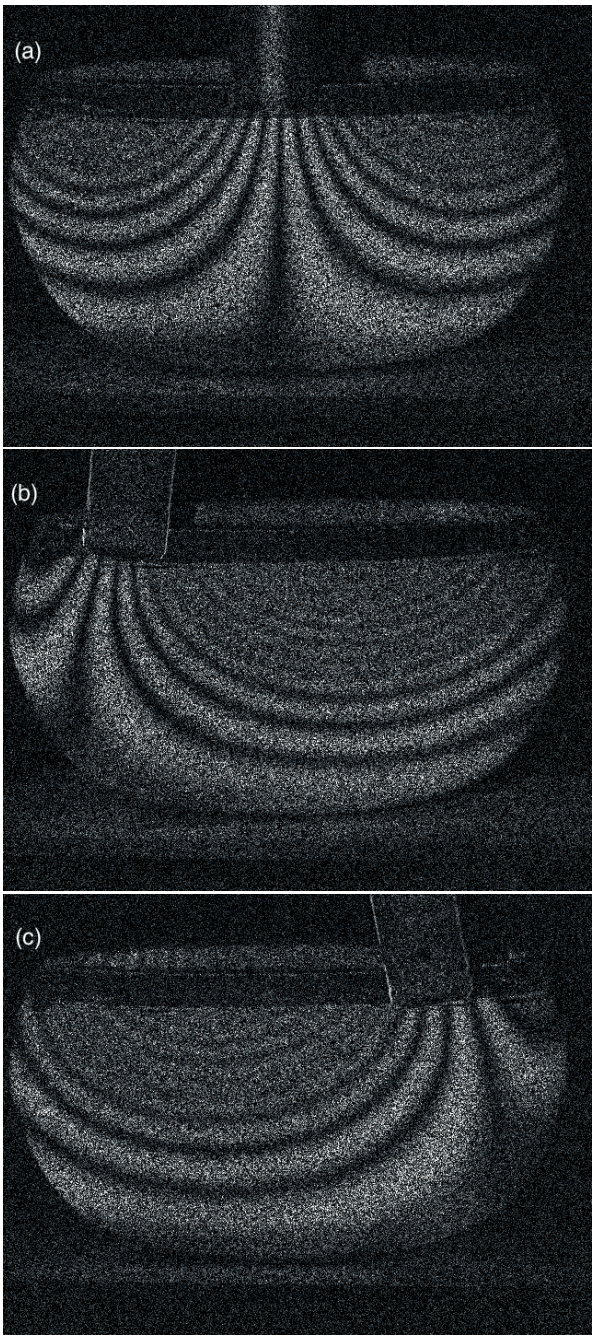

Figure 1: HSESPI images of the singing bowl during normal play (a) with the puja centered in the camera frame; (b) with the puja to the left of center; (c) with the puja to the right of center.

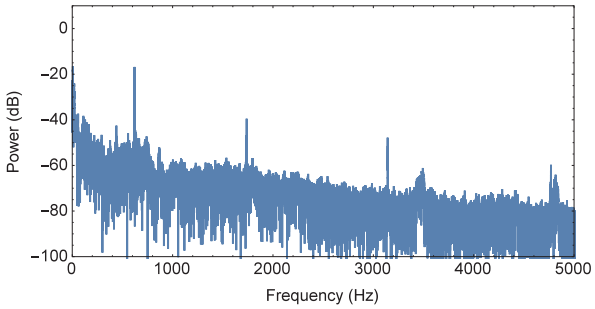

Figure 2: Power spectrum of the sound produced when a stationary singing bowl is struck with the puja.

The bowl was then mounted on a platform rotated by a variable speed motor. A wooden puja was mounted next to the bowl and touched the outer rim as the bowl rotated. The bowl revolved at two different speeds: first at 0.4 revolutions per second and then at 1.1 revolutions per second. While rotating at a slower speed a pure ringing was heard while there was a clear audible chatter when rotating at a faster speed. The audio signals for both speeds are shown in Fig.3.

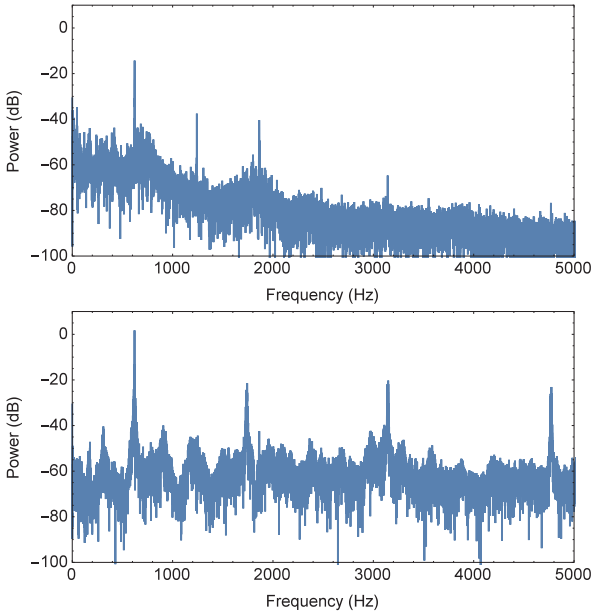

Figure 3: Power spectrum of the sound produced by the singing bowl as it is being played: (a) at 0.4 bowl revolutions per second, with no audible chatter, and (b) at 1.1 bowl revolutions per second, with a distinct audible chatter.

This power spectrum shows four clearly identifiable resonances, at approximately 621 Hz, 1735 Hz, 3144 Hz, and 4770 The ratio between the first two resonances can be predicted by modeling the bowl as a ring, with only approximately 1% difference between predicted and experimental ratios. The model becomes less accurate with the higher resonances, with the difference between the measured and predicted frequencies increasing to approximately 7% for the third resonance and approximately 14% for the fourth.

When no chatter is audible, the dominant frequency component appears at the first resonance frequency. Some harmonics of this frequency are evident in the spectrum, however, these are a product of the non-sinusoidal deflection shape at large amplitudes and do not represent resonances of the bowl. When chatter is heard, the higher resonances of the bowl appear in the power spectrum. This indicates that the bowl is ringing freely, and therefore, the contact between the puja and the bowl during chatter is similar to the contact made when striking the bowl.

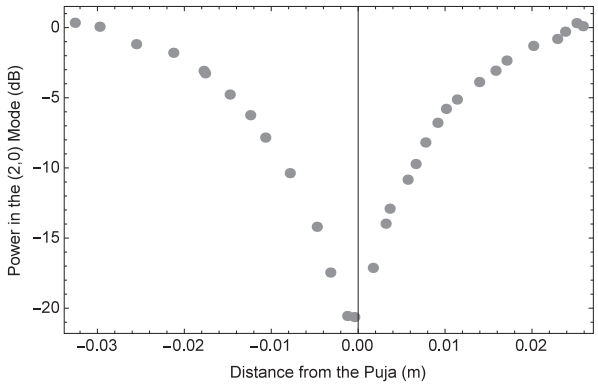

Figure 4: Power in the first resonance frequency recorded by the LDV vs. distance from the puja. Positive distance is in the direction of the bowl's rotation (clockwise). The zero position on the x-axis represents the point of contact.

To determine the position of the puja with respect to the position of the node of the (2,0) mode, which is the point of minimum displacement on the bowl, we measured the displacement of the bowl using a laser doppler vibrometer (LDV). We directed a LDV at the inner rim of the bowl and measured several points near the point of where puja contacted the bowl. A camera recorded a digital image of the puja and the point where the laser was incident on the bowl. From these images the distance from the puja to the point of measurement was calculated.

Figure 4 is a plot of the power in the displacement at the first resonance frequency as a function of position on the bowl. This plot indicates that the position of the node lies within 1.0 $\pm$0.5mm of the where the puja contacts the bowl. In this plot, the puja is ahead of the node in the direction of rotation.

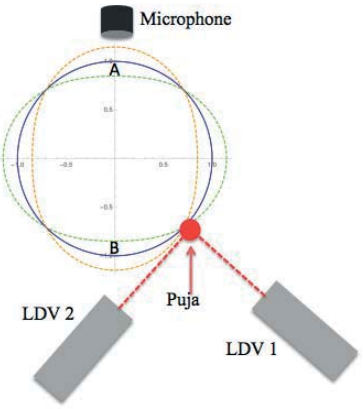

Figure 5: Experimental arrangement for determining the position of the node relative to the puja.

To confirm the position of the node with respect to the point of contact with the puja, we measured the phase difference between the motion of the bowl at one antinode and the puja. In the experimental arrangement shown in Fig. 5, one LDV was directed normal to the puja in the radial direction of the bowl and a second LDV was directed normal to the puja in the tangential direction. A microphone was placed near an antinode on the bowl, labeled as point A. By comparing the radial displacement of the puja to the displacement of the bowl, we were able to measure the relative phase between the puja and the bowl at the antinode. Measurements were made at speeds before and after chatter occurs, with the bowl rotating clockwise and counterclockwise. The tangential displacement of the puja was also studied to gain insight into the stick-slip motion.

4. ANALYSIS

In the final experiment described above, the microphone was placed close to the antinode at point A in Fig. 5. This motion is in phase with the oscillations of the antinode at point B. Figure 6 is a plot of the relative radial phase of the puja when the bowl is rotated at a speed of approximately 0.35 revolutions per second. Measurements when the bowl was rotated clockwise and counter-clockwise are shown. The sinusoidal pattern is attributable to a slight asymmetry in the mounting of the bowl and the pattern repeats four times per revolution of the bowl. It can be determined from Fig. 6 that the relative phase of the puja with respect to the displacement at the antinodes when the bowl is rotating clockwise is π out of phase with the relative phase when the bowl is rotating counter-clockwise.

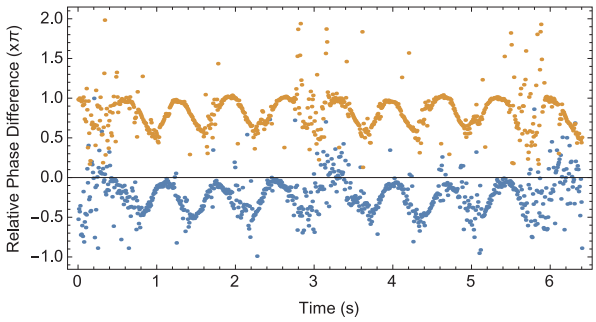

Figure 6: The relative phase of the puja in the radial direction when the bowl is rotating counter-clockwise (orange) and clockwise (blue). The bowl was rotating at 0.35 revolutions per second and periodic chattering occurred.

The radial motion of the puja is in phase with the antinode at point B when the bowl is rotating clockwise and out of phase when the bowl is rotating counter-clockwise. This indicates that the puja leads the node in the direction of rotation. Figure 7 is a schematic showing where the puja contacts the bowl with respect to the node and direction of rotation.

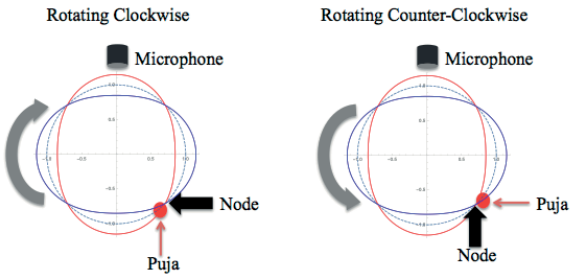

Figure 7: The location of the node relative to the contact point of the puja for clockwise and counter-clockwise rotation.

The second LDV was directed normal to the puja in the tangential direction to measure the stick-slip motion. A graph of typical tangential displacement is shown in Fig. 8. The results of this experiment suggest that a simple stick-slip mechanism

can be used to model the tangential motion of the puja. However, there is clearly a more complicated motion than is normally assumed. Further investigations of the tangential motion are needed to better understand this process.

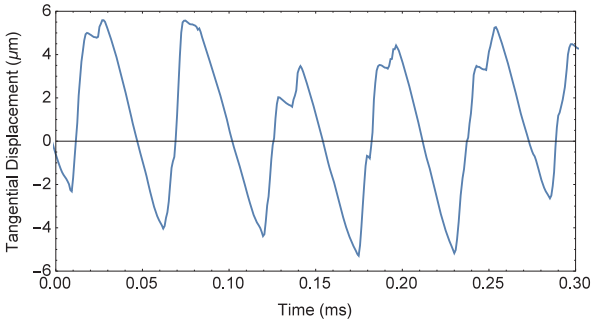

Figure 8: The tangential displacement of the puja when the bowl is rotating counter-clockwise at approximately 0.25 revolutions per second.

5. CONCLUSIONS

In the work reported here, we experimentally investigated the motion of the singing bowl and confirmed some of the predictions made in Ref. 3. When the singing bowl is played, it has a deflection shape that is dominated by the (2,0) mode, and the deflection shape rotates around the bowl with the puja. The puja forces a point of minimum displacement on the bowl, which lies in the vicinity of the contact point of the puja. From the results of the experiments described here, it appears that the point of contact of the puja is not at the node of the deflection shape, but rather the puja leads the node in the direction of rotation. Therefore, as the angular velocity of the puja increases, the amplitude of the radial displacement of the rim of the bowl increases, forcing the puja to briefly lose contact with the bowl and produce chatter.

6. REFERENCES

[1] Eva Judy Jansen, *Singing Bowl: A Practical Handbook of Instruction and Use*, Binkey Kok Pubications, 1990.

[2] A.P. French, "In vino veritas: A study of wineglass acoustics," *Am. J. Phys.*, vol. 51, pp. 688–694, 1983.

[3] O. Inacio, L.L Henrique, and Antunes. J., "The dynamics of tibetan singing bowls," *Acta Acustica united with Acustica*, vol. 92, pp. 637–653, 2006.

[4] Thomas R. Moore, Daniel W. Zietlow, Christopher W. Gorman, Donald C. Griffin, Connor P. Ballance, and David J. Parker, "Transient motion of a circular plate after impact," *J. Acoust. Soc. Am.*, vol. 125, pp. 63–69, 2008.

MODELING STRING BOUNDARY CONDITIONS AND STRING COUPLING IN LUTE INSTRUMENTS

Florian Pfeifle
University of Hamburg, Systematic Musicology, Germany
florian.pfeifle@uni-hamburg.de

ABSTRACT

An idiosyncratic feature of all lute instruments is the specific fixation of the strings leading to certain physical boundary conditions. Alongside the structural functionality of the string adjustment, the bridge and the nut, fixing the taut string at both ends, the string fixation transmits vibrational energy from the strings to the instrument's resonator and vice versa. An effect arising from this bi-directional coupling is a moving string fixation leading to time varying boundary conditions. In addition to this, the specific fixation of the strings leads to differing admittances in the respective transverse polarization of the string, giving rise to non-linear energy transfer between the polarizations. In this treatise, several fixtures are modeled, showing the influence of the boundary conditions on the string motion as well as the mechanical coupling strength in the respective direction of motion. The strings are modeled using finite difference approximations for the spatial domain and a locally symplectic integration scheme for the time domain discretization. The numerical results are compared to measurements taken with a high-speed camera and a piezoelectric transducer, giving insight to the feasibility of the proposed model parameters and showing the influence on the resulting sound.

TIME-DOMAIN SIMULATIONS OF A TEN-STRING BRAZILIAN GUITAR

Guilherme Paiva[1], François Gautier[2], Frédéric Ablitzer[2], José Maria C. Santos[3]
[1] Laboratoire d'Acoustique de l'Université du Maine, France/University of Campinas, Brazil
[2] Laboratoire d'Acoustique de l'Université du Maine, France
[3] University of Campinas, Brazil
pitupaiva@gmail.com
francois.gautier@univ-lemans.fr
frederic.ablitzer@univ-lemans.fr
zema@fem.unicamp.br

ABSTRACT

The Brazilian guitars are originally countryside traditional instruments played in different regions of Brazil where several variations of body shapes, types of wood, numbers of strings and tunings are normally found. The present work is focused on the viola capira (portuguese for countryside guitar), which is the most common type and plays a substantial role in traditional and recent Brazilian music. In general, it has ten steel strings arranged in five pairs which are coupled to the soundboard through the bridge in the same way of classical guitars. In order to analyse the interaction between the body and the strings of the instrument, a physical modelling based on an hybrid approach is developped; body modes are identified using experimental modal analysis and are coupled to the modes of an array of strings. A set of time-domain simulations is performed in order to reveal some specificities of the string-body coupling on the Brazilian guitars in terms of sympathetic resonances and beating phenomena.

INVESTIGATION OF TANPURA STRING VIBRATIONS USING A TWO-DIMENSIONAL TIME-DOMAIN MODEL INCORPORATING COUPLING AND BRIDGE FRICTION

Jamie Bridges and Maarten Van Walstijn

Sonic Arts Research Centre
Queens University Belfast, Belfast
jbridges05@qub.ac.uk

ABSTRACT

Tanpura string vibrations have been investigated previously using numerical models based on energy conserving schemes derived from a Hamiltonian description in one-dimensional form. Such time-domain models have the property that, for the lossless case, the numerical Hamiltonian (representing total energy of the system) can be proven to be constant from one time step to the next, irrespective of any of the system parameters; in practice the Hamiltonian can be shown to be conserved within machine precision. Models of this kind can reproduce a jvari effect, which results from the bridge-string interaction.

However the one-dimensional formulation has recently been shown to fail to replicate the jvaris strong dependence on the thread placement. As a first step towards simulations which accurately emulate this sensitivity to the thread placement, a two-dimensional model is proposed, incorporating coupling of controllable level between the two string polarisations at the string termination opposite from the barrier. In addition, a friction force acting when the string slides across the bridge in horizontal direction is introduced, thus effecting a further damping mechanism.

In this preliminary study, the string is terminated at the position of the thread. As in the one-dimensional model, an implicit scheme has to be used to solve the system, employing Newtons method to calculate the updated positions and momentums of each string segment.

The two-dimensional model is proven to be energy conserving when the loss parameters are set to zero, irrespective of the coupling constant. Both frequency-dependent and independent losses are then added to the string, so that the model can be compared to analogous instruments. The influence of coupling and the bridge friction are investigated.

1. INTRODUCTION

The tanpura is a traditional Indian stringed drone instrument which exhibits an interesting tonal characteristic known as the "jvari". Raman[1] theorised that the jvari (which consists of a descending formant of sustained high frequencies) also exhibited by the veena and sitar is a result of the curved bridge of these instruments. Investigation into the jvari has also been carried out by Bertrand[2] and Valette[3]. Bertrand conducted experiments using compression sensitive equipment to measure the displacement of a string vibrating against a curved barrier and was able to produce graphs showing the time varying formant phenomenon. Valette was able to predict the Helmholtz motion of the string and the precursor effect on the nut force signal due to the barrier. Despite the fact that this work has been done, a computer model which can fully simulate the behaviour of the real instrument is yet to be made, this indicates that the jvari is not yet fully understood. Current models can produce jvari like behaviour but do not capture the strong dependence of the jvari on the thread presence and placement in the tanpura. To be able to explain the jvari better more physical effects will have to be considered when attempting to describe the tanpura. This paper deals with trying to implement some previously unconsidered effects into an existing model.

When the strings are able to collide with the rigid barrier a non-linear effect is introduced. This non-linear contact effect can lead to non-physical energy jumps if the traditional Newtonian equations are used as the basis for numerical models without suitable precautions being taken [4]. These energy jumps can lead to a build up of energy which gives an unstable model. Methods which can be used to deal with this problem include energy methods and symplectic schemes. Energy preserving methods aim to conserve an energy like quantity, depending on the starting point of the model this can either lead to conserving the discrete time analogue to the total energy (Hamiltonian) [5] or an energy like quantity which does not exactly equal the true energy [6, 7]. Symplectic methods [8, 9] are ones in which the sum of all of the exterior products of the differential steps of the matched pairs of position and momentum is conserved as the system evolves over time. The already existing model which uses the Hamiltonian of the system as a basis to ensure energy conservation [10] will be briefly discussed. After this the method of expanding the model to have two oscillation planes and coupling will be detailed followed by a discussion of transverse bridge friction.

2. METHODOLOGY

An energy conserving method which preserves the Hamiltonian of the system is utilised beginning with a lossless, stiff string[11] vibrating in one dimension transverse to the string with simply supported boundary conditions. The string's dynamics can be described in the Newtonian manner:

$$\rho A\frac{\partial^2 y}{\partial t^2} = \tau\frac{\partial^2 y}{\partial z^2} - EI\frac{\partial^4 y}{\partial z^4} + k_c\lfloor(y_c - y)^\alpha\rfloor \qquad (1)$$

In this equation y is the displacement of the string, z is the distance along the string and y_c is the bridge profile as a function of z. k_c is the stiffness of the barrier, EI is the Young's modulus of the string material, α is a coefficient which defines the exponent of the force equation for the bridge repulsion, A is the cross sectional area of the string and ρ is the mass density of the string. The term $\lfloor(y_c - y)^\alpha\rfloor$ indicates that this term is zero when the string is not in contact with the barrier and has the value calculated when the string is touching the barrier. This term will always be non-negative as when the string is touching the barrier $y_c - y \geq 0$. When converted to the Hamiltonian

form and discretised this gives (for a fuller description of the derivation refer to [10]):

$$H^n = c_1[(q^n)^t(q^n)+(y^n)^t D(y^n)+\zeta 1^t\lfloor(y_c-y^n)^{\alpha+1}\rfloor \quad (2)$$

The discretisation here involves breaking the string up into M segments. H^n is the Hamiltonian over a spatial step at time step n, q^n is the scaled momentum vector at time step n of size $M-1$, y^n is the displacement vector of size $M-1$ at time step n, all y and q are at the same time step in (2), D is the spatial differentiation matrix which takes into account terms due to stiffness and tension, c_1 and ζ are constants created by combining other constants. The vectors for momentum and position are of length $M-1$ because the last point M is fixed by the boundary conditions and it is therefore never updated.

$$c_1 = \frac{2\rho A\Delta x}{\Delta t^2} \quad (3)$$

and

$$\zeta = \frac{k_c\Delta t^2}{2\rho A(\alpha+1)} \quad (4)$$

where Δx is a discretised spatial step and Δt is the times between samples. (2) can be rewritten as:

$$H^n = \Delta x\Big[\frac{(p^n)^t(p^n)}{2\rho A}+\frac{\tau}{2\Delta x^2}(D_1y^n)^t(D_1(y^n))+ \frac{EI}{2\Delta x^4}(D_2(y^n))^t(D_2(y^n))+\frac{k_c}{\alpha+1}1^t\lfloor(y_c-y^n)^{\alpha+1}\rfloor\Big] \quad (5)$$

so that the terms of the D matrix can be more easily interpreted. D_1 represents spatially differentiating once and D_2 twice. It can be shown[10] that the Hamiltonian is the same over two time steps, this proves that this method is energy conserving. Using Hamilton's equations of motion a scheme for finding the dynamics of the string can be constructed. After some rearranging and redefining (which can be looked up in [10]) the equation:

$$F = (I+D)s+2(Dy^n-q^n)+\zeta s^{-1}(\lfloor(y_c-y^n-s)^{\alpha+1}\rfloor -\lfloor(y_c-y^n)^{\alpha+1}\rfloor) = 0 \quad (6)$$

can be constructed where

$$s = y^{n+1}-y^n = q^{n+1}+q^n \quad (7)$$

and I is the identity matrix. By using a Newton Raphson solver[12, 13] to converge on a value for s which solves (6) the momentum and position for each string element at the next time step can be determined. Losses are introduced by discretising their force equations and then adding them in to (6) to give:

$$F = \big[(1+\frac{\gamma\Delta t}{2})I+(1+\frac{2\eta}{\Delta t})D\big]s+2(Dy^n-q^n)+ \zeta s^{-1}(\lfloor(y_c-y^n-s)^{\alpha+1}\rfloor-\lfloor(y_c-y^n)^{\alpha+1}\rfloor) = 0 \quad (8)$$

The combined continuous domain loss equations are defined as:

$$F_l = \eta(\tau\frac{\partial^3 y}{\partial t\partial z^2}-EI\frac{\partial^5 y}{\partial t\partial z^4})-\rho A\gamma\frac{\partial y}{\partial t} \quad (9)$$

These losses are resistive and Kelvin-Voigt terms which come from vibration and moving through a fluid, η and γ roughly define the friction inside the string and the string going through the air. (8) is solved in the exact same way as (6) to give the update equation taking into account losses. F_l cannot cause the model to become unstable as when it is added in $\frac{\partial H}{\partial t}\leqslant 0$ [10].

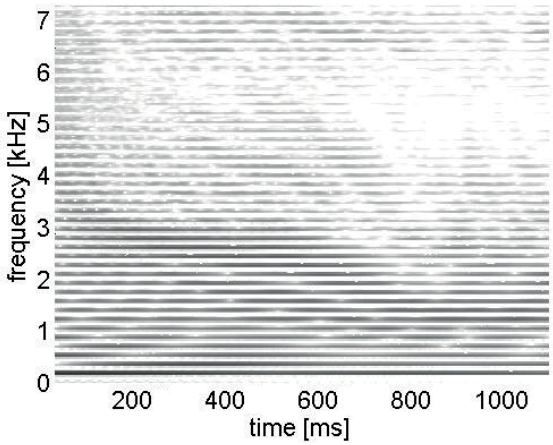

Figure 1: Spectrogram of the nut force in the y direction.

Figure 1 shows a spectrogram of the nut force in the one dimensional model, the jvari is characterised by the high frequency formant whose spectral centroid changes over time. This has the form of an intial drop in frequency followed by a plateau and then another drop. The initial condition that lead to this spectrogram was the string being set in a triangular shape with its maximum half way along the string. All simulations discussed in this paper were run with this initial condition. The constants used in the model to generate Figure 1 were; string length of 0.628m, mass per unit length of 5.5842×10^{-4}Kg/m, tension of 31.4675N, stiffness of $8.3498\times10^{-5}\mathrm{Pam}^4$, frequency independent damping coefficient of 0.1, frequency dependent damping coefficient of 1×10^{-8}, sampling frequency of 4×44100Hz and 200 string segments.

3. EXPANSION TO TWO DIMENSIONS AND INTRODUCING COUPLING

When a string is plucked it is rare that it will be plucked in a manner which excites it along only one of the axis as shown in Figure 2. Even if the string was plucked in such a manner there would still be energy transferred between oscillations along each axes as the bridge and nut in a real instrument do not hold the string perfectly steady and slight asymmetries in these parts will give a transfer of energy. This can be observed on a string instrument through simple observation by plucking a string and seeing the "whirling" which takes place (whirling referring to the tendency of the string to move in a spiralling motion around the z axis as shown in Figure 2). As can be seen in Figure 2 the string will move across the bridge when whirling, this introduces a frictional force in the x direction.

To add nut coupling into a tanpura model first the model must be generalised so that the string can vibrate in the two directions. In the absence of coupling a string vibrating in two dimensions can be considered to be two separate strings as no energy can be transferred between them. This means that energy conservation (within machine precision) in the lossless case is assured as both strings conserve energy and are separate systems. As the two strings are representing two planes of oscillation of the same string they have the same physical parameters associated with them and are chosen to have the same number of string segments to keep the formulation of the new model sim-

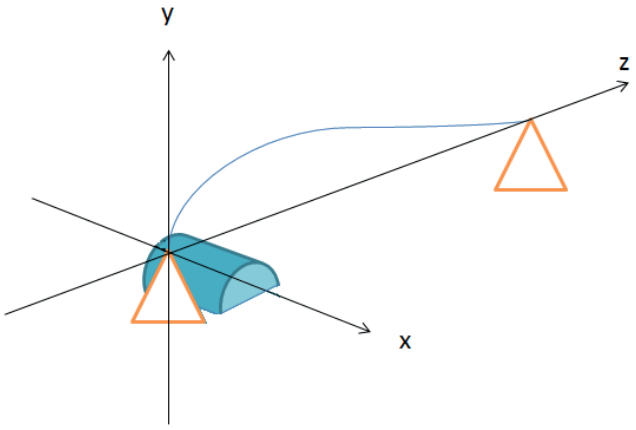

Figure 2: Diagram of the extended model. The triangles represent the points at which the string is terminated, the cylinder section the bridge and the blue line the string.

ple. The extension to two polarisations can be achieved simply though scaling up the vectors and matrices to include the other string. In (5) y^n will be replaced by:

$$r^n = \begin{pmatrix} x^n \\ y^n \end{pmatrix} \tag{10}$$

where x^n and y^n are the vectors of length $M-1$ containing all of the x and y positions of the string segments at time step n. p^n is replaced by:

$$p^n = \begin{pmatrix} {p_x}^n \\ {p_y}^n \end{pmatrix} \tag{11}$$

where ${p_x}^n$ and ${p_y}^n$ are the vectors of length $M-1$ containing all of the p_x and p_y values of the string segments at time step n. For the two dimensional string the second derivative approximation matrix is:

$$D_{2,2} = \begin{pmatrix} D_{2,1} & 0 \\ 0 & D_{2,1} \end{pmatrix} \tag{12}$$

where 0 represents a $M-1 \times M-1$ matrix of zeros and $D_{2,1}$ is the one dimensional spatial derivative matrix of the size $M-1 \times M-1$:

$$D_{2,1} = \begin{pmatrix} -2 & 1 & 0 & \cdots & \cdots & 0 \\ 1 & -2 & 1 & & & \vdots \\ 0 & \ddots & \ddots & \ddots & & \vdots \\ \vdots & & \ddots & \ddots & \ddots & 0 \\ \vdots & & & 1 & -2 & 1 \\ 0 & \cdots & 0 & 0 & 1 & -2 \end{pmatrix} \tag{13}$$

Using these equations in the relevant places (8) can again be used to approximate the dynamics of the system in exactly the same way as in the one dimensional case, having the effect of solving two completely strings at the same time. The barrier force now has additional zeros corresponding to the entire length of the x position vector in the relevant place as the string will not experience the repulsive barrier force in this direction. Now the update equations read:

$$r^{n+1} = s + r^n \tag{14}$$

and

$$q^{n+1} = s - q^n \tag{15}$$

where

$$s = \begin{pmatrix} s_x \\ s_y \end{pmatrix} \tag{16}$$

To introduce coupling a simple approach was adopted, the forces acting on the unfixed points closest to the nut on each string vibration axis were chosen to depend upon spatial gradients at the position of the other. There are other methods for introducing coupling such as that used by Pate[14] in the context of electric guitars. (17) shows how the second spatial derivative matrix, $D_{2,2}$, is altered with this in mind.

$$D_{2,2} = \left(\begin{array}{ccc|ccc} & & & 0 & \cdots & 0 \\ & D_{2,1} & & \vdots & \ddots & \vdots \\ & & & 0 & \cdots & \theta \\ \hline - & - & - & + & - & - & - \\ 0 & \cdots & 0 & & & & \\ \vdots & \ddots & \vdots & & & D_{2,1} & \\ 0 & \cdots & \theta & & & & \end{array}\right) \tag{17}$$

The entries in the matrix at the points $(2M-2, M-1)$ and $(M-1, 2M-2)$ have the value θ which has the effect of enabling the transfer of energy between the strings, this can be more clearly seen by looking at the explicit equations for the second derivative approximations at these points (all y_m are at the same time point).

$$\frac{d^2 y_{M-1}}{dx^2} \approx \frac{y_{M-2} - 2y_{M-1} + \theta y_{2M-1}}{\Delta x^2} \tag{18}$$

and

$$\frac{d^2 y_{2(M-1)}}{dx^2} \approx \frac{y_{2(M-1)-1} - 2y_{2(M-1)} + \theta y_{M-1}}{\Delta x^2} \tag{19}$$

When $\theta = 1$ these equations are functionally the same as considering the system as one string. In the context of this model this results in all energy being completely transferred to the other string at the nut end point (this was also observed through testing the model). When $\theta = 0$ the strings are uncoupled and are two separate systems with no transfer of energy possible. Between 0 and 1 some energy will be transferred between the strings which is effectively coupling. θ can also lie between -1 and 0, as a wave would pass through the negative twice to return to the string where it originated the negative will cancel out. The sign of θ can be observed in the direction which the coupling force pushes the other string along its displacement axis.

When coupling is added the lossless model can be proven to still be energy conserving within machine precision in an identical way to that shown by Chatziioannou and van Walstijn[10] so long as the matrix D remains symmetric. With $\theta = 0$ the spectrogram of the nut force in the y direction would be identical to that shown in Figure 1, Figure 3 shows the spectrogram with the coupling included. Figure 3 was simulated using identical parameters (except for the introduction of the second dimension and coupling) as the simulation which generated Figure 1. A value for θ of 0.1 was assumed and used throughout, this value was chosen as it fell within the required limits and gave noticeable effects. When Figures 1 and 3 are compared some subtle differences can be observed between the spectrograms, Figure 3 has a less steep drop off at the end of the jvari and the higher frequency content above the jvari varies over time in a different manner between the two.

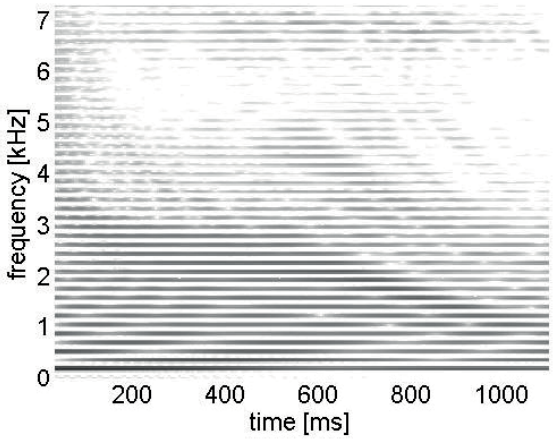

Figure 3: Spectrogram of the nut force in the y direction with coupling present.

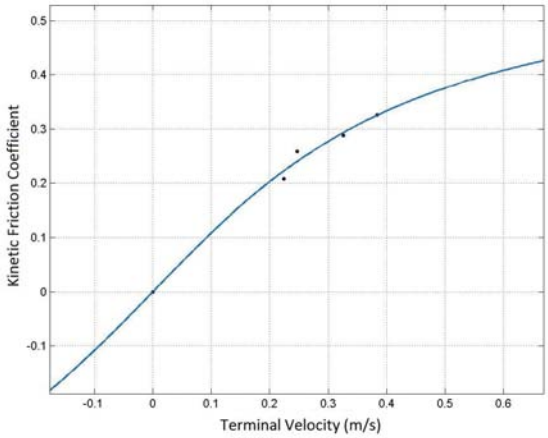

Figure 4: Graph showing the fitted atan curve (blue line)to the data gained from the experiment (black dots) detailed in section 3.3. The R-square value of the fit is 0.9913 indicating a good match.

4. BRIDGE FRICTION

4.1. Defining the tangential bridge friction and incorporating it into the model

When the string moves across the bridge in the x direction it will experience a frictional force. The form used for the kinetic friction coefficient that defines this force is a modified version of that detailed by Desvages[15], with the sticking component removed as sticking was assumed not to occur in the system being considered. This leaves the kinetic friction coefficient being defined as:

$$\mu(v) = c_1 \arctan(c_2 v) \tag{20}$$

where v is the relative velocity between the objects moving across each other, c_1 and c_2 are constants which characterise the interaction between the two materials sliding across each other. The force equation which is used in the model is:

$$F_{\mathrm{bf}} = -F_{\mathrm{n}}\mu(v_x) \tag{21}$$

The normal force, F_{n}, is the opposite of the bridge force so (20) can be rewritten in a discretised form as:

$$\begin{aligned} F_{\mathrm{bf}} = -\zeta {s_x}^{-1}(\lfloor (y_c - y^n - s_y)^{\alpha+1} \rfloor \\ -\lfloor (y_c - y^n)^{\alpha+1} \rfloor) c_1 \arctan(c_2 v_x(s_x)) \end{aligned} \tag{22}$$

The barrier friction term is added into the formulation in the same way as the other losses. The contribution of F_{bf} to F depends on both s_x because of the tangential velocity term and s_y from the barrier force term.

4.2. Finding the values of c_1 and c_2

To include the bridge friction an experiment had to be carried out to find the values of the constants in the definition of the kinetic friction as suitable data for the required materials could not be found. The experiment was carried out by allowing a tanpura bridge to slide down the three unwound strings on a guitar and taking a video of this. Unwound guitar strings were chosen as they are the most similar to tanpura string. The video was then analysed to find the velocity of the bridge over time, as the camera was only capable of taking videos at 30fps and the bridge moved quite fast there was a high uncertainty in the bridge position. Because of this uncertainty in the velocity the terminal velocity of the bridge was judged to be a more accurate measure than the velocity at each time point as it could be calculated over multiple time points. When the position against time plot became straight the linear section was fitted with a straight line and the gradient of this was taken to be the terminal velocity. Each iteration of the experiment gave a data point which consisted of a terminal velocity and the normal force. The equation which governs the bridge sliding down the guitar neck is:

$$F_{\mathrm{g}} - \mu(v)F_n = ma \tag{23}$$

where F_{g} is the gravitational force acting on the tanpura bridge, F_n is the normal force, m is the mass of the tanpura bridge and a is the acceleration of the tanpura bridge.
The normal force can be re-expressed as:

$$F_{\mathrm{n}} = F_{\mathrm{g}} \cos(\phi) \tag{24}$$

where ϕ is the angle that the guitar neck is held at compared to the horizontal axis. At terminal velocity $a = 0$ and so the equation for $\mu(v)$ can be rewritten as:

$$\mu(v) = \frac{1}{\cos(\phi)} \tag{25}$$

This allows the kinetic friction coefficient to be fitted by combining (19) and (24) into

$$c_1 \arctan(c_2 v) = \frac{1}{\cos(\phi)} \tag{26}$$

Using the angles and velocities measured as well as by noting that an additional point can be added at (0,0) because there is no kinetic friction at zero velocity the data can be fitted to an $arctan$ function using MATLAB's cftool, this is shown in Figure 4. The coefficients were determined to be $c_1 = 0.39$ and $c_2 = 2.84$. These result are reasonable (for most smooth materials the kinetic friction coefficient limit is between 0.3 and 0.7) but due to the rough nature of the experiment are estimates.

Figure 5 shows the spectrogram of the simulation run with the same parameter values as in Figure 3, apart from the addition of the barrier friction. It can be seen that the bridge friction has an effect on the shape of the simulated jvari, the second drop in the spectral centroid frequency is steeper in Figure 3.

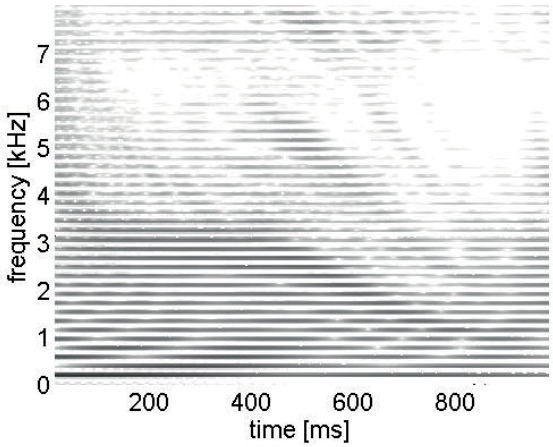

Figure 5: Simulation run with barrier friction.

5. EXAMINING THE SPECTROGRAMS OF SIMULATIONS WITH VARIED BRIDGE-THREAD DISTANCE

Spectrograms of the force in the y direction at the nut were taken to observe the jvari with different bridge centre positions. These simulations were run with the same parameters as the ones that were used to generate the other figures in this report.

It can be seen from Figure 6 that varying the bridge position has a significant effect on the shape of the jvari in the model. Changing the bridge position is analogous to varying the thread position in a real tanpura . Both involve the distance between the thread and the bridge maximum varying. Some general trends can be observed from the spectrograms, as the distance between the thread and the bridge is increased the plateau of the jvari is shortened and the central frequency of the plateau is increased. As the distance is increased the the steepness of the initial and final drops in the frequency of the jvari also increase. It can be qualitatively observed that the jvari is highly dependant on thread position in a real tanpura but experiments would have to be carried out to check whether the model correctly predicts how the jvari varies.

6. CONCLUSIONS AND FUTURE WORK

In this paper it has been shown that already existing models of the tanpura can be expanded to contain two polarisations of oscillation with coupling between them and that this new model retains the characteristic of being energy conserving to within machine precision in the lossless case. Bridge friction was also added to the model and rough estimates for necessary parameters were found by experiment. Both adding friction and coupling were shown to have an impact on the shape of the jvari but experiments will have to be carried out to ascertain a better value for θ and to check to see whether the coupling is frequency dependant. If the coupling is found to be frequency dependent then the model will have to be altered as the coupling included here is frequency independent.

7. REFERENCES

[1] Chandrasekhara Venkata Raman, "On some Indian stringed instruments," *Proceedings of the Indian Association for the Cultivation of Science*, vol. 7, pp. 29–33, 1921.

[2] Daniel Bertrand, *Les chevalets "plats" de la lutherie de l'inde*, Direction de la Musique et de la Danse Mission de la Recherche Musicale er Choregraphique, 1992.

[3] C. Valette, C. Cuesta, M. Castellengo, and C. Besnainou, "The tampura bridge as a precursive wave generator," *Acta Acustica united with Acustica*, vol. 74, no. 3, pp. 201–208, 1991.

[4] S. Bilbao, *Numerical Sound Synthesis*, Wiley & Sons, Chichester, UK, 2009.

[5] S. Bilbao, "Numerical Modeling of String/Barrier Collisions," in *ISMA*, Le Mans, France, 2014.

[6] Juliette Chabassier and Patrick Joly, "Energy preserving schemes for nonlinear Hamiltonian systems of wave equations: Application to the vibrating piano string," *Computer Methods in Applied Mechanics and Engineering*, vol. 199, no. 45, pp. 2779–2795, 2010.

[7] M. van Walstijn and V. Chatziioannou, "Numerical Simulation of Tanpura String Vibrations," in *Proc. International Symposium on Musical Acoustics*, 2014.

[8] J. M. Sanz-Serna, "Runge-Kutta schemes for Hamiltonian systems," *BIT Numerical Mathematics*, vol. 28, no. 4, pp. 877–883, 1988.

[9] R. Abraham, *Foundations of Mechanics*, W. A. Benjamin, Inc, 1967.

[10] Vasileios Chatziioannou and Maarten van Walstijn, "Energy conserving schemes for the simulation of musical instrument contact dynamics," *Journal of Sound and Vibration*, vol. 339, pp. 262–279, 2015.

[11] J Ahn and D Stewart, "An euler-bernoulli beam with dynamic frictionless contact: penalty approximation and existence," *Numerical Functiona; Analysis and Optimization*, vol. 28, no. 9-10, pp. 1003–1026, 2007.

[12] C. Baker C. Phillips, *The Numerical Solution of Nonlinear Problems*, Oxford University Press, 1981.

[13] V. Chatziioannou and M. Van Walstijn, "Sound Synthesis for Contact-Driven Musical Instruments via Discretisation of Hamiltons Equations," in *ISMA*, Le Mans, France, 2014.

[14] Arthur Pat, Jean-Loc Le Carrou, and Benot Fabre, "Predicting the decay time of solid body electric guitar tones," *The Journal of the Acoustical Society of America*, vol. 135, no. 5, pp. 3045–3055, 2014.

[15] C. Desvages S. Bilbao, "Physical modelling of nonlinear player-string interactions in bowed string sound synthesis using finite difference methods," in *ISMA*, Le Mans, France, 2014.

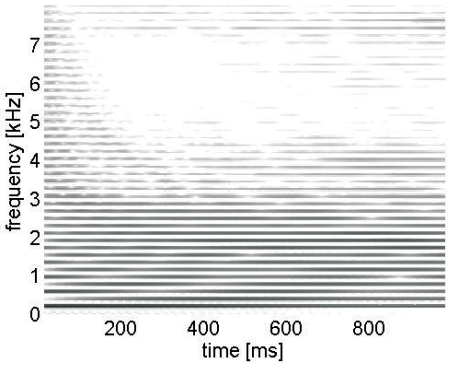

(a) distance from thread to centre of bridge 2.5mm

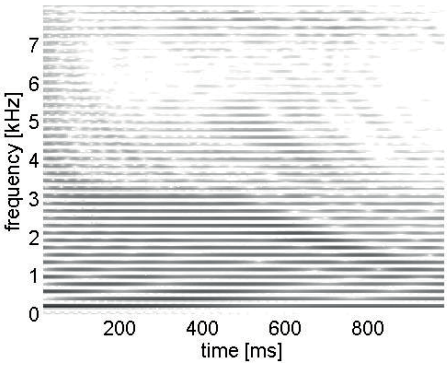

(b) distance from thread to centre of bridge 4mm

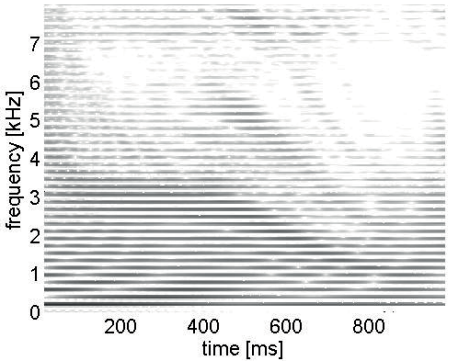

(c) distance from thread to centre of bridge 5mm

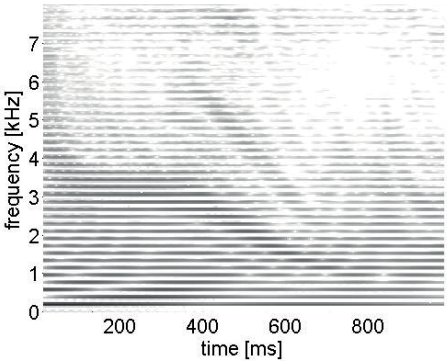

(d) distance from thread to centre of bridge 6mm

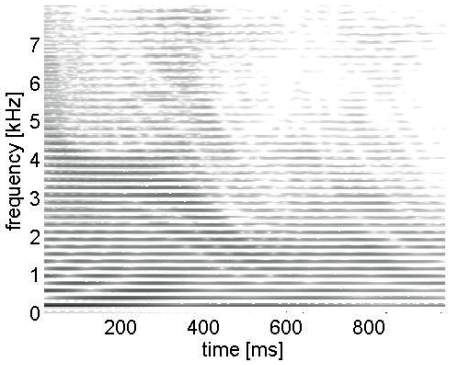

(e) distance from thread to centre of bridge 7.5mm

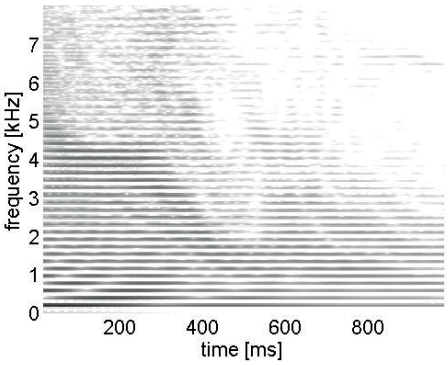

(f) distance from thread to centre of bridge 9mm

Figure 6: Spectrograms of simulated plucks with different bridge positions

PHYSICALLY-BASED DYNAMIC MORPHING OF BEAM SOUNDS

Thomas Hélie[1], *Denis Matignon*[2]
[1] CNRS UMR 9912 – IRCAM, France
[2] University of Toulouse, ISAE-Sup'aéro, France
thomas.helie@ircam.fr
denis.matignon@isae.fr

ABSTRACT

This paper addresses the time-domain simulation of beams made of materials that mutate according to the dynamics. The physical model is based on a standard linear Euler-Bernoulli equation, combined with parameterized nonlinear damping models inside a class that preserves the eigen-modes of the conservative problem. Typical mutations between metal, glass or wood are achieved through a local-in-time interpolation of damping characteristics with respect to the energy. This results in a structured nonlinear beam model which proves to be passive. It is recast in the formalism of Port-Hamiltonian Systems, which naturally provides a power-balanced decomposition into conservative, dissipative and source parts and from which a guaranteed passive simulation can be derived. The paper is organized as follows. First, the linear Euler-Bernoulli model of a beam is recalled. A class of linear damping models that preserve the eigen-modes is proposed. The power balance of this model is derived. Second, a modal decomposition is derived, a pole analysis is presented with a special focus on the dependence on the damping parameters. Third, this linear model is recast in the formalism of Port-Hamiltonian Systems: both the infinite-dimensional problem and the finite-dimensional approximation based on a mode truncation are examined. A guaranteed passive simulation and numerical results are provided. Fourth, the extended class of nonlinear damping models based on interpolating functions is introduced. The consistency with the (linear) modal decomposition is examined. The nonlinear Port-Hamiltonian System is provided. Finally, numerical results for various configurations of mutating characteristics are examined, together with sounds.

ROLE OF MODAL APPROACH FOR SOUND SYNTHESIS OF NONLINEAR SYSTEMS: THE CASE OF PLATES

Michele Ducceschi and Cyril Touzé

UME - ENSTA ParisTech
828, Boulevard des Marchaux, 91762 Palaiseau Cedex, France
ducceschi@ensta.fr

ABSTRACT

Time-domain simulation of musical instruments has shown promising results in recent years. Particularly attractive from a sound synthesis perspective is the resolution of system displaying some degree of nonlinearity, because of the richness of the perceptual information that nonlinearities produce.

In this work, the focus is on one such system, namely a flat (circular or rectangular) plate which, to a first approximation, can efficiently simulate the sound of a gong [1, 2]. From a dynamical perspective, in spite of very different geometries, plates and gongs behave similarly, meaning that the degree of nonlinearity is set by how large the amplitude of vibrations of the flexural waves is. In particular, plates and gongs may attain linear, weakly nonlinear and strongly nonlinear regimes when the amplitude of vibrations is, respectively, much smaller, of the same order of and larger than some defining thickness parameter [3, 4].

The dynamics of plates is well described by a set of two coupled Partial Differential Equations (PDEs) known as the von Kármán equations. For rectangular plates, a family of conservative Finite Difference schemes was developed by Bilbao [5]. An alternative approach is offered in this work, where the von Kármán equations are discretised along the modes of the system in order to reduce the original PDEs to a set of coupled Ordinary Differential Equations (ODEs). This is approach is referred to as *modal approach*, and it used for here in the context of sound synthesis of nonlinear systems [6]. Salient features of this approach include

- implementation of complex decay ratios with no extra effort using modal damping;
- simulation of circular plates without bothering with the problems related to particular spatial grids (a frustrating aspect for Finite Difference schemes);
- fast computational times for linear and weakly nonlinear regimes.

This work intends to show that the modal approach could be applied to a large class of nonlinear problems, against the common misconception that modes are only useful in treating linear problems. Sound examples and videos are shown in order to complete the presentation.

1. REFERENCES

[1] C. Touzé, S. Bilbao, and O. Cadot, "Transition scenario to turbulence in thin vibrating plates," *Journal of Sound and Vibration*, vol. 331, no. 2, pp. 412–433, 2012.

[2] A. Torin and S. Bilbao, "A 3D multiplate environment for sound synthesis," Maynooth, Ireland, 2013.

[3] C. Touzé, O. Thomas, and A. Chaigne, "Asymmetric nonlinear forced vibrations of free-edge circular plates, part I: theory," *Journal of Sound and Vibration*, vol. 258, no. 4, pp. 649–676, 2002.

[4] O. Thomas and S. Bilbao, "Geometrically nonlinear flexural vibrations of plates: In-plane boundary conditions and some symmetry properties," *Journal of Sound and Vibration*, vol. 315, no. 3, pp. 569–590, 2008.

[5] S. Bilbao, "A family of conservative finite difference schemes for the dynamical von karman plate equations," *Numerical Methods for Partial Differential Equations*, vol. 24, no. 1, pp. 193–216, 2008.

[6] M. Ducceschi and C. Touzé, "Modal approach for nonlinear vibrations of damped impacted plates: Application to sound synthesis of gongs and cymbals," *Journal of Sound and Vibration*, vol. 344, pp. 313 – 331, 2015.

PHYSICAL MODELING AND NUMERICAL SIMULATION OF HUMAN PHONATION

Manfred Kaltenbacher[1], Stedan Zörner[1], Andreas Hüppe[1], Petr Sidlof[2]
[1] Vienna University of Technology, Austria
[2] Technical University of Liberec, Czech Republic[3] University of Campinas, Brazil
manfred.kaltenbacher@tuwien.ac.at
stefan.zoerner@tuwien.ac.at
andreas.hueppe@tuwien.ac.at
petr.sidlof@tul.cz

ABSTRACT

The human phonation is a complex interaction of fluid mechanics, solid mechanics and acoustics. As the lungs compress, air flows through the larynx passing the vocal folds which form a narrow constriction, the glottis. The air flow forces the vocal folds to vibrate resulting in a pulsating air stream, which is the main sound generating mechanism for phonation. Hence, our modeling approach is to resolve, within the larynx and adjacent regions, the physical details of the phonation process in space and time by means of partial differential equations (PDEs). Due to limitations in computer resources and current numerical methods, full coupling between all three fields for realistic 3D geometries is currently not feasible. Therefore, we concentrate on prescribed flow computations, evaluate the acoustic sources and perform acoustic computations of the generated sound. In this way the fluid-solid interaction problem, whose accuracy critically depends on reliable geometrical and material parameters of all layers of the vocal folds, is circumvented. We apply the open source program OpenFoam for solving the 3D incompressible Navier-Stokes equations, and CFS++ (in-house research code) to compute the acoustic sources as well as sound propagation. The main findings of our current simulations can be summarized as follows. The dominant acoustic sources of the fundamental frequency as well as its harmonics are located inside the glottis and the highest amplitudes are found in a thin layer right above the surface of the vocal folds. For the non-harmonic frequencies, the acoustic sources are concentrated in the vortical decay region. The simulated formant frequencies for the /i/ and /u/ vowels compared well with the formant frequencies measured on human subjects. Furthermore, the simulations suggested that the false vocal folds induce an amplification of higher harmonics in the radiated acoustic field.

DISCRETE-TIME CONSERVED QUANTITIES FOR DAMPED OSCILLATORS

Vasileios Chatziioannou

Institute of Music Acoustics
University of Music and Performing Arts
Vienna, Austria
chatziioannou@mdw.ac.at

Maarten van Walstijn

Sonic Arts Research Centre
Queen's University Belfast
Belfast, UK
m.vanwalstijn@qub.ac.uk

ABSTRACT

Numerical sound synthesis is often carried out using the finite difference time domain method. In order to analyse the stability of the derived models, energy methods can be used for both linear and nonlinear settings. For Hamiltonian systems the existence of a conserved numerical energy-like quantity can be used to guarantee the stability of the simulations. In this paper it is shown how to derive similar discrete conservation laws in cases where energy is dissipated due to friction or in the presence of an energy source due to an external force. A damped harmonic oscillator (for which an analytic solution is available) is used to present the proposed methodology. After showing how to arrive at a conserved quantity, the simulation of a nonlinear single reed shows an example of an application in the context of musical acoustics.

1. INTRODUCTION

Physics-based sound synthesis usually relies on numerical approximations of the underlying equations of motion of a vibrating system. Various time-stepping methods can be employed to this cause. In the field of Music Acoustics finite difference time domain methods provide an efficient and flexible framework for numerical simulations [1]. Of particular importance, during the formulation of such numerical schemes, is the stability of the algorithms. Stability analysis has lately been carried out using energy methods [2], which are applicable to more general systems, compared to frequency domain approaches [3]. In particular, they offer the possibility of analysing nonlinear models, whose application in musical instrument simulation has recently seen a great increase [4]. The main idea behind energy methods is for the numerical scheme to posses a conserved discrete quantity that can be used to bound the solution size. This inherently links to Hamiltonian systems (without losses), where the conserved quantity H corresponds to the (constant) system energy.

There are however a number of possible shortcomings with this approach. Firstly, for some systems dissipation plays a crucial role in the dynamics, and conservation of the internal system energy does not so readily apply. One particularly challenging example is the numerical simulation of shock waves in tubes, in which there is a need for adding further, artificial dissipation in order to avoid spurious oscillations [5]. Examples of simpler relevant sub-systems of musical acoustics interest are bow-string interaction and reed excitation of woodwinds; in both cases the oscillations are driven by a continuous energy supply. Naturally, such forced systems cannot be formulated in a stable manner without dissipative terms, and the energy is conserved only in a global sense. As shown in [1], stability of numerical schemes for the simulation of such systems can still be defined through energy analysis, by requiring non-negativity of a numerical energy-like quantity. Nevertheless, it is logical to seek extended application of the principle of conservation in numerical modelling, which is possible by defining a more general energy-like invariant that accounts for both the dissipation from and the work injected into the modelled system. Similar ideas have been expressed in recent studies [4, 6], but explicit calculation of a numerical invariant for dissipative systems has not been demonstrated so far.

This paper explores the idea of a conserved numerical energy quantity in the presence of damping through a simple harmonic oscillator model. Using an unconditionally stable finite difference scheme as a starting point, the defined conserved quantity is tested in finite-precision realisations. The proposed methodology is first presented for the linear case and subsequently extended to include nonlinear interactions. The inclusion of a driving force is analysed leading to a numerical energy balance consisting of the system (kinetic and potential) energy, the power input due to the driving force and energy loss due to friction. The methodology is exemplified by simulation of a lumped reed (with lay beating) as a sub-system of the clarinet.

2. THE DAMPED HARMONIC OSCILLATOR

The equation of motion for the displacement y of a damped harmonic oscillator is given by

$$\frac{\mathrm{d}^2 y}{\mathrm{d}t^2} + \gamma \frac{\mathrm{d}y}{\mathrm{d}t} + \omega_0^2 y = 0 \tag{1}$$

where γ is the damping and ω_0 the resonance frequency of the oscillator. Multiplying by the mass m of the oscillator yields

$$m\frac{\mathrm{d}^2 y}{\mathrm{d}t^2} + m\gamma \frac{\mathrm{d}y}{\mathrm{d}t} + ky = 0 \tag{2}$$

where $k = m\omega_0^2$ is the stiffness. This second order ordinary differential equation (ODE) defines an initial value problem that can be solved using either analytic or numerical methods. Note that in the case of more elaborate models, involving nonlinear interactions, an analytic solution may not be available. Two initial conditions have to be specified for this second order equation, namely $y(0)$ and $\dot{y}(0)$, where the dot signifies differentiation with respect to time. This dissipative system can be written in Hamiltonian form (see, e.g., [7]) as

$$\frac{\mathrm{d}y}{\mathrm{d}t} = \frac{\partial H}{\partial p} \tag{3a}$$

$$\frac{\mathrm{d}p}{\mathrm{d}t} = -\frac{\partial H}{\partial y} - \gamma p \tag{3b}$$

where H is the total energy (Hamiltonian) of the system and $p = \partial L/\partial \dot{y}$ the conjugate momentum, where L is the Lagrangian of the system [8]. Note that the specific form of (3)

using the Hamiltonian is required for obtaining a provably stable time-stepping scheme when modelling a system with non-analytic forces (which does not work when the derivative terms are first explicitly evaluated before discretisation to render the more standard first-order schemes [9]).

Defining the kinetic and potential energy as

$$T(p) = p^2/(2m), \qquad V(y) = ky^2/2 \tag{4}$$

yields

$$H(y,p) = T(p) + V(y). \tag{5}$$

The required initial condition for system (3) of first order ODE's is the pair $(y(0), p(0))$. In the undamped case (for $\gamma = 0$) this is clearly a Hamiltonian system, which conserves the total energy H [8]. In the presence of damping, energy is dissipated according to

$$\begin{aligned}\frac{\mathrm{d}H}{\mathrm{d}t} &= \frac{\partial H}{\partial y}\frac{\mathrm{d}y}{\mathrm{d}t} + \frac{\partial H}{\partial p}\frac{\mathrm{d}p}{\mathrm{d}t} = \frac{\partial H}{\partial y}\frac{p}{m} - \frac{p}{m}\left(\frac{\partial H}{\partial y} + \gamma p\right) \\ &= -\frac{\gamma p^2}{m} \leq 0\end{aligned} \tag{6}$$

which induces the following conservation law

$$H + \int \frac{\gamma p^2}{m}\,\mathrm{d}t = \text{const.} \tag{7}$$

In this paper only the case $\gamma/2 < \omega_0$ is studied. This corresponds to an underdamped system, that admits an oscillatory solution. Although higher damping values may be encountered in mechanical systems they are less relevant to sounding objects and will not be treated here. Under the above assumption for γ, taking the Laplace transform [10] of (1) yields the characteristic equation

$$s^2 + \gamma s + \omega_0^2 = 0 \tag{8}$$

which is solved by $s = \gamma/2 \pm \mathrm{j}\,\omega_\gamma$, with $\omega_\gamma = \sqrt{\omega_0^2 - (\gamma/2)^2}$ being the frequency of the damped oscillator. The exact solution can then be written as

$$y(t) = Ae^{-\gamma t/2}\cos(\omega_\gamma t + \theta) \tag{9}$$

where the initial amplitude A and the phase θ of the oscillation can be obtained from the initial conditions.

3. DISCRETISATION

Time stepping methods involve the approximation of the continuous function $y(t)$ by a discrete function $y^n, n \geq 0$, such that $y^n \approx y(n\Delta t)$, where Δt is the time step. Using the following difference and averaging operators

$$\delta_{t+}y^n = \frac{y^{n+1} - y^n}{\Delta t}, \qquad \mu_{t+}y^n = \frac{y^{n+1} + y^n}{2} \tag{10}$$

that are centred at time $t = (n + 1/2)\Delta t$ and approximate a first order time differentiation and an identity operator respectively, equation (6), which describes the evolution of the system energy, is discretised as

$$\delta_{t+}H^n = -\frac{\gamma}{m}(\mu_{t+}p^n)^2. \tag{11}$$

By integrating (11) via summation over time from $\kappa = 0$ to n, one obtains the discrete conservation law:

$$K^n = H^{n+1} + \sum_{\kappa=0}^{n} \frac{\gamma}{m}\left(\mu_{t+}p^\kappa\right)^2 \Delta t = \text{const.} \tag{12}$$

which is the discrete equivalent of (7).

3.1. Discretising Hamilton's equations

An energy-conserving scheme—in the sense of equation (12)—centred at time $t = (n + 1/2)\Delta t$, whose properties have been recently demonstrated for a class of nonlinear Hamiltonian systems [9], can be obtained by applying mid-point derivative approximations to (3):

$$\delta_{t+}y^n = \frac{T(p^{n+1}) - T(p^n)}{p^{n+1} - p^n} \tag{13a}$$

$$\delta_{t+}p^n = -\frac{V(y^{n+1}) - V(y^n)}{y^{n+1} - y^n} - \gamma\mu_{t+}p^n \tag{13b}$$

leading to the following (second order) numerical scheme

$$\begin{aligned}p^{n+1} = {} & \frac{1 - k\Delta t^2/4m - \gamma\Delta t/2}{1 + k\Delta t^2/4m + \gamma\Delta t/2}p^n \\ & - \frac{k\Delta t}{1 + k\Delta t^2/4m + \gamma\Delta t/2}y^n\end{aligned} \tag{14a}$$

$$y^{n+1} = y^n + \frac{\Delta t}{2m}(p^{n+1} + p^n). \tag{14b}$$

This scheme—which, in this linear case, is equivalent to both the trapezoidal rule and the midpoint rule—can be proven to be unconditionally stable [9] (a fact that also holds in the nonlinear case, which is not true for either the trapezoidal or the midpoint rule).

An energy relation can be derived directly from Eq. (13) by multiplying (13a) by $p^{n+1} - p^n$ and (13b) by $y^{n+1} - y^n$ and substituting by parts to get

$$H^{n+1} = H^n - \frac{\gamma}{m}\left(\mu_{t+}p^n\right)^2 \Delta t \tag{15}$$

which replicates (11) exactly. Note that this derivation holds for any potential function V and hence also applies to nonlinear systems (as demonstrated in Section 4).

Simulation results for a 100 g mass with $\omega_0 = 2\pi 440$ rad/s and $\gamma = 300\ \mathrm{s}^{-1}$ are compared with the analytical solution on Figure 1. The bottom plot shows the error in the conservation of the invariant quantity K, defined as $K^n_{\text{err}} = K^n - K^0$. The sampling rate for all simulations in this paper is equal to 44.1 kHz.

3.2. Driven oscillator

The energy balance defined in (7) for the continuous case and (12) for the discrete case can be extended to incorporate the action of an external driving force f_{ex}. In that case Hamilton's equations become

$$\frac{\mathrm{d}y}{\mathrm{d}t} = \frac{\partial H}{\partial p} \tag{16a}$$

$$\frac{\mathrm{d}p}{\mathrm{d}t} = -\frac{\partial H}{\partial y} - \gamma p + f_{\text{ex}} \tag{16b}$$

with

$$\frac{\mathrm{d}H}{\mathrm{d}t} = \frac{pf_{\text{ex}} - \gamma p^2}{m} \tag{17}$$

and, discretising the external force using $\mu_{t+}f^n_{\text{ex}}$, the discrete conservation law transforms into

$$\begin{aligned}K^n = {} & H^{n+1} + \sum_{\kappa=0}^{n}\left(\gamma\left(\mu_{t+}p^\kappa\right)^2 - \left(\mu_{t+}p^\kappa\right)\left(\mu_{t+}f^\kappa_{\text{ex}}\right)\right)\frac{\Delta t}{m} \\ & = \text{const.}\end{aligned} \tag{18}$$

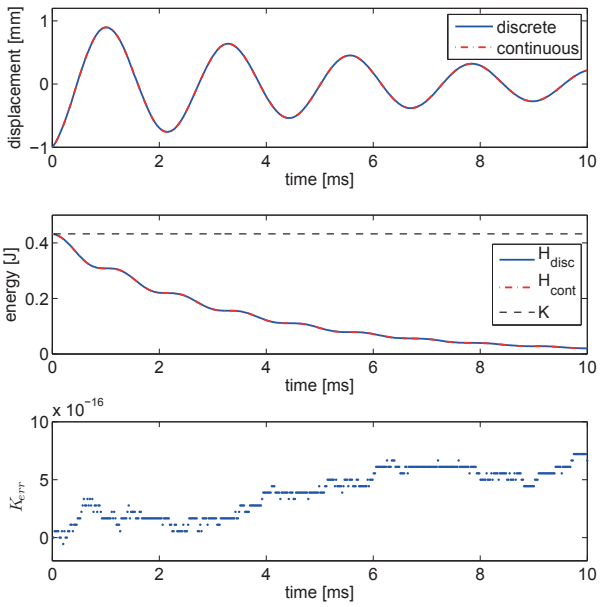

Figure 1: Evolution of the displacement and system energy for a damped oscillator, along with the invariant quantity. The bottom plot shows the error in the discrete conservation law (12) due to machine precision. Initial conditions are $y(0) = -1$ mm and $\dot{y}(0) = 1$ m/s.

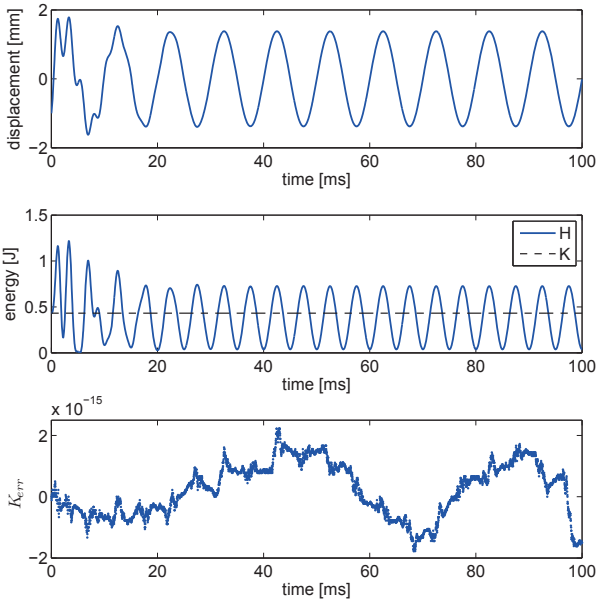

Figure 2: Evolution of the displacement and system energy for a driven oscillator, along with the invariant quantity. The bottom plot shows the error in the discrete conservation law (18) due to machine precision. Initial conditions are as in Fig. 1.

This now accounts for both the energy dissipated due to friction and the energy fed into the system by the external force. Driving the oscillator of the previous section with a force of the form

$$f_{\text{ex}} = A\sin(\omega_{\text{ex}} t) \tag{19}$$

with $A = 1000$ N and $\omega_{\text{ex}} = 2\pi 100$ rad/s yields the results plotted in Figure 2.

4. NONLINEAR INTERACTIONS

Things become more interesting when nonlinear forces are acting on the system. In that case there is (in general) no analytic solution to the differential equation and the problem has to be treated numerically. Motivated by nonlinear interactions in musical acoustics, the nonlinear force introduced into the system is a conditional repelling force that becomes active when the displacement is greater than a certain value. The hardness of such an impact can be modelled by the contact-related stiffness k_b and a power law constant α [11] yielding

$$f_{\text{NL}} = -k_b \lfloor y^\alpha \rfloor \tag{20}$$

where $\lfloor y^\alpha \rfloor = h(y)\, y^\alpha$, $h(y)$ denoting the Heaviside step function. Thus the potential energy of the system takes the form

$$V(y) = \frac{k}{2} y^2 + \frac{k_b}{\alpha + 1} \lfloor y^{\alpha+1} \rfloor. \tag{21}$$

The Hamiltonian form of the system is the same as in (16), with this new potential V used to calculate the total energy H.

For the numerical approximation of the Hamiltonian system (16), substituting the potential energy from (21) the same procedure as in Section 3 can be used, using mid-point derivative approximations to discretise Hamilton's equations at time $t = (n + 1/2)\Delta t$. This leads to the following nonlinear equation

$$F(x) = \left(1 + \frac{\gamma \Delta t}{2}\right) x + \frac{\Delta t^2}{2m} \frac{V(x + y^n) - V(y^n)}{x} - \frac{\Delta t}{m} p^n - \frac{\Delta t^2}{2m} (\mu_{t+} f_{\text{ex}}) = 0 \tag{22}$$

with $x = y^{n+1} - y^n = (\Delta t/2m)(p^{n+1} + p^n)$. Thus solving for x the scheme can be updated in y and p. The nonlinear equation (22) can be shown to have a unique solution (see [12]) and the conserved quantity is the same as in Section 3.2, now taking into account the updated potential energy from (21) when calculating H.

4.1. Application to sound synthesis

The methodology presented above for discretising nonlinear systems and monitoring their energy balance can be applied to several settings in sound synthesis simulations. In this case, it is assumed that the external driving force is known. In practise f_{ex} may be due to interaction between different objects, or supplied real-time by a performer. Applying a periodic driving force usually results in a steady-state displacement signal preceded by a transient oscillation, like that observed in Figure 2.

For instance, if the pressure difference that drives a clarinet reed is considered given in the form of a time series $p_\Delta(t)$, it is possible to sample it and calculate the force driving the reed, in order to simulate its oscillations. Defining M as the mass per unit area of the reed, the equation of motion becomes

$$M \frac{\mathrm{d}^2 y}{\mathrm{d}t^2} + M\gamma \frac{\mathrm{d}y}{\mathrm{d}t} + M\omega_0^2 y + k_c \lfloor (y - y_c)^\alpha \rfloor = p_\Delta \tag{23}$$

where k_c is defined as contact stiffness per unit area and y_c is the point after which the reed-mouthpiece interaction becomes significant [13]. The driving force per unit area corresponds to the pressure difference across the reed. The results of such a

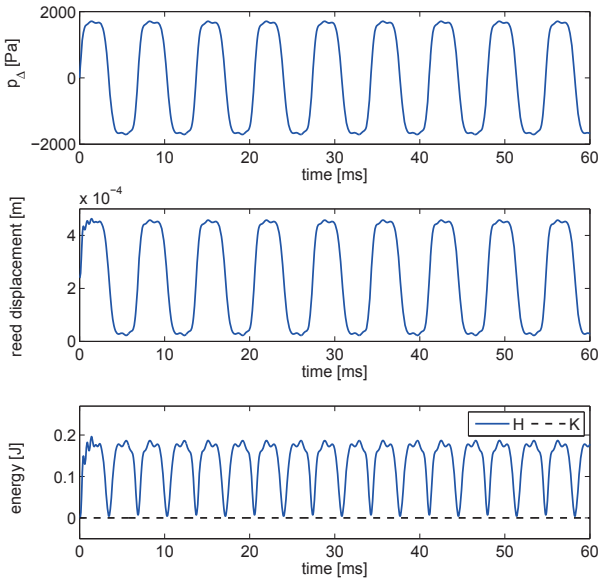

Figure 3: Evolution of the displacement and energy for a single reed, driven by a clarinet-like pressure difference p_Δ (as shown on the top plot). Initial conditions are $y(0) = 0$ and $\dot{y}(0) = 0$.

simulation, implemented by solving equation (22) at each time step, are shown in Figure 3. The pressure difference p_Δ is synthesised taking into account a typical clarinet spectrum at 146 Hz (Note D3) [14], by defining the amplitudes of the first seven harmonics as

$$\{A_1, A_2, \dots A_7\} = \{2000, 40, 400, 40, 100, 40, 28\} \text{ Pa}.$$

The contact is modelled using $k_c = 8.23 \times 10^{10}$ and $\alpha = 2$ and the reed parameters are given on Table 1. It can be observed that the conserved quantity K remains constant, in accordance with equation (18), which shows that no 'artificial' energy is fed into or lost from the system, besides that due to the external driving and frictional forces. Figure 4 plots the error in the conservation of K^n, defined as $K_{\text{err}} = K^{n+1} - K^n$. This demonstrates that in practical simulations, the global energy is not exactly preserved per time step, but varies by a small (quantised) amount due to finite precision; as explained in [1], such plots are also a useful debugging tool.

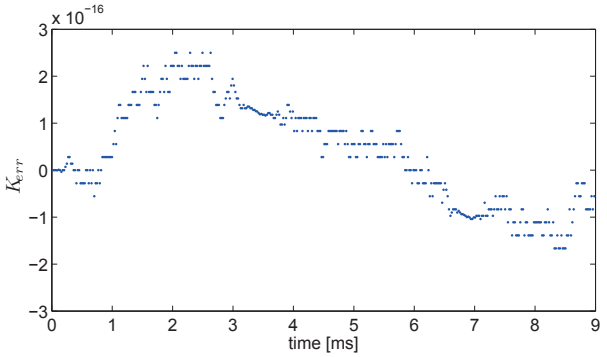

Figure 4: Evolution of the energy error K_{err} during the first 9 ms of the clarinet reed simulation.

Table 1: Parameters used in the single-reed simulation.

parameter	value	unit
ω_0	$2\pi 2000$	rad/s
γ	3000	1/s
y_c	2.4×10^{-4}	m
M	0.05	kg/m^2

5. DISCUSSION

Conservation of energy has been recognised as a key principle within stability analysis of time-stepping algorithms for a few decades [15]; more recently it has emerged as such in the context of simulation of non-linear phenomena in musical instruments [4]. Such an approach has evolved within the consideration of lossless systems, where the energy of the system is indeed conserved. A simple extension has been presented here, where a similar conservation law is formulated for damped oscillators. Conserved quantities, involving the damping parameter γ and the external driving force f_{ex}, have been calculated for a discretisation approach that is known to be unconditionally stable. It has been verified that the error in the conservation of these quantities is within the order of machine accuracy.

Such a test is an additional tool to verify the validity of a numerical approximation. Frictional forces lead to a monotonically decreasing energy and as such can conceal a potential instability of a numerical simulation. Even when conserved quantities can be theoretically established, in practice their conservation may depend on the range of the model parameters [9]. Testing for such an energy drift is usually carried out in conservative systems, by monitoring the constant system energy. The conserved quantity K proposed here can serve as a similar tool in the analysis of damped systems.

6. REFERENCES

[1] S. Bilbao, *Numerical Sound Synthesis*, Wiley & Sons, Chichester, UK, 2009.

[2] R. Richtmyer and K. Morton, *Difference Methods for Initial-Value Problems*, Wiley & Sons, New York, 1967.

[3] J. Strikwerda, *Finite difference schemes and partial differential equations*, SIAM, Philadelphia, 2007.

[4] S. Bilbao, "The changing picture of nonlinearity in musical instruments: Modeling and simulation," in *Proc. Int. Symp. Musical Acoustics*, Le Mans, 2014.

[5] A. Cook and W. Cabot, "A high-wavenumber viscosity for high-resolution numerical methods," *Journal of Computational Physics*, vol. 195, no. 2, pp. 594–601, 2004.

[6] C. Desvages and S. Bilbao, "Physical modeling of nonlinear player-string interactions in bowed string sound synthesis using finite difference methods," in *Proc. Int. Symp. Musical Acoustics*, Le Mans, France, 2014, pp. 261–266.

[7] U. Dressler, "Symmetry property of the Lyapunov spectra of a class of dissipative dynamical systems with viscous damping," *Physical Review A*, vol. 38, no. 4, pp. 2103–2109, 1988.

[8] V. Arnold, *Mathematical methods of classical mechanics*, vol. 60, Springer, New York, 1978.

[9] V. Chatziioannou and M. van Walstijn, "Energy conserving schemes for the simulation of musical instrument contact dynamics," *Journal of Sound and Vibration*, vol. 339, pp. 262–279, 2015.

[10] D. Pollock, *A Handbook of Time-Series Analysis, Signal Processing and Dynamics*, Acad. Press, London, 1999.

[11] S. Papetti, F. Avanzini, and D. Rocchesso, "Numerical methods for a nonlinear impact model: A Comparative study with closed-form corrections," *IEEE Trans. Audio, Speech and Language Process.*, vol. 19, no. 7, pp. 2146–2158, 2011.

[12] V. Chatziioannou and M. van Walstijn, "An energy conserving finite difference scheme for simulation of collisions," in *Sound and Music Computing (SMAC-SMC 2013)*, Stockholm, 2013, pp. 584–591.

[13] V. Chatziioannou and M. van Walstijn, "Estimation of clarinet reed parameters by inverse modelling," *Acta Acustica united with Acustica*, vol. 98, no. 4, pp. 629–639, 2012.

[14] N. Fletcher and T. Rossing, *The Physics of Musical Instruments*, Springer, New York, 1991, 2nd edition: 1998.

[15] S. Li and L. Vu-Quoc, "Finite difference calculus invariant structure of a class of algorithms for the nonlinear Klein-Gordon equation," *SIAM Journal on Numerical Analysis*, vol. 32, no. 6, pp. 1839–1875, 1995.

EXPLORING THE DECAY PROPERTIES OF GUITAR SOUNDS FROM MOBILITY MEASUREMENTS

Bertrand David[1], François Gautier[2], Marthe Curtit[3]
[1] Télécom ParisTech, Institut Mines-Télécom, CNR S LTCI , France
[2] Laboratoire d'Acoustique de l'Université du Maine, France
[3] Institut Technologique Européen des Métiers de la Musique, Le Mans, France
bertrand.david@telecom-paristech.fr
francois.gautier@univ-lemans.fr
marthe.curtit@itemm.fr

ABSTRACT

With the goal of providing the instrument maker useful and fast numerical tools to characterize the final objects, we herein propose a processing system to evaluate the decaying properties of guitars with only a few impact measurements. Our method relies on a hybrid synthesis technique first developed by J. Woodhouse (Acta Acustica, 2004). This technique is able to derive synthetic signals of guitar plucks with a very light computational load and makes use of mobility measurement at the bridge. The obtained signal thus includes the complexity and the singularity of the mechanical and acoustical behavior of the guitar body, without having to estimate or model it. In preceding studies (B. David, ISMA, 2014), some preliminary results have been obtained. It was in particular shown that with only a one-dimensional measurement of the mobility it was possible to well represent the decay properties for all the notes of a specific string. This paper extends those results by dealing with different instruments, by comparing the accuracy of the prediction for several strings and by using 2-dimensional measurements of the mobility. The decaying properties are studied with the help of High Resolution (ESPRIT) method and are "summarized" with the help of the Energy Decay Curve feature. This leads to a representation of the whole guitar compass with a so-called decay profile, which allows us to assess at once the properties of the instrument, its timbre homogeneity in terms of extinction and eventually detect and objectivize possible defects like the well known "dead tones".

CONNECTED MUSICIANS - EXAMPLES OF NEW SUPPORTIVE TECHNOLOGIES FOR MUSICIANS' PERFORMANCE ANALYSIS AND DAILY ROUTINE

T. Grosshauser, D. Bannach, A. Calatroni and G. Tröster

Institute for Electronics
ETH Zurich
Switzerland
Grotobia|Calatron|Dbannach|Gerhartr@ethz.ch

ABSTRACT

Many technologies are used in musical instrument teaching and learning, starting with audio and video recordings, up to mobile phones equipped with several apps. In this paper, we try to show possibilities to integrate further technologies in musicians' daily routine up to performance research. We describe several body worn and musical instrument integrated sensor setups in combination with a new app for data recording, storage and server connectivity, server based data distribution, visualization and several possibilities for real-time feedback. The system is a further development of PART (Performing ARts Technologies) system including, but not limited to the following musical instruments: Stringed instruments, clarinet, trumpet, cornet, trombone, drums and piano, but setups for several more instruments are available or further developed continuously. In general, for nearly every musical instrument and problem statement a specific modular set of sensors can be developed, adapted or already exists. Till now, the measured parameters include mainly motion, force, pressure and posture. Beside the further developed PART setup, some applications for string instruments and trumpet are described in this paper.

1. INTRODUCTION

More and more technologies are added to the mainly audio and video based systems in musical instrument playing and performance research and analysis (see Ng et al. [1], Baader et al. [2], [3] and Grosshauser et al. [4]). In trumpet and trombone playing Bertsch et al. in [5], Mayer et al. in [6], Petiot in [7] and Grosshauser et al. in [8] introduced sensor based systems to measure lip pressure while playing. For PART[1] (see Grosshauser in [9]), the most important parameters are:

- unobtrusive measurements and fixation of the electronics to the musician or musical instrument,
- possibility to capture nearly all relevant parameters while music making,
- easy to use, adapt and individualize,
- stand alone operation mode and wireless app/server connectivity,
- server based data storage, sharing, visualization and analysis,
- app based real-time feedback and visualization.

Although the system still is in development, several components are finished and ready to use in daily musicians' routines like practicing, teaching or rehearsing (distributed by Bonsai Systems[2]). Further developments including several new sensors or combined sensor systems (stand alone or data streaming) are described in the following comprising wireless data transmission based on Bluetooth low energy (BLE), improved server- and app connectivity, data sharing, saving, visualization and real-time feedback.

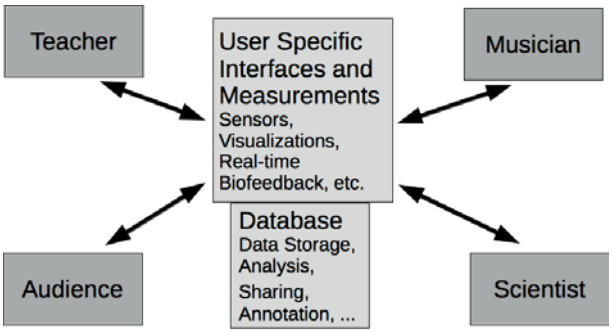

Figure 1: The central unit in the PART system is the user-centric (here musical instrument teacher, musician, scientist and audience or music enthusiasts) interface, including individually adaptable sensors, app and server connectivity providing data storage and visualization and several more features like data sharing and real-time feedback.

2. BASIC SETUP AND TECHNICAL DESCRIPTION OF THE FEATURES

Fig. 1 shows the underlaying idea of providing different kinds of data for audience, musicians, teachers and scientists. Server based online interfaces and apps allow the access to the recorded data. The data can be any sensor data, audio and video. The sensors (nearly any sensor can be integrated) can be used for motion capture, pressure and force measurement up to posture recognition. On the software side, the app allows adjustable individual real-time feedback, data visualization, recording, distribution, server up- and download and automatic sensor recognition and connectivity.

Fig. 2 shows a possible data flow sequence and technical features. These start with the sensors, online and offline data storage on the sensor boards while recording, wireless data transmission to e.g. mobile phones (in streaming mode or offline after the recording), server connectivity, real-time feedback and several more possibilities.

A priority was to simplify the usage and to reduce set up time of the complete system for simple integration into daily

[1] https://www.fb.com/PerformingArtsTec

[2] http://www.Bonsai-Systems.com

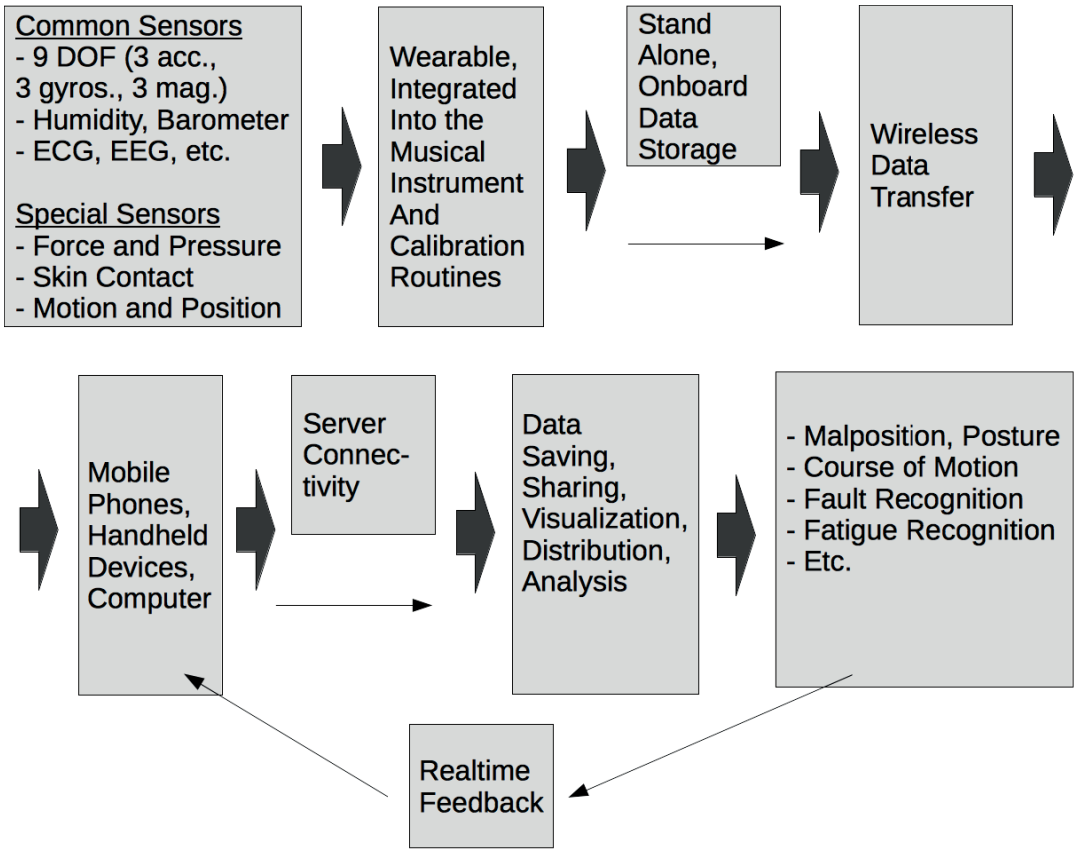

Figure 2: This figure shows the principle data flow from the sensors (motion and posture, pressure and force measurement and combination of all of these including calibration routines), the wireless data transfer including memory on the sensor nodes for stand alone use, app and server connectivity with versatile features including real-time biofeedback.

teaching and practicing scenarios. Beside daily usage, the precision of the sensors and possibilities of extensive data calculation on the sensor board, in the apps and on the server creates many possibilities in scientific experiments, on stage, or daily music making and teaching. Most relevant parameters (like force, motion and posture) can be captured of single musicians but also of music groups.

Preparation and Setup of PART

First, regarding to the specific problem statement, the relevant sensors or complete sensor setups are chosen. After doing so, all sensors are connected with the data logging app. After the app is started, all available BLE sensors in a range of around $20\,m$ are shown. The individual set of sensors chosen for experimentation or measurements is composed by tapping on their icons shown in the app. The wireless connection is established automatically. In a second step, different visualizations can be selected and if necessary, thresholds for real-time feedback can be adjusted. All data of each selected sensor can be recorded and saved in *.csv file format to allow further calculations in standard statistic programs. Additionally, sharing and saving the recorded data via email, online storage service providers or automatic server upload is possible. If the server upload is used, a web based interface provides multi-modal online data management, visualization, alignment, analysis and annotation.

2.1. Application Scenarios

In the following chapters, some basic applications for the complete system and several sensor systems are described.

2.1.1. String Instruments: Miniatur- IMU Based Right Hand Measurements

The measured and calculated parameters in the following examples are all based on 9 DOF (9 degree of freedom) IMUs (inertial measurement units) measurements. The measured parameters are:

- Bow position
- String level
- Bow rotation
- Bow to string angle

String Level and Bow Position

Several sensor based bow position measurement methods exist like in Demoucron et al. in [10], but mostly additional sensors have to be attached to the bow with a certain influence while playing, like shortening the playable overall length of the bow hair.

In our scenario, a 9 DOF IMU (see fig. 3) is fixed on the upper half of the forearm (see sensor nr. 1 in fig. 4) to reduce the influence of the wrist movement on the bow position measurement. After the sensors are fixed, a short calibration routine

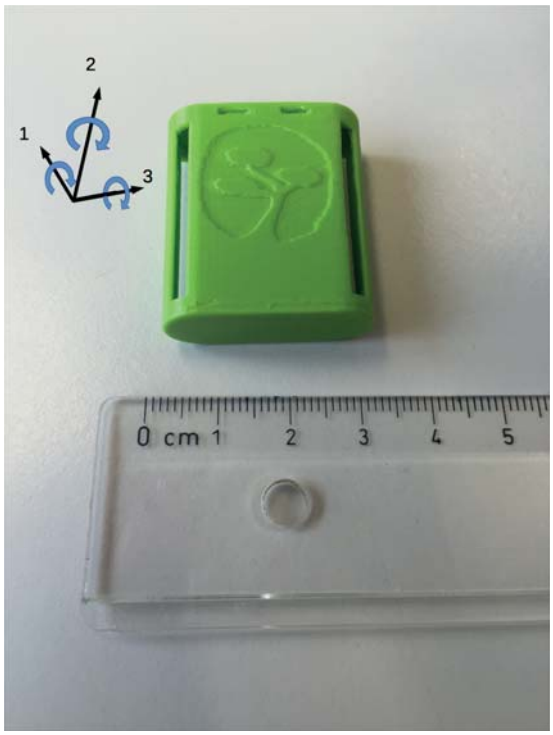

Figure 3: This figure shows the 9 DOF IMU, dimension is 10 x 29 x 33 mm, weight is 9 gr including rechargeable battery (chargeable via micro USB connector) providing yaw, pitch, roll (arrows 1, 2, and 3), w, x, y, z quaternions and raw data of the three axes accelerometer, three axes gyroscopes and three axes magnetometer. Different casings are available for several situational fixation possibilities.

is done, first a defined starting position e.g. bow position frog on the g-string and a second posture like bow position frog on the e-string. The IMU measurement resolution is $0.1°$angular degree, sampling frequency is up to 80 Hz.

With the z-axis rotation data of sensor 1 (see fig. 4) the bow position of 4 bow strokes from frog to tip on G, D, A and E string with a stop every 5cm (see blue line in fig. 5) is measured. The accuracy of position capturing is 1 cm with little body movements. Strong body movements while playing decreased the accuracy, but it is sufficient for stable middle, upper and lower bow half recognition (the most used terms regarding bow position in daily string instrument playing). The red line in fig. 5 represents the 4 string layers. Especially for beginners learning legato bowing these measurement method and data are useful.

Body movements mainly change the orientation data, which are not used in this setup, although a certain influence remains. To decrease this, a second sensor (see sensor nr. 2 in fig. 4) is fixed on the violin to measure the movement of the musician and the instrument relative to the forearm. By doing so, the accuracy is increased even with larger body movements.

Bow to String Angle Measurement and Bow Rotation

Sensor nr. 2 and 3 (see fig. 4) is used for bow to string angle detection.

First the sensors are calibrated both together in a fixed position, e.g. on the bow or the violin. Sensor nr. 2 is fixed on the violin, sensor nr. 3 on the bow. After the calibration, the two sensors measure the deviation of the orientation of each sensor

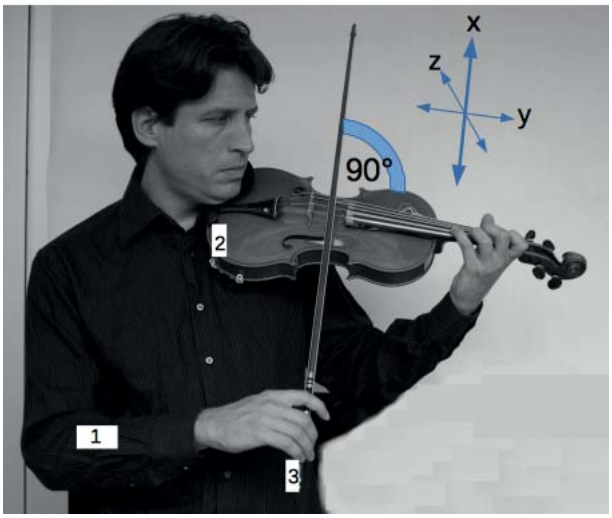

Figure 4: This figure shows the placement of three 9 DOF IMUs on the violin and the body. The first is on the fore arm, the second on the violin and the third is on the frog of the bow. Each 9 DOF IMU transfers the data to the app on a mobile device. Due to this topology, each node can act autonomously (battery, processor unit and onboard memory) and can be added or removed without disturbing the other sensors.

to each other in the z-axis (orientation). If the bow and the sensor nr. 2 is parallel it is a $90°$ bow to string/violin angle. As soon as bow to string angle changes, the positive or negative difference of the sensors alias the deviation to the $90°$ angle is shown. Fig. 6 shows the string to bow angle changes during several bow strokes. Further the rotation of the bow and the string levels (see red line in fig. 5) are measured and clearly recognizable.

Fig. 7 shows the rotation of the bow along the bow stick. This is a further parameter measured with IMU nr. 3 (see fig. 4), an additional parameter to describe the full motion of a bow while playing.

2.1.2. Brass Instruments: Trumpet and Cornet

In this section the PART system is used for lip pressure measurement in trumpet and cornet playing (see fig. 8), introduced by Grosshauser et al. in [11]. The setup consists of two modules, one (see no. 2 in fig. 9) with three miniature load cells and a 9 DOF IMU with 3 axes accelerometer, 3 axes gyroscopes, 3 axes magnetometer, (providing yaw, pitch roll and w, x, y, z quaternions) the other one (see no. 1 in fig. 9) with three adjustable screws to secure the force closure between mouth piece and instrument. The intersection between the mouthpiece and the trumpet is sealed with a silicone tube, part no. 3 (all parts in the following description see fig. 9). The three screws no. 4 are inserted into part no. 1. These screws push part no. 1 and 2 apart from each other by touching the tip of the miniature load cells. By doing so, the mouthpiece is pushed around 1 mm out of the trumpet and the lip pressure is transmitted to the load cells directly via the screws (no. 4), which are tightly fixed on the instrument (part no. 1).

The 9DOF IMU allows conclusions about the position and orientation and the acceleration of the instrument in all 3 dimensions while playing. The sampling frequency is up to 80 Hz. The final force resolution is below 1 gr, or below 0.01 N. A LiPo Battery is used for power supply, rechargeable via a micro USB adapter. The overall weight of the complete setup is 50 gr.

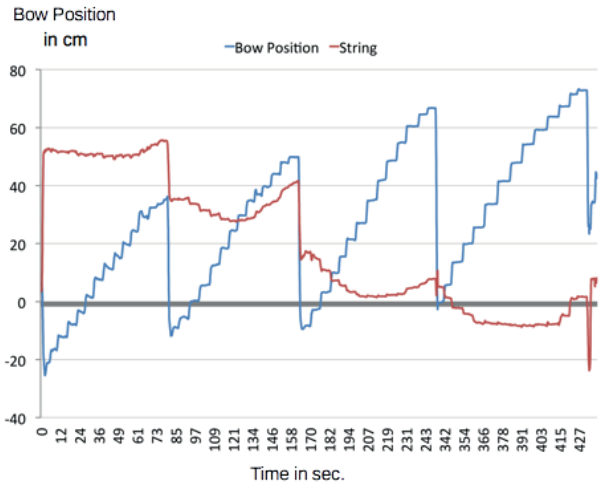

Figure 5: This figure shows a bow stroke on G, D, A and E string. The 9 DOF IMU is fixed on the forearm, the blue line are the roll data "bow position", showing a bow stroke with a stop every 5cm. IMU pitch data "string" show the bow level on each string from left to right according to the strings G, D, A and E (red line).

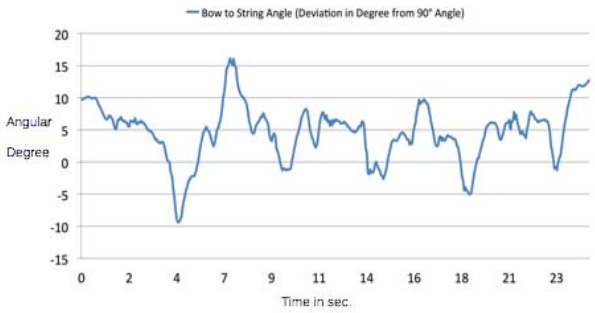

Figure 6: This figure shows the deviation of the 90° angle angle during a bow stroke on the E string. One 9 DOF IMU is fixed on the bow, the other one on the violin.

3. CONCLUSIONS AND FUTURE WORK

The basic work flow and usage of the extended PART system is demonstrated with several examples. It shows, that these additional technologies could be applied in daily teaching, practicing and performance science. Based on a plug-and-play process to use the sensors needed by simply adding them into an existing setup, the ease of integration into daily work- and practicing flow is shown. It is demonstrated with string instrument and trumpet scenarios. The main application fields right now are teaching, practicing, learning and performance research but also many experiments could be carried out in music medicine and physiology, and last but not least new possibilities for writing and composing music for completely new and augment musical instruments are given.

4. ACKNOWLEDGMENTS

Special thanks to www.bonsai-systems.com for providing us the data logging app and further technical support.

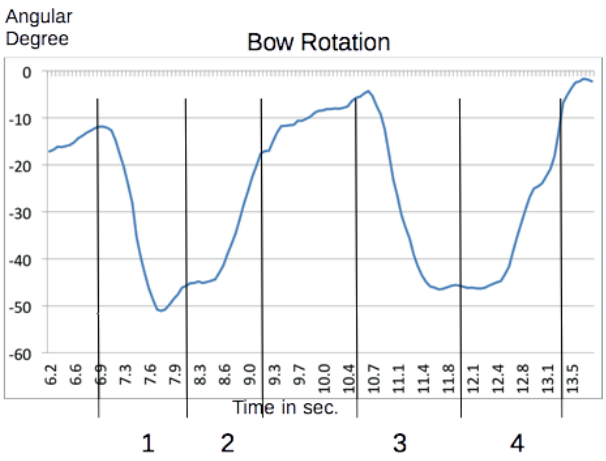

Figure 7: This figure shows the bow rotation of 4 up- and down legato bow strokes around the x-axis. Nr. 1 and 3 are down bows, 2 and 4 up bows.

Figure 8: This figure shows the lip pressure sensor fixed on a trumpet and real-time data visualization with the logging app. The first row shows the sum of the 3 pressure sensors, the second row data of each sensor.

5. REFERENCES

[1] K. Ng, "3d motion data analysis and visualisation for technology-enhanced learning and heritage preservation," in *AIKED'09: Proceedings of the 8th WSEAS international conference on Artificial intelligence, knowledge engineering and data bases*, Stevens Point, Wisconsin, USA, 2009, pp. 384–389, World Scientific and Engineering Academy and Society (WSEAS).

[2] Andreas Baader, Oleg Kazennikov, and Mario Wiesendanger, "Coordination of bowing and fingering in violin playing," in *Cognitive Brain Research*, 2005.

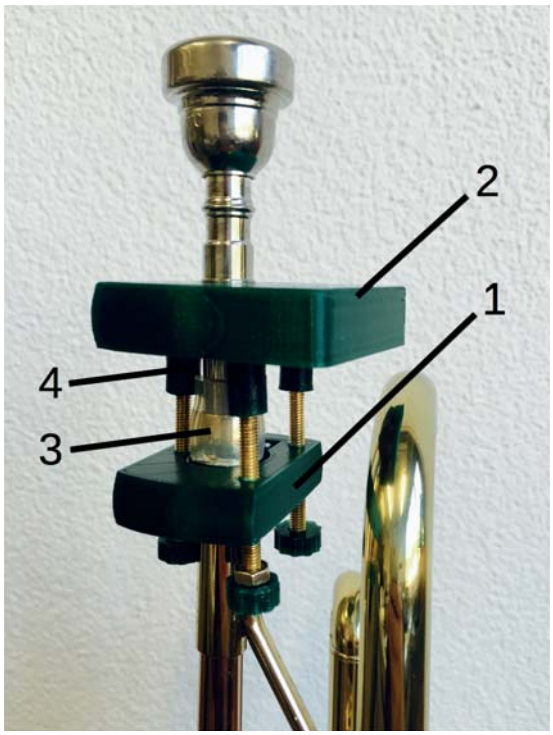

Figure 9: This figure shows the sensor module for lip pressure measurement fixed on a trumpet. Part 1 is the lower fixation part housing the three adjustable screws (4), touching the three load cells placed in part 2. These are the 3 contact points for force transmission from mouth piece to instrument. Between mouthpiece and trumpet there is a 1 mm gap (the mouthpiece is pulled around 1 mm out of the trumpet from the normal fixed position), sealed with a silicon tube (3). Module 2 includes the PCB with three miniature load cells, a 9 DOF IMU (providing yaw, pitch roll, w, x, y, z quaternions and raw data of the 3 axes accelerometer, 3 axes gyroscopes, 3 axes magnetometer), a BLE module and a rechargeable battery, chargeable via USB micro connector.

[3] W. Goebl and C. Palmer, "Tactile feedback and timing accuracy in piano performance," *Experimental Brain Research*, vol. Volume 186, pp. 471–479, 2008.

[4] Tobias Grosshauser and Gerhard Tröster, "Further finger position and pressure sensing techniques for strings and keyboard instruments," in *New Interfaces for Musical Expression, NIME13*, 2013.

[5] M. Bertsch and A. Mayer, "3d transducer for measuring the trumpet mouthpiece force," in *roceedings of the Forum Acusticum Budapest*, 2005.

[6] A. Mayer and M. Bertsch, "A new 3d transducer for measuring the trumpet mouthpiece force," in *Proceedings of Second Congress of Alps-Adria Acoustics Association and First Congress of Acoustical Society of Croatia*, 2005.

[7] J. F. Petiot, "Measurements of the force applied to the mouthpiece during brass instrument playing," in *Proceedings of the SMAC03 (Stockholm Music Acoustics Conference 2003)*.

[8] Tobias Grosshauser, Bernhard Hufnagl, Gerhard Tröster, and Ardina Mornell, "Sensor based hand weight and pressure measurements in trombone playing," in *SMAC Stockholm Music Acoustics Conference*, 2013.

[9] T. Grosshauser, *ENTDECKEN, ERFORSCHEN, VERSTEHEN: Unterstützende Technologien im Instrumentalunterricht*, vol. Gesund und motiviert musizieren ein Leben lang of *üben & musizieren - texte zur instrumentalpädagogik*, Schott Verlag, 2015.

[10] M. Demoucron, A. Askenfelt, and R. Causse, "Measuring bow force in bowed string performance: Theory and implementation of a bow force sensor," *Acta Acustica united with Acustica*, vol. 95, pp. 718–732(15), July/August 2009.

[11] Tobias Grosshauser, G. Tröster, M. Bertsch, and A. Thul, "Sensor and software technologies for lip pressure measurements in trumpet and cornet playing - from lab to classroom," in *SMC 2015, Sound and Music Computing Conference*.

HEARING PROTECTION FOR MUSICIANS

Esther Rois-Merz
Audienz, Austria
info@audienz.at

ABSTRACT

For a musician's career it is important to protect own hearing. Professional products therefore should always be custom made. There are several brands doing so called „linear filtering" by providing band pass filtering for a standard ear channel resonance at 2,7 kHz. They shall now damp the whole frequency range in a regular way, so that sound quality can be preserved while hearing is protected. But: looking at the individual acoustics of an ear channel resonance with its deviation of almost one octave at the peak, the damping can theoretically never be really regular. That includes sound discoloration, which is – in most cases - not beneficial for musical purpose. Several validating tests for hearing protector devices will be presented and referenced to the belonging standards. Every validation test has its pros and cons. To eliminate some disadvantages, a study with a miniature microphone in the ear channel shows results on eight individual ears. The results are some aspects of the impact of the damping with regard to music, which can now be heard because of the recording by the microphone in the ear channel. These results are challenging for audiologists adapting custom made hearing protection for musicians. Individual solutions with different filtering of the two ears are sometimes demanded from certain instrumentalists like flutists or violinists. Regular damping is not always what a musician is looking for: a clarinetist next to a piccolo player for example will be happy getting more damping in the higher frequency range. And last but not least: regular verification as proposed from the industry (leak test and damping verification at 500 Hz) fail completely in music application, where subjective test methods are most advantageous, but need profound expertise.

THE ROLE OF BIOMECHANICS AND NEUROMECHANICS IN DYNAMIC PERFORMANCE: A PRACTICAL INTEGRATION FOR MUSICIANS

Robert Friberg, Leigh Anne Hunsaker
Hardin Simmons University, United States of America
rfriberg@hsutx.edu
hunsaker@hsutx.edu

ABSTRACT

An interactive two-part session in which posture and effective motor control will be explained and demonstrated in an accessible, hands-on manner for performers and teachers. Recent and ongoing research on the relevant components of dynamic posture will be reviewed. Limitations of traditional approaches to teaching posture in the music studio will be examined, with recommendations for identifying, examining, and planning an intervention to improve dynamic posture. Musicians are invited to bring their modern or period instruments to participate in the sessions. Participants and observers in this two-part session will 1. Observe the interaction between the biomechanical and neuromechanical components of dynamic performance; 2. Recognize components of an efficient static posture; 3. Utilize principles of applied physiology, biomechanics, and motor control to modify posture; 4. Apply a rubric for identifying biomechanical and neuromechanical dysfunctions of posture and designing an individual program for performers. 5. Receive an individualized plan to improve dynamic posture in their performance medium.

USING A DUAL ELECTRONIC SPECKLE-PATTERN INTERFEROMETER TO STUDY COUPLED VIBRATIONS IN DRUMHEADS

Randy Worland and Benjamin Boe

Department of Physics
University of Puget Sound, Tacoma, Washington, USA
worland@pugetsound.edu

ABSTRACT

A dual electronic speckle-pattern interferometer (ESPI) system is described that allows images of operational deflection shapes of two sides of a vibrating object to be viewed simultaneously and recorded. Experimental details of the system are discussed and applied to the study of musical drums with two heads at either end of a cylindrical shell. In particular, methods for determining the degree of coupling and the phase relations between the two oscillating heads are shown. A variable length drum has been constructed and used to investigate the coupling of membrane vibrational patterns as a function of the distance between the heads. It is shown that the coupling vs. length data depend strongly on the shapes of the vibrational patterns. These coupling trends are illustrated and further interpreted with the use of a finite element model of the drum, which shows the role of the enclosed air motion within the shell.

1. INTRODUCTION

Many musical instruments exhibit vibrating surfaces on opposite sides of an air cavity (e.g. violins and guitars). These surface vibrations may be coupled to varying degrees by the enclosed air and the supporting mechanical structures. Drums containing membranes at opposite ends of a cylindrical shell (e.g. tom toms, snare drums, and bass drums) provide particularly good examples of this type of coupling in the context of a relatively simple geometry (Figure 1).

Figure 1. Tom toms (left) and snare drum (right) contain circular membranes at opposite ends of a cylindrical shell.

The first four normal mode shapes of a single ideal membrane are shown in Figure 2. The modes are identified by the number of nodal diameters and circles (*m*,*n*) respectively. Modes containing at least one nodal diameter are doubly degenerate, with two orthogonal orientations having the same frequency [1]. In real drums, slightly non-uniform tension in a head may lift this degeneracy resulting in closely spaced frequency pairs [2]. Non-uniform tension can also act to distort the symmetry of the nodal diameters and circles predicted for the ideal membrane.

In the coupled drum system, both membranes exhibit operating deflection shapes that are linear combinations of the ideal membrane modes, and which can still be adequately identified by the number of nodal diameters and circles, at least for the lower frequency resonances.

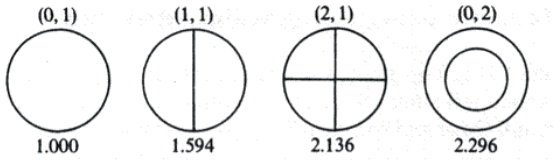

Figure 2. The first four normal mode shapes of an ideal membrane, with relative frequencies indicated below. The integers (*m*,*n*) designate the number of nodal diameters and circles respectively.

When one side of a drum is struck (the "batter" head), both sides vibrate. The coupling of the two heads is provided acoustically by the enclosed air and mechanically by the shell [3, 4]. In the current work, only the coupling due to the enclosed air is considered. The degree of coupling of the vibrational patterns on the two membranes depends on several factors including drum geometry (diameter and length), head materials, and tensions. With identical heads (as used in the experiments described below) strongly coupled shapes will have similar vibrational amplitudes when driven at a resonant frequency. Weakly coupled cases will result in an amplitude ratio that deviates from unity. "Uncoupled" cases have essentially no detectable motion on one head, while the other displays a resonant pattern. The degree of coupling also varies with the shapes of the vibrational patterns and the relative phase relation between the two heads. The lowest frequency (fundamental) mode always couples strongly, displaying the (0,1) shape, with both heads moving in phase [3]. Higher frequency resonances exhibit varying degrees of coupling, with membrane motions that are either in, or out of, phase with each other.

An optical system has been built to create interferometric images of both vibrating drumheads simultaneously. When the drum is excited acoustically at a resonant frequency, the operating deflection shape of each head can be recorded along with amplitude and phase information as described in Section 2 below.

2. EXPERIMENTAL SETUP

The optical system is based on the electronic speckle-pattern interferometer (ESPI) shown in Figure 3 and described in Reference 5. Light from a helium-neon laser is split into reference and object beams, which are then expanded using microscope objectives (not shown). The object beam reflects off the vibrating surface, while the reference beam travels a similar distance without encountering the object. The beams are recombined at the CCD camera and the resulting signal is processed [6] to create speckle-pattern interference images in

real time on the computer monitor. When the object is driven acoustically at a resonant frequency, the ESPI images show operating deflection shapes with nodal lines in white. Gray fringes indicate contours of equal amplitude motion normal to the surface of the object.

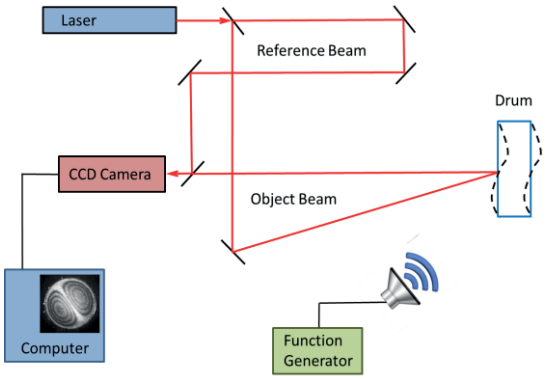

Figure 3: Schematic diagram of the electronic speckle-pattern interferometer (ESPI) used to image one vibrating surface. In the resulting images nodal lines appear white; gray fringes represent equal amplitude contours.

2.1 Dual ESPI system

In order to record images of both heads of a drum simultaneously, a dual ESPI system was constructed by adding a second, identical, setup directed at the opposite side of the drum as shown in Figure 4. With this arrangement, coupling of the drumhead vibrations can be observed. In particular, the operating deflection shapes and orientations can be compared in real time. In addition, the gray contour fringes can be counted to provide an estimate of the relative amplitudes of the two heads. It should be noted that in the case of coupled oscillators the *relative* amplitude does not depend on the location of the driving speaker. In practice, the speaker location is chosen to provide maximum clarity of the fringes.

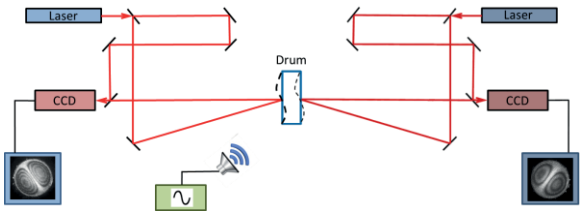

Figure 4: Dual ESPI system showing speckle-pattern images of both drumheads.

Due to the fact that the two CCD cameras view the drum from opposite directions, one image must be flipped horizontally before the relative orientation of the two images can be judged. In the lab this is achieved in real time by viewing one of the two computer monitors in a mirror (Figure 5). After the images are recorded, one is rotated digitally prior to presentation. Thus the images shown in Figure 4 will be viewed as in Figure 5, with alignment clearly visible in this particular case.

Drumhead resonant frequencies are initially determined using a spectrum analyzer with a microphone input as the drum is struck. Coupled vibrational patterns are then identified by scanning the acoustic driving frequency near these resonances while observing the ESPI images on both monitors (one via the mirror). Coupled patterns show very similar shapes and orientations, and both patterns reach their maximum amplitudes at the same frequency. The strength of the coupling may be qualitatively determined from the amplitude ratio, which is obtained by counting fringes in equivalent regions of the images.

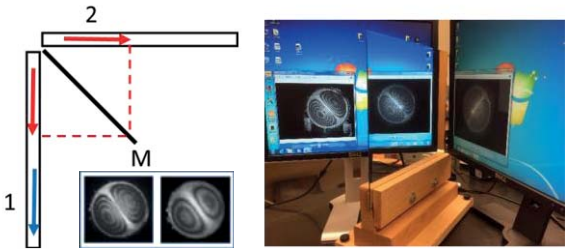

Figure 5. Computer monitors 1 and 2 display ESPI images from opposite heads of a drum. Mirror M is used to reverse the image from monitor 2 so the relative orientations can be viewed in real time.

2.2 Phase determination

As described above, The ESPI system produces white regions in the images where the object beam is unchanged during the drum head oscillation, i.e. at the nodal lines. However, these image pairs by themselves (e.g. Figure 5) do not provide phase information. Corresponding regions of the coupled vibrations shown in Figure 5 must be either in, or out of, phase with each other [7, 8]; this relative phase can determined by adding a moving mirror into the object beams of both sides of the system as described below.

A mirror in the object beam is attached to a mechanical oscillator [9] that is powered by the same function generator that drives the speaker (Figure 6 shows one side of the system). Thus, the mirror oscillates at the same frequency as the drumhead. In this configuration, nodal regions of the membrane no longer appear white. Instead, portions of the drumhead moving with the same amplitude and phase as the mirror now appear white. Because drumhead motion exhibits opposite phases on either side of a nodal line, the white line in the image will shift to one side or the other when the mirror motion is activated. This shift of the white regions, applied to both sides of the system, can be used to determine the relative phase of the two sides of the drum, and the ambiguity of phase in Figure 5 can be removed.

A decade resistance box is used in series with the mechanical oscillator to control the amplitude of the mirror motion, so that it can be adjusted to match a portion of the drumhead motion. A double pole double throw knife switch is used to reverse the phase of the mechanical oscillator as needed. Thus, each mirror can oscillate either in, or out of, phase with the driving speaker (and with the other mirror). The phases of the mirrors relative to each other can be verified by direct visual observation of their motion at low frequency (e.g. a 1 Hz square wave) and large amplitude.

However, in general no portion of the drumhead will be in phase with the driving speaker due to the time of flight of sound from the speaker to the drumhead. In such cases no white region will be seen in the images. The phase of the drumhead relative to the speaker cone is easily adjusted by varying the speaker location (i.e. its distance from the membrane.)

The appropriate speaker distances, which vary with driving frequency, are integer multiples of acoustic half wavelengths

and can be roughly estimated assuming straight line motion of sound from speaker to drumhead. However, in practice it is easiest to simply move the speaker by hand with the mirror motion activated, while watching the monitor for a clear signature (i.e. a white line that clearly deviates from the stationary mirror nodal line.) When this signature is observed, the amplitude of the mirror motion can be adjusted using the resistance box in order to maximize the clarity of the image. Reversing the mirror phase provides a way to double check the initial interpretation of the image, as the white line should now shift in the opposite direction.

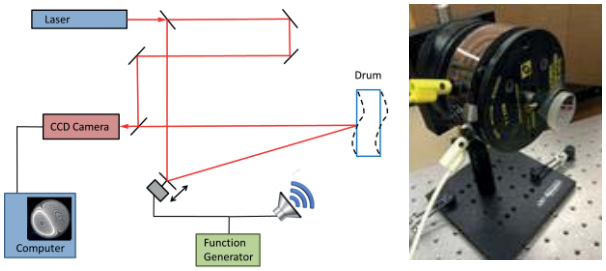

Figure 6. Moving mirror in object beam indicated with arrow (left). Mechanical oscillator (right) is driven from the same signal as the speaker that excites the drumhead.

Figure 7 shows three representative ESPI images of a single drumhead driven at a (2,1) resonance. The two nodal diameters and the nodal perimeter circle are visible in the first image, taken with no mirror motion. Viewing the nodal diameters as roughly vertical and horizontal, one expects motion in quadrants one and three to come toward the viewer when quadrants two and four move away (and vice versa). The next two images show the white regions shifted due to mirror motion of opposite phases, in agreement with this assumption. By observing similar images for both sides of the drum, and knowing the relative phases of the mirrors themselves, the relative phase of the drumhead motion can be determined unambiguously.

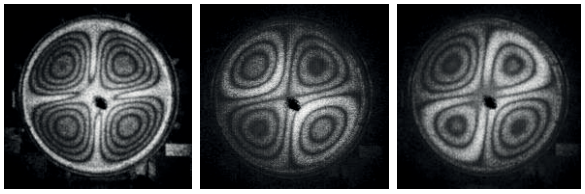

Figure 7. ESPI image of a (2,1) resonance pattern on a single drumhead (left). The same pattern with the mirror motion engaged (center and right). Mirror phase is reversed between center and right images. Note that the perimeter, which is always stationary, is not white in the moving mirror images.

3. FINITE ELEMENT MODEL

A finite element model of the drum, including the two heads and the enclosed air, was developed using commercial software [10]. The shell, which can play a role in the coupling process [3, 4], and the external air were not modelled. The model was used for qualitative comparison with experimental results and to explore the parameter space in terms of drum sizes and membrane tensions to investigate in the lab. Most importantly, the model provided insight as to the probable behavior of the air column inside the shell and its role in the coupling process.

Inputs to the model include drum geometry (diameter and length), head material properties (density, Young's modulus, and Poisson's ratio) and the membrane tensions. For this work identical membrane materials were used. In most cases the tensions in the two heads were set to differ from one another by a few percent. The model produced the following outputs: normal mode frequencies and shapes (including relative orientations), relative amplitudes, and relative phases for both heads and the enclosed air column. Visual representations of the mode shapes appear as in Figure 8, with nodal lines and planes depicted in green.

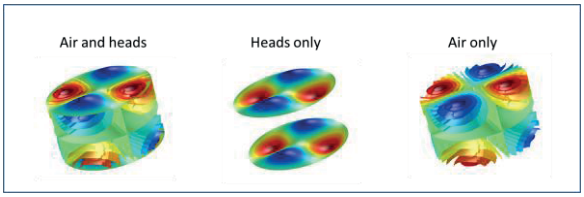

Figure 8. Representative images from the finite element model showing normal mode shapes for the two membranes and the enclosed air column. Nodal lines and planes are represented in pale green. Membrane images show displacements; air images show planes of equal pressure.

4. DRUM EXPERIMENTS

4.1 Variable length drums

Two variable length drums were constructed (Figure 9) allowing the heads and their tensions to remain fixed while coupling vs. length experiments were performed.

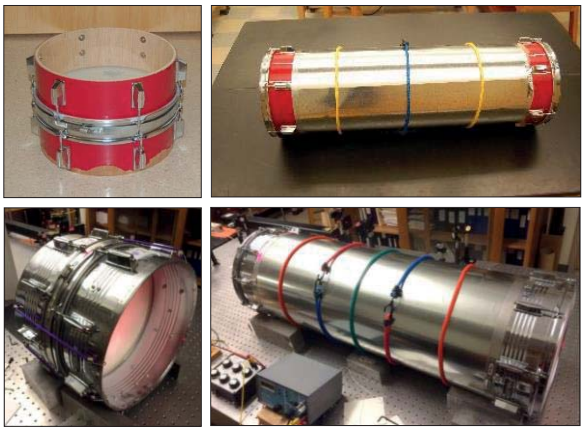

Figure 9. Variable length drums with shells replaced by sheet metal. 12" diameter tom tom (top) and 14" diameter snare drums (bottom). Lengths vary from about 2 to 110 cm. Heads face each other (left) for very small separations.

The first drum constructed was a 12" diameter tom tom cut in half to produce two shorter shells, each with a single head. The two sections were then connected using various lengths of sheet metal formed into a cylindrical shape and attached with modified hose clamps. The second variable length drum consisted of two 14" diameter snare drums, each with the snares and corresponding head removed. Again, these two drums were connected to sheet metal cylinders of various lengths, up to a maximum length of just over one meter. These drums could also be connected with the heads facing each other for very short lengths, as small as 2 cm. Identical single-ply Mylar heads [11] were used in all cases.

Drumhead tensions were adjusted via the standard tuning lugs spaced evenly around the perimeter (see Figure 1). The membrane tensions were tested for uniformity and for overall pitch using a commercially available mechanical gauge [12] that is placed directly on the head. Prior to assembly of the full drum, pitch and tension uniformity were also verified using a spectrum analyzer with a microphone input.

4.2 Experimental results

Several coupling trends were identified in the lab using the dual ESPI system with the variable length drums. These trends were qualitatively consistent with the predictions of the finite element model, including the shapes, amplitude ratios, and phase relations in the cases that were clearly coupled.

4.2.1 Coupling vs. length

The coupling strength of the vibrational patterns as a function of drum length L varies with shape. For patterns including only nodal diameters (in addition to the single nodal circle at the perimeter) the coupling strength decreases rapidly with drum length. These "diameter shapes" include (1,1), (2,1), and (3,1), etc. patterns. The finite element model suggests this behavior is due to air motion that "sloshes" back and forth azimuthally and can therefore be localized near a single head, as described by Rossing *et al*. [3, 4].

Figure 10 shows experimental ESPI images of (1,1) shapes on both heads of a drum with lengths varying from 2 cm to 55 cm. The fringe ratio begins at approximately one with the heads very close together and deviates from unity as the length is increased. At a length of 55 cm no vibrational pattern is visible on the head shown on the left. The resonant frequencies (not shown) also decrease moderately with increasing separation.

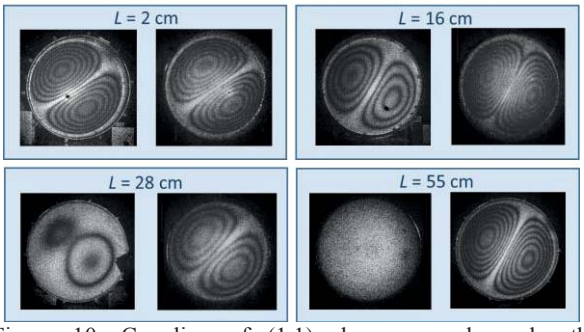

Figure 10. Coupling of (1,1) shapes vs. drum length. Amplitude ratios are inferred from the relative number of fringes on each head. The ESPI images show coupling strength varying from strong, at L = 2 cm, to barely visible at L = 28 cm. At L = 55 cm no coupling is observed.

The finite element model also shows how this (1,1) trend differs from that of the (0,1) fundamental (Figure 11). Shapes containing only circular nodal lines couple with longitudinal air motion, resulting in coupling between the heads over much larger lengths. Unlike the diameter shapes, these "circle shapes" do not conserve air volume and require some degree of longitudinal air motion. In particular, the fundamental (0,1) shape, with heads in phase, couples strongly for all lengths studied in the lab (up to 110 cm) as well as for all corresponding cases examined numerically with the finite element model.

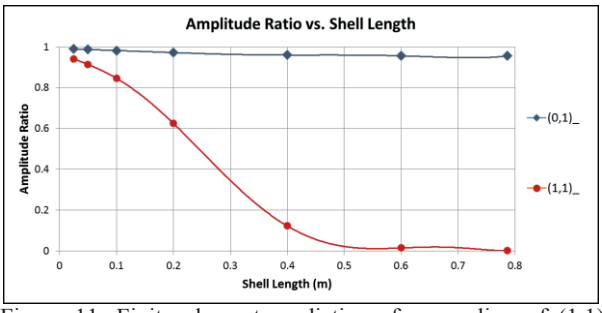

Figure 11. Finite element predictions for coupling of (1,1) shapes (red) and (0,1) fundamental shapes (blue) as a function of drum length. The (0,1) shapes couple strongly at all lengths via longitudinal air motion.

4.2.2 Diameter shapes vs. m

At a fixed length, the coupling strength of "diameter shapes" decreases with the number of diameters, m. Experimental ESPI images for the first four m values of a drum of length L = 6 cm are shown in Figure 12. The amplitude ratios, as determined by the relative numbers of contour fringes, clearly show the coupling strength decreasing as m varies from one to four. These results are qualitatively consistent with the finite element model, which is used to plot similar predictions in Figure 13.

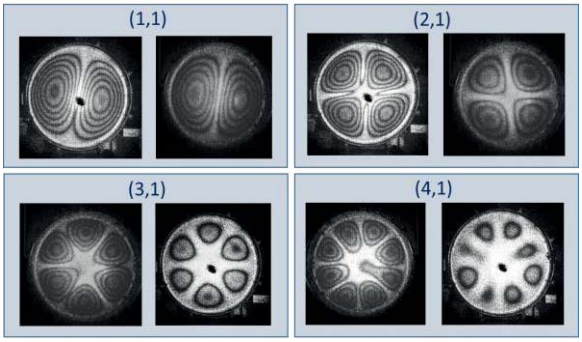

Figure 12. ESPI images showing coupling of "diameter shapes" at a fixed length of L = 6 cm. Equal amplitude fringes show the coupling strength decreasing as the number of nodal diameters (m) increases from 1 to 4.

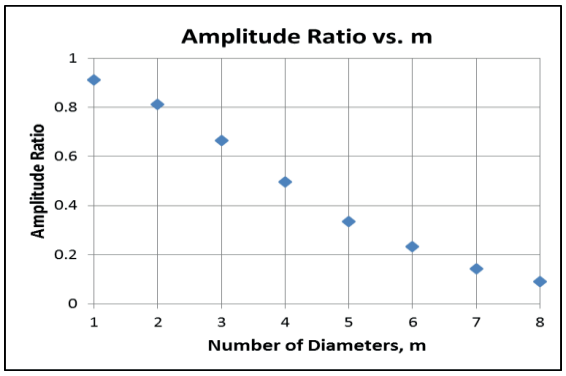

Figure 13. Amplitude ratio vs. number of nodal diameters at fixed drum length, calculated from the finite element model. Strongest coupling (amplitude ratio near unity) occurs with one diameter (1,1) and decreases steadily with increasing m.

5. CONCLUSIONS

A dual ESPI system has been constructed enabling opposite heads of a drum to be imaged simultaneously. Various aspects of the coupled vibrations can be determined including the approximate degree of coupling, relative orientation of the operating deflection shapes, and relative phase. A finite element model has been created using commercial software that agrees qualitatively with the experimental results and provides plausible representations of the air motion inside the drum shell. Variable length drums have been constructed and used to investigate membrane coupling trends as function of shell length.

Qualitative membrane coupling trends have been identified based on the characteristic shapes having either nodal diameters or nodal circles on the membranes. “Combination shapes” containing both nodal diameters and circles are also observed in the lab but are not addressed in this paper. Diameter shapes generally couple strongly only over small lengths and with small numbers of diameters. This may be explained by a localized “sloshing” motion of the enclosed air that need not extend from one head to the other. “Circle shapes,” without nodal diameters, do not conserve volume and appear to couple with longitudinal air motion. Thus, these patterns couple over the full range of lengths investigated.

Acknowledgments

The authors thank Thomas Moore of Rollins College for helpful advice on the method of determining relative phase.

6. REFERENCES

[1] T.D. Rossing, ed., Springer Handbook of Acoustics, Springer, pp. 642-648, 2007.

[2] R. Worland, “Normal modes of a musical drumhead under non-uniform tension,” J. Acoust. Soc. Am., Vol. 127, pp. 525-533, 2010.

[3] T.D. Rossing, I. Bork, H.Zhao, and.O. Fystrom, “Acoustics of snare drums,” J. Acoust. Soc. Am, Vol. 92, pp. 84-94, 1992.

[4] T.D. Rossing, “Science of Percussion Instruments,” World Scientific, pp. 26-30, 200.

[5] Moore, T.R. and Zietlow, S.A., “Interferometric studies of a piano soundboard,” J. Acoust. Soc. Amer., Vol. 119, pp. 1783-1793, 2006.

[6] National Instruments LabVIEW (www.ni.com/labview/).

[7] J.B. Marion, Classical Dynamics of Particles and Systems, 2nd ed., Academic Press, pp.408-415, 1970.

[8] K.R. Symon, Mechanics, 3rd ed., Addison-Wesley, pp. 191-200, 1971.

[9] Pasco Mechanical Wave Driver (www.pasco.com).

[10] COMSOL Multiphysics with acoustics and structural mechanics modules (www.comsol.com/).

[11] Remo Coated Ambassador heads (www.remo.com).

[12] DrumDial Precision Drum Tuner (www.drumdial.com).

INTERFEROMETRIC STUDIES OF THE BRAZILIAN CUÍCA

Tatiana Statsenko, Vasileios Chatziioannou, Wilfried Kausel

Institute of Music Acoustics
University of Music and Performing Arts Vienna, Austria
statsenko@mdw.ac.at

ABSTRACT

Electronic speckle pattern interferometry (ESPI) has been implemented for investigation of the vibrational behavior of the Brazilian cuíca. An advanced filtering and processing of time-averaging ESPI data has been applied to a friction drum, which has not been studied by means of laser interferometry before. Asymmetry in the operating deflection shapes of the cuíca has been observed and discussed. The obtained results were compared to finite element method computer simulations and single-point laser Doppler vibrometer deformation measurements. Vibrational shapes of the cuíca occurring under harmonic excitation are presented along with corresponding simulated mode shapes followed by the discussion of irregular patterns. The results of ESPI show an agreement with simulations and provide quantitative data on absolute values of the deformation amplitude.

1. INTRODUCTION

Drums are generally played by striking with hands or sticks. However, some percussion instruments, such as the cuíca, the lion's roar and the buhai, are excited by friction, which is applied on a wooden stick or a string, attached to the center of a membrane which is stretched on one open end of a cylindrical body. The playing principle of friction drums can be compared to violin bowing as it involves the stick-slip process which occurs when one object is sliding relative to another. This comprises continuous and transient actions, resulting in a complex and nonlinear response [1]. However, at low excitation amplitudes it is possible to describe the operating deflection shapes of the membrane with relation to normal modes, whereas at large amplitude they may show distinctly nonlinear or chaotic behavior.

The acoustical properties of the cuíca have been covered in a limited number of works and require more advanced examination, which can be given by non-contact optical methods, such as electronic speckle pattern interferometry (ESPI) and laser Doppler vibrometry (LDV), widely used in non-destructive investigation of vibrating objects [2]. Both techniques have been applied to musical instruments [3–6] and show high agreement with theoretical predictions on modal shapes, allowing full-field contactless measurements without special preparation of instruments. LDV uses the Doppler effect of a shifted frequency which occurs when light is reflected from the moving object. ESPI is an interferometric technique based on coherence properties of light diffracted from a rough surface. Microscopic variations in surface height produce scattered light in all directions and, due to high coherence of the laser, the amplitudes of the waves sum up. Imaging results in a granular pattern with spatial distribution of the intensity which solely depends on the diffraction limit of the camera [7]. Though speckles carry information on object movement, they reduce image quality and create 'salt and pepper' noise, so the main challenge is to retrieve the deformation phase change, which is highly affected by random phase distribution.

Time-averaging ESPI has evolved from holographic interferometry and provides fast and quantitative analysis on vibrations and small displacements of the whole object. It is a well-known optical method for non-contact deformation analysis with a conventional camera and a low-power continuous laser, which makes acquisition easy and does not require any specific conditions [7, 8]. The term "time-averaging" comes from the capturing procedure, since the acquisition time of a conventional detector is much higher than the period of vibration of the object under investigation.

The principal aim of this study was to investigate the vibration modes of a nonlinear friction drum under harmonic excitation with a simple low-cost experimental setup based on time-averaging speckle interferometry and supplemented with extensional advanced data processing.

2. CUÍCA

The cuíca is a Brazilian friction drum, brought from Africa and widely used in samba music as a rhythm and solo instrument [9]. The modern cuíca, shown in Figure 1, is made of an aluminum tube with ribs and a single drumhead made of animal skin.

Figure 1: Modern cuica, produced by Meinl Percussion. The photo is taken from the manufacturer's website.

The body can be also made of a gourd (folk cuíca), wood or fiberglass. A thin bamboo stick is bound to the center of the membrane, and the sound is produced by gentle rubbing of the stick with a piece of damp cloth in one hand, while the other hand alters the pitch by pressing against the center of the drum. If the second hand is not touching the drumhead, this results in an open tone [10]. In the sitting position the drum is horizontally placed on a knee of a performer, while for standing it is held at chest height, carried with a strap. The cuíca produces a high pitched sound recalling an animal voice with large dynamic range.

In the present paper, a 15 cm diameter cuíca drum from Meinl Percussion is investigated. The membrane is made of goat skin, approximately 0.3 mm thick. Harmonic excitation at low amplitudes does not reflect real playing conditions, yet it helps to visualize mode shapes and avoid excessive nonlinearities.

3. TIME-AVERAGING ESPI

Among various experimental techniques of ESPI, a reference-updating method was chosen because of its simplicity in implementation and higher intensity contrast compared to classical time-averaging interferometry [11]. An induced linear decorrelation of speckle phases between frames is introduced and subsequent images are being subtracted, revealing correlation fringes, which express levels of equal displacement of the object between two captures. This subtraction procedure eliminates decorrelation noise which generally occurs when the time between two compared frames increases. The output images can be displayed on the screen in real time and the shape of correlation fringes gives information about operating deflection shapes of the object at different frequencies.

3.1. Theory

Consider two interfering coherent light beams with spatially random phases, and a phase difference ϕ_0. One beam is reflected from an object, and another one is a reference beam originating from the same source. Due to the imaging system both beams are speckled and, in order to simplify the equations, a single pixel index is assumed. Assuming a linear phase shift in the reference beam and the external excitation of the object, the phase variation ϕ due to harmonic motion at frequency ω_0 can be temporally described as:

$$\phi(t) = \phi_0 + \gamma t + \xi \sin(\omega_0 t), \tag{1}$$

where γ is a coefficient directly linked to the velocity of the object due to the introduced linear movement and ξ describes harmonic motion and contains information about the vibration amplitude of the object A:

$$\xi = \frac{4\pi A}{\lambda}, \tag{2}$$

where λ is the wavelength of light. The time-averaged intensity of the n-th frame in a series of images measured by the detector is [11]:

$$\langle I_n \rangle = I_\mathrm{O} + I_\mathrm{R} + \beta \langle \cos(\phi_n + \gamma t + \xi \sin \omega_0 t) \rangle, \tag{3}$$

where I_O and I_R are intensities of two interfering beams, β is intensity modulation, and ϕ_n is a random phase defined for every pixel. It is assumed that if the time between two consecutive exposures is relatively short, the random phase changes only due to the linear shift. When two subsequent images taken during vibration are being subtracted, the resulting output intensity is:

$$I_\mathrm{sub}(\xi) = \beta \left| \frac{1}{t_\mathrm{exp}} \int_0^{t_\mathrm{exp}} \cos[\phi_n + \gamma(t_\mathrm{cam} + t) + \xi \sin \omega_0 t] \, \mathrm{d}t - \frac{1}{t_\mathrm{exp}} \int_0^{t_\mathrm{exp}} \cos[\phi_n + \gamma t + \xi \sin \omega_0 t] \, \mathrm{d}t \right|. \tag{4}$$

Generally, the exposure time t_exp and the time between two captures t_cam are not equivalent, so they are distinguished from each other. Equation (4) does not have a general analytic solution. However, it can be approximated by:

$$I_\mathrm{sub}(\xi) = |\mu \beta J_0(\xi)|, \tag{5}$$

where the coefficient μ depends only on parameters given by the linear movement and camera characteristics:

$$\mu = \frac{4}{\gamma t_\mathrm{exp}} \left| \sin(\frac{\gamma}{2} t_\mathrm{cam}) \sin(\frac{\gamma}{2} t_\mathrm{exp}) \sin(\frac{\gamma}{2}(t_\mathrm{exp} + t_\mathrm{cam}) + \phi_n) \right|. \tag{6}$$

The random phase ϕ_n immensely affects intensity and overall image quality. Low-pass filtering does not solve the problem, since it reduces fringe contrast. However, there are other ways to improve the images. The speckle size is given by the illumination wavelength and camera characteristics which can be adjusted so that each pixel accumulates several speckles. Image quality can be further enhanced by the averaging of several images, since the averaging of n frames decreases the speckle noise $\sqrt{n}$ times [12].

Therefore, nodes corresponding to $\xi = 0$ give maximum output intensity and are easily detected in an ESPI picture. Moving parts are defined by correlation fringes, given by Equation (5), with peak values rapidly decreasing as amplitude increases. However, phase and deformation amplitude values cannot be easily retrieved by taking the inverse of $|J_0(\xi)|$. The Bessel function is quasi-periodic, so the resulting phase map would be "wrapped"over a single interval from zero to the first root of the Bessel function. In phase-shifting ESPI the phase unwrapping procedure to obtain full-field data consists of adding integral multiples of 2π to the phase, preserving spatial continuity of the surface [13]. In reference-updating ESPI, regional inversion of the Bessel function, involving detection of minimum and maximum levels of the intensity within each side lobe region, is more appropriate due to different peak levels of the side lobes.

The proposed phase retrieving algorithm consists of enumeration of isolated contours and an order assignment of the corresponding side lobes of the Bessel function. For each area, maximum values are found and unwrapped. Contours of black correlation fringes are converted to phase data in the same fashion. First order regions can be processed on a pixel base, giving higher spatial resolution. The process assumes continuity of the object and provides no ambiguity of the side lobe order detection. Higher precision is achieved through pixel-by-pixel inversion based on retrieved data, but needs more computational time. The resulting absolute phase values can be easily converted to deflection amplitudes, providing quantitative data on vibration amplitude for every pixel.

3.2. Experimental setup

Consider the setup shown in Figure 2. Light from a laser source is split in two beams, one serving as an object illumination and a second being a reference beam. A mirror, mounted on a piezoelectric transducer (PZT), is introduced in the reference arm and provides an adjustable temporal optical path difference. A ground glass placed on the path of the reference beam serves as a diffuser which generates a scattered field and facilitates the alignment procedure. The two beams are combined upon the surface of the camera, therefore the average speckle size of both beams is the same. Rotation of polarizers controls the intensity of both beams. A continuous wave 532 nm laser operated at a power of 0.2 W. The frame rate of the camera was 11 fps for a resolution of 2050×2448 pixels.

The cuíca was fixed on the same table as all optical elements, and the bamboo stick was sinusoidally excited by a

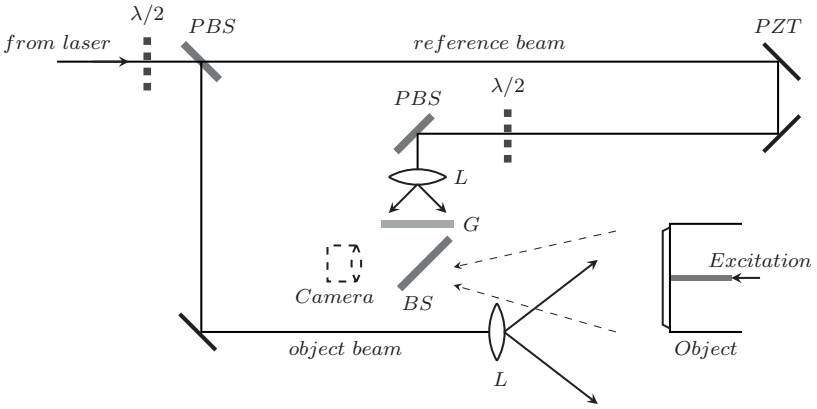

Figure 2: Setup for an ESPI measurement. Light from the laser is divided into two beams by a polarizing beamsplitter (PBS). Both beams are expanded by lenses (L). Half-wave plates ($\lambda/2$) are added to control the relative intensity of the beams. A reference beam is passing through the ground glass (G), and then the two beams are combined by a beamsplitter (BS) and directed to the camera. A PZT-mirror adds a linear phase shift during image capturing.

shaker mounted behind the instrument so that the only moving parts of the instrument were the stick and the membrane. The amplitude and frequency of the shaker were controlled by a frequency generator. The contrast of ESPI images was adjusted by changing the relative intensity of the beams, the amplitude of the PZT and the number of frames recorded during each cycle of the PZT. The image capturing and the PZT driving were done using LabVIEW software.

4. RESULTS

Along with experiments, the normal modes of the cuíca were studied using the finite element method (FEM) implemented in COMSOL Multiphysics. The investigation was done for a pretensioned membrane with a radius of 75 mm, clamped along the borders. Harmonic excitation was applied to a circular area of 5 mm in diameter, shifted by 1.4 mm from the center. The parameters used for the simulation of the membrane are shown in Table 1. They were chosen from analogous membrane materials and adjusted while comparing the model to the experimental values [14, 15].

Parameter	Value
Pre-tension	4470 N/m
Young's modulus	50 MPa
Density	1260 kg/m^3
Poisson's ratio	0.3

Table 1: Parameters for COMSOL modeling.

4.1. ESPI

Analysis has been done for excitation frequencies from 200 Hz to 2000 Hz. An unwrapping procedure was preceded by averaging, normalization and digital filtering of sequences of frames, all performed in MATLAB. Series of images were averaged in order to decrease speckle noise. The procedure of normalization involved division by the averaged reference frame, taken without any external excitation. Normalization removed undesirable diffraction effects and artifacts caused by dust. Spatial filtering was followed by localized Fourier transform filtering (LFF), based on the method described by Li [16]. The difference from LFF is that there is no Gaussian smoothing, and filtering is performed on the inverted images which positively affects the output contrast. The results of phase unwrapping for three vibrational states of the cuíca are presented in Figure 3 together with FEM simulations.

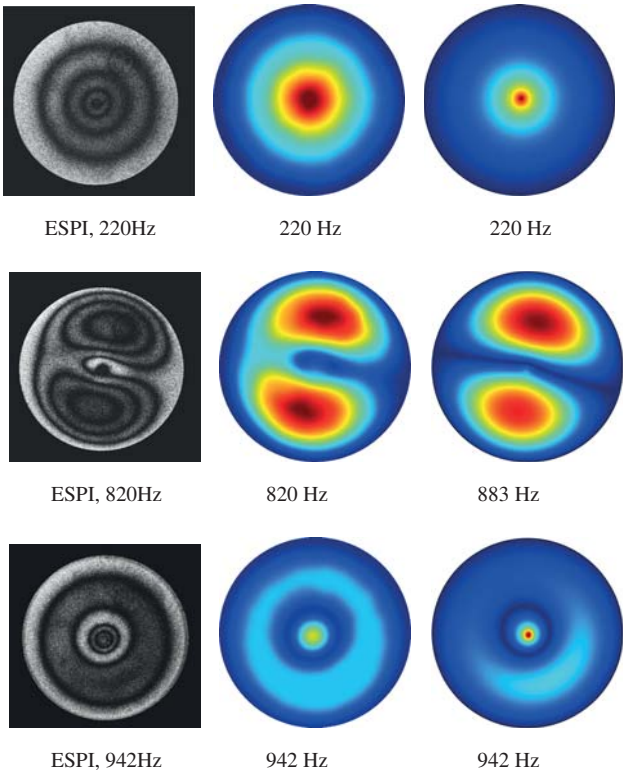

Figure 3: Unwrapping of two ESPI patterns and comparison to FEM predictions. Left: temporally averaged ESPI images. Middle: unwrapped data. Right: corresponding simulations.

The simulation was performed for exact experimental values of the frequencies where it was possible, but for certain values there was a discrepancy between experimental data and corresponding normal modes. Therefore, the closest solutions have been chosen. The wooden stick is connected not to the exact

center of the membrane, which causes asymmetry of the operating deflection shapes. This asymmetry may also be reinforced by inhomogeneity of the membrane and a slight tilt of the bamboo stick which changes the vector of the applied force. Thus, operating deflection shapes which imply only circular nodes become highly asymmetric with increasing excitation force. Such an example is shown in Figure 4 for the vibration amplitude at 872 Hz. The same result can be achieved for a totally symmetric object, when an additional component of the direction of applied force is introduced in the plane of the membrane. Such a small variation in location and direction of the applied force drastically changes the deformation shape of the membrane. Regarding the real tension of the membrane, it cannot be easily modeled. Since goat skin is not perfectly homogeneous, it changes along its area randomly. Simple altering of the tension in one direction did not give an effect similar to the one observed.

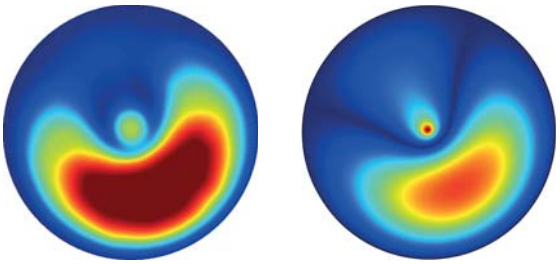

(a) Experiment (b) Simulation

Figure 4: Highly asymmetrical operating deflection shape at 872 Hz and the simulated deformation at the same frequency.

Figure 5 shows asymmetry in the vibrational shapes of the cuíca at high frequencies. Processed ESPI images are compared to corresponding operating deflection shapes calculated in COMSOL. Even without unwrapping, the main modes of vibration can be clearly seen in enhanced filtered images since the side lobe peak intensity decreases with rising deformation amplitude.

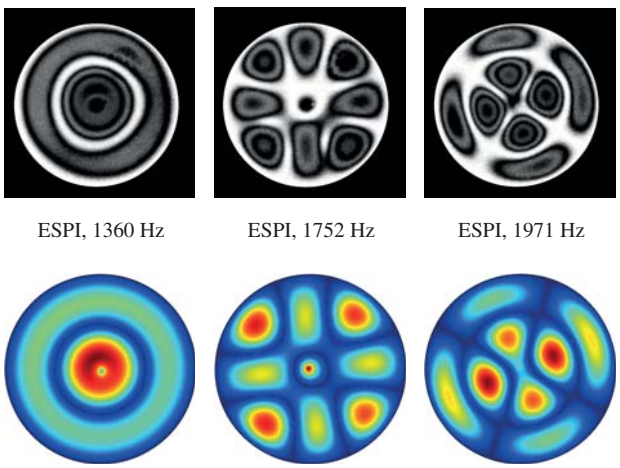

ESPI, 1360 Hz ESPI, 1752 Hz ESPI, 1971 Hz

(0,2) 1360 Hz (4,1) 1755 Hz (2,2) 1975 Hz

Figure 5: Slight asymmetry in the vibration shapes and corresponding FEM simulations. Top: temporally averaged and filtered ESPI images. Bottom: FEM simulations.

Such filtered ESPI images can be used for an initial modal analysis of vibrating structures and reveal vital information on the operating deflection shapes of the object under study. The presented experimental setup requires only basic infrastructure in order to be restored. It is thus suitable for application across a range of scientific disciplines and research institutions.

4.2. LDV verification

A single-point laser Doppler vibrometer was used in order to verify the obtained phase values. Table 2 shows a comparison between LDV results and unwrapped data at three single points chosen randomly on the surface of the membrane for two different frequencies. The average discrepancy is about 35 nm, which is in the order of $\lambda/15$.

	260 Hz		750Hz	
Point	ESPI, μm	LDV, μm	ESPI, μm	LDV, μm
1	0.074	0.08	0.29	0.25
2	0.176	0.2	0.17	0.2
3	0.1	0.09	0.26	0.28

Table 2: Comparison of the results of ESPI and LDV measurements for two frequencies at three different points on the membrane.

5. CONCLUSIONS

The vibration modes of a Brazilian cuíca drum were investigated under harmonic excitation between 200 Hz and 2000 Hz by means of time-averaging ESPI followed by digital processing, which gave an adequate agreement with FEM modeling and LDV single-point results. The proposed filtering and processing algorithms give high-contrast ESPI images and competent quantitative data on absolute values of deformations due to external excitation. For several frequencies, the observed operating deflection shapes are similar to simple clamped membrane normal modes. However, non-symmetry of the cuíca notably affects deformation shapes, which can be visualized on a computer screen in real time while changing frequency and excitation force.

Future work will involve the analysis of nonlinear behavior and transient events by means of high-speed ESPI in order to describe excitation processes in friction drums.

6. ACKNOWLEDGEMENTS

The authors would like to thank Alexander Mayer for technical assistance and development of data acquisition software in LabVIEW. This research work has been funded by the European Commission within the ITN Marie Curie Action project BATWOMAN under the 7th Framework Programme (EC grant agreement no. 605867).

7. REFERENCES

[1] A. Akay, "Acoustics of friction," *The Journal of the Acoustical Society of America*, vol. 111, pp. 1525–1548, 2002.

[2] P. Hariharan, *Basics of Interferometry*, Academic Press, 2007.

[3] E. V. Jansson, "An investigation of a violin by laser speckle interferometry and acoustical measurements,"

Quarterly Progress and Status Report, vol. 13, no. 1, pp. 25–33, 1972.

[4] T. D. Rossing, "Acoustics of percussion instruments: Recent progress.," *Acoustical Science and Technology*, vol. 22, pp. 177–188, 2001.

[5] G. Bissinger and D. Oliver, "3-D Laser Vibrometry on Legendary Old Italian Violins," *Sound and Vibration*, pp. 10–14, 2007.

[6] R. Perrin, D. P. Elford, L. Chalmers, G.M. Swallowe, T. R. Moore, S. Hamdan, and B. J. Halkon, "Normal modes of a small gamelan gong," *The Journal of the Acoustical Society of America*, vol. 136, no. 4, pp. 1942–1950, 2014.

[7] R. Jones and C. Wykes, *Holographic and Speckle Interferometry*, Cambridge University Press, 2nd edition, 2001.

[8] W. C. Wang, C. H. Hwang, and S. Y. Lin, "Vibration measurement by the time-averaged electronic speckle pattern interferometry methods.," *Applied Optics*, vol. 35, no. 22, pp. 4502–4509, Aug. 1996.

[9] J. Schneider, *Dictionary of African Borrowings in Brazilian Portuguese*, Buske Verlag, 1991.

[10] C. Eduardo and F. Kumor, *Drum circle: A Guide to World Percussoin*, Alfred Music Publishing, 2001.

[11] T. R. Moore and J. J. Skubal, "Time-averaged electronic speckle pattern interferometry in the presence of ambient motion. Part I. Theory and experiments.," *Applied optics*, vol. 47, no. 25, Sept. 2008.

[12] J. W. Goodman, *Laser speckle and related phenomena*, Springer, 1975.

[13] K. Creath, "Phase-shifting speckle interferometry," *Applied Optics*, vol. 24, no. 18, 1985.

[14] N. H. Fletcher and T. D. Rossing, *The physics of musical instruments*, Springer, 1998.

[15] W. K. Schomburg, "Membranes," in *Introduction to Microsystem Design*, vol. 1, pp. 29–52. 2011.

[16] C. Li, C. Tang, H. Yan, L. Wang, and H. Zhang, "Localized Fourier transform filter for noise removal in electronic speckle pattern interferometry wrapped phase patterns.," *Applied Optics*, vol. 50, no. 24, pp. 4903–11, Aug. 2011.

MICROPHONE ARRAY METHODS FOR MUSICAL ACOUSTICS

Rolf Bader
Institute of Systematic Musicology, Germany
r_bader@t-online.de

ABSTRACT

Measuring the radiating sound pressure at surfaces and sound holes of musical instruments can be performed using microphone arrays recording the radiated sound field around the instrument and back-propagating the measured pressures to the radiating surface or holes. Among the advantages of such a measurement setup are the preservation of the radiating surface by not attaching piezos or the like adding additional mass, the possibility to measure both, surfaces and sound holes at the same time, or when using a reasonable amount of microphones with high sampling rate to display transients at sound onsets. The main problem although is the back-propagation itself as this is an ill-posed problem. The main methods of multipole methods like the Minimum Energy Method (MEM), Helmholtz-Lease-Square (HELS) methods or Acoustic Holography (AH) try to overcome this ill-posedness using different approaches which again have pros and cons. While AH uses an angular spectrum back-propagating this spectrum with respect to its phases it has problems with evanescent waves which might appear with low frequencies already. HELS is using one virtual radiation point with many spherical harmonics overcoming the evanescent problem but with poor convergence and the need of very many harmonical functions. MEM uses as many virtual monopoles sources on the surface as there are microphones also overcoming evanescent waves with the need to distort these monopoles to overcome the ill-posedness of the problem. The paper shows examples of these methods for stringed, bowed and wind instruments.

EMERGENCE OF INHARMONIC COMPONENTS IN CLASSICAL GUITAR SOUNDS

Vincent Fréour[1], François Gautier[1], Bertrand David[2], Marthe Curtit[3]
[1] Laboratoire de Mécanique et d'Acoustique, Aix-Marseille Université, France
[2] Institut Mines-Telecom, Telecom ParisTech, France
[3] Institut technologique européens des métiers de la musique, Le Mans, France
vincent.freour@mail.mcgill.ca
francois.gautier@univ-lemans.fr
marthe.curtit@itemm.fr

ABSTRACT

Inharmonic components due to body modes are present in the transient phase of classical guitar sounds. The aim of this paper is to investigate their emergence using high resolution analysis methods. Using a wire breaking technique, the near field radiated pressure is recorded in various plucking conditions on classical guitars. An analysis-synthesis approach making use of the ESPRIT method is presented and some indicators of body-sound emergence are proposed and calculated. The influence of the conditions of excitation on the body-sound emergence is first characterized. In a second step, the calculation of these indicators of emergence is performed over a large pool of instruments, including high-end hand-made guitars, as well as entry-range industrial instruments. The main result show an overall greater sensitivity of high end guitars to the excitation conditions with regards to the emergence of the body sound at tone onset, hence allowing an objective categorization of the instruments.

PRECISE CELLO BOWING PENDULUM

Robert Mores

Faculty Design Media Information
University of Applied Sciences Hamburg, Germany
robert.mores@haw-hamburg.de

ABSTRACT

A cello bowing pendulum for precise measurement of physical parameters of bowing is presented. It is designed to hold and play bows of any style and to perform the bowing on a strict line. Such a strict line follows the bowing paradigm of musical play but also eases the instrumentation of the applied bowing forces. Two eccentric suspensions translate the initially circular track of a gravity pendulum into the desired straight line. An adjustable fraction of the weight serves as bow force, while the stringed cello is resting beneath the pendulum on a weighing scale which measures this bow force. The tractive force for bowing and the bow force are orthogonally arranged and can be adjusted and measured with centinewton precision. Secondly, bow velocity is not predefined by a driving entity but is controlled by the slip-stick interaction. A potential tractive force is intentionally combined with a damping unit so that the resulting mechanical impedance will instantaneously adapt to what the actual slip-stick process recommends including a resulting bow velocity. This adaptive operation is similar to what musicians sense during bowing and therefore appears to be a valid approach for related performance-based studies of musical acoustics. Such adaptive operation also appears to be preferable for investigations of bifurcation regimes, of reciprocal inter-instrument pitch-synchronization, of physical slip-stick interaction parameters and of maximum and minimum bow force. The paper contains the pendulum construction principle, operational modes and ranges as well as first results from regime transitions.

1. INTRODUCTION

Aim of the instrumentation is to facilitate measurements on slip-stick interaction in a valid and reliable form. Target investigations are (i) bow force limits, (ii) susceptibility to external factors, for instance inter-instrumental synchronization, (iii) characteristics of regimes and their stability.

For these fields of exploration, bowing should not be stimulated by a machine with fixed parameters of force and velocity. Electrical motors or comparable driving entities usually feature the property of high mechanical impedance. Such high-impedance predetermined bow driving is insensitive to what happens at the bowing point. This compares to what takes place when a totally inexperienced person bows a string the first time. The produced sound testifies non-optimal or non-typical operation, there is little susceptibility to sense the driving parameters necessary for a favourable sound. In terms of validity it is desirable to simulate what experienced musicians do when they sense the bow-string contact-point. Musicians will adapt their playing according to the response they feel in their hand and arm. A mechanical bowing installation with adaptive driving parameters is expected to reveal the physical parameters relevant to musical play.

The range of earlier bowing machines is diverse. Lawgreen (1980) used an electrical motor for propulsion of a wagon which holds the bow and controls the direction of bowing. Pickering (1991) started with a similar idea but used a grooved wheel to guide the bow in operation. The wheel was also used to define the bow force while investigating local temperature at the contact-point. Cronhjort (1992) used the drive system of a wire printer for propulsion and direction control. The construction, which only facilitates measurements on violins, as been used by Schoonderwaldt et al. (2008) to investigate bow-force limits. Schumacher and Garoff (1996) also used a motor-driven bow and a construction with micrometer screws to define bow pressure. With this construction Woodhouse et al. (2000) measured friction force with the help of force transducers at the string termination points. Galluzzo and Woodhouse (2014) presented yet another construction to investigate onsets. The heavy-load machine controls bow force and velocity.

These constructions have in common that they drive the bow or its substitute, a rod, by some kind of motor. Motors usually have a high mechanical impedance to perform their task. A high impedance, however, implies, that the driving motor is not necessarily susceptive to what happens to a load when moved or driven in any kind. High impedance together in combination with predefined velocity or acceleration raises issues of validity when exploring slip-stick interaction:

a) Parameter dynamics between onset and steady-state tones. For steady-state tones and the related quasi stable energy flux the possibly measured friction force translates to acoustic radiation and heat. During onset, however, the measured friction force additionally feeds the process of building up the energy for the starting string oscillation. This additional energy necessary to build up the oscillation is felt by a musician in terms of a tactile resistance, which he or she will adapt to via increased bow force and/or bow velocity.

b) The process of building up the oscillation is multi-dimensional. In order to achieve valid findings for investigated slip-stick scenarios any resulting bow force variation or velocity variation during onset should rather be modelled adequately before being used parametrically during operation. The approach here is not to model these parameters but to let the slip-stick interaction between bow and string co-define the necessary parameters, adaptively and instantaneously.

c) For understanding the stability of slip-stick regimes, it might be desirable to investigate the likelihood to reside in a certain regime or the likelihood to transit from one regime to another. Such likelihood can be measured when the driving control parameters adapt to what the slip-stick interaction wants. Such likelihood is otherwise difficult to measure, when transitions between regimes are predefined by high-impedance motion control.

d) Adaptive driving seems to be preferable also for investigations on mutual inter-instrument synchronization. Imagine an impulse of an external sound source arriving at a cello top and proceeding to the bridge and the string in the very

moment of an upcoming stick-slip transition. This impulse is likely to co-define the moment of such transition, and therefore the pitch. For such investigations the slip-stick interaction should not be ruled by predefined parameters and a high-impedance driving unit but should rather be left on its own.

e) The wolf note is another example of necessary adaption. Musicians are able to control the parameters of playing so that the wolf note can be avoided. They will sense the bow-string contact-point while controlling the parameters bow force, bow velocity, and bow-to-bridge distance to finally overcome the wolf note.

2. CONSTRUCTION PRINCIPLE

The target of the instrumentation setup is to measure physical parameters and to study slip-stick regimes in valid operational modes, i.e. in a way that comes close to what musicians do while performing. Therefore the free choice of real bows and the straight movement of such bows across their entire length are preferable. Additionally, bow-to-bridge distance, bow force, traction force, bow position and velocity should be measurable rather precisely. The main reason for preferring a pendulum arrangement against other alternatives is its potential of low friction movements. Another reason is its potential to use geometric principles for achieving steady bow forces across the entire bow length.

2.1 Geometry of height compensation

A conventional gravity pendulum inherently implies circular movements, and the centre of mass is elevated at its points of return relative to its middle position. This factor at first aggravates the target of straight movements. However, with an eccentric suspension *(ES)* the initially circular path can be converted into a straight path, at the point of attachment, see point *A* of *ES* along its movement across the positions *left* to *middle* to *right*, Fig. 1. The straight path corresponds to a circle of infinite radius, and the construction principle shown here is restricted to using an *ES* with a height to base line ratio of 1/2, see unit size *a* in Fig. 1. The pendulum requires the use of two rods or strings, one from *O1* to *B* and one from *O* to *C*. The left side of the Figure shows the construction principle using dividers, and the right side assists the analytical solution.

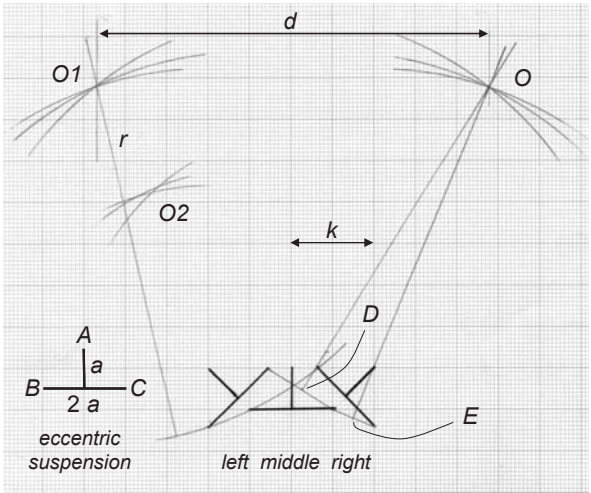

Figure 1: Construction principle for a pendulum of virtually infinite radius.

Construction with dividers: point *B* of the *ES* must follow a circular line, therefore point *B* in the *left*, *middle* and *right* position of *ES* is equidistant to the center *O1*. Reversely constructed, the circles around *B* of the *ES* in the three positions must intersect at *O1*. Likewise, the circles around *C* of the *ES* in the three positions deliver *O*. However, while constructing with dividers, the intersection of all three circles can be found for quite a range of radius *r* due to the limited precision of instruments. Out of that range, the three intersections of the three circles will not coincide, see area at *O2* in the Figure. The true *r* remains uncertain with this construction method, but a sufficiently accurate *r* can be found for an instrumentation setup.

Analytical solution: the range of operation, i.e. point *A* in *ES* strictly follows a straight line, is defined in terms of *k* multiples of *a*, precisely, $2 \cdot k \cdot a$. For the application, the bow length should be less than the total range of operation $2 \cdot k \cdot a$. While the pendulum will be able to continue the desired movement slightly beyond the indicated end positions *left* and *right*, these end positions are preferred for ease of use in an analytical approach. Furthermore, point *C* in the middle position of *ES* is the origin of the Cartesian coordinate system, normalized to the fundamental size *a* in *ES*. This setup delivers three coordinates.

$$\begin{array}{lll} C \text{ at } ES \text{ in } \textit{left} \text{ position} & x = a \cdot \left(\sqrt{2} - 1 - k\right) & y = a \\ C \text{ at } ES \text{ in } \textit{middle} \text{ position} & x = 0 & y = 0 \\ C \text{ at } ES \text{ in } \textit{right} \text{ position} & x = a \cdot (k - 1) & y = a \cdot \left(1 - \sqrt{2}\right) \end{array} \quad (1)$$

Please note that a general analytical solution is followed here, even though the illustration only shows the case of $k = 2$. The lines between these positions and the corresponding radii form isosceles triangles of individual heights, which are oriented perpendicular to mentioned lines and which intersect at center *O*, see Figure 1. Only two interceding heights of triangles are needed to determine the coordinates of *O*. This relation can be used for construction. Using this relation for the analytical solution requires determination of positions *D* and *E*.

$$\begin{array}{lll} D & x = a/2 \cdot \left(\sqrt{2} - 1 - k\right) & y = a/2 \\ E & x = a/2 \cdot (k - 1) & y = a/2 \cdot \left(1 - \sqrt{2}\right) \end{array} \quad (2)$$

These positions together with the slope of the heights of the two selected triangles

$$\begin{array}{ll} \text{slope of the line } \overline{DO} & k + 1 - \sqrt{2} \\ \text{slope of the line } \overline{EO} & k - 1 \,/\, \sqrt{2} - 1 \end{array} \quad (3)$$

form the functions

$$\begin{aligned} f_{DO}(x) &= a/2 \cdot \left[1 + \left(k + 1 - \sqrt{2}\right)^2\right] + a \cdot \left(k + 1 - \sqrt{2}\right) \cdot x \\ f_{EO}(x) &= a/2 \cdot \left[1 - \sqrt{2} + (k-1)^2 \,/\, \left(1 - \sqrt{2}\right)\right] + a \cdot k - 1 \,/\, \sqrt{2} - 1 \cdot x \end{aligned} \quad (4)$$

Solving these equations for the intersection of these functions will deliver the coordinates of center *O*, where the *x*-coordinate co-determines half of the distance *d* between *O* and *O1*, $d = 2 \cdot a \cdot (1 + x)$, which is necessary for the physical construction of the pendulum. The radius of the notation of *O* in polar coordinates directly delivers the radius *r* of the pendulum (remember that the origin of the coordinate system is at *C* of *ES* in the middle position due to the a priori definition). The radius *r* grows over-proportionally with *k* due to the quadratic components in the offsets in f_{DO} and f_{EO}, see Figure 2. The construction example in Figure 1 uses $k = 2$ and therefore

r = 8.69 a. For the implementation of a cello bowing pendulum, one might choose the parameters a = 12 cm and k = 3.5 to obtain an operating range of 84 cm, radius r = 2.32 m and the distance d = 1.3 m.

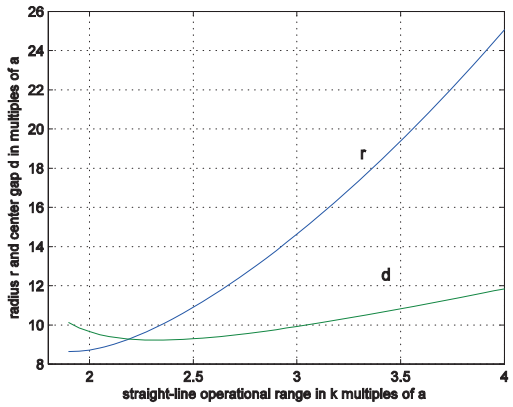

Figure 2: Pendulum geometry as derived from (4), required radius r and center gap d in multiples of basis width a versus the pendulum's maximum straight-line operational range in k multiples of basis width a.

Figure 3 illustrates the overall principle of the bowing pendulum. Two of the described *ES* systems (*ES* and *r* drawn to scale in units of a = 12 cm) are employed to hold the bow-mounting device of mass *M1* at both its ends, see *strings b* and *c*. Both ends of this device are guided on a straight line by construction, and so is the bow-mounting device. Note, that this straight line and traction forces applied through *strings d* and *e* are arranged orthogonally to the direction of gravity, which translates to the direction of bow force.

2.2 Weight compensation

The mass of the device, *M1*, emulates the mass of a cellist's arm in the range of 3 to 4 kg. It follows the straight line paradigm and its level above ground will not change. Therefore this mass will not contribute to variations of the potential energy and associated restoring forces. However, the two *ES* and the rods or strings holding them still follow a circular line of a conventional pendulum and therefore contribute to variations of potential energy. Even though the mass of these parts is only a small fraction of *M1* the pendulum will still target the middle position from either side, effectively representing a residual restoring force. This residual force disturbs the aim to operate an instrumentation setup at well definable forces and it aggravates precise measurement of these forces. Therefore, the residual force is compensated for by a counter-pendulum and its mass *M3* which is attached to *M1* by *string d*, see Figure 3. In effect, the pendulum can now be positioned at any position within its $2 \cdot k \cdot a$ range of operation without facing any restoring forces, it will simply remain where positioned.

2.3 Bow force adjustment and bow elasticity compensation

While mass *M1* is principally held by the pendulum, an adjustable fraction of its weight serves as bow force. The bow force is adjusted by fine tuning of the length of the *strings b* and *c*. Length variations of 1 mm correspond to bow force variations of several Newton in the implemented system while thin steel strings of length r are used to hold the two *ES* and the attached mass *M1*. Such length variation will not hamper the mentioned orthogonal arrangement of applied forces given a sufficient width of the total arrangement, here 6 m, not drawn to scale in Figure 3.

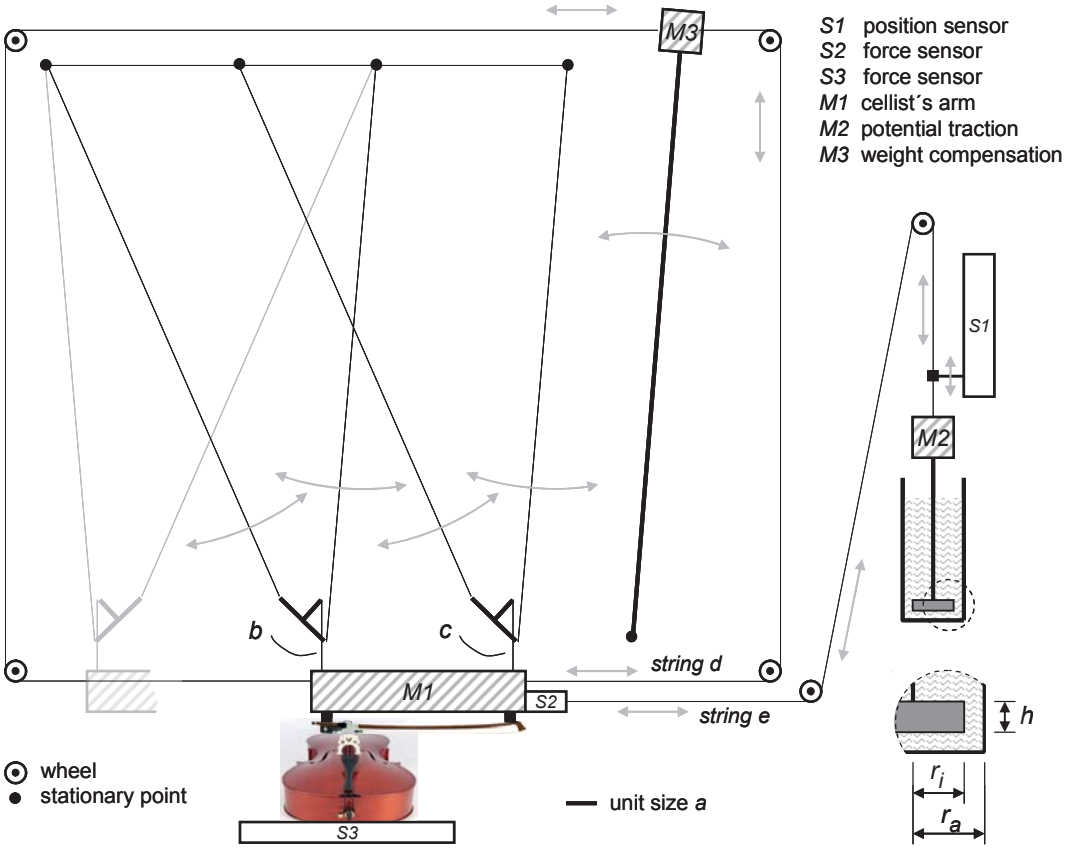

Figure 3: Schematic of the pendulum's total arrangement.

Bow force adjustments directly translate to the attached bow at its rather stiff ends, frog and tip. Along the bow hair, however, the force will be lower than at its ends when following the straight line paradigm and given the elasticity of bow and hair. In the middle section the bow will usually have to *dive deeper* towards the strings as compared to the end sections to achieve comparable forces. This can be observed while bowing. Such desirable diving can be applied, when relaxing the straight line paradigm. While point *A* of *ES* follows a straight line, see Figure 1, other points along the section from *A* to the base line *BC* will follow a circle the radius of which will range from infinity—close to *A*—to fractions of *r* depending on *k*—close to the base line *BC*. Therefore, altering the height of *ES* will allow to adjust a desirable curvature that would facilitate steady-state bow forces across the entire length for individual bows. In the implemented setup the height of *ES* can be lowered by up to 10% of its target value which comfortably allows to do all necessary adjustments. Note that this kind of adjustment also relaxes the need of precisely finding or precisely implementing the radius *r*.

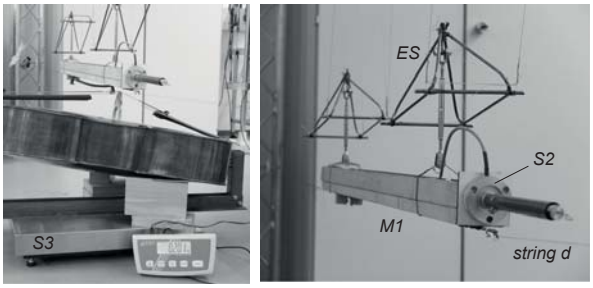

Figure 4: Implemented pendulum, in operation (left) and the compensated pendulum (right).

2.4 Adaptive driving entity

The introduction listed several issues of validity why it is not preferable to simply use a strong motor to apply the necessary traction force to the bow. The disturbing property is the high impedance. A motor of such high impedance is unlikely to adapt to the dynamics of a low-impedance load.

For the purpose of the targeted investigations, the driving unit is of low impedance and designed to adapt to the dynamics of the load. Its impedance will decrease with increasing bow velocity, similar to what a musician experiences.

The Hagen-Poiseuille relation for fluids is adapted to the laminar flow of a fluid along a non-rotating cylinder (Petzoldt 2015). A cylinder of height h and radius r_i is moved in a cylindric vessel of radius r_a, see Figure 3. This geometry is used in the derived Hagen-Poiseuille relation and delivers the force-velocity relation in dependence of the fluid's viscosity η in Pa·s

$$\eta = \frac{F_d}{2 \cdot \pi \cdot h \cdot v} \cdot \left[\ln\left(\frac{r_a}{r_i}\right) + \frac{r_i^2 - r_a^2}{r_i^2 + r_a^2} \right] \qquad (5)$$

while using SI units. This formula considers shear friction only and no turbulence and will therefore predict for low velocity only.

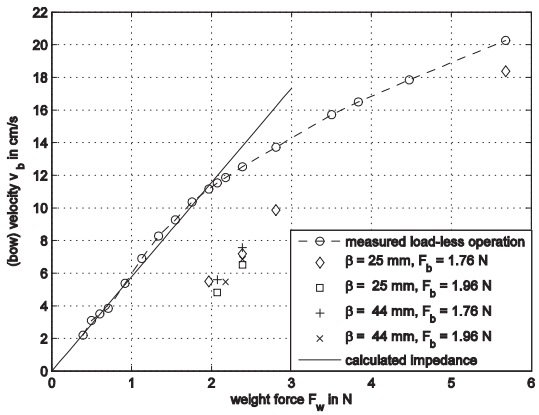

Figure 5: measured and calculated impedance of the driving entity for load-less operation, and measured velocity-weight-force relations for some load cases on the open D-string of a cello.

Figure 4 illustrates the source impedance for a damping device with r_a = 2 cm, r_i = 1.6 cm, h = 0.01 m, and filled with water, η = 1 Pa·s at 20 °C. The prediction roughly matches the measured values for low velocity. This velocity versus force curve indicates the velocity that is reached with a certain weight force represented by $F_w = M2 \cdot g$. This is the point of equilibrium where the weight force F_w is equivalent to the shear friction force F_d of the fluid. In other words, this curve represents the source driving characteristics without any load (*string e* is disconnected). In the case of a load, for example the few individual cases at F_w = 2 N and v_b = 5 cm/s, the potential force F_w will be in equilibrium with the sum of F_d and F_t, with F_t being the tractive force applied to the bow unit. F_d for the achieved bow velocity is now somewhat less than 1 N, and F_t is approximately 1.2 N. Variations in the slip-stick process will translate to variations of F_t and the corresponding bow velocity will adapt. The slope of such adaption is roughly 6 cm/s per N. The adaption is also observable for the four slightly different load cases leading to slightly different bow velocities at the given weight force F_w = 2.4 N. Load cases are denoted by the bow-to-bridge distance β relative to the string length and by the bow force F_b.

Range and relations of F_w and velocity reasonably relate to the impedance of a human arm. For a wider view of human body parts impedance see Mizrahi (2015). The velocity-dependent force can well be felt when manually driving *M2*, and the response feels like the resistance when bowing a cello string.

3. PARAMETER INSTRUMENTATION

3.1 Sensors, signaling and precision

Three parameters are measured in the system simultaneously. Sensor *S1* measures the position s_b of the bow. Bow velocity v_b and bow acceleration a_b can be derived from s_b.

Sensor *S2* measures the tractive force F_t applied to the bow unit via *string e*. *S2* does not measure tractive forces applied via *string d*, which are meant to compensate the two-sided residual restoring forces of the pendulum. However, the four wheels used to guide *string e* constitute a little frictional force when in motion, F_p , see Figure 5. F_p is kept very low, in the range of 0.1 ... 0.3N, depending on adjustments of tension in *string d*. F_p is also very stable across velocity v_b and across position s. F_p can be measured separately for each session to be used for post-calibration of data. The pendulum can be moved in a load-less mode of operation, i.e. without any contact between bow and instrument, and the measured tractive force F_t will directly

correspond to the pendulums friction F_p . For measurements of the static or dynamic friction between bow and string, F_f, sensor *S2* will finally capture F_f only indirectly, $F_f = F_t - F_p$. In cases of non-stationary velocity, the acceleration force $F_a = M1 \cdot a$ (*a* now stands for the acceleration and not for the unit length in *ES* geometry) has to be accounted for, see the arrow shaded in gray in Figure 6. Such non-stationary operations require an $F_f = F_t - F_p - F_a$ correction term.

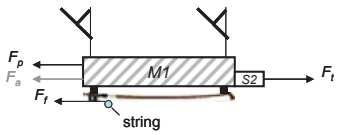

Figure 6: Frictional force at the bow F_f in relation with traction force F_t, frictional force of the compensation strings F_p, and possibly acceleration force F_a.

Sensor *S3* measures the bow force, F_b. Indeed, the high-precision industrial weigh scale measures the entire cello including the mounting jig used to hold the cello. However, relative measurements capture the additional bow force and its variations. Remember, that *string e* and therefore the force F_t are arranged strictly orthogonal to the gravitational force F_b so that even the momentum caused by F_t will not alter measurements of F_b.

All sensor signals are electrically converted prior to sampling: The DC signal from *S1* is converted to frequency, the *S2* Wheatstone bridge is operated with AC and the *S3* weighting scale signal is converted to frequency. All signals are captured at f_a = 192 kHz. For sensor types see appendix.

Precision is limited mechanically and electrically. The precision of position s_b is limited by the elasticity of *string e*, by limited precision of *S1*, and by limited stability of the VCO. The precision of F_f is limited by the contribution of F_p in F_t and by an initial calibration procedure. The precision of F_b is limited by the precision and linearity of the weighting scale and by the drift of the VCO. For details see Appendix A. Table 1 lists the overall maximum errors.

Table 1: Parameters measured and related maximum errors

physical property		sensor	maximum error
s_b in cm	bow position	*S1*	± 0.18 cm
v_b in cm/s	bow velocity	derived from s_b	± 0.025 cm/s
F_t in N	traction force	*S2*	± 0.15 N ± 1 %
F_b in N	bow force	*S3*	± 0.11 N

In terms of dynamical response, sharp impulses were applied to the sensors and the individual response time measured after all procedural steps of conversion, analysis and normalization. More precisely, a traction force impulse of 10 N has been applied to sensor *S2* (half of its operational range but three times the range needed in instrumentation), a weight impulse of 10 N has been applied to *S3* (1/60 of its operational range but twice the range needed for instrumentation), and a displacement step of 3 cm has been applied to *S1* (only 1/20 of its operational and instrumental range due to impedimental mass load). The response time $T_{10/90}$ is measured at the 10 % and 90 % fractions of the total impulse or step total amplitude and is less than 10 ms in all cases, see Table 2.

Table 2: Parameter measurement dynamic response

physical property		sensor	impulse / step	$T_{10/90}$
s_b	bow position	*S1*	3 cm step	~6 ms
F_t	traction force	*S2*	10 N impulse	~0.8 ms
F_b	bow force	*S3*	10 N impulse	~8 ms

For sound recording a piezo of 1 gram weight is directly mounted to the bridge.

3.2 Operational range

The implemented construction facilitates bowing of all four classical instruments from violin to double bass. Bow velocity can be comfortably adjusted from zero to v_b = 30 cm/s. Bow forces can be adjusted from zero to 5 N and is typically limited by the bow stiffness. Adjustments allow to enforce stationary bow forces along s_b within a corridor of ± 0.01 N (can be monitored directly at *S3* even though the captured signal has the maximum error as outlined in Table 1) but also gradients of F_b. The bow-bridge-distance can be adjusted and measured in the submillimeter range. The bow in motion maintains a predefined track sufficiently well even though there is no external force to keep the targeted distance to the bridge. Note that the forces along the long *strings e and d* have only little potential of guiding any direction. Such stability of distance is not surprising and cellists know that shifting the bow towards a different β requires to resolutely change the bow-string angle.

3.3 Compact data representations

For meaningful and sparse representation of data, signals are averaged across non-overlapping windows of 12.5 ms. This is about the time span of one slip-stick period on the lower strings of a cello and of a few slip-stick periods on the higher strings. The recorded sound is analyzed in terms of pitch frequency using the YIN algorithm (Cheveigné and Kawahara, 2002) in order to classify between Helmholtz motion and non-Helmholtz regimes. A bow stroke finally generates data tuples of 200 to 1500 times four numbers, depending on bow velocity.

4. REGIME-TRANSITION EXAMPLE

Figure 7 represents an example of operation where the bow force is intentionally adjusted to gradually decline along the bow position s_b. The two sound samples are provoked by varying the weight force F_w which is not the measured traction force F_t in the trace below.

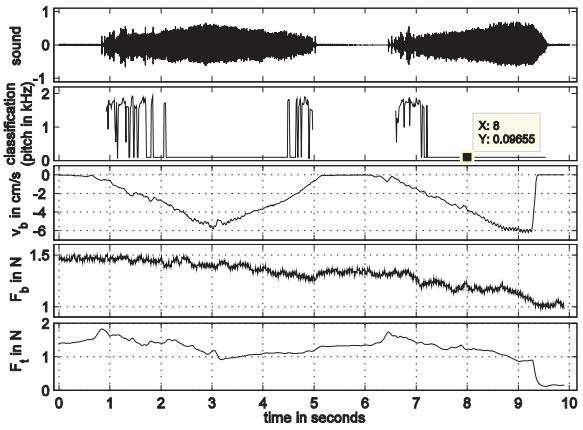

Figure 7: Traces of parameters for transitions between bifurcation and Helmholtz motion (resolution 12.5 ms), from the top: sound, classification (Helmholtz-motion at nominal pitch of open G string versus bifurcation at higher pitches), bow velocity (v_b<0 for upstroke), bow force, and traction force.

Figure 8 represents the populations of bow velocity v_b versus bow force F_b. Using the classification data for Helmholtz versus non-Helmholtz motion reveals the related parameter ranges necessary to establish either regime. Three features can be observed here. (i), there are gaps between the regimes,

suggesting, that there is no smooth transition but rather a jump from one regime to the other. This gap denotes the maximum bow force and can be extracted from the data. (ii), there are also visible gaps within a class, suggesting that there exist subclasses of stability with related preferred bowing parameters. Obviously, the slip-stick process co-moderates the resulting velocity for a given bow force. Note that these populations can be disclosed by the adaptive driving unit only. (iii), a hysteresis can be observed while plotting Figure 8 in timely sequence. This further endorses the observation of stability of regimes, or, in other words, the hesitation to transit to another regime.

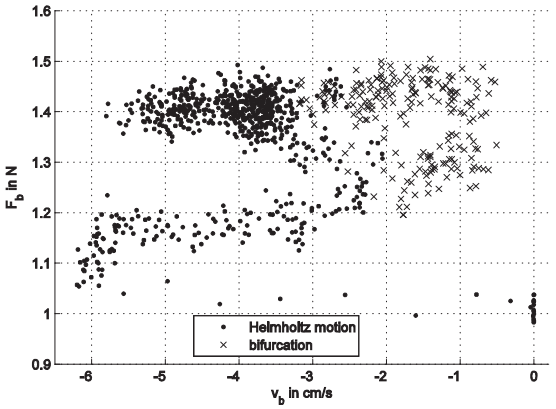

Figure 8: Bow force versus bow velocity populations for Helmholtz motion (dots) and for bifurcation-regimes (cross), same data as in Figure 7, populations reveal visible (i) gaps between regimes, (ii) gaps within regimes, (iii) hysteresis between transitions.

5. SUMMARY

A pendulum is presented that allows precise measurement of bow velocity and bow forces. Bow forces comply both traction force and bow force. Measurements can be taken during the bowing of all kinds of stringed instruments and all styles of bows. While restoring forces of the pendulum are compensated for, precise measurement of mentioned bow forces is facilitated at maximum errors of about 0.1 N. The dynamic response time is less than 10 ms for all parameters measured. An example of transitions between Helmholtz motion and bifurcation regimes demonstrates that stability issues can now be explored which was not possible with earlier constructions. This is due to the adaptive bow driving mechanism which emulates the musician's sensitivity with respect to the bow-string interaction and resistance. The pendulum is fully described to facilitate reconstruction by others, but researchers are also welcome to directly use the existing construction.

6. REFERENCES

Cheveigné, A., H. Kawahara: Yin, a fundamental frequency estimator for speech and music. Journal of Acoustical Society of America, 111 (2002) 1917–1930.

Cronhjort, A.: A computer-controlled bowing machine (MUMS). STL-QPSR 33 (1992) 61–66.

Galluzzo, P. M., J. Woodhouse: High-performance bowing machine tests of bowed-string transients. Acta Acustica united with Acustica 100 (2014) 139–153.

Lawgren, B.: On the motion of bowed violin strings. Acustica 44 (1980) 194–206.

Mizrahi, J.: Mechanical Impedance and Its Relations to Motor Control, Limb Dynamics, and Motion Biomechanics. J. Med. Biol. Eng. 35 (2015) 1–20.

Petzoldt, T.: Ringspaltgleichung für Viskosimeter (equations for annular gaps in viscometers, with derivation), published on the IMETER company webpage, URL http://www.imeter.de/adienstleistungen/dienstviskositaet/75-viskositaet-im-ringspalt.html, downloaded June 16, 2015.

Pickering, N. C.: A new light on bow action. Journal of the Violin Society of America 11 (1991) 83–92.

Schoonderwaldt, E., K. Guettler, A. Askenfelt: An empirical investigation of bow-force limits in the Schelleng diagram. Acta Acustica united with Acustica 94 (2008) 604–622.

Schumacher, R. T., S. Garoff: Bowing with a glass bow. Journal of the Catgut Acoustical Society 3 (1996) 9–17.

Woodhouse, J., R. T. Schumacher, S. Garoff: Reconstruction of bowing point friction force in a bowed string. Journal of Acoustical Society of America 108 (2000) 257–368.

7. APPENDIX

These are more details on sensor devices and related error components for the three physical properties measured.

For the Novotechnik TP1-800 , representing *S1*, non-linearity, hysteresis, resolution and repeatability amount to ± 0.5 mm. Signal conversion and post-sampling processing introduce an additional error of ± 0.1 mm. Calibration introduces an additional maximum uncertainty of ± 0.2 mm. Additionally, the elasticity of string *e* introduces an additional uncertainty of ± 1 mm for the given length and the range of forces applied. The total maximum error in measuring the bow position s_b is therefore ± 1.8 mm.

Note that the error for bow velocity v_b is smaller than for the position s_b since error components contributing to the absolute position error are not relevant after derivation. The limited resolution of *S3* and the signal conversion maximum error contribute most to the residual estimated uncertainty of ± 0.25 mm for the velocity v_b.

For the Burster 8520, representing *S2*, non-linearity, hysteresis and repeatability amount to ± 0.1 N. Signal conversion and post-sampling processing introduce an additional error of ± 0.05 N. Calibration introduces an additional uncertainty of ± 1% maximum. The total maximum error in measuring traction force F_t is therefore ± 0.15 N ± 1 %.

For the Kern-DE 60K1D, representing *S3*, non-linearity, hysteresis, resolution and repeatability amount to ± 0.05 N maximum. Signal conversion and post-sampling processing introduce an additional error of ± 0.04 N maximum. Calibration introduces an additional uncertainty of ± 0.02 N maximum. The total maximum error in measuring bow force F_b is therefore ± 0.11 N.

MICROPHONE ARRAY MEASUREMENTS OF THE GRAND PIANO

Niko Plath, Florian Pfeifle, Christian Koehn, Rolf Bader
Institute of Systematic Musicology, University of Hamburg, Germany
niko.plath@uni-hamburg.de
florian.pfeifle@uni-hamburg.de

ABSTRACT

This treatise is concerned with a measurement method and current results of an on-going project performed at the Institute for Systematic Musicology in Hamburg, Germany. A series of measurements are taken on four concert grand pianos in eight different stages of production, starting with the glue-laminated soundboard planks and ending with the completely assembled piano in concert tuned state. The majority of the sound energy radiated by a grand piano originates from the soundboard, which amplifies the vibrations of the strings via the bridge. Due to the large size of the soundboard as well as its irregular shape, measuring deflection shapes is a nontrivial task. Common measurement methods such as piezoelectric accelerometers can affect the acoustic vibrations of the soundboard due to the added mass. To this end, a noninvasive microphone array method is utilized for the present work. The array consists of 105 microphones successively placed in 18 positions parallel to the soundboard, resulting in a total number of 1890 measurements of which 1289 microphones cover the actual surface. The Soundboard is excited using an acoustic vibrator at 14 positions associated with string termination points on the bass and main bridge. The utilised SineSweep technique is capable of separating the linear part of an impulse response of a weakly non-linear system from several non-linear parts, representing the harmonic distortion of various orders. The measured sound pressure is back-propagated to the radiating soundboard surface using a minimum energy method. The resulting deflection shapes due to the forced oscillation can be visualized up to 4 kHz. Impedance curves are calculated for the 14 input locations on the bridge. The empirical findings will contribute to the formulation of a real-time physical model to help piano makers estimate the impact of design changes on the generated sound.

INVESTIGATING CHIME BAR VIBRATIONS USING HIGH-SPEED STEREOPHOTOGRAMMETRY

Timo Grothe[1], *Rainer Barth*[2]

[1]Erich-Thienhaus-Institut, Hochschule für Musik Detmold, Detmold, Germany
[2] Institut für Leichtbau und Kunststofftechnik, Technische Universität Dresden, Dresden, Germany
grothe@hfm-detmold.de

ABSTRACT

Stereophotogrammetry is an optical distance measurement method. Using digital image correlation, the 3D coordinates of control points on a surface are calculated from a stereocamera recording. The use of highspeed cameras allows to obtain time resolved displacement data suitable for structural vibration analysis. The technique appears to be attractive to study musical instruments under realistic performance conditions: The measurement is non-invasive and both rigid-body motion as well as acoustically relevant vibrations are obtained from one video sequence. However, the spatial resolution is far less compared to interferometric measurement methods, and depends strongly on the specific measurement setup, namely, the size of the measurement window, the distance from the measurement object, and the lighting situation. This contribution presents a feasibility study on a Double Bass Chime Bar in A ($f_0 = 110$ Hz) and discusses potential fields of use of the method in musical acoustics research.

1. INTRODUCTION

Experimental vibrational analysis of musical instruments is mostly carried out using a defined excitation, i.e. a hammer or a shaker. After a series of sequential single point measurements with an accelerometer or laservibrometer, modal shapes, frequencies and damping can be estimated. Most mechanical musical instruments have been studied already in this fashion [1].
However, the vibration measurement on musical instruments *under playing conditions* is challenging: On the one hand, the realistic musical excitation by a musician is very difficult to measure without disturbance. On the other hand, the instrument usually is moved during performance and mounted sensors would not only disturb the structure, but also the musician. One walkaround is to use artificial excitation mechanisms, such as artificial hammering, plucking [2], bowing [3] machines, that assure musician-like but well defined and reproducible excitation. A disadvantage of this approach is, that transient behaviour along with artistic articulation are not measurable. To overcome these limitations and measure the vibrations of musical instruments during musical performance, contact-free, time- and space resolved simultaneous measurements of many points on the musical instrument structure are necessary. These requirements are in principal met with Highspeed Stereophotogrammetry (HSSP).
With this method, the 3-D coordinates of arbitrary control points on the body surface can be calculated from pixel data of two digital cameras, which face the object under certain angles. The spatial resolution and accuracy achievable with this image correlation based method is scarce compared to interferometrical methods. The technical specifications of the high-speed cameras limit the measurement: Space- and time resolution, as well as measurement time depend on each other and are constrained by the camera sensor size, the distance between the two cameras, and between cameras and measurement object, the size of the measurement plane, the speed and size of the buffer storage and the lighting conditions. Thus, the feasability of the method has to be identified with respect to the specific measurement task. HSSP has recently been used successfully for applications in vibration analysis of structures with strong rigid body movement, such as rotor blades [4, 5, 6].
To the knowlegde of the authors, very few studies have been carried out that used HSSP to monitor acoustically relevant vibrations (e.g. [7], [8]).

2. MATERIAL AND METHODS

To study the feasability of HSSP in vibrational analysis of musical instruments, the chime bar is well suited due to its plane rectangular surface. Furthermore, its vibrational characteristics have been studied in great detail (e.g. [9]).

2.1. Measurement setup and data acquisition

As a preparation prior to the optical measurement small circular stickers of a reto-reflecting material are tacked in an irregular pattern onto the surface to be measured (Figure 1 a).
The HSSP measurement system PONTOS (Fa. GOM, Braunschweig, Germany) was used in the measurement. Two high-speed cameras are mounted on a rail, such that their angle of cut is 25 degrees on the measurement surface (Figure 1 b). Due to buffer limitations the measurement time depends on the frame rate. The measurement time can be prolonged by reading fractions of the full sensor per shot.
For this feasability study, the framerate was set at 2 kHz which is the maximum framerate of the system. The image size was set to 256x1024 pixel, which is a quarter of the full sensor size. With these settings, 2.5 s could be recorded. For times of exposure smaller than 0.5 milliseconds, a powerful light source has to be used. The PONTOS system comprises six LED flashes around each camera lense, triggered with the camera shutter.
The surface of the Chime Bar has a length of 500 mm and a width of 50 mm. The distance between the cameras and the bar surface was 0.75 m. Once camera and measurement object is fixed, the calibration procedure is done by taking a sequence of pictures from a calibration plate under different tilt angles. The warping of the calibration pattern in the sensor images is then evaluated to span a measurement volume. Inside this volume 3 D cartesian coordinates can be assigned to any measurement point on the surface. Subpixel accuracy is achieved by an image postprocessing algorithm, that detects the centers of the ellipses that the circular reflecting stickers produce on the two camera sensors. The raw data from the HSSP measurement is a point cloud in x, y and z for each frame of the video recording.

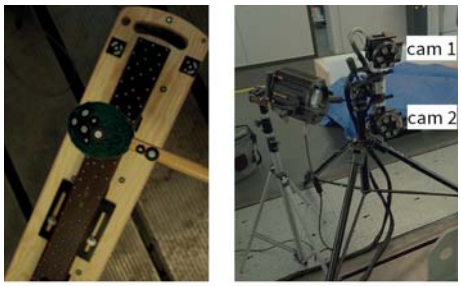

Figure 1: Setup for HSSP measurements on a Chime Bar
a) Retoreflecting stickers mark the measurement points on mallet and chimebar surface.
b) Stereophotogrammetry system PONTOS (Fa. GOM) Measurements were carried out at ILK (Technische Unversität Dresden)

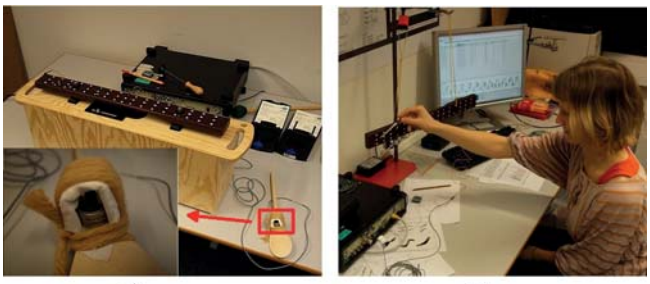

Figure 2: Comparison measurements with an accelerometer a) excitation with a modified mallet, b) roving hammer modal testing experiment.

2.2. Postprocessing of the raw data

The Chime Bar is mounted on loosely to a resonator box by two pins perpendicular to its surface. The pins are padded with a soft rubber and felt such that the rigid body motion of the bar can have strong components of what would be called ”heaving” and ”rolling” motions in a ship.
To analyze the acoustically relevant bending motions of the bar, the rigid body motion was determined frame by frame principal coordinate analysis. Projecting the raw data on the time dependent principal coordinate system yielded new coordinates x', y' und z' of the measurement points. These were interpolated on a rectangular grid $(x'_{i,j}|y'_{i,j})$. The result of the post-processing is for discrete, equidistant measurement points i, j, the deflection of the Chime Bar $z'_{i,j}(t)$ perpendicular to its surface. The post-processing of the HSSP raw data was done using MATLAB.
The (freely choosable) resolution of the measurement grid was $\Delta x' = 36$ mm, $i = 1..12$; und $\Delta y' = 10$ mm, $j = 1..4$.

2.3. Comparison Measurements

For comparison purposes measurements with an accelerometer have been carried out on the same Chime Bar at various excitation levels. After integrating the measurement results twice they can be compared with the processed optical displacement data. Two experiments have been carried out: First, in a typical musical situation as in the HSSP measurement. A wooden stick with a force sensor wrapped in tissue and wool served as a mallet to determine typical excitation forces at various musical dynamic levels (Figure 2 a). Second, a classical modal analysis experiment of the bar only. The Chime Bar was unmounted from the resonator box and excited at several points by an impact hammer and the vibration was recorded by an accelerometer in a fixed position at the edge (Figure 2 b). When comparing modal analysis results, this second measurement will be referred to as EMA.

2.4. Modal Analysis

Fron the postprocessed optical displacement data $z'_{i,j}(t)$ of the Chime Bar a modal analysis was carried out using Operational Modal Analysis (OMA). This is a stochastic system identification method which bases on a singular value decomposition of a matrix of concatenated spectral density vectors representing system responses measured simultaneously at several measurement points on the structure. Modal shapes, frequencies and damping values can be determined without explicit knowledge of the excitation function [10]. This is useful for the present HSSP experiment, where the Chime Bar is struck with a normal mallet and the excitation force is unknown. For the identification of modes, the curve-fit-frequency-domain algorithm (CFDD) implemented in the commercial software PULSE Labshop Type 7760, V 18.1 (Brüel&Kjær, Nærum, Denmark).
The combination of applying this modal analysis method on high-speed stereophotogrammetry data will be called HSSP-OMA in the following.

3. RESULTS

The advantage of the HSSP-method is that the displacements at various points are measured simultaneously. When looking at single point measurements, however, the limited dynamic range compared to contact-free interferometrical methods is obvious. Figure 3 shows displacement levels and decay curves for two different excitation locations of the Chime Bar, the sensor was mounted near an edge of the bar. The data are shown in Figure 3, where the suppression of the $4^t h$ partial when striking the bar in the middle (L/2) and the dampening effect of the acoustical resonator on the bar vibrations are clearly visible
The displacement magnitudes in the Chime Bar range from millimeters at the fundamental frequency to less then a micrometer above 1 kHz when playing *forte*, and down to a few nanometers when playing *pianissimo* (Figure 4). That is well below the noise floor of the HSSP-measurement. For the setup described above, the noisefloor in z' was 6.8 ± 1.2 micrometer RMS (mean and standard deviation, averaged over the 48 grid points).
For comparison, typical displacements in modal hammer measurement from the EMA experiment are shown in Figure 4, where the Chime Bar was disconnected from the resonator.
The OMA takes advantage of the fact, that all displacements are measured at the same time. Despite the limited signal to noise ratio, this feasability study on HSSP-OMA shows an excellent agreement in the modal frequencies as compared to the classical EMA method. However, the limitations of the sampling rate do not appear to be important given the low spatial resolution in this measurement setup.

Table 1 shows a comparison of EMA and HSSP-OMA modal analysis results. The indices (n,m) in the first column describe the modal shape in terms of the number of nodal lines perpendicular (n) and parallel (m) to the wood fiber direction of the bar. The acoustically relevant partials of the Chime Bar in the range $f < f_s/2$ are the fundamental $f_0 = 109.3$ Hz and the fourth partial at $f_4 = 438.2$ Hz $\approx 4\, f_0$ (see Table 1). At these frequencies, the Chime Bar performs bending motions with two

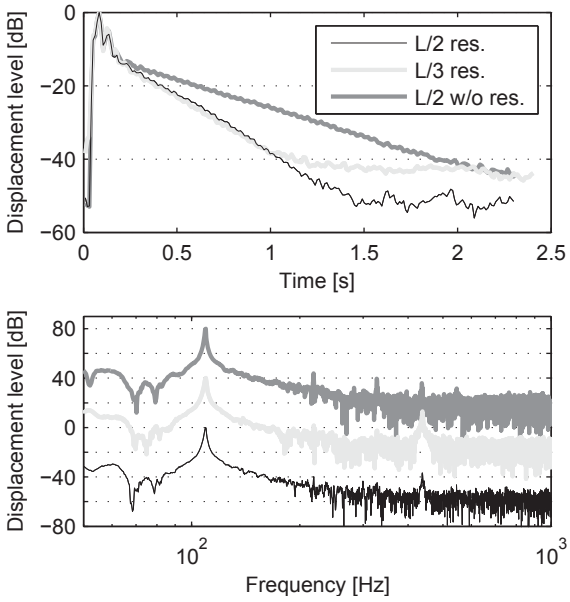

Figure 3: Displacement levels for three strikes in *mezzoforte* on a Chime Bar as measured with HSSP. The striking position were approx. L/2 and L/3 measured from the edge, the measurement point is near the edge of the bar. For the third strike (L/2 w/o res.), the resonator hole was covered with a sheet of paper. Curves are shifted vertically for better readability.

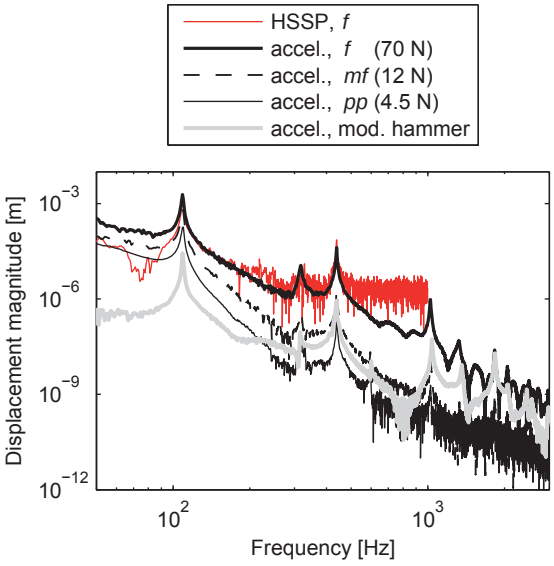

Figure 4: Displacement magnitudes of the Chime Bar directly measured with HSSP and integrated from accelerometer measurements. The bar is struck with a normal mallet (HSSP), a modified mallet equipped with force sensor, and a modal hammer. Values in brackets are the peak forces measured with modified mallet.

and three nodal lines, respectively, perpendicular to the longitudinal axis of the bar. With a low signal-to-noise ratio of about 16 dB at the fourth partial, the (3,0) modal shape still is clearly detected from HSSP-OMA (Figure 5). The occurence of the (1,1) torsional mode depends on the offset of the striking position with respect to the longitudinal center line. The fact that no modal shape could be identified with the OMA algorithm is possibly due to a centered strike. The signal-to-noise ratio of the respective (1,1) peak around 320 Hz is only slightly lower than that of the (3,0) peak around 440 Hz (see Figure 5). The mould on the bottom side of the bar is cutted by the instrument makers to tune these two modes to a harmonic frequency ratio [11]. Further, also the tenth partial can be tuned to an integer ratio with the fundamental. In the present study we find $f_{10} = 1038$ Hz $\approx 9.5\, f_0$ only in the EMA measurement. It is possible, that the mass added to the bar by the accelerometer in this measurement has lowered this modal frequency.

In contrast to the classical roving hammer method (EMA) are the results of the OMA not based on a lab experiment, but stem from a fully contact-free monitoring of the bar vibrations under realistic playing conditions. While the EMA lab test will reveal all possible modal shapes, the HSSP-OMA method only detects the relevant vibrational modes that are excited when playing the instrument. From the results it can be seen, that the (1,1) torsional mode and the (2,0) lateral mode (column 3 and 5 in Table 1) not only are inefficient radiators [11], but also are excited weakly in a normal musical excitation. Aside from the modal shapes, the OMA also reveals relative amplitudes of the modes and their time decay (not shown here).

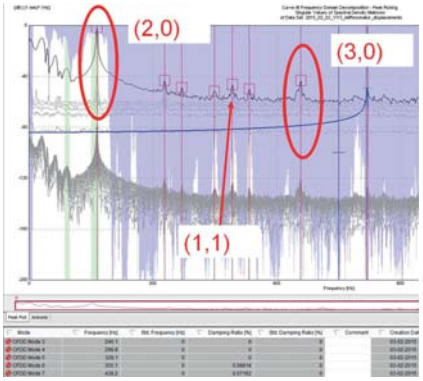

Figure 5: Screenshot of the Modal Analysis (OMA) on high-speed stereophotogrammetry data of a struck Chime Bar using the Brüel&Kjær s software PULSE Labshop.

4. OUTLOOK

With the Chime Bar an example for a simple musical instrument structure has been chosen intentionally for this feasability study. Not only the geometry can be measured easily, also the impulsive manner in which it is played approaches a broadband excitation, an assumption the operational modal analysis is based on.

Potential uses in musical acoustics depend critically upon the size of the structure and the displacement magnitudes at the vibrations of interest. The noise-floor of HSSP measurement is determined by the size of the measuring field and the minimum possible camera distance. With appropriate lenses, spatial resolutions in the nanometer range are possible [13]. To detect eigenfrequencies in musical instrument structures that are driven quasi-periodically, the harmonic components of the excitation must be treated separately. Implementations for this approach are reported in the literature [12]. HSSP is to the authors knowlegde the only method that allows for contact-free simultanenous measurements of fully transient structural vibrations

	EMA Impact hammer + Accelerometer	OMA Mallet + Photogrammetry	Literature [9]
(2,0)			
f_0 [Hz]	109,2	109,3	
f_0 / f_{nom}[Cent]	-13	-11	
ζ [%]	0,21	0,50	
(1,1)		*not found*	
f [Hz]	315,2		
f / f_0 [-]	2,89		2,48
ζ [%]	0,45		
(3,0)			
f [Hz]	438,9	438,2	
f / f_0 [-]	4,02	4,01	4,03
ζ [%]	0,24	0,07	
(2,0)*		*not found*	
f [Hz]	599,0		
f / f_0 [-]	5,49		7,01
ζ [%]	0,26		
(4,0)		$f > f_{Nyquist}$	
f [Hz]	1038		
f / f_0 [-]	9,50		10,70
ζ [%]	0,28		
(2,1)		$f > f_{Nyquist}$	
f [Hz]	1361		
f / f_0 [-]	12,46		11,09
ζ [%]	0,45		

Table 1: Modal Analysis of a Chime Bar. Comparison of results of the photogrammetric measurements (column 3) with the roving hammer measurements (column 2) and literature data (column 4). EMA: experimental modal analyis, OMA: operational modal analysis, * lateral mode

at musical instruments under playing conditions. The combination HSSP-OMA is especially interesting because it allows for the characterisation of the instrument while interacting with the player in a mostly disturbance-free manner during performance, rather than studying only the instrument itself under lab conditions. This can be a basis to study performance differences between musicians playing the same instrument, and may be useful to validate complex physical models that are used in digital sound synthesis with great success [14]. If the drawback of the relatively low spatial resolution in the range of micrometers can be overcome, HSSP-OMA can be a very useful measurement technique to investigate in detail the relationships between the construction of musical instruments, their excitation and finally their produced sounds.

5. ACKNOWLEDGEMENT

The authors wish to thank Polina Zakharchuk for the carrying out comparison measurements, and Jason Kunio as well as Richard Schlombs of Brüel und Kjær for extensive support with PULSE Reflex and the friendly resourcing of test licenses. Jörn Jaschinski, and Malte Kob are acknowledged for support with the HSSP-measurements, and helpful discussions on modal analysis.

6. REFERENCES

[1] Neville Fletcher and Thomas Rossing, *The Physics of Musical Instruments*, Springer, 2005.

[2] Thorsten Smit, Friedrich Türckheim, and Robert Mores, "A highly accurate plucking mechanism for acoustical measurements of stringed instruments," *The Journal of the Acoustical Society of America*, vol. 127, no. 5, pp. EL222–EL226, 2010.

[3] Andreas Cronhjort, "A computer-controlled bowing machine (mums)," *STL-QPSR*, vol. 33, pp. 61–66, 1992.

[4] Troy Lundstrom, Javad Baqersad, Christopher Niezrecki, and Peter Avitabile, "Using high-speed stereophotogrammetry techniques to extract shape information from wind turbine/rotor operating data," in *Topics in Modal Analysis II, Volume 6*, R. Allemang, J. De Clerck, C. Niezrecki, and J. R. Blough, Eds., Conference Proceedings of the Society for Experimental Mechanics Series, pp. 269–275. Springer New York, Jan. 2012.

[5] Sergio E Obando, Javad Baqersad, and Peter Avitabile, "Improved modal characterization using hybrid data," *SOUND AND VIBRATION*, vol. 48, no. 6, pp. 8–12, 2014.

[6] NS Ha, HM Vang, and NS Goo, "Modal analysis using digital image correlation technique: An application to artificial wing mimicking beetle's hind wing," *Experimental Mechanics*, pp. 1–10, 2015.

[7] Sten Urban, "Resonanzverhalten von Saiten einer Laute unter Berücksichtigung der Instrumentenmoden," Tech. Rep., Technische Universität Dresden, 2008.

[8] Timo Grothe, Rainer Barth, Malte Kob, and Jörn Jaschinski, "Hochgeschwindigkeits-stereophotogrammetrie eines klingenden stabes," in *Fortschritte der Akustik, 41. Jahrestagung für Akustik (DAGA2015), Nürnberg*, 2015.

[9] Ingolf Bork, Antoine Chaigne, Louis-Cyrille Trebuchet, Markus Kosfelder, and David Pillot, "Comparison between modal analysis and finite element modelling of a marimba bar," *Acta Acustica united with Acustica*, vol. 85, no. 2, pp. 258–266, 1999.

[10] Bart Peeters and Guido De Roeck, "Stochastic system identification for operational modal analysis: a review," *Journal of Dynamic Systems, Measurement, and Control*, vol. 123, no. 4, pp. 659–667, 2001.

[11] Ingolf Bork, "Practical tuning of xylophone bars and resonators," *Applied Acoustics*, vol. 46, no. 1, pp. 103 – 127, 1995, Musical Instrument Acoustics.

[12] Prasenjit Mohanty and Daniel J Rixen, "Operational modal analysis in the presence of harmonic excitation," *Journal of sound and vibration*, vol. 270, no. 1, pp. 93–109, 2004.

[13] Wei Huang, Chengfu Ma, and Yuhang Chen, "Displacement measurement with nanoscale resolution using a coded micro-mark and digital image correlation," *Optical Engineering*, vol. 53, no. 12, pp. 124103–124103, 2014.

[14] S. Bilbao, A. Torin, and V. Chatziioannou, "Numerical modeling of collisions in musical instruments," *Acta Acustica united with Acustica*, vol. 101, no. 1, pp. 155–173, 2015-01-01T00:00:00.

STEADY STATE SOUND PRODUCTION AND INVESTIGATIONS ON CLASSIC GUITARS

Hellmut Schmücker
H. E. S., Germany
hellmut.schmuecker@mac.com

ABSTRACT

The discussion about the quality of a guitar goes back to the early days of this instrument. Because its growing popularity in the last decades numerous experiments and theoretical investigations have been published in order to better understand the instrument and to improve the quality of the tone production. The possibilities and tools to investigate the functionality and properties of a guitar have developed dramatically in recent years due to the application of fast and cheap computers. Mathematical procedures and modelling according to finite element methods allow to simulating any instrument. Here, a more practical approach is presented. The guitar is slightly modified to produce the sound in the very same way the string tension acts on the bridge. The guitar under test is agitated with steady state signals or, for range measurements, as sweep-sine or MLS signals. With these defined state signals, analysis is by far more easy to accomplish. Shown are comparative frequency response between famous old guitars and new models, influence of string tension and weight distribution, temperature and humidity. All results are verified by conventional analysis methods.

AN AUTOMATIC ACQUISITION SYSTEM FOR MEASURING THE DIRECTIONAL CHARACTERISTIC OF MUSICAL INSTRUMENTS

Martin Lahmer, Alexander Mayer

Institute of Music Acoustics
University of Music and Performing Arts Vienna, Austria
martin_lahmer@gmx.at, mayer@mdw.ac.at

ABSTRACT

Obtaining data on the directional characteristics of musical instruments can be both time-consuming and demanding in terms of equipment. This paper explains the construction of an affordable automatic turntable system, for measuring the radiated sound as a function of angle and frequency in one plane. An initial test was carried out on two brass instruments excited by an artificial mouth and two stringed instruments driven by a shaker. The second part of this paper deals with the further processing of the obtained values. As the sound pattern data can be stored in an online database (MySQL), the directional characteristics are accessible via a web-interface. The user is able to display the measurements as single plot (e.g. for each angle), as polar-plot or colormap. This interface represents the first part of a planned Musical Instrument Measurement Database (MIMD) for collecting diverse measurement data of different kind of musical instruments.

1. INTRODUCTION

For the sound of an instrument or even of orchestras sound radiation and the effect of the room is a significant criterion and like other sound sources musical instruments have a more or less pronounced directional dependence of sound radiation. It varies significantly depending on the frequency spectrum. The simplest case is a spheric source radiation when sound is expanded in all directions equally. Usually, this case will occur if the sound source is a "breathing sphere" or it is small in comparison to the radiated wavelength. This occurs at low frequencies and the constant radiation remains virtually unaffected. In the case of higher frequencies the directional characteristic is affected by numerous influences like the position of the player, the direction of the musical instrument, the acoustical consistence of the instrument, etcetera. [1][2].

In Figure 1 the omnidirectional sound radiation for individual frequency regions of some brass wind instruments is given. This measurements were taken by Jürgen Meyer [1]. The spheric radiation depends much on the form of structure and the dimension of the individual bells so long as the bell is the transducer. For instance, the bell of a Tuba is relatively wide in comparison to that of a Trumpet. So a Tuba spreads sound omni directionally at lower frequencies (about 30 Hz up to 90 Hz) compared to a Trumpet (about 180 Hz up to 500 Hz).

In 1970, Meyer and Wogram measured and documented the directional characteristic of Trumpets, Trombones, and Tubas [3]. It turned out that it is necessary to define those angular regions for which the sound level does not sink by more than 3 dB or more than 10 dB respectively below the directed maxima. The 3 dB limit describes the *half width*. This is the difference where the sound intensity is just half the value related to the maximum. For simplification sound pressure above the 3 dB limit was taken as quasi equal. Otherwise a level difference of 10 dB is perceived as approximately one-half the loudness. Figure 2 illustrates the directional characteristic of a Tuba within the 3 dB limit. As it can be seen, the effective radiation angle will narrow if the frequency raises.

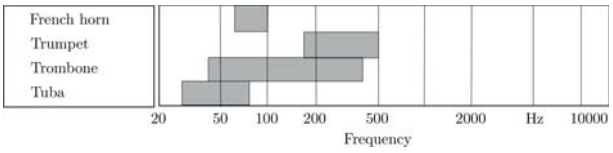

Figure 1: Spheric sound radiation of brass instruments by Meyer [1].

Finally, a quantity called the statistical directivity factor is important for room acoustical considerations. It represents a relationship between sound pressures actually present, to those which would be caused by a sound source of equal total power with omnidirectional characteristics at the same distance. The statistical directivity factor can be given in dependence on direction: Values larger than 1 indicate directions with, on the average, stronger radiation; values less than 1 indicate directions of below average radiation. For example, an ideal dipole reaches a value of approximately 1.7 in the direction of strongest radiation. On the boundary of the 3 dB region, the statistical directivity factor drops to 0.7; on the boundary of the 10 dB region, to 0.3 of the maximum value. For sound level considerations it is advantageous to convert the statistical directivity factor to a dB value. The quantity is designated as directivity index. It specifies how much the sound level is higher in the direction considered than it would be for an omni-directionally radiating sound source of equal power [1].

Obtaining the data on the directional characteristics of musical instruments can be done in various ways. The basic method will use a single microphone, the test item has to be turned in defined angles, for each being excited at the frequency bandwidth of interest. If multichannel recording is possible, a multitude of microphones can be placed on a ring or better on a sphere around the test item. For measurements excluding the influence of the surrounding room, both set-ups should be placed inside an anechoic chamber. This paper describes the implementation of a single microphone automated measuring system. After setting up the system the device-under-test will be excited and rotated without human supervision. As carrier a massive turntable was equipped with step-motors. Lastly, the storage and the processing of measured data and the control of the turntable and its step-motors have to be combined externally outside the chamber by a computing system. Here a Personal Computer (*PC*) with *LabVIEW* from *National Instruments* was used. With it, the PC is capable of communicating with the

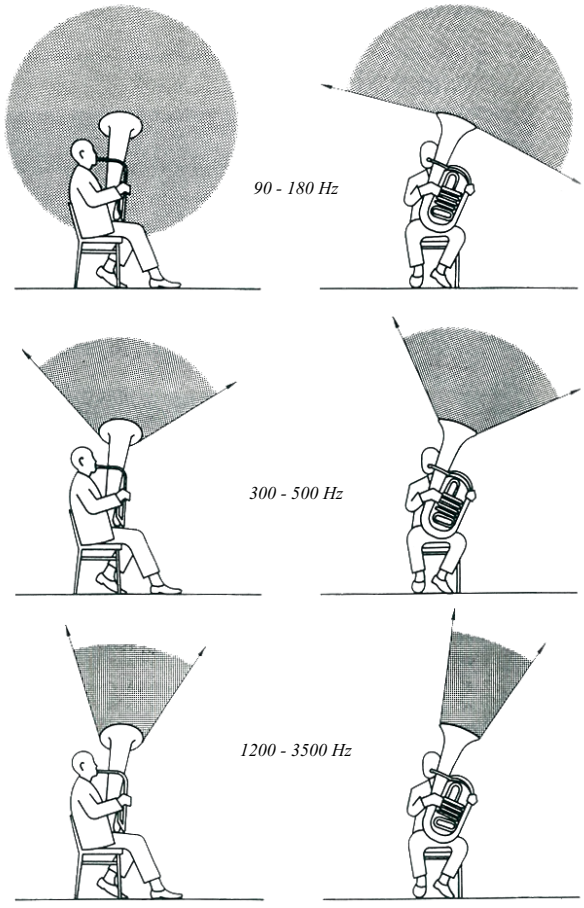

Figure 2: Main radiation area (0 to -3 dB) of a Tuba by Meyer [3].

Step-Motor-Control (*SMC*), executing the acoustical measurements and processing the acquired information.

2. TURNTABLE-SYSTEM WITH STEP-MOTORS

For this project an existing turntable was chosen for modification. It consists of a huge bearing ring of a semi-trailer coupling with a diameter of about 65 cm which was attached on a heavy metal-frame. The actual table board can be placed on the bearing ring by four screws, however, other installations can be mounted on the bearing ring too. For instance, a stable construction with a Tuba to be measured is shown in Figure 3. This build-up was made of a flexible assembly kit with mounting rails. It was the final mechanical set-up for the acoustical acquirement of Tubas.

2.1. Mechanical Design

For automatic motion it is necessary to install at least one motor onto the turntable construction. To ensure conformity between required effort and engine performance the tensile force was measured at the outer edge of the bearing ring with a spring balance. It turned out that the mean force was at about 200 N, however, the top force was measured at about 400 N at some points of the wheel. This can be explained by the fact that the semi-trailers coupling ring is not ideal and possesses higher friction losses at several points. Multiplied with the radius of the ring (33 cm) the resulting maximum load torque amounts 132 N m.

Figure 3: Turntable system with a stable construction for fixing a Tuba.

Therefore, the selected motor must meet this criterion, so that the platform can rotate smoothly. A few stepper motors with a nominal holding torque of 44 N cm were available at the institute. It should be mentioned that the holding torque nearly corresponds to the driving torque at lower stepper frequencies. Since comparing these torques results in a high discrepancy, a convenient power transmission had to be found. For this use a nearly 1:300 gear reduction was calculated by dividing load torque by the motor torque. A geared belt drive was chosen to achieve the required power transmission. Figure 4 shows a hypothetical example of a gear belt drive which connects the bearing ring on the turntable-construction with a toothed belt wheel placed on the axis of the stepper. With 12 teeth and a belt pitch of 5 mm the belt wheel has a perimeter of 60 mm. This leads to a radius of 9.549 mm. It was possible to attach a timing band with 411 teeth and a length of 2055 mm onto the edge of the semi-trailers bearing ring. So a provisional "belt pulley" was created with a radius of about 327.063 mm since the complete diameter of the turning ring is 654 mm.

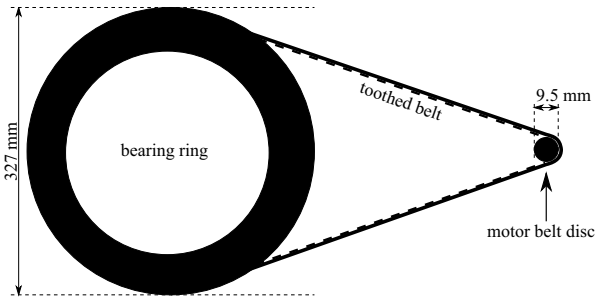

Figure 4: Example of a gear belt drive with a reduction of about 1:35.

As a result of this, the Gear Ratio (GR) which is also known as mechanical advantage, can be calculated where the input belt wheel has radius r_i and the output belt wheel has radius r_o, or rather the number of output teeth (N_o) is divided by number of input cogs (N_i):

$$GR = \frac{\omega_i}{\omega_o} = \frac{r_o}{r_i} \approx \frac{N_o}{N_i} = \frac{411}{12} = 34.25. \qquad (1)$$

As it can be seen in Equation (1) the resulting mechanical advantage ($GR = 1 : 34.25$) is too small to drive the turntable's bearing. Furthermore, the gear will not be able to stabilize the

system if the motor is turned off. For that reason, another gearing mechanism had to be combined with the pre-designed system. In this case, a worm gear for further reduction was selected. The self-locking feature and the property of achieving a high gear transmission ratio are few advantages of worm gears. For this use, a worm with a module of 1.0 was purchased. A module of 1.0 signifies dimension of a cog. The more force is applied on the cogs the higher should be their module. Since the worm is a special form of a helical gear the angle of the helical toothing is defined by the winds around the wheel axle. The cog/tooth is referred to in this case as a gear or a start. One start indicates that one rotation of the worm screw will rotate the worm wheel by one cog. A higher gear/start stands for a faster turn and vice versa. To complete the worm gear an adapted worm wheel had to be combined. Here, one with 20 teeth and a hub diameter of 23 mm was used. Comparing the amount of teeth of the worm wheel (N_{wheel}) with the starts of the worm (N_{worm}) will lead to the gear transmission ratio:

$$GR = \frac{N_{wheel}}{N_{worm}} = \frac{20}{2} = 10. \quad (2)$$

Equation (2) depicts that the mechanical advantage of the planned worm gear accomplishes a ratio of 1:10. So the worm gear and the belt drive were united and finally, the collective gear ratio reached a reduction of 1:350. Of course, this was only an ideal result because friction losses of the advanced gearing mechanism derogated the transmission.

The principal composition of the gear unit is charted in Figure 5. This graph shows how the torque is transmitted from the step motor to the terminal turntable ring in ground plan on the left side. First, the force is transported over the motor shaft to the worm. After this, it is converted 1:10 to the connected worm wheel thereafter, over an axis the power is finally transferred to the turntable's gearing ring by the driving wheel. This last transmission had a ratio of 1:35. Thereby the direct transmission ratio of 1:350 can be calculated. For completeness the sheer plan of the gear mechanism is shown on the right side of Figure 5. It also shows the transmission of power from the step motor with its worm gear, via worm wheel and the connected axis, to the closing driving wheel connected with the bearing ring.

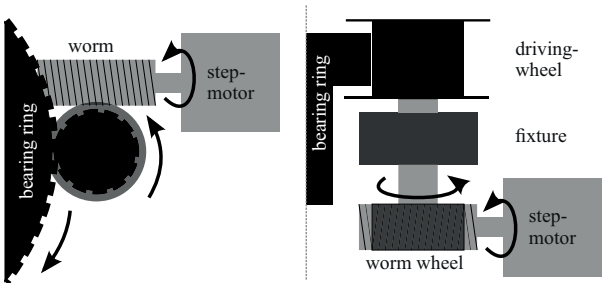

Figure 5: Principle of the designed gearing mechanism. Left: ground plan, right: sheer plan.

As mentioned above, the bearing ring of the semi-trailer's coupling ring is not ideal and so the outer edge of it is not absolute circular. To compensate these unevenness of the ring the motor was not fixed stable onto the mounted driving belt instead, it was pulled against the edge by a spring. The needed load of the spring gained the mechanical losses of the system. So it was decided that an additional motor should reinforce the existing engine. The total torque was doubled and the stepping losses were compensated by the mutual engagement of both engines.

The translated torque of both engines ($2 * 0.44\ Nm = 0.88\ Nm$) on the driving belt of the ring is now $308\ Nm$ which conforms the required expenditure of energy (about $132\ Nm$) more than enough. It has to be taken into account that the angular velocity of the turntable system is slowed by the reduction of a factor of 350 (cf. Formula of gear ratio with ω_i as motor velocity and ω_o as output velocity in Equation (1)). That leads to increasing the rotational speed of both motors simultaneously to balance the velocity decrease. As mentioned above, increasing the stepper frequency leads to lowering the step motor torque. In addition, unbalanced load could destabilise the system and induce disparate force actions on the bearing. That would require a higher torque of the gear and accordingly of the step motors. After all, it is of use to have an overpowered system which can deal with possible force problems.

2.2. Step Motor Control Interface

The Step Motor Control (*SMC*) - Unit is responsible for the automatic process of regulating the step motor drive. The unit has following tasks to do:

- Controlling the two stepper motors by stimulating convenient signals.
- Communicating with the supervising processor unit over a serial interface.
- Monitoring, whether step losses and accordingly degree losses would occur.
- Providing a manual control of the turntable with buttons and a seven-segment display.
- Managing the power for all integrated components.

As micro-controller an *Arduino Mini* - Board(rev5) was applied for controlling all tasks the SMC have to do. It is a small micro-controller board assembled with an *ATmega328*, intended for use on breadboards. Since the whole acquisition concept is a research project, in addition, that such board is relatively cost-efficient, the Arduino Mini seems to be the most adequate solution for this cause. For the SMC two *A4988 Stepper Motor Driver Carrier* from *Pololu Robotics and Electronics* were selected. The driver board features adjustable current limiting, over-current and over-temperature protection, and five different micro-step resolutions (down to 1/16-step). Since a high gear reduction is applied, there is no use of micro-stepping and only the full-step mode should be executed. It operates from 8 35 V and can deliver up to approximately 1 Ampere per phase without a heat sink or forced air flow, or 2 Ampere per coil with sufficient additional cooling. The SMC applies the Electronic Industries Alliance (*EIA*) standard RS-232 as serial interface. As main function the serial communication has to exchange several instructions from and to the supervising computer.

2.3. Exciting Brass Instruments

For oscillating the air column in the tube of brass wind instruments a convenient stimulation system is required. Therefore, a loudspeaker had to be adapted for this use. Since also Tubas with an immense volume of air should be measured, a low frequency speaker with a rated output power of 50 Watt from *RS-Components* was chosen. It has an impedance of 8 Ohm and a diameter of 5.25 Inch. This large-dimensioned speaker was covered in a box made of plywood. A circle of the size of the membrane was cut out of the front plate besides a holed plastic

cone was placed over the hole in order to focus the sound energy. The mouthpiece of the brass instrument could be mounted with clips, and between both parts a rubber ring was placed for tightening. Additionally, a probe microphone which serves as reference, was integrated in the plastic cone as near as possible to the mouthpiece plane. It is a 1/8 Inch pressure microphone (type: 40DP) from *G.R.A.S.* which has a linear frequency range ($\pm$1 dB) from 10 Hz up to 30 kHz. Figure 6 shows the completed High Air Pressure Artificial Mouth (HAPAM) box in blue.

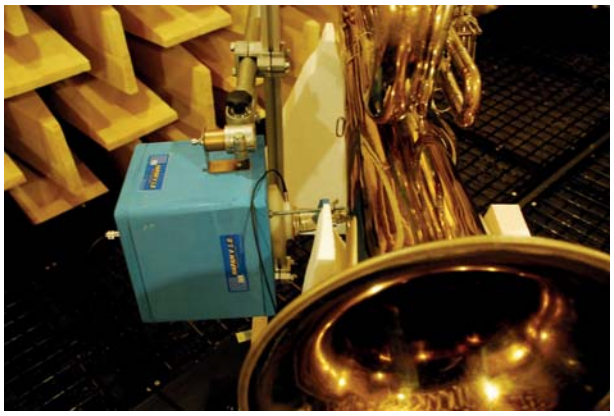

Figure 6: HAPAM mounted on a Tuba.

2.4. Exciting Stringed Instruments

For exciting stringed instruments a *Brüel & Kjær Measurement Exciter Type 4810* in conjunction with an impedance head (*PCB 288D01*) was chosen. The strings are damped by soft foam, the push rod was placed on the bridge of the musical instrument. As excitation reference the force output of the impedance head was evaluated.

2.5. Final Measurement Set-Up

A *ROGA RG-50 ICP*® 1/4 Inch probe microphone is placed in front of the musical instrument to be rotated and measured. It has a linear frequency response ($\pm$1 dB) from 30 Hz up to 4 kHz. Since lower frequencies should be measured too, it should be noted that the microphone has an accuracy of $\pm$1.5 dB down to 4 Hz. It is connected with the suitable *PCB Series 440* sensor signal conditioner with gain of 1x, 10x, 100x. The G.R.A.S. microphone which interacts as reference in the excitation device HAPAM, is connected with a *BSWA Tech Co. MC702* pre-amplifier. Both pre-amplifiers were connected with a port which is linked with a 19 Inch rack terminal tower outside the chamber. For the measurement of stringed instruments the HAPAM and the reference microphone was exchanged to the above mentioned shaker and impedance head setup. The input signal for HAPAM's loudspeaker or the shaker is amplified by *Orion Profi Mosfet Amplifier* from *Zoffmusic*. Next, a converted XLR connector supplies the SMC with power besides the communication is realised over a RS-232 link. For analog data transfer a data acquisition interface card (DAQ) from *National Instruments* which is compatible to LabVIEW came into use.

2.6. Supervising Computer Program with LabVIEW

Controlling the rotation of the step motor controller and conducting the measurements were applied by a program based on designing software *LabVIEW*. The cycle of the acquisition can be divided in several parts. First of all, a top layer sequence can be defined. This level describes functions from the initialisation to the conclusion of the measured data abstractly. It can be said that the top layer also provides information about the process of the SMC's micro-controller program by the reason that both program cycles work synchronously. The second layer describes one acoustical measurement at a given position of degrees. It is encapsulated in the top layer between approaching of the desired positions of the turntable. It will be applied while the end position has not been achieved. The third and last one is the data processing layer which computes all acquired information.

3. MEASURING PROCEDURE

After setting up the music instrument and corresponding excitation device onto the turntable, all connections to the PC must be set. Now the user will be able for setting up the desired measurement parameters, like step-angle θ, full or half circle, excitation bandwidth B and the duration of measurement d. According to the bandwidth and duration the software generates a logarithmic or linear stepped sine signal, depending on the chose of the user. The sampling frequency as the buffer size of the DAQ - device is fixed by fs = 50000 samples per second and the buffer size B = 5000 samples. As each output buffer will contain the data of a sine at one frequency, the length of duration influences directly the number of output buffers and therefore also the frequency resolution. As soon, the start button is hit, the software ensures, that the turntable moves to the position $\theta = 0$ degrees. As soon the position is reached, the SMC prompts the control-software to start excitation and recording of the response. As soon, the stepped sine excitation ends, also the recording comes to stop. The SMC receives the command to increment the position by the stepp-angle θ. This procedure repeats until the the last position has been reached. In the first glance the obtained data is stored as transfer response into a text file.

3.1. Transfer Response

The Transfer Response relates output sound pressure to input sound pressure. Since the transfer response is similar to the acoustical admittance of a musical system, it also can be associated with the input impedance [4]. Further measurements of the directional sound radiation on brass instruments were based on the acquisition of single transfer responses (Equation (3), where n is the index of frequency and θ the angle of measurement).

$$T_{brass}[n,\theta] = \frac{p_o[n,\theta]}{p_i[n]} \tag{3}$$

Considering the transfer response measured on stringed instruments [5] the output sound pressure is related to the input force of the shaker onto the bridge and can be described as:

$$T_{string}[n,\theta] = \frac{p_o[n,\theta]}{F[n]} \tag{4}$$

Both methods describe the resonance profile of the music instrument. Each transfer response is now transferred into an binary format and stored as measurement dataset in an*MySQL* online database. The dataset represents a collection of vectors T[n,θ]. As for the directivity measurement the resonance profile is not of interest, but the variation in terms of radiation angle θ, all

data is normalized to one measurement. For the analysis presented the transfer data of $\theta = 0$ degree has been chosen as normalization reference. The normalization factor K[n] is derived by Equation (5), all vectors will be normalized by Equation (6).

$$K[n] = \frac{1}{T[n,0]} \tag{5}$$

$$T_{norm}[n,\theta] = K[n] * T[n,\theta] \tag{6}$$

All calculations are done by the web-server, the most algorithms are programmed using *PHP*, a server-side scripting language. *JAVA Scripts* where used, where fast user-interaction is required. As user-interface a common web-browser is needed. All line-graphs are translated to the web-browser readable XML-based vector image format *SVG*. For displaying colour-maps, the written script transfers the data into portable network graphics (*PNG*).

4. WEBINTERFACE

In the first glance the web-interface was only meant to display and share the data of the directivity patterns recorded. Soon the idea of a Musical Instrument Measurement Database (*MIMD*) came into mind, where different kind of measurements of music instruments can be stored (current url: `http://iwk.mdw.ac.at/am/mimd`). The present version of *MIMD* can handle and display input impedance and transfer response measurements. Directivity graphs can be calculated by referring to a collection of corresponding transfer response data.

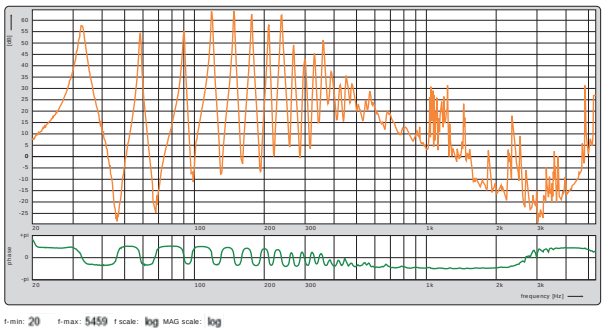

Figure 7: Input impedance of a tuba in B

4.1. Single Measurement Display

The acoustic input impedance of brass wind instruments is often used to specify and analyse quality indicators as the intonation [6]. The results of BIAS measurements can be loaded and displayed (Figure 7). Other than the graphic output of the BIAS Software the web-interface will also plot the corresponding phase graph below the impedance plot. The user can adjust the graphic output in terms of frequency bandwidth and linear or logarithmic scaling on both axis. As the data is displayed as a vector graph, lossless zooming in is only limited by the frequency resolution of the measurement. In the current state of the software the graph can only be downloaded as svg-file. Future programming will allow to load more than one measurement data sets to allow a direct comparison of impedance curves. The algorithm can also be used to display admittance measurements of stringed music instruments. As the transfer data is stored in the same data-format as the acoustic impedance, the tool can also display the single transfer data (Figure 8). For taking single point measurements interactively a moveable measurement bar is planned.

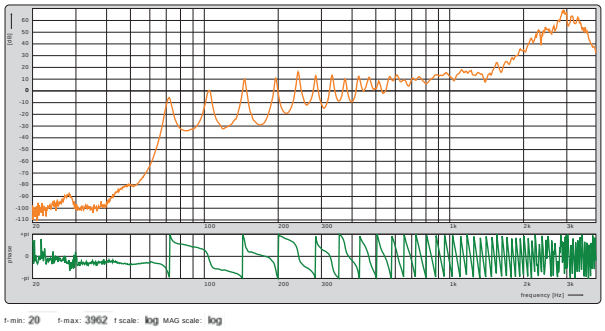

Figure 8: Single transfer respond of a tuba in B

4.2. Directivity Pattern Display

To observe the directivity pattern the user can choose of two different plot-types. A polar-plot diagram offers a two dimensional vector graph at one frequency (Figure 9). Using a slide-bar above the graph the value of frequency is changeable. As here a quick response to the user changes is essential the data is transferred to the client computer. A *JAVA Script* handles the graphic output and updates the plotted svg-graph corresponding to the set value of frequency. For a total view of the directivity data, a two dimensional color map or directivity sonogram was chosen as output (see Figure 10). The output pixel-map can be adjusted by the user. By default the highest appearing amplitude is mapped to the color red, the lowest to blue. By defining a value for ”Ceiling” all amplitude values above, will be mapped to the same red-color value. By imputing a value higher than zero into the ”Floor” input field, all amplitudes below this limit will be mapped to the same blue-value. All existing amplitude values in between this two limits will be mapped linearly to the color-field displayed below the main graph. Also a limitation of the frequency bandwidth is possible by changing the values of ”f-min” and ”f-max”. A fifth input field provides a remapping of the data whether the zero-degree line is centred horizontally or at the top or bottom limits of the pixel-map.

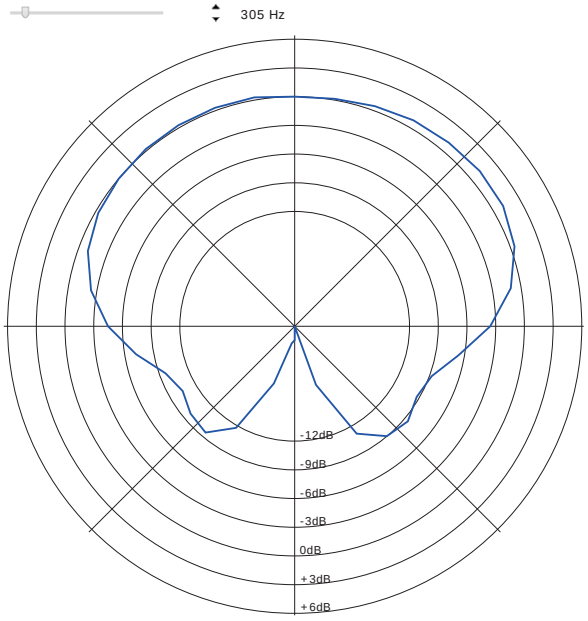

Figure 9: svg pattern of a tuba in B at 305 Hz

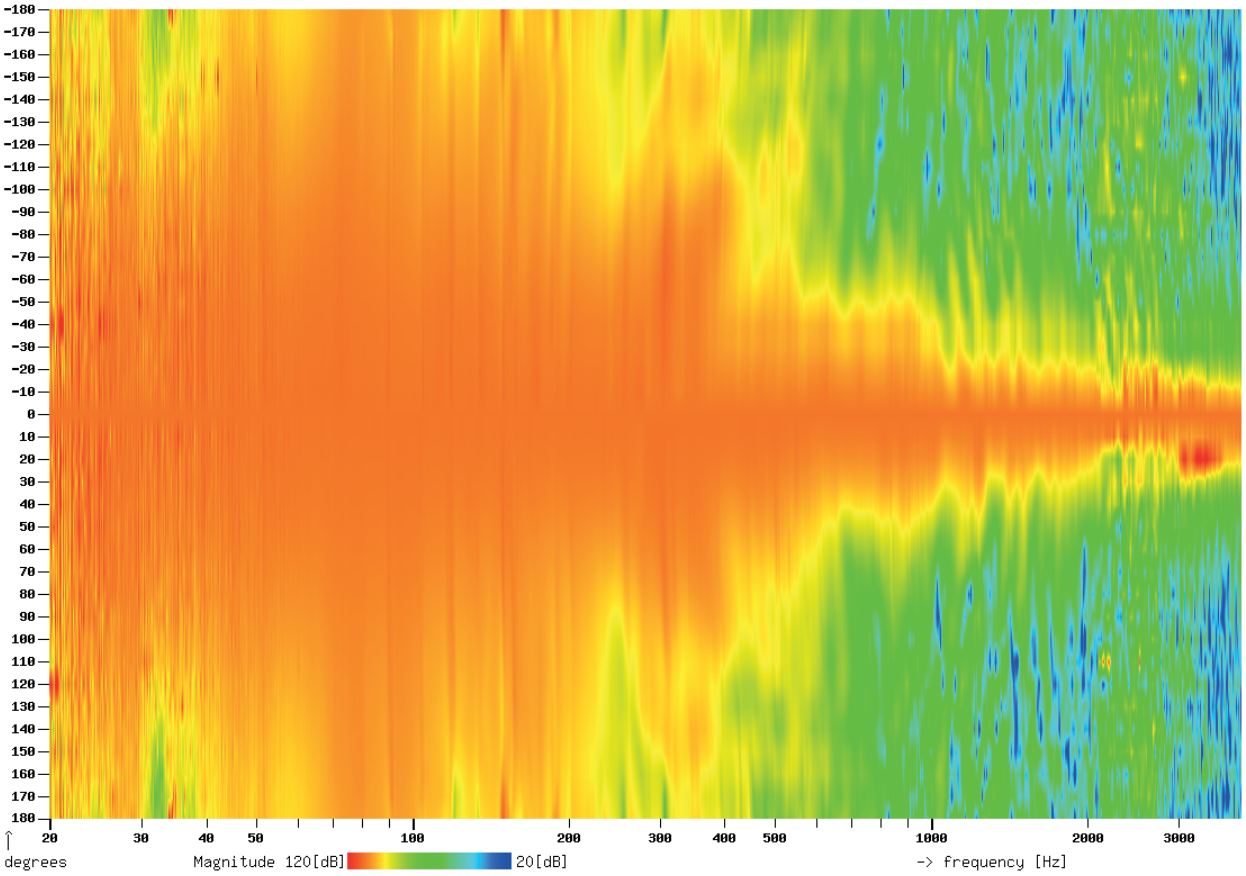

Figure 10: Directivity sonogram of a Tuba in B, Ceiling: 120 dB, Floor: 20 dB, f-min: 20 Hz, f-max: 3962 Hz and 0 degree measurement positioned in the horizontal centre.

5. CONCLUSION

The presented hardware in conjunction with the developed software offers a widely user-friendly device for measuring two-dimensional directivity patterns of brass wind- and stringed instruments. An extension to obtain directivity data in three dimensions is planned.

The current version of the web-interface allows to display several kinds of single measurement data as well directivity patterns. Future features will include data exporting functions and multi-curve display. Depending on the response to the presented database, extensions for collecting construction data of music instruments, general descriptions, sounds and photos will be processed.

6. REFERENCES

[1] Jürgen Meyer and Uwe Hansen, *Acoustics and the Performance of Music: Manual for Acousticians, Audio Engineers, Musicians, Architects and Musical Instrument Makers*, Springer Science+Business Media, LLC, 5 edition, 2009.

[2] Jürgen Meyer, "Musikalische Akustik," in *Handbuch der Audiotechnik*, pp. 123–180. Springer-Verlag Berlin Heidelberg, 2008.

[3] Jürgen Meyer and Klaus Wogram, "Die Richtcharakteristiken von Trompete, Posaune und Tuba," *Das Musikinstrument*, vol. 19, pp. 171–80, 1970.

[4] Stephen Elliott, John Bowsher, and Peter Watkinson, "Input and transfer response of brass wind instruments," *Journal of the Acoustical Society of America (JASA)*, vol. 72, no. 6, pp. 1747–1760, 1982.

[5] Paul Geissler, Otto Martner, Carsten Zerbs, and Martin Schleske, "Psychoacoustic investigations on the possibility of aurally identical violins," in *Proceedings of the Stockholm Music Acoustics Conference 2003, SMAC 03*, Stockholm, 2003, KTH Speech , Music and Hearing, vol. 1, pp. 59–62, Roberto Bresin.

[6] Werner Winkler and Gregor Widholm, "Bias - blas instrumenten analyse system," in *15 Jahre Institut für Wiener Klangstil (1980-1995)*, Eduard Melkus, Ed., pp. 95–106. Institut für Wiener Klangstil, Wien, 1996.

REED CHAMBER RESONANCES IN FREE REED INSTRUMENTS: PROBLEMS AND POSSIBILITIES

James Cottingham
Coe College, United States
jcotting@coe.edu

ABSTRACT

This paper presents an overview of recent research on reed chamber resonances in free reed instruments. Western free reed instruments such as the accordion, harmonica, and harmonium do not normally employ pipe resonators to determine the pitch, but all do feature some sort of reed chamber or cavity in which the reed is mounted. This is necessary to provide a secure mounting for the reed and to properly direct the airstream. The reed chamber will necessarily have resonances which can affect the tone quality and may have some effect on the pitch. Since the cavity volumes are small, however, the resonances will have high frequencies, and the effects on the reed vibration generally tend to be small. An exception to this can occur in the accordion or harmonica for higher pitched reeds, for which a resonance of the reed chamber can be close to the vibration frequency of the reed tongue. In this case the cavity air vibration can become large enough to influence the self-excitation mechanism, possibly interfering with tongue vibration and the resulting musical tone, and in some case preventing the sounding of the reed at all. Builders typically attempt to alleviate this situation by modification of the reed chamber. In the harmonica, if the effect is not too great, skilled players, already accustomed to pitch bending, may be able to overcome this difficulty in some cases by appropriate changes in the vocal tract. In the case of the accordion, Tonon has recently described and implemented means of modifying the internal construction to include a player-controlled internal resonating chamber of variable frequency to enable pitch-bending by the player somewhat similar to that available to the harmonica player.

BIONIC PITCH BENDERS FOR FREE REED INSTRUMENTS

John Granzow, Thomas Rossing, Peter Egbert
Stanford University, United States
jcotting@coe.edu

ABSTRACT

3D printed vocal tracts modelled from MRI scans of an expert musician performing note bends on a diatonic harmonica are shown to precisely reproduce the same pitch changes. The geometry of the vocal tract acoustically coupled to the reeds is now investigated as an exterior replica or even used as a prosthetic to demonstrate a difficult musical technique. This process is discussed within the history of vocal tract models, and interrogated through a critique of Norbert Wiener's contentious claim that 'the best material model for a cat, is another cat, or preferrably the same cat'. We finish with a discussion of how this tool chain of magnetic resonance imaging and numerically controlled fabrication affords novel research in performance techniques through physical simulation.

EXPERIMENTAL STUDY OF THE SOUND PRODUCED FROM A CONCERT ACCORDION

Maria Jesus Elejalde Garcia, Erica Macho Stadler, Ricardo Llanos Vazquez, Asier Agos Esparza
University of the Basque Country, Spain
mariajesus.elejalde@ehu.eus
erica.macho@ehu.eus
ricardollanosvazquez@gmail.com
asieragos@gmail.com

ABSTRACT

Western free-reed musical instruments include various families: accordions, concertinas, reed organs and mouth organs. In the accordion, each free reed is riveted on a metal plate, named “reed plate”. The reed plate is normally made of aluminium and the reed tongue is a piece of steel. The non-riveted end of the reed is free to vibrate from one side to the other of a slot carved on the reed plate under the reed. These boundary conditions are similar to those of a cantilever beam. An accordion reed is only activated when air driven by the bellows comes from the same side of the plate on which the reed is riveted (inward-striking reed or inward-sliding reed). As it has little damping, the reed vibrates with a frequency just below the lowest resonance frequency of the clamped-free bar. Apart from this, due to the non linearity of the problem, a great number of harmonics are found for that frequency instead of the non-harmonic overtones expected for a clamped-free bar. On the reverse of the reed plate there is another identical reed with its corresponding slot. One of the reeds sounds when opening the bellows and the other reed sounds when closing the bellows. In the case of medium or large reeds, the opposite side of the slot is completely covered by a strip made of leather or plastic that moderates the airflow and avoids the passage of air through the hole in the reed tongue that it is not activated. Bigger reeds produce lower notes. A small mass is placed on the tips (free end) of the accordion's lowest reeds to attain low frequencies without being too long. Accordion reeds are usually tuned by removing material at the free end (to raise the pitch) or removing it in the middle (to lower the pitch). Reed tongues must be carefully contoured: a sharp change of section should be avoided as this is liable to cause a “stress raiser” which can result in a fracture forming. Accordion players distinguish between bellows attacks and finger attacks. In bellows attacks the button (or key) is pressed first and the bellows are moved after. In finger attacks, the bellows are set in motion (by pulling or squeezing them) and soon afterward the button is pressed down. In this work, we present the relationships between the control of a concert accordion, the generated sounds, and how these are perceived are analysed. We explore the mass load effect on sound timbre and the fine differences in timbre for bellows attack and finger attack.

EXPERIMENTAL STUDY OF FREE REED INITIAL TRANSIENTS

James Cottingham[1], *Daniel Wolff*[2]
[1] Coe College, United States
[2] University of North Carolina Greensboro, United States
jcotting@coe.edu
dmwolff@uncg.edu

ABSTRACT

Attack transients of harmonium-type free reeds from American reed organs have been studied in some detail. Oscillation waveforms were obtained using a laser vibrometer system, variable impedance transducer proximity sensors, and high speed video with tracking software. Although the fundamental transverse mode is dominant, the presence of higher transverse modes and torsional modes in the initial transient has been established. Typically the motion of the reed tongue begins with an initial displacement of the equilibrium position, often accompanied by a few cycles of irregular oscillation. This is followed by a short transitional period in which the amplitude of oscillation gradually increases and the frequency stabilizes at the steady state oscillation frequency. In the next stage, the amplitude of oscillation continues to increase to the steady state value. Spectra derived from the waveforms in each stage have been analyzed, showing that the second transverse mode and the first torsional mode are both observed in the early stages of the transient, with the torsional mode often appearing earlier. Measurements on reed tongues of different design have been made to further explore the significance of the torsional mode in the initial excitation. [Work partially supported by United States National Science Foundation REU Grant PHY-1004860.]

PIANO HAMMER-STRING CONTACT DURATION: HOW THE BASS HAMMER IS RELEASED FROM THE STRING

Anatoli Stulov

Institute of Cybernetics at Tallinn University Technology, Estonia
stulov@ioc.ee

ABSTRACT

We associate the bass hammer-string contact duration with the time of propagation of compression wave traveling through the hammer body from the contact point to the hammer kernel and back. Based on the hereditary model of the microstructured wool felt, it has been revealed that the stiffness of felt is a nonlinear function of the compression and it is strongly determined by the rate of the felt loading. This means that the speed of the compression wave that propagates through the felt depends on the wave form and on its amplitude. It has been shown that the pulse of a smooth form, and which has no discontinuity on its front propagates with constant speed until the accumulation of nonlinear effects results in the eventual continuous wave breaking. After that moment the shock has been formed, and now the velocity of the shock wave depends on the value of the jump discontinuity across the wave front. It has been shown that the front velocity of the shock wave is greater than the velocity in a linear medium. Therefore, the total time of wave propagation, which is related with a duration of the hammer-string contact, decreases as the dynamic level of the hammer impact is raised. As result, for the first bass hammers the contact duration is shorter than the round-trip time to agraffe, and hence, no reflected wave is needed to assist the hammer for going away from the string.

1. INTRODUCTION

The process of the string excitation by a hammer impact is under investigation for a plenty of years. There are many studies devoted to this problem. We may recollect the well known reviews by Hall [1], Suzuki and Nakamura [2], and Fletcher and Rossing [3].

By now, it is well known that the duration of the hammer-string contact time is one of the main parameters in determining the spectral content of the sound produced by a piano. The problem of the contact duration between the hammer and the string, and discussion what can cause the hammer to rebound is a central point of many papers. The prevailing view about this question is presented in [4, 5, 6].

The common understanding of the dynamics of the hammer-string interaction is expressed in [5]: "*When the hammer has less mass than the string, it will most likely be thrown clear of the string by the first reflected pulse.*"

Nevertheless, the assumptions that only the first reflected wave can rebound the hammer from the string is not quite true. For example, in [7] it was found that the contact duration for *A1* note is less than the round-trip time to agraffe. In addition, in [1], and in [6] it is definitely stated that the hammer can rebound from the string without the assistance of any reflected wave.

This problem was also considered in [8], and by using the nonlinear hysteretic hammer felt model it was shown that the bass hammers, which are relatively light compared to the string, may lose string contact due to the hammer elasticity, and without the assistance of waves traveling along the string, and reflecting back from the agraffe.

This fact is illustrated by Fig. 1.

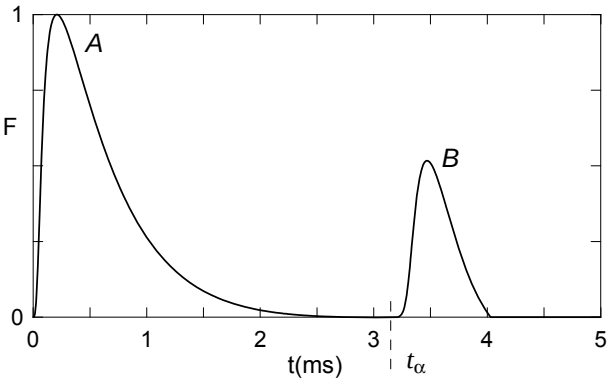

Figure 1: Normalized force history of the hammer-string interaction. Hammer number $N = 6$ (note D_1: $f = 36.71$ Hz); initial hammer impact velocity is 5 m/s. t_α is the moment of reflected wave arrival.

The numerical simulation of the hammer-string interaction shows that the acting force exerted by the hammer impact consists of two pulses. The first pulse A displays the process of loading and unloading of the hammer during the impact. The moment of arrival of the first reflected wave from the agraffe is marked by t_α. It means that the hammer has time enough to decompress fully, and moves away from the string without the assistance of reflected wave.

After the moment t_α the reflected wave arrives to the contact point, and one can see the beginning of the second, or repeated contact between the hammer and the string (pulse B). This process is presented in Fig. 1 definitely.

The goal of the current paper is to understand the physics of the hammer unloading through the traveling waves, but traveling not along the string, but by means of compression waves propagated inside the hammer body, which stiffness is essentially nonlinear.

2. COMPRESSION WAVES IN THE FELT

We associate the contact duration with a time, which is needed for a wave traveling with velocity c to spread for a distance $L = 2\lambda$, where λ is the felt thickness. The simple scheme of wave propagation through the hammer body is shown in Fig. 2.

In order to analyze the process of compression wave propagation in the hammer felt, and to estimate the speed of that wave, the constitutive equation of the microstructured wool felt

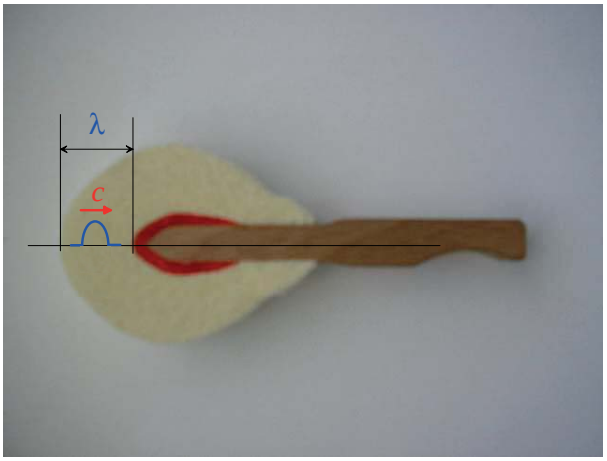

Figure 2: Hammer wave parameters.

material was derived in [9] in the form

$$\sigma(\varepsilon) = E_d \left[\varepsilon^p(t) - \frac{\gamma}{\tau_0} \int_{-\infty}^{t} \varepsilon^p(\xi) \exp\left(\frac{\xi - t}{\tau_0}\right) d\xi \right]. \quad (1)$$

Here σ is the stress, $\varepsilon = \partial u/\partial x$ is the strain, u is the displacement, the constant E_d is the dynamic Young's modulus of the felt, p is the parameter of nonlinearity, γ is the hereditary amplitude, and τ_0 is the relaxation time.

Because this approach is based on the piano hammer model [10, 11], we are limited to describing only the compression wave propagation ($\varepsilon(x,t) > 0$).

The one-dimensional strain wave propagation in the wool felt is considered in [9]. By using the classical equation of motion

$$\rho \frac{\partial^2 u}{\partial t^2} = \frac{\partial \sigma}{\partial x}, \quad (2)$$

where ρ is the felt density, and the constitutive equation (1), a nonlinear partial differential equation with third-order terms is derived in the following form

$$\rho \frac{\partial^2 u}{\partial t^2} + \rho\tau_0 \frac{\partial^3 u}{\partial t^3} - E_d \left\{ (1-\gamma) \frac{\partial}{\partial x} \left[\left(\frac{\partial u}{\partial x} \right)^p \right] + \tau_0 \frac{\partial^2}{\partial x \partial t} \left[\left(\frac{\partial u}{\partial x} \right)^p \right] \right\} = 0. \quad (3)$$

The dimensionless form of this equation is obtained by using the non-dimensional variables that are introduced by the relations

$$u \Rightarrow u/l_0, \quad x \Rightarrow x/l_0, \quad t \Rightarrow t/\alpha_0, \quad (4)$$

where

$$\alpha_0 = \tau_0/\delta, \quad l_0 = \tau_0 \sqrt{E_d/\delta\rho}\,, \quad (5)$$

and parameter δ is defined as $0 < \delta = 1 - \gamma \leqslant 1$.

In terms of non-dimensional strain variable $\varepsilon(x,t)$ Eq. (3) reads

$$(\varepsilon^p)_{xx} - \varepsilon_{tt} + (\varepsilon^p)_{xxt} - \delta\varepsilon_{ttt} = 0. \quad (6)$$

Several samples of felt pads were subjected to the static stress-strain tests in mechanical laboratory at the Faculty of Civil Engineering at the Tallinn University of Technology. The average value of the static Youngs modulus of the pads was estimated as $E_s = 0.06$ MPa. The value of the felt density was determined as $\rho \approx 10^3$ kg/m^3.

For numerical simulation the reasonable value of the static Young's modulus of the felt is chosen to be $E_s = 0.05$ MPa. The values of hereditary parameters are chosen as $\gamma = 0.99$ and $\tau_0 = 14$ μs, which are close to the values of the same parameters for bass piano hammers [12].

Taking into account the relationship $E_s = \delta E_d$ that is derived in [9], we obtain

$$\delta = 0.01, \quad E_d = 5 \text{ MPa}, \quad c_s = 7 \text{ m/s}, \quad c_d = 70 \text{ m/s}. \quad (7)$$

Here velocity $c_s = \sqrt{E_s/\rho}$ corresponds to the static Young's modulus E_s (very slow loading), and velocity $c_d = \sqrt{E_d/\rho}$ corresponds to the dynamic Young's modulus E_d (very fast loading).

By using these values of material constants, the space scale l_0 and time scale α_0 that were used in (4) are

$$l_0 = 10 \text{ mm}, \quad \alpha_0 = 1.4 \text{ ms}. \quad (8)$$

The numerical analysis of the strain wave propagation is presented in [9]. This calls for solution of the boundary value problem of Eq. (6). A boundary value of the strain prescribed at $x = 0$ is selected in the following form

$$\varepsilon(0,t) = A \left(\frac{t}{t_m} \right)^3 e^{3(1 - t/t_m)}, \quad (9)$$

where t_m defines the time coordinate corresponding to the maximum of the pulse amplitude A.

This form of a pulse is continuous and smooth, and it is very similar to the force history pulse shown in Fig. 4a in [12]. The front of a pulse satisfies necessary conditions $\varepsilon(0,0) = \varepsilon_t(0,0) = \varepsilon_{tt}(0,0) = 0$.

The effect of the value of initial pulse amplitude A on the pulse evolution is presented in Fig. 3. The material parameters are selected as $\delta = 0.2$ and $p = 1.5$. The numerical solution is presented for three sequential time moments, and for three different values of the initial amplitude A of the boundary value (9).

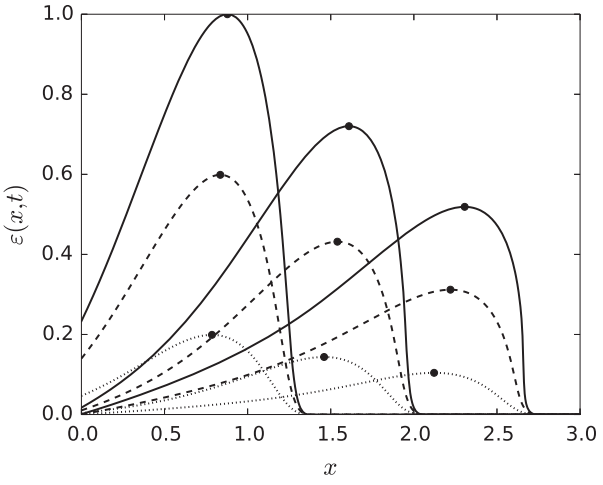

Figure 3: Nonlinear evolution of a pulse ($t_m = 1/2$) for time moments $t = 2$, $t = 3$ and $t = 4$. Pulses of an initial amplitude $A = 0.1$ are shown by solid lines, $A = 0.06$ by dashed lines, $A = 0.02$ by dotted lines. Bullets show the position of the pulse maximum. The results have been normalized relative to the largest amplitude ($A = 0.1$).

One can see, that in this case the front velocity is a constant value $V_f = c_s$, and does not depend on the pulse amplitude. On the other hand, it is also evident that for larger amplitudes

the maximum point, or the crest of a pulse (shown by bullets), propagates faster than the front of a pulse.

Therefore a forward-facing slope of a pulse becomes steeper with a distance of propagation, and accumulation of this effect results in the finally pulse breaking. This means that the shock wave will be formed at the moment when the forward-facing slope of a pulse becomes vertical, and therefore the value of discontinuity across the wave front is defined by the amplitude of a pulse crest.

3. SHOCK WAVE PROPAGATION

Here we consider propagation of a pulse with a finite jump discontinuity on the front through the felt material. For any rate of loading the felt material is defined with the aid of the nonlinear constitutive equation (1) in the form

$$\sigma(U) = E_d \left[(U_x)^p - \frac{\gamma}{\tau_0} \int_{-\infty}^{t} (U_x)^p \, e^{(\omega - t)/\tau_0} d\omega \right]. \quad (10)$$

Here the values of parameters are: $p > 1$, and $0 \leqslant \gamma < 1$.

The conservation law

$$\frac{d}{dt} \int_{x_1}^{x_2} \rho U_{tt}(x,t) dx = \sigma(x_2,t) - \sigma(x_1,t) \quad (11)$$

gives a correspondence between the shock conditions and the shock velocity V_s

$$[\sigma] = -\rho V_s [U_t], \quad (12)$$

where the brackets indicate the jump in the quantity [13].

The constitutive equation in the form (10) gives a relationship

$$[\sigma] = E_d [U_x]^p. \quad (13)$$

By using (12), (13), and taking into account the kinematic identity $[U_t] = -V_s[U_x]$, one can find the relationship between the anticipated front velocity V_s and the value of the discontinuity $[U_x]$ across the wave front

$$\upsilon = \frac{V_s}{c_d} = [U_x]^{\frac{p-1}{2}}, \quad [U_x] = [\varepsilon] = \varepsilon_0 = \text{const} > 0. \quad (14)$$

The dependence of non-dimensional front velocity on the value of discontinuity across the wave front is shown in Fig. 4a.

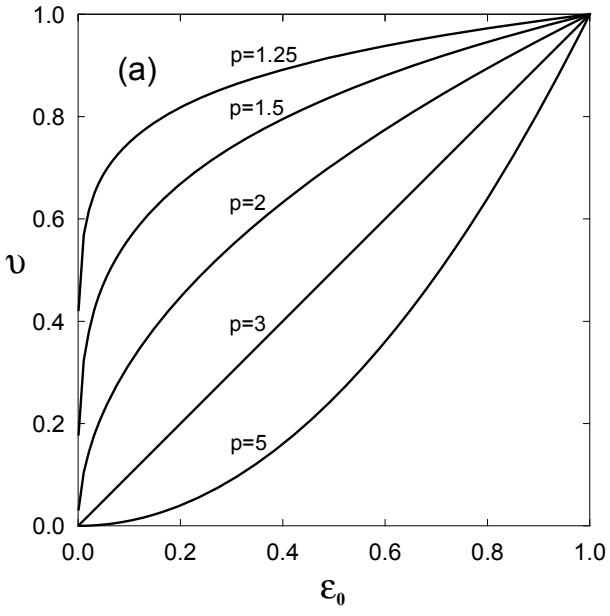

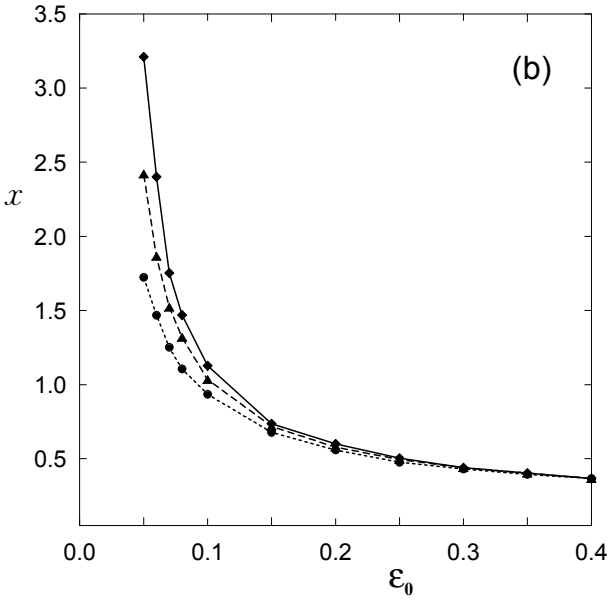

Figure 4: Shock wave parameters as functions of the value of discontinuity ε_0 across the wave front. (a) Non-dimensional front velocity υ shown for various values of parameter p. (b) Non-dimensional distance x of the shock formation shown for various values of parameter δ = 0.01 (diamonds), δ = 0.2 (triangles), and δ = 0.6 (bullets).

As it was mentioned above, in the linear case, and for the continuous smooth pulse ($\varepsilon_0 = 0$), the front velocity is a constant value $V_f = c_s$. In case of the shock wave propagation ($\varepsilon_0 > 0$), the front velocity V_s is always greater than V_f, because $c_d > c_s$ (see relationships (7)).

By numerical simulation of the strain wave propagation, whose initial form is given by the smooth and continuous boundary value (9), the distances, at which the shock pulse is formed, were specified, and the values of discontinuity across the wave front at these points were determined. These dependencies of the distance x of the shock wave appearance as a function of the value of discontinuity ε_0 across the wave front for various values of parameter δ are presented in Fig. 4b.

4. CONCLUDING REMARKS

Resuming the results presented above, we can state that the strain (compression) wave, which originally is continuous and smooth enough, initially propagates through the felt material with a constant speed $V_f = c_s$, until the shock pulse is formed. After that moment the pulse propagates with a velocity $V_s > V_f$, and this shock velocity depends on the value of the discontinuity ε_0 across the wave front, which, in turn, depends on the initial level of the hammer impact.

Finally, using the data obtained, we can estimate the average velocity V_{av} of the wave propagating through the hammer felt. We associate this velocity V_{av} with compression wave velocity c shown in Fig. 2.

For a numerical example we have chosen the nonlinear parameter p = 1.5, and the distance of wave propagation $L = 2\lambda$ = 32 mm, which is equal approximately to the double thickness of the felt of first bass hammer. The values of other parameters, such as the space scale l_0 and the time scale α_0, are the same as presented in (7) and (8). The non-dimensional parameters x and υ are obtained by using the results presented in Fig. 4.

ε_0	$x(1)$	X(mm)	t_1(ms)	L_x(mm)	$\upsilon(1)$	V_s(m/s)	t_2(ms)	t_*(ms)	V_{av}(m/s)
0.05	3.20	32.0	4.57	0	0.473	47.3	0	4.57	7.0
0.075	1.75	17.5	2.50	14.5	0.523	52.3	0.28	2.78	11.5
0.10	1.13	11.3	1.15	20.7	0.562	56.2	0.37	1.52	21.0
0.15	0.74	7.4	1.06	24.6	0.622	62.2	0.39	1.45	22.0
0.20	0.60	6.0	0.86	26.0	0.669	66.9	0.40	1.26	25.4

Table 1: Parameters of traveling compression wave.

The other parameters displayed in Table 1 are determined by relations

$$X = xl_0,\ \ L_x = L - X,\ \ V_s = \upsilon c_d,\ \ t_1 = X/c_s,$$

$$t_2 = L_x/V_s,\ \ t_* = t_1 + t_2,\quad V_{av} = L/t_*. \qquad (15)$$

Here X is the distance that the wave propagates through a felt with a "normal" speed c_s in the time t_1, L_x is the part of a whole distance $L = 2\lambda$ (see Fig. 2) through which the wave propagates in the time t_2 with the velocity V_s, and t_* is the total time of propagation. The velocity V_{av} is the "average" speed of traveling wave.

Analysis of the data presented in Table 1 shows that the wave with a small initial amplitude, which results in the value of jump discontinuity across the wave front ε_0 = 0.05, propagates through the whole distance as a smooth pulse. This small amount of the compression amplitude one can relate with pp dynamical level of a hammer blow, which corresponds to the velocity of the hammer impact V = 1 m/s, approximately.

On the contrary, the value of discontinuity across the wave front ε_0 = 0.2 can be created only by a very hard ff level of a hammer blow, which corresponds to the initial hammer velocity V = 7 m/s, approximately.

The total time of the wave propagation t_* one can associate with the duration of contact between the hammer and the string. After this moment t_* the hammer felt is unloaded completely, and the hammer has lost the contact with the string.

Thus, with the growth of the level of the hammer impact and the shock pulse appearance, the average speed V_{av} of wave propagation increases.

Therefore, we can state that the duration of the hammer-string contact decreases as the dynamic level of the hammer impact is raised, and this effect is appeared due to a peculiar property of the piano hammer felt, which is called the nonlinear hammer stiffness.

5. ACKNOWLEDGMENT

This research was supported by the European Regional Development Fund (Project TK124 (CENS)).

6. REFERENCES

[1] D. E. Hall, "Piano string excitation III: General solution for a soft narrow hammer," *J. Acoust. Soc. Am.*, vol. 81, no. 2, pp. 547–555, 1987.

[2] H. Suzuki and I. Nakamura, "Acoustics of pianos," *Appl. Acoustics*, vol. 30, pp. 147–205, 1990.

[3] N. H. Fletcher and Th. D. Rossing, *The Physics of Musical Instruments*, Springer, New York, 2nd edition, 1998.

[4] D. E. Hall, "Piano string excitation in the case of small hammer mass," *J. Acoust. Soc. Am.*, vol. 79, no. 1, pp. 141–147, 1986.

[5] Th. D. Rossing, *The Science of Sound*, Addison-Wesley, 2nd edition, 1990.

[6] A. Askenfelt and E. V. Jansson, "From touch to string vibrations. III: String motion and spectra," *J. Acoust. Soc. Am.*, vol. 93, no. 4, Pt.1, pp. 2181–2196, 1993.

[7] T. Yanagisawa and K. Nakamura, "Dynamic compression characteristics of piano hammer felt," *J. Acoust. Soc. Jpn.*, vol. 40, no. 11, pp. 725–729, 1984.

[8] A. Stulov, "Piano hammer - string interaction," in *Proceedings of ICA 2004*, Kyoto, Japan, 2004, pp. 2127–2130.

[9] D. Kartofelev and A. Stulov, "Propagation of deformation waves in wool felt," *Acta Mechanica*, vol. 225, pp. 3103–3113, 2014.

[10] A. Stulov, "Hysteretic model of the grand piano hammer felt," *J. Acoust. Soc. Am.*, vol. 97, no. 4, pp. 2577–2585, 1995.

[11] A. Stulov, "Dynamic behavior and mechanical features of wool felt," *Acta Mechanica*, vol. 169, pp. 13–21, 2004.

[12] A. Stulov, "Experimental and computational studies of piano hammers," *Acta Acoustica united with Acoustica*, vol. 91, no. 6, pp. 1086–1097, 2005.

[13] G. Whitham, *Linear and Nonlinear Waves*, Wiley-Interscience, New York, 1974.

ENERGY BASED SIMULATION OF A TIMOSHENKO BEAM IN NON-FORCED ROTATION. INFLUENCE OF THE PIANO HAMMER SHANK FLEXIBILITY ON THE SOUND.

Juliette Chabassier[1], *Marc Duruflé*[2]
[1] Modartt, France
[2] Inria, France
juliette.chabassier@pianoteq.com
marc.durufle@inria.fr

ABSTRACT

A nonlinear model for a vibrating Timoshenko beam in non-forced unknown rotation is derived from the virtual work principle applied to a system of beam with mass at the end. The system represents a piano hammer shank coupled to a hammer head. An energy-based numerical scheme is then provided, obtained by non classical approaches. A major difficulty for time discretisation comes from the nonlinear behavior of the kinetic energy of the system. This new numerical scheme is then coupled to a global energy-preserving numerical solution for the whole piano. The obtained numerical simulations show that the pianistic touch clearly influences the spectrum of the piano sound of equally loud isolated notes. These differences do not come from a possible shock excitation on the structure, nor from a changing impact point, nor a "longitudinal rubbing motion" on the string, since neither of these features are modeled in our study.

DOUBLE POLARISATION IN NONLINEAR VIBRATING PIANO STRINGS

Jin Jack Tan, Cyril Touzé, Benjamin Cotté

IMSIA,
Institute of Mechanical Sciences and Industrial Applications,
ENSTA-ParisTech - CNRS - EDF - CEA,
Université Paris-Saclay,
828 Boulevard des Marchaux, 91762 Palaiseau Cedex, France
jtan@ensta.fr

ABSTRACT

The present work studies the double polarisation phenomenon observed in vibrating piano strings. From the experimental viewpoint, it is known that when a string is given an initial displacement in one transverse direction (e.g. hammer excitation in the vertical plane), the second transverse displacement (e.g. in the horizontal plane) is also excited after a few milliseconds and the amplitude can be of similar order to the first transverse displacement. This phenomenon contributes to a characteristic piano sound feature called the "double decay". The purpose of this study is to investigate the role of nonlinearities in inducing double polarisations. The nonlinear vibrations of the strings are studied with a two-degrees-of-freedom (dofs) system extracted from the Kirchhoff-Carrier string equations. The method of multiple scales is used to study the free vibrations of two polarisations having nearly equal eigenfrequencies and thus presenting a 1:1 internal resonance. For an imperfect string with slightly different eigenfrequencies between the two polarisations, it is found out that depending on the energy of the excitation, an uncoupled transverse mode can develop into a coupled mode where there is energy exchange between the two transverse polarisations. The coupled mode is stable and the string oscillates in an elliptic path. Numerical experiments are also carried out, confirming the findings of the analytical approach.

1. INTRODUCTION

This study on the double polarisation of piano strings is contained in a larger project which aims at developing a physically-based time-domain piano sound synthesis model. The work was pioneered by Chabassier [1] who proposed a refined complete model of a grand piano [2, 3]. However a few points still need additional developments. For example, one tonal feature that was not observed in the simulated sound is the double decay, i.e. where the temporal signal exhibits two envelopes with different decay rates. It is understood that one of the contributing factors of double decay is the double polarisation of piano strings, as first reported by Weinreich [4]. The double polarisation phenomenon is not modeled in Chabassier's work which may explain the absence of double decay in her modeled piano sound. The double polarisation can be caused by various factors, such as nonlinearities of piano strings, asymmetry and complex boundary conditions, coupling to unison strings etc. [5, 6, 7, 8, 9].

In this contribution, we focus on the nonlinearity experienced by piano string vibrating at large amplitudes as a possible cause for explaining the birth of double polarisation. More particularly the two fundamental eigenfrequencies of a string with double polarisation are known to have close values, thus showing a 1:1 internal resonance. It is also known from other studies on nonlinear vibrations [10, 11] that thanks to a 1:1 internal resonance, energy can be exchanged between vibration modes so that even if the motion is initiated along one polarisation only, the nonlinearity can make this motion unstable, so that eventually a coupled vibration arises with the two polarisations involved. The objective of the present contribution is thus to clearly establish if the nonlinearity can be the cause of this coupling, as well as to highlight the main parameters governing the transfer of energy. The 1:1 internal resonance has already been studied in the case of forced vibrations, see *e.g.* [12, 10, 11]. Here our interest is in the case of free vibration for which only Manevitch and Manevitch present a detailed investigation [13]. The complete problem will hence be fully revisited and applied to the specific case of strings.

The article is organised as follows. First, a system of nonlinear Kirchhoff-Carrier string equations is presented in section 2 and solved via the multiple scales method in section 3. The results are presented and discussed in section 4. The paper continues with a numerical experiment to demonstrate the double polarisations in section 5 before wrapping up with conclusion in section 6.

2. KIRCHHOFF-CARRIER EQUATION

The Kirchhoff-Carrier equations for a freely vibrating fixed-fixed string with two polarised displacements u_1 and u_2 read [14, 15, 11]:

$$\rho A \ddot{u_1} - (T_0 + N)\, u_1'' = 0, \tag{1a}$$

$$\rho A \ddot{u_2} - (T_0 + N)\, u_2'' = 0, \tag{1b}$$

where N is the axial tension created by the large amplitude motions and the coupling with the transverse motion. It reads:

$$N = \frac{EA}{2L} \int_0^L \left({u_1'}^2 + {u_2'}^2 \right) \mathrm{d}x. \tag{2}$$

In this set of equations, L is the length, A the crosse section area, E Young's modulus, T_0 the tension and ρ the density. Among others, underlying assumptions are that the inertia of the longitudinal component is negligible, see *e.g.* [16, 14] for more details. Following [11], the equations can be made nondimensional for a more general treatment.

The solutions of the nondimensional equations can be ex-

pressed in modal form:

$$u_1(x,t) = \sum_{k=1}^{K} \Phi_k(x) p_k(t), \qquad u_2(x,t) = \sum_{k=1}^{K} \Phi_k(x) q_k(t), \tag{3}$$

where $\Phi_k(x)$ are the mode shapes, and $\{p_k(t), q_k(t)\}_{k\geq 1}$ the modal coordinates. Restraining only the fundamental mode in the truncation for each polarisation (*i.e.* $K = 1$) and using the usual projection (Galerkin) technique, on obtains the following two dofs nonlinear system for the two modal coordinates p, q related to each polarisation:

$$\ddot{p} + \omega_1^2 p + \varepsilon \left[\Gamma_1 p^3 + C_1 p q^2\right] = 0, \tag{4a}$$

$$\ddot{q} + \omega_2^2 q + \varepsilon \left[\Gamma_2 q^3 + C_2 q p^2\right] = 0, \tag{4b}$$

where ε is a small parameter arising from the nondimensionalisation [11], $\varepsilon = EAd^2/T_0L^2$, with d the diameter of the string. For a perfect string, the two eigenfrequencies are equal so that $\omega_2 = \omega_1 = \pi$ [11]. The same holds for the nonlinear coefficients, in a perfect case we have $\Gamma_1 = \Gamma_2 = C_1 = C_2 = \pi^4/2$. However, acknowledging that such perfect string does not exist in reality, a detuning parameter σ_1 is introduced so that the two eigenfrequencies of the two modes are possibly slightly different,

$$\omega_2 = \omega_1 + \varepsilon\sigma_1. \tag{5}$$

Following the same lines, the system will be studied with general and different nonlinear coefficients so as to draw the complete picture for the nonlinear string. In a given experimental case, a procedure would be needed for identifying these coefficients.

3. MULTIPLE SCALES METHOD

The system in equation (4) is solved by the multiple scales method which describes the original system to be function of multiple independent time scales. Introducing the "fast" and "slow" time scales:

$$T_0 = t, \tag{6a}$$

$$T_1 = \varepsilon t, \tag{6b}$$

p and q can take the following form,

$$p(t) = p_0(T_0, T_1) + \varepsilon p_1(T_0, T_1) + O(\varepsilon^2), \tag{7a}$$

$$q(t) = q_0(T_0, T_1) + \varepsilon q_1(T_0, T_1) + O(\varepsilon^2), \tag{7b}$$

where p_0 and q_0 can be written as:

$$p_0 = A(T_1)\exp(i\omega_1 T_0) + c.c, \tag{8a}$$

$$q_0 = B(T_1)\exp(i\omega_2 T_0) + c.c, \tag{8b}$$

where $c.c$ stands for complex conjugates. A and B are unknown complex functions of T_1. Substituting equation (7) into (4) and grouping all the resonant terms for 1:1 resonance up to order ε, one obtains the solvability conditions. By writing A and B in polar form:

$$A(T_1) = a(T_1)\exp(i\alpha(T_1)), \tag{9a}$$

$$B(T_1) = b(T_1)\exp(i\beta(T_1)), \tag{9b}$$

the solvability conditions can be broken down into a set of four dynamical equations (two for amplitude a and b, two for the phases α and β):

$$a' = -\frac{C_1}{2\omega_1} a b^2 \sin(\gamma_2 - \gamma_1), \tag{10a}$$

$$\gamma_1' = \frac{3\Gamma_1}{\omega_1} a^2 + \frac{C_1}{\omega_1} b^2 \left[2 + \cos(\gamma_2 - \gamma_1)\right], \tag{10b}$$

$$b' = \frac{C_2}{2\omega_2} b a^2 \sin(\gamma_2 - \gamma_1), \tag{10c}$$

$$\gamma_2' = \frac{3\Gamma_2}{\omega_2} b^2 + \frac{C_2}{\omega_2} a^2 \left[2 + \cos(\gamma_2 - \gamma_1)\right] + 2\sigma_1, \tag{10d}$$

where

$$\gamma_1 = 2\alpha, \qquad \gamma_2 = 2\beta + 2\sigma_1 T_1. \tag{11}$$

The introduction of equation (11) is necessary so that the system is made autonomous (not directly dependent on any time scales).

3.1. Uncoupled solutions

Let us first consider the uncoupled solutions. They correspond to the motions of the strings that are either in the horizontal direction, or in the vertical one. The first set of uncoupled solutions is found by setting $b = 0$, in Eqs. (10). The 4-dofs system then degenerates into a two dofs and reads:

$$a' = 0, \tag{12a}$$

$$\gamma_1' = \frac{3\Gamma_1}{\omega_1} a^2, \tag{12b}$$

The equations can be easily integrated to give:

$$a = C_a, \tag{13a}$$

$$\alpha = \frac{3\Gamma_1}{2\omega_1} a^2 T_1 + \alpha_a, \tag{13b}$$

where C_a and α_a are both integration constants independent of T_1. Using this result, the solution p_0 can be expressed as:

$$p_0 = 2a\cos\left[\omega_{NL} t + \alpha_a\right], \tag{14}$$

where

$$\omega_{NL} = \omega_1 \left(1 + \varepsilon \frac{3\Gamma_1}{2\omega_1^2} a^2\right). \tag{15}$$

The first order solution is thus a periodic orbit where only p is involved in the vibration since setting $b = 0$ implies $q = 0$. The nonlinear frequency of oscillation ω_{NL} depends on the amplitude a, a usual feature in nonlinear oscillations. For a positive value of Γ_1, which is the case for strings, the nonlinearity is of the hardening type, *i.e.* the oscillation frequency increases with the amplitude.

A similar exercise can be done for the other uncoupled case, i.e. $a = 0$ and one would obtain a similar result for q_0,

$$q_0 = 2b\cos\left[\omega_{NL} t + \beta_b\right] \tag{16}$$

where

$$\omega_{NL} = \omega_2 \left(1 + \varepsilon \frac{3\Gamma_2}{2\omega_2^2} b^2\right) \tag{17}$$

One can notice the similarity between the two solutions, coming from the fact that the uncoupled solutions are ruled out by classical Duffing equations. The nonlinearity is completely governed by coefficients Γ_1 and Γ_2. Figure 1 shows the backbone curve (amplitude-frequency relationship, Eqs. (15)-(17)) for $\varepsilon = 0.163$, a typical value for a string that has been computed using standard values from [1]. The value $\Gamma = 0$ is used

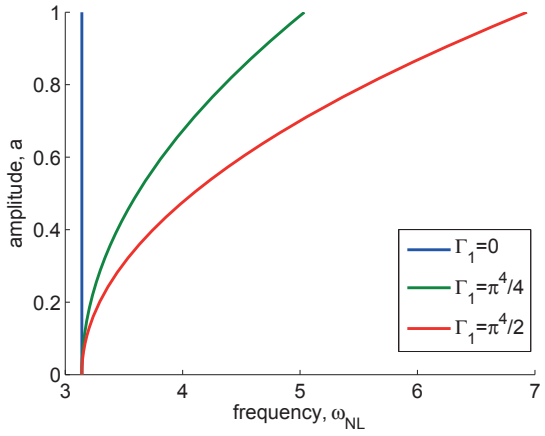

Figure 1: Relationship between a and ω_{NL} for various Γ_1 at $\omega_1 = \pi$, $\varepsilon = 0.163$.

as an eyeguide to recall that for linear vibrations, the oscillation frequency is independent from the amplitude. The values $\Gamma = \pi^4/2$, $\omega = \pi$ are the standard values for perfect strings. Finally $\Gamma = \pi^4/4$ is plotted as an intermediate case between the linear string and the perfect nonlinear string. The figure allows one to estimate the deviation (in radian frequency) of the oscillations with respect to the linear eigenfrequency, as a function of the vibration amplitude.

3.2. Coupled solutions

Let us now investigate the coupled solutions of the conservative system given by Eqs. (10). Stationary oscillations occurs at a given energy level so that coupled solutions can be searched for fixed amplitudes, by imposing $a' = b' = 0$. This is also in the line of the uncoupled cases where periodic solutions were found for fixed amplitudes and only phase variations, from which the nonlinear amplitude-frequency relationship were derived. From equation (10a) and (10c), it is obvious that for coupled solutions to exist (i.e. $a \neq 0$, $b \neq 0$), one must have mandatory $\sin(\gamma_2 - \gamma_1) = 0$. This implies in particular that $\cos(\gamma_2 - \gamma_1) = \pm 1$. Interestingly, for each case of the possible value of the cosine, the two polarisations p and q are related in a different manner. For $\cos(\gamma_2 - \gamma_1) = +1$, a simple algebra on the system shows that the solutions p and q are related by the following relationship:

$$\frac{q}{p} = \pm\frac{b}{a}, \tag{18}$$

while for $\cos(\gamma_2 - \gamma_1) = -1$, p and q are related by:

$$\frac{q^2}{4b^2} + \frac{p^2}{4a^2} = 1. \tag{19}$$

These particular forms expressed by the coupled solutions has already been commented by Manevicth and Manevitch [13], who refers to them respectively as "normal mode" (NM) (former case, Eq. (18)), and "elliptic mode" (EM) (latter case, and Eq. (19)). This peculiar relationship expressed for each time between the solution amplitudes leads to a particular motion which is sketched in Figure 2 in the (p, q) (displacements) plane. The elliptic mode appears particularly interesting for us as it corresponds to the whirling motion observed in piano strings [9].

The nonlinear amplitude-frequency relationships defining the backbone curves for coupled solutions can be found out

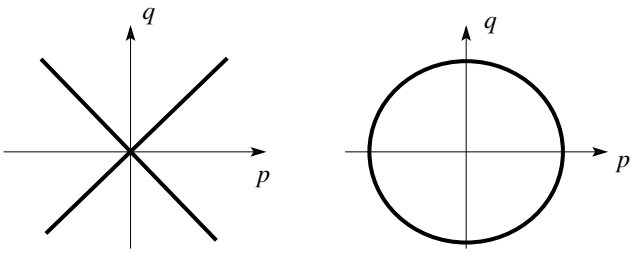

(a) normal mode (b) elliptic mode

Figure 2: Illustrations of the two modes of coupled solutions. Image not to scale.

by setting $\cos(\gamma_2 - \gamma_1) = \pm 1$ in Eqs. (10b)-(10d), where the right-hand sides become constants, so that one can retrieve α, β and subsequently the nonlinear frequency ω_{NL} for the coupled modes as:

$$\omega_{NL} = \omega_1 \left[1 + \varepsilon \left(\frac{3\Gamma_1}{2\omega_1^2} a^2 + \frac{rC_1}{2\omega_1^2} b^2\right)\right]. \tag{20}$$

In this equation (and in the remainder of the article), the parameter r is such that $r = 3$ for normal mode, and $r = 1$ for elliptic modes respectively. As can be seen in equation (20), the nonlinear frequency is influenced by the amplitude of both polarisations a and b. The equation forms a surface on the 3D space defined by (a, b, ω_{NL}). However curved line solutions are awaited instead of a whole surface family. Noting that $\gamma_2 - \gamma_1 = n\pi$ from the necessary conditions of existence for coupled solutions, one has thus $\gamma_2' - \gamma_1' = 0$. Using such relation, one can obtain:

$$\left[\frac{rC_1}{\omega_1} - \frac{3\Gamma_2}{\omega_2}\right] b^2 + \left[\frac{3\Gamma_1}{\omega_1} - \frac{rC_2}{\omega_2}\right] a^2 = 2\sigma_1. \tag{21}$$

This relationship expresses the link between the amplitudes a and b for both normal ($r = 3$) and elliptic ($r = 1$) coupled modes. The conjuction of Eqs (20) and (21) define the backbone curves for the coupled modes.

Let us now investigate how the coupled solutions can be related to the uncoupled ones. By setting $a = 0$ or $b = 0$ in Eq. (21), it can be seen that either of the uncoupled modes can branch into the coupled modes provided the following conditions are met:

For uncoupled mode $a \neq 0$

$$a^2 \geq \frac{2\sigma_1}{\frac{3\Gamma_1}{\omega_1} - \frac{rC_2}{\omega_2}}, \tag{22}$$

For uncoupled mode $b \neq 0$

$$b^2 \geq \frac{2\sigma_1}{\frac{rC_1}{\omega_1} - \frac{3\Gamma_2}{\omega_2}}, \tag{23}$$

These equations provide a limit value, in terms of amplitudes of the uncoupled modes, for which the coupled solutions can develop. Below these limit value, only uncoupled solutions exist. It must be noted that in certain cases, the RHS of both the equations can have two positive values of which the lower one indicates the bifurcation point where the uncoupled solution branches into the coupled solution while the higher one indicates the point where the coupled solution collapse and enter the uncoupled solution [13].

3.3. Stability analysis

To obtain the stability of the coupled modes, Eqs (10) can be reduced to a 3-DOF system by taking the difference between the two phases or even further to a 2-DOF system as demonstrated by Manevitch and Manevitch [13]. The advantage of using such an approach is that the coupled solutions are then real fixed points of the 3- or 2-dofs systems, so that the usual tools from dynamical system theory can be used for investigating stability. One can thus construct the Jacobian matrix of the corresponding system and solve for the eigenvalues. Using either system will result in the same following stability criteria for the coupled modes:

$$\frac{\omega_2\Gamma_1}{C_2\omega_1} + \frac{\Gamma_2\omega_1}{C_1\omega_2} < 2 \qquad \text{for normal modes,} \tag{24a}$$

$$\frac{\omega_2\Gamma_1}{C_2\omega_1} + \frac{\Gamma_2\omega_1}{C_1\omega_2} > \frac{2}{3} \qquad \text{for elliptics modes.} \tag{24b}$$

It is interesting to see that the stability of the coupled solutions does not depend on the energy but rather on the physical parameters of the system (i.e. eigenfrequencies and nonlinear constants). It also means that regardless of level of excitation, exhibition of stable normal or elliptic modes are pre-determined.

To conclude the analytical study, let us investigate the stability of uncoupled solutions and demonstrate how uncoupled solutions can become unstable in favour of a coupled one. As noted by Manevitch and Manevitch [13], the stability of the uncoupled solutions is determined by the energy of the system. Using the same approach as for the coupled case does unfortunately not give a useful criteria for the stability of uncoupled solutions, which are found to be always unstable. Furthermore, Manevitch and Manevitch do not give an explicit proof of the stability of uncoupled solutions in [13]. The underlying problem is that when setting either $b = 0$ or $a = 0$ in the system, the degeneracy is ill-conditioned so that the phase space shrinks down to a two dofs system where the perturbation brought by the other oscillators are not defined and thus cannot be studied. The solution is found from the forced and damped vibration cases by canceling the damping terms and identifying the external excitation frequency to the nonlinear oscillation frequency ω_{NL}. Using the existence conditions derived in [10] from a geometric analysis in phase space, one can obtain the following *instability regions* for the uncoupled solutions:
For uncoupled mode $a \neq 0$

$$\omega_{NL} = \omega_2 + \varepsilon r \frac{C_2}{2\omega_2} a^2 \tag{25}$$

For uncoupled mode $b \neq 0$

$$\omega_{NL} = \omega_1 + \varepsilon r \frac{C_1}{2\omega_1} b^2 \tag{26}$$

where $r = 1$ and $r = 3$ define the lower and upper bound of the instability region, that are simply related to the connection with either elliptic mode or normal mode. The instability affecting the uncoupled mode $a \neq 0$ originates from the eigenfrequency of the other uncoupled mode, ω_2 and vice versa. This is because the existence of another uncoupled solution upsets the stability of the original uncoupled solution. It is also interesting to note that the point where the uncoupled solution changes its stability (either in losing or restoring it) is also the point where the uncoupled solution branches into a coupled solution (or a coupled solution leaves and enters the uncoupled solution). Finally, the stability of the uncoupled solutions are seen to depend on the coupling nonlinear coefficients C_1 and C_2 only, as can be expected.

4. RESULTS AND DISCUSSIONS

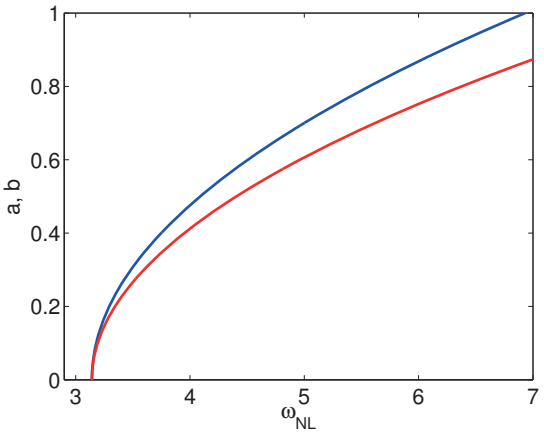

Figure 3: Amplitude-frequency relationships for the strings, perfect case with $\omega_1 = \omega_2 = \pi$ (no detuning: $\sigma_1 = 0$), and equal nonlinear coefficients $C_1 = C_2 = \Gamma_1 = \Gamma_2 = \pi^4/2$. The black — and blue — lines (overlapped with each other) indicate the two uncoupled modes while the red — line indicates the elliptic mode. $\varepsilon = 0.163$.

In this section, several case studies are made to demonstrate the properties of the system. Firstly, a perfect string case is considered (i.e. $\sigma_1 = 0$, $C_1 = C_2 = \Gamma_1 = \Gamma_2$). For this case, the two amplitude-frequency relationships for uncoupled solutions given by Eqs. (15) and (17) are exactly the same so that the backbones in Fig. 3 collapse on the same curve (black and blue curves, only the blue being visible). For the coupled solutions, Eqs. (21) for the normal mode ($r = 3$) degenerates, indicating that no normal modes are possible in the perfect case. On the other hand, elliptic modes does however exist, and Eqs. (21) shows that they have same amplitude : $a = b$. Reporting in Eq. (20), one obtains the backbone curve for the coupled, elipitc modes in the perfect case as: $\omega_{NL} = \omega_1(1 + 2\varepsilon\frac{\Gamma_1}{\omega_1}a^2)$. This shows that coupled solutions have a stronger hardening behaviour than uncoupled ondes, as reported in Fig. 3 with a red line. It must be noted that a 2D representation has been chosen for simplicity, by using the same axis for both amplitudes a and b, whereas the whole solutions should be plotted in a 3D space. In such 3D space (a, b, ω_{NL}), uncoupled solutions are restricted respectively to the planes (a, ω_{NL}) and (b, ω_{NL}), whereas the coupled elliptic solutions is in the plane $a = b$.

Finally, examining the different stability conditions found in the previous section for both coupled and uncoupled modes leads to the conclusion that all the solutions reported in Fig. 3 are stable. This leads to the important conclusion that if the motion is excited on a given polarization, then it will stay on it for every time so that no whirling motion of the string would be observed. The coupled elliptic solutions could be observed only if very specific initial conditions are given to the string so that the motion is initiated along this mode.

Let us now turn to the more realistic case of an imperfect string. The most simple imperfection with a slight detuning between the two eigenfrequencies of the polarisation is investigated, by setting $\sigma_1 = 1$, and keeping all the nonlinear coupling coefficients equal: $C_1 = C_2 = \Gamma_1 = \Gamma_2$. The backbone curves are represented in Fig. 4, where now the two uncoupled solutions (black and blue lines) are different and originates respectively from ω_1 and $\omega_2 = \omega_1 + \varepsilon\sigma_1$. Eqs (21) shows once again

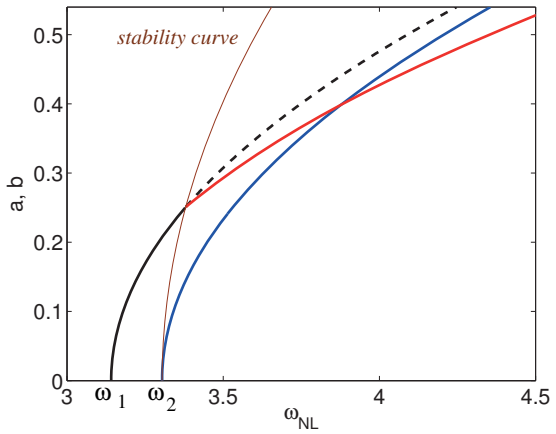

Figure 4: Amplitude-frequency relationships for periodic solutions of the nonlinear string, imperfect case with $\sigma_1 = 1$, all other coefficients being the same as in Fig. 3: $C_1 = C_2 = \Gamma_1 = \Gamma_2 = \pi^4/2$, $\omega_1 = \pi$, $\varepsilon = 0.163$. Black —— : uncoupled solution $a \neq 0$, blue —— uncoupled solution $b \neq 0$, red —— coupled elliptic mode. Dashed lines - - indicates instability. In brown is given the instability limit predicted by Eq. (25).

that in this case normal modes are not likely to exist. Only elliptic modes are possible. The instability condition for uncoupled solutions, provided by Eq. (25)-(26), shows that:

- The uncoupled solutions with $b \neq 0$ are always stable.
- On the other hand, uncoupled solutions with $a \neq 0$ can be unstable and branch on an elliptic mode, recovering also the criteria given by Eq. (22).

The instability region for uncoupled mode with $a \neq 0$ given by Eq. (25) has two curves. The one for normal mode ($r = 3$) is not relevant. Finally only the instability line with $r = 1$ is meaningful, and is represented as a brown line in Fig. 4. The crossing between the sdof uncoupled solution and the instability limit occurs exactly when condition (22) is fulfilled. From this point, uncoupled solutions are unstable, and the branch of elliptic mode solutions (red line) emerges. Once again a 2D representation has been chosen for simplicity, the reader must however keep in mind that the red line is neither in the plane (a, ω_{NL}), nor in (b, ω_{NL}), but really develop in the full 3D space and is not contained within a plane. In particular the crossing between the coupled solution (red line) and uncoupled ($b \neq 0$, blue curve) is only a matter of the representation used but does not exist in the full 3D space.

The important conclusion that can be drawn from this study is that as soon as an imperfection is taken into account, an unstable region in the backbone curve for uncoupled modes exist. Once the limit amplitude exceeded, uncoupled solutions are unstable so that even though an initial condition is given for that polarisation, an energy transfer will occur so that eventually the system would settle on the stable elliptic mode. Interestingly, one can notice from Eq. (25) that the smallest the detuning σ_1, the smallest the amplitude limit for unstable solutions occurs. Hence in order to observe easily this phenomenon, the detuning need not be zero, but should be as small as possible.

5. NUMERICAL EXPERIMENTS

The main analytical findings of the previous section is now compared to direct numerical simulations of the original system given by Eqs. (4). More particularly, the mots interesting case of the imperfect string is considered, with a slight detuning between the two eigenfrequencies of the two polarisations. The equations of motion are directly integrated numerically in time with a fourth-order Runge-Kutta method. The experiment is carried out with varying level of initial excitation on the first mode only, mimicking the case of a piano string being struck with a hammer of increasing velocities, and hence exciting the string in only one polarization. The values of the case previously studied in Fig. 4 are selected. The analytical study predicts that the uncoupled solution should be stable as long as $a < 0.25$. A first case is thus studied below this limit value, with an initial condition in displacement only, with $p(t = 0) = 0.4$ and $q(t = 0) = 1e - 4$. Note that, from Eqs. (9)-(14), a factor 2 between a (resp. b) and the amplitude solution in time for $p(t)$ (resp. $q(t)$), is present, so that the limit amplitude for stability for $p(t = 0)$ is 0.5. The direct time integration is represented in Fig. 5. One can observe that below the amplitude where instability occurs, the second coordinate $q(t)$ stays at negligible values around $1e - 4$.

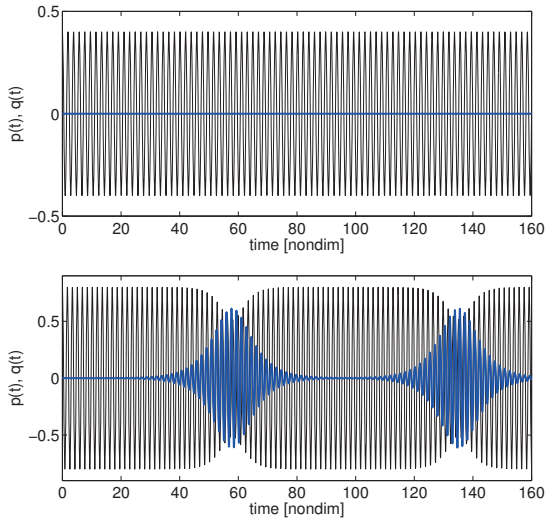

Figure 5: Time responses from direct numerical integration of Eqs. (4) and for varying levels of initial displacements $p(t = 0)$. At the top, $p(t = 0) = 0.4$, below the instability limit; at the bottom, $p(t = 0) = 0.8$, above the instability limit. Black —— line correspond to $p(t)$ and blue —— line to $q(t)$.

For an initial condition above the instability limit, $p(t = 0) = 0.8$, one can observe that an energy exchange between the two modes occurs and $q(t)$ reaches values up to 0.6. The energy then gets back and forth between the two oscillators, a typical feature of nonlinear conservative oscillations [12]. This numerical experiment confirms the instability of the uncoupled solution. It also shows that, for a given piano string, and for amplitude of excitation that are above a certain threshold that can be predicted, a motion initiated along a single polarisation can be transformed into a coupled whirling motion, as observed experimentally.

6. CONCLUSION

A detailed study has been conducted to examine the two polarisations of nonlinear vibrating strings, and to show if the geometric nonlinearity due to large-amplitude vibration can be responsible of the coupling between the two polarizations, even

though the motion is initiated along a single direction. An analytical study has been conducted using a two-modes approximation for the Kirchhoff-Carrier equation, and then the method of multiple scales. The frequency-amplitude relationships of the two polarisations and the ways whirling motion can take place are identified. The main finding of the anlytical study reveals that an imperfection is needed in order to make uncoupled solutions unstable. When all the coefficients are equal, in the mathematical case of a perfect string, then the periodic solutions are all stable. When a detuning is considered between the two eigenfrequencies, which is always the case in practice, then uncoupled solutions can become unstable and whirling motions of the string can take place even though the motion is initiated along one polarisation only. These results also clearly demonstrate that the geometric nonlinearity can be a potential cause for the whirling motions observed in real piano strings. Future work will consider experimental validations of these findings. The imperfections brought by the specific boundary conditions of the piano string will also be studied in order to assess their role in the appearance of double polarisation.

7. ACKNOWLEDGEMENT

The research work presented in this paper has been funded by the european commission within the Initial Training Network (ITN) Marie Curie action project BATWOMAN, under the seventh framework program (EC grant agreement no. 605867).

8. REFERENCES

[1] J. Chabassier, *Modélisation et simulation numérique d'un piano par modèles physiques*, Ph.D. thesis, École Polytechnique, 2012.

[2] J. Chabassier, A. Chaigne, and P. Joly, "Time domain simulation of a piano. Part 1 : model description.," *ESAIM: Mathematical Modelling and Numerical Analysis*, vol. 48, no. 05, pp. 1241–1278, 2013.

[3] J. Chabassier, P. Joly, and A. Chaigne, "Modeling and simulation of a grand piano," *Journal of the Acoustical Society of America*, vol. 134, pp. 648, 2013.

[4] G. Weinreich, "Coupled piano strings," *J. Acoust. Soc. Am.*, vol. 62, pp. 1474, 1977.

[5] T. C. Hundley, H. Benioff, and D. W. Martin, "Factors contributing to the multiple rate of piano tone decay," *J. Acoust. Soc. Am.*, vol. 64, no. 5, 1978.

[6] H. Suzuki and I. Nakamura, "Acoustics of pianos," *Applied Acoustics*, vol. 30, pp. 147, 1990.

[7] J. Burred, *The acoustics of the Piano*, Ph.D. thesis, Professional Conservatory of Music Arturo Soria, 2004.

[8] C. Karatsovis, *Acoustic Features of Piano Sounds*, Ph.D. thesis, University of Southampton, 2011.

[9] A. Chaigne, J. Chabassier, and N. Burban, "Acoustics of pianos: physical modeling, simulations and experiments," in *Proceedings of SMAC 2013, Stockholm, Sweden*, 2013.

[10] C. Touzé, O. Thomas, and A. Chaigne, "Asymmetric nonlinear forced vibrations of free-edge circular plates. part I: Theory," *Journal of Sound and Vibration*, vol. 258, pp. 649–676, 2002.

[11] O. Thomas, A. Lazarus, and C. Touzé, "A harmonic-based method for computing the stability of periodic oscillations of non-linear structural systems," in *Proceedings of the ASME 2010 IDETC conference, Montreal, Canada*, 2010.

[12] A.H. Nayfeh and D.T. Mook, *Nonlinear Oscillations*, Wiley, 1979.

[13] A. Manevitch and L. Manevitch, "Free oscillations in conservative and dissipative symmetric cubic two-degree-of-freedom systems with closed natural frequencies," *Meccanica*, vol. 38, pp. 335–348, 2003.

[14] S. Bilbao, "Conservative numerical methods for nonlinear strings," *The Journal of the Acoustical Society of America*, vol. 118, no. 5, pp. 3316–3327, 2005.

[15] T. Hélie and D. Roze, "Sound synthesis of a nonlinear string using volterra series," *Journal of Sound and Vibration*, vol. 314, no. 12, pp. 275 – 306, 2008.

[16] P. Morse and U. Ingard, *Theoretical Acoustics*, Princeton University Press, 1968.

COMPARISONS BETWEEN MEASURED AND PREDICTED VIBROACOUSTICS CHARACTERISTICS OF AN UPRIGHT PIANO SOUNDBOARD

Benjamin Trévisan, Pierre Margerit, Kerem Ege, Bernard Laulagnet
Laboratoire Vibrations Acoustique – IN SA de Lyon, France
benjamin.trevisan@insa-lyon.fr
pierre.margerit@insa-lyon.fr
kerem.ege@insa-lyon.fr
bernard.laulagnet@insa-lyon.fr

ABSTRACT

The piano soundboard is an orthotropic plate made of spruce, ribbed by multiple stiffeners (the ribs) parallel to the grain direction of the main panel's wood and two addition beams (the bridges) nearly in a perpendicular direction. This complex structure transforms the piano string vibration (coupled to the soundboard at the bridge) into sound; its vibrations and radiations are therefore of primary importance for the sound characteristics of the instrument. Several vibroacoustics models have been developed these last decades using different methodologies: finite element / numerical modeling (Berthaut et al., Applied Acoustics, 2003 ; Chaigne et al., JASA, 2013 ; Chabassier et al., JASA, 2013) or reduced models using global descriptors (Boutillon and Ege, JSV, 2013). An analytical model recently developed at LVA (Trévisan et al., ISMA 2014 / NOVEM 2015) is particularly well-adapted for a parametrical study and appears as an alternative to time-consuming numerical methodologies. The model is based on a variational approach that takes into account plate and superstructures energies. The soundboard vibration is decomposed on the corresponding orthotropic simply supported unribbed plate modes. The aim of this analytical tool is ultimately to help piano manufacturers to predict the influence of structural modifications of the soundboard (number/dimensions of ribs/bridges…) on the sound of the instrument. In order to validate the methodology and hypotheses done in the analytical model, we present and compare in this communication measured/predicted vibroacoustics quantities obtained for a same structure and under same (supposed) conditions: a Pleyel P131 upright piano soundboard fixed on its wooden rim. The quantities compared are modal basis in the low-frequency domain [0-400Hz] and point mobility along the bridge for a larger frequency band [0-5kHz]. Results on vibrations are very satisfying demonstrating the validity of the model. Experimental radiation results (soundboard radiated power) will also be given and compared to predicted quantities.

ENERGY ANALYSIS OF STRUCTURAL CHANGES IN PIANOS

Antoine Chaigne

Institute of Music Acoustics
University of Music and Performing Arts
Vienna, Austria
chaigne@mdw.ac.at

Juliette Chabassier, Marc Duruflé

Magique 3D Team
Inria Bordeaux Sud Ouest, France
juliette.chabassier@inria.fr
marc.durufle@inria.fr

ABSTRACT

The leading idea of this theoretical paper is to examine the effects of structural changes in the piano on the basis of energetic quantities relative to its constitutive parts. These energies are global quantities which characterize the intrinsic properties of the instrument, irrespective of the observation point. The evolution of the various energy terms with time are calculated with a help of a recent piano model which couples together the hammer, the nonlinear strings, the soundboard and the acoustic space [1]. Some parameters, which play a major role in the history of the piano are particularly examined: string tension and diameter, soundboard thickness and rigidity, hammer mass and velocity. The results show that direct links can be established between the energetic quantities and the tonal properties of the piano sounds, in terms of temporal envelope and spectral content. They also shed useful light on the energy exchange between the constitutive parts of the instrument, and on its acoustical efficiency. This study is intended to have potential applications as a theoretical guideline for piano making, restoration and reproduction of historic instruments.

1. INTRODUCTION

This paper reports the first part of a study, whose aim is to establish links between physical construction parameters and sound properties in pianos. The leading idea of the project is to investigate to what extent the future sound qualities of a piano can be predicted by a set of geometrical and material data related to its different constitutive parts and on their assembly conditions. The results of this study could be used for the initial sketch in the design of a new instrument, and for prediction of the effects of structural changes in piano restoration. It should also be useful for a better understanding of the evolution of sound quality in piano history.

Twenty years ago, a systematic exploration of piano parameters was done by the author, though this study was restricted to the string-hammer system only [2]. More recently, French developed a theoretical framework for describing the effects of structural modifications in the soundboard-soundbox system in guitars [3]. Here, the study is based on a recent piano model developed by Chabassier which couples together the nonlinear strings, the hammer, the vibrating soundboard and the acoustic field [4, 1].

This piano simulation model is discretized in time and space and yields, as a result, the time history of a number of physical quantities: sound pressure, soundboard vibrations, strings and hammer motion, energetic quantities. It allows the variation of one single geometrical or material parameter at a time, independently of the others. The model is based on a *dynamical* (and not *static*) behavior of the instrument. This enables us to investigate the effects of structural changes that would often be impossible to achieve in the reality. However, in its present state, the model does not have the capacity of reproducing all the necessary fine adjustments made in the development of a real piano. In this respect, it can be viewed as a complementary tool of the usual piano design procedure in a workshop.

In this paper, focus is put on energetic vibratory and acoustic quantities. These quantities are obtained through spatial integration of the dynamic variables in each domain of the constitutive elements of the piano. As a result, we obtain functions of time, only. The advantage of examining such quantities is that is yields a *global* assessment of the instrument as a source, irrespective of the listening (or recording) point. They also shed useful light on the energy exchanges due to the coupling between all parts of the instruments.

The paper starts with a summary of the model, which has already been described elsewhere extensively [4, 1]. Attention is paid to energetic quantities which are thereafter thoroughly discussed. The results are given for one single note (Steinway D, C♯5, Nr 53, fundamental f_1=555 Hz). The study is concentrated on some selected parameters of strings (tension at rest, diameter), hammer (mass, striking velocity) and soundboard (thickness, elasticity). These parameters are known to have important effects on piano tones, and have evolved significantly in the history of piano making [5, 6]. However, as far as we are aware, they have not been yet the subject of any systematic theoretical study in the past, essentially because of the absence of a reliable model where the main elements of the piano are coupled together.

2. MODEL AND METHOD

2.1. Model

In its present state, the piano model starts with the impact of a hammer of mass M_H with initial velocity V_H on a string (or on a set of 2 to 3 strings, depending on the note). The complex mechanism that transmits the action of the player from key to hammer is ignored. The strings vibrate both transversely and longitudinally, these two regimes being non-linearly coupled. Transverse and longitudinal string forces are transmitted to the soundboard at the bridge. The soundboard is modeled as a dissipative orthotropic Reissner-Mindlin plate. The ribs and bridges are modeled as local heterogeneities in thickness and rigidity (see Figure 1). The soundboard radiates sound in a closed box surrounding the instrument (see Figure 2). The other parts of the instrument are assumed to be rigid. The box is delimited by absorbing regions (Perfectly Matched Layers, or PML) so that no outgoing waves return back to the piano.

The equations of the model are discretized in time and space. The stability criteria of the numerical formulation are based on energy conservation. The input set of parameters of the simu-

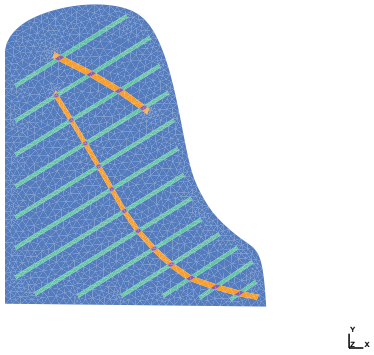

Figure 1: Model of a Grotrian-Steinweg soundboard. The ribs and bridge are modeled as local heterogeneities in thickness and rigidity.

lations is composed of the geometrical and material data of the constitutive elements of the piano: hammer, strings, soundboard and air (see Table 1). The main output files are physical functions of time (string displacement, hammer force, soundboard acceleration, sound pressure, energetic quantities) and most of them can be heard after appropriate digital-to-analog conversion, which allows an auditory evaluation of the structural modifications. Soundboard's eigenfrequencies and mode shapes also are available. In total, the numerical model requires heavy calculations. As an example, the order of magnitude for the number of degrees of freedom (dof) is 1.4×10^5 for the soundboard, and 2.3×10^7 for the acoustic space.

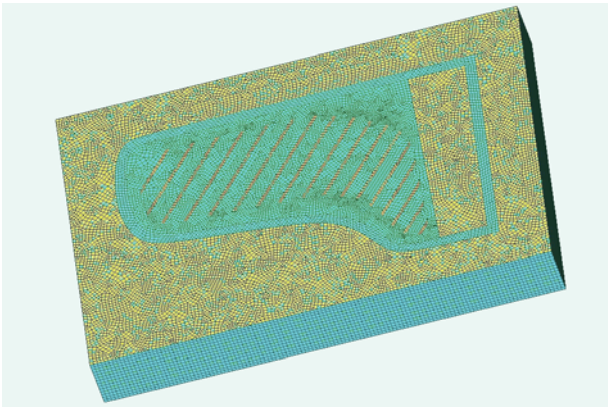

Figure 2: Closed box delimiting the acoustic field radiated by a Steinway D piano (seen from bottom). The box is delimited by absorbing regions (PML).

The equations of the model and their numerical treatment were presented in detail in previous papers, and will not be developed further here [4, 1]. However, since the results and the discussion that follows mainly refer to energetic quantities, these expressions are now briefly reviewed.

2.2. Energetic quantities

At the origin of time, the initial energy imparted to the piano is the kinetic energy of the hammer:

$$\mathcal{E}_0 = \frac{1}{2} M_H V_H^2. \tag{1}$$

The energy of the constitutive elements of the piano are obtained through spatial integration over their respective domains. As a result, we obtain the evolution with time of a scalar quantity that fully characterizes each element, irrespective of the observation point. For simplicity, the dissipation terms are ignored in the energetic quantities given in this section, although these terms are present in the simulations. The expression of the various sources of losses in the piano model are reviewed in the Appendix (see Section 6).

2.2.1. String energy

The energy $\mathcal{E}_s(t)$ of a non-dissipative nonlinear string s is given by:

$$\mathcal{E}_s(t) = \mathcal{E}_{s,kin}(t) + \mathcal{E}_{s,pot}(t) \tag{2}$$

where the kinetic energy is:

$$\begin{aligned}\mathcal{E}_{s,kin}(t) = {} & \frac{\rho A}{2} \int_0^L \left(\frac{\partial u_s}{\partial t}\right)^2 dx \\ & + \frac{\rho A}{2} \int_0^L \left(\frac{\partial v_s}{\partial t}\right)^2 dx + \frac{\rho I}{2} \int_0^L \left(\frac{\partial \varphi_s}{\partial t}\right)^2 dx,\end{aligned} \tag{3}$$

and the elastic potential energy [7]:

$$\begin{aligned}\mathcal{E}_{s,pot}(t) = {} & \frac{T_0}{2} \int_0^L \left(\frac{\partial u_s}{\partial x}\right)^2 dx + \frac{EA}{2} \int_0^L \left(\frac{\partial v_s}{\partial x}\right)^2 dx \\ & + \frac{EI}{2} \int_0^L \left(\frac{\partial \varphi_s}{\partial x}\right)^2 dx + \frac{AG\kappa}{2} \int_0^L \left(\frac{\partial u_s}{\partial x} - \varphi_s\right)^2 dx \\ & + (EA - T_0) \int_0^L \left[\frac{1}{2}\left(\frac{\partial u_s}{\partial_x}\right)^2 + \right. \\ & \left. \left(1 + \frac{\partial v_s}{\partial x}\right) - \sqrt{\left(\frac{\partial u_s}{\partial x}\right)^2 + \left(1 + \frac{\partial v_s}{\partial x}\right)^2}\right] dx,\end{aligned} \tag{4}$$

In these expressions, u_s is the vertical transverse displacement, v_s the longitudinal displacement and φ_s the rotation of the cross-sections. The string is defined by the following parameters: length L, density ρ, cross-sectional area A, flexural inertia I, tension at rest T_0, Young's modulus E, torsional modulus G, and shear correction factor κ (Timoshenko's parameter). Examples of parameters are given in Table 1 for the note C♯5. In the absence of internal dissipation, and for no coupling with air and soundboard, $\mathcal{E}_s(t)$ is constant after the hammer has left the string, and is then equal to the total energy imparted by the striking hammer.

2.2.2. Hammer energy

The hammer strikes the string at position x_H. As a result, the hammer force F_H imparted to the string is described by:

$$F_H(t) = K_H \Phi\big(\langle u_s \rangle(t) - \xi(t)\big). \tag{5}$$

where K_H is a stiffness coefficient, and Φ is a standard nonlinear power function of the distance d between the hammer position ξ and the position of the string $\langle u_s \rangle$ averaged over the length of the hammer-string contact [8, 9]. The force F_H is limited in time to the instants where the hammer is in contact with the string i.e., when the string-hammer distance is smaller than the reference distance obtained when the string is just touching the undeformed felt, at the origin of time. Defining then further the function $\Psi(d) = \int_d^{+\infty} \Phi(s)\, ds$, one can

show that the energy of the hammer interacting with the string s is written [4]:

$$\mathcal{E}_H(t) = K_H \Psi\big(\langle u_s \rangle(t) - \xi(t)\big) + \frac{M_H}{2}\left(\frac{d\xi}{dt}(t)\right)^2. \quad (6)$$

This expression again is valid for a non-dissipative hammer only. In the model, a dissipative term is added to the stiffness term in Eq. (5) to account for the relaxation of the felt (see Appendix).

2.2.3. Soundboard energy

Similarly to the strings, the energy $\mathcal{E}_p(t)$ of the soundboard is:

$$\mathcal{E}_p(t) = \mathcal{E}_{p,kin}(t) + \mathcal{E}_{p,pot}(t) \quad (7)$$

where the kinetic energy is:

$$\mathcal{E}_{p,kin}(t) = \iint_\omega \rho_p\, \delta \left(\frac{\partial u_p}{\partial t}\right)^2 dx\, dy + \iint_\omega \rho_p \frac{\delta^3}{12} \left|\frac{\partial \underline{\theta}_p}{\partial t}\right|^2 dx\, dy, \quad (8)$$

and the elastic potential energy:

$$\mathcal{E}_{p,pot}(t) = \iint_\omega \frac{\delta^3}{12} \mathbf{C}\, \underline{\varepsilon}(\underline{\theta}_p) : \underline{\varepsilon}(\underline{\theta}_p)\, dx\, dy + \iint_\omega \delta\, \underline{\kappa}^2 \cdot \underline{G}\, |\underline{\nabla} u_p + \underline{\theta}_p|^2 dx\, dy. \quad (9)$$

Here, ρ_p is the density of the soundboard, and δ its thickness. Both quantities can be space-dependent, which is necessary for representing brigdes and ribs. u_p is the transverse displacement, $\underline{\theta}_p$ is the local rotation vector, and $\underline{\varepsilon}$ is the linearized strain tensor. $\mathbf{C}$ is an orthotropic elasticity tensor which, again, depends on space. This tensor can then also account for the presence of bridge and ribs. It is easily possible to modify this tensor in order to change the elastic properties of the soundboard (consecutive to a pre-stress due to the crown, for example) without changing its mass. In the simulations, additional terms account for the dissipation inside the material.

2.2.4. Acoustic energy

Finally, the acoustic energy $\mathcal{E}_a(t)$ radiated by the instrument is given by:

$$\mathcal{E}_a(t) = \iiint_\Omega \frac{\rho_a}{2} |\underline{v}_a|^2\, dx\, dy\, dz + \iiint_\Omega \frac{\mu_a}{2} p^2\, dx\, dy\, dz, \quad (10)$$

where ρ_a is the air density, and μ_a its compressibility. $\underline{v}_a$ is the acoustic velocity and p is the sound pressure.
All energetic quantities (2)-(4) and (5)-(10) yield valuable insight into the time history of the transmission of energy from string to soundboard, and, in turn, from the soundboard to the acoustic space, over the duration of a piano tone. Derivations of these quantities versus time allow further to describe the phenomena in terms of power. From the ratio between soundboard and total energy (resp. between acoustic and total energy), we gain useful information on the vibrational (resp. acoustical) efficiency of the instrument, and on the variations of these efficiencies consecutive to structural modifications.

2.3. Selection of notes and parameters

The program is able to simulate the 88 notes of a modern grand piano. Amongst these, particular notes were simulated in the past and compared for validation to measurements on a Steinway D grand piano: D♯1, C2, F3, C4, C♯5, G6 (see [1]). Other measurements on a large variety of pianos are currently under way. The objective of the present paper is not to reproduce one given instrument, but rather to exhibit the main principles of energy analysis. Therefore, the effects of structural changes are analyzed below for one single note (C♯5), and for a simple soundboard of constant thickness. Refined modifications related to ribs and bridges are left for a future report. The investigated modifications reported here are inspired by the main tendencies observed in the history of piano making. In addition, the change of parameters were selected to be made easily in the present version of the simulation program.

- The variation of string tension is a key feature observed in the history piano making. In the past, low string tension was imposed because it was entirely withstood by the soundboard. With the evolution of more powerful and louder instruments, the strings of modern pianos are now fixed on cast iron frames, thus allowing higher tension. In order to keep the same pitch in the present study, the diameter of the strings is modified so that the transverse velocity of the waves is kept constant. The inertia coefficient is modified accordingly.
- Another currently observed evolution is related to the mass of the hammers, which generally tend to increase throughout the history of piano making. The initial velocity of the hammer is also used as a varying parameter, for comparison.
- The thickness δ of the soundboard is an essential parameter which influences both its mass and rigidity. As a consequence, it has an extreme influence on the transmission of energy from strings to soundboard and from soundboard to air. A fortunate aspect of the present piano model lies in the possibility of modifying this parameter over a wide range of values, without considering the consequences in terms of soundboard weakness and risks of breaking. Since the prime purpose here is to observe the physical consequences of structural modifications, the range of thickness goes here far beyond those observed on real pianos.
- In our model, the rigidity of the soundboard can also be modified, independently from its mass and structure, just by modifying the elastic constants. This might correspond to *virtual* materials, but also to the effect of crown in real pianos. It is generally admitted that increasing the soundboard rigidity contributes to produce a louder sound, and thus we want to verify this point and quantify it in terms of physical quantities.

3. RESULTS AND DISCUSSION

The numerical simulations reported below are made for a "complete" piano, where the 3 strings (note C♯5) are coupled to a Steinway D grand piano soundboard (without ribs and bridges), this soundboard being coupled to the acoustic field. The other parts of the piano (case, keybed, frame) are supposed to be rigid. The sound duration is 1 s. A list of the main parameters for the note C♯5 is given in Table 1.

3.1. Variations of string tension and diameter

Figure 3 shows the time evolution of the total energy of the piano, for three different tensions of the strings. All other parameters remain unchanged, except the diameter of the string which varies in proportion to the square root of the tension in order to keep the same pitch. All three curves start with the

Hammer	
Mass M_H	7.9 g
Velocity V_H	3 m/s
Stiffness K_H	2.8 10^{10} SI-units
Striking position x_H	0.039 m
String	
Length L ($\times$ 3)	0.3255 m
Cross-sectional area of strings A	6.66 10^{-7} m^2
Tension T_0	687 N
Density ρ	7850 kg/m^3
Young's modulus E	2.0 10^{11} N/m^2
Torsional modulus G	8.0 10^{10} N/m^2
Shear correction factor κ	0.85
Moment of inertia I	3.5 10^{-14} m^4
Soundboard (Spruce)	
Density ρ_p	380 kg/m^3
Thickness δ	10 mm
Longitudinal modulus E_L	11.0 10^9 N/m^2
Transverse modulus E_T	650 10^6 N/m^2

Table 1: Main parameters used for the reference note C♯5.

same initial energy ($\mathcal{E}_0 = 0.0355$ J) imparted by the hammer. The middle curve corresponds to the nominal tension $T_0 = 687$ N, while the upper and the lower curves correspond to $T_0/2$ and $3T_0/2$, respectively. The three curves show a more or less rapid decrease up to 0.1 s, and then stabilize. However, the initial decrease is much more pronounced for the nominal and high tension that for the low tension. For low tension, the energy is maintained longer confined in the strings.

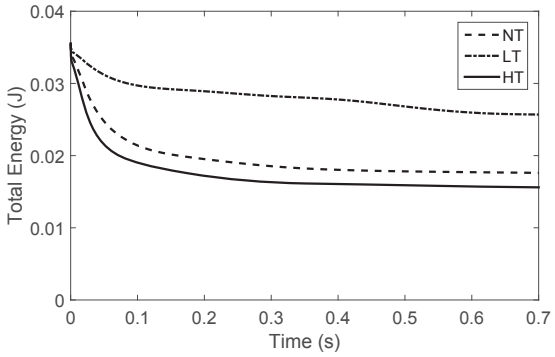

Figure 3: Time evolution of the total energy of the piano for three different tensions of the strings. Note C♯5. Upper curve: $T_0/2$ (Low Tension); middle curve: T_0 (Normal Tension); lower curve: $3T_0/2$ (High Tension).

This result is a direct consequence of the impedance matching at the bridge. As seen in Figure 4, the maximum of the relative soundboard energy ratio follows the same order as the tensions, which shows that more string energy is transmitted to the soundboard when the tension is higher. Another significant feature of this figure is that the soundboard energy is damped more rapidly for high string tension than for low tension, which means that the structural and radiation losses are higher in relative value. This can be explained by the fact that both the internal viscoelastic losses in the soundboard and the radiated energy vary as the square of the velocity (see Appendix).

Finally, it is seen in Figure 4 that the relative acoustic energy radiated by the piano follows the same time evolution as the soundboard, for each tension. This is due to the fact that the soundboard is identical in the three cases.

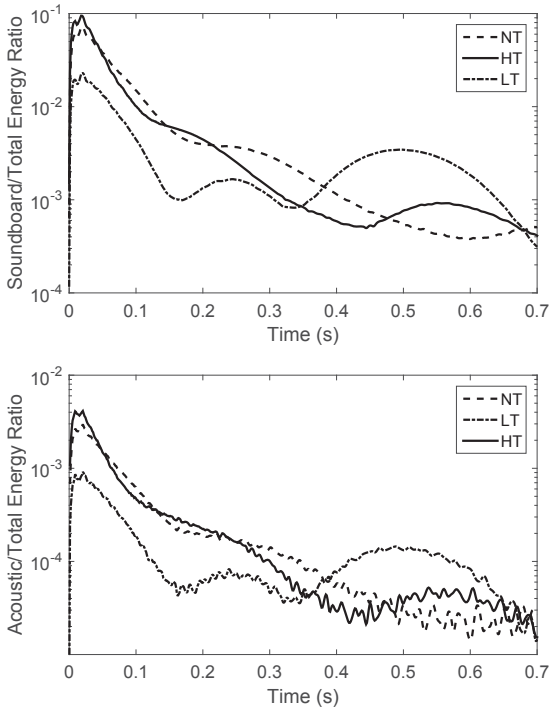

Figure 4: Time evolution of the relative soundboard energy (top) and acoustic energy (bottom) for three different tensions of the strings. High tension: solid line; normal tension: dashed line; low tension:dash-dotted line. Note C♯5.

Simulations of the sound pressure at a given fixed point in space (z=38 cm above the soundboard) are coherent with these results (see Figure 5). For this figure, as for the following ones, the origin of the axes ($x = 0$, $y = 0$, $z = 0$) is situated on the lowest left corner of the soundboard (bass range). As expected, the maximum of the pressure increase with strings' tension, and the decay time is longer for low tension. This result is of prime importance, since the pressure is the acoustic variable that we hear. However, from the point of view of piano manufacturing, the results based on energy considerations presented in Figure 4 have a more general meaning, since they are valid for the instrument (the sound source) as a whole.

3.2. Variations of soundboard thickness and rigidity

In this section, the energetic quantities and sound pressure envelopes are compared for three different soundboards: the reference soundboard (TSB) whose parameters are listed in Table 1, a thin soundboard (VTSB) of thickness δ= 7 mm, and a rigid soundboard (RIG) with the reference thickness, but where all elasticity moduli are multiplied by a factor of 2.

Figure 6 illustrates the effects of thickness and rigidity changes on the eigenfrequencies of the three soundboards. In each case, the simulations are made taking the 800 first modes of the soundboard into account. The theory predicts that the asymptotic modal density is nearly inversely proportional to the thickness and to the square root of the elasticity moduli [10]. This is coherent with the results obtained here, where the maximum frequency of the modes for the thin soundboard is 3413 Hz, i.e, 0.8 times the 800th eigenfrequency of the reference soundboard (4229 Hz). Similarly, the 800th eigenfrequency of the rigid soundboard is 5981 Hz, which is 1.4 times higher than the

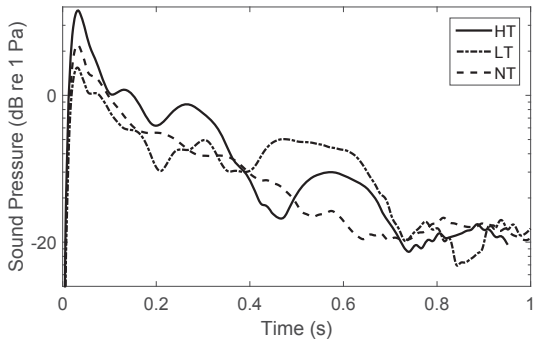

Figure 5: Time envelope of the sound pressure at a point of coordinates (x=0.85; y=1.46; z=0.38) m for three different strings' tensions. The x-axis is parallel to the keys, the y-axis is perpendicular to it in the soundboard plane, and the z-axis is perpendicular to the soundboard. The origin of the axes is at the lowest left corner of the soundboard (bass side). High tension ($3T_0/2$): solid line; normal tension (T_0): dashed line; low tension ($T_0/2$): dash-dotted line.

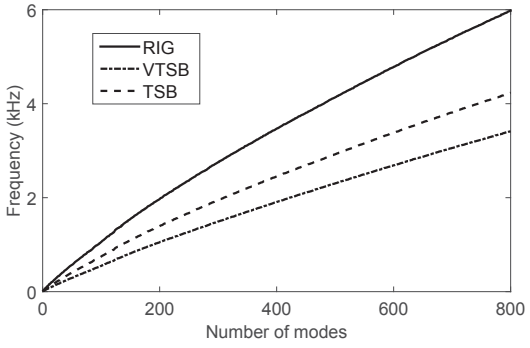

Figure 6: Soundboard eigenfrequencies in three different cases: Reference (TSB, dashed line), thin soundboard (VTSB, dash-dotted line), rigid soundboard (RIG, solid line).

reference soundboard. Before moving to other considerations, let us point out that these modifications of the eigenspectrum are responsible for changes in tone color since most of the soundboard modes are excited during the transients of piano tones.

Figure 7 shows the time evolution of energy ratios for the three soundboards during the initial part of a piano tone (0.4 s). The thin soundboard (VTSB) has the highest soundboard/total energy ratio, and its maximum is reached the most rapidly (after 14 ms). This is due to the fact that the velocity profile of this soundboard is higher than for the reference one. However, this ratio also shows the most rapid decrease, again because the losses in the soundboard increase with the square of the velocity (see Appendix). The rigid soundboard (RIG) also has more energy than the reference one (TSB), due this time to an increase in potential elastic energy (see Eq. 9), and its decay times lies between the two others. Examining now the acoustic/total energy ratios shows substantial differences: here the rigid soundboard generates almost the same acoustic energy as the thin one, but this energy lasts significantly longer. As shown in the bottom of the figure, this result is due to a more efficient structural-acoustic coupling for the rigid soundboard than for the others, and less rapid losses. This is in accordance with the general theory of vibroacoustics which predicts that the

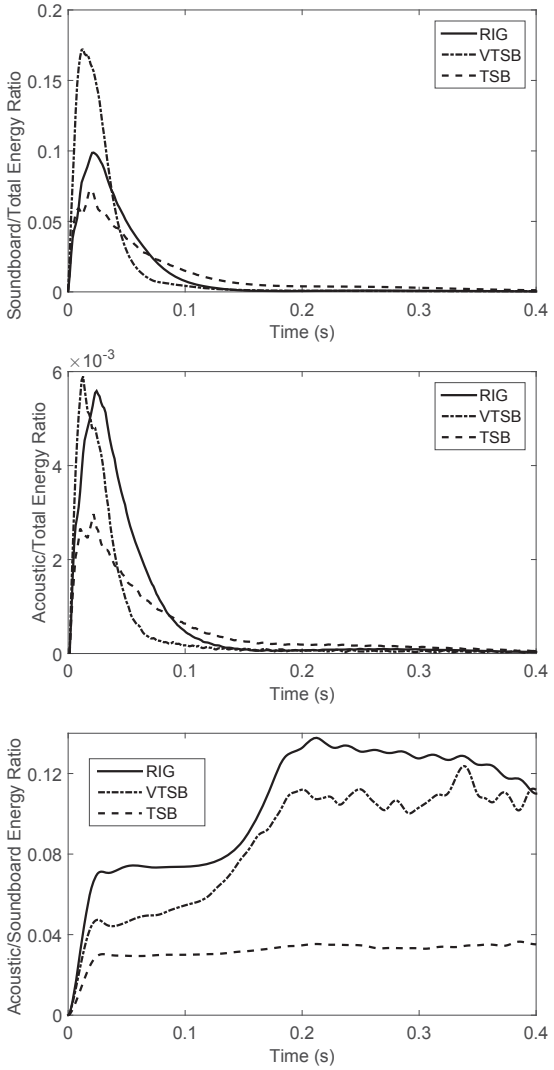

Figure 7: (Top) soundboard energy vs total energy. (Middle) radiation efficiency of the instrument: Ratio acoustic energy vs total energy. (Bottom) Vibroacoustic coupling: ratio acoustic energy vs soundboard energy. Time evolution. TSB (dashed line): reference soundboard; VTSB (dash-dotted line): thin soundboard; RIG (solid line): rigid soundboard.

acoustical efficiency of a plate increases with the stiffness [11]. In this presented case, the gain in acoustical efficiency due to stiffness exceeds the decrease due to reduction of the mean velocity, compared to the thin soundboard. In piano making, it is well-known that imposing an initial dome shape (or crown) to the soundboard is a good way to enhance the radiation of the instrument through increase of stiffness, without change of mass. Attaching ribs to the soundboard produces similar effects, though with a slight increase of mass.

The results based on energy considerations for the source are confirmed on the time envelope of the sound pressure at the point of coordinates (x=0.85; y=1.46; z=0.38) m (see Figure 8). For this particular selected point, the rigid plate yields the louder sound. Although it decreases faster than the reference sound during the initial transient, it stays in average louder for the entire duration of the tone. The sound pressure simulated with the thin soundboard also starts with a louder sound than the reference one but, in this latter case, it decays significantly

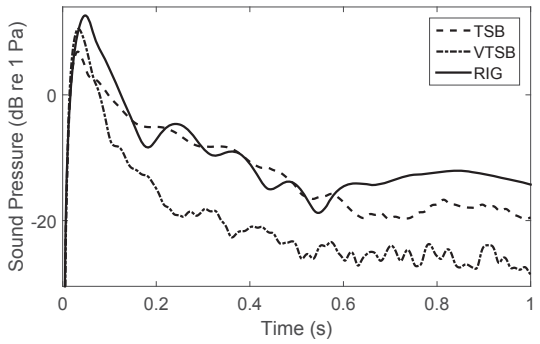

Figure 8: Time envelope of the sound pressure at the point of coordinates (x=0.85; y=1.46; z=0.38) m for three soundboards. Solid line: rigid soundboard (RIG); dashed line: reference soundboard (TSB); dash-dotted line: thin soundboard (VTSB).

faster.

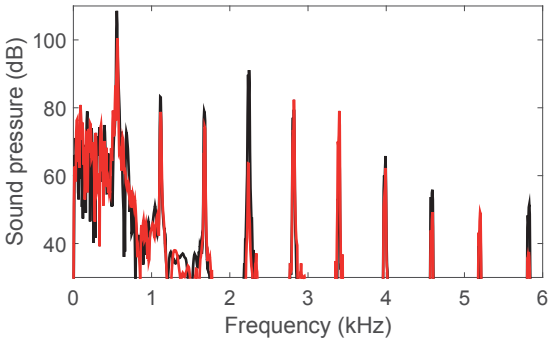

Figure 9: Spectra of the sound pressure simulated at the point of coordinates (x=0.85; y=1.46; z=0.38) m. Initial transient (duration 0.4 s). RIG (black) and VTSB (red) soundboards.

Modifying the properties of the soundboard has additional consequences on the sound spectrum. Figure 9 shows a comparison between the spectra calculated at the same point in space for the rigid and thin soundboards, respectively. In accordance with the eigenfrequencies displayed in Fig. 6, we can see on the lower part of the initial transient spectra that the excited frequency band of the soundboard modes is broader for the rigid soundboard than for the thin one. Similarly, on the upper part of the spectra, it can be seen that the magnitude of the strings' partials is higher in the rigid case compared to the thin one. Both these two effects contribute to substantially change the timbre of the tones. This is confirmed when listening to the simulated sound pressure.

3.3. Variations of hammer mass and velocity

In this section some properties resulting from changes in hammer mass and/or initial velocity are investigated. Such modifications have many consequences on piano tones. However, due to the lack of place, we limit ourselves to their effects in terms of acoustical efficiency. Figure 10 shows the evolution of the total energy of the sound (note C♯5) for three different situations: the reference case, a hammer with normal velocity and mass divided by 2, and a hammer with normal mass whose initial velocity divided by 2. In contrary with the previous situations

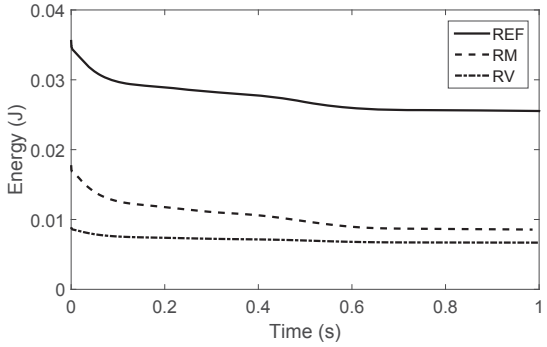

Figure 10: Temporal evolution of the total energy for the note C♯5. Solid line: reference case (REF); dashed line: reduced hammer mass $M_H/2$ (RM); dash-dotted line: reduced initial velocity $V_H/2$ (RV).

(variations of string's tension and soundboard properties) the initial energy is different in the three cases, according to Eq. 1. While Figure 10 does not show salient effects, it is not the case

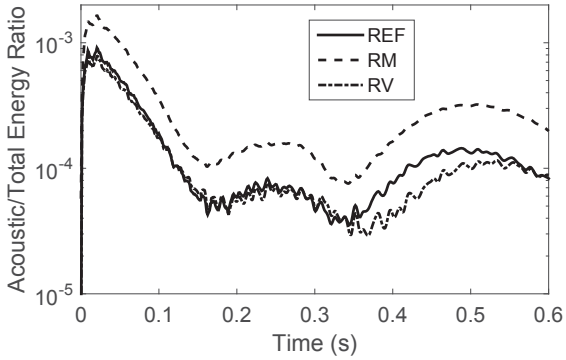

Figure 11: Relative acoustic energy. Solid line: reference case; dashed line: reduced hammer mass $M_H/2$; dash-dotted line: reduced initial velocity $V_H/2$.

for Figure 11 which shows the relative acoustic efficiency of the selected piano note in these three cases. Surprisingly, the hammer with reduced mass yields a significantly higher relative acoustic energy, whereas this relative energy only slightly depends on the hammer velocity. The relative soundboard energy (not shown here) shows similar features so that one has to seek upstream in the transmission chain of the piano, at the hammer-string level, for understanding this effect. In fact, as pointed out by the author in a previous study [2], reducing the hammer mass not only results in a decrease of the maximum hammer force, but also in a decrease in the hammer force duration, as seen in Figure 12. In contrast, reducing the hammer velocity induces almost only a reduction of force amplitude, with only a slight increase in the duration of the force pulse. As a consequence of pulse shortening, the slopes of the string's displacement increase. Since the force at the bridge is nearly proportional to the first spatial derivative of the displacement, it can be seen in Figure 13 that the bridge force pulses for the small hammer mass case have nearly the same amplitude as the reference one. In conclusion, this explains why both the soundboard and acoustic energy are comparable in these two cases. Finally, since the input energy is smaller in the case of reduced hammer mass, the soundboard and acoustic relative energy ratios are higher.

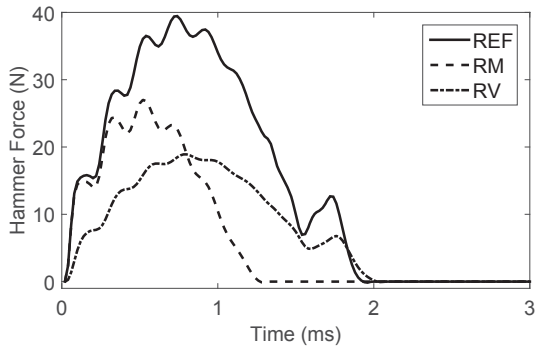

Figure 12: Hammer forces. Solid line: reference case; dashed line: reduced hammer mass $M_H/2$; dash-dotted line: reduced initial velocity $V_H/2$.

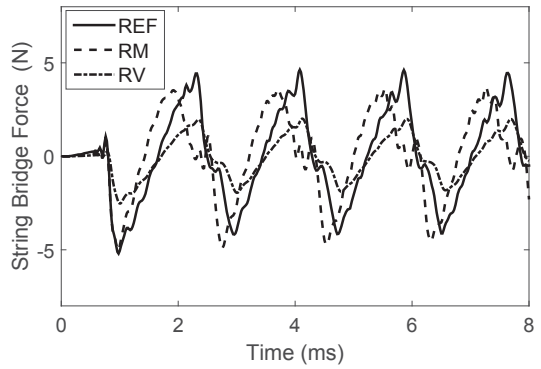

Figure 13: String forces at the bridge. Solid line: reference case; dashed line: reduced hammer mass $M_H/2$; dash-dotted line: reduced initial velocity $V_H/2$.

4. CONCLUSIONS AND FUTURE WORK

In this paper, the effects of structural changes related to hammers, strings and soundboard in a piano were analyzed in terms of energy. From the time evolution of acoustic, soundboard and total energies, it was shown how elementary modifications of structures affect the amplitude, decay time and spectral content of the sounds radiated by the piano. This analysis shed useful light on the energy transfer from strings to soundboard and air. One objective is to take advantage of these preliminary results to analyze real instruments in a historical perspective. It can be seen on historic pianos that several of the previously examined features coexist. Pianos built during the first half of the nineteenth century, for example, are characterized by reduced string tension, reduced hammer mass and thin soundboard, compared to modern pianos. One goal is then to measure and quantify the tonal differences between historic and modern instruments, and to relate them to intrinsic differences of structures. Another natural extension of this study is to use energy analysis for investigating refined aspects of piano manufacturing, such as the design of ribs and bridges, the choice of strings' material and the use of leather for the piano hammers.

The work presented in this paper was motivated by the interest to bring some light into the *global* energetic behavior of the piano. However, the *local*, or *note by note*, consequences of structural changes should not be forgotten. It has been seen, for example, that the eigenfrequencies of the soundboard increase with its rigidity. As a consequence, the soundboard mobility will vary over a large frequency range significantly. This feature might induce some heterogeneities in the strings-soundboard coupling and, in turn, in the sound quality.

The piano model used in this study is characterized by an accurate description of the losses, for each element (see the Appendix below). The modal approach used for the soundboard, in particular, allows a mode by mode adjustment of the damping. This feature should facilitate the simulation of soundboards made of different materials, and their comparisons in terms of tone quality. Finally, from a theoretical point of view, an important work remains to be done in order to determine to what extent the losses in strings and soundboard depend on their geometry, so that adjustments can be done in the model accordingly.

5. ACKNOWLEDGEMENTS

This project was supported by a Lise-Meitner-Fellowship of the Austrian Science Fund (FWF) [Project number M 1653-N30].
Numerical experiments presented in this paper were carried out using the PLAFRIM experimental testbed, being developed under the Inria PlaFRIM development action with support from LABRI and IMB and other entities: Conseil Régional d'Aquitaine, FeDER, Université de Bordeaux and CNRS (https://plafrim.bordeaux.inria.fr/).

6. APPENDIX: ENERGY LOSSES IN THE PIANO

This section summarizes, without demonstrations, the lossy terms used in the model for describing the dissipation phenomena in hammers, strings and soundboard. For simplicity, the expressions below are given in the case of a single string. The reader can refer to previous papers for details on the calculations, and for a more general formulation of the losses [1, 4].

6.1. Losses in a string

In order to account for frequency-dependent losses in a string in a convenient way, additional terms of the form:

$$r_u \frac{\partial u_s}{\partial t} - \eta_u \frac{\partial^3 u_s}{\partial t\, \partial x^2} \tag{11}$$

are added in the string equation [12]. The coefficients r_u and η_u are usually derived from experiments. Similar expressions are used for v_s and φ_s. As a consequence, one can show that the rate of energy loss for the transverse motion of the string is given by:

$$\frac{d}{dt}\mathcal{L}_u = r_u \int_0^L \dot{u}_s^2 \, dx + \eta_u \int_0^L \frac{d\dot{u}_s}{dx}^2 dx, \tag{12}$$

with analog expressions for v_s and φ_s. In total, the rate of energy in the string is given by:

$$\frac{d}{dt}\mathcal{E}_s = K_H \langle \dot{u}_s \rangle \Phi\big(\langle u_s \rangle(t) - \xi(t)\big) - \frac{d}{dt}\mathcal{L}_s \tag{13}$$

where the first term on the right-hand side accounts for the transfer of energy from hammer to string, and where the sum of energy losses in the string is of the form:

$$\mathcal{L}_s = \mathcal{L}_u + \mathcal{L}_v + \mathcal{L}_\varphi. \tag{14}$$

6.2. Losses in the hammer-string system

In order to account for the relaxation losses in the hammer felt, a dissipative term of the form

$$R_H \frac{d}{dt}\Phi\big(\langle u_s\rangle(t) - \xi(t)\big) \tag{15}$$

is added on the right-hand side of Eq. (5). Due to the action-reaction law, the energy gained by the string is now compensated by a decrease of hammer energy. As a consequence, taking further string and hammer losses into account, leads to the following energy rate for the isolated hammer-string system:

$$\begin{aligned} &\frac{d}{dt}\mathcal{E}_{s,H} = -\frac{d}{dt}\mathcal{L}_s - \frac{d}{dt}\mathcal{L}_H \\ &\text{with } \frac{d}{dt}\mathcal{L}_H = R_H\Phi'\big(\langle u_s\rangle(t) - \xi(t)\big)\left[\langle \dot{u}_s\rangle - \dot{\xi}\right]^2, \end{aligned} \tag{16}$$

where $\mathcal{L}_H$ is the energy loss in the hammer felt. When the hammer-string system is coupled to the soundboard at the bridge, an additional source of loss has to be considered for this system, as shown below.

6.3. Losses in the soundboard

In the present model, a modal approach is applied to the soundboard. The soundboard modes are calculated first, and the internal losses are assumed to be small enough so that each modal displacement q_n is described by a damped oscillator equation of the form:

$$m_n\ddot{q}_n + r_n\dot{q}_n + k_n q_n = f_n, \tag{17}$$

where f_n is the modal projection of the string force at the bridge. For each soundboard mode, the rate of energy is given by:

$$\frac{d}{dt}\mathcal{E}_{p,n} = f_n\dot{q}_n - r_n\dot{q}_n^2. \tag{18}$$

In total, since the modes are assumed to be decoupled, the rate of energy for the soundboard becomes:

$$\frac{d}{dt}\mathcal{E}_p = \sum_{n=1}^{N} f_n\dot{q}_n - \sum_{n=1}^{N} r_n\dot{q}_n^2 = \frac{d}{dt}\mathcal{E}_B - \frac{d}{dt}\mathcal{L}_p, \tag{19}$$

where $\mathcal{E}_B$ is the coupling energy between the string and the soundboard at the bridge, and $\mathcal{L}_p$ is the loss of energy in the soundboard. The energy of the soundboard is truncated to N modes (N=800 for the examples given in the present paper, see Fig. 6). To ensure the conservation of energy for the string-hammer-soundboard system, the rate $-\frac{d}{dt}\mathcal{E}_B$ has to be added in the right-hand side of Eq. (16). Finally, when the soundboard is coupled to the acoustic space, it is subjected to a loss rate of acoustic energy of the form $-\frac{d}{dt}\mathcal{E}_a$ to be added in the right-hand side of Eq. (19).

6.4. Decreasing energy for the complete piano

In summary, we can write the following balance of energy for all constitutive parts of the piano:

$$\begin{aligned} \frac{d}{dt}\mathcal{E}_{s,H} &= -\frac{d}{dt}\mathcal{L}_H - \frac{d}{dt}\mathcal{L}_s - \frac{d}{dt}\mathcal{E}_B, \\ \frac{d}{dt}\mathcal{E}_p &= \frac{d}{dt}\mathcal{E}_B - \frac{d}{dt}\mathcal{L}_p - \frac{d}{dt}\mathcal{E}_a. \end{aligned} \tag{20}$$

By summation, we find the total energy rate:

$$\begin{aligned} \frac{d}{dt}\mathcal{E}_{tot} &= \frac{d}{dt}\left(\mathcal{E}_{s,H} + \mathcal{E}_p + \mathcal{E}_a\right) \\ &= -\frac{d}{dt}\left(\mathcal{L}_s + \mathcal{L}_H + \mathcal{L}_p\right). \end{aligned} \tag{21}$$

Finally, through integration of Eq. (21), and considering further that the total energy is equal to $\mathcal{E}_0$ at the origin of time, while the lossy terms are equal to zero, we find:

$$\mathcal{E}_{tot}(t) = \mathcal{E}_0 - \left(\mathcal{L}_s + \mathcal{L}_H + \mathcal{L}_p\right)(t) = \mathcal{E}_0 - \mathcal{L}(t), \tag{22}$$

which corresponds to the energy curves shown in Figs. 3 and 10.

7. REFERENCES

[1] J. Chabassier, A. Chaigne, and P. Joly, "Modeling and simulation of a grand piano," *J. Acoust. Soc. Am.*, vol. 134, no. 1, pp. 648–665, 2013.

[2] A. Chaigne and A. Askenfelt, "Numerical simulations of piano strings. II. Comparisons with measurements and systematic exploration of some hammer-string parameters," *J. Acoust. Soc. Am.*, vol. 95, no. 3, pp. 1631–1640, 1994.

[3] M. French, "Structural modifications of stringed instruments," *Mech. Syst. and Signal Proc.*, vol. 21, pp. 98–107, 2007.

[4] J. Chabassier, A. Chaigne, and P. Joly, "Time domain simulation of a piano. Part 1: model description," *Mathematical Modelling and Numerical Analysis*, vol. 48, no. 5, pp. 1241–1278, 2014.

[5] M. Novak Clinkscale, *Makers of the piano, 1700-1820*, Oxford University Press, Oxford, 1993.

[6] M. Novak Clinkscale, *Makers of the piano, 1820-1860*, Clarendon Press, Oxford, 1999.

[7] J. Chabassier and P. Joly, "Energy preserving schemes for nonlinear Hamiltonian systems of wave equations. Application to the vibrating piano string.," *Comp. Meth. in Appl. Mech. and Eng.*, vol. 199, pp. 2779–2795, 2010.

[8] X. Boutillon, "Model for piano hammers: Experimental determination and digital simulation," *J. Acoust. Soc. Am.*, vol. 83, no. 2, pp. 746–754, 1988.

[9] A. Stulov, "Experimental and computational studies of piano hammers," *Acta Acustica united with Acustica*, vol. 91, no. 6, pp. 1086–1097, 2005.

[10] J. P. D. Wilkinson, "Modal densities of certain shallow structural elements," *J. Acoust. Soc. Am.*, vol. 43, no. 2, pp. 245–251, 1968.

[11] F. Fahy, *Foundations of Engineering Acoustics*, Academic Press, London, 2000.

[12] S. Bilbao, *Numerical sound synthesis. Finite differences schemes and simulation in musical acoustics.*, J. Wiley, Chichester, 2009.

DESIGNING ON SUBJECTIVE TOLERANCE TO APPROXIMATED PIANO REPRODUCTIONS

Federico Fontana, Stefano Zambon, and Yuri De Pra

Dipartimento di Matematica e Informatica
University of Udine, Italy
federico.fontana@uniud.it

ABSTRACT

Results from three experiments are presented, showing that the perceived acoustic and vibrotactile quality of a reproduced piano does not require models simulating every aspect of the original instrument with great accuracy. It was found that high-quality loudspeaker array passive listening at the pianist's position admits distortion of the sound field. Furthermore, pianists during playing seem to compensate for errors in the auditory scene description. Finally, they are particularly sensitive to the existence of vibrotactile musical feedback on their fingers meanwhile tolerant about the precision with which this feedback is reproduced. Based on these results we are currently working on a lightweight portable physics-based digital piano design, that should improve upon the experience a pianist with no keyboards at hand makes when interacting with a touch-screen piano software running on smartphones and laptops.

1. INTRODUCTION

Musical instrument models often expose surprisingly high levels of accuracy to the performer. Since they are employed especially to enable digital implementations which reproduce the original instrument features only partially, one wonders whether the model can be integrally transferred and, thus, appreciated in the digital counterpart. Even more radically, one may wonder whether a performer has a neat perception of the original accuracy while playing the real instrument.

Aspects of the performer's acoustic sensitivity to an instrument quality have been put into question by carefully designed experiments [1]. Fritz and colleagues have revisited a common belief about the superiority of old Italian violins [2]. The accurate perception of a piano has been criticized since long [3], but perhaps not so many times. An insightful experiment was performed by Galembo and Askenfelt, who showed that a blindfolded group of expert pianists easily recognized three previously played different pianos by randomly performing over them, conversely they lost much of their own recognition ability when just listening to the same pianos [4]. Goebl and colleagues investigated on the long-debated question about the influence of touch to piano sound production [5]. Experiments like these suggest that a musical instrument sound designer should commit him or herself to uncompromised quality only after making sure that a model under study is perceptually worth that quality.

With specific regard to the piano, the question becomes more complicate once the real instrument is substituted by a system made of digital and electro-acoustic components. Irrespectively of their quality, such components in fact further bias the perception of the sound effects that are produced by a model. A reduced keyboard mechanics working in absence of hammers and strings is likely to influence the otherwise subtle cutaneous and haptic sensations to the fingertips, but to what extent do these sensations influence a performer's self-confidence with the instrument? The replacement of a soundboard with a loudspeaker set inevitably changes the acoustics of a piano, but do performers and listeners experience a measurable decay in the sound quality and localization?

In the following we summarize the results of four experiments that we have recently conducted on the piano, with the help of other researchers. Two such experiments were intended to understand the sensitivity and possible salience of cutaneous cues during playing. The remaining two aimed at understanding the perceptual consequences of corrupting the instrument's acoustic field pointing to the performer, in terms of perceived sound accuracy and localization. The results justify to test the quality of digital implementations whose distance from the real instrument is increased, trading off the resulting minor accuracy with improved portability and reduced costs. Currently we are working on an augmented table interface prototype which implements this design approach.

2. EXPERIMENTS

In general the experiments put the focus on the multimodal relationships existing between the performer and his or her instrument. Once such relationships are strengthened by years of practice and repeatable experiences, a change in some feedback modality should bring a comparable experiential novelty unless that change is imperceptible. We have investigated this and other facts by experimenting on the dependencies between the auditory and somatosensory experience, holding a visual scenario consisting of a real piano or alternatively a digital keyboard.

2.1. Perception of interactive vibrotactile feedback [6]

Keyboard makers have long since given empirical evidence of the importance of haptic cues in defining the quality of an instrument. First of all touch, mostly depending on the keys' material along with their dynamic response due to the connection mechanism with the strings, confers a unique haptic signature to a piano. Besides the mentioned Galembo experiment [4], the relationships between the perceived quality of a piano and the haptic signature of its keyboard have been understood only to a limited extent. It is generally acknowledged that the use of a simplified keyboard mechanics along with keys made of plastic material, such as those found in consumer digital pianos, inevitably translate to a less rewarding experience for the pianist. Yet, the subjective effects of an impoverished keyboard on the perceived sound quality have not been quantified to date.

Even less is known about if and how the same quality is influenced by vibrotactile feedback arriving at the pianist's fingers

Figure 1: Setup for loudness estimation on the grand piano using a KEMAR mannequin.

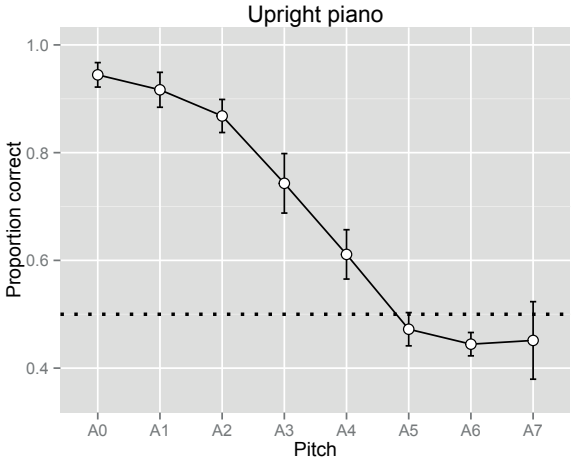

Figure 2: Mean proportions correct for the upright piano configuration. Chance performance given by dashed line. Error bars present within-subjects confidence intervals.

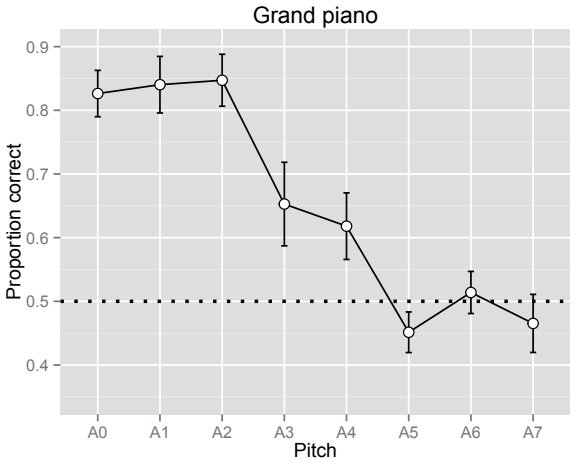

Figure 3: Mean proportions correct for the grand piano configuration. Chance performance given by dashed line. Error bars present within-subjects confidence intervals.

once the more prominent somatosensory experience of striking the keys has ceased, leaving space to the vibrations traversing the instrument until the keys are released. In a related study [7], one of the present authors conducted a pilot experiment on a digital piano modified with the addition of vibrotactile feedback. On the other hand, while investigating the perception of vibrations on a grand piano, Askenfelt and Jansson provided quantitative evidence that even *ff* notes generate partial components whose magnitude hardly exceeds the known vibrotactile thresholds at the fingers [8]. Their measurements, hence, support the claim that neither a piano keyboard nor the keybed or the pedals should be able to convey prominent vibrotactile cues to the pianist.

We measured the pianists' sensitivity to piano key vibrations at the fingers while playing an upright or a grand Yamaha Disklavier piano. We took advantage of the switchable quiet mode to either provide vibrations or not in both pianos during playing. Subjects had to be prevented from hearing the Disklaviers; therefore, MIDI OUT data were used to control a Pianoteq software piano synthesizer that was configured to simulate a grand or an upright piano. The synthesized sound was provided by means of isolated headphones. The loudness of the acoustic pianos at the performer's ear was estimated by recording with a KEMAR mannequin all the A keys played at various velocities (Figure 1 shows the grand piano setup).

The test was a yes-no experiment. The task was to play a loud, long note (*mf* to *fff* dynamics, lasting 4 metronome beats at 60 BPM) and then to report whether vibrations were present or not. Only the A keys across the whole keyboard were considered, in this way reducing the experiment's duration while maximizing the investigated pitch range. A randomized sequence of 128 trials was provided, made up of 16 occurrences of each A key. Half of the trials were in the "vibration OFF" condition, corresponding to the Disklavier set to quiet mode. The total duration of the experiment was about 20 minutes per participant.

2.1.1. Summary of results and discussion

Proportions of correct responses, given by

$$p(c) = \frac{(\text{“yes”} \cap \text{vibes present}) + (\text{“no”} \cap \text{vibes absent})}{\text{total trials}},$$

were calculated for each participant individually for each A key. Average results for the upright and grand configurations are presented respectively in Figures 2 and 3, showing a similar trend. For the lowest three pitches (A0 to A2), the subjects could easily discriminate between the trials with and without vibrations. In the middle register the proportion of correct responses was still over 60%, while it finally dropped to chance level at A5 ($f_0 = 880$ Hz).

Our findings complement the Askenfelt and Jansson results [8] especially in the low range up to 110 Hz, where detection was clearly easier than in the range of highest sensitivity, where only two thirds of the subjects were successful at detecting key vibrations. This may be explained by the nature of the vibratory signal which was not sinusoidal, unlike in the threshold measurements by Verrillo. More in general the pianist is engaged in an enactive experience where every key depression produces a distinct audio-haptic contact event, immediately followed by the transmission of vibrotactile cues from the keyboard, caused by the vibrating strings and resonating body of the instrument. Such cues are subjected to disparate temporal, spatial and spectral summation or interference effects, depending on the sequence of played notes and chords, as well as on the position of the hands on the keyboard. For all such effects the literature provides only sparse data.

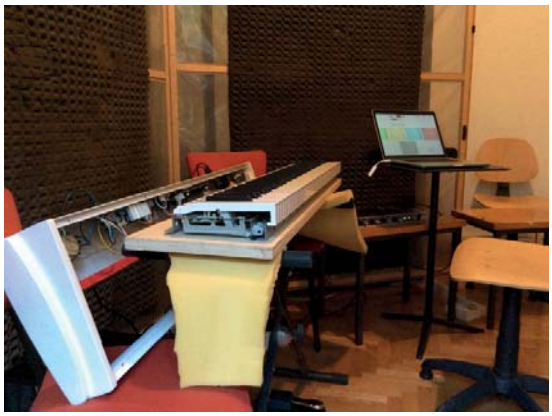

Figure 4: Experimental setup.

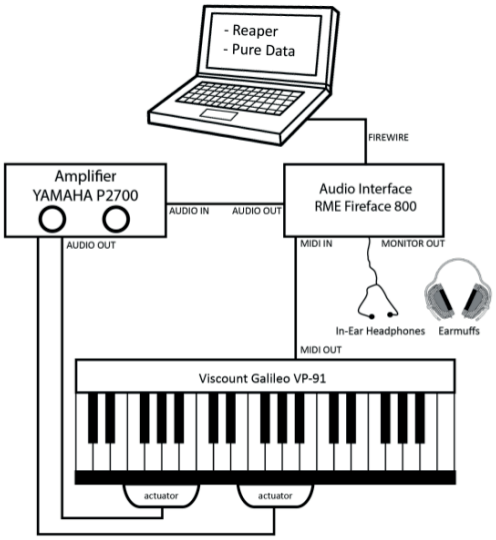

Figure 5: Schematic of the setup.

The effects of active pressing force on vibrotactile perception are not thoroughly known, but there is evidence that vibrotactile magnitude sensation increases under a passive static force. Promising results have been very recently obtained in this sense by Papetti and colleagues [9].

2.2. Interactive reproduction and subjective evaluation of real vs. synthetic vibrotactile cues [11]

On the light of the previous experiment, recently we have investigated on the quality of the vibrotactile feedback. In other words, we hypothesized that pianists appreciate the reproduction of real as opposed to simplified synthetic key vibrations. The experiment required to disassemble a digital piano keyboard, and instrument it so as to convey vibratory signals to the user (see Figure 4); then, to record key vibrations on an acoustic piano and to synthesize simplified counterparts, which were organized in two respective sample banks.

Audio-tactile stimuli were produced at runtime: the digital keyboard played by the participants sent MIDI messages to the computer, where a piano synthesizer plug-in generated the related sounds and, in parallel, a sampler plug-in played back the Disklavier grand piano vibration samples then processed by an amplitude & spectral equalizer plug-in (see Figure 5).

Subjects wore earphones and ear-muffs on top of them, in the same fashion as the mannequin did during a previously made loudness matching procedure. In this way they were not exposed to the sound coming by air conduction from the transducers, as a by-product of their vibration.

Three vibration conditions were assessed relative to a non-vibrating standard stimulus A:

B: recorded real vibrations;

C: recorded real vibrations with 9 dB boost;

D: synthetic vibrations.

Synthetic vibrations consisted of noise filtered around the fundamental note, possessing similar amplitude envelope across time. Sound feedback was generated by a Pianoteq piano synthesizer playing the same configuration as in the previous experiment. The task was to play freely on the digital keyboard and assess the playing experience on five attribute rating scales: Dynamic control, Richness, Engagement, Naturalness, and General preference. The dynamics and range of playing were not restricted in any way.

Subjects could switch freely among setups α and β: Setup α was always the non-vibrating standard, while setup β was one of the three vibration conditions (B, C, D). The rating of β was given in comparison to α. The presentation order of the conditions was randomized. Also, participants were not aware of what could actually change in the different setups, and in particular they did not know that sound feedback would not be altered. The free playing time was 10 minutes per couple of conditions (A, B), and participants were allowed to rate the five attributes at any time during the session by means of a point & click graphical user interface (GUI). In the end, each subject gave one rating in each attribute scale for each vibration condition.

2.2.1. *Summary of results and discussion*

Ratings were given on a continuous Comparison Category Rating scale (CCR), ranging from -3 to +3, which is widely used in subjective quality determination in communications technology. Inter-individual consistency was assessed for each attribute scale by computing the Lin concordance correlations ρ_c for each pair of subjects. The average ρ_c were 0.018 for general preference, 0.006 for dynamic control, -0.04 for richness, -0.02 for engagement, and -0.04 for naturalness. In all scales, a few subjects either agreed or disagreed almost completely and, due to this large variability, ρ_c was not significantly different from 0 for any of the scales ($t(54) < 0.77, p > 0.05$). The low concordance scores indicate a high degree of disagreement between subjects.

Responses were positively correlated between all attribute scales. The weakest correlation was observed between richness and dynamic control, (Spearman correlation $\rho_s = 0.18$), and the highest between general preference and engagement ($\rho_s = 0.75$). The partial correlations between general preference and the other attribute scales were as follows: $\rho_s = 0.39$ for dynamic control, $\rho_s = 0.72$ for richness, and $\rho_s = 0.57$ for naturalness.

Results are plotted in Figure 6, and the mean ratings for each scale and vibration condition are given in Table 1. On average, each of the vibrating modes was preferred to the non-vibrating standard, the only exception being condition D for Naturalness. For conditions B and C Naturalness received faintly positive scores. The strongest preferences were for Dynamic range and Engagement. General preference and Richness had very similar mean scores though somewhat lower than Engagement and Dynamic control. Generally, C was the most preferred

Vibration	Dyn.	Rich.	Eng.	Nat.	Pref.
B	0.92	0.30	0.50	0.26	0.24
C	1.28	0.67	1.21	0.17	0.81
D	0.87	0.42	1.00	-0.23	0.29

Table 1: Mean ratings over all subjects for each attribute and vibration condition.

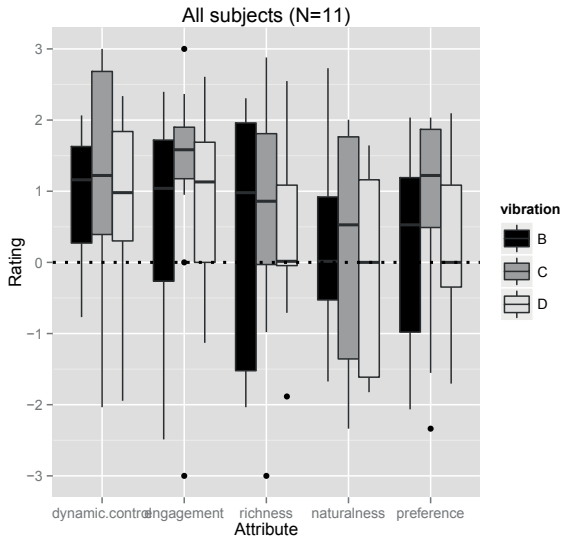

Figure 6: Results of the quality experiment. Boxplot presenting median and quartiles for each attribute scale and vibration condition.

of the vibration conditions: It scored highest on four of the five scales, although B was considered the most natural. Interesting enough, B scored lowest in all other scales.

Heterogeneity was observed in the data, as might be expected due to the high degree of variability in the inter-individual agreement scores ρ_c. A k-means clustering algorithm was used to divide the subjects *a posteriori* into two classes according to their opinion on General preference. Eight subjects were classified into a "positive" group and the remaining three into a "negative" group. The results of the respective groups are presented in Figure 7. A difference of opinion is evident: The median ratings for the "winning" setup C are nearly +2 in the positive group and -1.5 in the negative group for General preference. In the positive group, the median was > 0 in all cases except one (Naturalness, D), whereas in the negative group, the median was positive in only one case (Dynamic control, B).

We concluded that key vibrations increase the perceived quality of a digital piano. Although the recorded vibrations were perceived as the most natural, amplified natural vibrations were overall preferred and received highest scores on all other scales as well. The other interesting outcome is that the vibrating setup was considered inferior to the non-vibrating standard only in Naturalness for synthetic vibrations. This suggests that pianists are indeed sensitive to the match between the auditory and vibrotactile feedback.

The high degree of disagreement between subjects suggests that intra- and inter-individual consistency is an important issue in instrument evaluation experiments. Due to only one attribute rating per subject and condition, intra-individual consistency could not be assessed in the present study and will be left for a future revision. However, the heterogeneity in the data was similar across all attributes and conditions, making it hard to believe it was caused by inconsistency alone. Roughly two thirds of the subjects clearly preferred the vibrating setup, perhaps less rewarded by the synthetic vibrations, while the remaining one third had quite the opposite opinion. It is interesting that both the jazz pianists, having probably more experience of digital pianos than the classical pianists, were in the "negative" minority: would a vibrating digital keyboard be perceived as less pleasant than a neutral one, reflecting a preference of those pianists to the digital piano's traditional tactile response?

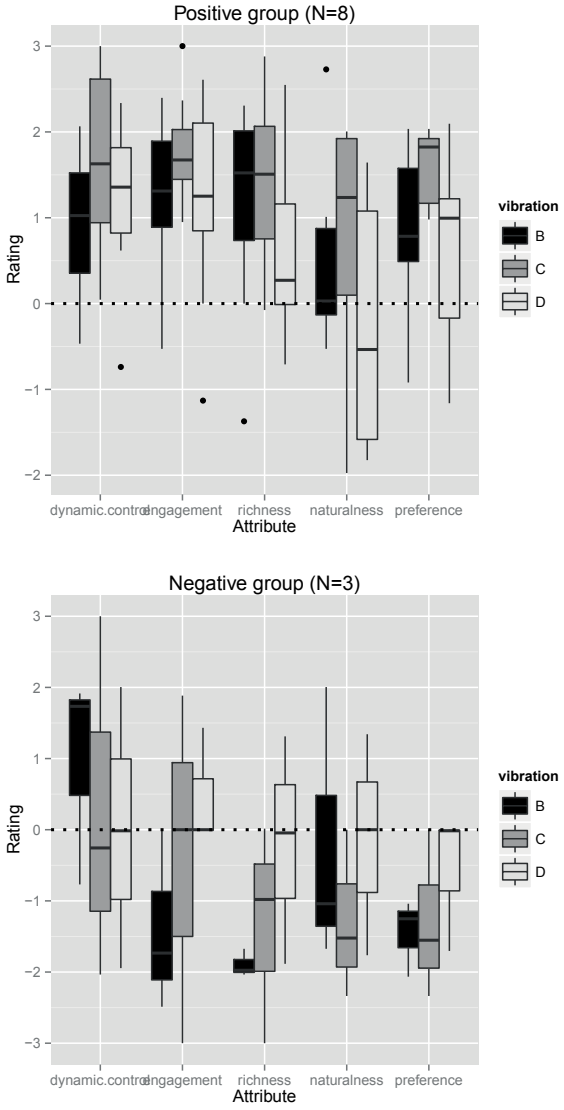

Figure 7: Quality results for the positive and negative groups.

2.3. Sensitivity to loudspeaker permutations [12]

Performers declare to be especially sensitive to changes in the sound coming from their instrument. On the other hand, the role and importance played by the auditory cues when a piano is perceived to sound different is not obvious. Recent literature marks the difference existing between playing as opposed to listening to a piano: such two activities would in fact lead the pianist to develop different impressions about the quality of the instrument [13, 5].

This research considered a collection of accurately recorded multi-channel piano notes, that were presented to a group of pi-

Figure 8: Recording session: microphone setup.

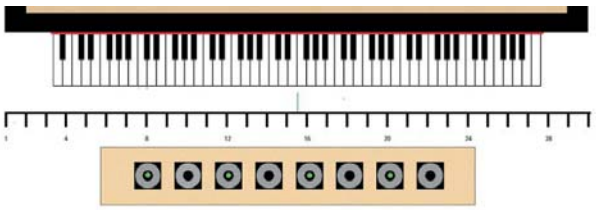

Figure 9: Microphone/loudspeaker alignment.

anists via a calibrated array of eight small loudspeakers. Distortions were introduced during the listening test by exchanging the output channels, and subjective impressions about the realism of the sound and the auditory scene were gathered along with the apparent listening position. Our analysis suggests that only the largest permutations, in a sense that will be defined later, cause significant corruption of both qualities furthermore without clear implications on the auditory scene description.

Six *mezzo forte* piano notes (C4, E4, C2, A4 major, D4, C5) were selected from a huge collection, result of a recording session made in July 2012 at the Viscount International SpA semi-anechoic room based in Mondaino (RN) - Italy, using a Seiler model 1849 piano that was tuned and prepared for the occasion, and then played by a professional pianist and sound designer consulting for the company. Such notes were collated together one after the other, hence forming a slow scale lasting about thirty seconds.

Fig. 8 illustrates the recording setup consisting of a linear array of 30 Bruel&Kjær model 4188 omnidirectional microphones, calibrated and made available by Angelo Farina's acoustics research group at the University of Parma, along with an M-Audio multi-channel sound interface. The array was positioned in such a way to capture the soundfield in front of the cover, which was left open. The reproduction was realized avoiding any signal processing, by just reporting eight equally-spaced recorded channels onto a single-pressure chamber linear array made with 2.5" Ciare loudspeaker units.

Fig. 9 shows the alignment between the microphone and the loudspeaker array, with the piano keyboard taken as reference: the eight loudspeakers, hence, reproduced the recorded channels no. 8, 10, 12, 14, 16, 18, 20 and 22, respectively. From here on we will associate such recorded channels respectively to the loudspeakers 1, 2, 3, 4, 5, 6, 7, 8, numbered left to right.

Ten reproduction patterns were prepared using the eight channels: two of them were formed respectively by quadruplicating two, and duplicating four recorded channels over the loudspeakers; the third one was left untouched; the remaining seven were obtained by permutations of the inputs. All patterns are listed in Table 2.3 below.

Pattern no.	Configuration	Label
1	11118888	Magnified stereophony
2	11336688	Magnified quadraphony
3	12345678	Original
4	21436587	Swapped adjacent ones
5	34127856	Swapped adjacent pairs
6	56781234	Swapped quadruples
7	73258146	Random no. 1
8	78345612	Swapped edge pairs
9	87654321	Reverse panning
10	51843276	Random no. 2

The experiment was set up in a silent, dry room (approximately $3 \times 3 \times 2.75$ meters) having walls partially covered with damping foam. In addition to the active array, four loudspeakers were located each at one corner of the room, furthermore two additional eight-channel arrays were put in front of the listener: the presence of such idle systems added uncertainty in the listeners about the sources that were going to be used during the experiment.

Subjects had to sit on a chair at the center of the room, approximately one meter far from the loudspeaker array. While sitting, every subject was given a tabletop computer on which (s)he could respectively rate the *realism of the sound* R_S and the *realism of the auditory scene* R_A on a scale ranging 1 (poor) to 7 (excellent), as well as choose his or her own *relative position* R_P in the virtual scene among nine possible listening points, labeled A to I in alphabetical order. Before the test, the subject was given verbal instructions about the scale (s)he was going to listen to, as well as about the use of the graphical interface.

The test consisted of listening to a balanced random distribution of the patterns, each repeated five times for a total of fifty trials. During each trial, every subject listened to the musical scale and then rated R_S, R_A and R_P by selecting the corresponding value in the graphical interface; finally, (s)he submitted her or his selections by pushing a software button. After each submission a new trial was started: this procedure allowed in particular for rating a scale and go to the next one by submitting before the end of the current sound, or conversely to pause at the end of a trial by delaying the respective submission. In this way subjects could optimize the flow of the test, which took approximately 40 minutes to be completed.

2.3.1. Summary of results and discussion

Fig. 10 (above) plots, for each pattern in the respective box, the median of the corresponding rate R_S, the 25$^{\text{th}}$ and 75$^{\text{th}}$ percentiles with their extreme datapoints, the average values and the outliers. The same boxes are displayed for each pattern rated R_A, below in the figure. Both plots have been obtained using the `boxplot` function of Matlab.

An informal inspection suggests the existence of a significant decay in both sound and scene realism *only* when the patterns 7,8 and 10 are displayed. In all other cases the decay appears to be not significant.

2.4. Active sound localization

Similarly to the explanation given for motivating the stability of the perceived realism in presence of loudspeaker permutations in the previous array, independently of the existence of a

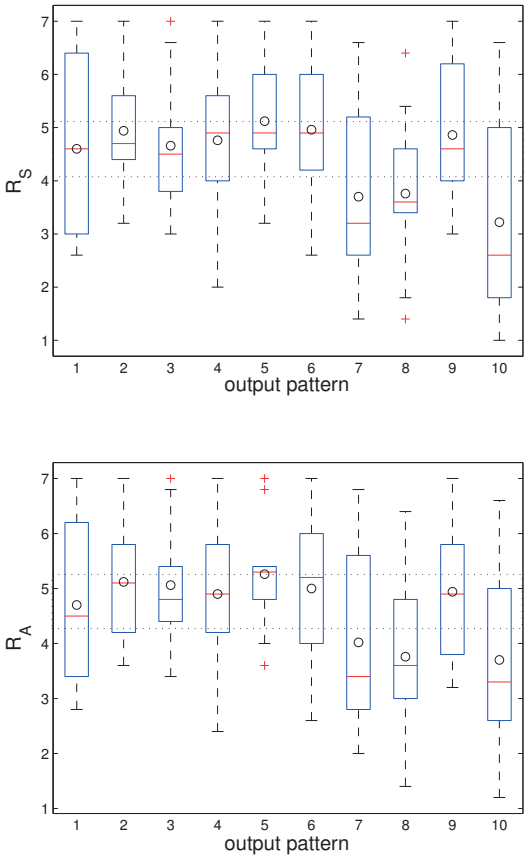

Figure 10: Boxplots showing median, 25th and 75th percentiles with their extreme datapoints, average values ('○') and outliers ('+') for each output pattern rated R_S (above) and R_A (below), respectively. On either boxplot, the rectangle in dashed line gathers average values within the respective HSD range, edged by the largest average.

precedence effect we conjecture that the localization of a note during playing is locked to the corresponding key position by the somatosensory cues of hand proprioception. Holding this locking effect, then the same position can be robustly recalled during listening: this previously learnt process may suppress the auditory localization of the same note via lateralization cues, in particular resolving any potential incongruence between the proprioceptive and auditory information.

Here we illustrate some preliminary results of an experiment using the same stimuli as before, this time employing a 14 channel array of 2.5" Ciare loudspeaker units, in which we asked subjects to localize the direction of arrival of piano notes. Subjects either passively listened to the stimuli, or conversely they activated them by playing the corresponding key on the Galileo keyboard—see Sec. 2.2. The array channels were manipulated so to create also reversed, random, and monophonic sounds.

Figure 11 shows that subjects during active playing gave higher scores to manipulated sound fields. The significance of these scores is left to a future analysis, along with any further discussion on the support of the active playing task to the sound localization.

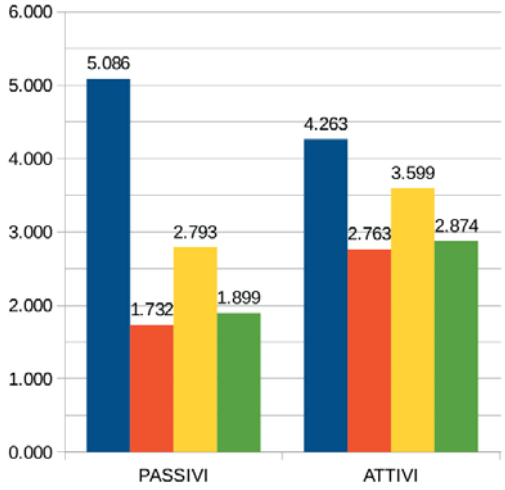

Figure 11: Histograms showing perceived degree localization for listening (left) vs. playing performers (right) respectively for normal (blue), reversed (red), random (yellow), and monophonic (green) array listening.

3. AUGMENTED TABLE INTERFACE

Recently there has been a lot of attention, both in the musical interface research community and in the industry, in developing keyboard-like interfaces which are highly portable and that can be the right companion for computing devices such as smartphones and tablet PCs. Such devices usually provide touch-screen interfaces, but they suffer from limitations in size, high latency and are in general not sensitive to force variations. Therefore, we focused on developing an interface that aims to augment any surface, e.g. a common table, into an immaterial digital keyboard, requiring no more space than the portable computing device to operate.

In this work we aimed at developing a prototype which can capture the musical gestures using mostly a common camera, following standard algorithms for finger and hand tracking [14]. In this way, the augmented interface could be built without any additional hardware making it the best solution in terms of portability. While there are already some solutions that work in a similar way, such as Augmented Piano by Amit Ishai and Moshe Liran Gannon [1], they all suffer from high failure rate in the detection algorithms and high latency.

Our primary goal was to provide a system which could detect precisely notes and velocities, working with a total latency lower than 30 milliseconds. Unfortunately, this requirements are very strict for a generic mobile computing platforms such as smartphones or tablets, mainly because of the extra latency imposed by either the video and audio processing pipelines of the underlying operative systems. Therefore, we centered our prototype on a Linux-based single-board PC, which is similar in terms of computing hardware to the aforementioned devices but gives us the flexibility that we need in terms of software development. Moreover, we were able in this way to experiment with enhancements that rely on external hardware, such as the use of piezoelectric microphones to improve detection latency or tactile transducers for haptic rendering on the surface. However, it is important to notice that the features provided by them are optional and the system is still functional just with video

[1] https://sites.google.com/site/pianoreality/

input from a camera.

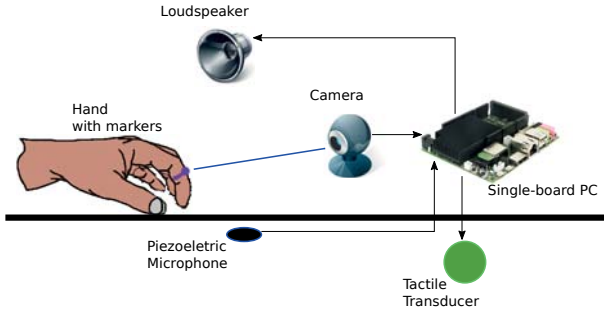

Figure 12: Test picture

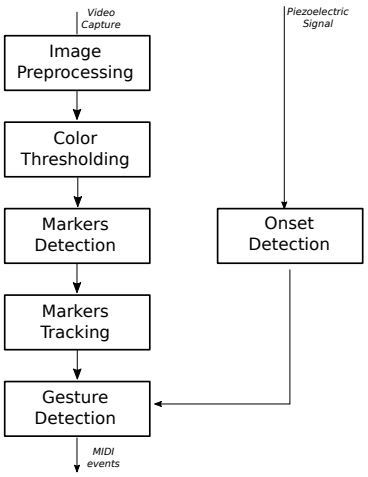

Figure 13: Data flow

3.1. Prototype Architecture

We chose to employ the Udoo single-board PC [2] as the computing core of our system. While maintaining a compact size, the board features a quad-core ARM Cortex-A9 processor clocked at 1GHz, plus an additional ARM Cortex-M3 processor compatible with the Arduino Due environment. The board also features an integrated codec for audio connections and a WiFi module which comes useful when integrating a device like a PC or smartphone for e.g. control with a graphical user interface. We tried several solutions for the camera and finally settled on the Playstation Eye Camera, a compact and cheap consumer device which is still capable of capturing video with a low latency and a high frame-per-second (FPS) rate (60FPS at 640x480 resolution).

The connection between the components of the system can be seen in Fig. 12. Besides the main board and the camera, there is an optional input in the form of a piezoelectric microphone placed on the table. The output hardware components are a generic loudspeaker or headphones, plus an optional tactile transducer driven by a separate DAC on the board controlled by the Cortex-M3 processor.

The system runs on top of a Linux system based on a highly customized Debian Wheezy distribution. The most difficult part has been the integration of the RealTime Linux Kernel patch [15], since the sources provided by the board manufacture are not aligned with the mainline Linux Kernel. With this modification we were able to reduce the audio latencies from 40ms to 4ms, thus resulting in a minimum impact on the overall latency of the system. The audio synthesis system is driven by the JACK audio server [16] and is composed by a sample-based synthesis engine [3], able to reproduce e.g. a high-quality piano soundfont with a polyphony of 256 notes. We implemented a dedicated service in the form of a Jack audio program to obtain the haptic output signal from the audio, by filtering and downsampling the output of the synthesizer. The result is then encoded and sent over a serial communication bus connected to the Cortex-M3 processor, where a separate piece of software, written using the Arduino language, is in charge of collecting the data and driving one of the additional DACs accessible on the board.

3.2. Gesture Recognition Algorithm

At its core, the system tracks the movement of the fingers using the video stream obtained from the camera. Using only this information, it is very hard to obtain latencies lower than 30-40ms, due to the low frame rate and buffering involved in video processing. Therefore, we included the option to use the data acquired by a contact microphone placed on the surface to improve the overall latency. The audio signal obtained in this way is analyzed using an onset detector calibrated to find the peaks at medium-high dynamics, thus enabling the triggering of Note ON events in advance compared to when the video-only algorithm would have detected them.

We wrote a C++ program using the popular OpenCV library [17] for most of the vision-related tasks. The algorithm implemented requires coloured markers placed on rings that can be worn on the fingers, excluding the thumb, and a camera placed in a fixed position in front of the hand. Processing follows standard motion-tracking techniques [14] and is summarized by the dataflow diagram presented in Fig. 13.

During an initial one-time calibration phase, the colour of the tracking markers is analyzed finding a two-dimensional threshold on Hue and Saturation by looking at the histogram of a predefined region, using an interval having half-length of a standard variation σ for Hue and three times σ for Saturation, since Hue is a more reliable feature to track. A second calibration is performed to estimate the pose of a keyboard drawn on a sheet of paper, in order to have a map from camera coordinates to keyboard keys.

At run-time, each image is first preprocessed by applying a conversion from RGB to HSV color space. Then, a two-dimensional thresholding operation, using the limits derived from the calibration, is applied to obtain a binary image where the selected pixels correspond to the tracked colors. A sequence of dilate and erode filters is applied to the result so that false positives are minimized and noise inside the tracked area is reduced. A number of predefined (e.g. four) markers are then detected in the binary image using a standard algorithm by Suzuki et al. [18] which gives as a result a set of closed contours. For each contour, a single relevant and stable point is extracted by using features based on the momentum of the detected area such as the barycenter.

The detected video coordinates are then fed to a tracking algorithm based on a Kalman filter, where we used a dynamic system of dimension four, with two states assigned to position and two to velocity. The usage of this algorithm reduces significantly detection artifacts that can result in sudden jumps of the

[2] http://www.udoo.org/
[3] http://www.fluidsynth.org/

tracked position, which can severely impact gesture and velocity detection in the following phase. At the same time, however, the filtering process might add some latency, so the parameters of the Kalman filter have to be calibrated in order to get a good compromise. Finally, the tracked positions are analyzed at each frame for detecting musical relevant gestures, which are then converted to MIDI events such as Note ON/Note OFF or continuous controls. Note triggering works using two virtual contacts placed vertically above the table and measuring the time between the crossing of the two contacts. After an event is triggered, the horizontal coordinates are mapped from camera to keyboard space using the transformation obtained from the calibration step, so the exact key pressed can be detected.

If the piezoelectric audio is taken into account, the trigger of the events is formed by the logical or of the two detection systems, with some extra logic that takes care of not detecting a single event more than one time. Typically, the audio-based detection works with medium to high dynamics, while only the video is used for lower dynamics, which luckily do not suffer much from higher latency. Overall, detection latency using the audio trigger is around 10ms, of which 4ms are fixed and due to the audio buffer size and the rest vary depending on dynamics of the hit and type of the surface. Video-only latency is harder to estimate but we judged it to be around 35-40ms from empirical comparison with other systems.

4. ACKNOWLEDGMENTS

Alberto Amendola, Federico Avanzini, Yuri De Pra, Hanna Järveläinen, Giorgio Klauer, and Stefano Papetti have collaborated to the mentioned experiments. The authors acknowledge support from the Proof of Concept Network national project entitled ”Virtual piano system on a tablet pc” (”Sistema di pianoforte virtuale su tablet pc”) called by the AREA Science Park in Trieste, participated by the University of Udine and Julia SRL, and co-financed by Viscount SpA through the University of Verona, all from Italy.

5. REFERENCES

[1] D Murray Campbell, “Evaluating musical instruments,” *Physics Today*, vol. 67, no. 4, pp. 35–40, 2014.

[2] Claudia Fritz, Joseph Curtin, Jacques Poitevineau, Palmer Morrel-Samuels, and Fan-Chia Tao, “Player preferences among new and old violins,” *Proceedings of the National Academy of Sciences*, vol. 109, no. 3, pp. 760–763, 2012.

[3] Mary Cochran, “Insensitiveness to tone quality,” *The Australasian Journal of Psychology and Philosophy*, vol. 9, no. 2, pp. 131–133, 1931.

[4] A. Galembo and A. Askenfelt, “Quality assessment of musical instruments - Effects of multimodality,” in *5th Triennial Conference of the European Society for the Cognitive Sciences of Music (ESCOM5)*, Hannover, Germany, Sep. 8-13 2003.

[5] Werner Goebl, Roberto Bresin, and Alexander Galembo, “Once again: The perception of piano touch and tone. Can touch audibly change piano sound independently of intensity?,” in *Proceedings of the International Symposium on Musical Acoustics (ISMA2004)*, Nara, Japan, Mar. 31 – Apr. 4 2004, pp. 332–335.

[6] F. Fontana, F. Avanzini, H. Järveläinen, S. Papetti, F. Zanini, and V. Zanini, “Perception of interactive vibrotactile cues on the acoustic grand and upright piano,” in *Proc. Joint ICMC/SMC Conf.*, 2014.

[7] F. Fontana, S. Papetti, V. dal Bello, M. Civolani, and B. Bank, “An exploration on the influence of vibrotactile cues during digital piano playing,” in *Proc. 8th Sound and Music Computing Conference (SMC2011)*, Padua, Italy, July 6-9 2011, pp. 273–278, Padova University Press, Available at `http://www.padovauniversitypress.it/`.

[8] A. Askenfelt and E. V. Jansson, “On vibration and finger touch in stringed instrument playing,” *Music Perception*, vol. 9, no. 3, pp. 311–350, 1992.

[9] S. Papetti, H. Järveläinen, and G.-M. Schmid, “Vibrotactile sensitivity in active finger pressing,” in *World Haptics Conf.*, 2015.

[10] Andrew M. Galica, Hyun Gu Kang, Attila A. Priplata, Susan E. DAndrea, Olga V. Starobinets, Farzaneh A. Sorond, L. Adrienne Cupples, and Lewis A. Lipsitz, “Subsensory vibrations to the feet reduce gait variability in elderly fallers,” *Gait & Posture*, vol. 30, no. 3, pp. 383 – 387, 2009.

[11] F. Fontana, F. Avanzini, H. Järveläinen, S. Papetti, G. Klauer, and L. Malavolta, “Interactive reproduction and subjective evaluation of real vs. synthetic vibrotactile cues on a digital piano keyboard,” in *Proc. SMC Conf.*, 2015, To appear.

[12] F. Fontana, Y. De Pra, and A. Amendola, “Sensitivity to loudspeaker permutations during an eight-channel array reproduction of piano notes,” in *Proc. SMAC/SMC 2013*, Stockholm, Sweden, Jul. 30 - Aug. 3 2013.

[13] Anders Askenfelt, Alexander Galembo, and Lola L. Cuddy, “On the acoustics and psychology of piano touch and tone,” *The Journal of the Acoustical Society of America*, vol. 103, no. 5, pp. 2873, 1998.

[14] Ali Erol, George Bebis, Mircea Nicolescu, Richard D Boyle, and Xander Twombly, “Vision-based hand pose estimation: A review,” *Computer Vision and Image Understanding*, vol. 108, no. 1, pp. 52–73, 2007.

[15] Steven Rostedt and Darren V Hart, “Internals of the rt patch,” in *Proceedings of the 2007 Linux symposium*. Citeseer, 2007, vol. 2, pp. 161–172.

[16] Paul Davis and T Hohn, “Jack audio connection kit,” in *Proceedings of the 1st Linux Audio Developer Conference*. Institute for Music and Acoustics, ZKM, Karlsruhe, Germany, 2003.

[17] Gary Bradski et al., “The opencv library,” *Doctor Dobbs Journal*, vol. 25, no. 11, pp. 120–126, 2000.

[18] Satoshi Suzuki et al., “Topological structural analysis of digitized binary images by border following,” *Computer Vision, Graphics, and Image Processing*, vol. 30, no. 1, pp. 32–46, 1985.

PERFORMANCE SPACE: THE SPOTLIGHT AND ITS IMPLICATIONS FOR PERFORMANCE PSYCHOLOGY

Aaron Williamon
Royal College of Music, London, United Kingdom
aaron.williamon@rcm.ac.uk

ABSTRACT

Professional training in music often lacks repeated exposure to realistic performance situations, with musicians learning all too late (or not at all) how to manage the stresses of performing and the demands of their audiences. This lecture will explore the physiological and psychological differences between practising and performing, specifically examining cardiovascular and neuroendocrine responses in musicians when performing under pressure. It will also introduce the Performance Simulator, an innovative new facility which operates in two modes: (i) concert and (ii) audition simulation. Initial results demonstrate that the Simulator allows musicians to develop and refine valuable performance skills, including enhancement of communication on stage and effective management of high state anxiety.

RHYTHM PERCEPTION IN THE CONTEXT OF MUSIC AND DANCE

Yi-Huang Su
Technical University of Munich, Germany
yihuang.su@tum.de

ABSTRACT

Multisensory cues in a music performance – such as the sounds of the instruments and the musicians' gestures – are important means of communication amongst ensemble musicians, which can also be used by the audience to form multimodal experiences of music. There is, however, a similar and yet less understood scenario that also involves visual observation of movements and auditory perception of music: dance. As dancers coordinate their movements with the musical rhythms, both streams of information may converge temporally into a multimodal percept from the audience's perspective. Here, I will present some of my recent investigations in this scenario: How do observers extract temporal information from dancelike movements? Do similar processes as found in auditory rhythm perception also underlie visual perception of structured human movements? How does visually perceived rhythmicity interact with perception of auditory rhythms? In one study, we found that observers make use of the underlying periodicity in movement trajectories for temporal estimation of dancelike movements, which seems analogous to the benefit of a regular beat in processing auditory rhythms. Regarding the cross-modal effects, I will show that observing a humanlike figure bounce periodically induces a visual beat percept, which can modulate or improve beat perception of auditory rhythms in parallel. Furthermore, the profile of multisensory gain suggests the presence of an integrated audiovisual beat in rhythm perception and synchronization. Finally, the extent of temporal integration between auditory and visual rhythms appears to depend on the perceived congruency between the two streams. Together these results reveal an audiovisual interplay in the rhythm domain involving sounds and movements, which may be based on their sensorimotor correspondence in perception. It remains to be verified whether musicians, dancers, and the audience may employ (partially) overlapping cross-modal mechanisms for communication, synchronization, and perception.

ENABLING SYNCHRONIZATION: AUDITORY AND VISUAL MODES OF COMMUNICATION DURING ENSEMBLE PERFORMANCE

Laura Bishop[1], *Werner Goebl*[2]
[1] Austrian Research Institute for Artificial Intelligence (OFAI), Austria
[2] University of Music and Performing Arts Vienna, Austria
laura.bishop@ofai.at
goebl@mdw.ac.at

ABSTRACT

Ensemble musicians exchange nonverbal auditory and visual cues (e.g. breathing, head nods, changes in tempo/dynamics) during performance to make their intentions more predictable and help enable synchronization. The predictability of performers' intentions is higher in some musical contexts (e.g. within phrases) than in others (e.g. following held notes or long pauses), and recent research suggests that musicians' use of auditory and visual cues may change throughout a performance as the predictability of co-performers' intentions fluctuates. We present two studies that investigate the nature of cues given in high-predictability and low-predictability musical contexts, and that test musicians' abilities to use these cues during duet performance. Study 1 tested pianists' reliance on auditory and visual cues in musical contexts where timing was more or less precisely specified by the score. Pianists performed the secondo part to three duets with recordings of pianists or violinists playing the primo parts, as the presence and absence of auditory and visual visual signals from the primo were manipulated. Asynchronies between primo recording and participant secondo performances were then calculated. The results showed increased reliance on visual cues when uncertainty about co-performers' intentions was high (i.e. at re-entry points following long pauses), but a strong reliance on auditory cues otherwise. Study 2 used motion capture to map the head and hand gestures that pianists and violinists use to cue each other in at the starts of pieces. This study is currently ongoing, but forwards-backwards head acceleration is hypothesized to indicate the timing of starting note onsets, and gesture duration is hypothesized to indicate piece tempo. This research aims to enhance our understanding of which cues and modes of communication are important across different performance contexts, and is expected to benefit ongoing efforts to develop an intelligent accompaniment system capable of responding to human performance cues in real-time.

PERCEPTUAL RELEVANCE OF ASYNCHRONY BETWEEN ORCHESTRAL INSTRUMENT GROUPS IN TWO CONCERT HALLS

Henna Tahvanainen, Aki Haapaniemi, Jukka Pätynen, Tapio Lokki

Department of Computer Science
Aalto University School of Science, Finland
henna.tahvanainen@aalto.fi

ABSTRACT

Timing in a music ensemble performance is asynchronous by nature. Asynchrony is generated by the players themselves, and further delays to listeners are introduced by the location and orientation of the instruments on stage. While the musicians aim to an accurate mutual synchronization, deviating from the perfect synchrony may even produce desirable effects. For one, the timbre can appear broader as with orchestra string sections. The perceived asynchrony within an ensemble varies between 20 to 50 ms.

This paper studies the perceptual relevance of asynchrony between three orchestral instrument groups in two concert halls. Perfect synchrony was compared to 1) the bass-register instruments (double basses and timpani) played first with delays of 20 ms for middle-register instruments (cellos, bassoon), and 40 ms for treble-register instruments (winds, brass, violas, violins), and 2) the treble-register instruments played first with delays of 20 ms for middle-register, and 40 ms for bass-register instruments.

Listener preference was investigated with a paired comparison online listening test using binaural renderings of the concert halls over headphones. The results were analysed with a probabilistic choice model with latent preference groups. The analysis shows that listener preference generally depends on the asynchrony: the bass-register instrument starting first is the most preferred option in both halls while the treble-register starting first is the least preferred. The results also imply that preference on timing depends on the concert hall, and this requires future listening tests with a spatial audio system in order to reproduce the spatial characteristics of the concert halls more accurately.

1. INTRODUCTION

Perfect synchrony is practically never obtained across all players of a music ensemble. Musicians aim to synchronise their playing by their internal clock, as well as acoustic and visual cues, such as body movements of other players [1, 2]. In many cases, these cues are obstructed. For example, the maximum distance between two members of a symphony orchestra on stage translates to a propagation delay of about 30 to 50 ms which hampers the synchronisation by hearing [1]. In addition, different string sections are typically on different sides of the stage, which makes visual cues from other players difficult to follow.

Consequently, asynchrony in ensemble performance is mostly unintended. A typical value of asynchrony between players is 20 to 50 ms [3, 4, 5, 6, 7, 8, 9]. For example, the asynchrony of the bowing onsets within a string ensemble members settles somewhere between ± 30 ms respective to nominal synchrony [9]. Asynchrony of a few milliseconds can be heard, but determining the temporal order of two sounds requires a time difference of about 15 to 20 ms [10]. Furthermore, asynchrony is more difficult to detect when the lead sound is louder than the lagging sound, and this is thought to be caused by forward masking [11, 12].

Asynchrony can also be intentional, and it is often employed in ensembles for expressiveness. For instance, in string, wind, and piano duets, the melody line is typically played about 20 ms earlier in order to emphasize the melody [4, 5, 7, 13]. In jazz ensembles, the drummer often advances the melody instruments at every other beat, and this makes the music swing [6]. Informal discussions with several conductors have revealed that they occasionally utilize intentional asynchrony within the orchestra in order to achieve a desired musical expressiveness, such as the enhancement of bass.[1]

Playing in asynchrony may have benefial effects. For example, asynchrony is applied in orchestra auralisation to create instrument sections that sound natural, for example to obtain a wider timbre for string sections [14, 15]. Furthermore, when the orchestra plays in synchrony the frequencies of higher harmonics of the bass-register instruments and the fundamentals of the treble-register instruments coincide [16, 17, 18], and this may lead to undesirable simultaneous masking effects [12]. In this case, the perceived loudness of the bass-register instruments lies solely on their low frequency components which may not radiate sufficiently as the wavelengths at the low frequencies are much greater than the dimensions of the instruments [16, 19]. Thus, playing in asynchrony may help in making bass-register instruments more audible.

This study explores the perceptual relevance of intentional asynchrony within a symphony orchestra via binaural renderings in online listening test. An anechoic loudspeaker orchestra is auralised in two concert halls. The musical instruments are divided into three groups according to their register, and artificial asynchrony is introduced between the groups. The results indicate that listeners prefer asynchrony to synchrony and the preferred asynchrony is such that the bass-register instruments start to play before mid- and treble-register instruments. It seems this preference is hall-dependent, but further testing with a larger selection of concert halls is required using a spatial sound system.

2. METHODS

2.1. Participants

Thirty nine subjects (5 female) performed the online listening test (mean age=32, SD=9). 61 % reported to have taken part

[1] See for example the video "'Die Kunst des Dirigierens"' with Herbert von Karajan and Vienna Philharmonic Orchestra between 1:00-1:37 – www.youtube.com/watch?v=Shc-4AZVaNk

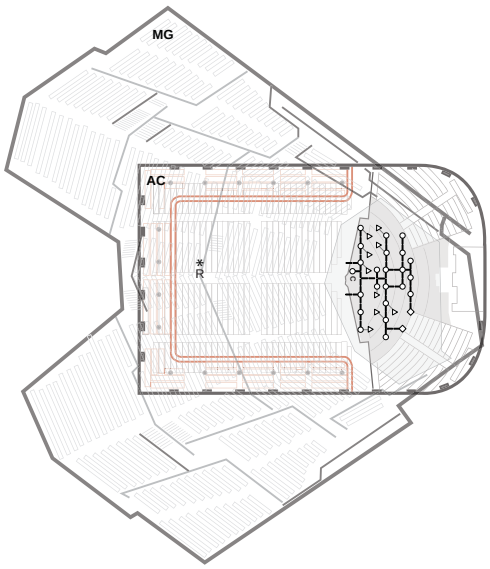

Figure 1: Plans of the concert halls superimposed with the loudspeaker orchestra position. The measurement position is marked with R and it is located at 19 m from the stage edge.

Table 1: The properties of the measured unoccupied concert halls. Reverberation time RT, and strength G are averaged over 63-8000 Hz octave bands. Clarity C_{80} is averaged over 500-1000 Hz octave bands. SDE stands for the frequency of maximum attenuation of the seat-dip effect. Note that the level of the frequency response in AC has been reduced by 2 dB.

Abbr.	Name	N	RT [s]	G [dB]	SDE [Hz]	C_{80} [dB]
AC	Amsterdam Concertgebouw	2040	2.1	-1.4	125	-2.7
MG	Munich Gasteig	2400	2.0	-1.5	99	-0.1

in listening tests before, and 82 % reported they play a musical instrument. 28 % reported they prefer listening to classical music 5 or more points on a scale of 0 to 10. Because of the online listening test, the participants could not be screened with audiometry and were thus assumed to have normal hearing. The participants used their own headphones that ranged from cheap in-ear models to professional open-ear models.

2.2. Stimuli

The stimuli for the experiment consisted of an anechoic symphony orchestra auralised in two concert halls: Amsterdam Concertgebouw (shoebox), and Munich Gasteig (fan). Their hall plans are shown in Fig. 1 and some objective parameters are listed in Tab. 1.

These concert halls were chosen because they have very similar spectral responses, when the level of the overall response in AC is reduced by 2 dB. The left-hand side of Fig. 2 shows the 20-ms and the full frequency response in both halls. The middle and the right-hand side show the time-frequency development of the frequency response at 10-ms time-window increments in AC and MG, respectively.

The symphony orchestra comprised a 24-channel loudspeaker orchestra (LSO) on stage [20]. The LSO positions on stage are shown in Fig. 3 with the corresponding channel numbers. The

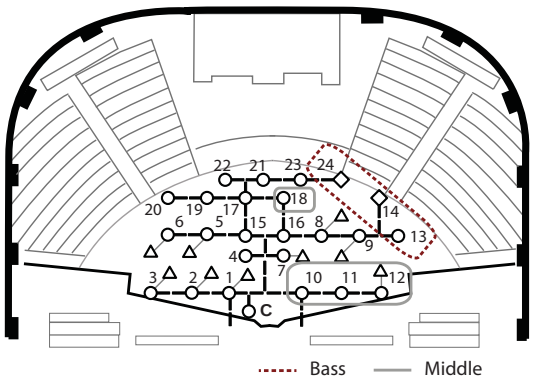

Figure 3: The position of the loudspeaker orchestra on stage with the channel numbers. The bass-register instrument (double bass and timpani) and the middle-register instruments (cellos, bassoon) are shown for this study. All the other loudspeakers contain the treble-register instruments (violas, violins, clarinets, horns, oboe, flute). The content of each channel is shown in Table 2.

Table 2: The instrument registers and their corresponding loudspeaker orchestra channel numbers.

Register	LSO Channel	Instruments
Bass	13	double bass
	14	double bass
	24	timpani
Middle	10	cello
	11	cello
	12	cello
	18	bassoon
Treble	1-6	violin
	7-8	viola
	9	viola, cello
	15	violin, flute
	16	viola
	17	clarinet
	19-20	trumpet
	21-22	trombone
	23	empty

content of the channels is listed in Tab. 2. The orchestra played the opening chord of Beethoven's 7th symphony (see Fig. 4 for score).

In brief, the stimuli were created in the following manner: the room impulse responses (RIRs) from each loudspeaker (24 channels) on the concert hall stage were measured using the logarithmic sine sweep technique with a G.R.A.S. probe at the measurement position R located 19 m from the stage edge. The RIRs were then analysed with the Spatial Decomposition Method that estimates the direction of arrival of the sound field at discrete time samples [21]. The directional estimates were then allocated to a 3D spatial sound system with 24 channels, with directions matching the nearest loudspeaker in the set-up. The binaural RIRs were obtained by filtering the loudspeaker set-up with head-related transfer functions (HRTFs) of subject no. 40 in the CIPIC database [22]. Then, the binaural RIRs were convolved with anechoic musical instrument recordings.

Because the CIPIC HRTFs are obtained in anechoic con-

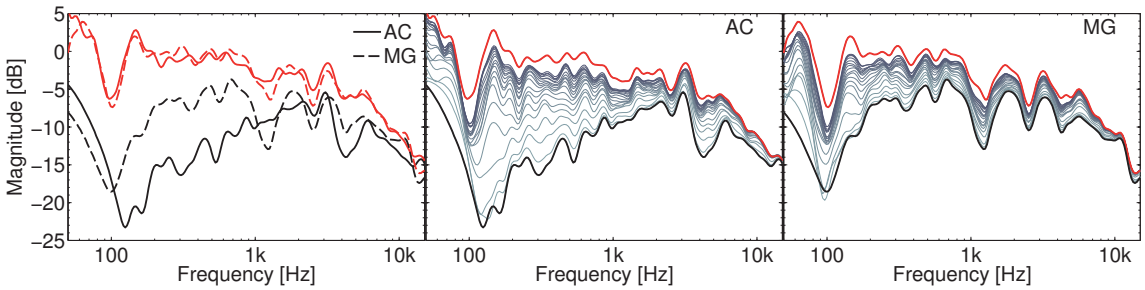

Figure 2: The time-frequency development of the frequency response of the concert halls. The top curve shows the frequency responses of the whole impulse response. The thin curves show the frequency responses at 10-ms increments with the lowest cure in bold starting at 20 ms after the direct sound. The second highest curve in bold shows the frequency response at 200 ms after the direct sound. Note that the level of the frequency response in AC has been reduced by 2 dB.

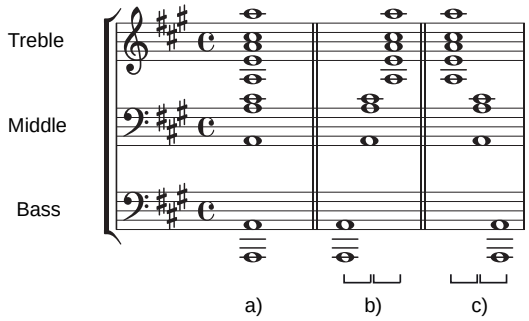

Figure 4: Score for a) perfect synchrony SYNC, b) bass-register first BMT, and c) treble-register first TMB.

ditions, the HRTFs were preprocessed with an equalisation response to better resemble listening in a normal room. The equalisation response was obtained by 1/3-octave smoothing the average of eight HRTFs on the lateral plane at 45 degree intervals, and raising the smoothed average to the power of $\alpha = 0.6$ (for more details, see [23]). Several listeners have informally evaluated the equalisation to produce a plausible binaural reproduction using CIPIC responses.

Furthermore, due to the positioning of the loudspeakers on the stage and the corresponding path length differences to the measurement position, the initial delays of the RIRs vary between the LSO channels. While this corresponds to the situation with an actual orchestra, it was undesired for the present study where exact control over the timing between channels was required. Therefore, the LSO channel IR's were synchronized by the position of their initial peaks. Similarly, the relative timing of the anechoic orchestra channels were adjusted to have synchronous physical onsets of notes. A perfect synchrony between the instruments was obtained by finding an energy threshold for both the instrument and room impulse onsets.

The convolved audio was divided into three instrument groups based on note heights/instrument registers: bass, middle, and treble, see Table 2. Various delays were applied for the three instrument groups by shifting the convolved tracks in time and summing the result. Three timings were used with delays of 0 ms, 20 ms, and 40 ms across groups. The 20-ms time difference between consecutive instrument groups was chosen based on earlier research on existing asynchrony within ensembles [4, 5], as well as on the threshold for the time difference of two events whose temporal order can be judged [10].

The first timing represents perfect onset synchrony and it is referred to as SYNC. The second timing is a case where the bass-register (B) instruments start earlier and are followed by middle-register (M) instruments after 20 ms and treble-register (T) instruments after 40 ms, and it is referred to as BMT. The third case represents the opposite case where treble-register instruments start earlier with the same relative delays (TMB). The timings are also shown in Fig. 4.

2.3. Design

The experiment was a paired comparison (two-alternative choice) test with ties allowed. The listeners were presented with 20 pairs of stimuli on a web page. They were asked to listen to each pair and to choose which of the two samples they prefer. It was also possible to choose a tie with "'Cannot say"'. The samples could be listened to as many times as needed, and all pairs were available simultaneously. Furthermore, the listeners were asked to listen with headphones in a quiet place.

The test consisted of pair combinations of six stimuli (2 halls $\times$ 3 timings = 15 pairs) in a random order. In addition, three pairs with identical samples were randomly added to the sequence in order to monitor the use of ties, and whether the listeners were listening accurately. Two additional pairs were included in the beginning of the test as the training pairs and they were excluded from the analysis.

The online listening test was implemented with HTML5 and JavaScript. Because 16-bit wav-files (sampling rate 48 kHz) and HTML5 <audio>-tags were used for playback, some browsers (e.g., Internet Explorer, Safari) could not be used in the listening test.

The listener was also asked at the end of the listening to comment freely on the basis for their preference. At the end of the web page, the listener was also asked to provide some background information including headphone type, experience in classical music, listening tests, and playing musical instruments.

2.4. Analysis methods

The results of the paired comparison experiment were analysed with a probabilistic choice model developed by Bradley, Terry [24] and Luce [25], that is based on a logistic distribution of response differences. The BTL-model describes the probability of an item to be preferred over the others with a specified attribute. The previous auditory perception studies include various attributes, such as unpleasantness [26, 27]; eventfulness [27]; spaciousness, brightness, naturalness, distance [28]; and level of bass and articulation [29]. In this case, the dimension is *preference*.

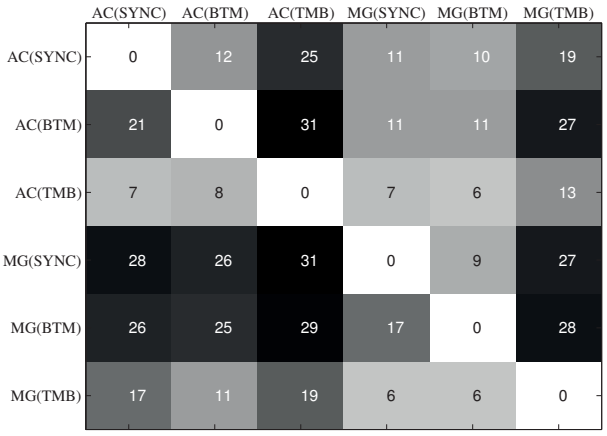

Figure 5: The preference matrix. The number indicates the absolute frequency with which the sample in the row was preferred over the sample in the column. A darker colour indicates a higher frequency. Since each participant was presented the pair once, the maximum frequency is 39.

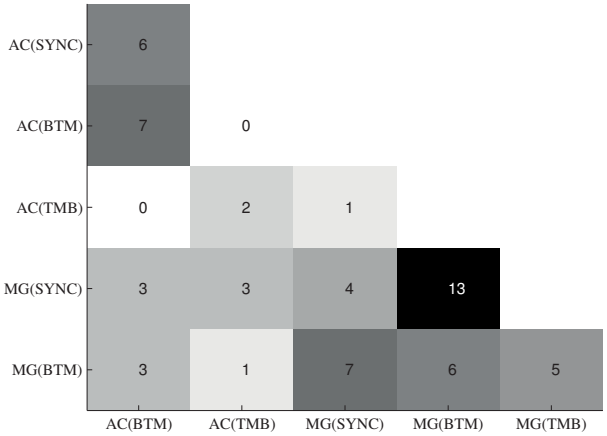

Figure 6: Number of ties for each comparison pair. A darker colour indicates a higher frequency. Note that matrix is triangular, because the presentation order of the pairs has been ignored.

Allowing ties in the paired comparison experiment makes the analysis of the results more complicated [30, 31, 32]. While a number of packages (for an example for R and Matlab see [33]) are available for the analysis of paired comparison experiments, most of them consider the two-alternative forced choice procedure only, and prohibit ties in the data. In the simplest treatment, the ties can be neglected, split, or apportioned either randomly, or according to some criterion [34]. Rao and Kupper [30] proposed that when the difference between two responses is below a certain threshold, a tie is declared. Davidson [31] proposed that the probability of a tie is proportional to the geometric mean of the preference probabilities. For the data in this study the probabilities do not differ significantly between the Davidson model for ties (implemented in the psychotools-package in R) and discarding the ties. Thus, the ties have been discarded in the following BTL-models.

Moreover, untrained listening test subjects may not necessary form a homogeneous group, and thus the data may include latent preference groups [35, 34]. Consequently, the data was segmented using a latent class model developed by Courcoux et al [35]. This approach includes a Monte Carlo significance test procedure in order to determine the adequate number of classes or groups. Here, 100 Monte Carlo random samples with size of the number of subjects (39) were drawn for models with an increasing number of latent groups. The segmentation that best fits the data can be found with a likelihood ratio statistic between the groups. The BTL-model can then be applied to each latent group separately.

3. RESULTS

Combining the individual data of all the participants yields a preference matrix in Fig. 5 without the ties. It shows the absolute frequencies of the preferred samples. The bottom-left quadrant has the highest frequencies, showing that MG is generally preferred over AC.

The portion of ties was about 10% of all the answers and they are plotted in Fig. 6. The most ties occur in MG between SYNC and BMT (about 33 %), while between other pairs the percentage of ties is about 18% or less.

The top plot of Figure 7 shows the results of the BTL-model of all the answers. The BTL-model shows that MG appears to be preferred with all timings. By implementating the segmentation, a model with three latent groups was found to best fit the data. The bottom plot of Figure 7 shows the BTL-model for each of the three latent groups. The first two groups with 6 and 19 subjects, respectively, prefer MG over AC in general. The third group consists of 14 subjects that somewhat prefer AC to MG. As for the preference of timing, the first group prefers BMT timing in MG. In the second group the only significant result is the SYNC and BMT are clearly most preferred in MG. In the third group, none of the timing adjustments is clearly preferred.

Based on the top plot of Fig. 7, it appears that the differences between hall acoustics were a more dominating feature than synchrony for the preference. Hence, the preference of timing adjustment in each hall is not clearly observed in the BTL-model. Therefore, the between-concert-hall pairs were excluded and the effect of timing was analysed in each hall separately. In a similar manner to all the data, this subset of data can be segmented. In AC, the 39 subjects are best-fitted to a two-group model, and in MG to a single-group model. The BTL-model for these groups is shown in Fig. 8. In AC, eight listeners prefer the TMB timing, while the other 31 listeners prefer the BMT. In MG, the BMT timing is most likely preferred, but is not significantly different from the preference of SYNC.

Neither age, sex, preference of classical music, nor experience in listening tests or playing a musical instrument were significantly different between the obtained groups.

4. DISCUSSION

The results indicate that synchrony between symphony orchestra instrument groups is relevant for preference. In general, the case when the treble-register instruments started to play (TMB) first, was the least preferred. One of the explanations could be that the percussive timpani is played later than most instruments which gives a sensation of being ”off-beat”. However, there was a group of eight people in AC that actually preferred the treble-register instruments starting first. It is possible that these listeners prefer a soft attack of the timpani, as some of them reported. The soft attack is likely caused by forward-masking of the other instruments.

The results further indicate the preferred timing, or asynchrony, may differ across concert halls. In the two halls studied, the bass-register instruments playing first (BMT) was gen-

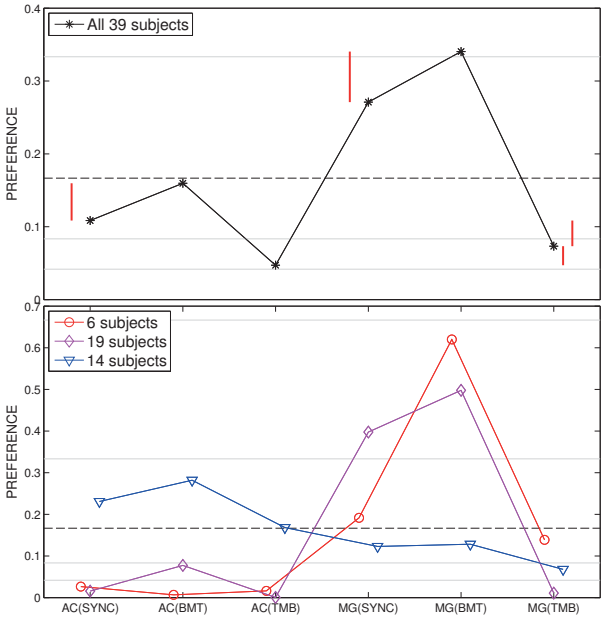

Figure 7: The BTL-model for the probability of preference over all stimuli before and after grouping. The results are displayed on a ratio scale, where the sum of ratios is normalised to unity. The black dashed line indicates the probability of chance (1/6). The 95% confidence intervals are not shown in order to retain clarity. The non-significant differences between the values are indicated with vertical lines on top plot. For the bottom plot, the thin lines indicate the doubling of the probability (on a logarithmic scale). If two values fall within the same area formed by two lines, generally no significant difference exists between the values.

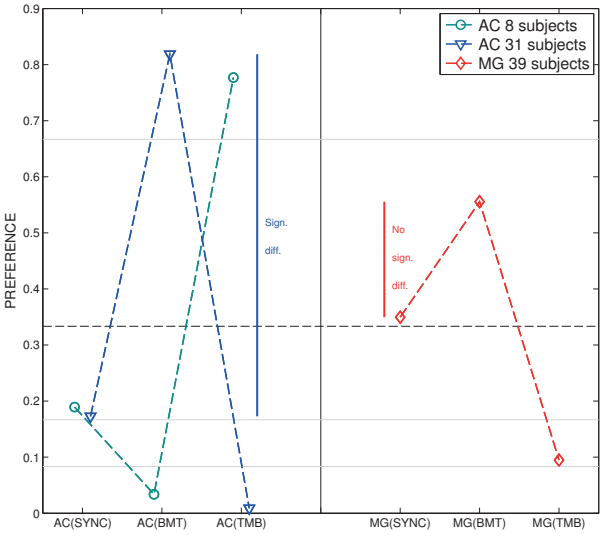

Figure 8: The BTL-model for the probability of preference over timing for each hall separately. The significances of the value differences are indicated with vertical lines.

erally preferred but in MG the difference to perfect synchrony (SYNC) is insignificant. The high amount of ties in MG between BMT and SYNC shows that adjusting the timing may not be as important in MG as in AC, as long as it is natural (not ”off-beat”).

The preference differences between the concert halls may be at least partially explained by the seat-dip effect. Namely, the time-frequency responses of the two halls differ in the temporal increase of the level at both low and mid-high frequencies from about 100 Hz until 1 kHz (see Fig. 2), and this frequency range is mostly affected by the seat-dip effect [36]. The seat-dip effect refers to the attenuation that the direct sound arriving at grazing angles to the seats undergoes at low frequencies. This leads to a more audible lack of bass in some concert halls than in others [37, 38, 29]. The effect is observed as a dip in the frequency response by 20 ms after the direct sound, and it is caused by a destructive interference between the direct sound and reflections from the tops of the seat backs. Depending on the further reflections in the concert hall that do not arrive at the listener at grazing angles, the dip can diminish. Previous research shows that the perception of bass can be enhanced if direct sound lack the low frequencies, but early frequencies retain it [39].

In MG, the seat-dip effect at 20 ms is a narrow band dip centred around 100 Hz. While the magnitude of frequency response increases steadily with time, the response retains its shape, including the dip. On the contrary, in AC the dip is at a slightly higher frequency and it covers a wide frequency range. What is more, the frequency response in AC becomes flatter with time and the dip becomes smaller. Consequently, in AC the main boost of the low and mid-high frequencies is delayed. This means that when the orchestra plays simultaneously, the low frequencies are initially hampered by the seat-dip effect. If the bass-register instruments anticipate a little, their low and mid-high frequencies will arrive at the listener closer in time with the treble instruments.

In other words, it is more difficult to play in AC than in MG, since timing of the instruments is crucial. The bass-register instruments should play first in AC because of the strong time-frequency development of the frequency response. And when asynchrony is applied to playing chords in AC, the effect is much more salient than in MG where the time-frequency development of the frequency response mostly consists of increasing level.

An alternative explanation is that AC might benefit from the bass-register instruments starting first due to some masking effects. Because the mid-high frequency response is delayed, the higher partials of the bass-register instruments are less masked by the treble-register instruments, when the bass-register instruments start to play earlier.

The overall preference of MG over AC is not in line with the other published results on concert hall preference [40]. One of the reasons could be the chosen stimuli. The stimuli consisted of onlyone chord which makes it susceptible to small variations. For example, in MG the timpani can be heard sharper than in AC, which is likely to increase overall preference towards MG.

Another reason for the inconsistent preference results could be the reproduction method. The correct spatiotemporal development in the concert hall auralisations is essential and its quality may deteriorate from the lack of both individualised HRTFs and head tracking, as well as the lack of headphone equalisation. Finally, the listeners participated in the test in an uncontrolled environment. Thus, there may have been many kinds of distractions. Consequently, a listening test in a controlled environment with a more elaborate spatial sound reproduction is required to confirm the results of the internet experiment. Further listening tests could also focus on the possible enhancement of bass with asynchronous playing.

5. CONCLUSIONS

Intentional asynchrony within three groups of symphony orchestra instruments were studied via binaural renderings of concert halls. The results show that in a shoebox-shaped hall AC, it is preferable to play chords asynchronously so that the double basses and timpani start first, and are then followed by the cello and bassoon, and finally by violins, violas, woodwinds and brass. In a fan-shaped hall MG, there is no clear preference towards sychrony or asynchrony as long as the low frequencies are not too late. However, in neither of the halls the treble-register instruments should start first. The preference differences can at least partially be account for by the seat-dip effect and the subsequent time-frequency development of the frequency response.

6. ACKNOWLEDGMENTS

The research leading to these results has received funding from the Academy of Finland, project no. [257099].

7. REFERENCES

[1] G. M. Naylor, "The achievement of ensemble," *Applied Acoustics*, vol. 23, no. 2, pp. 109–120, 1988.

[2] P. E. Keller and M. Appel, "Individual differences, auditory imagery, and the coordination of body movements and sounds in musical ensembles," *Music Perception*, vol. 28, no. 1, pp. 27–46, 2010.

[3] D. Deutsch, "Hearing music in ensembles," *Physics Today*, vol. 63, no. 2, pp. 40–45, 2010.

[4] R. A. Rasch, "Synchronization in performed ensemble music," *Acustica*, vol. 43, no. 4, pp. 122–131, 1979.

[5] L. H. Shaffer, "Timing in solo and duet piano performances," *The Quarterly Journal of Experimental Psychology*, vol. 36, no. 4, pp. 577–595, 1984.

[6] A. Friberg and A. Sundström, "Swing ratios and ensemble timing in jazz performance: Evidence for a common rhythmic pattern," *Music Perception*, vol. 19, no. 3, pp. 333–349, 2002.

[7] W. Goebl and C. Palmer, "Synchronization of timing and motion among performing musicians," *Music Perception*, vol. 26, no. 5, pp. 427–438, 2009.

[8] G. P. Moore and J. Chen, "Timings and interactions of skilled musicians," *Biological Cybernetics*, vol. 103, no. 5, pp. 401–414, 2010.

[9] J. Pätynen, S. Tervo, and T. Lokki, "Temporal differences in string bowing of symphony orchestra players," *Journal of New Music Research*, vol. 41, no. 3, pp. 223–237, 2012.

[10] I. J. Hirsh, "Auditory perception of temporal order," *The Journal of the Acoustical Society of America*, vol. 31, no. 6, pp. 759–767, 1959.

[11] W. Goebl and R. Parncutt, "The influence of relative intensity on the perception of onset asynchronies," in *Proceedings of the 7th International Conference on Music Perception and Cognition, Sydney, Australia*, 2002.

[12] B. Moore, *An introduction to the psychology of hearing*, Brill, 2012.

[13] W. Goebl and R. Parncutt, "Asynchrony versus intensity as cues for melody perception in chords and real music," in *Proceedings of the 5th Triennial ESCOM Conference, Hanover, Germany*, 2003.

[14] M. C. Vigeant, L. M. Wang, and J. Holger Rindel, "Investigations of orchestra auralizations using the multichannel multi-source auralization technique," *Acta Acustica united with Acustica*, vol. 94, no. 6, pp. 866–882, 2008.

[15] J. Pätynen, S. Tervo, and T. Lokki, "Simulation of the violin section sound based on the analysis of orchestra performance," in *Proceedings of IEEE Workshop on Applications of Signal Processing to Audio and Acoustics (WASPAA 2011)*, New Paltz, NY, USA, 2011, pp. 173–176.

[16] J. Meyer and U. Hansen, *Acoustics and the Performance of Music*, Springer, New York, NY, USA, 2009.

[17] N. Nishihara and T. Hidaka, "Loudness perception of low tones undergoing partial masking by higher tones in orchestral music in concert halls," *Journal of the Acoustical Society of America*, vol. 132, no. 2, pp. 799–803, 2012.

[18] L. J. Trainor, C. Marie, I. C. Bruce, and G. M. Bidelman, "Explaining the high voice superiority effect in polyphonic music: Evidence from cortical evoked potentials and peripheral auditory models," *Hearing Research*, vol. 308, pp. 60–70, 2014.

[19] A. Askenfelt, "Eigenmodes and tone quality of the double bass," in *Dept for Speech, Music, and Hearing – Quarterly Progress and Status Report*, Roayl Institute of Technology, Stockholm, Sweden, 1982, vol. 23, pp. 149–174.

[20] J. Pätynen, *A Virtual Loudspeaker Orchestra for Studies on Concert Hall Acoustics*, PhD dissertation, Aalto University School of Science, Espoo, Finland, 2011.

[21] S. Tervo, J. Pätynen, and T. Lokki, "Spatial decomposition method for room impulse responses," *Journal of Audio Engineering Society*, vol. 61, no. 1, pp. 1–13, 2013.

[22] V. R. Algazi, R. O. Duda, D. M. Thompson, and C. Avendano, "The CIPIC HRTF database," in *IEEE Workshop on the Applications of Signal Processing to Audio and Acoustics (WASPAA2001)* , New York, NY, USA, 2001, pp. 99–102.

[23] J. Pätynen, S. Tervo, and T. Lokki, "Amplitude panning decreases spectral brightness with concert hall auralizations," in *Proceedings of the 55th International Conference of the Audio Engineering Society: Spatial Audio*, Helsinki, Finland, 2014.

[24] R. A. Bradley and M. E. Terry, "Rank analysis of incomplete block designs: I. The method of paired comparisons," *Biometrika*, pp. 324–345, 1952.

[25] R.D. Luce, *Individual Choice Behaviour. A Theoretical Analysis.*, Wiley, New York, 1959.

[26] W. Ellermeier, M. Mader, and P. Daniel, "Scaling the unpleasantness of sounds according to the btl model: Ratio-scale representation and psychoacoustical analysis," *Acta Acustica united with Acustica*, vol. 90, no. 1, pp. 101–107, 2004.

[27] B. De Coensel, S. Vanwetswinkel, and D. Botteldooren, "Effects of natural sounds on the perception of road traffic noise," *The Journal of the Acoustical Society of America*, vol. 129, no. 4, pp. EL148–EL153, 2011.

[28] S. Choisel and F. Wickelmaier, "Evaluation of multichannel reproduced sound: Scaling auditory attributes underlying listener preference," *The Journal of the Acoustical Society of America*, vol. 121, no. 1, pp. 388–400, 2007.

[29] H. Tahvanainen, J. Pätynen, and T. Lokki, "Studies on the perception of bass in four concert halls," *Psychomusicology: Music, Mind and Brain*, 2015.

[30] P. V. Rao and L .L. Kupper, "Ties in paired-comparison experiments: A generalization of the Bradley-Terry model," *Journal of the American Statistical Association*, vol. 62, no. 317, pp. 194–204, 1967.

[31] R. R. Davidson, "On extending the Bradley-Terry model to accommodate ties in paired comparison experiments," *Journal of the American Statistical Association*, vol. 65, no. 329, pp. 317–328, 1970.

[32] D. E. Critchlow and M. A. Fligner, "Paired comparison, triple comparison, and ranking experiments as generalized linear models, and their implementation on GLIM," *Psychometrika*, vol. 56, no. 3, pp. 517–533, 1991.

[33] F. Wickelmaier and C. Schmid, "A Matlab function to estimate choice model parameters from paired-comparison data," *Behaviour Research Methods, Instruments, and Computers*, vol. 36, no. 1, pp. 29–40, 2004.

[34] H. T. Lawless and H. Heymann, *Sensory Evaluation of Food: Principles and Practices*, Springer Science & Business Media, 2010.

[35] Ph. Courcoux and M. Semenou, "Preference data analysis using a paired comparison model," *Food Quality and Preference*, vol. 8, no. 5, pp. 353–358, 1997.

[36] H. Tahvanainen, J. Pätynen, and T. Lokki, "Analysis of the seat-dip effect in twelve European concert halls," *Acta Acustica united with Acustica*, vol. 101, no. 4, pp. 731–742, 2015.

[37] T. Schultz and B. Watters, "Propagation of sound across audience seating," *Journal of the Acoustical Society of America*, vol. 36, no. 5, pp. 885–896, 1964.

[38] G. Sessler and J. West, "Sound transmission over theatre seats," *Journal of the Acoustical Society of America*, vol. 36, no. 9, pp. 1725–1732, 1964.

[39] A. Walther, P. Robinson, and O. Santala, "Effect of spectral overlap on the echo threshold for single reflection conditions," *Journal of the Acoustical Society of America*, vol. 134, no. 2, pp. EL158–EL164, 2013.

[40] L. L. Beranek, *Concert Halls and Opera Houses: Music, Acoustics, and Architecture*, Springer- Verlag, New York, USA, 2nd edition, 2004.

PLAYING SLOW IN REVERBERANT ROOMS – EXAMINATION OF A COMMON CONCEPT BASED ON EMPIRICAL DATA

Zora Schärer Kalkandjiev and Stefan Weinzierl

Audio Communication Group
TU Berlin, Germany
zora.schaerer@tu-berlin.de, stefan.weinzierl@tu-berlin.de

ABSTRACT

During the performance of music the room acoustical environment has a substantial influence on the player's perception of the music. This presumably affects his way of playing, the more so if one assumes an inner reference that he wants to convey to the audience. Reducing the tempo in very reverberant rooms is a strategy that is often reported by musicians and it was, for example, recommended by J. J. Quantz in his famous music treatise in 1752. In this paper, the data collected in a field study conducted with a cellist in 7 European concert halls and a laboratory study conducted with 12 musicians in 14 virtual performance spaces is used to investigate in how far this strategy is actually followed in practice. A software-based analysis of the recordings of the musicians as well as room acoustical measurements in the halls were the basis for a statistical analysis of the influence of parameters like T_{30}, or ST_{late} on the tempo of the pieces played in each concert hall. The results suggest that the adjustment of tempo strongly depends on the basic tempo of the performed music and that there are different types of strategies adopted by musicians. These are elucidated by statements collected in interviews that were conducted with the performers during the experiments.

1. INTRODUCTION

The way musicians perceive their own tonal rendition depends on the rooms they perform in, since the acoustics of a performance space has a strong effect on the sound of the music that is played. It is likely that performers make certain adjustments in their way of playing to adapt to the room acoustical surrounding. An interrelation that is frequently named by musicians is that reverberant rooms require a reduced tempo. In his work on flute playing, already J. J. Quantz gave a detailed description of how notes are blurred if they are played too fast in reverberant rooms and advocated a reduced tempo under these conditions [1]. This kind of adjustment was similarly recommended by music scholars in their treatises of the 20th century [2] [3].

There are only few empirical investigations on the influence of reverberance on the playing tempo of musicians and they have yielded partly conflicting results. An early study carried out with the Cleveland Orchestra used the duration of whole movements as measure for the tempo played in halls with reverberation times of between 1 s and 2.1 s [4]. The results did not confirm the expected negative linear relation between tempo and reverberation time but instead implied a negative correlation between the room acoustical quality and the duration of the movements. An investigation using a MIDI grand piano played by different performers in a room with variable acoustics used the inter-onset-intervals of the recorded MIDI tones as measure for the tempo [5]. Surprisingly, no influence of any of the room acoustical parameters (reverberation time, late reverberation level, ratio between direct sound and early reflections, spectral properties of reverberation) on the mean tempo of the music pieces could be demonstrated. In a laboratory study carried out in an anechoic room, soloists of different instruments played musical phrases in room acoustical environments simulated with 6-channel loudspeaker reproduction [6] [7]. Interestingly, most of the musicians not only reduced their playing tempo (measured by the mean phrase duration) in very reverberant rooms but also under anechoic conditions.

All studies mentioned above were focused on the reverberation time as the only room acoustical measure for reverberance, disregarding other features that are perceptually more relevant from the performer's perspective. Moreover, a sufficiently large variance of room acoustical conditions should be provided in order to cover the whole range of possible performance venues and to identify also non-linear interrelations.

In the studies presented here, two different approaches were taken to further explore the relation between reverberance and tempo: A case study with a renowned solo cellist was carried out in real concert halls and a laboratory study using computer models of concert spaces that were auralised by means of dynamic binaural synthesis was conducted with twelve performers of six orchestral instruments. In both studies, the musicians' performances of different pieces were recorded, a software-based analysis of the recordings was employed to quantify the tempo of the music performances and room acoustical parameters typically used to predict reverberance were determined in the performance spaces. This was the basis of a statistical analysis designed to investigate the effect of the room acoustical conditions on the tempo, thereby taking into account the influence of the basic tempo of the performed pieces and, in the laboratory study, the played instrument and the performers' individuality. The two studies are described in detail in [8] and [9], respectively.

2. METHODS

2.1 Recordings and performance analysis

The case study was carried out in collaboration with the cellist Jean-Guihen Queyras who performed the *Six Suites for Violoncello Solo* by J. S. Bach in seven European concert halls (6 suites × 6 movements = 36 pieces). He was recorded with a boundary layer microphone (Schoeps BLM 03 C) that was placed 11.5 cm from his cello spike, so it was positioned almost in the centre of the hemispherical directivity of the microphone. Thus, the distance between instrument and microphone remained constant and inclinations of the cello during the performances did not cause any loudness fluctuations in the recordings. Because of the short distance between instrument and microphone the influence of the sound of the rooms could be neglected.

The laboratory study took place in the fully anechoic chamber of the TU Berlin (V = 1850 m^3, f_c = 63 Hz) and was conducted with six instruments each played by two professional solo musicians: violin, cello, clarinet, bassoon, trumpet and trombone. The musicians played excerpts of approx. 1 minute duration of two pieces of their own choice that had a calm and lively character, respectively (see [9] for a list of the pieces). They were recorded with a miniature microphone (Sennheiser MKE 1) that was attached directly to the instruments (see Figure 3).

The method for deriving a description of the tempo chosen by the musicians in their performances on the basis of the recordings was aimed at a perceptually meaningful analysis. By means of a software-based analysis five technical tempo related features on note- and beat-level were extracted from the software [10]. To predict the tempo of musical pieces as perceived by listeners, two of these technical features were used as predictor variables in a regression formula with 90% explained variance that was obtained in [11].

2.2 Room acoustical parameters

In all the studies on the effect of room acoustics on music performance mentioned above, the reverberation time *RT* was used as a measure for the duration of reverberation. When evaluating the comments and recommendations of musicians and music scholars, it is however not entirely clear, if it is the total duration of reverberation that mostly influences the choice of tempo. According to [12] the early decay time *EDT* and the late support ST_{late} are more appropriate parameters to predict the reverberance perceived by listeners and musicians, respectively. The late sound strength G_l was recently recommended as a parameter similar to ST_{late} but with less measurement uncertainty [13]. Finally, the blurring of tones as described by Quantz might also be related to the clarity of a concert hall, which is predicted by the parameter C_{80}. To investigate the influence of reverberance on the musical tempo, all of the five above mentioned room acoustical parameters were taken into account.

In the field study, room acoustical measurements according to [12] were carried out in the seven concert spaces (see [8] for a detailed description of the halls). The aim of the study was to determine the room acoustical conditions during the cellist's concerts as exactly as possible in order to draw valid conclusions about their influence on his way of playing. Thus, computer models of the concert spaces were constructed and their room acoustical properties were fitted to the measurements taken in the real halls (this routine is described in detail in [8]). Then, the presence of an audience as well as a source with the directivity of a cello was simulated in the models [14] [15] before carrying out room acoustical measurements. The directional source was thereby placed at 0.6 m height at the same stage position where the cello had been during the concerts and the receiver was positioned at 1.2 m height and 0.4 m from the source. The five room acoustical parameters used as independent variables in this paper were determined with the above source-receiver-setup and are denoted by the subscript *vlc* in the following. The values measured for the concert spaces of the field study are shown in Figure 1.

The 14 concert halls simulated in the laboratory study were computer models based on existing halls [16] [17] [18] [8] representing typical performances spaces for Western classical music (see [9] for a detailed description of the halls). The room acoustical properties of these models were determined with a receiver placed at the centre of each stage 2.5 m from the stage edge at a height of 1.2 m and with sources conforming to the directivities of the instruments involved in the experiments [14] [15] that were placed at their respective typical distance from the receiver [9]. The parameters measured in the room models using the described source-receiver-setup are denoted by the subscript *ins* in the following. The five parameters used in this paper to describe the reverberance of the simulated halls are shown in Figure 2.

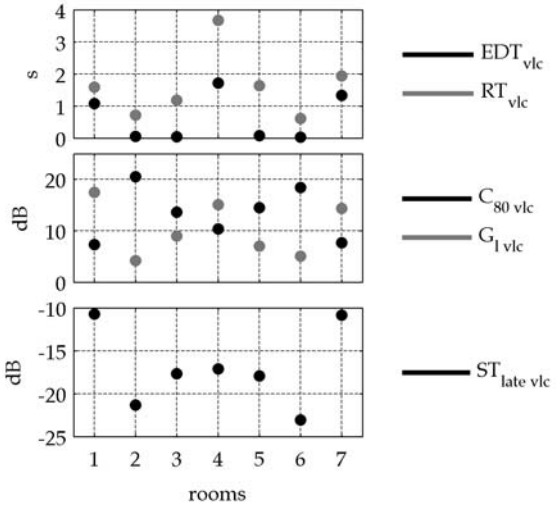

Figure 1: Room acoustical parameters measured on stage of the concert halls of the field study using a source with the directivity of a cello and a source-receiver distance typical for a cellist and his instrument.

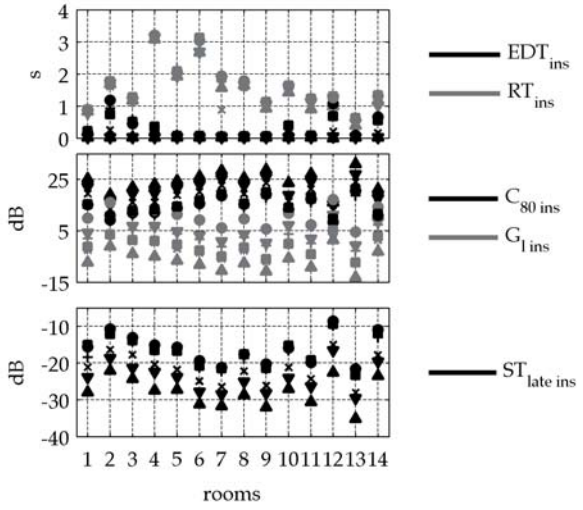

Figure 2: Room acoustical parameters measured on stage of the concert halls of the laboratory study using sources with the directivity of the involved instruments (×: Vl, +: Vlc, ▼: Cl, ▲: Fg, ●: Trp, ■: Trb) and a source-receiver distance typical for a musician and his instrument.

2.3 Experimental procedures

The cellist in the field study was recorded during his regular performances of the *Six Suites for Violoncello Solo*, which took place over the course of one year. After each concert, a guided interview was conducted, in which he was asked to describe the room acoustics of the hall he had performed in as well as his way of playing and conscious adjustments that he had made.

The room acoustical environments in the laboratory study were simulated on the basis of the computer models by means of dynamic binaural synthesis [19]. The method for acquiring binaural room impulse responses (BRIRs) from the models is

described in detail in [9] and yielded one dataset for each of the 14 rooms for head rotations between ±50°and head elevations between -30° and 21° with a resolution of 2° and 3°, respectively. During the experiment, the head movements of the musicians were detected by head tracking (Polhemus Patriot) in order to select the appropriate BRIR from the dataset and to convolve it in real-time with the anechoic input signal recorded at the instrument. It was only the response of the room that was thereby simulated, since the direct sound of the instrument was produced in the real experimental environment. The simulation was presented to the performers with extra-aural headphones (AKG K-1000) that barely impeded the instrument's direct sound path to the performer's ears. The frequency responses of the recording microphone and the headphones were equalised, the latter was compensated individually for each musician [20]. Prior to the recording session, the performers were given 10 minutes to become familiar with each virtual room. Then, they were recorded playing excerpts of two music pieces and interviewed with the same questions that had been used in the field study. The warm-up, the recording of the same two pieces and the guided interview was repeated in each of the randomly presented virtual rooms.

Figure 3: Left: Microphone attached to a violin in the laboratory study. Right: Violinist playing in a simulated concert hall while wearing extra-aural headphones.

2.4 Statistical analysis

The aim of the statistical analyses was to reveal the effect of the five room acoustical parameters on the tempo chosen by the musicians when playing the 36 pieces in 7 concert halls (field study) and the 2 pieces in 14 concert halls (laboratory study) in separate analyses for each of the two datasets. By using hierarchical linear models (HLMs) as analysis method [21], the nested structure of the data (pieces, rooms / pieces, musicians, rooms) was accounted for, since variances were considered on each level of the data.

Before the actual analysis, the variances on each level were compared separately for both datasets by using intercept-only HLMs, i.e. models with no regressors that only consider the grouping structure of the data. This showed that for the laboratory dataset the variance on the room level was very small compared to the variance on the other levels. This implies that the variance of the musicians' individual adjustments to the room acoustics was greater than the variance of their averaged adjustments, i.e. that the players' reaction patterns to the room acoustical environment were highly individual. Since the room level variance was so small, indicating that the room level was not relevant in the hierarchical structure, this level was omitted in the further analysis [21].

Since high correlations between the five room acoustical parameters would have caused problems of multicollinearity, the parameters were not used as five predictors in single HLMs but rather as single predictors in five HLMs. Furhtermore, the results of previous studies have indicated that the relation between tempo and reverberance might be inversely quadratic [6]. To explore this evidence, the room acoustical parameters were used as squared predictors in further HLMs. In total, ten HLMs were calculated for each dataset with the restricted maximum likelihood method and standardised independent and dependent variables by using one of the five room acoustical parameters shown in Figure 1 and Figure 2 either as squared or as linear predictor.

The resulting models were compared by calculating their explained variance on the room and musician level, respectively, with the following formula [22]:

$$R^2_{\text{level 2}} = 1 - \frac{\sigma^2_{\text{M1 | level 2}} + \frac{\sigma^2_{\text{M1 | rest}}}{n}}{\sigma^2_{\text{M0 | level 2}} + \frac{\sigma^2_{\text{M0 | rest}}}{n}} \qquad (1)$$

$\sigma^2_{\text{M1 | level 2}}$ and $\sigma^2_{\text{M1 | rest}}$ are the level 2 (room / musician) variance and the residual variance of the target model M1. $\sigma^2_{\text{M0 | level 2}}$ and $\sigma^2_{\text{M0 | rest}}$ are the variance on the respective levels in an intercept-only model M0 with no predictors. *n* is the number of groups (rooms / musicians).

3. RESULTS

Figure 4 and Figure 5 show the regression coefficients β (black *) with 95% confidence intervals for the single regressors in each HLM calculated with the data of the field and the laboratory study, respectively. The figures show the regression coefficients for that version of each predictor (linear or squared) that had the higher explanatory power. Each β illustrates the extent and significance of the effect of each room acoustical predictor on the *tempo* derived from the recordings with CIs not crossing the zero-line being considered as a significant effect.

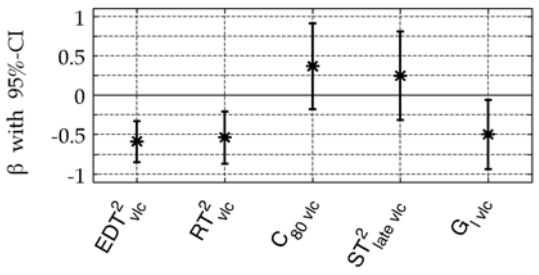

Figure 4: Field study – Standardised regression coefficients with 95% confidence intervals (CIs) for the five room acoustical parameters (x-axes) predicting the response variable *tempo*. CIs not crossing the zero-line indicate significant coefficients ($p < 0.05$).

As can be seen in Figure 4, the cellist in the field study significantly reduced his tempo in rooms with long EDT_{vlc} and RT_{vlc} as well as high $G_{\text{1 vlc}}$. Similar to the results of [6], he also reduced his tempo with low EDT_{vlc} and RT_{vlc}. The difference between the effects of EDT_{vlc} and RT_{vlc}, on the one hand, describing the duration of reverberation (quadratic relation) and $G_{\text{1 vlc}}$ on the other hand, describing the strength of reverberation (linear relation), indicate that these parameters are related to different perceptual qualities on the side of the musician. It is noteworthy that the strongest effect on *tempo* can be observed for EDT_{vlc}^2 with an explained variance of 74.36%. In the interviews conducted after the concerts, the cellist not only reported to slow down in reverberant environments to avoid a muddled sound, which is in line with Quantz. He furthermore mentioned the prolongation of pauses under such conditions, which additionally contributes to a reduced overall tempo. His

slowing down in rooms with short duration of reverberation might be due to the prolongation of notes as a strategy to compensate for the lack of sound decay, as it was addressed by other musicians in [23].

Figure 5 shows that in the laboratory study the *tempo* averaged over musicians and pieces was significantly reduced in rooms with long RT_{ins} and significantly increased in rooms with high and low $G_{l\,ins}$. Again this indicates a separate perception of duration and strength of reverberation, but the linear and quadratic relations between these aspects and *tempo* are contrary to the results of the field study. Furthermore, a strong tendency for a positive effect of $C_{80\,ins}{}^2$ and $ST_{late\,ins}{}^2$ can be observed. The strongest effect on the mean *tempo* of the musicians of the field study can be observed for RT_{ins}. It is apparent that the effects in Figure 5 are much smaller than in Figure 4 (different scaling of the y-axes). This is due to the fact that the HLM coefficients in Figure 5 were calculated for the *tempo* averaged over musicians and pieces, while at the same time the adjustment strategies of the performers were very individual. To be able to compare the explanatory power of the predictor RT_{ins} to the one of $EDT_{vlc}{}^2$ as predictor for the data of the field study, an HLM was calculated for the laboratory dataset with RT_{ins} as predictor and the individual musicians as additional factor to take into account their individual adjustment strategies. This resulted in an explained variance of 8.73%.

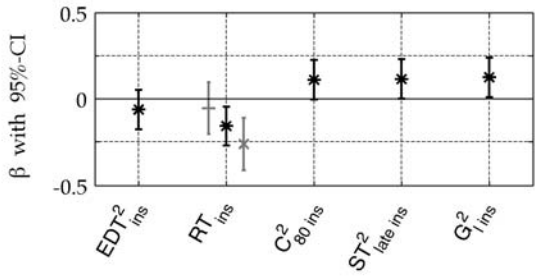

Figure 5: Laboratory study – Standardised regression coefficients with 95% confidence intervals (CIs) for the five room acoustical parameters (x-axes) predicting the response variable tempo. The coefficients of the HLM with room acoustical predictors only are shown as black *, coefficients of an HLM with ‚basic tempo' as additional factor are shown in grey (−: ‚fast'; ×: ‚slow'). CIs not crossing the zero-line indicate significant coefficients ($p < 0.05$).

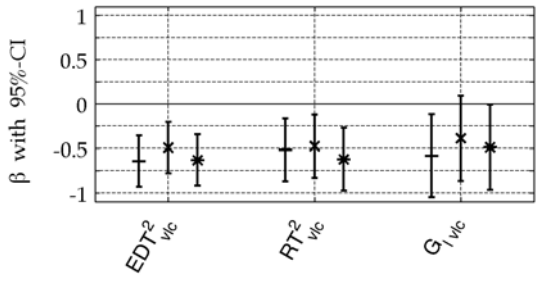

Figure 6: Field study – Standardised regression coefficients with 95% CIs for the room acoustical parameters separately predicting the *tempo* of the movements classified by the factor 'basic tempo'. –: variable, ×: slow, *: fast. CIs not crossing the zero-line indicate significant coefficients ($p < 0.05$).

To investigate the interaction of the basic tempo of the played pieces with the influence of the room acoustical parameters on *tempo*, the movements of each suite played by the cellist in the field study were classified as 'variable' (movements 1 and 5), 'slow' (movements 2 and 4) and 'fast' (movements 3 and 6). Then, 3 HLMs were calculated by using each of the significant room acoustical parameters shown in Figure 4 as predictor and the basic tempo as additional factor. Figure 6 shows the resulting regression coefficients with 95% CIs and illustrates that the effect of the reverberance on *tempo* was slightly stronger for the movements with 'variable' and 'fast' basic tempo, while the 'slow' movements were less affected.

The grey – and × in Figure 5 show the regression coefficients of an HLM with RT_{ins} as predictor and the basic tempo of the two pieces ('fast', 'slow') played by the performers in the laboratory study as additional factor. The difference between the two pieces regarding the effect of the other room acoustical parameters was very small, so these coefficients are not shown here. It becomes apparent that on average the musicians played the slow pieces quite considerably slower than the fast pieces in rooms with long RT_{ins}. In the guided interviews of the laboratory study, almost all musicians reported to prolong pauses in reverberant environments. However, it was explained that this strategy was used primarily for slow pieces, while for fast pieces the focus rather lay on clear, short articulation. Thus, these statements support the statistical evidence very clearly.

In Figure 7 the influence of RT_{ins} on the 'slow' and 'fast' pieces played in the laboratory study is shown separately for each instrument. It can be seen that it was the celli, the bassoons, the trumpets and the trombones who significantly reduced the *tempo* of the slow pieces in rooms with long reverberation time. The *tempo* of the fast pieces played by the bassoons and the brass players was not affected by RT_{ins}. In the case of the celli, the short articulation described above as a strategy for fast pieces in reverberant environments was apparently accompanied by a faster *tempo*., which was confirmed by an interview statement of one of the cellists in the study. The clarinets did not adjust the *tempo* of any of the pieces to the reverberation time of the rooms while the violins reacted similarly to the cellist of the field study: They played the fast pieces slower with increasing RT_{ins}, while the *tempo* of the slow pieces was not adjusted.

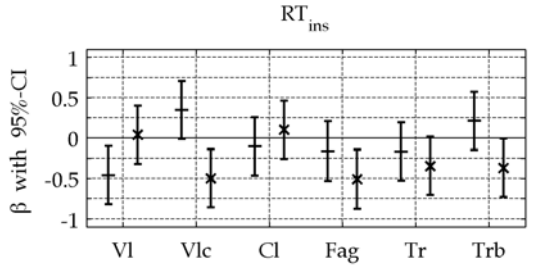

Figure 7: Laboratory study – Standardised regression coefficients with 95% CIs for RT_{ins} separately predicting the *tempo* of each instrument (x-axes) and each piece (–: 'fast'; ×: 'slow'). CIs not crossing the zero-line indicate significant coefficients ($p < 0.05$).

4. CONCLUSIONS

On the basis of data collected in a field and in a laboratory study, statistical analyses with hierarchical linear models were carried out in this paper to elucidate the effect of five room acoustical parameters describing different aspects of reverberance on the tempo played in music performances.

Based on their effect on the way of playing, the duration and the strength of reverberation were obviously perceived as different acoustical qualities by the musicians. Significant effects were

found for the early decay time, the reverberation time and the late sound strength, while the clarity and late support seem to be indicators of minor importance. For the data of the field study, the strongest influence was shown for EDT_{vlc}^2 (R^2 = 74.36%), for the data of the laboratory study it was RT_{ins} (R^2 = 8.73%). The amount of variance explained by a single room acoustical parameter in the field study is quite surprising since in real concert situations there are many other factors potentially influencing the performance. It must be considered, though, that some of these factors might be correlated with the room acoustics, for example, visual impressions of the size of the room and the stage. Thus, the auditory and visual impressions taken together might have a stronger impact than the isolated auditory information alone. The latter was the case in the laboratory study, where the musicians additionally had to allocate cognitive capacity in order to imagine the simulated room they heard and to get used to the experimental situation. This might explain the considerably lower amount of explained variance reported above.

The results of the field study data showed a significant negative effect of EDT_{vlc}^2, RT_{vlc}^2 and $G_{l\,vlc}$, while the effect of these parameters was slightly lower for the slow movements than for the movements with fast and variable basic tempo. Averaged over musicians, a significant negative effect of RT_{ins} and a significant positive effect of $G_{l\,ins}^2$ on the *tempo* were found for the laboratory study data. On average, the musicians of the laboratory study played the slow pieces with reduced *tempo* with increasing RT_{ins}, while the *tempo* of the fast pieces was not adjusted. Comparing the effect of RT_{ins} on the two pieces for the six instruments showed clear differences, implying specific adjustment strategies of the players.

In summary, this study was able to confirm that the reverberance of performance venues has significant effects on the playing tempo of musicians. The strategies how to adapt to the acoustical environment, however, seem to be largely individual. While some musicians reduce the tempo only for faster pieces to avoid a muddled sound, others seem to put more focus on a short articulation with an even faster tempo as a possible consequence. Moreover, the interrelation between reverberance and speed is not necessarily linear: Some musicians (as the cellist in the field study) use a slower tempo also in very dry room acoustical environments, presumably because of more prolonged tones as a compensation for a lack of room acoustical decay.

5. ACKNOWLEDGEMENTS

The studies reported in this paper were supported by the German National Academic Foundation and the German Research Foundation (DFG WE 4057/9-1). The authors wish to thank the musicians who participated in the experiments. Furthermore, the authors thank Dr. Steffen Lepa for his valuable advice on statistical issues.

6. REFERENCES

[1] J. J. Quantz, Versuch einer Anweisung, die Flöte traversière zu spielen, Kassel et al.: Bärenreiter, 1983.

[2] I. Galamian, Principles of Violin Playing and Teaching, Englewood Cliffs: Prentice-Hall, 1962.

[3] P. Borciani, Das Streichquartett, Milan: Ricordi, 1973.

[4] F. F. Winckel, "Optimum Acoustic Criteria of Concert Halls for the Performance of Classical Music," *J. Acoust. Soc. Amer.*, vol. 34, no. 1, pp. 81-86, 1962.

[5] S. Bolzinger, O. Warusfel and E. Kahle, "A study of the influence of room acoustics on piano performance," *Journal de Physique IV, Colloque C5, supplement au Journal de Physique III*, vol. 4, pp. 617-620, 1994.

[6] K. Ueno, K. Kato and K. Kawai, "Effect of room acoustics on musicians' performance. Part I: Experimental investigation with a conceptual model," *Acta Acustica/Acustica*, vol. 96, pp. 505-515, 2010.

[7] K. Kato, K. Ueno and K. Kawai, "Effect of room acoustics on musicians' performance. Part II: Audio analysis of the variations in performed sound signals," *Acta Acustica/Acustica*, vol. 101, no. 4, pp. 743-759, 2015.

[8] Z. Schärer Kalkandjiev and S. Weinzierl, "The influence of room acoustics on solo music performance: An empirical case study," *Acta Acustica/Acustica*, vol. 99, no. 3, pp. 433-441, 2013.

[9] Z. Schärer Kalkandjiev and S. Weinzierl, "The influence of room acoustics on solo music performance. An experimental study," *Psycholmusicology: Music, Mind and Brain*, 2015.

[10] A. Lerch, Software-Based Extraction of Objective Parameters from Music Performances, Munich: Grin Verlag, 2009.

[11] S. Weinzierl and H.-J. Maempel, "Zur Erklärbarkeit der Qualitäten musikalischer Interpretationen durch akustische Signalmaße," in *Gemessene Interpretation. Computergestützte Aufführungsanalyse im Kreuzverhör der Disziplinen*, H. von Loesch and S. Weinzierl, Eds., Mainz et al., Schott, 2011, pp. 213-236.

[12] ISO 3382-1, Acoustics - Measurement of room acoustic parameters - Part 1: Performance spaces, Geneva: International Organization for Standardization, 2009.

[13] J. J. Dammerud, Stage Acoustics for Symphony Orchestras in Concert Halls, Doctoral Thesis, University of Bath, 2009.

[14] R. Schneider, Simulation einer musikalischen Aufführung durch die Auralisation von Musikinstrumenten mit korrekter Richtcharakteristik, Master's Thesis, Technical University of Berlin, 2011.

[15] M. Pollow, G. Behler and F. Schultz, "Musical instrument recording for building a directivity database," in *Fortschritte der Akustik - Tagungsband der 36. DAGA*, Berlin, 2010.

[16] S. Weinzierl, Beethovens Konzerträume. Raumakustik und symphonische Aufführungspraxis an der Schwelle zum modernen Konzertwesen, Frankfurt am Main: Verlag Erwin Bochinsky, 2002.

[17] L. Beranek, Concert Halls and Opera Houses - Music, Acoustics and Architecture, 2nd ed., Berlin et al.: Springer, 2004.

[18] T. Hidaka and N. Nishihara, "Objective evaluation of chamber-music halls in Europe and Japan," *J. Acoust. Soc. Amer.*, vol. 116, no. 1, pp. 357-372, 2004.

[19] A. Lindau, T. Hohn and S. Weinzierl, "Binaural resynthesis for comparative studies of acoustical environments," in *Proc. of the 122nd AES Convention*, Vienna, 2007.

[20] A. Lindau and F. Brinkmann, "Perceptual evaluation of headphone compensation in binaural synthesis based on non-individual recordings," *J. Audio Eng. Soc*, vol. 60, no. 1/2, pp. 54-62, 2012.

[21] J. Hox, Multilevel Analysis, 2nd ed., New York/Hove: Routledge, 2010.

[22] T. A. B. Snijders and R. J. Bosker, "Modeled variance in two-level models," *Sociological Methods & Research*, vol. 22, no. 3, pp. 342-363, 1994.

[23] D. Blum, The Art of Quartet Playing. The Guarneri Quartet in Conversation with David Blum, Ithaca: Cornell Universtiy Press, 1987.

FLEXIBLE SCORE FOLLOWING: THE PIANO MUSIC COMPANION AND BEYOND

Andreas Arzt[1,2]*, Werner Goebl*[3]*, Gerhard Widmer*[1,2]

[1]Department of Computational Perception, Johannes Kepler University, Linz, Austria
[2]Austrian Research Institute for Artificial Intelligence (OFAI), Vienna, Austria
[3]Institute of Music Acoustics, University of Music and Performing Arts, Vienna, Austria
andreas.arzt@jku.at

ABSTRACT

In our talk we will present a piano music companion that is able to follow and understand (at least to some extent) a live piano performance. Within a few seconds the system is able to identify the piece that is being played, and the position within the piece. It then tracks the performance over time via a robust score following algorithm. Furthermore, the system continuously re-evaluates its current position hypotheses within a database of scores and is capable of detecting arbitrary 'jumps' by the performer. The system can be of use in multiple ways, e.g. for piano rehearsal, for live visualisation of music, and for automatic page turning. At the conference, we will demonstrate this system live on stage. If possible, we would also like to encourage (hobby-)pianists in the audience to try the companion themselves. Additionally, we will give an outlook on our efforts to extend this approach to classical music in general, including heavily polyphonic orchestral music.

1. INTRODUCTION

Score following, also known as real-time music tracking, is a big challenge. It involves listening to a live incoming audio stream, extracting features from the audio that capture aspects of the 'sound' of the current moment, and tracking the most likely position in the score – regardless of the specific tempo chosen by the musicians on stage, of tempo changes due to expressive timing, and robust to varying sound quality and instrument sounds.

Real-time music tracking originated in the 1980s (see [1, 2]) and has attracted quite some research in recent years [3, 4, 5, 6, 7, 8, 9]. Although there still are many open research questions (such as on-line learning of predictive tempo models during a performance), score following is already being used in real-world applications. Examples include Antescofo[1], which is actively used by professional musicians to synchronise a performance (mostly solo instruments or small ensembles) with computer realised elements, and Tonara[2], a music tracking application focusing on the amateur pianist and running on the iPad.

In this paper we will summarise some recent developments of our music tracking system. First, in Section 2 below, we will describe a system that allows flexible music tracking on a big database of piano music. In Section 3 we will discuss some of the challenges we encountered when we prepared our music tracker to follow orchestral music live at a world-famous concert hall. Finally, in Section 4, we will discuss further steps of how to combine these two concepts – flexible score following on a database, and tracking orchestral music (or any other kind of instrumental classical music) –, and possible application enabled by this technology.

2. THE PIANO MUSIC COMPANION

The piano music companion is a versatile system that can be used by pianists, and more widely by consumers of piano music, in various scenarios. It is able to identify, follow and understand live performances of classical piano music – at least to some extent. The companion has two important capabilities that we believe such a system must possess: (1) automatically identifying the piece it is listening to, and (2) following the progress of the performer(s) within the score over time.

The companion is provided with a database of sheet music in symbolic form. Currently the database includes, amongst others, the complete solo piano works by Chopin and the complete Beethoven piano sonatas, and consists of roughly 1,000,000 notes in total. When listening to live music, the companion is able to identify the piece that is being played, and the position within the piece. It then tracks the progress of the performers over time, i.e. at any time the current position in the score is computed. Furthermore, it continuously re-evaluates its hypothesis and tries to match the current input stream to the complete database. Thus, it is able to follow any action of the musician, e.g. jumps to a different position or an entirely different piece – as long as the piece is part of the database. See Figure 1 for a very brief technical description. More information can be found in [10] and [11].

The piano music companion enables a range of applications, for both listeners and performers. Musicians might use this system as a convenient way to query and show the sheet music. They can just sit down at the piano, play a few notes, and the piano music companion will show the respective piece, at the correct position. The companion will take care of turning the pages at the appropriate times, and will also recognise jumps to a different positions or pieces and show the sheet music accordingly. For listeners of classical music, the main purpose of the piano music companion is to enrich the experience of classical music concerts. This might be achieved e.g. by providing information synchronised to the music, in various formats (text, images, videos). We will discuss this in a bit more detail in Section 3 below.

3. ADVENTURES IN THE CONCERTGEBOUW

So far, in our research we were focusing mainly on classical piano music, which resulted in the piano music companion briefly described above. The multi-national European research project PHENICX[3] then provided us with the unique opportunity (and

[1] repmus.ircam.fr/antescofo
[2] tonara.com
[3] http://phenicx.upf.edu

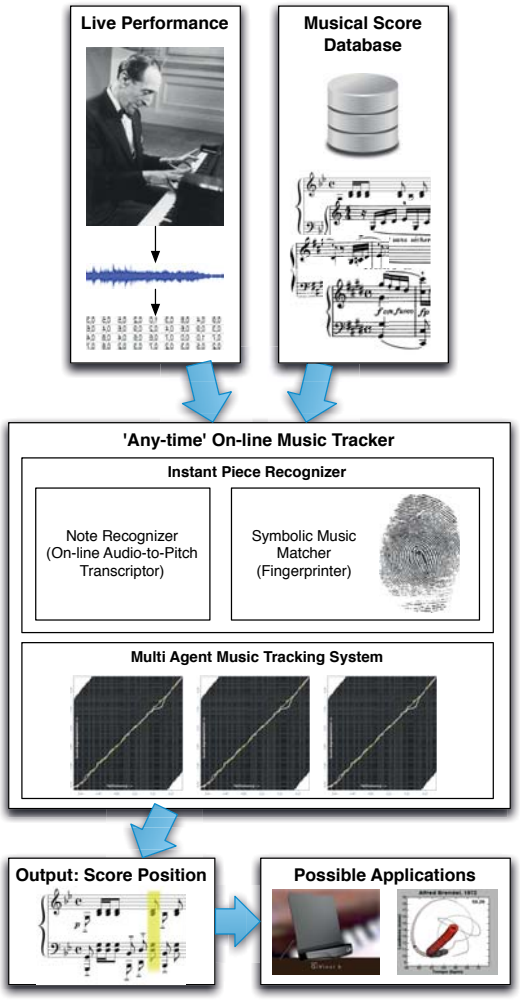

Figure 1: The piano music companion takes as input a live audio stream. It first tries to transcribe this stream into symbolic information (*Note Recogniser*). Then, it matches this information to a database of sheet music, also represented in symbolic form, via a fingerprinting algorithm (*Symbolic Music Matcher*). The output of this stage is fed to a *Multi Agent Music Tracking System* which is based on an on-line version of the dynamic time warping algorithm. This component tries to align the incoming audio stream to (synthesised versions of) the sheet music at the respective positions provided by the fingerprinter. At each point in time the best position (regarding alignment costs) is returned.

challenge) to work with the famous Concertgebouw Orchestra, and to demonstrate our score following technology in the context of a big, real-life symphonic concert.

The event took place on February 7th, 2015, in the Concertgebouw in Amsterdam. The Royal Concertgebouw Orchestra, conducted by Semyon Bychkov, performed the *Alpensinfonie* (Alpine Symphony) by Richard Strauss. This concert was part of a series called 'Essentials', during which technology developed within the project can be tested in a real-life concert environment. For the demonstration a test audience of about 30 people was provided with tablet computers and placed in the rear part of the concert hall. The music tracker was used to control the transmission and display of additional information, synchronised to the live performance on stage (a similar study was presented in [12]). The user interface and the visualisations were provided by our project partner Videodock[4].

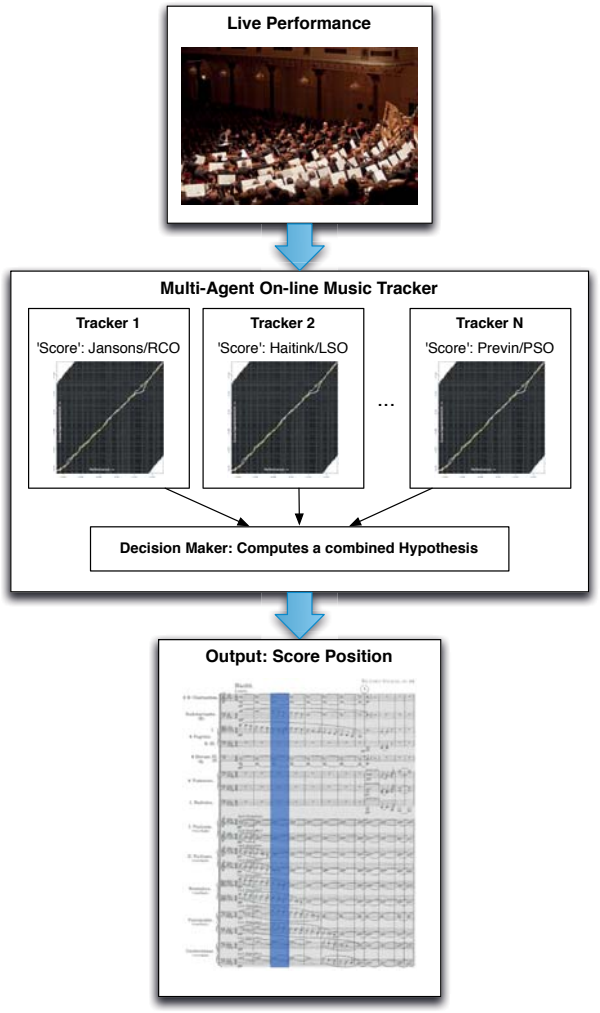

Figure 2: The Multi-agent Tracker. The live input is fed to N independent instances of the tracking algorithm. Each aligns the input to its own score representation, based on different performances of the same piece. Then, the individual hypotheses are combined and the estimate of the current position in the score is returned.

During the concert the audience was presented with 3 different kinds of visualisations. The sheet music was shown synchronised to the live performance, with highlighting of the cur-

[4] http://videodock.com

rent bar and automatic turning of the pages. Textual information, prepared by a musicologist was shown at the appropriate times, helping the audience to understand the structure of the piece. Additionally, artistic videos were shown, which were telling the story of the *Alpensinfonie*.

As this was a live experiment during a real concert, our main goal during the preparation was to make sure that the algorithm will not get lost at any point in time. In the end, this led to a method that increased both the robustness and also the accuracy of the tracking process, with the main idea being to use multiple actual performances (which are preprocessed automatically) as the basis of the tracking process, instead of a single synthesised version of the score (see Figure 2 for a brief explanation). For further information about the experiment at the Concertgebouw we refer the reader to [13], and to [14] for a larger scale evaluation of the multi -gent tracking system.

4. OUTLOOK: THE COMPLETE CLASSICAL MUSIC COMPANION

In the previous two sections above we introduced a flexible piano music tracker and a robust tracking algorithm for orchestral music – and basically any other kind of classical music. Our vision is to finally combine the capabilities of these two systems, resulting in a prototype of what we call the *Complete Classical Music Companion*.

In the end, we envisage a mobile application on a tablet computer or a mobile phone that is at your fingertips anytime and anywhere and can act as your personal classical music companion. Always ready to listen to classical music, and trying to identify and to understand what it is listening to, it can provide you with all kinds of information, guide you, and help you understand the performance. It can provide you with background information about the composer and the historical background of the piece. During the performance it can present information synchronised to the live performance, provided by musicologists and adapted to your level of expertise. It can also show you the sheet music or more abstract representations of the piece (e.g. regarding the structure or the instrumentation).

In the future, we are planning not to limit ourselves to information about the piece, but would also like to include live analysis of the performance itself. As a first step, we will try to build an on-line version of the visualisation presented in [15], which tries to capture two important aspects of an expressive performance – tempo and loudness – and visualises them in a 2-dimensional space.

The biggest obstacle right now is that one important component, the *Note Recogniser* (see Figure 1), is limited to piano music only. Already the transcription of polyphonic piano music to a symbolic representation (on-line!) is a very difficult task, and so far we do not have a solution that works sufficiently well for e.g. orchestral music.

Another big challenge still is the data preparation for the companion. For every single piece both a symbolic version (e.g. MusicXML) and images of the sheet music – synchronised to each other – are needed. Unfortunately, optical music recognition programs are far from being capable of automatically transforming sheet music into MusicXML in sufficient quality, especially for complicated orchestral scores. Currently we are slowly adding new pieces, which involves a lot of manual effort, but in the long run a different solution is needed – either crowd based or in cooperation with a music publisher.

5. CONCLUSIONS

In this paper we summarised our efforts towards building a *Complete Classical Music Companion*. We already have a working prototype for piano music only, which we will demonstrate during the conference. Also, we have successfully demonstrated that our music tracker is well-suited to follow orchestral performances under real-life conditions.

There are still a few parts missing to enable us to finally build a prototype of the system we have in mind. Main future work will be concentrated on filling these gaps, the most important one being to find a way to make the transcription component work with a wider range of instruments.

6. ACKNOWLEDGEMENTS

This research is supported by the Austrian Science Fund (FWF) under project number Z159 and the EU FP7 Project PHENICX (grant no. 601166).

7. REFERENCES

[1] Roger Dannenberg, "An on-line algorithm for real-time accompaniment," in *Proc. of the International Computer Music Conference (ICMC)*, Paris, France, 1984.

[2] Barry Vercoe, "The synthetic performer in the context of live performance," in *Proc. of the International Computer Music Conference (ICMC)*, Paris, France, 1984.

[3] Andreas Arzt, Gerhard Widmer, and Simon Dixon, "Automatic page turning for musicians via real-time machine listening," in *Proc. of the European Conference on Artificial Intelligence (ECAI)*, Patras, Greece, 2008.

[4] Arshia Cont, "A coupled duration-focused architecture for realtime music to score alignment," *IEEE Transactions on Pattern Analysis and Machine Intelligence*, vol. 32, no. 6, pp. 837–846, 2009.

[5] Christopher Raphael, "Music Plus One and machine learning," in *Proc. of the International Conference on Machine Learning (ICML)*, Haifa, Israel, 2010.

[6] Takuma Otsuka, Kazuhiro Nakadai, Toru Takahashi, Tetsuya Ogata, and Hiroshi G. Okuno, "Real-time audio-to-score alignment using particle filter for co-player music robots," *EURASIP Journal on Advances in Signal Processing*, vol. 2011, no. 2011:384651, 2011.

[7] Nicola Montecchio and Arshia Cont, "A unified approach to real time audio-to-score and audio-to-audio alignment using sequential montecarlo inference techniques," in *Proc. of the IEEE Conference on Acoustics, Speech and Signal Processing (ICASSP)*, Prague, Czech Republic, 2011.

[8] Zhiyao Duan and Bryan Pardo, "A state space model for on-line polyphonic audio-score alignment," in *Proc. of the IEEE Conference on Acoustics, Speech and Signal Processing (ICASSP)*, Prague, Czech Republic, 2011.

[9] Filip Korzeniowski, Florian Krebs, Andreas Arzt, and Gerhard Widmer, "Tracking rests and tempo changes: Improved score following with particle filters," in *Proc. of the International Computer Music Conference (ICMC)*, Perth, Australia, 2013.

[10] Andreas Arzt, Sebastian Böck, and Gerhard Widmer, "Fast identification of piece and score position via symbolic fingerprinting," in *Proc. of the International Society for Music Information Retrieval Conference (ISMIR)*, Taipeh, Taiwan, 2012.

[11] Andreas Arzt, Sebastian Böck, Sebastian Flossmann, Harald Frostel, Martin Gasser, and Gerhard Widmer, "The complete classical music companion v0.9," in *Proc. of the AES Conference on Semantic Audio*, London, England, 2014.

[12] Matthew Prockup, David Grunberg, Alex Hrybyk, and Youngmoo E. Kim, "Orchestral performance companion: Using real-time audio to score alignment," *IEEE Multimedia*, vol. 20, no. 2, pp. 52–60, 2013.

[13] Andreas Arzt, Harald Frostel, Thassilo Gadermaier, Martin Gasser, Maarten Grachten, and Gerhard Widmer, "Artificial intelligence in the concertgebouw," in *Proc. of the International Joint Conference on Artificial Intelligence (IJCAI)*, Buenos Aires, Argentina, 2015.

[14] Gerhard Arzt, Andreas Widmer, "Real-time music tracking using multiple performances as a reference," in *Proc. of the International Society for Music Information Retrieval Conference (ISMIR)*, Malaga, Spain, 2015.

[15] Jörg Langner and Werner Goebl, "Visualizing expressive performance in tempo-loudness space," *Computer Music Journal*, vol. 27, 2003.

REAL-TIME ESTIMATION OF INSTRUMENT CONTROLS WITH MARKER BASED IR CAMERAS.

Alfonso Perez-Carrillo[1], *Marcelo Wanderley*[2]
[1] Music Technology Group, University Pompeu Fabra, Spain / McGill University, Canada
[2] McGill University, Canada
alfonso.perez@upf.edu
marcelo.wanderley@mcgill.ca

ABSTRACT

Scientific analysis and understanding of musical performances is an ambitious challenge at the intersection of a wide array of disciplines ranging from motor-learning and cognitive sciences to music pedagogy. Recently, the availability of technology and methods to measure many aspects of the musical performances allow for a better understanding of the mechanisms behind musical practice. Among these aspects, it is of special interest in this work the measurement of instrumental controls. Several methods have been reported in the last years adapted to a specific kind of instrument. Most of these methods are generally intrusive and in many cases they need for data post-processing so that instrumental controls can not be computed in real-time, which in some applications is crucial. We present a method based on high speed video cameras that track the position of reflective markers. The main advantages with respect to previous solutions are that 1) the degree of intrusivity is very low, while 2) it is able to compute the instrumental parameters in real-time based on the geometrical position of the markers and 3) it allows for the measurement of several instruments and performers. The main problem with such optical systems is marker occlusion. Each marker needs to be identified by at least three cameras placed at different angles and planes in order to correctly determine its 3D coordinates. Marker identification is made robust by the use of rigid bodies (RB), a six degrees-of-freedom (6DOF) rigid structure defined by the position of a set of markers and associated with a local system of coordinates (SoC). The position of the markers is constant relative to the local SoC and their global coordinates can be obtained by a simple rotation and translation from the local to the global SoC. Even if some of the markers are occluded, their position can be reconstructed from the others. The method has been successfully applied to bowed strings by tracking the position of bow and strings and it is being adapted to the guitar, which presents extra difficulties as the hands of the performer are flexible skeletons rather than rigid bodies.

PIEZOELECTRIC FILM SENSORS FACILITATE SIMULTANEOUS MEASUREMENT OF BOWING PARAMETERS AND BRIDGE VIBRATIONS DURING VIOLIN PLAYING

Gunnar Gidion, Reimund Gerhard
Applied Condensed-Matter Physics, Institute of Physics and Astronomy,
University of Potsdam, Germany
gidion@uni-potsdam.de
reimund.gerhard@uni-potsdam.de

ABSTRACT

In violin playing, an important part of the interaction between the player and the instrument is mediated by the bow. The bridge, on the other hand, transfers the bowed-string vibrations to the violin body. For the present investigations, both the action of the bow and the bridge are detected by thin polymer-film sensors with piezoelectric properties. By combining this technology with conventional acoustic and optical means of detection, aspects and measures of playability (especially the minimum bow force) can be referred to the respective bridge and body vibrations. Results are discussed in terms of the theoretical framework of Woodhouse and in comparison to the experimental work of Schoonderwaldt and Demoucron.

TOWARDS BRIDGING THE GAP IN A MUSICAL LIVE PERFORMANCE

Oliver Hödl[1], Fares Kayali[1], Geraldine Fitzpatrick[1], Simon Holland[2]
[1] Vienna University of Technology, Austria
[2] Open University, United Kingdom
oliver.hoedl@igw.tuwien.ac.at
fares@igw.tuwien.ac.at
geraldine.fitzpatrick@tuwien.ac.at
simon.holland@open.ac.uk

ABSTRACT

Performances across diverse musical genres conventionally happen with a clear one-way structure; musicians perform while spectators listen, except when they sing along, for instance. In most cases, the audience's opportunities for participation are limited to relatively inexpressive forms of interaction such as clapping, swaying and interjecting. By contrast, recent emerging technologies for audience participation allow spectators to collaborate in expressive and targeted ways with performing artists to influence and shape musical live performances in real time. Already, a rich variety of custom-built instruments, devices and systems have been devised for audience participation with the potential to facilitate richly collaborative performance.

The artistic potential of such technology-driven audience participation is high both for musicians and their audiences. Furthermore, it can bridge the gap between the active role of musicians and the passive role of spectators. Participative technologies can qualitatively change the overall experience in new positive directions for all involved.

However, if not considered carefully, audience participation can be annoying, may fail, and may lead to frustration. While the reasons for this can be manifold, we posit that the chances of successful audience participation are greatly facilitated by well-considered design.

To this end, we systematically analysed a vast number of existing approaches of audience participation in musical and non-musical domains. In addition, we conducted two case studies at live performances to shed light on conceptual and compositional constraints within the process of designing audience participation.

Our insights are presented as a collection of structured design aspects able to characterise participatory music performances and their broader contexts. As a result, we propose the design toolkit "LiveMAP", which stands for "Live Music Audience Participation", and which supports the design and creation of participatory elements in a musical live performance.

TAPPINGFRIEND – AN INTERACTIVE SCIENCE EXHIBIT FOR EXPERIENCING SYNCHRONICITY WITH REAL AND ARTIFICIAL PARTNERS

Werner Goebl[1,2] *and Dominikus Guggenberger*[3]

1) Austrian Research Institute for Artificial Intelligence (OFAI), Vienna Austria
2) Institute of Music Acoustics, University of Music and Performing Arts Vienna, Austria
3) http://www.dominikusguggenberger.at/, Vienna, Austria

ABSTRACT

TappingFriend is an interactive science game aimed to provide a playful experience of synchronization and cooperation between one or two humans and a virtual partner – the maestro. The players tap in time with the maestro on little drums and the system provides immediate feedback on their synchronization success by showing their taps relative to the maestros taps and by counting the taps that were on time, too early or too late. One aim of the game may be to achieve as many on-time taps as possible. The maestro's degree of cooperation differs between play modes, and players experience the different levels of cooperativity while tapping. Players have to develop different strategies to stay on beat with their fellow players and the virtual partner, the maestro. The four different play modes offer different levels of cooperation by the maestro: in the first play mode, the maestro keeps a strict beat and does not react to either of the two players. In the second play mode, the maestro changes his tempo and gets faster or slower or both; thus, in these two modes the players have to adapt to stay in sync. In the third play mode, the maestro establishes himself a cooperative tapping behavior by employing a simple phase and period correction model: he "listens" to the taps of his fellow players and adapts his tapping tempo and phase to stay as closely together as possible. In the fourth play mode, the maestro cues in with four beats and leaves the two players on their own. This exhibit implements current sensorimotor models of temporal coordination that are based on current research on synchronization and communication in music ensembles.

1. INTRODUCTION

Sensorimotor synchronization refers to the ability of humans to entrain to an external beat such as a metronome click [1, 2] by finger tapping, dancing, or during music making, to name a few. This human ability is unique among primates and is believed to be one of the driving forces of human evolution [3]. Being in sync with others creates a sensation of affiliation with the counterpart [4], increases social bonding and group cohesion [3] even in groups of 4-year old children [5], and is one of the most fundamental mechanisms in music making. Therefore, the aim of this interactive science exhibit is to promote the experience of sensorimotor synchronization among human dyads together with a virtual partner in a simple and intuitive way.

A simple form of rhythmic entrainment is finger tapping to an external stimulus, as implemented in the current exhibit. In TappingFriend's first two play modes, the virtual partner, the "maestro," either keeps a strict beat or changes the tempo of the beat by getting faster, slower, or both. The two tappers have to adapt strongly to stay in sync with the maestro. In cognitive terms, they employ phase and period correction processes for successful synchronization [1]. While in these two play modes, the maestro does not react to the tappers and leaves all adaptation to the two tappers. In the third cooperative play mode, the maestro uses a simple timing adaption model to try to minimize synchronization error with his fellow tappers [6]. The tappers may experience, how much easier it is to tap with a cooperative partner than with an uncooperative partner. They can deliberately change the overall tempo by keeping their taps on the early or late side. In the fourth play mode, the two tappers are left on their own to tap together as they wish.

2. EXHIBIT DESIGN

TappingFriend (German: "Im Takt bleiben")[1] is designed for one or two human players and an artificial partner, the "maestro." It is a free-standing, self-contained exhibit with a touch screen in portrait orientation that provides an interactive user interface and a display of performance success. For each of the two users, a small modified drum is placed at each side of the screen to act as a tapping interface. The players (either alone or in pairs) start a trial by pressing the "start" button on the touch screen and tap on the drums after four cue-in clicks by the maestro. During the synchronization phase, the maestro produces 17 taps, corresponding to four bars in a standard binary meter. The tappers receive acoustic and visual feedback from their actions. The acoustic feedback is relayed by a speaker mounted below each drum with a drum sound at different pitches for the two players. The maestro's sound is a sharp, high-pitched woodblock sound. Visual feedback is given in real time on the screen and provides detailed yet intuitive information on the timing accuracy of each of the two tappers separately by displaying the individual taps relative to each other on a time axis as well as counts of taps that were on time, too early or too late (see below).

2.1. Software Design

The graphical user interface (see Fig. 1) is kept clear and simple with only a few elements for play mode selection, parameters and visual feedback of play progress and success. Most prominent is the central dark-grey tapping panel that displays the detailed timing information for the maestro (yellow) and the two players (black). The time on the vertical axis evolves from top to bottom, analogous to an hourglass. To deviate from a more common visualization of time evolution from left to right, typically found in scientific publications, was a deliberate design decision that was immediately well received by scientifically lay people and researchers alike. For simplicity, the tapping

[1] http://www.ofai.at/music/imtaktbleiben

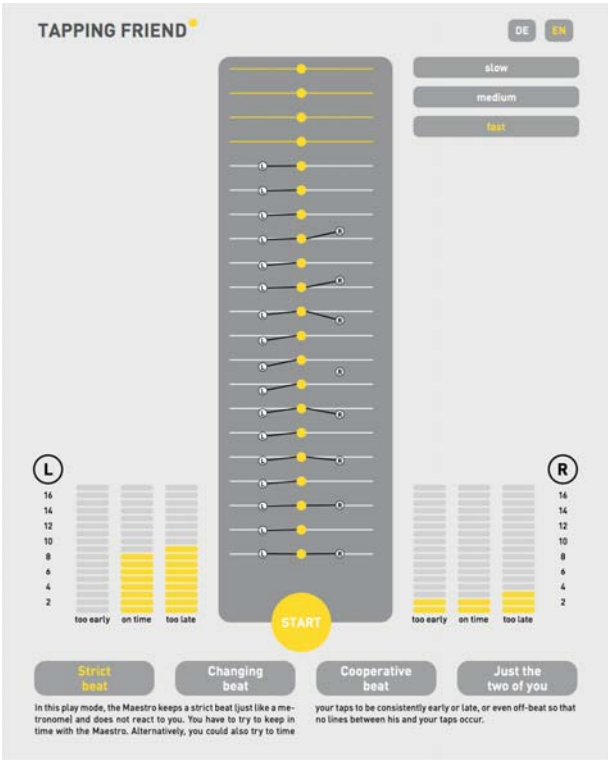

Figure 1: Screen shot of the first play mode in which the maestro (yellow) maintains a strict beat. In the main panel, the time elapses from top to bottom. In this particular trial, the left tapper ("L") managed to stay in synchrony with the maestro fairly well (as displayed in the left success panel: 8 taps on time, 9 too early) while the right tapper ("R") attempted to entrain in half the period, resulting low success scores.

panel does not display time units as in a scientific graph (such as a tick for each second); however, time evolution is clearly felt during tapping, even without time units.

The tapping panel is initially filled with the four cue-in taps (yellow horizontal lines with open circles) and 17 planned taps (white horizontal lines with open circles) of the maestro. During a trial, the circles are filled yellow when a click of the maestro occurs; the taps of the two players are visualized with black circles at each side, labelled with an upper-case initial for each tapper ("L" for left tapper, "R" for right, see Figure 1). These circles are visually connected to the maestro's taps with lines, when a tap falls within the attention window surrounding a maestro's beat (see below).

On each side to the bottom of the tapping panel, the players receive feedback of individual tapping success by visually presenting counts of beats that are on time, too early, or too late. The success heuristics of these counts are defined as follows (see also Figure 2): a tap within ±30 ms is classified as "on time," corresponding roughly to the threshold of perceiving two musical events as separate [7]. We also defined an attention window of a third beat around each click of the maestro within which a tap is either classified as "too early" or "too late." (Thus, at a medium tempo of 500 ms inter-tap interval the attention window is 333 ms wide.) A tap outside the attention window is defined as "off beat" and is not included in the success display. Taps are visually connected to the taps of the maestro with a solid line when they are not off beat.

On the top right, the users select the language of the software (currently English and German) and the tempo of the maestro. The three tempo options are slow, medium, and fast which are set to inter-tap intervals of 600, 500, and 400 ms, corresponding to 100, 120, and 150 bpm, respectively. The medium tempo is chosen to reflect a generally preferred tapping tempo of humans [8, 9] that also corresponds to typical rates of human locomotion [10]. The slow and fast alternatives are 20% slower or faster than the medium tempo.

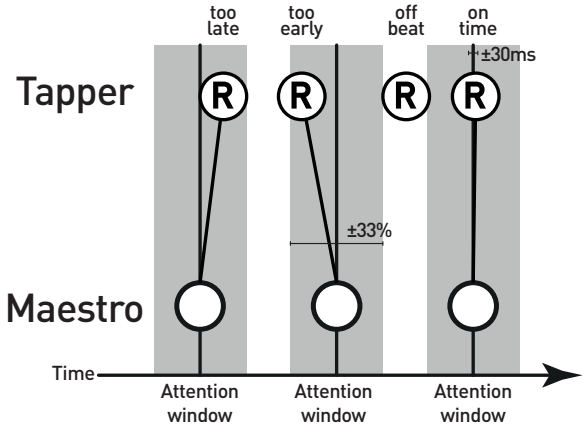

Figure 2: Schematic of the success heuristics of Tapping Friend. A tap within ±30 ms is classified "on time," a tap within the attention window (± a third of a beat) is considered "too early" and "too late," respectively, everything else "off beat."

2.1.1. *Play modes*

TappingFriend has four play modes that feature different levels of cooperation by the maestro and for the two players. In the first play mode ("Strict beat"), the maestro maintains a strict beat like a metronome and does not cooperate with the co-tappers. The yellow circles of the maestro always cover the planned beats exactly.

In the second play mode ("Changing beat"), the maestro changes the tempo by getting faster, slower, or both, but still does not react to the tappers. The tappers have to adapt strongly to stay on time with the maestro (see Figure 3). The tempo change is set to 5% when there is a change only in one direction ("faster" and "slower") and to 8% when two directions of change are involved ("faster–slower" and "slower–faster"). These values of tempo change are chosen to be clearly above the just noticeable difference for tempo change, which are around 3% [11].

2.1.2. *Synchronization model*

In the third play mode ("Cooperative Beat"), the maestro behaves cooperatively and reacts to the taps of the two players by trying to compensate for part of the timing error that occurs between the players' taps and the maestro. To this end, we implement a simple linear timing model that uses phase and period correction as two separate processes [6].

We denote the time instances of the maestro's clicks as m_n and the taps of the players as t_{1n} and t_{2n}; the asynchrony between the maestro and the tappers is defined as the mean of the two players' taps inside the attention window (see Figure 2):

$$A_n = \frac{1}{2}\sum_{i=1}^{2}(t_{in} - m_n). \qquad (1)$$

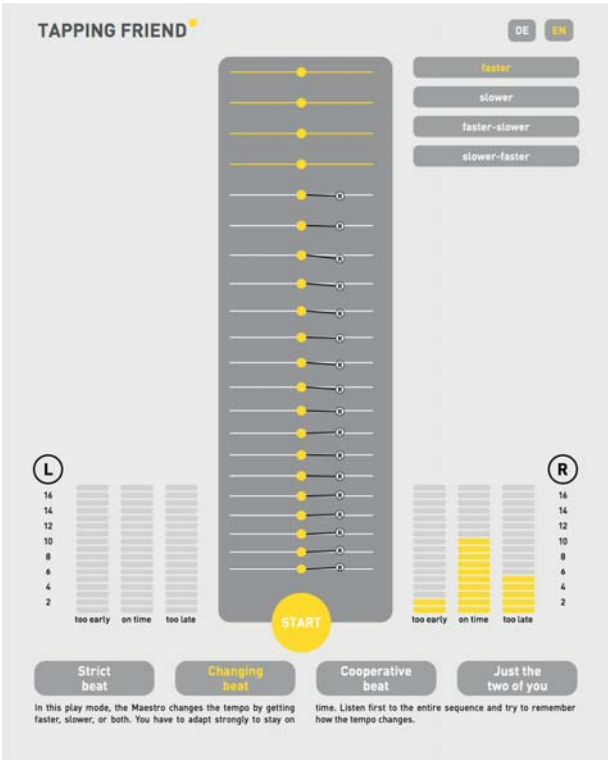

Figure 3: Screen shot of the second play mode in which the maestro changes the tempo (and gets faster as in this example trial).

Each future tap of the maestro m_{n+1} is estimated as:

$$m_{n+1} = m_n + T_n - (\alpha + \beta)A_n, \tag{2}$$

where T_n is the current period of the maestro, α the phase correction parameter, and β the period correction parameter. The current period T_n of the maestro is updated as:

$$T_{n+1} = T_n - \beta A_n. \tag{3}$$

The parameters are set to $\alpha = 0.33$ and $\beta = 0.20$ in accordance to results from the literature for optimal synchronization conditions [6].

When two players are tapping simultaneously, the tempo correction models takes information from both tappers into account. In the possible case of multiple taps inside the attention window, the timer kernel takes those taps into account that are closest to the maestro's tap and ignores the others. Since the period of the maestro is likely to change in this play mode, the yellow circles of his taps deviate from the white circles that denote the strict continuation of the initial period (see Figure 4).

In the fourth play mode ("Just the two of you"), the maestro plays the first four beats to set an initial tempo and then leaves the two one their own. The tappers are free to either try to keep the same tempo or to invent rhythms on their own. Synchronization success is now computed between the two tappers in the same way as before. Likewise, taps close to each other are connected by lines directly from one tapper to the other (see Figure 5).

The TappingFriend software interface has been implemented in JavaFX 8.0 (by the first author), which features a versatile and responsive graphical front-end and makes use of the internal 60-fps pulse of the JavaFX environment.

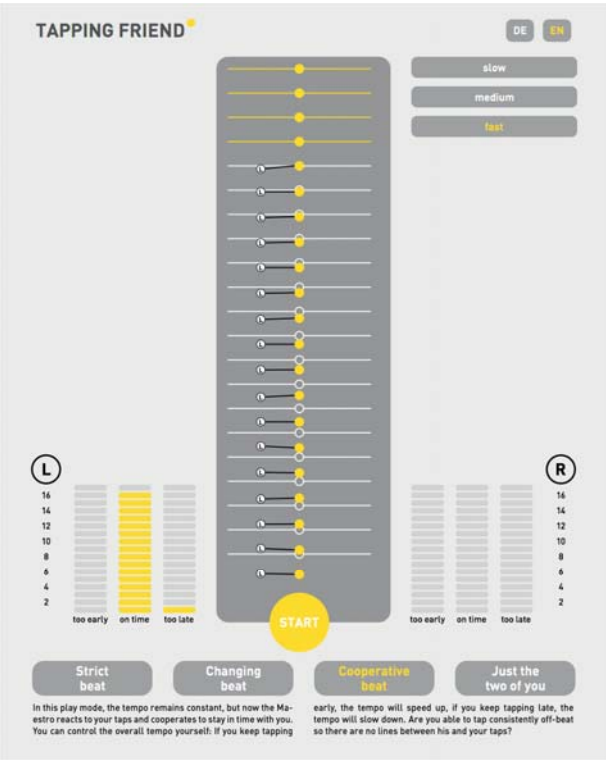

Figure 4: Screen shot of the third play mode. As the maestro adapts his taps to the co-tappers, the yellow circles may not align with the white horizontal lines, leaving empty circles that denote a strict continuation of the initial tempo.

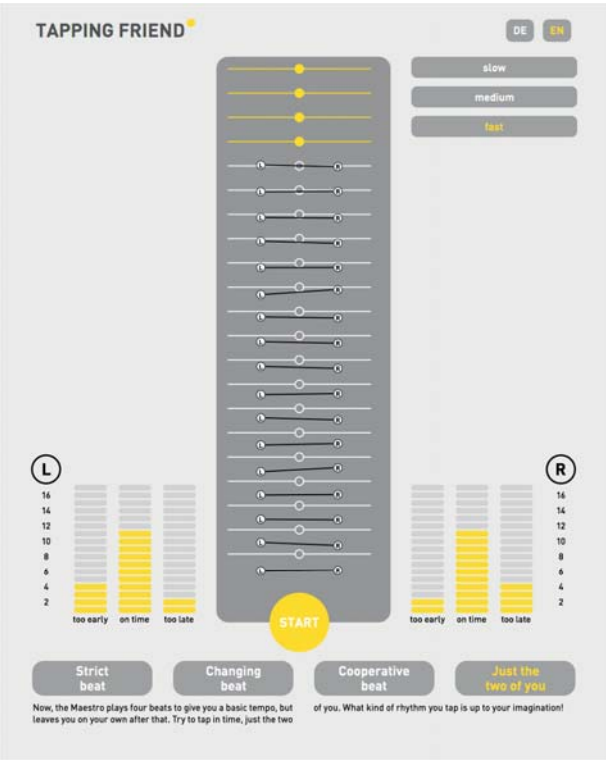

Figure 5: Screen shot of the fourth play mode in which the two players are left on their own after the maestro cued the initial tempo. Synchronization success is now displayed between the two players rather than between a player and the maestro.

2.2. Hardware

TappingFriend contains an embedded silent computer (Zotac ZBox CI320 Nano, 128GB SSD, 4GB RAM) running a Linux operating system (Ubuntu 14.04) with a 19-inch TFT LCD touch screen by Elo (1280 × 1024 pixels). The two drums are simple plastic drums with 10 cm diameter covered with touch-sensitive conductive tissue that is connected to an Arduino board (Uno) controlling the sensitivity of tap detection. This board is daisy-chained with another Arduino board (Leonardo) that triggers the TappingFriend software by emulating keyboard events. A repeated tap can be triggered after a refractory period of 40 ms.

2.2.1. Audio and Video Latency

To measure the delay between a physical tap produced by a player, the acoustical feedback produced by the speakers and the visual feedback on screen, we recorded the signal from an accelerometer (1 cm diameter) glued on the drum skin, the speaker signal, and the signal from a photo sensor on three tracks on a Focusrite Scarlett 18i8 sound card (44.1 kHz with 16-bit word length). For this specific test, we programmed a black rectangle below the photo sensor to change its color from black to white each time a tap was received. Fifty-five subsequent taps were recorded and the onset time differences between the accelerometer signal, the audio, and the video signal manually determined in a common audio software (Audacity 2.1.1). These measurements revealed an average audio latency (from physical action to sound) of 36.1 ms (SD = 6.4 ms), thus, satisfying the requirements of real-time systems [12]. The visual delay (from physical action to the brightness change) was 64.4 ms on average (SD = 10.9 ms). These latency values are lower than those of a piano key that takes between 35 ms at extremely loud to 220 ms at very soft keystrokes from key surface movement to the actual sound onset [13].

2.2.2. Audio precision

To assess the precision of the metronome produced by the exhibit, we recorded for each of the three tempi five metronome sequences without any other taps and determined the onset timing automatically with an onset detection function implemented in Matlab. The average inter-tap intervals were 600.2, 500.0, and 400.0 ms for the three tempi, respectively. The mean coefficients of variance (standard deviation of inter-tap intervals relative to their mean) were 0.0054, 0.0042, and 0.0029 ms, respectively. Given that these values also comprise variability of the onset detection function, they certify a sufficiently precise performance of the current software-hardware combination.

3. CONCLUDING REMARKS

The exhibit is planned to be presented at the "Forschungsfest 2015" (September 2015) near the Vienna Naschmarkt. After that it will join the interactive traveling exhibition "Wirkungswechsel"[2] of the Science Center Netzwerk[3] and will be presented across Austria over the upcoming years.

TappingFriend currently logs each trial by storing the timing information of the maestro and the two players and the play mode number on hard disk. According to the ethical standards of the Declaration of Helsinki (1964), no other information is stored that may identify individuals. This data will be used to evaluate the usage of this exhibit, as well as the overall synchronization capabilities of the users. The software may also be used in controlled timing studies in the future.

4. ACKNOWLEDGEMENTS

This outreach activity has been realized within a scientific research project supported by the Austrian Science Fund (FWF, P 24546). The science exhibit is made possible through generous support by the Vienna Business Agency (Wirtschaftsagentur Wien)[4] and the Kapsch Group.[5] We wish to thank Daniel Fabry for developing the hardware interface. We are grateful to Sarah Funk and Barbara Streicher (Science Center Netzwerk) for precious input during the development of TappingFriend and to Laura Bishop and Barbara Streicher for valuable comments on earlier versions of this text.

5. REFERENCES

[1] B. H. Repp, "Sensorimotor synchronization: A review of the tapping literature," *Psychol. Bull. Rev.*, vol. 12, no. 6, pp. 969–992, 2005.

[2] B. H. Repp and Y.-H. Su, "Sensorimotor synchronization: A review of recent research (2006–2012)," *Psychol. Bull. Rev.*, vol. 20, no. 3, pp. 403–452, 2013.

[3] W. T. Fitch, "The biology and evolution of music: A comparative perspective," *Cognition*, vol. 100, pp. 173–215, 2006.

[4] M. J. Hove and J. L. Risen, "It's all in the timing: Interpersonal synchrony increases affiliation," *Soc. Cognition*, vol. 27, no. 6, pp. 949–961, 2009.

[5] S. Kirschner and M. Tomasello, "Joint music making promotes prosocial behavior in 4-year-old children," *Evolution and Human Behavior*, vol. 31, pp. 354–364, 2010.

[6] B. H. Repp and P. E. Keller, "Sensorimotor synchronization with adaptively timed sequences," *Hum. Movement Sci.*, vol. 27, pp. 423–456, 2008.

[7] W. Goebl, *The Role of Timing and Intensity in the Production and Perception of Melody in Expressive Piano Performance*, Doctoral thesis, Institute of Musicology, 2003, available online at http://iwk.mdw.ac.at/goebl.

[8] L. van Noorden and D. Moelants, "Resonance in the perception of musical pulse," *J. New Music Res.*, vol. 28, no. 1, pp. 43–66, 1999.

[9] R. Parncutt, "A perceptual model of pulse salience and metrical accent in musical rhythms," *Music Percep.*, pp. 409–464, 1994.

[10] H. G. MacDougall and S. T. Moore, "Marching to the beat of the same drummer: the spontaneous tempo of human locomotion," *J. Appl. Physiol.*, vol. 99, pp. 1164–1173, 2005.

[11] A. Friberg and J. Sundberg, "Time discrimination in a monotonic, isochronous sequence," *J. Acoust. Soc. Am.*, vol. 98, no. 5, pp. 2524–2531, 1995.

[12] C. Bartelette, D. Headlam, M. Bocko, and G. Velikic, "Effect of network latency on interactive musical performance," *Music Percept.*, vol. 24, no. 1, pp. 49–62, 2006.

[13] W. Goebl, R. Bresin, and A. Galembo, "Touch and temporal behavior of grand piano actions," *J. Acoust. Soc. Am.*, vol. 118, no. 2, pp. 1154–1165, 2005.

[2] http://www.wirkungswechsel.at/

[3] http://www.science-center-net.at/

[4] http://viennabusinessagency.at/

[5] http://www.kapsch.net/

ROUGHNESS OF VIOLIN TONES – THE PERCEPTION OF IRREGULARITIES

Zdenek Otcenasek, Jan Otcenasek

Musical acoustics research centre (MARC), Music and Dance Faculty,
Academy of Performing Arts in Prague, Czech Republic
otcenasek@hamu.cz

ABSTRACT

The article presents the results of a second part of a larger experimental study on the perception of different types of changes in the time courses of rough violin sound signals**.** In the first part of the study, the sounds of a bowed, open violin string (G), played with different bow speeds and force, resulting in sounds differing in roughnesses, were simultaneously documented by a high speed video camera and recorded. The recordings were used as stimuli in a ranking and rating and pair comparison listening test. The roughness dissimilarity ratings and perceived difference verbal attribute descriptors were connected with stimuli positions in a MDS perception space (for the details of the test conduct and evaluation, see [13]). In the presented second part, the revealed multidimensionality of perceived roughness is studied in the context of time course changes in both the audio and the string motion signals. The signal analysis reveals connection of the two of the possible dimensions of roughness (cracked and buzzing percepts) to a signal variability. The cracked percept is connected to irregularities in both signals, and the buzzing percept, to a superposition of regular waveforms of neighboring harmonics (one bark harmonic triads) in two barks of the audio signal.

1. INTRODUCTION

Roughness plays a role in the perception of musical sounds, such as those of a violin, for example. Unpleasantly rough tones of a beginner violinist, or an effort in attaining desirable rough tones of electric guitars might represent instances of a roughness related sound-quality evaluation which can be directly important to musicians.

The roughness psychoacoustic quality is used to describe a complex phenomena associated with subjective perception of different temporal changes in sound. Some roughness concepts regard roughness as a result of envelope fluctuations in time and spectral domain and link auditory roughness to the sound waveform, other have suggested physiological bases of roughness (e.g. interference of multiple harmonics of a complex tone at the basilar membrane [1], higher order auditory grouping [2] or neural bases of roughness [3]). Roughness is also studied in relation to the concept of dissonance, sub-harmonic components of the sound, and with character of aperiodicities in sound signal, e.g. in [4, 5].

Since the causes of roughness can arise from several physical reasons, it is suggested that perceived roughness is multidimensional (e.g. in [6, 7]. Also studies of pathologic voice quality based on listening tests e.g. [7] show results of more than one factor or dimensionality in roughness ratings). The results of listening tests focused on timbre of violin tones have also revealed roughness multidimensionality (buzzing, subharmonicity [8]).

The violin (or the bowed instruments generally) sound due to repeating slip-stick release cycle of the string under the bow. The time courses of the string waveform were explored in detail in multiple studies of bowed violin string motion, e.g. [9]. The string exhibits irregularities or aperiodicities in oscillation caused by irregularities in the timing and magnitude of the string release during play. This results in various time changes in sound signal waveforms which are also joined with distinct perceptual quality. Both periodic and aperiodic modulations and subharmonicity were described in the string movement (various extent of jitter, shimmer and spikes). These time changes are dependent to a large extent on the used bowing technique (on bowing place, speed, pressure force, broadness of the bow hairs in contact, e.g. [10, 11]).

In relation to these results, the goal of the entire experiment was to use different regimes of bowing to obtain a variety of different string motions and roughness forms [9] to explore the multidimensionality of perceived roughness. The goal of the presented research was to investigate the relation between the forms of roughness, the string motion and the radiated sound and relate some forms of roughness (described with suitable verbal descriptors) to the character of the sound signal and string motion near the violin bridge.

2. SUMMARY OF THE EXPERIMENT

2.1 The experiment overview

The experiment was conducted in the first part of the study (for further information on the experiment see [13]). Different types of rough violin sounds were generated by changes in the bowing technique (performed by a musician) in the first part of the experiment. The tones were played on an open G string, on a single violin, and recorded with a Neumann KU100 dummy head. Corresponding string movements were recorded with a Phantom SpeedSense 9060 high speed camera (60kfps). Both recordings were synchronized (see Fig. 1).

Figure 1: The setup of the sound and string movement recording

An acceptable number of 9 sounds was selected by rejecting similarly sounding recordings in a listening pre-test in order to obtain samples representative of different roughness types. The selected sounds were evaluated by listeners in two listening tests

(headphones, mono). Roughness dissimilarity and verbal attribute descriptors were collected in a pair comparison test. Roughness as an entirety was evaluated in a ranking and rating listening test. Tests were done with 20 participating subjects: 10 sound engineers and musicians (the *experts* group), and 10 participants without special musical or listening experience, (the *non-experts* group).

2.2 The experiment results summary

The obtained dissimilarity values were analyzed using a multidimensional scaling method (MDS [12]). Both tests had a statistically significant agreement among all respondents, but the stress values (D) of the *experts* differed from the *non-experts* in solutions with a same dimensionality (see the more distinct elbow for the experts solution line at number 4 in Fig. 2), indicating that experts considered more sound quality attributes: While a 2D solution was sufficient for the non-experts, a solution with less than 4D was not suitable for unbiased preservation of the dissimilarities obtained for the experts (only the more distinct and detailed experts 4D MDS sound configuration is used in the second stage of the experiment in result**,** see chapter 3.)

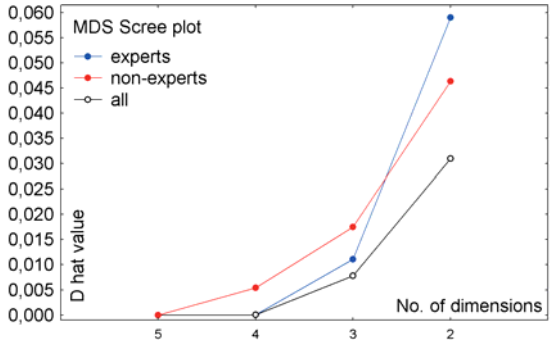

Figure 2: *non-experts*, *experts* and *all* MDS solution scree plots (from 5 to 2 dimensions)

The respondents used slightly different spontaneous verbal descriptors for the same sound qualities in the pair comparison test. Synonymous meanings were merged after post-test consultations with respondents, and the most frequently used descriptor was chosen as a representative label of a certain sound quality attribute. A frequency of occurrence (F_{occ}) of every attribute was computed for each sound stimulus (summarized in Table 1). These values of F_{occ} were embedded to the 4D experts perception space using a linear regression.

The embeddings were used for the interpretation of the the perceptual space configuration and consecutively for a search for the physical aspects of the obtained dimensionality

Fig. 3 displays the spatial directions along which the embedded, separate perceptual attributes increase. The gradients are displayed as colored lines from the positions of sounds with minimal to maximal frequency of occurrence (a small and a large circle) labelled with identical colour in the inscription (the positions are marked with the sound numbers).

Table 1: The overall roughness and F_{occ} of the attributes

Sound. no	Roughness			F_{occ} (Pair comparison test)							
	Rank+rate test										
	all	experts	non-exp.	Cracked	Strident	Buzzing	Rustle	Blear	Dark-Bright	Narrow	Quinted
1	4.6	4.4	4.8	1	1	1.5	2.5	4	4.5	1	0
2	9.5	9.4	9.5	10	3	0	0.5	1	3	3	0
3	3.3	2.1	4.4	0	3	7.5	0	0	1	0	0
4	1.9	2.4	1.5	0	0	2.5	1.5	4.5	6	6	0
5	6.1	6.4	5.8	4	2.5	0.5	3	4	5	3	0
6	8.3	7.9	8.7	7	8	0	1	0.5	0	1	0
8	5.3	3.9	6.6	0	2.5	7	1	1	1.5	9	0.5
9	2	1.5	2.4	0	0.5	4	0.5	3	3.5	1	0
10	4.4	4.6	4.1	1	1	4.5	1	2	2	3	8

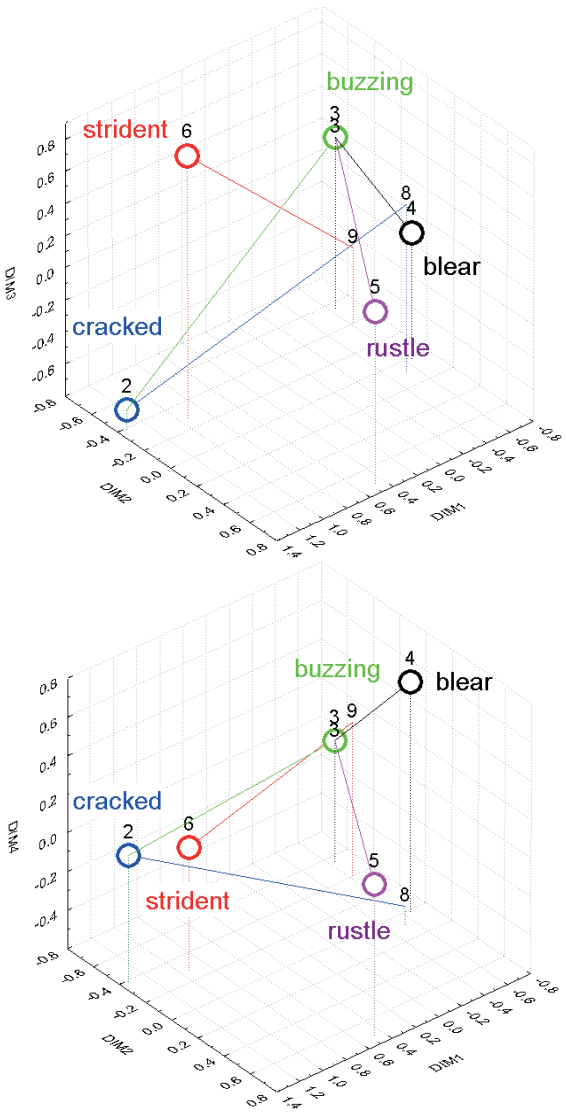

Figure 3: Attribute gradations (marked in different color) from minimum (no circle) to maximum (large circle). Digits mark the positions of sounds in the experts perception space. Top figure: dimensions 1, 2, 3, bottom figure: dimensions 1, 2, 4.

The presented F_{occ} and regression lines were used for the analysis of the roughness causations in the presented second part (see chapter 3).

The obtained generally known psychoacoustic dimensions (the roughness jugged as an entirety in the rating test, the dark-bright

and narrow dimensions) were also embedded into this space (see Fig. 4).

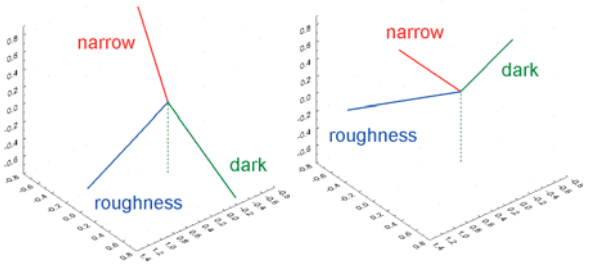

Figure 4: Gradation of regular psychoacoustic dimensions (in different colours), only the positive half-axis from the space midpoint (0, 0, 0, 0) is shown. Left figure shows dimensions 1, 2, 3, right dimensions 1, 2, 4.

Angles between the regression lines were computed to assess the relations between the embedded attributes and to ease the orientation in the 4D perceptual space (for summary of the results, see Table 2). The embedded attribute angles revealed the multidimensionality of roughness (the cracked and buzzing percepts constitute the roughness percept as an entirety) [13].

Table 2: Angles between the attribute regression lines

	strident	buzzing	rustle	blear	dark-bright	narrow	roughness
cracked	65	127	95	100	93	85	32
strident		88	101	129	133	27	61
buzzing			125	130	133	79	116
rustle				39	51	105	82
blear					16	121	104
dark-bright						125	103
narrow							89

The right angles (90±15°, red in Table 2) between buzzing-strident, cracked-rustle, strident-rustle and cracked-bleary attributes indicate these sound attributes are potentially discrete psychoacoustic dimensions or quantities (see Table 3.)

Table 3: Potential discrete psychoacoustic dimensions (left column: sound quality attributes, right: sound quality renditions)

Attributes:	Perceived sound quality description:
bleary	blurred and cloudy sounding
buzzing	buzzzing like sound
strident	Piercing, cutting, and gradation of sharpness
cracked	interrupts and time variations in sound

Oblique angles (20~70° and 110~160°, black in Table 2) may indicate non-discrete attributes, but can also result from insufficient number of used stimuli in the 4D perception space (where a certain attribute direction might be inhomogeneously filled-in), and can also arise from a need of higher real space dimensionality than used.

2.3 Sound perception implications summary

The embeddings of all of the attributes into the perception space revealed:

· Roughness (as an entirety) is not collinear with any of the other obtained attributes.

· The cracked and buzzing percept both contribute to the perceived roughness (more in cracked and less in buzzing, 32° and 64° angles respectively).

· Neither rustle or bleary contribute to roughness (90±15° right angles).

· The strident quality increases with an increase in narrowness (27° angle) and brightness (47° angle; brightness is opposite to darkness (133° angle)) and also to roughness (61° angle). This is in accordance with previous studies of sharpness [14, 15], since the strident percept is a gradation of sharpness. In these studies, sharpness was similarly related to: 1) dark, gloomy ↔ clear, bright; 2) narrow ↔ wide, full; 3) rough, harsh ↔ soft, delicate

· Narrowness is independent to buzzing, cracked and rustle (all are angled 90±15° to narrowness) and also is almost opposite to bleary (121°).

· Darkness and bleary are nearly collinear (16° angle). More bleary sounds were also darker.

· Buzzing is partially opposite to bleary (130° angle) and darkness (133° angle). The bleary and dark sounds were less buzzing.

3. THE CAUSATIONS OF ROUGHNESS

One of the results of the described first experiment part is that roughness is a two dimensional phenomena in the used stimuli context, and the perception of roughness judged as an entirety might be predicted from the amount of the cracked and buzzing percepts. The next part of the study focused on the possible causations of these attributes.

The following analysis is based on the time courses of the microphone signal and the string movement near the bridge. The time course of the violin string motion represents a trajectory of a chosen location on the string. The tracking was performed using a software, tracing the best correlating pattern in a defined area between frames (movement of defined pixel patterns on a surface)

3.1 The *cracked* percept and irregularities

The time courses of highly cracked sounds displayed visible periodicity irregularities in both the string motion and in the sound signal.

The values of the autocorrelation function 1st maximum used as a measure of signal invariability (Fig. 5) clearly differentiated the highly cracked sounds. But the lesser cracked and buzzing sounds could not be discriminated using this method (see Fig. 6).

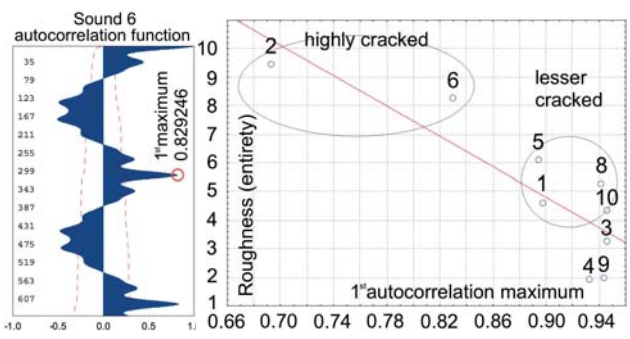

Figure 5: Left: An example of the autocorrelation function and 1st maximum values (the peak in the middle right) Right: The sounds ranked along the values of the 1st maximum of the autocorrelation function and roughness.

The string movement and the sound signals variability was therefore analyzed using a different approach. Sequential correlations of neighbouring time windows with the length of one tone period (SC1P) were used for a between period variability evaluation. The signals were divided into segments with the duration of one period (based on the f_0 of the signal) and the samples of every segment were correlated to the succeeding one using spearman correlation. Time courses with less time changes between the segments had higher correlation coefficients between adjacent periods. The resulting SC1P coefficients are shown in Fig. 6 to 9.

In Fig. 6 and 7 the SC1P values for every sound (colored circles) are ranked on the y-axis according to the overall roughness of the sound, and grouped by the most frequent attribute for every sound (the buzzing sounds are in the left graph, the cracked/other sounds are in right graph). The label displays 2 most frequent attributes for each sound. Sound 4 features the lowest overall roughness rating, and is shown in both graphs.

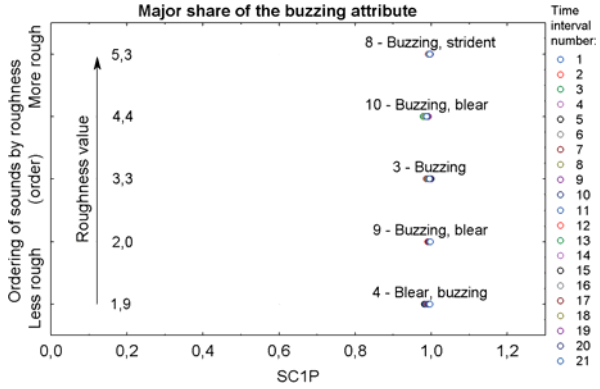

Figure 6: SC1P and sound roughness values for the 21 time segments (each segment represented by a circle) of each sound waveform with a major share of the buzzing percept

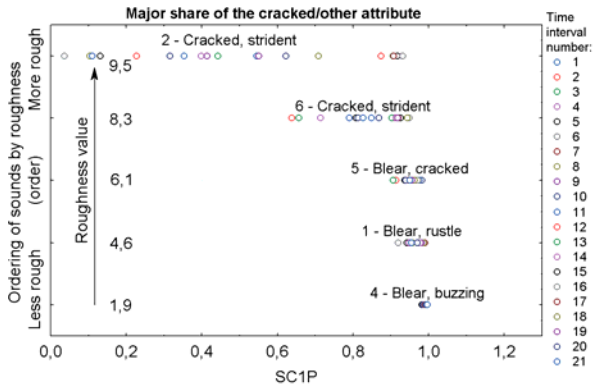

Figure 7: SC1P and sound roughness values for the 21 time segments (each segment represented by a circle) of each sound waveform with a major share of the cracked and other percepts

While the mean SC1P values of sound signals with cracked/other qualities decrease with increasing perceived roughness (and their variance increases), the SC1P values in sound signals with buzzing remain relatively high and with relatively little variance as the values of the roughness rating of the sounds increase.

The SC1P results for the string movements also correspond to these results (see the SC1P values of all sounds in Fig. 8; the cracked sounds 2, 6, 5, 1 have both relatively lower mean and greater variance of SC1P values, and the buzzing sounds 3, 8, 10, 9 show relatively lower variance and higher mean values).

The SC1P correlation values remain relatively high and invariable in the time courses of both signals in sounds with increasing extent of the buzzing attribute, and do not increase with increasing extent of buzzing.

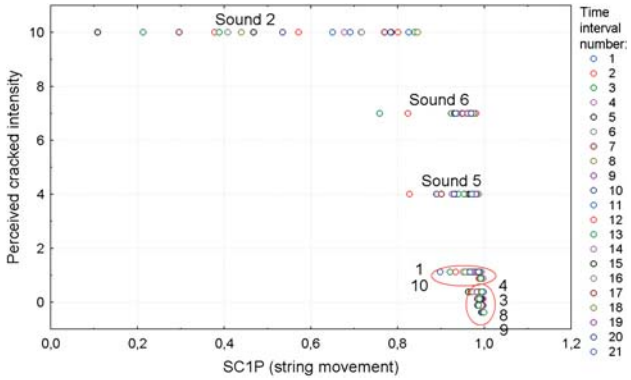

Figure 8: The SC1P values of the string movement for all of the studied sounds (the sounds 4, 3, 8, 9 in red ovals have value 0 of the cracked attribute and the sounds 1, 10 have value 1).

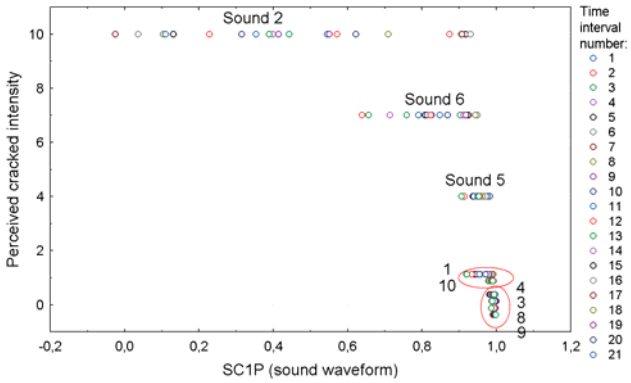

Figure 9: The SC1P values of the sound signals for all of the studied sounds (see legend in Fig.8).

The SC1P values for the string and for the sound signal are similar in values and trends, although there are distribution variations, which have yet to be investigated.

3.2 The *buzzing* percept and harmonics in a bark

The buzzing sounds display very little between period changes in the time courses (see SC1P results in 3.1). Since the spectral waterfalls show more harmonic components with higher amplitudes in the frequency ranges above 3 kHz (when compared with the other sounds) a further approach was used to analyze the signals. The study focused on the interactions of harmonics within a single bark, following to the relationships already reported in previous studies [16, 17]. The sound signals were bandpass filtered using a one bark wide filter. The bark number was chosen with regards to the f_o of the considered sound and the requirement of a three harmonics content (The appropriate bark is centered around the f_o multiples. The 2940 to 3450 Hz band contains the 15th, 16 th, 17 th harmonics in a 196 Hz open G string tone). Listening to this sound filtered in one bark featuring three harmonics showed that its buzzing considerably differs from an unfiltered one. A broader filtering in the two bark 2950 - 4050 Hz range (TBB) resulted in a more buzzing-like sound, therefore this TBB filtering was used. An example of a TBB signal time course is shown in Fig. 10 Top

(shown for sound 5). The lines between the red circles in the graph mark an amplitude of the envelope rise. The length of the line specifies the rise amplitude used as a characteristic of the buzzing extent. The values are gathered in the Table 4 (the first number in the *Rise* row marks the lowest rise found in the TBB bandpass filtered signals / the second marks the highest; *Aver.Rise.* presents the averages of the rise values).

The amplitude variability off TBB signals was also analyzed by a correlation method. A one period autocorrelation window was used likewise to the SC1P. Fig. 10 bottom shows an autocorrelation function example of TBB filtered signal for sound 5 (only the positive autocorrelation values are presented). The displayed red circle (with a value) marks further characteristic employed for buzzing extent estimation (see values in the *Correlat.* row in Table 4).

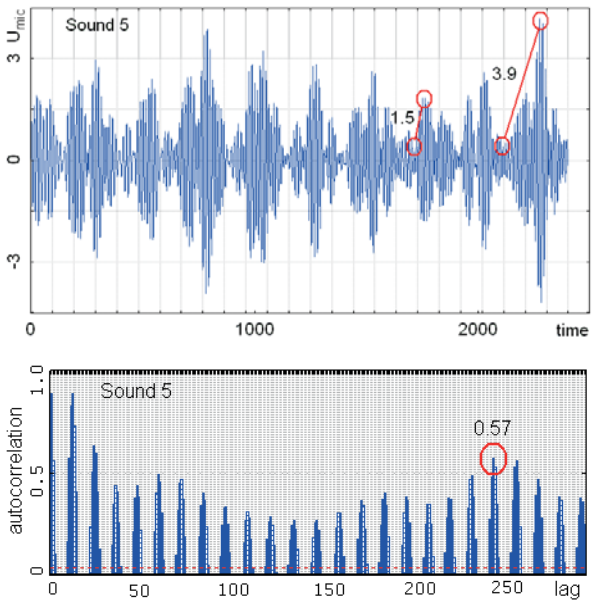

Figure 10 Top: The time course of the sound signal after the two bark bandpass filtering (TBB) in the 2940 to 4040 Hz range. Bottom: Positive values of the autocorrelation function of one 5.1 ms period (196 Hz) of TBB filtered signal.

Table 4: The buzzing value and the characteristic used for the buzzing amount estimation

Sound	**3**	**8**	**10**	**9**	**4**	**1**	**5**	**2**	**6**
Buzzing	**7.5**	**7**	**4.5**	**4**	**2.5**	**1.5**	**0.5**	**0**	**0**
Rise	**4.8 /5.7**	**4.2 /5.6**	**2.3 /3.8**	**2.3 /3.5**	**1.5 /2**	**2.8 /5.2**	**1.5 /3.9**	**3.5 /11.8**	**1.7 /6**
Aver.Rise	**5.3**	**4.9**	**3.2**	**3**	**1.8**	**4**	**2.8**	**4**	**3.5**
Correlat.	**0.86**	**0.87**	**0.86**	**0.89**	**0.8**	**0.66**	**0.57**	**0.37**	**0.26**

The steadiness of the risings (a regularity of the filtered signal) is demonstrated by a low variation in the rise values obtained in different time sections. The values in Table 4 show that the sounds with high correlation value and with smaller average rise value invoke smaller buzzing sensation (compare e.g. the sound 3 and 9). Low correlation values also characterize the cracked percepts. The buzzing sound quality percept is conditioned by regularity of harmonic triads in a bark. A higher unfiltered signal variability could suppress the buzzing causation by disrupting the interactions of the harmonic triads in the two barks by the multiple cracked irregularities (small correlations and large differences between the lowest and the highest rise will occur, see sounds 1, 5, 2, 6 in Table 4). The harmonic triad interactions are also influenced by the harmonic levels (the harmonics in one bark had to have roughly comparable levels (level uniformity)).

4. CONCLUSIONS

The results of the listening tests show that roughness judged as an entirety (in the used violin tone context) might be predicted from the amount of the cracked and buzzing percepts (see [13] and a summary in 2.3). The presented results links the causations of these attributes to a between period variability in both studied signals.

The between period similarity decreases in violin tones with a major share of the cracked percept with increasing perceived roughness in both the string movement course and the sound signal waveform. This decrease in similarity mainly occurs due to irregularities in time courses of the sound signal waveforms. The between-period similarity analyzed by sequential correlations of neighbouring time windows with one tone period length (SC1P) appears to be an overall indicator of the cracked roughness quality (in the cracked dimension).

On the other hand, an increase in the buzzing quality was not directly accompanied by an increase in the SC1P values (sounds with high buzzing quality have high SC1P coefficients already). The causes of the buzzing perception might be explained more reasonably based on the characteristics gathered in Table 4. Three sufficiently stable harmonics in one bark in the time course might form an amplitude modulation by superposition. The results of the two barks filtering analysis (TBB) indicate that the buzzing percept is caused by the modulation interactions in the two neighboring barks. The buzzing sound quality is perceived with more intensity if the pulsations of TBB filtered signals have higher rises and the risings are regular. The average of the rise values obtained in the TBB time sections with duration of one tone period duration of the tone fundamental frequency has shown to be a suitable characteristic of the rising height in this study. The value of the autocorrelation function in the same time section is a suitable characteristic of the risings regularity.

5. ACKNOWLEDGMENTS

Supported by the Ministry of Education, Youth and Sports of the Czech Republic in the Long Term Conceptual Development of Research Institutes grant of the Academy of Performing Arts in Prague: The "Sound quality" project.

6. REFERENCES

[1] H. Fastl, E. Zwicker: Psychoacoustics facts and models, Springer, Berlin (1990)

[2] Ch.G. Tsai: Auditory Grouping in the Perception of Roughness Induced by Subharmonics: Empirical Findings and a Qualitative Model, Proc. Int. Symposium Musical Acoustics. Nara, Japan (2004)

[3] M.J. Tramo, P.A. Cariani, B. Delgutte, L. D. Braida: Neurobiological Foundations for the Theory of Harmony in Western Tonal Music, The Biological Foundations of Music, 92-116 (2001)

[4] J. Kreiman, B.R. Gerratt: Perception of aperiodicity in pathological voice“, J. Acoust. Soc. Am. 117, 2201-2211 (2005)

[5] K. Omori, H. Kojima, R. Kakani, D.H. Slavit, S. Blaugrund: Acoustic characteristics of rough voice: subharmonics, J. of Voice. 11, 40-47 (1997)

[6] C.G. Tsai, L. C. Wang., S.F Wang, Y.W. Shau, T.Y. Hsiao, W. Auhagen: Aggressiveness of the Growl-like Timbre: Acoustic Characteristics, Musical Implications and Biomechanical Mechanisms, Music Perception. 27 (3), 209-221 (2010)
[7] J. Kreiman, B.R. Gerratt, G.S. Berke. The multidimensional nature of pathologic vocal quality, J. Acoust. Soc. Am., 96, 1291-1302 (1994)
[8] J. Stepanek, Z. Otcenasek,: Interpretation of Violin Spectrum Using Psychoacoustic Experiments, Proc. Int. Symposium Musical Acoustics. Nara, Japan (2004)
[9] M.E. McIntire, R. Schumacher, J. Woodhouse: "Aperiodicity in bowed-string motion", Acta Acustica, 49(1) 13-32 (1981)
[10] J. Woodhouse, P.M. Galluzzo: The bowed string as we know it today, Acta Acoustica, 90, 579-589 (2004)
[11] M.E. McIntire, J. Woodhouse: On the fundamentals of bowed-string dynamics. Acta Acustica, 43, 93-108 (1979)
[12] J. B. Kruskall: Nonmetric multidimensional scaling: a numerical method. Psychometrika 29, 115-129, (1964)
[13] Z. Otčenášek, J. Otčenášek,. Perception of different Types of roughness of violin tones. In: Proceedings of the International Symposium on Musical Acoustics, - Le Mans, France. p. 557-62, (2014) www.conforg.fr/isma2014/cdrom/data/articles/000102.pdf
[14] J.Štěpánek, Interpretation and comparison of perceptual spaces, Proceedings of Inter-Noise 2005, Rio de Janeiro (2005), http://zvuk.hamu.cz/vyzkum/publikacni.php
[15] J. Štěpánek, Z. Otčenášek, Acoustical correlates of the main features of violin timbre perception, Electronic proceedings CIM05 Montréal 2005, Québec, Canada, http://zvuk.hamu.cz/vyzkum/publikacni.php
[16] Z.Otčenášek, J.Štěpánek, "Glossy" and "Buzzing" in timbre of violin sounds, 6 CFA, Lille (2002), str.691-694, http://zvuk.hamu.cz/vyzkum/publikacni.php
[17] J.Štěpánek, Z.Otčenášek, Interpretation of Violin Spectrum Using Psychoacoustic Experiments, CD of Proceedings of the International Symposium on Musical Acoustics (ISMA2004), Nara, Japan, 4-S2-1 (2004), http://zvuk.hamu.cz/vyzkum/publikacni.php

TOWARDS THE COMPARABILITY AND GENERALITY OF TIMBRE SPACE STUDIES

Saleh Siddiq[1], Christoph Reuter[1], Isabella Czedik-Eysenberg[1], Denis Knauf[2]

[1]Musicological Department, University of Vienna, Austria
[2]Vienna University of Technology, Austria
saleh.siddiq@univie.ac.at

ABSTRACT

This article describes an empirical meta study that was carried out to assess the comparability of timbre spaces [1]. A recent comparison of three popular timbre spaces revealed a lack of consistency among those studies [2]. It is most likely caused by the stimuli-sets that were vastly different from study to study. Thus far, instruments were reduced to a single tone, compared at the same pitch, and only (re-)synthesized sounds were used.
These findings raise the question whether an empirical meta timbre space would rather comply with the results of the original timbre spaces or confirm the inconsistency. Based on the original stimuli of the compared timbre spaces [3][4] [5], and additional natural instrument sounds out of the *Vienna Symphonic Library*, a hearing experiment was performed. By the means of multidimensional scaling, the obtained dissimilarity matrix was graphed into a new meta timbre space and eventually structured through a hierarchical clustering.
The inconsistency is confirmed. The meta timbre space yields a clear clustering of stimuli-sets. Apparently, there is a greater timbral resemblance among the different instrument sounds from the same stimuli-set than among the sounds of the same instrument across the different stimuli-sets. Hence, the timbral differences between the stimuli-sets prevail as primary discrimination cue and thus, impair the comparability and generality of timbre space studies.

1. INTRODUCTION

Although most people intuitively "know" what timbre, or tone quality, is, it in fact remains a very elusive phenomenon when it comes down to the hard facts. Timbre can be associated with many facets of music like instrumentation, pitch range, articulation, and musical dynamics. Hence, it is impossible to describe timbre with a distinctive sound feature—as compared to other characteristics such as pitch (~periodicity) or loudness (~intensity). Timbre research can be basically divided into two main branches: the investigation of sound production (i.e. musical acoustics) and the investigation of sound perception (i.e. music psychology) [6]. A popular focal point of musical acoustics is the acoustics (which in this case means timbre) of musical instruments in terms of identification and discrimination. So far, several acoustic parameters have been identified as contributors to musical instrument timbre (see [6] for a brief summary), and it's a complex interaction of these features that makes up the instrument sound. This knowledge about timbre from an acoustical perspective is reflected in a definition provided by Stumpf as early as 1890 [7]. Stumpf's definition was, in fact, an adaptation of a definition previously published by Helmholtz [7][8][9]. Helmholtz then considered the harmonic spectrum as the only physical correlate of timbre. Stumpf accepted it as the main feature, labeled it "Klangfarbe im engeren Sinn" (roughly translated: timbre in a narrow sense), and further packed all the other (temporal) features, such as noise, transients, fluctuations, musical phrases etc. together and labeled them "Klangfarbe im weiteren Sinn" (timbre in a wider sense).
While the acoustic components of timbre are thus well explored, there's still not much known about their psychological correlates that are actually used by the ear to perceive an impression of timbre. Since the publications of Helmholtz' "On the Sensations of Tone" (1863) [8]—especially the English translation by (1875) Ellis [9]—and Stumpf's "Tonpsychologie II" (1890, unfortunately never translated), timbre has gained attention by empirical scientists. Since then, several approaches have emerged in order to describe the perception of timbre. Thereof, especially the so-called *timbre spaces* (TS) have generally been accepted. TS are (most often Euclidean) virtual spaces that translate timbral dissimilarities into spatial distances. That means, the closer two sounds are located in such a space, the stronger their timbres resemble each other. Although most of those studies were somehow productive, there are some common noticeable drawbacks: (1) musical instrument sounds were generally (re-)synthesized instead of being actually recorded. (2) Instruments were reduced to a single tone, (3) they were, in each case, compared on the same pitch that (4) inevitably had to be out of range for many instruments (imagine trying to find a common pitch for double bass and flute or even piccolo). Musical instruments obviously can't be properly represented through a single tone. Such methodical weaknesses considerably reduce the data basis, thus minimizing the chance of significant data overlap between two studies, and, as a consequence, have a negative impact on the comparability and therefore the validity of the studies.

1.1 Comparison of Timbre Spaces

If it is assumed that TS studies yield significant results about timbre similarities of musical instruments, then the same instruments should appear in roughly the same spatial regions across the different studies and thus, the spatial relations between all the instruments should be consistent across the studies as well.
In an earlier meta study, the results of three of the most popular TS studies by Grey 1975 [3], Krumhansl 1989 [4], and McAdams et al. 1995 [5] were compared [2]. These TS were chosen not only because of their popularity and significance but also because they contain a decent number of the same instruments (comparing flute A with flute B obviously makes more sense than comparing flute A with double bass B) and the coordinates of all three Euclidean dimensions were, somehow, accessible.
The 3D-coordinates of all instruments were extracted from every TS, uniformly scaled (the lowest value becoming 0, the highest 100) and aligned, and finally graphed into a new 3D scatter plot. The result was a meta TS (MTS, see Figure 1) that revealed a notable inconsistency among the compared TS. That

means that the same instruments, across all studies, were located in widely different regions of their respective spaces.

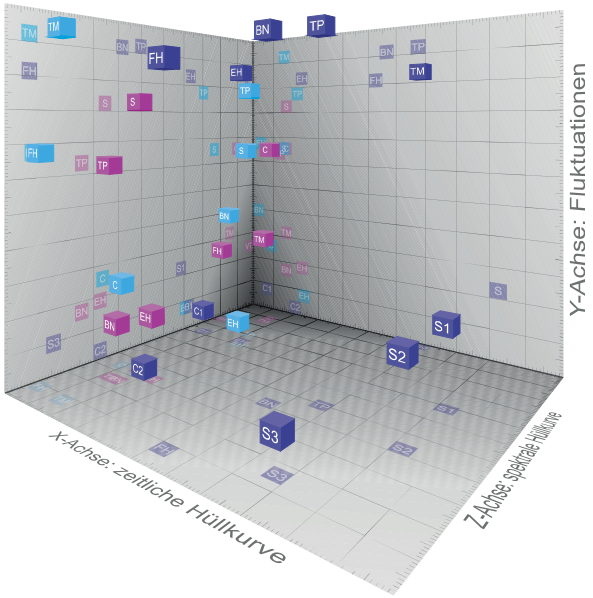

Figure 1: Meta timbre space (MTS). Colors: blue = Grey (GRY), cyan = Krumhansl (KRH), magenta = McAdams (MCA); dimensions: x = temporal envelope, y = fluctuations, z = spectral envelope; abbrev.: BN = bassoon, C = clarinet, EH = cor anglais, FH = french horn, S = strings, TM = trombone, TP = trumpet.

2. QUESTION

These results, and the fact that same instruments are obviously often represented by very different stimuli, raise a new question: Will an empirical TS, based on the original stimuli from the compared studies, support the inconsistency or instead reconcile with the original TS? Or to put it another way: How much of an influence do the utilized stimuli have on the comparability and generality of TS studies?

3. METHODS

To investigate the question, the same TS as in the earlier comparison [3][4][5] were now compared in an empirical meta study [1]. The methods basically match those of the compared studies. By means of a hearing experiment (pairwise comparison) and a multidimensional scaling (MDS), a meta TS was ascertained [3][4][5][10]. For the first time, the new empirical meta TS (EMTS), allows to compare the stimuli of different TS as well as actually recorded instrument sounds of the *Vienna Symphonic Library* (VSL) in the same context. On top of that, a hierarchical clustering was performed in order to closely examine the (spatial) arrangement and relations of the sounds.

3.1 Stimuli

This study includes every instrument that is represented in each of the compared TS. Hence, the following seven instruments were tested: bassoon, clarinet, English horn, French horn, strings (i.e. celli), trombone, and trumpet. The utilized 24 stimuli were exactly the same stimuli used in the original studies by Grey (1975) [3] (including three celli, two clarinets; thus a total of ten stimuli) and Krumhansl (1989) [4] (seven stimuli; McAdams et al. (1995) [5] utilized the same set of stimuli) and moreover actually recorded instrument sounds (seven stimuli) from the *Vienna Symphonic Library* (VSL). According to the stimuli from the original studies, the pitch was Eb4 (roughly 313 Hz).

3.2 Subjects

A total of 35 subjects, including 15 females and 20 males, participated in the experiment. Their ages ranged from 19 to 72 (Ø=30.9, SD=13.3). The subjects had to assess their amount of musical experience by completing a short questionnaire before the experiment. 24 subjects were musicians (including playing instruments, singing, and conducting), eight were formerly active and three were non-musicians (Ø=19.6 years of experience, SD=14.2).

3.3 Procedure

The experimental session lasted roughly 45 to 60 minutes and consisted of four phases: an instruction and familiarization phase, a training phase, the actual experimental phase, and the questionnaire. The instructions were presented orally as well as in written form on the screen. Subjects were allowed to ask any question to avoid possible misconceptions. After that, all 24 stimuli were presented in a randomly ordered sequence in order to familiarize the subjects with the range of timbre variation among the test sounds. Unlimited repetitions were allowed but the order of presentation was random every time.

The timbral dissimilarity of the stimuli was rated subjectively in a pairwise comparison. Subjects did their ratings on a one-dimensional ten-point-scale (0 = most similar, i.e. identical; 9 = least similar). The succession of both the sounds within a pair and the pairs themselves was fully randomized for each subject. The randomized order of the sounds within a pair enabled us to cut the session duration in half by dropping all complementary ordered pairs (i.e. B–A instead of A–B) while still controlling the confounding influence of the order of presentation. Identical pairs (A–A) were excluded as well. Hence, the experimental phase consisted of ((24·23):2=) 276 pairs. Each trial could be repeated as often as needed. Subjects were allowed to take unlimited breaks at any time during the session, provided they were not in the middle of a trial.

The preceding training phase, consisting of 20 trials (randomly drawn out of the available 276 pairings), was identical to the actual test, so subjects could get accustomed to the procedure and hopefully develop some kind of a consistent rating strategy.

The experiment was performed on a specially developed browser-based software. The stimuli were presented through external sound cards (Roland Quad-Capture UA55) and electrostatic headphones (Koss ESP 950 with amplifier E 90).

3.4 Evaluation

The perceptual ratings of each subject were stored in a separate symmetric dissimilarity matrix. In fact, the matrices were half-matrices (i.e. only the upper triangle) because leaving out the complementary pairs led to an empty lower half-matrix. Since systematic asymmetries have never been found [10], leaving out the lower half, the complementary pairs respectively, is not a constraint. The individual half-matrices were averaged into an overall half-matrix. Using the median instead of mean value considerably lowered the stress value of the subsequently calculated spatial configuration. The calculation was carried out by means of a non-metric multidimensional scaling (MDS). Based on the eigenvalues, a four-dimensional configuration proofed to be an appropriate fit (Kruskal's stress = 0,0362). Thereon, eventually, a hierarchical clustering was performed in order to in depth study the spatial arrangement of the sounds.

4. RESULTS

The ascertained new empirical meta TS (EMTS, see Figure 2) strongly confirms the previously found inconsistency. It is visible to the naked eye, that, in the EMTS, sounds of the same instruments do not reside in the same spatial regions. So the sounds of the same instruments (e.g. flute A and flute B) do not possess significant timbral similarities, which hence causes the expected instrument-clusters not to evolve. That would be enough to state that there's a lack of comparability among and thus a lack of generality to (the compared) TS-studies.

Furthermore, another striking phenomenon was found: while the VSL-sounds tend spread over the whole space, the Grey-stimuli (GRY) and Krumhansl-stimuli (KRH) primarily group on opposing sides of the space. In other words: the sounds group into some kind of "stimuli-set-clusters" instead of the aforementioned expected instrument-clusters. The hierarchical clustering (see Figure 3) reveals a strict division into three main clusters. Interestingly, (1) the clarinets (VSL and KRH) set themselves apart as a separate cluster. The rest splits into (2) an almost exclusive GRY-cluster (only disturbed by the VSL bassoon) and (3) a KRH-cluster. The latter one is spread wider since it also contains most of the VSL-sounds.

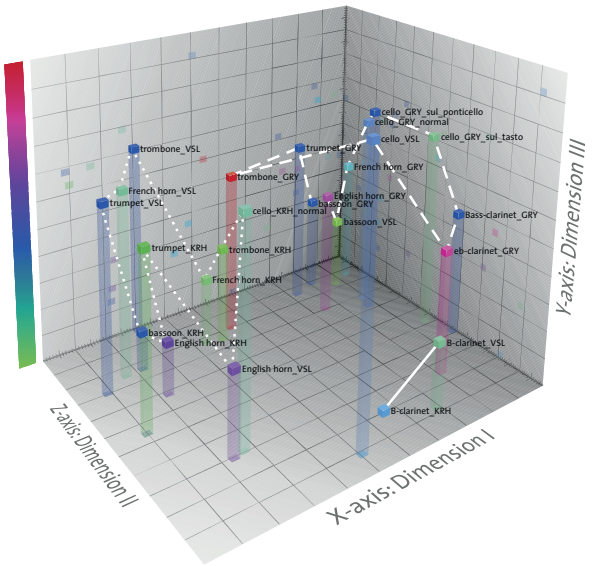

Figure 2: Empirical meta timbre space (EMTS). Color scale = dimension IV, red = high value, green = low value. No physical correlates of timbre were attached to any of the dimensions. The three main clusters are highlighted by the white lines: solid = b-clarinets (VSL & KRH), dotted = KRH-cluster, dashed = GRY-cluster.

5. DISCUSSION AND OUTLOOK

The results of this empirical meta study do not comply with the data of the compared studies, but rather confirm the inconsistency among those studies that was found in an earlier comparison. Possible reasons for this inconsistency could be, (1), subjective data diverging from study to study —although these are unlikely to fully account for the vast differences—and (2) more probably, different distance models and MDS algorithms that were used to process the data (see [10] for an in-depth discussion). If we furthermore take the conspicuous grouping in stimuli-set-clusters into account, it seems likely that utilizing natural sounds might have the biggest impact on the validity of TS studies. In fact, the obvious systematic timbral toning (or—in this case—rather "tone*i*ng") of the stimuli-sets seems to stand out so much that it simply overrules the initially sought-after instrumental characteristics and become the primary cues of timbre discrimination. The timbral toning most probably stems from the process of (re-)synthesizing the stimuli, which further supports the notion that natural sounds from actually recorded instruments are better suited for studying musical timbre. The notion that the sound system might be the crucial factor can be dismissed, since the systematic timbral differences among the stimuli-sets were apparent even though the stimuli were presented through the same speakers (in this case headphones). Nonetheless, it is clear that the frequency response of loudspeakers always, more or less, influences timbre perception. Thus, diverging results from different studies may—not fully but to some extent–be also put down to different sound systems.

However, it needs to be stated that stimuli duration could have a biasing influence. The GRY-stimuli averaged 350 ms [3] while the KRH-stimuli averaged 673 ms [5]. The different durations, taken by themselves, are not a problem because (1.) they only contribute to the studied differences between the stimuli-sets and (2.) by a stimulus duration of max. 300 ms, the ear has reached its maximal performance. That means, even by the end of the shorter GRY-stimuli the impression of timbre through the ear is well established and any further increase of duration won't increase the quality of perception by the ear [11][12][13] [14]. But the problem became evident when the duration of the VSL-sounds had to be adjusted. Since manipulating the stimuli of the compared studies was not an option, the only question was then towards which stimuli-set the VSL-sounds would be tilted. The perceptual durations of the VSL-sounds were eventually matched with those of the KRH-stimuli. At first glance, this complies with the basal clustering. A further examination, however, shows that same instruments of both sets still do not possess considerable timbral similarities. If we examine the leafs of the tree model (i.e. the single items/instruments), the same instruments of different sets never share the same nodes (see Figure 3). So the durations apparently do not interfere with timbre perception but might be a factor on a more general level of over-all similarity. While different durations become confounding factors in meta studies that are bound to have some kind of impact, it might be fair to assume that they do not generally impair the validity of TS studies per se.

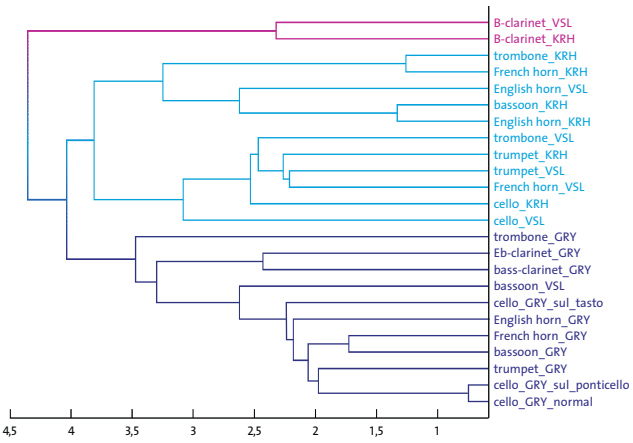

Figure 3: Dendrogram of the hierarchical clustering. The main clusters are seperated by color: magenta = clarinet-cluster, blue = GRY-cluster, cyan = KRH-cluster.

Other than that, the results indicate that natural sounds are better suited to yield reliable data with regards to timbral similarities of musical instruments. In other words: the usage of actually recorded sounds presumably would significantly enhance the external validity, reliability and thus generality of TS studies.

The next steps planned include further empirical studies, exclusively using real instrument sounds and taking musical dynamics and pitch as influencing variable of timbre. Therefor, musical instruments will be tested over a vast range of their respective ranges of pitch and dynamics. This considerable broadening of the data basis for each instrument will certainly lead to results that are (1) reproducible and hence reliable, (2) closely related to the actual circumstances in music, and thus will (3) yield more realistic and universal information about the perceptual similarities of the timbre of musical instruments.

6. ACKNOWLEDGEMENTS

Supported by funds of the Österreichische Nationalbank (Österreichische Nationalbank, Anniversary Fund, project number: 16473). Special thanks to the *Vienna Symphonic Library* for supporting our work with two free "Vienna Super Package" licenses.

7. REFERENCES

[1] Siddiq, S. et al., "Kein Raum für Klangfarben – Timbre Spaces im Vergleich", Fortschritte der Akustik – 40. DAGA 2014, Oldenburg, Germany, 2014

[2] Siddiq, S., "Timbre Space revisited – Was ist Fakt, was ist Mythos?" Proc. FAMA (of the DEGA), Detmold, Germany, pp. 51–52, 2014

[3] Grey, J. M., "An exploration of musical timbre using computer-based techniques for analysis, synthesis and perceptual scaling," Stanford University, Report No. STAN-M-2, Stanford, 1975

[4] Krumhansl, C., "Why is musical timbre so hard to understand?" Nielzen, S. and Olsson, O. (eds.), "Structure and perception of electroacoustic sound and music," Amsterdam, Netherlands, pp. 43–53, 1989

[5] McAdams, S. et al., "Perceptual scaling of synthesized musical timbres: Common dimensions, specificities, and latent subject classes," Psychological Research, 58(3): 177–192, 1995

[6] Auhagen, W., "Zu Fragen der Klangfarbenwahrnehmung und der Klanggestaltung durch Musiker," Eberl, K. and Ruf, W. (eds.), "Musikkonzepte – Konzepte der Musikwissenschaft. Bericht über den Internationalen Kongress der Gesellschaft für Musikforschung, Halle (Saale) 1998," Vol. 1, Kassel, Germany, pp. 86–100, 2000

[7] Stumpf, C., "Tonpsychologie," Vol. 2, Stuttgart, Germany, 1890

[8] Helmholtz, H. v., "Die Lehre von den Tonempfindungen als physiologische Grundlage für die Theorie der Musik," Braunschweig, Germany, 1st ed. 1863

[9] Helmholtz, H. v. and Ellis, A. J., "On the sensations of tone as a psychological basis for the theory of music," London, United Kingdom, 1st english edition, 1875

[10] McAdams, S., "Perspectives on the Contribution of Timbre to Musical Structure," Computer Music Journal, 83(3): 85–102, 1999

[11] Mertens, P.-H., "Die Schumannschen Klangfarbengesetze und ihre Bedeutung für die Übertragung von Sprache und Musik," Frankfurt/M, Germany, 1975

[12] Reuter, C., "Die auditive Diskrimination von Orchesterinstrumenten. Verschmelzung und Heraushörbarkeit von Instrumentalklangfarben im Ensemblespiel," Frankfurt/M, Germany, 1996

[13] Gefand, S. A., "Hearing. An introduction to psychological and physiological acoustics," Yew York, NY, 2004

[14] Yost, W. A., "Fundamentals of hearing. An introduction," San Diego, CA, 2007

MODELLING SIMILARITY PERCEPTION OF SHORT MUSIC EXCERPTS

Daniel Müllensiefen
Goldsmiths, University of London, United Kingdom
d.mullensiefen@gold.ac.uk

ABSTRACT

There is growing evidence that human listeners are able to extract considerable amounts of information from short music audio clips containing complex mixtures of timbres and sounds. The information contained in clips as short as a few hundred milliseconds seems to be sufficient to perform tasks such as genre classification (Gjerdigen & Perrott, 2008; Mace, Wagoner, Teachout, & Hodges, 2012) or artist and song recognition (Krumhansl, 2010). The ability to extract useful, task-related information from short audio clips also has been shown to vary between individuals and this variability has been the basis for the construction of a sound similarity sorting test (Musil, El-Nusairi, & Müllensiefen, 2013) as part of the Goldsmiths Musical Sophistication test battery (Müllensiefen, Gingras, Musil & Stewart, 2014) where participants are asked to sort 16 800ms clips into 4 groups by perceived similarity. In this talk we will present data to explain the individual differences in the ability to extract meaningful information from short audio clips and to compare audio extracts on the basis of sound information alone. In addition, we will present two approaches to identify audio features of the short sound clips that drive listeners judgements. The first approach (Musil, El-Nusairi, & Müllensiefen, 2013) makes use of timbre features in combination with powerful statistical prediction methods to approximate listener judgements. In contrast, the second approach (Müllensiefen, Siedenburg & McAdams, in prep.) relies on Tversky's theoretically motivated model of human similarity perception (Tversky, 1977) to explain listener judgements and makes use of 22 spectro-temporal audio descriptors from the clips using the Timbre Toolbox (Peeters et al., 2011). Non-negative matrix factorization was employed to decompose the clips-descriptor matrix into a matrix of binary features which were then fed into Tversky's ratio models of similarity perception. Results show a superiority of the second approach using Tversky's similarity model that explains a higher proportion of the variance in the listener judgements and requires considerably less parameter tuning. The results are discussed in the context of psychological approaches to similarity perception which seem to apply well to the perception of musical sound.

COMPARING RECORDED AND SIMULATED MUSICAL INSTRUMENT SOUNDS: PERSPECTIVES FOR A PERCEPTUAL EVALUATION

Alejandro Osses V., Armin Kohlrausch
Eindhoven University of Technology, Netherlands
a.osses@tue.nl
a.kohlrausch@tue.nl

ABSTRACT

To better understand the properties of a musical instrument, a common practice is to compare its recordings in controlled situations with a computational model that attempts to recreate such situations. In this study we present perceptual criteria we applied to evaluate the so-called hummer in two acoustic conditions, with and without first-order reflections. The hummer is a plastic corrugated tube that produces a clear pitch sensation when rotated at specific speeds. Our evaluation was based on estimates of the perceptual descriptors of loudness, loudness fluctuation, roughness and fundamental frequency. We discuss why we chose those descriptors, which limitations our analysis had and what aspects we consider important in order to extend this approach to the evaluation of other musical instruments.

INVESTIGATING THE COLLOQUIAL DESCRIPTION OF SOUND BY MUSICIANS AND NON-MUSICIANS

Jack Dostal
Wake Forest University, United States of America
dostalja@wfu.edu

ABSTRACT

What is meant by the words used in a subjective judgment of sound? Do musicians, scientists, instrument makers, and others mean the same things by the same expressions? These groups describe sound using an expansive lexicon of terms (bright, brassy, dark, pointed, muddy, etc.). The same terms and phrases may have different or inconsistent meanings to these different groups of people. They may even fail to be applied consistently when used by a single individual in various contexts. We would be better able to relate scientific descriptions of sound to musical descriptions of sound if the words used to describe sound had less ambiguous interpretations. To investigate the use of words and phrases in this lexicon, subjects with varying musical and scientific backgrounds are surveyed. The subjects are asked to listen to different pieces of recorded sounds and music and are asked to use their own colloquial language to describe the musical qualities and perceived quality differences in these pieces. Some of the qualitative results of this survey will be described, and some of the more problematic terms used by these various groups to describe sound quality will be identified.

PRE-ASSEMBLY VIOLIN AURALIZATION—LISTENING TO PLATE-TUNING TRENDS AND TO FINE MODEL-ADJUSTMENTS

Robert Mores
University of Applied Sciences Hamburg, Germany
robert.mores@haw-hamburg.de

ABSTRACT

Listening to violins before or during the manufacture process might be desirable for luthiers. Two different approaches are revisited and compared. One approach identifies the mutual dependencies between plate modes, body modes and cavity modes as empirically derived from pre-assembly and post-assembly measurements [Bissinger, J. Acoust. Soc. Am. 132, 465 (2012)]. The derived model uses the critical frequency as an intermediary key parameter to co-define body and cavity modes as well as the radiation efficiency at higher frequencies. The bridge rocking frequency serves as a secondary key parameter to define radiation in the frequency range above 2 kHz. While varying these parameters the resulting radiation filter allows to listen to trends that directly translate to mode 2 and mode 5 plate tuning but also to bridge tuning [Bissinger and Mores, J. Acoust. Soc. Am. 137, EL293 (2015)]. The other approach is based on sampling technology. The binaural impulse responses of an existing reference violin is sampled in the preferred listening position in a luthier's shop. Based on this sample, a luthier can modify individual resonances while editing in the frequency domain in order to explore fine adjustments for future models. A method has been developed to preserve the sampling quality while transforming such a partially modified violin spectrum into an audio-processable filter [Türckheim et al., DAFx-10 1-6 (2010)]. By means of real-time processing, a luthier can listen to the virtually modified violin while playing a silent violin. Both systems will be examinable during the poster session.

PART I. INTERACTIVE SESSION: IMPROVING DYNAMIC POSTURE FOR MUSICAL PERFORMANCE

Robert Friberg, Leigh Anne Hunsaker
Hardin Simmons University, United States of America
rfriberg@hsutx.edu
hunsaker@hsutx.edu

ABSTRACT

Given the almost universal assumptions in brass pedagogy that good posture allows freer air flow and reduces unnecessary tension, corresponding improvements in sound, flexibility, and articulation may be expected with improved posture. Published studies of posture in brass players, however, have not included systematic observations of the perceived quality of these aspects of performance. Recent work by Friberg and Hunsaker has explored this area of interest, finding significant results with short-term postural training. This session begins with a brief review of relevant research followed by an interactive session with audience participation. The neuromechanic of posture is the foundation for understanding efficient and effective movement. The biomechanics and more importantly, neuromechanics and their role in effective motor control, will be explained and demonstrated in a practical and usable manner for performers. Presenters will work with volunteers to establish efficient posture and movement while playing short excerpts of their choosing. Brass players are invited to bring both period and modern instruments. Other instrumentalists and vocalists are also welcome to participate.

PART II. INDIVIDUALIZED PROGRAMS FOR CONTINUING IMPROVEMENT

Robert Friberg, Leigh Anne Hunsaker
Hardin Simmons University, United States of America
rfriberg@hsutx.edu
hunsaker@hsutx.edu

ABSTRACT

The results of recent and ongoing research concerning the efficacy of long-term postural training for instrumentalists will be examined. The authors will discuss the limitations of traditional postural instruction in typical music school settings. Recommendations will be offered for performers and teachers who would like to increase their understanding and ability to implement efficient performance strategies for themselves and their students. Following this, Presenters will work with interested musicians, tailoring a program for their specific needs. Each participant will be screened for biomechanical and neuromechanical dysfunction related to posture. A specific program is developed to improve static and dynamic posture as it relates to performance. In addition, a model is provided for the application of the intervention principles for use with the participants' students.

AURALIZATION AS A TOOL FOR EVALUATING A MUSICAL INSTRUMENT

Matthew Boucher [1], *David Pelegrin-Garcia* [2], *Bert Pluymers* [1], *and Wim Desmet* [1]

[1] Dept. of Mech. Eng.
[2] Dept. of Physics & Astronomy
KU Leuven, Heverlee, Belgium
matt.boucher@kuleuven.be

ABSTRACT

When a musician is considering the purchase of a new instrument, the test room often does not have ideal acoustics, and a musician rarely has the opportunity to test the new instrument in a concert or recital hall before purchase. However, one of the most important criteria when choosing a musical instrument is its sound in a representative performance environment. If recorded in a relatively anechoic environment, the dry sound of an instrument can be merged with the acoustic reflections of a performance environment through a process known as auralization. The technique of auralization, therefore, allows the musician to evaluate the sound of the instrument without being influenced by non-musical cues, such as quality or knowledge of manufacturing. By reproducing the auralized sound, a musician can listen to his/her own playing as if it were played in a concert hall, for example, with the auralized sound quality being one aspect of total quality. Auralization techniques can then be a service offered to musicians by the instrument maker at the time of purchase in addition to testing in standard factory showrooms.

1. INTRODUCTION

At the time of purchasing a musical instrument, a musician starts with several instruments to test. By repeatedly playing typical repertoire on each instrument, unsuitable instruments are identified and removed from the pool of possibly suitable instruments. Eventually, one instrument is judged to be the best, and a happy musician goes home with a new instrument.

While this process seems simple enough, there are many factors that contribute to the decision process. For example, when choosing a tuba, it is suggested that intonation, tone, response and dynamics are all important playing criteria and that the evaluation may be different for low, middle and high tones [1].

As a further complication, non-musical cues, such as touch, can affect one's perception of sound during playing [2]. It has been shown that pianists can determine which piano they are playing even when their vision and hearing are intentionally impaired [3], indicating that the mechanical response of piano keys is an identifying factor of quality.

Another non-musical cue can be simple knowledge of how the instrument was made or materials of construction. Smith's experiment showed that a copper trombone bell was not distinguished from brass bells of varying thickness by a group of 10 professional trombonists during double blind tests. However, distinguishable playing characteristics were attributed to the copper bell during non-blind tests [4].

This provides motivation to separate the evaluation of sound from complicating factors such as touch and knowledge of fabrication. A simple way to do this is to record the playing and judge the instruments only based on a listening test without any visual or tactile clues. However, the listening test is then only valid to judge the instrument's sound in a particular recording room. Of more concern is that musicians, whether consciously or subconsciously, change their performance based on their acoustical environment [5].

For these reasons, isolating the sound of a musical instrument from non-musical cues and room effects is desired. This can be achieved through a technique known as auralization. The technique consists of recording a sound in a room with sound absorbing walls and then adding the perceivable effects of another acoustic environment. An added benefit is to judge the sound of the instrument in different musical settings [6].

In this work, the basics of the auralization techniques are outlined, and their application to the evaluation of a basstuba (in F) is demonstrated. Two excerpts of different musical styles, common to the tuba repertoire, are chosen and auralized. They are taken from: (1) *Vocalise*, Op. 34, No. 14 by Sergei Rachmaninoff, a lyrical, singing melody originally written for soprano or tenor voice that has been transcribed for various instruments, including the tuba and (2) the *Hungarian March* from Hector Berlioz's *The Damnation of Faust*, which is played at a higher dynamic level and requires a harder, march-like articulation.

Applying auralization in this context, the intent is to isolate the sound of the instrument so that it may be evaluated in the absence of non-musical cues. This work is intended to aid musicians and musical instrument manufacturers in the evaluation of a musical instrument at the time of purchase.

2. AURALIZATION

The basic process of auralization consists of recording a sound source in a room with sound absorbing materials on its walls and then blending this "dry" sound with the response of a particular performance environment. It is most often associated with the evaluation of concert halls, which has been the subject of lots of research [7]. Even though the usual goal is to compare the quality of different concert halls, the method is equally valid to evaluate different sources of sound in the same concert hall, which would be valuable in the case of a musician testing

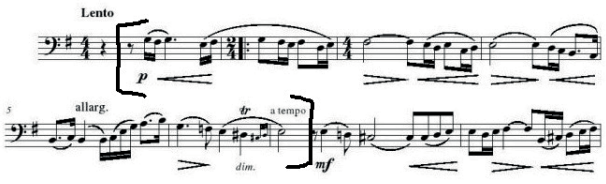

Figure 1: Excerpt from Rachmaninoff's *Vocalise*.

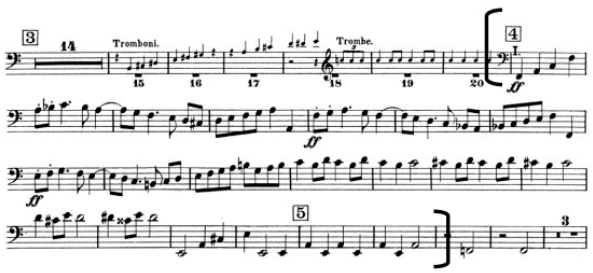

Figure 2: Excerpt from Berlioz's *Hungarian March*.

several instruments for purchase.

New challenges are presented in this case, of course, namely, that the same music should be reproduced exactly on each instrument. However, as is the case in most recording sessions, several takes are allowed, so it is assumed that experienced musicians are able to reliably reproduce high quality performances on different instruments. Any differences that remain are attributed to the characteristics of the instrument.

In this section, the main steps of the auralization technique are outlined: 2.1 the making of dry recordings, 2.2 taking into account room and listener effects of a typical musical environment, 2.3 adding these effects to the dry recordings and 2.4 listening and evaluation. The process is applied to the musical excerpts shown in Figs. 1 and 2.

2.1. Anechoic recording

An anechoic (*i.e.*, without echo) room is an acoustically dry room that is specifically designed for performing sensitive acoustic experiments. Such experiments include measuring the directivity of loudspeakers, human hearing tests and noise radiation measurements of machines. Although not achievable in practice, a perfectly anechoic room absorbs all sound energy at its walls at all frequencies, imitating an infinite space. This means that a listener inside an anechoic room in the presence of a sound source only hears the direct sound from the source and not the reflected sound from the walls of the anechoic room.

When a musical instrument is played in a normal room, the sound heard by a listener contains the sound of the musical instrument and the sound reflected from the walls of the room. The differences between a normal room and an anechoic room are illustrated in Figs. 3 and 4. If a musical instrument is played inside an anechoic room, only the sound starting from the source and traveling directly to the microphone is present; any reflected sound from the walls is absent.

The recording setup in the anechoic room of the KU Leuven

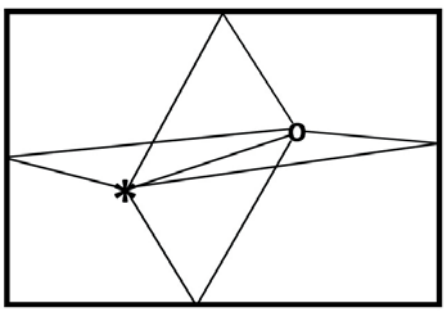

Figure 3: The sound in a normal room comes from the source ($*$) and reflections from the walls and arrives at the listener (**o**).

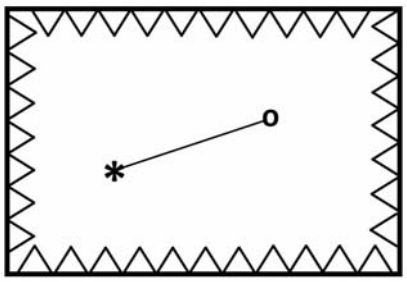

Figure 4: Only the direct sound is present in an anechoic room. The reflections are eliminated by the triangular wedges, which are made of absorbing materials.

Dept. of Physics & Astronomy is shown in Fig. 5. Two microphones are placed in front of the player at $+/-45^\circ$ and one microphone directly behind the player. All three microphones were placed at a distance of $150\,\mathrm{cm}$. The two front microphones were Behringer ECM8000 $1/2$" microphones, and the one behind was a Brüel & Kjaer type 4192 $1/2$" pressure-field microphone with measurement amplifier type 2160. A fourth microphone, a miniature Sennheiser MKE2 ($4.8\,\mathrm{mm}$), was placed on-axis at the opening of the bell using tape and string. The audio interface was a Roland UA-1010 Octa-Capture, and the Reaper Digital Audio Workstation was used, which allowed multitrack recording [8].

It is important to note that the choice of microphones has an impact on the quality of the recordings. For example, large diaphragm microphones (1") are more sensitive than microphones with smaller diaphragms ($1/2$" or below). While this allows the recording of more faint sound pressure levels (SPL), they can not be used to record very high SPLs, such as those arising at fortissimo passages played with the tuba at short distances. For auralization purposes, therefore, it is important to maximize the dynamic range of the recording, *i.e.*, the difference between the strongest signal peaks and the noise floor. Moreover, the frequency response of the microphones should be flat.

The directivity of the musical instrument should also be considered when making anechoic recordings, as it plays a role in the placement of the recording microphones. The directivity of a musical instrument describes how the low, middle and high tones radiate in different directions. Fortunately, due to the bass nature of the tuba, its sound radiates rather evenly in all directions over most of its playing range [9, 10], and the recordings at the three microphone positions are quite similar. Other instruments with more complicated directivity patterns (*e.g.*, violin or flute [9]) may need a more complex arrangement of micro-

Figure 5: Recording setup in anechoic room using 3 microphones.

RIR	all room effects including the positions of the source and listener, materials on walls, size and shape of room
HRIR	all effects due to the presence of a listener including shape of upper body, head and ear
BRIR	room and listener effects contained in RIR and HRIR

Table 1: Summary of different impulse responses.

phones [11]. Other sounds like mechanical noise or breathing from the player may also have a more complicated directivity pattern. With the intention of evaluating the auralized sound of the tuba, these additional sounds should be ignored as much as possible.

Under these conditions, anechoic recordings of a tuba performing the excerpts found in Figs. 1 and 2 were obtained, eliminating the room acoustics feedback given to the musician [1]. The next step in the auralization process is to determine the effects a real musical environment has on the sound of the instrument. This is done by using impulse responses.

2.2. Impulse responses

Once an anechoic recording is obtained, the relevant, perceivable aspects of listening to this sound as if it were performed on the stage of a concert hall must be added. This is done by using impulse responses that contain the effects of the room and listener's presence. There are three types of impulse responses that are relevant to the auralization of a musical instrument, the RIR, HRIR and BRIR, which are explained below.

A room impulse response (RIR) is the resulting sound in a room after a very short sound. In classical measurements of the RIR, the sound is recorded after the popping of a balloon. Short impulsive sounds are used, because they excite all frequencies evenly. This is why most acousticians clap their hands when they enter an acoustic space. They are performing a very crude measurement of the room impulse response.

The impulse response of a room depends on the size and shape of the room, the objects inside the room and the materials on its walls. If someone adjusts the position of reflecting panels on stage or if curtains are drawn or closed, all of these things change the RIR.

Even if the wall treatments and other objects do not change, a room impulse response is still dependent upon the source and receiver locations. At an opera, an RIR changes if the singer walks across the stage or if the listener changes seats. Therefore, the room impulse response contains all the sound effects that are determined by the room and the positions of the sound source and listener.

The RIR describes how the sound travels through a room and arrives at the location of a listener. However, this measurement is from a microphone, a physically different situation than if the sound were measured at the listener's eardrums. The presence of a human listener affects the sound waves arriving at the listener's location. For these reasons, a head-related impulse response (HRIR) is needed.

The HRIR gives the relationship between the sound at the eardrum of the listener and the sound as measured by a microphone in place of the listener. The two sounds are different, because the shape of the body, head and ear all affect the incoming sound. Sound coming from the left and arriving at the right ear must travel around the head, resulting in a different sound compared to a direct line of travel, likewise for the sound coming from the right, arriving at the left ear. Therefore, the HRIR contains all the information related to the physical presence of a human listener.

[1] It is recognized that an anechoic environment may itself be a form of feedback that may influence the musician. However, it has been reported that musicians are able to quickly adapt and perform well in this acoustically foreign environment [11].

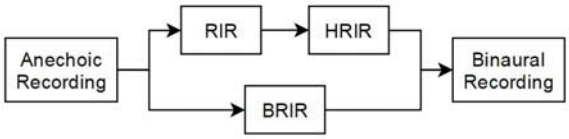

Figure 6: How to make a binaural recording.

The combination of both the RIR and HRIR gives the binaural room impulse response (BRIR), which contains the information of how a sound source on stage travels through the concert hall to the listener's location and arrives at the listener's eardrum. The different impulse responses are summarized in Table 1.

It should be noted that there are several databases of impulse responses available for academic use. Room impulse responses of different rooms are available [12, 13]. Head-related impulse responses can also be found [14, 15, 16].

The anechoic recording and the binaural room impulse response are the two main building blocks of the auralization process. How to combine them into a binaural recording is described next.

2.3. Processing

Adding room and head effects to an anechoic recording consists of a convolution process of the recorded signal with a binaural room impulse response. Convolution is a mathematical process of combining two sequences. Specifically, the sound at a particular time in the first sequence (the anechoic recording) results in a large amount of echoes that are determined by the impulse response. Each instance in time of the anechoic recording gives rise to a similar sequence of echoes. Finally, all the echoes overlap and are added together to get the total effect.

In digital audio workstations (DAW), the convolution process is similar to adding artifical reverb. The reverb in this case is the reflections measured inside a real concert hall. In addition to Reaper, the already mentioned DAW used to make the anechoic recordings, Audacity [17], Cubase [18] and Wavosaur [19] are other popular DAWs.

It is usually necessary to use a reverb or convolution plug-in with a DAW, and there are many available. Two examples are Freeverb (opensource) [20] and SIR2 (license required) [21]. They are provided as Virtual Studio Technology (VST) plug-ins that are compatible with most DAWs. Available from CATT-Acoustic, GratisVolver is available as a free stand-alone convolver [22].

While DAWs are quite user friendly, the convolution algorithm used is not always specified, and computation time-saving measures are often employed, which reduce the accuracy of the convolution process. For these reasons, Octave [23] is used in this work for the convolution process. Octave is an open-source software used primarily for advanced numerical computations. With the execution of only a few commands, an anechoic recording can be read, processed and listened to. The process of obtaining binaural recordings is summarized in Fig. 6.

By convolving the anechoic recordings with binaural room impulse responses, binaural recordings of both musical excerpts are calculated. The anechoic recordings as well as the binaural recordings using one chamber hall and one concert hall are available at `people.mech.kuleuven.be/~u0086891/Data`. Audio files for all four microphones are included.

2.4. Listening and evaluation

If this process of creating binaural recordings were repeated for other tubas, the binaural recordings could be compared. The musician trying out a new musical instrument could listen to Instrument A, playing several contrasting pieces of music in a few different musical environments. Next, Instrument B could be auralized under the same conditions. In this way, the musician could judge the musical characteristics of the instrument independent of several biasing factors, such as mechanical response and knowledge of manufacturing techniques.

Even though the sound has been successfully separated from any non-musical cues, determining the best sound is still quite involved. Therefore, the subjective evaluation is left to the musician purchasing the instrument.

On the other hand, if there are several evaluators, perhaps several representatives of the musical instrument manufacturer, other factors should be taken into consideration. Specifically, attributes have to be clearly defined, and some training is often needed. Returning to the suggestions found in [1], there are many attributes to consider. Intonation is obviously related to the frequency at which the instrument plays relative to accepted standards, but evaluating the tone of an instrument may not be as straightforward. A bright or a dark tone may be preferred, and this may differ for different musical styles. Even more problematic is that people have a range of opinions of what bright means and what dark means.

Once the attributes are well-defined, these can be judged and ranked for the different recordings using standardized blind listening tests like MUSHRA [24] or paired comparisons. The results of the listening tests can give customers and manufacturers more objective information when evaluating the auralized sound of the instruments.

3. DISCUSSION

It is possible to approximate the experience of playing an instrument in a concert hall by using real-time auralization. This technique is essentially identical to the offline convolution described in section 2.3. Instead of using a recording, the microphone input during live performance is directly processed by the convolution plugin, and the output is played through headphones worn by the player. In order to use this technique, headphones should be of high quality, open type and with a rather flat frequency response. The time delay between the instant a sound is played and the time for the sound to be processed by the audio interface, *i.e.*, the system's latency, should be lower than $5\,\mathrm{ms}$. In addition, the early samples of the BRIRs should be trimmed, accounting for the latency of the sound card and the propagation of sound between the instrument and the microphone. Despite the benefits of this technique, it brings back the effects of visual and tactile cues in judging the value of an instrument.

A critical requirement for accurate auralizations is the use of an anechoic room. Since construction of an anechoic room is quite expensive, it is not expected that these techniques can be immediately applied to the evaluation of musical instruments. However, anechoic rooms are standard facilities at acoustics research laboratories. Therefore, auralization of musical instruments can be a point of collaboration between research institutions and instrument makers.

4. CONCLUSIONS

This work applies the basics of auralization techniques to the evaluation of a musical instrument. The main concepts, including anechoic recordings, impulse responses and data processing, are described. Auralization is intended to be of use for musicians and instrument makers at the time of purchasing a new instrument. This method successfully isolates the sound perception from the non-musical cues experienced by a musician when testing an instrument. A musician can record several instruments and then listen to the binaural recordings in order to independently evaluate the playing quality of the instrument.

5. ACKNOWLEDGEMENTS

The research of Matthew Boucher is supported by the European Commission and the Marie Curie Initial Training Networks GRESIMO (No. 290050) and BATWOMAN (No. 605867), the Research Fund KU Leuven and the Fund for Scientific Research - Flanders (F.W.O.). David Pelegrin-Garcia gratefully acknowledges F.W.O.-V for supporting this research by financing his postdoctoral grant No. 1280413N. Alexander Lindau and the Audio Communication Group of TU Berlin are recognized for providing binaural impulse response data.

6. REFERENCES

[1] R. Bobo, *Choosing a tuba*, `http://www.rogerbobo.com/musical_articles/tubashopping.shtml`, 2006.

[2] D. M. Campbell, "Evaluating musical instruments," *Physics Today*, vol. 67, no. 4, pp. 35–40, 2014.

[3] A. Galembo, "Acoustics of extreme ranges of piano, part 2...," *Piano Tech. J.*, vol. 55, pp. 14–17, 2012.

[4] R. Smith, "The effect of material in brass instruments: a review," in *Proceedings of the Institute of Acoustics*, 1986, vol. 8.

[5] Z. Shärer Kalkandjiev and S. Weinzierl, "The influence of room acoustics on solo music performance: an empirical case study," *Acta Acust united Ac*, vol. 99, no. 3, pp. 443–441, 2013.

[6] M. Vörlander, *Auralization*, Springer, 1st edition, 2008.

[7] T. Lokki, "Tasting music like wine: Sensory evaluation of concert halls," *Physics Today*, vol. 67, no. 1, pp. 27–32, 2014.

[8] Reaper, `http://www.reaper.fm/`.

[9] J. Meyer, *Acoustics and the Performance of Music*, Springer, 5th edition, 2009, Translated by Uwe Hansen.

[10] PTB, `http://www.ptb.de/en/org/1/17/173/richtchar.htm`.

[11] J. Pätynen, V. Pulkki, and T. Lokki, "Anechoic recording system for symphony orchestra," *Acta Acust united Ac*, vol. 94, pp. 856–865, 2008.

[12] Aachen Impulse Response Database, http://www.ind.rwth-aachen.de/en/research/tools-downloads/aachen-impulse-response-database/.

[13] R. Stewart and M. Sandler, "Database of omnidirectional and b-format impulse responses," in *Proc. of IEEE Int. Conf. on Acoustics, Speech, and Signal Processing*, Dallas, Texas, 2010.

[14] MIT Sound Media Lab, http://sound.media.mit.edu/resources/KEMAR.html.

[15] UC Davis, http://interface.cipic.ucdavis.edu.

[16] IRCAM, http://www.ircam.fr/equipes/salles/listen/download.html.

[17] Audacity, http://audacityteam.org/.

[18] Steinberg Media Technologies GmbH, http://www.steinberg.net/en/products/cubase/start.html.

[19] Wavosaur, www.wavosaur.com.

[20] Freeverb3, http://freeverb3vst.osdn.jp/.

[21] Christian Knufinke, SIR Audio Tools, http://www.siraudiotools.com/ http://www.knufinke.de/sir.

[22] CATT-Acoustic, http://www.catt.se/.

[23] S. Hauberg J. W. Eaton, D. Bateman and R. Wehbring, *GNU Octave version 4.0.0 manual: a high-level interactive language for numerical computations*, 2015.

[24] Institute of Sound Recording, http://iosr.surrey.ac.uk/software/.

STUDY ON THE INFLUENCE OF ACOUSTICS ON ORGAN PLAYING USING ROOM ENHANCEMENT

Sebastià V. Amengual[1], *Winfried Lachenmayr*[2], *and Malte Kob*[1]

[1]Erich-Thienhaus-Institut
Hochschule für Musik Detmold, Germany
amengual@hfm-detmold.de, kob@hfm-detmold.de

[2]Müller-BBM GmbH, Germany
winfried.lachenmayr@mbbm.com

ABSTRACT

A pilot study on the influence of different reverberation on the musical performance of organ players is presented. Using an organ with MIDI output, three different organ players are recorded performing the same pieces while a room acoustics enhancement system is used to modify the acoustic conditions of the Detmold concert hall in real time.
Since the dynamics and tuning properties of the organ remain constant, the analysis focuses mainly on tempo features such as total duration, rests duration and tempo variability, as extracted from the MIDI files. A set of binaural recordings is obtained for future studies on the relation of performance variations and the acoustic feedback received by the musicians. Finally, the participants are interviewed individually after the experiment to obtain their impressions of the influence of the acoustics.
The results show that the reverberation has a direct influence on the musicians, leading to slower tempo and longer breaks between consecutive notes. However, this relation is conditioned by other factors such as the character of the piece, the level, the global tempo and the individual players.

1. INTRODUCTION

Organ music is usually played in very reverberant spaces such as churches or cathedrals, resulting in challenging conditions to achieve a good synchronization with other musicians such as choirs or ensembles. Moreover, in many cases, the organ console is located far away from the organ stops, increasing the performance difficulty due to the sound travel time. This implies that organ players in particular need to adapt to the environment, in order to achieve a good music performance in a variety of different spaces.

Organ music was originally composed to be played in churches or religious spaces, thus room acoustics are an inherent characteristic of organ music. However, nowadays organ music is also played or practiced in concert hall environments, with noticeably different conditions. The goal of this preliminary study is to find out in what way the performance is affected.

By means of a room acoustics enhancement system it is possible to modify the room acoustics in real time, in order to study the performance adjustments adopted by the musicians. In addition, using a concert organ equipped with a MIDI output the performance can be easily recorded to extract a set of features related with the properties of the musical performance.

2. STATE OF THE ART

The authors know of no formal studies specifically on the influence of acoustics on organ playing. Nevertheless, the study of musicians' performance adjustments to room acoustics is a topic under investigation and similar experiments have been completed focusing on piano performance, cello and other soloist instruments.

In [1, 2] Bolzinger et al. presented a series of experiments on the influence of acoustics on piano performance. The main finding of that study is the relation between intensity of the performance and reverberation, meaning that more reverberant environments lead to softer performances. However, they found no conclusive relation between acoustic conditions and tempo variations.

A similar experiment focusing on piano performance was presented by Kawai et al. in [3]. In this experiment, the authors present links between the musicians' adjustments and three room acoustic parameters - T_{30}, ST_{early} and ST_{late}. The main effect of reverberation is reported to be on the *full pedal time ratio*, meaning that longer reverberation time leads to a shorter use of the piano pedal, as the remaining room energy acts in a similar way to the pedal. From the perspective of stage support, the main effect is reported to be on the dynamics of the performance, agreeing with the results presented previously by Bolzinger et al. Nevertheless, in this case the analysis of the tempo features show that the tempo variations are highly piece dependent: The musical characteristics of the piece are a variable that have impact on the influence and depending on the character of the piece the musicians may or may not be affected by the acoustics.

Although the acoustic properties of organ and piano are quite different, the playing technique presents several overlaps and similar results could be expected. However, it is clear that the feet and pedals have a completely different role in organ playing (yet, special attention has to be given to pedal melodies). Moreover, the organ dynamic cannot be influenced as directly.

When investigating the influence of room acoustics on cello players, Schärer et al. [4, 5] conclude that musicians are affected individually and relates the reverberation time with the tempo. In this case, it is shown that very dry and very reverberant rooms lead to lower tempos.

3. SET-UP

To conduct an analysis on the influence of the acoustics during a music performance it is necessary to be able to generate dif-

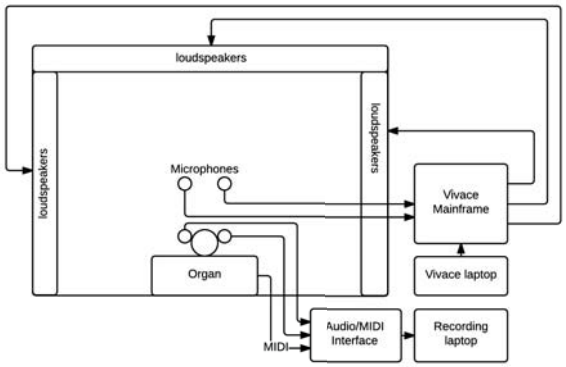

Figure 1: Schematic view of the implemented setup

ferent acoustic situations in real time and record the musician's reaction by means of acoustic and/or visual feedback. In this study, the acoustic conditions are generated using the electronic enhancement system *Vivace*, distributed by Müller-BBM ASG. The performance is captured using a MIDI connection implemented on the organ with respect to the instances at note on/off, and the acoustic signal at the musician's position is recorded by means of binaural recording.

3.1. Variable acoustics

To implement an electronic enhancement (or variable acoustics) system it is necessary to create a signal path: (1) capturing the signal from the instrument, (2) processing it by means of convolution with different spatial impulse responses and (3) playing back the generated reverb using a surrounding loudspeaker set-up (see Fig. 1 & 2).
The Detmold Konzerthaus is equipped with a *Vivace* system, which is a convolution engine that allows the user to define a set of desired room acoustic parameters as well as manipulation of the convolved impulse response. To feed the convolution engine, a pair of microphones in the ceiling and a pair placed close to the organ is used, in order to capture more direct sound of the instrument. After processing the signal, the artificial reverberation is played back through a virtual loudspeaker array (Iosono WFS with approximately 300 real loudspeakers) resulting in 56 virtual output channels.

3.2. MIDI recording

The most effective way to analyze the interaction between a musician and an organ is encoding all the keys and pedals pressed during the experiment. During this experiment the performance was encoded using a MIDI interface built on the organ and recording the data stream with a digital audio workstation (DAW).

The MIDI recording ensures that the recorded data matches completely with the action of the musician, avoiding errors that could occur in audio signal analysis. In addition, in this case, the keyboards and the pedal are encoded in different channels, allowing an easy separation and analysis of the pedal and hand notes.

Moreover, since the dynamics of the organ are constant – i.e. the MIDI velocity values are all maximum – the performance analysis is limited to temporal features.

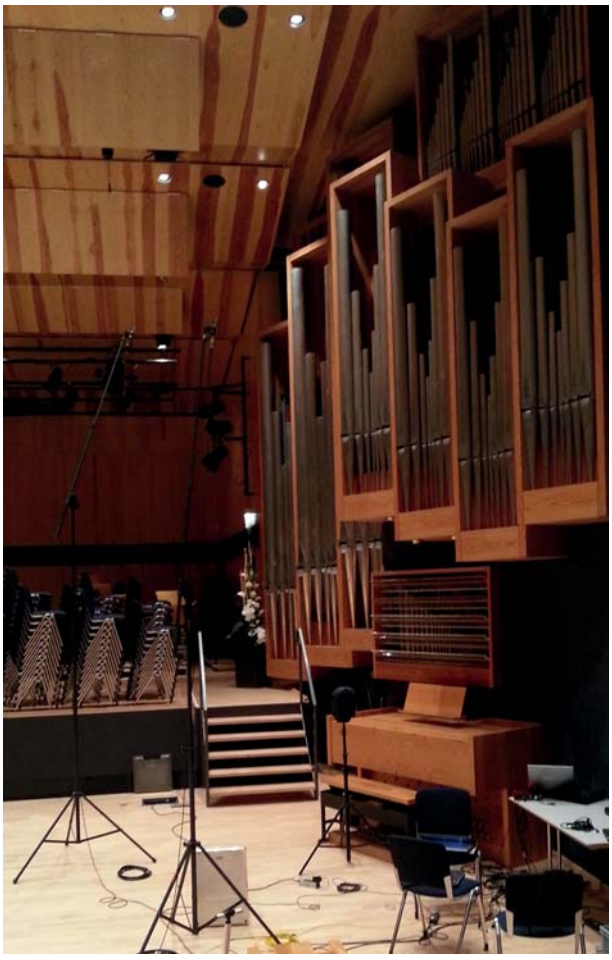

Figure 2: General view of the set-up in the concert hall

4. EXPERIMENT

4.1. Procedure overview

In the experiment the musician plays the same excerpt repeatedly while the acoustic conditions of the room are changed between iterations. Every excerpt is played in two variations (blind and non-blind) and it is played at least five times for each of the acoustic conditions:

- Blind test: In this variation, the musicians are not explicitely notified about the changes in the acoustics, which are randomly switched after each take. This allows the study of the "natural" adaptation of the playstyle.
- Non-blind test: After the blind test, several iterations are completed with explicit notifications on the acoustic changes. All the iterations of every different acoustic scenario are completed consecutively and a short training period is given before the trials/recordings. The data from this variation is used to quantify wether a bias is introduced in the playstyle by the *a priori* knowledge.

As the participant musicians are told about the general topic of the investigation (to study possible effect of the room on organ playing) and the conditions are briefly demonstrated in the beginning, there could be some bias involved i.e. that participants would play differently on purpose or subconsciously when a certain acoustic condition is active. Nevertheless it is not discussed *how* different acoustic settings could alter the playing

or articulation and the subjective opinions are the musicians' own vocabulary.

4.2. Acoustic conditions

Three different acoustic conditions are designed for the experiment:

- Natural reverb: Natural room reverberation without enhancement. The RT_{60} of the room is approximately 1.6 seconds.
- Soft increase: The reverberation is increased by approximately 0.5 seconds between 250 and 1500 Hz.
- Strong increase: The reverberation time is strongly increased at low and mid frequencies, between 5 seconds at 250 Hz to 1.5 seconds at 5 kHz.

In Figure 3 the different reverberation times are shown as a function of the frequency. The measurements are performed using the organ itself as an excitation source: by pressing all keys simultaneously most frequencies of the spectrum are covered. With releasing the keys, the decay is measured using an NTi XL2 Sound Level Meter and repeated a few times if single bands do not fulfill the signal-to-noise ratio requirement for the measurement. Possibly due to low frequency noise caused by the ventilation system or the organ itself, the results at 63/125 Hz are not reliable and therefore not included in the graph. Moreover, since the measurements are performed using the organ for exciting, it is not possible to achieve a sufficient dynamic range over 5 kHz, hence the reverberation is measured until 4 kHz only. However, the depicted frequency range contains most of the acoustic energy radiated by the organ and it is measured using the same radiation characteristics present during the real performances.

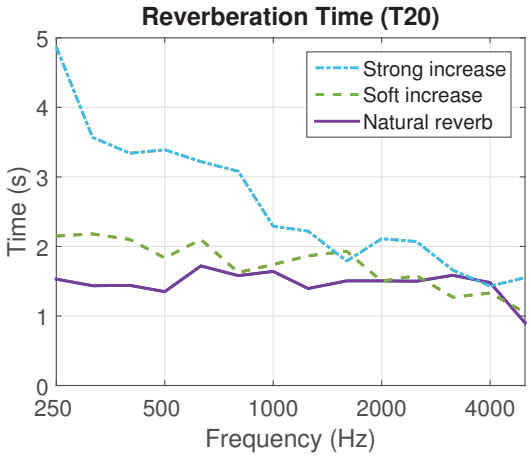

Figure 3: Reverberation times for the different acoustic conditions.

4.3. Participants

The participants in the experiment are three organ students from the Hochschule für Musik Detmold. The study level of the musicians is different, yet all of them are at a comparably high professional level.

Player Green is the first participant and only plays in two of the three conditions, "natural reverb" and "soft increase" (not in "strong increase" setting). The organ registration of this initial player then stays constant for the other two performers. As all musicians are given the same pieces and since two of them have to commemorate the piece, they are asked about any difficulties or insecurities that would inflict on their natural flow of playing. This is not the case, as everybody had studied the pieces before and refreshed it with some rehearsing.

4.4. Music pieces

The music pieces played during the experiment are two excerpts of a composition for organ solo:

- Mendelssohn A: Felix Mendelssohn Bartholdy, *Organ Sonate Op.65 No.2, Grave*, bars 1-4 (Fig. 4).
- Mendelssohn B: Felix Mendelssohn Bartholdy, *Organ Sonate Op.65 No.2, Adagio*, bars 24-30 (Fig. 5).

As mentioned before, the registration used by the musicians stays the same per piece, ensuring equal conditions for all players. One player suggested possible modifications regarding the registration and a take is recorded with this personal registration after completion of the tests. Table 1 contains supplementary information regarding the two pieces.

Piece	LAeq (dB)	Character	Avg. duration (s)
Mendelssohn A	78.2	Grave, lots of chords	13.5
Mendelssohn B	67.5	Pianissimo, legato	22.4

Table 1: Characteristics of the pieces used in the study.

5. ANALYSIS

This section describes in detail the different steps implemented to analyse the recorded performances.

5.1. Procedure

After completing the experiment, every recorded session results in a single MIDI file. The next steps are executed for each individual musician:

- Split & sort
- Importing the MIDI database
- Features extraction
- Analysis of the results

5.2. Split & sort

The files are split and sorted by acoustic condition, piece and musician, in order to build a database. "Defective" recordings with performance or technical errors are deleted.

5.3. Importing the MIDI dataset

The main tool used for the analysis is the MIDI Toolbox for Matlab [6]. Once the files are imported into the program the MIDI stream is represented as a Nx7 matrix, where N is the number of notes of the stream. Table 2 shows an example of the imported data stream corresponding to one take of the performance of *Mendelssohn A*.

Note that the onset and duration expressed in beats do not contain valuable information, since it is extracted from the encoded tempo embedded in the MIDI file, which is an arbitrary value. There are two channels containing information – channel 1 and 7 – which correspond to the keyboard and pedal notes respectively. The velocity of all the notes is the same as the keys are only quantized as "pressed" or "not pressed" (analog to an open or closed organ stop).

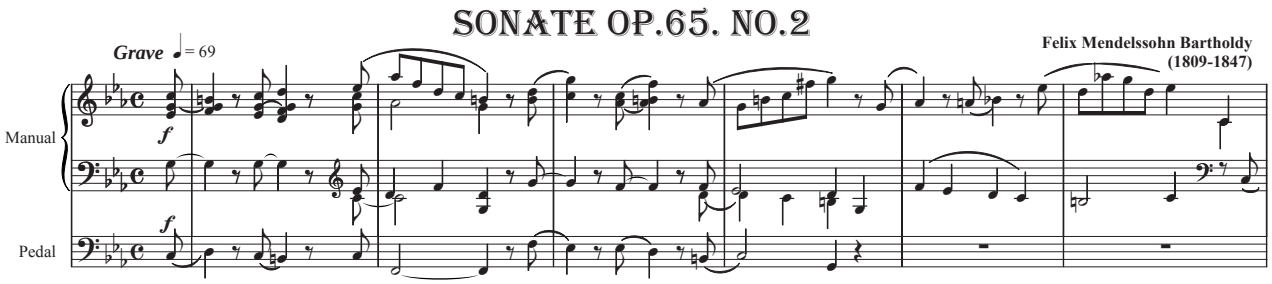

Figure 4: Music score of *Mendelssohn A*.

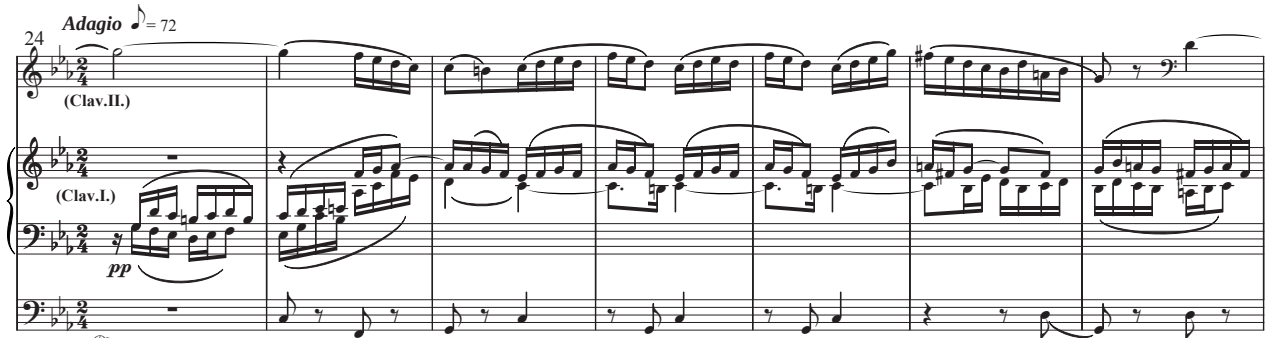

Figure 5: Music score of *Mendelssohn B*.

Onset (beats)	Duration (beats)	MIDI channel	MIDI pitch	Velocity	Onset (sec)	Duration (sec)
0	1.2250	7.00	48.00	127.000	0	0.6125
0.0333	0.6354	1.00	63.00	127.00	0.0167	0.3177
0.0490	0.9073	1.00	72.00	127.00	0.0245	0.4536
0.0781	2.0750	1.00	67.00	127.00	0.0391	1.0375
0.1063	1.9458	1.00	55.00	127.00	0.0531	0.9729
1.0240	1.1542	7.00	50.00	127.00	0.5120	0.5771
1.0281	1.0958	1.00	65.00	127.00	0.5141	0.5479
1.0427	1.1396	1.00	71.00	127.00	0.5214	0.5698
3.1719	1.0948	7.00	48.00	127.00	1.5859	0.5474
3.2031	0.4490	1.00	63.00	127.00	1.6016	0.2245
3.2469	1.7719	1.00	55.00	127.00	1.6234	0.8859
3.2490	0.8198	1.00	72.00	127.00	1.6245	0.4099

Table 2: Decoded MIDI stream of an excerpt of *Mendelssohn A*.

5.4. Features extraction

5.4.1. Average Tempo

The tempo related features are *total duration of the excerpt* (T_{time}) in seconds and *average tempo of the excerpt* (T_{tempo}) in beats per minute. They are extracted using the following expressions

$$T_{time}(s) = t_{last} - t_1 \tag{1}$$

$$T_{tempo}(bpm) = 60 \cdot \frac{N_{beats}}{T_{time}} \tag{2}$$

where t_{last} and t_1 are the onset times of the last and first notes of the excerpt, respectively, and N_{beats} is the number of beats of the excerpt. Note that the duration of the last note is not included in this feature.

5.4.2. Duration of rests

Since the most audible effect of the increased reverberation is produced after the offsets, a useful feature to analyze the influence of reverberation on the performance is the duration of the rests in the excerpts. The extracted features are *total time of rests* (T_{rest}) and *average duration of rests* ($T_{\mu rest}$), both computed in seconds.

$$T_{rest}(s) = \sum_{i=1}^{N} t_{rest}(i) \tag{3}$$

$$T_{\mu rest}(s) = \frac{T_{rest}}{N} \tag{4}$$

where t_{rest}(i) is the duration of every individual rest and N is the total number of analyzed rests.

5.4.3. Phrasing

The phrasing characteristics can be extracted following different methods, most of them based on beats histogram or distribution of strong beats. However, in this case all the beats have the same strength and different approaches have to be considered. Due to the character of the pieces used in this study, the following approaches can be implemented:

- Analysis of the duration of consecutive rests: In case of having rests in all the voices, the duration of consecutive rests can be measured, obtaining an estimation of the start/opening and stop/closing of different musical phrases.
- Analysis of a single voice: The analysis of a melodic voice allows the representation of the evolution in the duration of consecutive notes.
- Analysis of the pedal: Due to the easy extraction of the pedal voice the single voice analysis can be effortlessly implemented on the low notes.

6. INTERVIEWS AND SUBJECTIVE IMPRESSIONS

To gain insight in the musicians' impressions on the acoustic situations, short interviews are collected for the preceding set

of trials (i. e. after a block of 10-15 repetitions of one music piece), to 1) gather information and hints on what the musicians had experienced, heard or got affected by in a certain way and 2) analyze later if these impressions are truly resulting in a change of playing and could be measured through extracted features, or are possibly just imagined/random. The interviews are conducted in German and translated into English.

6.1. Organ players

Detailed interview content can be seen in tables 4 and 5 of the Appendix. To summarize, for *Mendelssohn A*, the effect of additional reverberation is supposedly heard by all three participants, reporting changes of playing mostly in terms of shorter articulation and longer breaks. Preference tends towards the "soft increase" reverberation setting. For *Mendelssohn B*, less dynamic and rather fluent, nobody reports to be significantly affected. By the most experienced player (Blue) there are a few remarks towards altering the registration depending on the acoustics.

6.2. Authors' impressions

The authors are trained in music and partly in audio production and therefore consider themselves expert listeners. During pretests consisting of the selection of appropriate music it quickly appears that an effect of the acoustics on the organ playing seems very dependent on the musical material and its character. With some pieces, the additional acoustics appear negligible (e. g. soft, fluent passages) while others seemed very prominent, both for player and audience (e. g. parts with big dynamic and breaks). Overall, the configuration "soft increase" seems to enhance the natural acoustics in the hall well, although depending on the music it is sometimes rather subtle.

The biggest immediate difference between the players seems to be the chosen overall tempo since this is not fixed but left to the musicians choice. This can be seen in the results and might be kept fixed by means of a metronom/click for further studies.

Player Blue (BL) appears to play a rather constant tempo regardless of the acoustics, Player Yellow (YE) on the other hand seems not as consistent in their behavior in general. In Mendelssohn A the musicians appear to notice the acoustic changes after the first 2-4 chords and then alter their playing, if at all. Overall, a slight difference in tempo and articulation and a noticeable difference in rest duration seems to happen. There is no big difference in behavior heard between blind and non-blind trials.

7. RESULTS

The results of the study seem to be highly dependent on the individual players and nature of the piece. While the results for *Mendelssohn A* show a tendency to play slower, with longer rests and notes, in the case of *Mendelssohn B* the performance is not affected by the acoustics (see Fig. 6 and 7). This corresponds to what the musicians reported.

The following subsections give a close view to the different analyzed features of *Mendelssohn A*.

7.1. Tempo

In *Mendelssohn A* the players tend to play slower when the reverberation is increased (Fig. 6a). However, the analysis of variance shows significance only for player OR. Player BL reports being affected - this is not visible here. Nevertheless, player BL shows the reported tendency in the non-blind case, meaning that the previous knowledge about the acoustic conditions seems to lead to an overrating of the effect of the acoustics.

7.2. Quaver rests

The duration of the first five quaver rests of *Mendelssohn A* has been measured and averaged in every take (Fig. 6b). The behavior of the players follows a similar tendency in this case, with longer rest duration when the effects of the reverberation are more evident. In this case, the statistical significance shows similar results (only player OR is significantly affected).

7.3. Notes duration

The duration of all the notes has been averaged in every take, using the same approach as in the quaver rests. By combining the effects on rests and notes duration, the origin of the tempo variations can be deduced (Fig. 6).

On one hand, player YE is playing longer rests (Fig. 6b) but the duration of the notes remain constant (Fig. 6c), which means that all the effect in the tempo variations is due to longer rests. On the other hand, players BL and OR tend to play longer notes with increased reverberation, and their tempo variations are made up from both longer notes and rests.

One way ANOVA					
		P-value			
		Mendelssohn A		Mendelssohn B	
Player	Test	Tempo	Rests	Tempo	Rests
BL	Blind	0.459	0.302	0.779	0.7957
OR	Blind	<0.01	<0.01	0.572	0.6413
YE	Blind	0.087	0.054	0.97	0.3485
BL	Non Blind	0.046	0.176	/	/
OR	Non Blind	<0.01	<0.01	/	/

Table 3: Resuts of the one way ANOVA analysis on the analyzed features. Abreviations BL, OR and YE stand for players blue, orange and yellow, respectively.

7.4. *A priori* knowledge

Although there are only two players which are recorded in blind and non-blind conditions, the results show a very different individual behavior. Player OR shows the same behavior and results with and without previous knowledge about the acoustic conditions. However, as mentioned previously, player BL shows a different behavior when having previous information about the acoustics and a detailed analysis is necessary to understand this situation: As shown in Fig. 3 in the acoustic condition "Strong increase" the reverberation is much more drastically lengthened than in "Soft increase". Therefore, player BL seems to naturally change the performance in the "Strong increase" scene, but in the case of "Soft increase", the changes are originated by the *a priori* knowledge on the acoustics, leading to an overrating of the effect of the reverberation, which is not present in the blind experiment.

8. CONCLUSIONS

This paper presents a pilot study on influence of acoustics on music performance. The proposed set-up using acoustic room enhancement in a concert hall and MIDI analysis has been

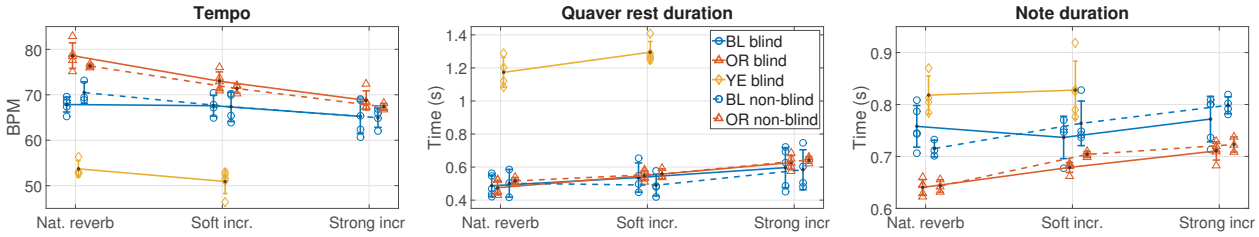

(a) (b) (c)

Figure 6: Performance results of *Mendelssohn A*, bars 1-4. Every color stands for a different player, solid and dashed lines represent blind and non-blind conditions, respectively. Point markers represent results of single takes.

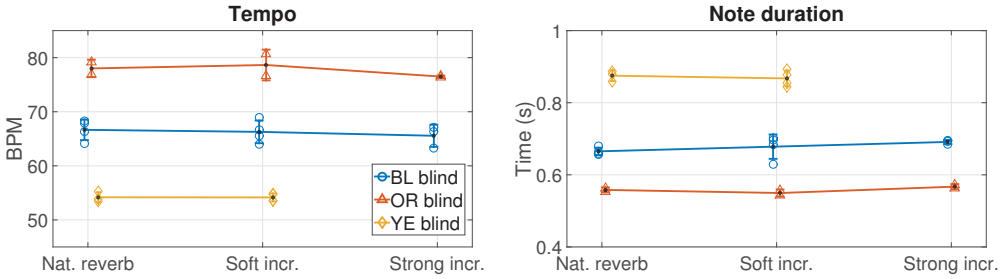

(a) (b)

Figure 7: Performance results of *Mendelssohn B*, bars 24-30. Every color stands for a different player, solid and dashed lines represent blind and non-blind conditions, respectively. Point markers represent results of single takes.

proven to be suitable in this experiments, in which all the information related to the performance can be encoded in a data stream. Results show different influence of acoustics depending on individual players and musical context. In some cases, there is no noticeable influence, and when a given musical and acoustic circumstances are met, increased reverberation time results in lower tempo and longer rests.

8.1. Further work

Further experiments are planned with a larger number of participants and musical pieces in order to create a representative categorization of musicians, classifying them according to the influence of acoustics on their playstyle. In addition, it is necessary to perform an extended study on the musical features that make a piece susceptible to performance adjustments.

The inclusion of a delay between pressing a key and sound generation is a variable that can be taken into account in order to increase the effect of the acoustics and approximate them to performance spaces such as churches or cathedrals. The delay can be implemented by using a digital organ synthesizer and playing back the synthesized sound through an electroacoustic system placed in a remote position, thus using the organ merely as a console. First experiments using this approach have been already implemented and the results are under analysis.

9. ACKNOWLEDGEMENTS

The authors wish to thank all the participants in the experiments for their collaboration. The research work presented in this article has been funded by the European Commission within the ITN Marie Curie Action project BATWOMAN under the 7th Framework Programme (EC grant agreement no. 605867).

10. REFERENCES

[1] S. Bolzinger and J. C. Risset, “A preliminar study on the influence of room acoustics on piano performance,” *Journal de physique III*, vol. 2, no. C1, pp. 93–96, 1992.

[2] S. Bolzinger, O. Warusfel, and E. Kahle, “A study of the influence of room acoustics on piano performance,” *Journal de physique IV*, vol. 4, no. C5, pp. 617–620, 1994.

[3] K. Kawai, K. Kato, K. Ueno, and Sakuma T., “Experiment on adjustment of piano performance to room acoustics: Analysis of performance coded into MIDI data.,” in *Proceedings of the International Symposium on Room Acoustics, ISRA 2013*, Toronto, Canada, 2013, Canadian Acoustical Association.

[4] Z. Schärer and S. Weinzerl, “Room acoustics viewed from the stage: Solo performers’ adjustments to the acoustican environment,” in *Proceedings of the International Symposium on Room Acoustics, ISRA 2013*, Toronto, Canada, 2011, Canadian Acoustical Association.

[5] Z. Schärer and S. Weinzerl, “The influence of room acoustics on solo music performance: An empirical case study,” *Acta Acustica united with Acustica*, vol. 99, pp. 433–441, 2013.

[6] T. Eerola and P. Toiviainen, *MIDI Toolbox: MATLAB Tools for Music Research*, University of Jyväskylä, Jyväskylä, Finland, 2004.

11. APPENDIX: MUSICIANS INTERVIEWS

Table 4: Musicians interview for *Mendelssohn A*

Player	Experience Level	Articulation	Rests/Tempo	Preference	Other
Blue	Completed so called concert exam studies in organ playing (additional 2-year degree after Master), therefore quite advanced.	The same phrases are played stronger or softer depending on the acoustics. The key releases are shorter with much reverb.	Hears when ”the room comes” and it of course affects the playing, e. g. if there is more reverb, one waits longer in breaks. When much reverb is there, the player waits longer after the break(s).	With the given registration, ”soft increase” was preferred over the other two. The setting ”strong increase” would require another registration (e. g. more 8-feet pipes to make it less transparent and give it a more romantic sound).	Sometimes the registration sounds better and fuller with more reverb, otherwise the mixture is too ”squeeky”. The player would put in more ground voice registers to create a fuller sound.
Orange	Last semesters of Bachelor studies.	With more reverb, there is no legato but instead more staccato articulation in the lower voice.	In the frame of the possibilities of the piece, the playing is changed to longer breaks and slower tempos when there is more reverb.	The ”soft increase” setting fits the best, with longer reverb (”strong increase”), it is too much and gets muddled up. Also, an acoustic feedback tone was heard.	Changes between acoustics are not confusing, one hears well in the breaks what is happening. After the first two chords, the player listens for what happens acoustically and reacts spontaneously and to musical taste.
Yellow	Half way through Bachelor studies, initial participant with lower experience level than the other players.	The reverb makes the ”impact” so the player lets the reverb do the impact – if present, otherwise one has to do it by playing.	If extra reverb is not present, the note before the break is played longer than one would usually – to make up for the missing reverb and to get overall the same desired expression.	Clearly better with extra reverb than without for this romantic (period) piece.	/

Table 5: Musicians interview for *Mendelssohn B*

Player	Experience Level	Articulation	Rests/Tempo	Preference	Other
Blue	Completed so called concert exam studies in organ playing (additional 2-year degree after Master), therefore quite advanced.	Left hand sounds stronger when there is more reverb. Regarding the registration the player would change the swell	In the right hand no big changes are noticable.	Overall it sounds nicer and more ”airy” with the setting ”strong increase”, so this was the preferred configuration	With the ”big acoustics” it sounds like a ”sound carpet / wash”.
Orange	Last semesters of Bachelor studies.	Player notices a difference when there is lots of reverb (”strong increase”). Then, the left hand gets ”mixed up” and one must play more transparent, e. g. smaller phrasing.	/	”Soft increase” sounds a bit more organic, but overall no big sonic difference.	The difference is suspected to be smaller because there are less breaks.
Yellow	Half way through Bachelor studies, initial participant with lower experience level than the other players.	Not much difference was noticed while playing due to nature and little dynamic of piece, maybe a small effect in the melody voice.	/	With artificial reverb is preferred ”a little better” when listening back to the own MIDI recording played back with and without extra reverb.	/

COUPLED ORGAN PIPES AND SYNCHRONIZATION – NUMERICAL INVESTIGATIONS AND METHODS

Jost Fischer, Rolf Bader
Institute of Systematic Musicology, University of Hamburg, Germany
jost.leonhardt.fischer@uni-hamburg.de
r_bader@t-online.de

ABSTRACT

We present a new approach to investigate the interaction of two organ pipes numerically. By solving the compressible Navier-Stokes equations under suitable boundary and initial conditions we can completely retrace the way of mutual interplay of the nonlinear coupled system of two organ pipes, which leads to synchronization. We give detailed insights into the concept of implementation and run such complex CFD/CAA simulations using parts of the open source C++ toolbox OpenFOAM. Our robust numerical results are in excellent accordance to data of real synchronization experiments with organ pipes. This opens a new window to analyze the nonlinear fluidmechanical and aeroacoustical mechanisms of sound generation, sound propagation and acoustical interaction of organ pipes. Especially the properties and functions of coherent turbulent fluidmechanical objects inside organ pipes, like the oscillating air sheet, the jet, and the primary vortex in the lower resonator region, as well as the influence of the upper labium are of our augmented interest. The shown techniques define a new step beyond the present research of interactions of wind driven musical instruments.

INTON – A SYSTEM FOR IN-SITU MEASUREMENT OF THE PIPE ORGAN

Milan Guštar, Zdeněk Otčenášek

Musical Acoustics Research Center
Academy of Performing Arts in Prague, Czech Republic
milan.gustar@hamu.cz

ABSTRACT

The article presents the design and capabilities of the *Inton* measurement system. The system is developed in MARC Prague for an in-situ repeatable unbiased acoustical documentation of sound condition of pipe organs and for the analysis of the organ pipe sounds in the process of organ building and voicing. The organ sound documentation is independent on the precise actual placing of the microphones in the space. In addition to the usual review of spectra of the individual pipes the system allows to evaluate balance of the tone sound quality within registers of an organ, to discover out-of-tendency tones and to asses the room acoustic parameters from the point of view of an organ position in the space without any other equipment. The system consists of a microphone set, microphone pre-amplifiers, A/D converters and two laptop computers with special software.
The system was already used for the subsequent objective and/or subjective evaluations and comparisons of documented sounds after a long time pause. Some organ builders in CZ employ Inton as a tool in various stages of the organ building or restoration techniques. The Inton measurement of room acoustics using the pipe organ as a sound source is used at present in a research project to extend the Inton utilities.

1. INTRODUCTION

Sounds of pipe organ are each time joined with properties of the space where the instrument is placed. That is why the organ sounds can not be measured in an anechoic room. The repeated in-situ recordings of pipe organ tones with one microphone in a fixed place in a room and the following signal analysis show changes of obtained results with barometric pressure, temperature and humidity. The sound spectra are changed due to the changes of sound radiation conditions in the room which also changes the standing wave trajectories and the sound pressure distribution (sound field) in the room [1]. Furthermore, it is not possible to place the microphone in an exactly equal position upon repetition. Then the comparisons of repeated measurement made with one microphone are not accurate enough. Therefore, „The method of the acoustical documentation of pipe organs“ was developed (first presented in [1], later extended [2] only in Czech). Both the operating procedures based on this method and the necessary hardware were joined in one measurement system presented in this article. The system design was realized in MARC Prague and the abilities were proven in cooperation with organ builder specialists. The system is frequently used in voicing process (voicing = intonace in Czech language), after that the name *Inton* was established.

Pipe organs are very complex musical instrument. In an organ assembly, the pipe voicing must keep both the suitable sound quality and loudness relationships of separate pipes of a tone between different registers and also the suitable harmony of the pipe soundings within the tones of a single register (balance of tones [7]). The suitable balance of tones is connected with room acoustics. The historical evolution of pipe organs brought a common convention in preferred organ sound, and the listeners of organ music expect some suitable fluent changes in tone sound according to the pitch changes. But a quantification of this expectation is difficult because the balance is based on intuitive subjective feelings only. Experienced organ voicers hold a concept about such fluent changes within tone sounds in their mind to realize it accordingly. The appraisal of actual tone balance by a voicer only in in-situ listening is exhausting. The correct balance evaluation is practically impossible after one hour listening without a pause. Therefore the Inton software was extended with a graphical balance screening utility based on spectral analysis of signals of individual pipe in registers. The utility also enables a detection of the tones which are out-of-tendency from the fluent changes of tone spectra needed for the loudness and sound quality balance of organ registers. If the sound of an organ is listened to, and subjectively judged after a time (e.g. by members of a committee after an organ repair or restore) the listeners usually do not agree with each other (a person memorizes only an individually stylized reflection of listened sounds). The Inton system allows tone comparisons in both in subjective listening tests and in objective spectral characteristic matching.

2. HARDWARE

The Inton hardware is a modular system built from standard components (see Fig. 1) allowing easy system configuration according to the specific measurement needs and the utilization and the re-use of the equipment which is readily available to the user. The Inton hardware consists of a microphone set, microphone pre-amplifiers, a multi-channel A/D converter, a server computer for audio data digitization and a client computer for system control, data processing, visualizations and archiving. Both computers are interconnected via wired or wireless ethernet network. All components are ordinarily market available without a special claim.

2.1 Microphones

The basic microphone set consists of three omni-directional microphones. The set acceptable minimises negative effects of standing waves. This basic microphone set is suitable for the objective acoustical documentation and analysis.
Recordings for the subjective listening tests require binaural microphones (dummy heads). As an alternative, standard microphone pairs in AB configuration with narrow base can also be used.

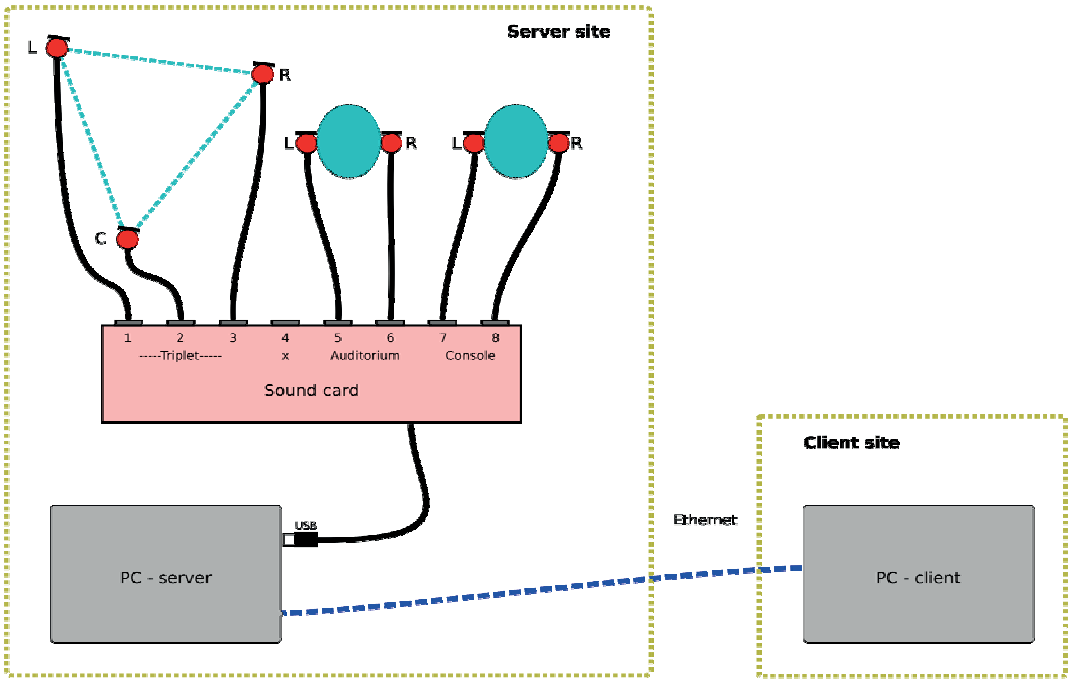

Figure 1: Inton hardware schematics

2.2 Pre-amplifiers & A/D converters

Microphone pre-amplifiers, phantom power supplies and A/D converters can be integrated in an external sound card with USB interface. Sound cards with 24 bits quantisation, sample frequency 96 kHz and flat frequency response 20 Hz – 20 kHz ± 0.5 dB fulfil requirements for the measurement dynamic and frequency range.

2.3 Computers

Digitized signals from the sound card are fed to a laptop computer with the software for data acqusition, transfer and storage (IntonASIOserver program). This *Server* computer with the sound card can be placed in the space with respect to optimal microphones wiring (usually placed on a typical listening place in a nave).

Data from the server are transmitted to the remote computer (client) via wired or wireless ethernet network. The *Client* computer with the special software (Intonclient program) serves for the data processing, analysis, visualization and archiving as well as for the system control. Separation of the client computer from the rest of the system facilitates physical manipulation with this control computer during the measurement. The client computer can be placed in a suitable position at the organ console to be easily accessible during the playing the keyboards or stop tabs manipulations. Wireless connection allows free manipulation with the client computer during measurement, e.g. the organ builder can control the process during the voicing the pipes inside of organ.

3. SOFTWARE

Software for the pipe organ sound recording and analysis is divided into two separate programs, each running on the dedicated computer.

3.1 Server

IntonASIOserver program is used for the acoustical signals digitization and transmission. Program runs autonomously on the server computer and is controlled using commands being sent form the client computer via UDP protocol. Audio data are transferred to the client computer via TCP channel.

3.2 Client

Intonclient program serves for the user interface, received data storage, immediate processing, automatic analysis, visualization and archiving. Inton graphical output allows fast visual evaluation of the tones spectral characteristics and registers evenness and balance (for more see [7]). Spectral analysis results can be stored in the numerical and the graphical form.

Recorded sound samples and analysed data are stored in the format suitable for the acoustical documentation results export into the central database of historical organs in the Czech Republic.

The client program can be run in two operational modes. In the *on-line* mode is the client computer connected via the ethernet network with the server which upon request sends digitalised audio signals for the processing, visualization and storage. In the *off-line* mode the client computer runs independently and allows the access to the stored data, the visualisation, post-processing and storage. In the *off-line* mode e.g. new analyses can be performed and added.

It is possible to customize the measurement parameters as well as the program user interface and the graphical output look.

Main program window contains graphical output of the spectral analysis results. Spectra of all tones from selected register can be displayed in various forms (Figs. 2 and 3). Each sound sample spectrum is displayed as a coloured bar placed above the corresponding key. The colours represent the frequency components amplitude; vertical positions correspond with the frequencies. The position of the bar bottom edge indicates the fundamental frequency of the tone.

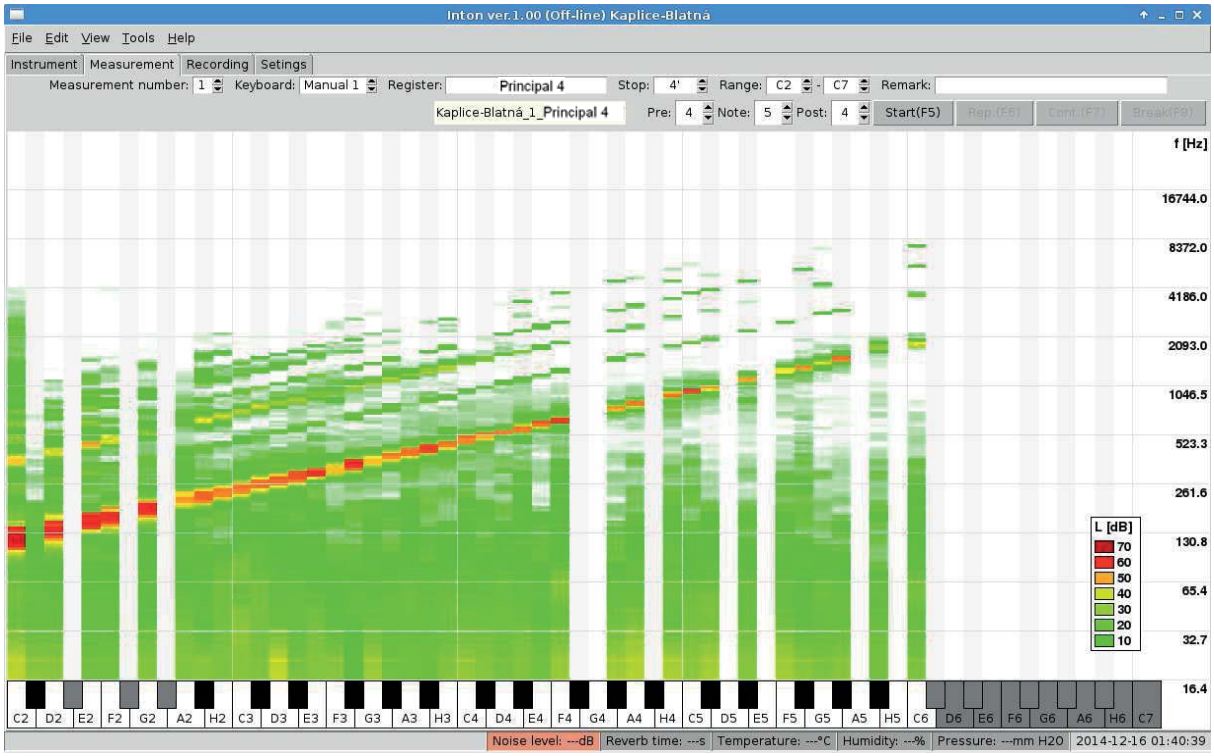

Figure 3: An example of FFT spectra of the Principal 4' register (grayed keyboard keys were assigned "not to play"; white columns above non gray keys show not played tones up to now; 2th left column presents a non sounding pipe; the tones A2, F3, G3, C5, A#5 are examples of out-of-tendency tones)

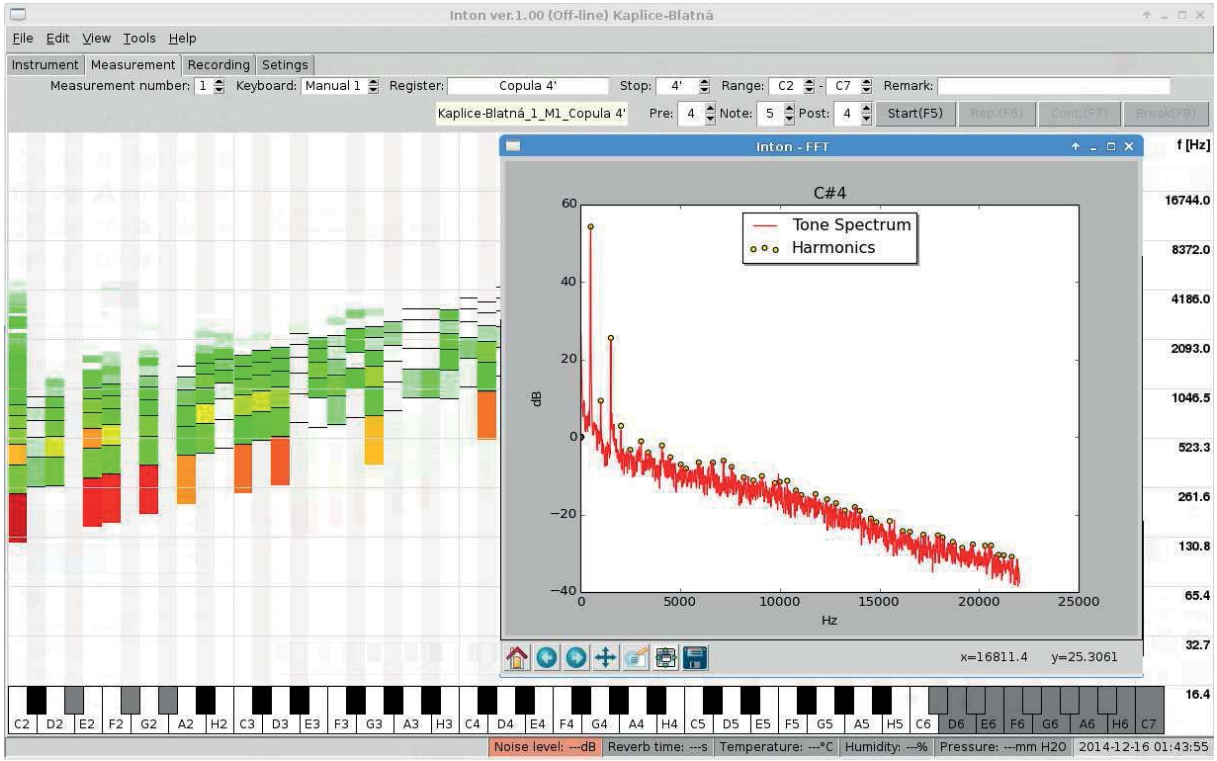

Figure 2: Harmonic spectra of the register and FFT spectrum with harmonics for selected tone C#4

The graph in Fig. 3 displays an example of different view on spectra for a selected tone (in this way an additional information can be displayed including time courses of separate microphone signals, fundamental frequency, harmonics spectra, etc.).

Program contains a simple audio recorder allowing the recording of sound examples or other samples without sound analysis.

Recorded sound samples and analysed data are stored in the format suitable for the acoustical documentation result exports into a central database.

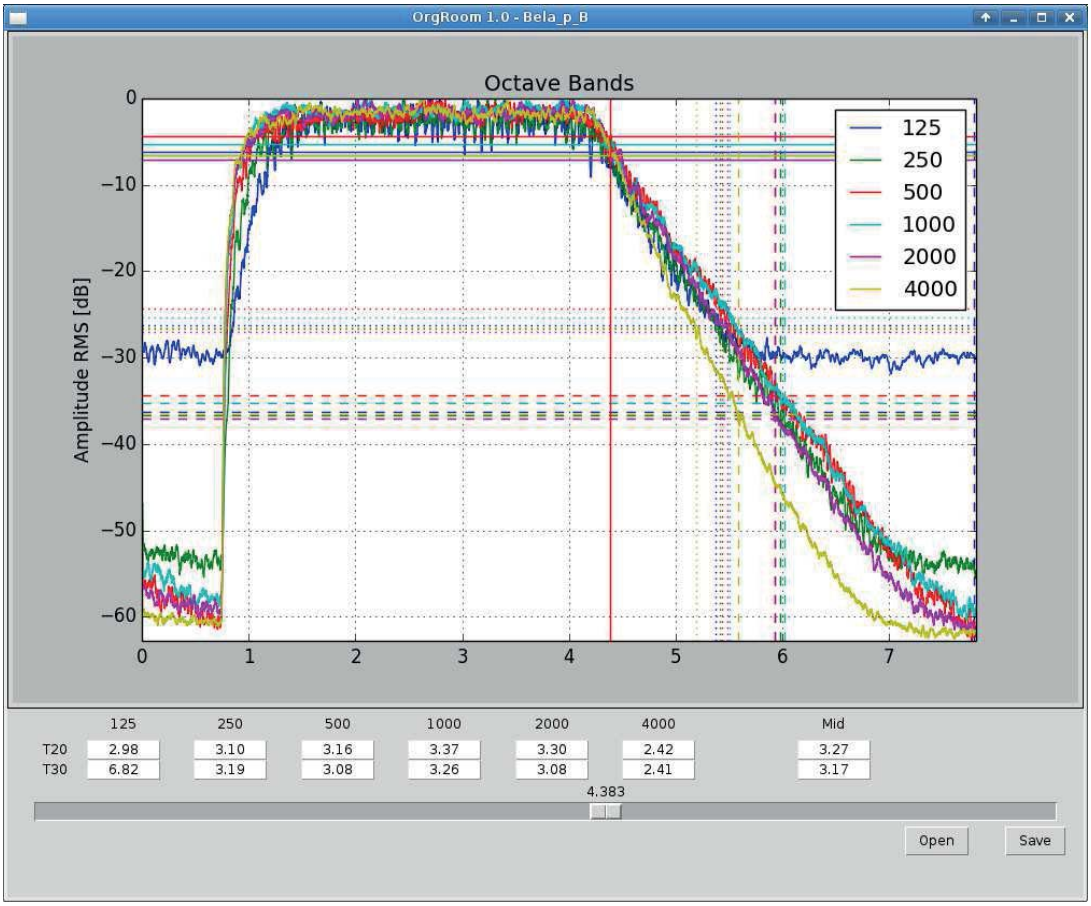

Figure 4: Time course of sound pressure decays (sound signals filtered in octave bands, middle frequencies see legend)

4. THE SYSTEM USE

The tones of individual registers are played by a Inton operator on a real organ keyboard and produced sounds are recorded by the Inton system. The user interface of the Inton software instructs the operator about the selected register and tone height to be played (as a single note or as a sequence of pre-selected tones assigned by operator on a keyboard of the user interface; an example of pre-selected tones see in Figs. 2, 3 bottom, the non played tone keys are on the keyboard in gray). The instant automatic signal analysis and the graphical presentation of the results in various forms are done automatically. The operator can select from different types of results visualization (an example of a spectral view see in separate frame in Fig. 3) during the organ building, restoration or documentation according to a process in progress (voicing, pipes adjustment, tuning, interventions effects assessment, etc.). One of these visualizations is a special 3D spectral graph of the register tones where an operator is able to evaluate visually the spectral characteristics, the tone evenness, a tendency of tone balance in a register and the out-of-tendency tones (an example see in Fig. 2). The recorded samples as well as the analysis results can be saved (automatically or manually) in the format suitable for the archiving and subsequent use.

The operator can export the aggregate acoustical organ documentation into the complex data repository which serves for storing various organ data and the recordings of individual pipe sound. Collected data taken at different times can be used off-line to identify the organ sound changes due to instrument wear, the quality or restoration work, etc.

5. ROOM ACOUSTICS MEASUREMENT

The process applied for the objective acoustic documentation of pipe organ also allows the measurement of room reverberation time based on the analysis of recorded organ tones decay (the organ tone room acoustics method). This procedure does not require any other expensive electronic equipment for the room acoustics measurement. The room acoustic properties with the pipe organ as a sound source are assessed with regard to the organ position in the space and thus can give more credible results than traditional methods with the artificial sound sources, which usually have a position outside of an organ pipe placing.

Fig. 4 shows graphs of the recorded sound pressure time course in octave bands 125 – 4 000 Hz with calculated reverberation times T20 and T30 for respective octave bands and total reverberation times T20Mid a T30Mid.

The comparison of room reverberation times T20Mid and T30Mid obtained using a loudspeaker (ISO 3382-1 method) and using the organ pipes (organ tone method) at selected locations shows differences of a few percent. From practice, the comparisons of the octave band reverberation times T20 and T30 also show differences of a few percent, except the band 4 000 Hz where the values are usually lower by 20 – 30 % for organ tone method (the ISO 3382-1 method with a loudspeaker outside of pipe locations poorly express the sound absorption and diffraction caused by the pipe bodies surrounding a sounding pipe).

6. CONCLUSION

The *Inton* system was developed and tested at Musical Acoustics Research Centre (MARC) of Academy of Performing

Arts in Prague and it is currently used by the cooperating institutions for the pipe organ acoustical documentation and for the creation of the database of historical organs in the Czech Republic.

The Inton system available in various configurations gives the advanced methods of pipe organ acoustical analysis not only to highly qualified researchers in acoustics but also to conservationists and organ builders in the organ restoration or building processes, or to musicologists and other users requiring a tool for the objective analysis or comparison of pipe organ sound.

ACKNOWLEDGMENTS

Supported by the Ministry of Culture of the Czech Republic in the DF12P01OVV012 project

7. REFERENCES

[1] Štěpánek, J., Otčenášek, Z. and Syrový, V., Acoustic documentation of church organs. In proceedings of SMAC 93, 516-519, 1993
http://zvuk.hamu.cz/vyzkum/dokumenty/SMAC93.pdf

[2] Otčenášek, Z., Syrový, V. and Urban, O., Technologický list čís. 15: Akustická dokumentace píšťalových varhan, verze 8&1, MARC HAMU v Praze, 2008

[3] Guštar, M. and Otčenášek, Z., Funkční vzorek zařízení pro analýzu zvuku varhan, Technologický list 49, MARC HAMU v Praze, 2013

[4] Guštar, M., Software pro analýzu zvuku varhan, Technologický list 60, MARC HAMU v Praze, 2014

[5] Otčenášek, Z., Moravec, O. and Guštar, M., Metodika akustické dokumentace s analyzačním zařízením a softwarem, Technologický list 58, MARC HAMU v Praze, 2014

[6] ČSN EN ISO 3382-1, 2009

[7] Otčenášek, Z., The balance of the spectra of the tones of one organ stop. In Proceedings 34. Deutsche Jahrestagung für Akustik DAGA 2008, Dresden, s. 423-425, 2008
http://zvuk.hamu.cz/vyzkum/dokumenty/Lit169.pdf

THE INFLUENCE OF NICKS ON THE SOUND PROPERTIES AND THE AIRFLOW IN FRONT OF FLUE ORGAN PIPE

Zdeněk Otčenášek, Viktor Hruška, Ondřej Moravec, Martin Švejda

Musical Acoustics Research Centre
Academy of Performing Arts in Prague, Czech Republic
zdenek.otcenasek@hamu.cz

ABSTRACT

Nicking is a well-known voicing technique of metal flue organ pipes widely used by Czech organ builders in history. Its effect is investigated in this paper. The sound analysis results and the PIV images of the airflow in front of the mouth were studied to achieve more advanced state of the art in organ pipe diagnostics. Both measurements were performed in steady state part of pipe sound. The results of the sound analyses are in accordance with organ builders experience – the depression of higher harmonics was observed in the frequency spectrum after pipe nicking. Airflow analysis shows significant differences in vector velocity maps – decrease of vector lengths near the flue.

1. INTRODUCTION

The sound of organ in baroque era has represented certain sound quality ideal of the period. Later, the sound of organ varies through the history. In the baroque era the clear and resolute sound timbre was required, in the romantic era more delicate sound was preffered. Hence the need of existing instruments modification (wind pressure elevation, pipes re-voicing). One of the commonly used methods of metal flue organ pipes voicing was creating (or enlarging) nicks on the languid (see Figure 1). The organ builders say the nicks makes pipe sound "more cultivated" or "less aggressive" which is equivalent to depression of higher harmonics in technical language. Also it is known, that the nicks should make flow more uniform and ordered. The aim of this paper is to document the differences in the sound quality and in the airflow in front of the pipe mouth before and after nicking.

Figure 1: detailed view of pipe mouth; languid with small baroque nicks (left), and with large romantic nicks (right)

2. METHOD

2.1 Measurement setup

The Principal 8' pipe B3 was documented. Measurements were taken in an anechoic room. The pipe was installed on an experimental windchest with electro-magnetic valves and small bellows supplied by electric ventilator. The wind pressure was 83 mm water gauge (≈ 814 Pa). Sound recordings (and subsequent airflow measurements) of the pipe in the original baroque state was taken. Then the large romantic nicks were made on the languid and all measurements were repeated. Acoustical and airflow measurements were done separately because of noisy optical measurement devices.

2.2 Acoustical measurement

Sound of the pipe was digitally recorded using 4 microphones. Two microphones were placed far from the pipe and two microphones near the pipe, one of them in the vicinity of mouth and the second one in the half length of pipe body. A schematic diagram of the microphone arrangement is shown in Figure 2.

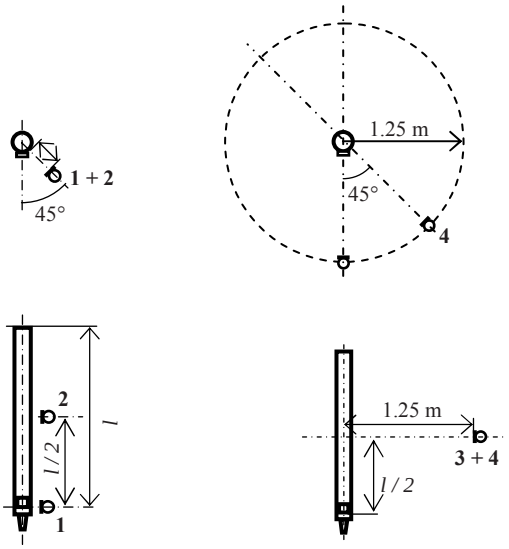

Figure 2: microphone arrangement during pipe sound recording

The recorded sound signals were analyzed. For each signal the standardised sound pressure level (SPL) and the frequency spectrum was computed, the fundamental frequency was identified and then the harmonic spectrum was computed. For each computed spectrum the frequency center of gravity (FCG) and frequency center of gravity of harmonic spectrum (FCGh) was computed.

Frequency center of gravity of harmonic spectrum (FCGh) is defined as

$$f_{cg} = f_1 \left(\sum_{k=1}^{N} kA_k \Big/ \sum_{k=1}^{N} A_k \right) \qquad (1)$$

where
N … total number of harmonic partials in spectrum
f_1 … fundamental frequency
A_k … amplitude of k^{-th} partial

FCG of FFT spectrum is defined similarly using FFT bins instead of harmonics.

2.3 Airflow measurement

2.3.1 Particle image velocimetry (PIV)

The airflow in front of the organ pipe mouth is closely tied with generated sound and physical characteristics of pipe [1, 3], which can be very helpful while diagnosing pipes. Airflow was investigated using phase-locked Particle Image Velocimetry (PIV) – a non-intrusive optical measuring technique. PIV experiments on flutes were earlier conducted e.g. by Bamberger [3] and Yoshikawa [1]. Principle of this technique is illustrated in Figure 3 [2]. The method obtains instantaneous velocity vector maps in a cross-section of a flow. The particle seeded flow is illuminated by a thin light sheet which is formed by laser beam passed through cylindrical lens. Double-pulsed laser flashes twice in an arbitrarily short time interval, which freezes particles in the flow. Snapshot pair is captured for each flash by a high-speed camera. The obtained image pair is then divided into sub-sections (interrogation area) and particles movement $\vec{v}$ is computed

$$\vec{v} = \frac{\Delta \vec{X}}{\Delta t} \qquad (2)$$

where $\Delta \vec{X}$ is the movement of particles in the specific interrogation area and Δt is the time delay between the flashes in the pair.

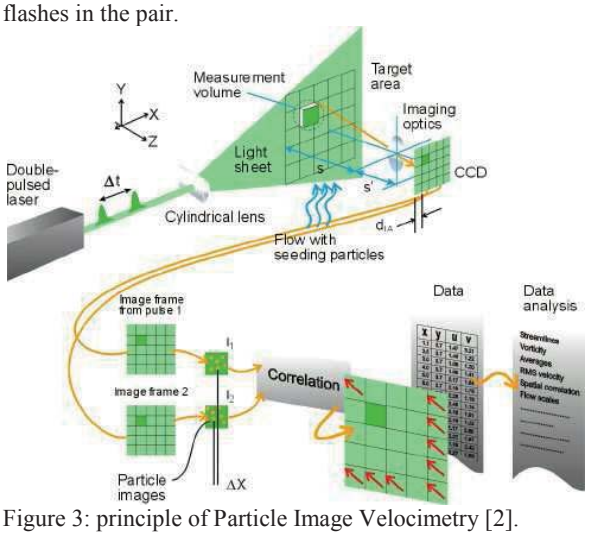

Figure 3: principle of Particle Image Velocimetry [2].

2.3.2 Planes of interest

Airflow was investigated in front of the pipe mouth. Measurements were conducted in two perpendicular planes: parallel to mouth (front view - 8 mm in front of the front labial edge) and perpendicular to the mouth center – side view. Graphical representation of investigated planes is shown in Figure 4.

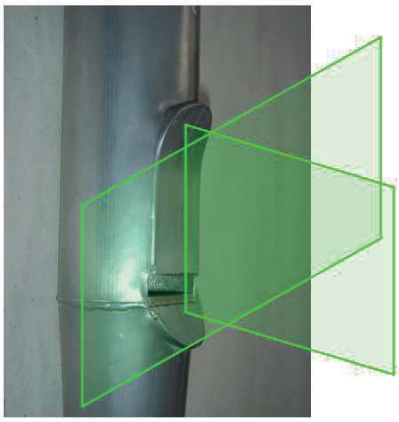

Figure 4: the planes of interest of the airflow measurement

2.3.3 Phase-locked PIV

Maximum repetition rate of used double-pulsed laser (Litron Nano-L 200-15) was 15 Hz. Since the measured pipe was tuned on 248 Hz it was not possible to directly acquire time-resolved data using this equipment. Phase-locked technique was used instead. Velocity maps were obtained repeatedly at the same phase of generated sound and resulting vector maps derived from image-pairs taken at this specific phase were then averaged. This method allows only investigation of steady state airflow.

2.3.4 Optical measurement setup

Optical measurement setup is shown in Figure 6. Sound of the pipe is captured using condenser microphone (SENNHEISER KM-6P) located at the specific position. The signal is pre-amplified and then filtered by the narrow band-pass filter (Brüel & Kjaer Spectrum shaper 5612) which passes only a signal of the fundamental harmonic. This signal is then processed by a shaper (Lindos L102) which produces a square-wave-like signal. The negative to positive zero crossings of this signal are used as the trigger events for camera (Phantom SpeedSense v611) and the laser. In order to obtain image pair in the desired phase of the generated sound delay is set via controlling PC. The PIV system (manufactured by Dantec Dynamics A/S) is synchronized via 80N77 Synchronizing box. The PIV system is controlled using Dynamic Studio software by Dantec Dynamics.

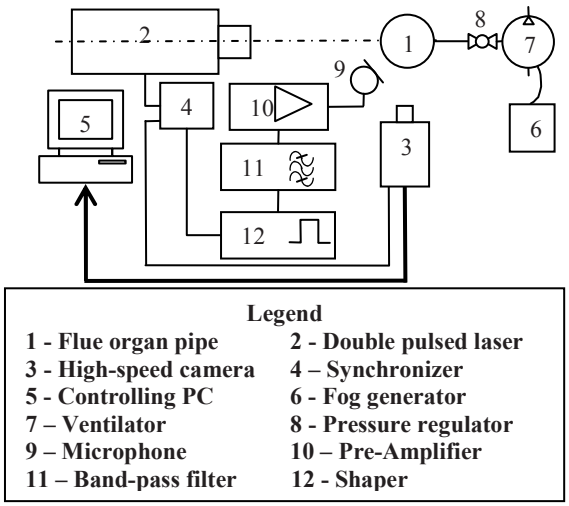

Figure 5: optical measurement setup

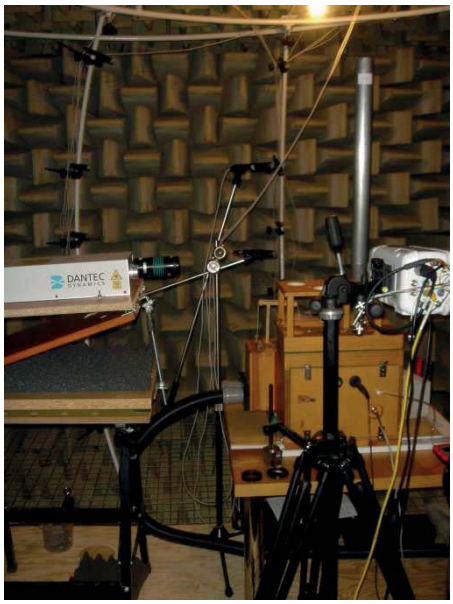

Figure 6: experimental setup of airflow measurement

2.3.5 Results computation

Velocity vector maps were obtained using Adaptive correlation analysis implemented in the software Dynamic Studio 3.41 [5]. Vorticity maps (Figure 12) in *z*-plane were also computed using Dynamic Studio according to the formula:

$$\omega_z = \frac{\partial V}{\partial x} - \frac{\partial U}{\partial y} \qquad (3)$$

where **V** is the scalar map with vertical values of vectors, **U** is the scalar map with horizontal vector values and *x*, resp. *y* is horizontal, resp. vertical coordinate.

3. RESULTS

3.1 Acoustical measurement

The fundamental frequency of the tone was 248.7 Hz. The fundamental frequency shift after nicking remains in the range of measurement uncertainty. The SPL of the sound recorded by individual microphones is summarized in Table 1. Changes of SPL values are very subtle, only the signal captured at the mouth showed slightly larger decrease of ca. 1.3 dB. The results of frequency analysis shows that languid nicking decreases amplitudes of higher partials (see Figure 7). This phenomenon is also documented by noticeable decrease of harmonic spectrum centre of gravity values (FCGh, see table 2). The decrease of corresponding value (FCG) is more than three times smaller. This implies that the noise part of the sound remains unchanged.

Table 1: standard sound pressure levels of the pipe with baroque and romantic nicks

	SPL [dB]	
mic No.	baroque	romantic
1	84.8	83.5
2	84.0	84.2
3	75.7	75.3
4	76.8	76.4

Table 2: frequency spectrum centre of gravity (FCG) of the pipe with baroque and romantic nicks and change ratio of its value (upper part); harmonic spectrum centre of gravity (FCGh) of the pipe with baroque and romantic nicks and change ratio of its value (lower part);

Frequency centre of gravity (FCG) [Hz]			
mic No.	baroque	romantic	rel. change
1	1602	1584	0.99
2	1587	1463	0.93
3	1554	1513	0.97
4	1394	1353	0.97
Centre of gravity of harmonic spectrum (FCGh) [Hz]			
mic No.	baroque	romantic	rel. change
1	568	506	0.89
2	483	412	0.85
3	512	457	0.89
4	482	434	0.90

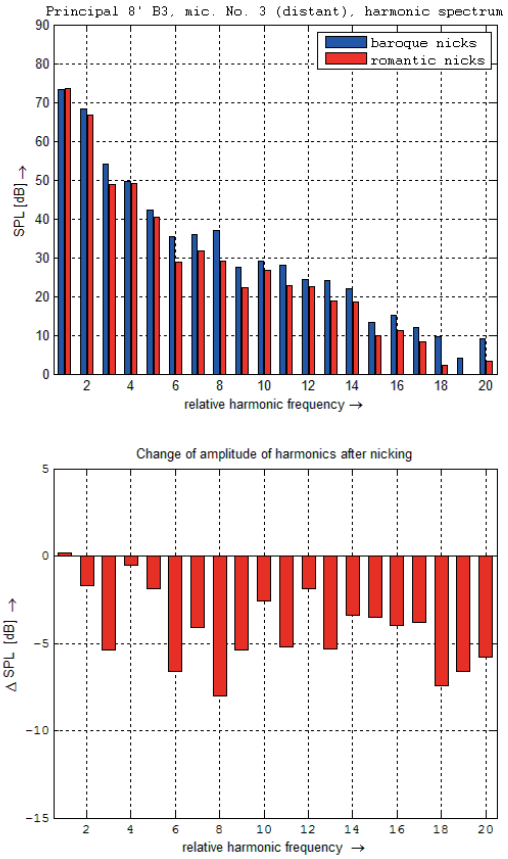

Figure 7: harmonic spectrum of sound of the flue pipe with baroque nicks and with romantic nicks (up), change of the amplitude of harmonics after nicking (down).

3.2 Airflow measurement

Images obtained while investigating airflow from side and front view are shown on Figure 8 and 9 respectively. Red rectangles mark areas for which resulting velocity maps are shown in the following images.

Vector maps were created by averaging of 250 maps for each of 12 phases. Only the maps in several crucial phases are shown to achieve better readability of results.

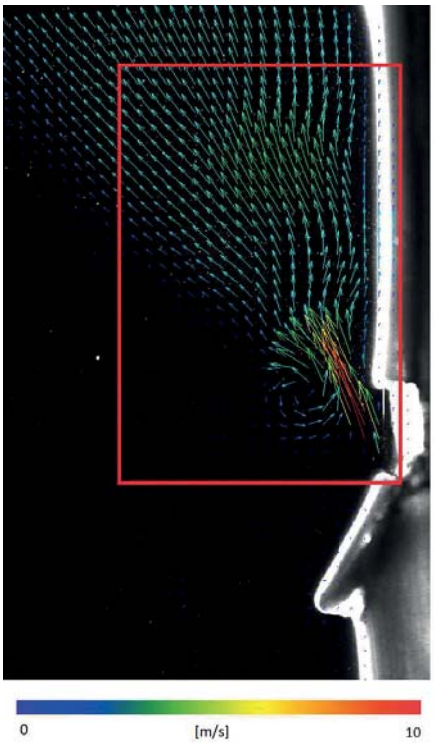

Figure 8: The area of interest in front of the mouth from the side view with averaged velocity vector map in 0°.

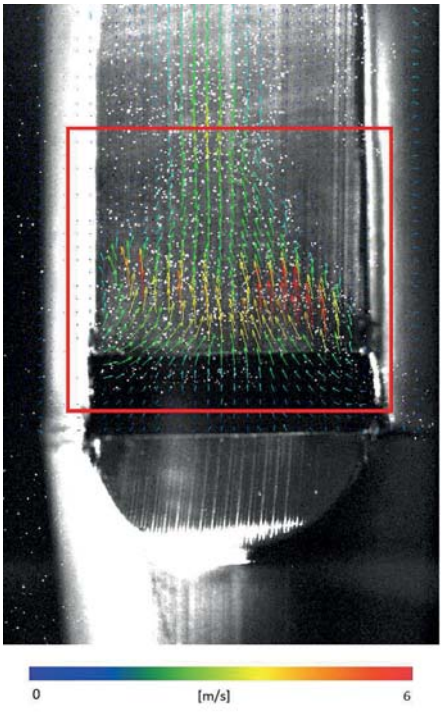

Figure 9: The area of interest in front of the mouth from the front view with averaged velocity vector map in 0°.

On Figure 10, resp. Figure 11 are shown velocity maps obtained from side, resp. front view. Blue velocity vectors correspond to baroque nicks, red vectors to romantic nicks. Color scale represents the relative difference of vectors lengths in the pair in the specific position (the greener area, the greater difference between vectors). It is evident that the velocity near the languid was decreased after creating romantic nicks.

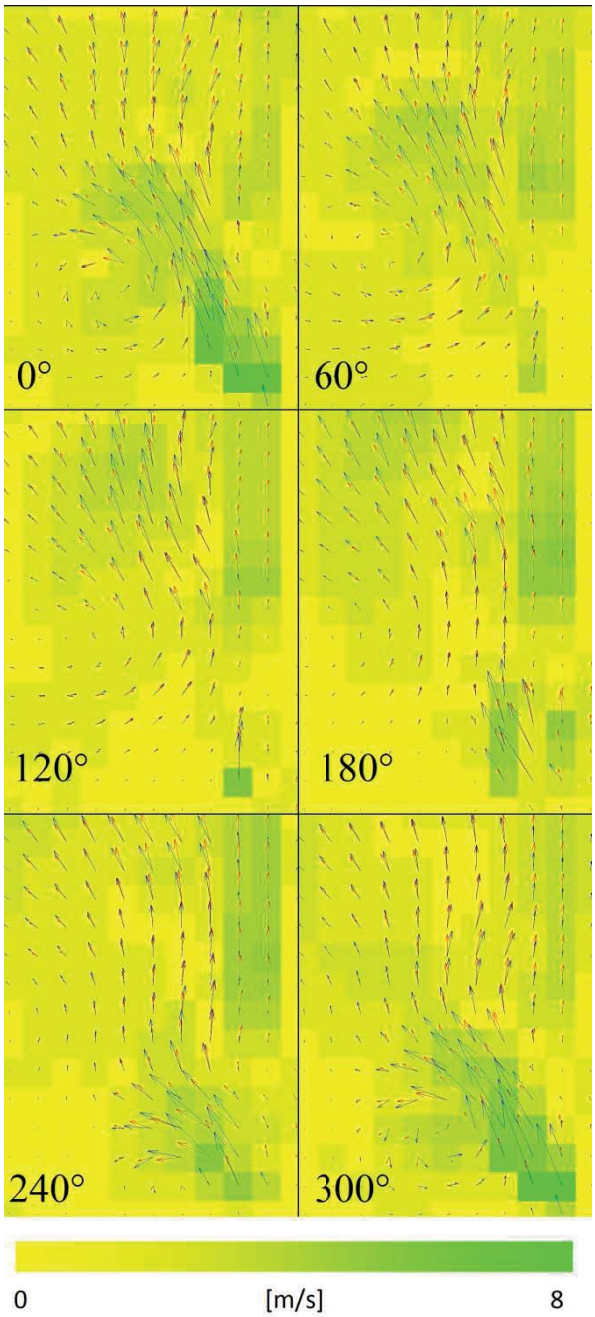

Figure 10: velocity maps in front of the mouth observed from side view in specific phases of generated sound, underlying color corresponds to the local velocity difference between baroque and romantic nicks

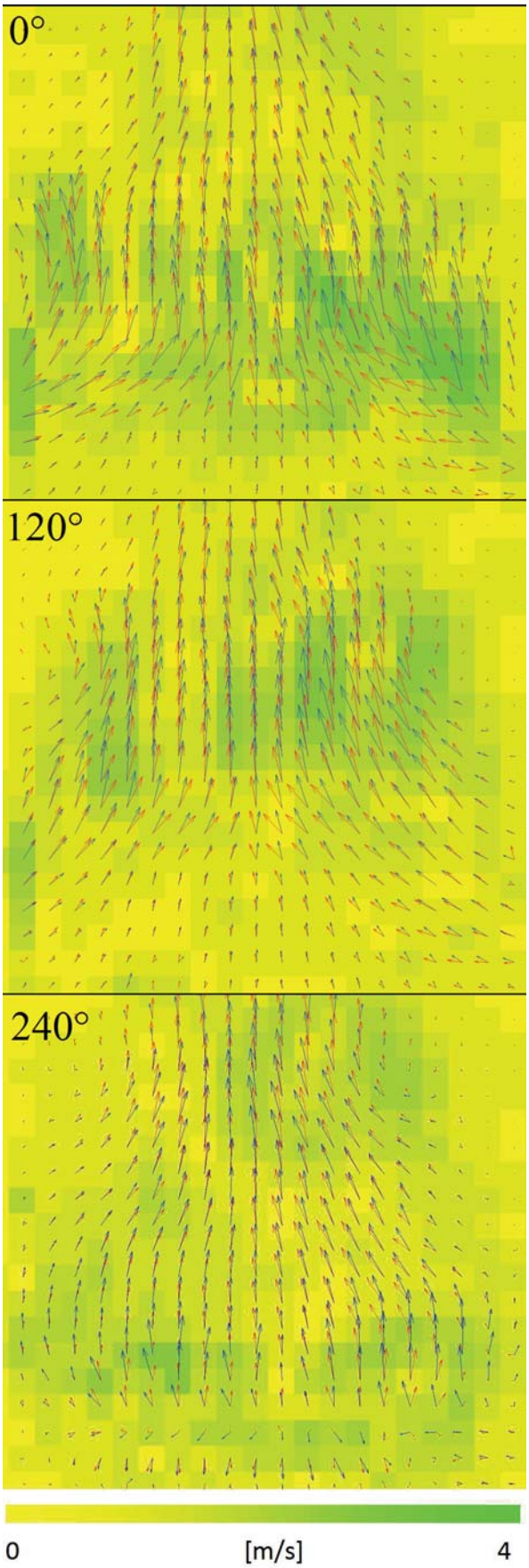

Figure 11: Velocity maps in front of the mouth observed from front view in specific phase states of generated sound.

3.2.1 Vorticity

Vorticity maps were computed by Dynamic Studio according to equation 3. On Figure 12 there are shown vorticity maps derived from averaged velocity maps at 0° (which corresponds to the most outward striking jet state) of generated sound for baroque nicks (left) and romantic nicks (right). Original velocity maps are also shown for better clarity.

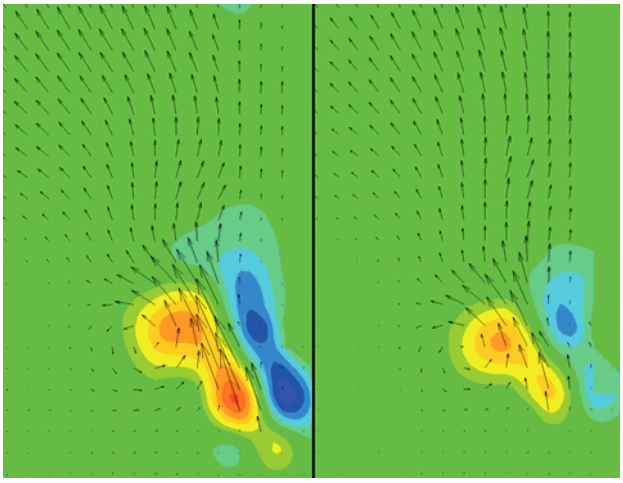

Figure 12: vorticity maps in front of the mouth observed from side view. Baroque mouth (left), romantic mouth (right). Blue, resp. red colors represent negative, resp. positive values.

4. DISCUSSION AND CONCLUSION

Changes in the sound frequency spectrum as a consequence of metal flue pipe languid nicking were documented. Also the changes in the airflow in front of the pipe mouth and the vortex layer creation were shown.

Given the usual values of the flow speeds in wooden and metal organ pipes, the air could still be considered incompressible. Therefore a good approximation from simple continuity equation U_0A = const., where U_0 is the mean flow velocity and A the area of the slit, is obtained. Nicks slightly extend the flue cross-section without removing the flue edge completely so the tone production at the languid remains unchanged. Then from the continuity equation results the decrease of U_0 without destroying any of sound producing mechanisms (see Figure 10 and 11).

The fundamental frequency shouldn't be affected by nicking, because the pipe and its eigenfrequencies are still the same. On the other hand audible and measurable differences in the acoustic spectra were expected. Excitation of higher harmonics is associated with nonlinear behavior of the jet (vortex-layer formation among others - for further discussion see [4]). This is documented in amplitude decrease in obtained vorticity maps after creating nicks (see Figure 12) - jet-vortex layer formation is less significant with nicks, which suppresses the tone production mechanism documented by Yoshikawa et al. [1].
On top of that it is considered a stronger attenuation of higher frequencies as a result of mainly inertive (inductive) pipe impedance, which can affect the signal to noise ratio in the less excited higher harmonics. Acoustic measurements (see Figure 7) confirmed these asssumptions – nicking decreased amplitudes of higher partials of the tone.

5. ACKNOWLEDGMENTS

Research supported by the MKCR project No. DF12P01OVV012 and presentation by the MSMTCR in the Long Term Conceptual Development of Research Institutes grant of the Academy of Performing Arts in Prague: The "Sound quality" project.

6. REFERENCES

[1] Yoshikawa, S., Tashiro H., Sakamoto, Y. "Experimental examination of vortex-sound generation in an organ pipe: A proposal of jet vortex-layer formation model". Journal of Sound and Vibration 331. (2012) 2558–2577.

[2] DANTEC DYNAMICS: Particle Image Velocimetry. (2015). [Online]. Available: http://www.dantecdynamics.com/docs/support-and-download/research-and-education/piv.pdf.

[3] Bamberger A. Vortex sound of flutes observed with Particle Image Velocimetry. In: Proceedings of ICA conference, Kyoto. 2004.

[4] Fabre, B., Hirschberg, A., Wijnands, A. P. J.: "Vortex Shedding in Steady State Oscillation of a Flue Organ Pipe" Acustica, vol. 82 (1996) 863-877.

[5] DANTEC DYNAMICS: Dynamic Studio User´s guide. (2015). [Online]. Available: http://fstroj.uniza.sk/web/ket/subory/DynamicStudio%20Manual.pdf.

DIGITAL GUITAR WORKSHOP – A PHYSICAL MODELING SOFTWARE FOR INSTRUMENT BUILDERS

Rolf Bader, Jan Richter, Malte Münster, Florian Pfeifle
Institute of Systematic Musicology, University of Hamburg, Germany
r_bader@t-online.de
janrichter.office@gmail.com
m.muenster@arcor.de
fkra003@uni-hamburg.de

ABSTRACT

Instrument builders have an ideal of sound in mind. Their experience in craftsmanship guides them through the production process. It is a more or less trial-and-error method. Each part of the instrument considered to be relevant to fit the imagination is going to be modified during the production process. The whole production process starting from a certain imagination of sound to the completed guitar and backwards represents an inverse problem. Still at best the solution would be inverse, where the builders would know how a geometry looks like producing the desired sound. The physical modeling software Digital Guitar Workshop (DGW) is a tool for guitar builders to do both, the trial-and-error as well as the inverse problem solution. Therefore 32 sample guitars were measured in terms of geometries of each part and radiation using microphone array techniques including the Minimum Energy back-propagation method. Selecting a preferred guitar out of the sample, builders can use a Graphical User Interface (GUI) to change properties of the instruments in detail like quantity, size and position of fan bracings, top and back plate thickness distribution, sound hole size and position, bridge size and position and much else. Builders can use the graphical soundboard to pluck a virtual tone which is calculated immediately to surveil the whole design process . The physical model of the guitar sound, simplified with respect to longitudinal waves and ribs, bases on the principles already widely publicized by R. Bader: Computational Mechanics of the Classical Guitar. (Springer 2005). Furthermore the builder can change an existing sound in the software by in- or decreasing sound strength within a chosen band and bandwidth with an equalizer. Subsequently the software proposes a geometry which meets this sound with best approximation. This inverse problem solution in the existing software version is a simple search algorithm using a large sample of pre-changed guitar geometries. The huge database shows large deviations in sound when changing the basic shape of the guitar and small deviations in detail by changing the fan bracing or plate thickness.Future work will be to improve the mentioned sound processing algorithm towards a mathematical solution.

REAL-TIME PHYSICAL MODELING OF LARGE INSTRUMENT GEOMETRIES USING COUPLED FPGAS

Florian Pfeifle
Institute of Systematic Musicology, University of Hamburg, Germany
Florian.Pfeifle@uni-hamburg.de

ABSTRACT

A recent methodology utilised to simulate and synthesize physical models of complete instrument geometries is extended to facilitate the implementation of larger physical models in real-time. The existing system utilises explicit finite difference methods to simulate and synthesize physical models of music instruments on Field Programmable Gate Array (FPGA) hardware. To extend the computational abilities of the existing system, it is enhanced by more recent FPGA hardware consisting of two FPGAs of the Virtex-7 family, a 2000T and a 690T which are connected to a personal computer via a PCIe interface protocol. A first implementation of a large scale geometry using explicit finite difference methods is compared to a specifically adapted pseudo-spectral implementation of a plate model, which is applied to simulate a geometrically correct model of a grand piano soundboard. A central interest of this work lies on the applicability to real-world problems arising in instrument acoustic research and instrument design. Thus, a dynamic configurability and contrallability of the models is sought after. To this end, an Input/Output protocol is utilised for real-time adaptability of the physical parameters of each model part. The simulation results of the soundboard model are compared to measurements taken on real grand piano soundboards in different production stages.

FEASIBILITY ANALYSIS OF REAL-TIME PHYSICAL MODELING USING WAVECORE PROCESSOR TECHNOLOGY ON FPGA

Math Verstraelen[1]*, Florian Pfeifle*[2]*, Rolf Bader*[2]

[1]Computer Architecture for Embedded Systems
University of Twente, the Netherlands
[2]Institut für Systematische Musikwissenschaft
Universität Hamburg

ABSTRACT

WaveCore is a scalable many-core processor technology. This technology is specifically developed and optimized for real-time acoustical modeling applications. The programmable WaveCore soft-core processor is silicon-technology independent and hence can be targeted to ASIC or FPGA technologies. The WaveCore programming methodology is based on dataflow principles and the abstraction level of the programming language is close to the mathematical structure of for instance finite difference time-domain schemes. The instruction set of the processor inherently supports delay-lines and data-flow graph constructs. Hence, the processor technology is well suitable to capture both digital waveguide as well as finite-difference oriented algorithm descriptions. We have analysed the feasibility of mapping 1D and 2D finite-difference models onto this processor technology, where we took Matlab reference code as a starting point. We analyzed the scalability and mapping characteristics of such models on the WaveCore architecture. Furthermore we investigated the composability of such models, which is an important property to enable the creation and mapping of complete musical instrument models. One part of the composability analysis has been to combine digital waveguide (FDN reverberation model) with finite-difference time-domain models (primitive six-string instrument model). The mapping experiments show a high efficiency in terms of FPGA utilization, combined with a programming methodology that matches in a transparent way with the mathematical abstraction level of the application domain. We used a standard FPGA board to get full-circle confidence of the carried-out analysis. The WaveCore compiler and simulator results have shown the scalability of the processor technology to support large models.

1. INTRODUCTION

The development of sound synthesis digitization is to a large extend relying on the availability of computational power and hence indirectly linked to the progress of Moore's law. Sound synthesis itself is built upon a production model. The nature of such a model can be abstract and hence based on the production of the desired sound itself (e.g. Digital Waveguide or wavetable techniques) or based on a model that physically represents the object that produces sounds such as Finite Difference Time Domain (FDTD). A historical overview and elaborate explanation of these techniques can be found in [1], [2], and [3]. Mapping of FDTD based physical models on processors is challenging because of the huge computational requirement. Despite the impressive evolution of general purpose processors which are multi-core nowadays and widely applied in mainstream computer platforms, these processors can still not meet the computational requirements for solving FDTD models within reasonable timespans, let alone real-time. As a result, the focus is on different processor technologies, like GPGPU (General-Purpose computing on Graphics Processing Units) [4] and FPGA (Field Programmable Gate Array). Solutions based on GPGPU can achieve impressive accelleration and offer flexibility because of the programming versatility. Feasibility of real-time simulation of physical models on GPGPU has been investigated by Hsu et. al. [5]. They have been able to map square shaped 2D membrane structures with grid sizes up to 81x81 points onto a GPGPU at 41.1 kHz real-time, and compared this against GPP performance. FPGA's enable parallel computing to the extreme and have the potention to meet the real-time computational requirements. The difficulty with FPGA's, however, is programmability. In principle an FPGA is a fabric of primitive logic gates and memory resources that can be configured (interconnected) in an almost arbitrary way. This implies that an FPGA "programmer" has to develop a processor soft-core that is subsequently mapped on the FPGA fabric. Such a soft-core often results in an ultimately efficient solution to the given application problem, but often lacks flexibility. Motuk et. al. [6],[7] designed FPGA-targeted soft-cores for solving plate equations and obtained impressive efficiency results with this. Using these soft-cores, however, makes it still not trivial to compose a complete instrument model. Pfeifle et. al. has to our knowledge been the first to design FPGA targeted soft-cores that implement complete instrument models, based on the composition of different FDTD models [8]. Our conclusion is that FPGA technology has the ability to implement computational intensive real-time physical models of musical instruments, but the problem is to make this technology sufficiently flexible (i.e. to design soft-cores that enable efficient and versatile model development) and accessible (i.e. without the steep learning curve to apply this technology).

2. SCOPE AND CONTRIBUTION

We focus on the application of FPGA technology for real-time musical instrument modeling in a broad sense. Our special interest is FDTD, but we also take into account that other techniques, like digital waveguide or "classical" analog electronics modeling should also be feasible. Our research object is WaveCore. This is a programmable soft-core processor technology that is specifically designed for audio and acoustics. Earlier work has showed that WaveCore can be applied efficiently for low-latency audio effects processing [9], applying digital waveguide and classical modeling techniques. In this paper we investigate the feasibility of applying the WaveCore technology to real-time physical modeling on FPGA. Our aim is to apply this technology to model complete musical instruments with good efficiency and to hide those technological aspects for

the developer that make FPGA difficult to use. The structure of this paper is as follows: we start with an introduction to the WaveCore processor. Then we explain how FDTD schemes can be mapped on WaveCore technology. Further we explain how different FDTD schemes (and possibly other algorithmic parts) can be composed into a larger scope, and conclude with a technology efficiency analysis.

3. DATA-FLOW MODEL AND RELATED PROCESSOR ARCHITECTURE

WaveCore is a many-core processor concept. This processor is a so-called soft-core, which means that the processor design is implemented as a hardware description in a Hardware Description Language (HDL). This HDL code can be targeted (synthesized) to silicon which can be either ASIC (Application Specific Integrated Circuit) or FPGA (Field Programmable Gate Array) technology. After targeting this softcore to the desired technology, the WaveCore processor behaves like a programmable Digital Signal Processor (DSP) chip. The WaveCore processor is programmable with a native language that is inspired by data-flow concepts. This WaveCore programming language is declarative. This means that a WaveCore program describes a function, and hides details about how this function should be executed which is the case in imperative programming languages like C or C++. A WaveCore program is a data-flow process graph: a network of processes, edges and a global scheduler. Each WaveCore Process (WP) is an entity that is periodically executed (i.e. "fired") by a global scheduler. Upon firing a process consumes one data-entity, called "token" from each connected "inbound-edge". Likewise, after process execution a process produces one token per associated "outbound-edge". A token consists of one or more "primitive token-elements" (PTE). Where one PTE is the atomic native 32-bit data element. A WP can have an arbitrary number of inbound and outbound edges (including zero). Each WP can have a different link to the global scheduler. This scheduler orchestrates the execution of the entire process graph by periodically generating "fire-events" to the linked processes through dedicated "fire-links". In the example process-graph in fig.1 there are two different fire-links, called Es1 and Es2. This implies that different WP's can be fired with different rates: a multi-rate process graph is therefore supported by the concept. A global scheduler concept leads to a very strict and predictable execution behaviour of the process-graph, provided that the execution time of the actors is predictable. A WaveCore process is allowed to be partitioned. Such a partition is called a WaveCore Process Partition (WPP). As can be seen in fig.1, an inbound or outbound edge can be divided and linked to different WPP's. Hence it is possible that multiple WPP's can contribute to the production/consumption of a single token. At the lowest level we define the "Primitive Actor" (PA). A PA is an indivisible process which is depicted in fig.2. As can be seen a PA has two inbound edges: $x1, x2$, a function f, one outbound edge y, a parameter p, a max-length delay Λ and an inbound edge τ which controls the actual delay-line length dynamically. Each PA consumes at most two PTE's, and produces one PTE upon execution of that particular PA. The production of a PTE can be delayed through a run-time controllable delay-line that is associated with each PA. The delay-line length Λ is specified at compile-time and can be run-time modulated with a third inbound signal, called τ, yielding a dynamically variable delay-length $\lambda^{n+1} = \Lambda.g(\tau^n)$. Hence is is possible to describe algorithms with time-varying delays (like flanging [9]) in a compact and efficient way. The maximum delay-length Λ is specified at compile-time and can have any arbitrary positive integer value including zero. A limited set of different PA functions are supported by means of the already mentioned function f (like addition, multiplication, division, etc.). The PA function types that are of importance in this paper are (1) C-type PA: $y^{n+1} = p$, (2) MAD-type PA: $y^{n+\lambda} = p.x_1^n + x_2^n$, (3) ADD-type PA: $y^{n+\lambda} = x_1^n + x_2^n$ (4) MUL-type PA: $y^{n+\lambda} = x_1^n.x_2^n$, and (5) AMP-type PA: $y^{n+\lambda} = p.x_1^n$. The C-type PA is insensitive to its $x1$ and $x2$ inbound edges and basically emits a programmable constant value to its outbound edge, each time that it is fired. This C-type PA can be linked to a token-element and hence to an inbound port or local WPP-input. Each PA can be programmed such that it emits it output PTE to an outbound port, or a partition output, or locally to a fellow-PA within the same WPP.

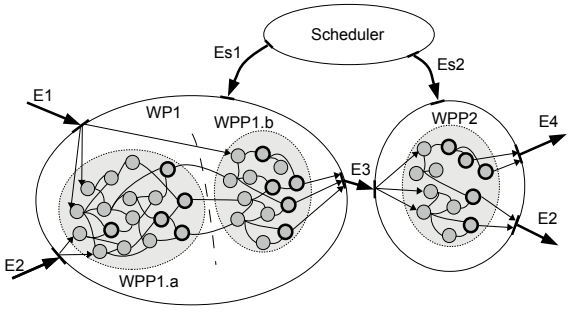

Figure 1: Data-flow oriented WaveCore programming model.

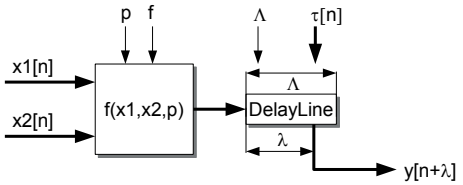

Figure 2: Primitive Actor (PA) model.

3.1. WaveCore processor architecture

The WaveCore processor itself consists of a cluster of so-called "Processing Units" (PU). A block diagram of this cluster is depicted in fig.3. Each PU embodies a small Reduced Instruction Set Computer (RISC). This PU-cluster is interconnected be means of a Network-on-Chip (NoC), called Graph Partitioning Network (GPN). The PU-cluster can be intialized (i.e. loading compiled WaveCore program code) through the "Host-Processor Interface" (HPI). This HPI is intended to be connected to a host-computer that can either be on the same chip (FPGA or ASIC) or an externally connected computer. The execution of the individual PU's within the PU-cluster is orchestrated by the Scheduler. In principle this Scheduler is a programmable sequencer which generates firing events to each individual PU, according to a compile-time derived cyclo-static schedule. Each PU is capable to access system memory space through the "External Memory Interface". Hence, each PU is individually responsible for moving token data and delay-line data from/to external memory. The WaveCore compiler (which is not further described in this paper) takes care of automated mapping of a WaveCore Process Graph onto the PU-cluster. Like mentioned each WP in the process graph can be partitioned into one or

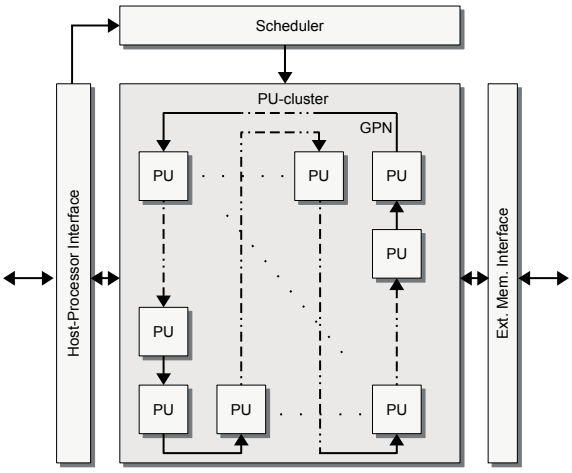

Figure 3: WaveCore processor: PU-cluster.

more WPP's. Each WPP is entirely mapped on a PU. It is supported that one WP is eventually mapped on a set of PU's. This property is used by mapping a finite-difference scheme, as we will explain further in this paper. The connections between the different WPP's are automatically mapped on the GPN network by the compiler.

3.2. Processing Unit architecture

Like mentioned, a PU embodies a small pipelined RISC processor. The block diagram of a PU is depicted in fig.4. This unit consists of two main parts: the "Graph Iteration Unit" (GIU) and the "Load/Store Unit" (LSU). The GIU is a small pipelined CPU which is fully optimized to sequentially fire PA's according to a compile-time derived static schedule. The instruction set for this CPU is defined in such a way that a compiled PA can be executed as a single instruction. This unit fires an entire WPP after that it receives a process-dispatch event from the global scheduler (through a fire-link), and hence executes each compiled PA within this WPP sequentially. The heart of the GIU is a single-precision (32-bits) floating-point ALU. The LSU takes care of external memory traffic. As such, the GIU is decoupled from external memory and hence insensitive to the associated latency.

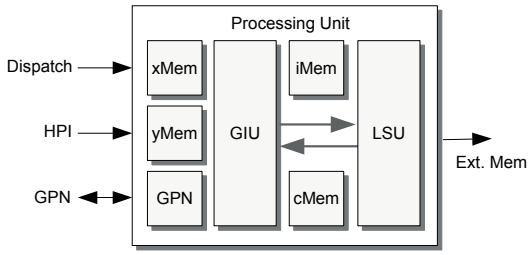

Figure 4: Processing Unit (PU).

4. DESCRIBING PHYSICAL GEOMETRIES IN WAVECORE PROCESSES

In this section we zoom in into the discretization of Partial Differential Equations (PDE) that are of importance for Finite-Difference (FD) modeling [2]. Next, we will analyze and explain how such a scalable and discrete model is translated to a WaveCore process.

4.1. Finite difference schemes of wave equations

We focus on finite difference schemes that originate from the generic wave equation as defined in (1). This equation models wave propagation in a medium, like a string (1-dimensional), plate (2-dimensional) or a 3D medium.

$$\lambda(s).\nabla^k u(s,t) = \epsilon(s)\frac{\partial^2 u(s,t)}{\partial t^2} + \mu(s)\frac{\partial u(s,t)}{\partial t} + f(s,t) \quad (1)$$

Where s represents the spatial coordinates (i.e. $< x >$ for a 1-dimensional geometry or $< x, y >$ for a 2-dimensional geometry). The parameter k represents the order of the differential equation. The first-order partial time derivative term models wave propagation losses. The term $f(s,t)$ enables model stimulation (e.g. plucking a string or striking a snare-drum). In our analysis we will investigate 2nd and 4th PDE orders. We allow the parameters λ, ϵ and μ to be dependent on the spatial coordinates in our analysis. However, we assume these parameters to be time invariant. Physically this means that non-uniformity of the medium is possible. The first step is to transform the space/time continuous eq.(1) into its space/time discrete counterpart. Therefore we introduce a grid in space: $s = \sigma\Delta s$, and time: $t = n\Delta t$. Furthermore we apply a central difference approximation which yields the following substitutions for the first and second partial time derivative:

$$\frac{\partial u}{\partial t} \approx \frac{u_\sigma^{n-1} + u_\sigma^{n+1}}{2\Delta t} \quad (2)$$

$$\frac{\partial^2 u}{\partial t^2} \approx \frac{u_\sigma^{n-1} - 2u_\sigma^n + u_\sigma^{n+1}}{\Delta t^2} \quad (3)$$

We substitute (2) and (3) into (1) and subsequently solve for u_σ^{n+1}. This yields the iteration function, as defined in (4)

$$u_\sigma^{n+1} = s_1(\sigma)\xi^n(\sigma) + p_1(\sigma)u_\sigma^n + p_2(\sigma)u_\sigma^{n-1} + p_3(\sigma)f_\sigma^n \quad (4)$$

Where we define $\xi^n(\sigma)$ as the spatial stencil computation function. This function accumulates the neighborhood node values, including centered node u_σ^n with discrete timestamp n. The definition of this spatial stencil depends on the dimensions of the models and the order of the differential equation. The general definition is given in equation (5).

$$\xi^n(\sigma) = \sum_k \alpha_k . u_{\sigma_k}^n \quad (5)$$

For a 2D geometry with 2nd order (membrane) we can expand this stencil computation function as follows:

$$\xi^n(i,j) = u_{i-1,j}^n + u_{i+1,j}^n - 4u_{i,j}^n + u_{i,j-1}^n + u_{i,j+1}^n \quad (6)$$

An illustration of a 2D node scheme with the stencil defined in (6) is given in fig.5.

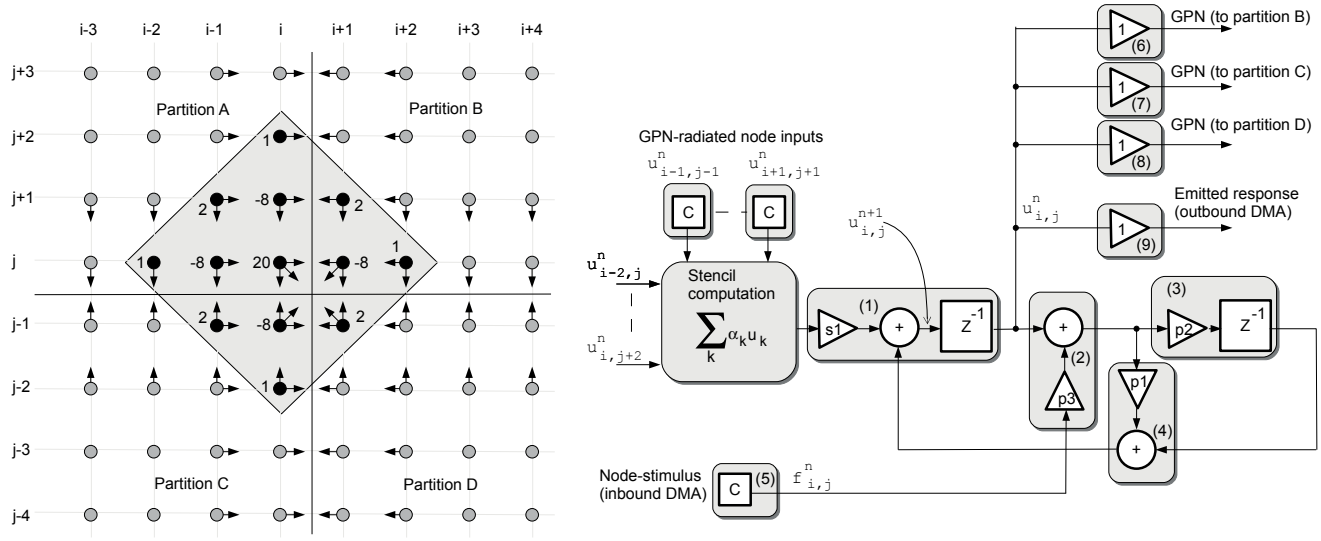

Figure 6: Node computation scheme

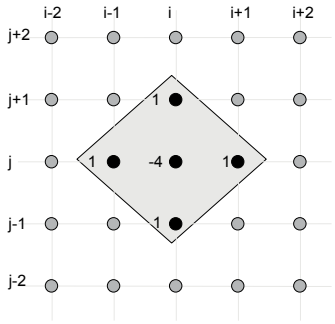

Figure 5: 5-points stencil within membrane model

4.2. Capturing finite-difference schemes into WaveCore processes

A finite-difference scheme as in fig.5, with node-computation defined in eq.(5) can be seen as a directed graph. The basic elements in such a graph are vertices (the nodes wherein the actual computation takes place) and edges. Data elements (i.e. tokens) are carried over the edges and consumed/produced by the vertices. A WaveCore process can also be seen as a directed graph, where the vertices are represented as Primitive Actors (PA), which are arbitrarily interconnected by edges. Hence, a finite-difference scheme can be mapped on a PA-graph. The graph structure of a FD-scheme is very similar to the associated WaveCore PA-graph structure. This is exactly the reason why a WaveCore process transparently represents the mapped FD-scheme. There are basically three main requirements for mapping a finite-difference scheme onto a WaveCore process: (1) scalability, (2) the ability to move stimulus data(f_σ^n) to the model for each node and for each time-stamp n, and (3) the ability to move node-data from the model for each node u_σ^n and for each time-stamp n. A WaveCore PU executes compiled PA's sequentially in time, and the PU clock frequency is limited. This implies that in many cases only a limited part of a FD-scheme (depending on its size) fits on a single PU. Therefore a FD-scheme needs to be partitioned and each partition must be mapped on a PU. Partitioning of the FD-scheme and mapping of partitions on different PU's inherently means that stencil-computation for partition-boundary nodes cannot be done without gathering one or more node-values that belong to the stencil from "neighbor" PU's. The GPN-network within the WaveCore PU-cluster is used for this purpose: partition boundary-node values are moved to neighbor partition(s) over this GPN network for every discrete timestamp. We call this phenomenon "radiation" since every partition radiates its boundary values to its direct environment. Note that the radiation intensity depends on the geometry (1D, 2D, 3D) and spatial stencil complexity (order of the PDE). This is shown for a 2D model of a fourth order differential equation (plate equation) in fig.6. Radiation of node values is illustrated with arrows (e.g. node $u^n_{i,j+2}$ within partition A radiates to partition B). As can be seen, in the worst-case some nodes need to radiate to three neighbor partitions. The example node at position (i, j) depends on 7 radiated node inputs from partitions B,C and D and 6 local node values. Node $u^n_{i,j}$ itself radiates to partitions B,C and D. Note that "radiation" is an inevitable side-effect of partitioning, which has also been described within the context of physical model mapping on FPGA by Motu et.al [7].

The actual mapping of a FD-node onto a PA-graph is depicted in fig.6. The stencil computation is implemented with a multiply-add type PA tree structure (shown as a "black-box"). The inputs of this part of the PA-graph are C-type PA's (if applicable: GPN radiation entry-points) and outputs from different local (i.e. within the same partition) nodes. The output of this stencil computation part feeds into the temporal difference

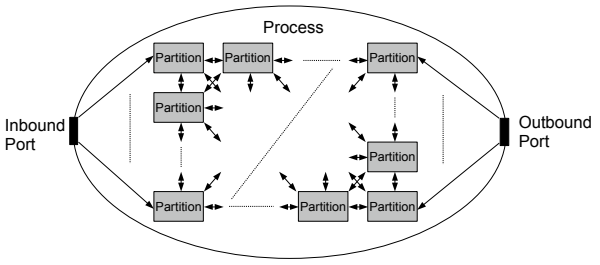

Figure 7: FD scheme represented as a WaveCore process

equation part. This part consists of four interconnected PA's (labeled 1,2,3,4). As can be seen, there is a transparent relationship between the node-PA graph structure and the implemented difference equation (4). The example node (i, j) itself radiates to three neighbor partitions. The PA's 6,7 and 8 are included for this purpose. The execution of each of these PA's (6,7,8) initiate a GPN-write transaction. Moving stimulus data (function f_σ^n) from outside to the model is implemented with C-type PA(5). This PA is linked to the inbound port of the associated WaveCore process. The LSU of the PU takes care that the required data is fetched from external memory through DMA and moved to the memory location that is allocated to PA(5). Moving node data from the model to outside is implemented with PA(9). This PA is linked to the outbound port of the associated WaveCore process. The LSU of the PU takes care that the PA(9) output data is moved to, and the input to PA(5) is moved from external memory space via DMA. The abstract representation of a complete FD-scheme as a WaveCore process (including stimulation and response emission) is depicted in fig.7.

5. COMPOSITION OF PHYSICAL GEOMETRY MODELS IN WAVECORE PROCESS-GRAPHS

The ability to capture finite-difference models in a scalable processor technology is an important requirement to build musical instrument models. This requirement on itself however is not sufficient. Other important requirements are (1) the ability to combine different geometry models where each model may run at a different sampling-rate, (2) the ability to move stimulus and response streaming data between the model and the external (e.g. analog or an externally connected computer that generates stimuli and post-processes generated model data), (3) real-time processing with low latency, (4) the ability to add processes which structures are not as regular as FD-schemes (e.g. traditional signal-processing functions or effects), (4) programming flexibility and processor architecture abstraction. In the following subsections we will demonstrate by three experiments how these requirements fit on the WaveCore programming model and processor technology.

5.1. Experiment 1: primitive six-string device in an acoustic room

We combined a simple guitar model with a virtual guitar player in an acoustic room and described this in a WaveCore process graph that is depicted in fig.8. The virtual guitar player is modeled as a process called "SixStringPlayer". The implementation is a low-frequency oscillator which output if connected to a tapped delay-line. As a result, this process emits a "downstrum" event at the LFO rate (sub-Hz frequency) by periodically generating a "pluck" token. This token consists of six PTE's (one PTE for each string). The guitar model is described in the "Fdtd_SixString" process. This process is composed of six 1D FD-scheme instances (each one coded as a WPP) that are connected to a "SixStringBody" WPP. The six string models are connected to the "pluck" port where each string receives one out of six PTE's from the associated inbound token. Each string is tuned in a way that the guitar model is tuned in an E-major chord. Each pluck event causes a raised-cosine shaped pluck at a fixed position in the associated string. The "SixStringBody" combines the outer edges of the six strings, combines these and routes these back to the same strings (simple interference model). Moreover, this WPP extracts a stereo audio signal from the combined string vibrations and links this stereo signal to the "SixStringOut" port of the process. The "SixStringOut" port of the "Fdtd_SixString" process is connected to a reverberation process called "FDN_reverb". This process implements a feedback-delay network that models a 3D space in an abstract way (zita_rev1, [10]). This is a simple model in terms of number of PA's, but fairly complex in terms of number of instantiated delay-lines (66 in total). This process yields a reverberated stereo output, called "DAC". Finally the "DAC" edge is connected to a process that is called "DAC". This is not a WaveCore process, but an abstract model of a Digital to Analog Converter. All processes in the graph are synchronized to a single rate called "AudioRate" which is generated by the global scheduler model in the same process graph. The WaveCore compiler translates the entire process graph to an object file. This object file can either be mapped to a target WaveCore processor platform or simulated by the WaveCore simulator. For this process graph we did both and noticed no differences between the simulated model and the real-time (48kHz sampling rate) WaveCore processing on the FPGA board (Digilent Atlys [11]) that we used.

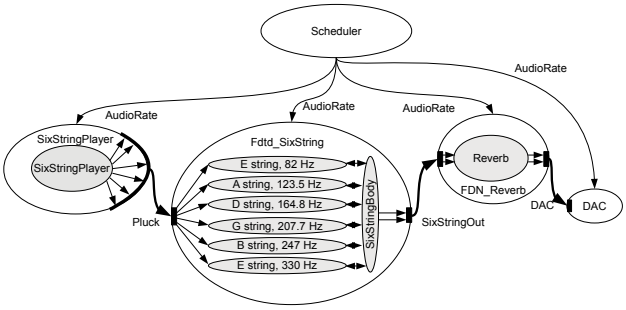

Figure 8: WaveCore Process Graph of six-string model.

5.2. Experiment 2: scalable 2D plate model

We wrote a 2D plate model generator with 2nd and 4th order differential equations, based on equation (4). This generator produces a scalable and partitioned WaveCore process graph which is depicted in fig.9. The purpose of this process graph

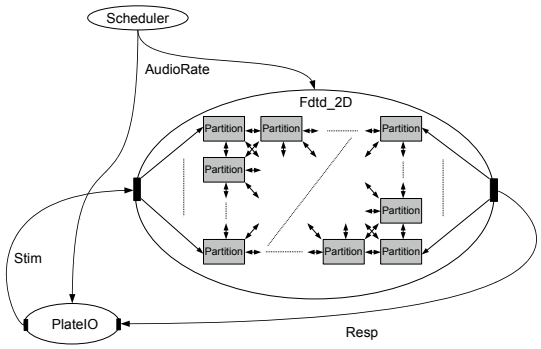

Figure 9: WaveCore Process Graph of 2D plate model with stimulus generation/response capturing.

is to demonstrate the scalability of FD-schemes as partitioned WaveCore processes. Furthermore, we analyzed the mapping characteristics using this model. The results of this analysis are summarized in a next section of this paper. We applied square-shaped partitioning where we tried to optimize the partition size in such a way that a partition just fits on a targeted

PU. The ”PlateIO” process enables verification of the model: this process injects stimuli into the model and captures emitted responses. We used the WaveCore simulator to verify the functional correctness of the generated model. A simulation snapshot is depicted in fig.10 We observed that a FD-scheme is

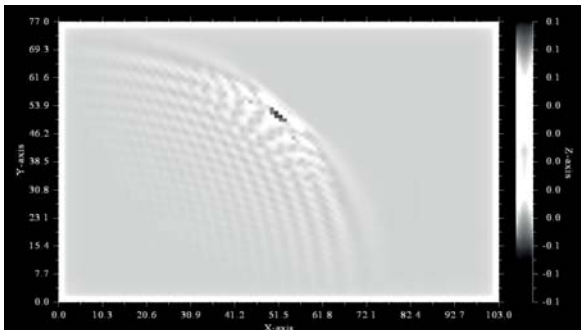

Figure 10: WaveCore simulation snapshot of 2D plate model.

uniformly scalable. The WaveCore compiler turned out to be robust and fast: it took less than a minute to compile an FD-model with over 8000 nodes to WaveCore object code.

5.3. Experiment 3: real-time 2D plate model on FPGA

We generated a 2D membrane model (2nd order PDE) and compiled this as a partitioned WaveCore process which is depicted in fig.11. Within this process graph we connected the analog

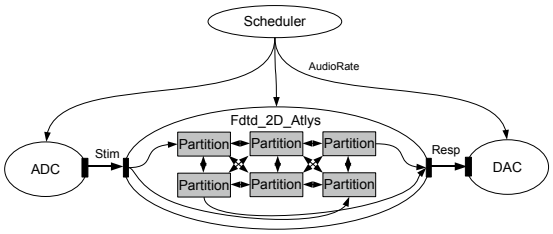

Figure 11: WaveCore Process Graph of 2D plate model on FPGA, connected to ADC/DAC.

stereo input of the FPGA to two opposite diagonal corners of the 2D node-grid. Likewise, we connected the other two diagonal corner node outputs of the 2D node-grid to the stereo output of the FPGA board. These analog I/O connections are modeled in the WaveCore process graph by the ADC and DAC processes. This model runs real-time at 48kHz audio sampling rate and ultra low latency where we connect an audio source to the analog input of the board and a speaker to the analog output of the board. We also simulated this process graph using the WaveCore simulator. We used an audio sound bite that we linked to the ADC process, and played the produced (by the DAC process) audio with a media player. We observed a similar audible result, compared with the FPGA setup.

6. MAPPING EFFICIENCY

The efficiency of a processor technology can roughly be divided into two aspects. The first aspect is the compiler efficiency: for a given application domain, how efficient are the algorithms mapped on the target processor architecture. The second aspect is what we call ”silicon efficiency”: how efficient is the given processor architecture w.r.t. silicon area. The overall efficiency is ultimately a metric on how efficient the algorithms within the target application domain are mapped on the overall processor technology. For physical modeling on WaveCore we have investigated mapping efficiency, silicon efficiency for FPGA and the overall efficiency.

6.1. Compiler efficiency

The mapping of a FD-scheme on the WaveCore processor is most efficient when all the PU's in the cluster execute arithmetic PA's for every PU instruction. This means that all processing effort is spent on the actual computation. Inefficiency is caused by a non-ideal locality of reference: we introduced the concept ”radiation” which implies explicit data movement and replication of node-data over partition boundaries. The compiler itself also generates inefficiency that is caused by a non-optimal memory allocation and pipeline scheduling. This inefficiency results in so-called ”bubbles” in the GIU pipeline (caused by data dependency conflicts of subsequent instructions) and additional instructions for operand pointer initialization. We inves-

Table 1: *FD-partition mapping on WaveCore PU*

Dim/ Spatial	Nodes	GPN-load (%)	Comp. Overh. (%)	Stim (%)	Resp (%)	ILP
1/2	292	0.06	4.51	1	1	5.56
2/2	169	3.22	4.10	1	100	11.10
2/2	169	3.66	4.93	1	1	7.14
2/4	81	4.54	6.39	1	100	20.00
2/4	81	4.72	8.22	1	1	16.67

tigated the compiler efficiency for FD-scheme partitions. We optimized these partitions in such a way that the size just fits a PU, where we fixed the PU instruction size to 2048. We investigated mapping capabilities for 1D schemes (2nd order) and 2D schemes (membrane and plate models). For each partition we investigated the mapping influence of model stimulation (stim.: the percentage of nodes that are stimulated for every discrete timestep) and response data movement (resp.: the percentage of node values that are moved from the model for every discrete timestep). Table 1 summarizes the PU-mapping efficiency figures. The ”GPN-load” figure expresses the percentage of clock-cycles in which GPN transactions (radiation) are initiated, relative to the overall thread-size. The ”Comp. Overh.” figures expresses the percentage of added instructions, due to compile inefficiencies. Ultimately, the ILP (Instruction Level Parallelism) number is an important metric which expresses the averaged number of required GIU instructions per FD-node.

6.2. Silicon efficiency

We mentioned that the WaveCore processor is implemented as a softcore and described in a HDL (Hardware Description Language). This HDL implementation is configurable at compile-time (within this context ”compilation” means the process of mapping the HDL description of the processor to the targeted technology). The most important configuration parameters are PU-cluster size (number of PU's) and PU memory configuration (i.e. instruction memory size per PU). The HDL description of a configured WaveCore processor instance can be compiled to a target technology: either FPGA or ASIC. The target technology, combined with application requirements dictates the opti-

mal processor configuration. Typically the most important constraints within a given technology are the amount of embedded memories, feasible clock frequency and the amount of logic-gates. The execution of a PU-thread is always linear: a PU does not support branches, loops or jumps in the program flow. This means that the number of instructions that can be executed during one sampling period can be expressed by eq.(7).

$$C_p(f_s) = \begin{cases} N_{pu}.C_{imem} & \text{if } f_s \leq f_d \\ N_{pu}.f_{clk}/f_s & \text{if } f_s > f_d \end{cases} \quad (7)$$

With $C_p(f_s)$ the PU-cluster capacity as function of the sampling frequency, N_{pu} the number of PU's in the cluster, f_{clk} the PU clock frequency, f_s the sampling frequency and C_{imem} the instruction memory capacity. This hyperbolic relation between PU capacity and sampling rate dictates the optimization of a PU-cluster for a given application domain and a given technology (e.g. FPGA), with $f_d = f_{clk}/C_{imem}$ as "drop-off" sampling frequency" (the capacity C_p drops for sample frequencies $f_s > f_d$). We used the relation in eg.(7), and the FPGA

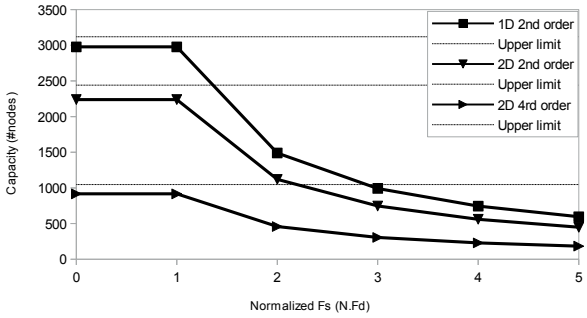

Figure 12: FDTD mapping capacity curves of WaveCore on Atlys FPGA board

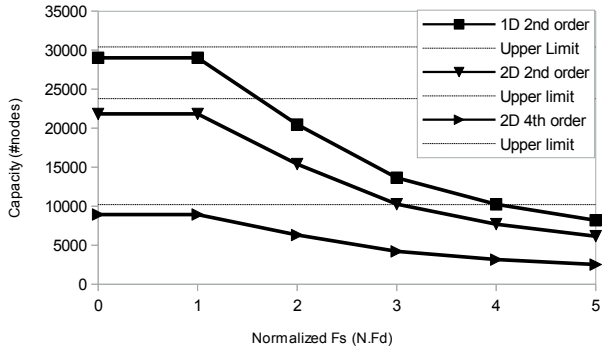

Figure 13: FDTD mapping capacity curves of WaveCore on ML605 FPGA board

constraints to derive PU-clusters for two target platforms: the Digilent Atlys board (Spartan6, LX45 device) and the Xilinx ML605 board (Virtex6). Our goal has been to utilize the available FPGA resources as much as possible. For the Atlys board we derived a PU-cluster which consists of 8 PU's and 2k instruction capacity per PU. For the ML605 board we derived a PU-cluster which consists of 55 PU's where 23 PU's have 4k instruction capacity each and the other 32 PU's have 2k instruction capacity each. The resulting FDTD mapping capacity profiles for both mentioned boards are depicted in fig.12 and fig.13. These capacity profiles represent the capacity (in #nodes) for the scalable 1D and 2D (2nd and 4th order) FD geometries that we analyzed in the previous sections of this paper, as a function of the normalized sampling frequency. The "upper-limits" in the figures represent the theoretically maximum performance, with no compiler efficiency losses. The actual performance depends on the achieved clock-frequency f_{clk}. The maximum f_{clk} depends to a large extend on the GIU pipelining and has an upper-limit that is defined by the floating-point arithmetic. For the Atlys board we found a feasible clock frequency: $86MHz < f_{clk} < 189MHz$, or $42kHz < f_d < 92kHz$. For the ML605 board we found a feasible clock frequency: $150MHz < f_{clk} < 338MHz$, or $37kHz < f_d < 82kHz$. The lowest clock-frequencies are obtained without any pipeline optimizations (push-button HDL compilation). The highest frequencies require careful pipeline optimizations.

6.3. Overall efficiency

Ultimately, the most interesting efficiency characteristics are determined by the ability to map real-life application cases (virtual instruments) onto a given processor technology. Estimation of model complexity is not straightforward since the complexity of a physical model of a musical instrument in terms of #nodes depends on may aspects, such as the frequency-dependent speed of sound on wood and other material and geometry dependent parameters. The required sampling rates for this application domain vary according to the nature of the modeled objects and may range up to approximately 500 kHz. An example of a realistic instrument model is the Banjo. This model is composed of 5 strings (560 nodes in total, 1D, 65kHz sampling rate), a membrane (2048 nodes, 2D circular shaped, 128kHz sampling rate), an air-filled cilindrical shaped 3D space (8192 nodes, 3D, 65kHz sampling rate) and the bridge (512 nodes, 2D, 128kHz sampling rate) which is the interface between the strings and the membrane. Pfeifle et. al. have been able to map a fully functional Banjo model using the methodology as described in [8] on the ML605 board where the majority of the FPGA resources are utilized. We made an estimation on the feasibility to map this model on the ML605 board using WaveCore technology, based on the obtained capacity curves in fig.13 and reasonable estimations of required composition interface overhead. The outcome of this (optimistic) estimation is that it is probably feasible to map an instrument of this complexity on the ML605 board where approx. 75% of the WaveCore cluster capacity would be utilized. However, a couple of performance/efficiency optimizations will need to be done to the technology. (1) The required minimum PU cluster clock frequency will be approximately 250MHz. (2) Automated partitioning of geometry parts to maximally utilize the PU capacity is necessary. (3) We found out that data memory allocation (performed by the WaveCore compiler) is too greedy, resulting in a too large data memory footprint. A more efficient data memory allocation however is conceptually possible.

7. CONCLUSIONS AND FUTURE WORK

We have investigated the feasibility of using WaveCore processor technology for real-time physical modeling purposes. We have focused on the ability to map FD-schemes with different dimensions and different PDE orders. Furthermore we focused on the ability to use this technology to compose virtual musical instrument models. We did this by demonstrating the process-graph oriented programming methodology that enables the combination of different processes that are possibly multi-rate and are possibly implementations of different modeling meth-

ods (e.g. FD-schemes, combined with FDN or arbitrary data-flow oriented structures). We observed a high level of transparency between the physical models and the actual implementation of such models in WaveCore language. We also observed a good efficiency, despite the fact that there is a reasonably high versatility in the programming capability and abstraction. In particular, the programming versatility and abstraction combined with a good mapping efficiency results in our conclusion that WaveCore is a promising processor technology for virtual instrument modeling. Future work is the mapping of one or more musical instrument models on a suitable FPGA platform where the biggest challenges seem to be high sampling rates for some geometry parts and high-bandwidth off-chip response data funneling. We have found possible optimization areas within the technology. Automated partitioning of large process-graphs is an important though currently missing step in the mapping process. Next to this we have found a few optimization options that can further enhance the efficiency of the processor technology.

8. REFERENCES

[1] Julius O. Smith, *Physical Audio Signal Processing for virtual musical instruments*, W3K Publishing, 1st edition, 2010.

[2] Stefan Bilbao, *Numerical Sound Synthesis: Finite Difference Schemes and Simulation in Musical Acoustics*, Wiley, 1st edition, 2009.

[3] Udo Zölzer, *DAFX: Digital Audio Effects*, Wiley, 2nd edition, 2011.

[4] Stefan Bilbao, Alberto Torin, Paul Graham, James Perry, and Gordon Delap, *Modular Physical Modeling Synthesis Environments on GPU*, 2014.

[5] Bill Hsu and Marc Sosnick-Pérez, "Real-time gpu audio," *Commun. ACM*, vol. 56, no. 6, pp. 54–62, June 2013.

[6] E. Motuk, R. Woods, and S. Bilbao, "Implementation of finite difference schemes for the wave equation on fpga," Philadelphia, United States, 2005, IEEE International Conference on Acoustics, Speech, and Signal Processing, pp. 237–240.

[7] E. Motuk, R. Woods, and S. Bilbao, "Fpga-based hardware for physical modelling sound synthesis by finite difference schemes," in *Proceedings of the IEEE field programmable technology conference*, Singapore, 2005, IEEE, pp. 103–110.

[8] F. Pfeifle and R. Bader, "Real-time finite-difference physical models of musical instruments on a field programmable array (fpga)," in *Proceedings of the 15th int. Conference on Digital Audio Effects (DAFx-12)*, York, UK, 2012.

[9] M. Verstraelen, G.J.M. Smit, and J Kuper, "Declaratively programmable ultra low-latency audio effects processing on fpga," in *Proceedings of the 17th int. conference on Digital Audio Effects*, Erlangen, Germany, 2014, DAFx 2014, pp. 263–270.

[10] Julius O. Smith, "Zita-rev1," Available at `https://ccrma.stanford.edu/~jos/pasp/Zita\_Rev1.html`, accessed Jan. 21, 2014.

[11] Digilent Inc., "Atlys Spartan-6 FPGA Development Board)," Available at `http://www.digilentinc.com/Products/`, accessed Jan. 21, 2014.

SOFTWARE SIMULATION OF CLARINET REED VIBRATIONS

Fritz Schueller, Carl Poldy

Private Researchers
Vienna, Austria

fritz.schueller@aon.at
carl.poldy@nativeprogramming.at

ABSTRACT

Electric Circuit Analysis Programs, such as MicroCAP [1] are useful for simulating acoustical and mechanical behaviour of musical instruments. As has been shown in [2], frequency dependent characteristics such as acoustical impedances of wind instruments can be simulated. Also pressure and volume-flow inside a tube can be demonstrated graphically [3]. A so called AC-analysis was used for these tasks.
In the present paper first the transient response of a purely mechanical device, the clarinet reed, is studied. MicroCAP offers the possibility to show several parameters on a time scale. For this a different analysis is used, namely TR-analysis (transient analysis).
The quasi-static relation between volume flow and pressure difference is the only acoustical-mechanical question that is dealt with in this paper.
The paper explains the electro-mechanical-acoustical analogies that are the basis for the simulations. Finally the suitability of the software-model used is demonstrated by checking the results against the literature [4], [5].

1. INTRODUCTION

1.1 The software model

The model of the reed used here is the most simple one. It consists only of lumped elements. As has already been shown [5], lumped elements are useful for understanding the basic properties of clarinet reeds.
In section 2 we compare the results of Walstijn and Avanzini [4], [5] with those from the software-models used here. Conclusions are given in section 3 and an outlook to future work in section 4.

1.2 Electro-mechanical analogies

The partial differential equations that describe electrical processes are very similar in many cases to those for describing mechanical and acoustical processes. Therefore using suitable mapping, mechanics and acoustics can be represented by electrical circuits. The analogy used here can be described as follows: The three main passive components of electricity L, C, R represent in mechanics mass, compliance and friction. More details and tables are given in the appendix.

2. COMPARISON WITH THE RESULTS OF WALSTIJN AND AVANZINI

2.1 Motivation

Walstijn and Avanzini [4] and [5] have studied the applicability of numerical simulations to clarinet reeds. Whereas [4] deals with a one-dimensional distributed model, [5] considers a lumped model (see Fig. 1 in [5], repeated here as Fig. 1). We keep to the symbols used by Walstijn and Avanzini if not otherwise mentioned.

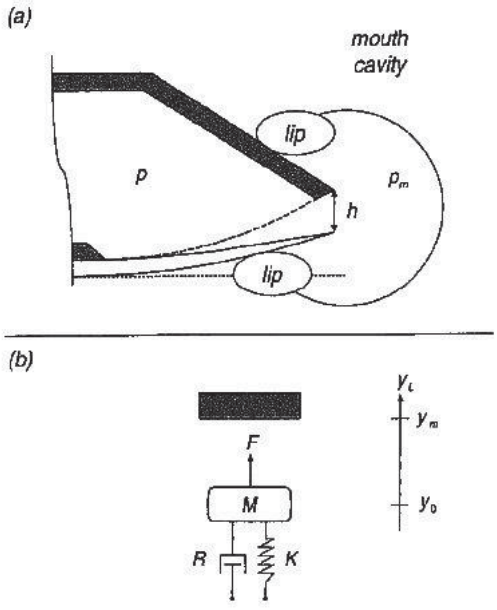

Figure 1. (a): Schematised view of a clarinet reed-mouthpiece-lip system. The dashed line indicates the profile of the mouthpiece lay, and p and p_m denote the mouthpiece pressure and the mouth pressure, respectively. (b): One-mass model of the reed tip vibration, with effective mass M, effective damping R, and stiffness K. The effective external force F exerted on the reed equals $S_d \Delta p$, where S_d is the effective driving surface, and $\Delta p = p_m - p$ is the pressure difference across the reed. The reed opening h is related to the reed tip position y_L by $h = y_m - y_L$, where y_m is the vertical position of the mouthpiece lay tip.

Fig. 1, The lumped model (Fig. 1 of [5])

2.2 Reed resonance peaks

These above mentioned two papers are good entry points for studying the applications of electronic Circuit Analysis Programs. First the excursion response of Fig. 2 of [5] is reconstructed. The reed model for this is shown in Fig. 2. Examples of typical values used are shown in the list of definitions. In MicroCAP the units are not given explicitly. "1m" does not mean 1 metre but 1 milli. SI-units are taken for granted. Depending on the physical dimension meant, 1m can stand for 1 mm, 1 mV or 1mA, etc.

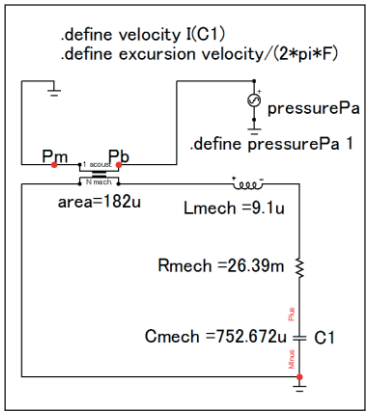

Fig. 2, Model used to reconstruct Fig. 2 of [5]

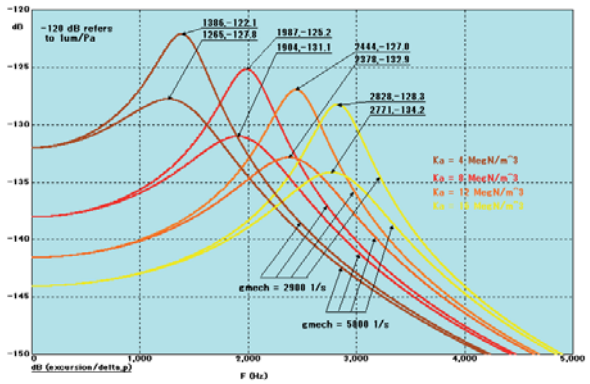

Fig. 3, Reconstruction of Fig. 2 in [5] with the original damping factor g_{mech}=2900, as well as doubled 5800

The following definitions show the syntax of MicroCAP for the physical constants and variables as well as the values used for the reproduction of Fig. 2 in [5].

```
.define delta_p v(Pm)-v(Pb)
.define R1value 1

.define width 13m              Table I of [4]
.define length 34m             Table I of [4]
.define area length*width

.define Ma 0.05                Table I of [4]

.define Lmech Ma*area

.define Ka 4Meg  (stepped to 8, 12, 16 Meg)

.define Cmech 1/Ka*area

.define gmech 2900             3.2 of [5]
.define Ra gmech*Ma            3.2 of [5]
.define Rmech Ra*area

.define excursion i(C1)/s
```

The symbol *s* in the excursion definition stands for *jω* in MicroCAP. The result is independent of the choice of R1. The signal generator delivers a cosine voltage. The result is also independent of the amplitude. During the AC-analysis the generator is swept from 0 to 5000 Hz. The lower curves of Fig. 3 show the excursion per *delta_p* for an increased value of g_{mech} of 5800/s. The reed length was chosen according to [4] Table I. The value of the area has no influence on the result of Fig. 2 in [5]. We see here that the peak is not the same as resonance frequency. They are only the same for symmetrical peaks (achieved by multiplying by frequency or plotting velocity instead of excursion).

2.3 Response comparisons

Fig. 7 of [5] shows the response of the freely resonating reed to a short Hanning pulse. The reconstruction (Fig.4) for the lumped model gives a similar result. The model for Fig. 4 is shown in Fig. 5.

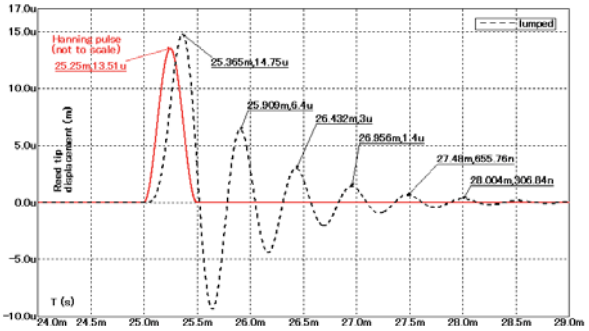

Fig. 4, Response of the reed to a short pulse

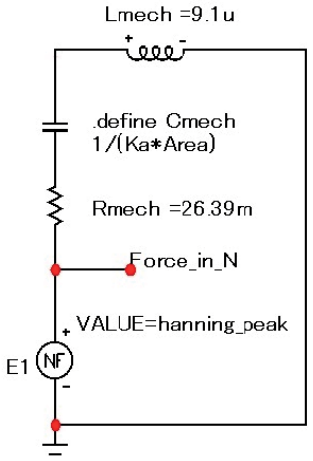

Fig. 5, Model to reconstruct the transient response.

A Hanning pulse of 0.5 ms was used. Its peak value was chosen in such a way that the maximum excursion equals the

one in Fig. 7 of [5]. The radian frequency of the exponentially decreasing reed oscillation ω_r corresponds to equation (11) in [5] - (ω_r^2 is a printing error, also in (10) of [5]). The corrected equation (11) is shown here as (1).

$$\omega_r\{\Delta p(n)\} = \sqrt{\frac{K_a\{\Delta p(n)\}}{M_a} - \frac{g^2}{4}} \qquad (1)$$

All this is in the small-signal range where the nonlinear model would be inappropriate.

2.4 Reed tip displacement

Here we compare the results of section 4.1 in [5] with those obtained using MicroCAP. The part d of Fig. 6 of [5] is recalculated in Fig. 6 of the present paper. The model is shown in Fig. 7. It is similar to Fig. 2, except that a DC-offset according to (24) of [5] is added, and the condenser is nonlinear. The vertical axis here corresponds to Fig. 8 of [4], with rest position of the reed at 0.85mm and hard-limit at 1.25mm, which will never be reached in the static state.

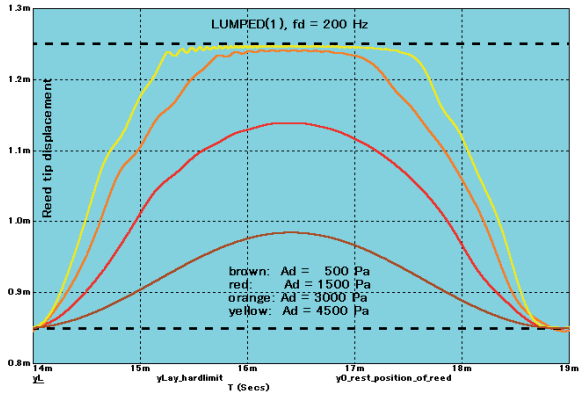

Fig. 6, Reed tip displacement as in [5], Fig. 6d

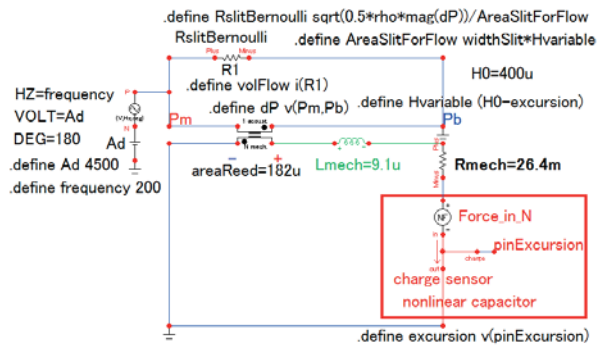

Fig. 7, The model used for the simulation in Fig. 6

The resistor *RslitBernoulli* is responsible for the pressure difference ΔP between the mouth (P_m) and the bore (P_b) of the clarinet. The simple model, without refinements, depends entirely on the Bernoulli effect $\Delta P = 1/2\ rho\ v^2$ to throttle the air flow, viscosity playing no role. Since the B. effect is essentially an expression of energy conservation in the air flowing, no viscosity effects in the narrow aperture are allowed, at least not while the aperture is open. Otherwise there would be energy exchange with the walls: contradicting the key mechanism for flow regulation.

The nonlinear characteristic used as input for these nonlinear simulations is shown in Fig. 8. Although the vertical axis represents force, it is expressed in Pa to ease comparison with Fig. 8a of [4] on which it was modelled.

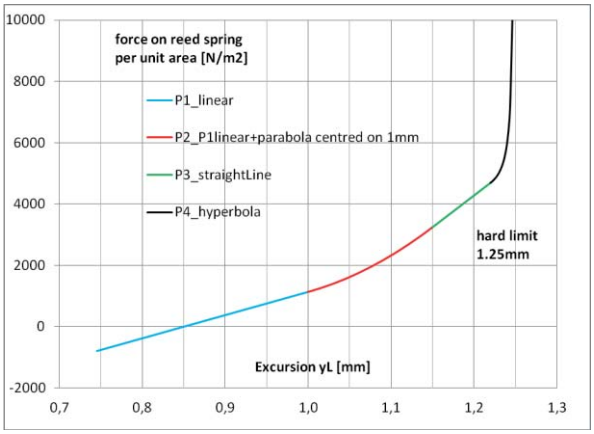

Fig. 8, The curve used for nonlinear simulations in the present paper. Physically the vertical axis P_{nonlin} really represents a force $F_{nonlin} = P_{nonlin} \times areaReed$.

Of course pressure is not an appropriate input parameter for describing a mechanical spring such as a reed, whether linear or nonlinear. We need that part of the force responsible for stretching the spring, whereas part of it is used for overcoming inertia and friction. The parameter actually used in the simulations was F_{nonlin} derived from static P_{nonlin} taking into account the effective area. In the simulation the force at any moment stretching the spring was deduced from the excursion, as shown in the circuit (Fig. 7).

In Fig. 9 we see the curve for K_a. It cannot be used reliably as input for a simulation. But it can readily be derived from Fig. 8 dividing P_{nonlin} [Pa] by *excursion* [m].

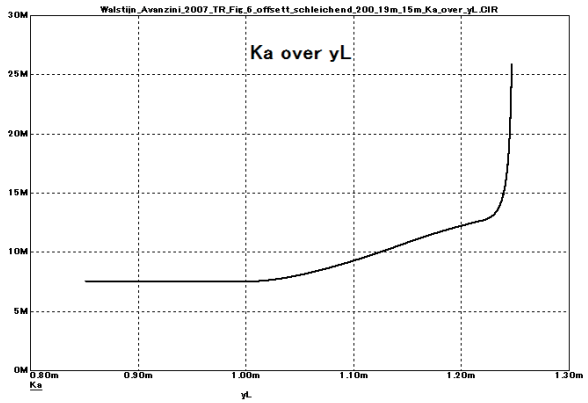

Fig. 9, K_a versus yL corresponding to Fig. 8

It is important to be aware that K_a is defined as depending on yL-*0.85mm* in the dynamic simulation of Fig. 6. But K_a itself as a function of Δp is only useful for static simulations. Because in the dynamic state yL not only depends on Δp but also on the momentary inertial and resistive forces of the reed mass L_{mech} and the resistance R_{mech} respectively.

2.5 Volume flow versus pressure difference

In [5] (section 5.2.1 and Fig. 8) the relation between volume flow and pressure difference is treated. There is some limit in the validity of (31) of [5]. Because for a positive volume flow u_f for $\Delta p>0$ it is required that $K_a > \Delta p/(ym - y0)$. The equation (31) is reproduced here as (2).

$$u_f = w\left[y_m - y_0 - \frac{\Delta p}{K_a(\Delta p)}\right]\sqrt{\frac{2\Delta p}{\rho}} \qquad (2)$$

Fig. 10 shows u_f versus $\Delta p>0$ using the force corresponding to Δp vs. yL of Fig. 8 in [4]. The result is similar to that of Fig. 8, "lumped (1)" in [5]. Additionally the effect of a softer reed is shown. The reed never closes completely due to the non-linearity which contains a hyperbolic function.

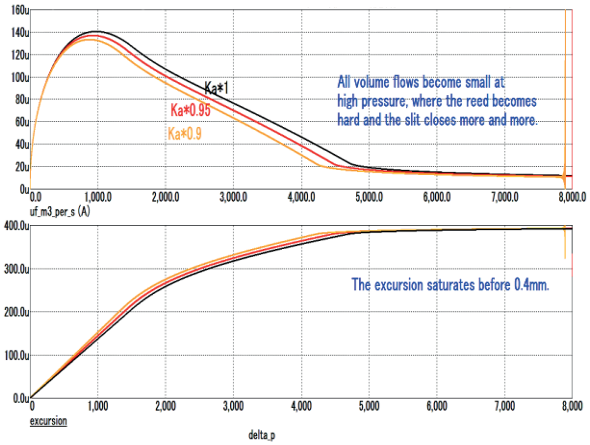

Fig. 10 Volume flow and excursion vs. pressure difference

3. CONCLUSION

It could be shown that a Circuit Analysis Program is well suited for studying mechanical and acoustical properties of a single reed generator for self sustained oscillations, as used e.g. in a clarinet. AC-analysis for frequency response of several parameters and TR-analysis for time dependent processes can be built up easily together with the needed models.

4. FUTURE WORK

That which was described here is just the beginning of the work on a refined model of the clarinet reed oscillator. It is used for testing of the reed part and the tools. One of the refinements is a distributed reed model similar to the one in [4]. This will then be coupled to a resonance tube. We intend to find out e.g. how many reed elements are needed to get a realistic simulation. This will include the behaviour of the reed generator depending on the distribution of stiffness, mass and resistance of the reed, the curve of the mouthpiece lay and the lip force and damping. A further goal is to develop a library of macros (elementary models) for the different parts of a clarinet or other woodwind instruments.

5. APPENDIX: UNAMBIGUOUS ELECTRO-MECHANICAL-ACOUSTICAL ANALOGIES

There are 3 domains, each with a clear-cut circuit region: electrical, mechanical, acoustical. The power of analogies is that any single concept which triggers the imagination (e.g. the concept "*velocity*") can be mapped from one domain to another without its perceived character changing. (We would never confuse velocity with deflection). But the units *do* change: the three velocity-like concepts *A*, *v*, *U* have different units [coulomb/s], [m/s], [m^3/s] (Table I).

Table I shows how the various expressions of any single notion are related, using the conventional symbols as far as possible. In choosing symbols for *quantities* we have some freedom (*vel*, *v*, *u* for velocity). But not in symbols for *units*. The use of S. I. units[1] (and their symbols) is mandatory (velocity is [m/s], not [miles/hour] and not [m/sec]). On the other hand symbols for *quantities* are just recommendations.

In mechanics there are 2 analogies:
(1) impedance analogy (volts ≡ force; el. current ≡ velocity),
(2) mobility analogy (volts ≡ velocity; el. current ≡ force).

We use analogy (1). It is more intuitive [6] and the extension to the acoustic domain, in which it is superior (topological similarity between circuit and physical arrangement) is easy: volts ≡ pressure, and I ≡ volume current. Nevertheless it must be admitted that (2) is topologically advantageous in mechanics. But it takes time to learn it.

We need in future to avoid confusion between two types of acoustic quantities: (1) *purely acoustic* quantities, e.g. acoustic stiffness K_{acoust} [Pa/(m^3/s)] common in general acoustics, but also sometimes used in reed literature[2]), and (2) *hybrid* quantities traditional in reed literature and appropriate here. *Impedances* (and impeding quantities such as stiffness) combine two different categories of variables[3]: "potential" and "motional" (here *pot* and *mot*). Examples of *pot* are force and pressure. Examples of *mot* are excursion, volume displacement, velocity, volume current [m^3/s].

"Pure-acoustic" stiffness K_{acoust} [Pa/(m^3/s)] is not the same as hybrid stiffness K_a [Pa/m] where the subscript "a" means "acoustic", but refers only to the *pot* quantity, the *mot* quantity in the denominator remaining mechanical. And yet both are called "acoustical". To derive the hybrid K_a from K_{mech} one multiplies K_{mech} by area *once*. To derive K_{acoust} one multiplies *twice*. In much of the reed literature the reader needs to do a lot of detective work to find out which one the author meant: pure acoustic or hybrid acoustic.

Table II collects more notions, mainly those used in the literature for acoustics and mechanics of wind instruments (see [4] and [5] and the references given there). Another source of confusion is the subscript *a*, which sometimes stands for "area" and sometimes for "acoustical".

[1] S.I. stands for Système International d'Unités)
[2] Fletcher [7], in his admittance Y_r (with negative real part), uses pure acoustic units [(m^3/s)/Pa].
[3] If *pot* is in the numerator *mot* is in the denominator: R_a = *pot*/*mot* = pressure/velocity [Pa/(m/s)].

Electricity			Mechanics			Acoustics		
Quantity	Symbol	Unit	Quantity	Symbol	Unit	Quantity	Symbol	Unit
Voltage	*U, u*	V	Force	*F*	N	Pressure	*p, P*	Pa = N/m^2
Current	*I, i*	A = C/s	Velocity	*v, u*	m/s	Volume Flow	*u, U, q*	m^3/s
Charge	*Q, q*	C = As	Excursion	*s, x, y*	M	Vol. Displacement	*Vol*	m^3
Inductance	*L*	H = Vs/A	Mass	*m*	Kg	Inertance, a. Mass	*M, M_a*	Pa.s^2/m^3 = kg/m^4
Capacitance	*C*	F = As/V	m. Compliance	*C_m*	m/N	a. Compliance	*C, C_a*	m^3/Pa
1/ Capacitance	*1/C*	1/F=V/As	m. Stiffness	*K_m*	N/m	a. Stiffness	*K, K_a*	Pa/m^3
Resistance	*R*	Ohm = V/A	m. Resistance	*R_m*	N/(m/s)=Ohm_m	a. Resistance	*R, R_a*	Pa/(m^3/s) = Ohm_a
Impedance	*Z*	Ohm = V/A	m. Impedance	*Z_m*	N/(m/s)=Ohm_m	a. Impedance	*Z, Z_a*	Pa/(m^3/s) = Ohm_a
Admittance	*Y*	Mho = A/V	m. Admittance	*Y_m*	(m/s)/N=Mho_m	a. Admittance	*Y, Y_a*	(m^3/s)/Pa = Mho_a
Power	*P*	W =VA	Power	*P*	W=Nm/s	Power	*P*	W=Pa.m^3/s = N.m/s
Energy	*W, E*	J = Ws	Energy	*W, E*	J=Nm	Energy	*W, E*	J= Pa.m^3 = N.m

Table I, Electro-mechanical-acoustical analogies

Hybrid System for impedance related quantities		
Quantity	Symbol	Unit
Hybrid Mass (or Hybrid Inertance)	*M_a*	kg/m^2
Hybrid Compliance	*C_a*	m/Pa
Hybrid Stiffness	*K_a*	Pa/m
Hybrid Friction	*R_a*	Pa.s/m
Hybrid Impedance	*Z_a*	Pa.s/m
Hybrid Admittance	*Y_a*	m/Pa.s

Table II, Hybrid system

Electrical definitions in MicroCAP			Used in these simulations and/or recommended by the authors		
Quantity	Symbol	Unit *)	Quantity	Symbol (.define)	Unit *)
Voltage	V, v	V	Mechanical Force	*Force*	N
Voltage	V, v	V	Acoustic Pressure	*P_m, P_b, delta_p*	Pa = N/m^2
Current	I, i	A	Mechanical Velocity	*velocity*	m/s
Current	I, i	A	Acoustic Volume Flow	*volflow*	m^3/s
Charge	Q, q	C = As	Mechanical Excursion	*yL*	m
Charge	Q, q	C = As	Acoust. Volume Displacement	*vol*	m^3
Inductance	L1, L2, ...	H = Vs/A	Mechanical Mass	*L_{mech}*	Kg
			Hybrid Mass	*M_a*	kg/m^2
Inductance	L1, L2, ...	H = Vs/A	Acoustic Mass, Inertance	*M_{aa}*	Pa.s^2/m^3 = kg/m^4
Capacitance	C1, C2, ...	F = As/V	Mechanic Compliance	*C_{mech}*	m/N
			Hybrid Compliance	*C_a*	m/Pa
Capacitance	C1, C2, ...	F = As/V	Acoustic Compliance	*C_{aa}*	m^3/Pa
1/ Capacitance	1/C1, 1/C2, ...	1/F = V/As	Mechanical Stiffness	*K_{mech}*	N/m
			Hybrid Stiffness	*K_a*	Pa/m
1/ Capacitance	1/C1, 1/C2, ...	1/F = V/As	Acoustic Stiffness	*K_{aa}*	Pa/m^3
Resistance	R1, R2, R3, ...	Ohm = V/A	Mechanical Friction	*R_{mech}*	kg/s = Ohm_m
			Hybrid Friction	*R_a*	Pa.s/m
Resistance	R1, R2, R3, ...	Ohm = V/A	Acoustic Resistance	*R_{aa}*	Pa.s/m^3 = Ohm_a
Impedance	Zel **)	Ohm = V/A	Mechanical Impedance	*Z_{mech}*	kg/s = Ohm_m
			Hybrid Impedance	*Z_a*	Pa.s/m
Impedance	Zel **)	Ohm = V/A	Acoustic Impedance	*Z_{aa}*	Pa/(m^3/s) = Ohm_a
			Damping factor, R_a/M_a (=R_{aa}/Maa =R_{mech}/L_{mech})	*g or g_{mech}*	1/s
			Reed damping factor =1/Q	κ_r used by Fletcher [7]	dimensionless

*) Not displayed in MicroCAP, **) Not defined in MicroCAP

Table III, Examples of symbols recommended by the authors to avoid ambiguity

Often in computer programming other (mostly longer) symbols are used, to avoid short variables that (1) might be reserved by the programming language for other purposes, and (2) would make the search function tedious.

Table III gives an overview of the definitions used as well as recommendations by the authors. The subscript *a* used *once* (as in K_a), means a hybrid impeding quantity. Used *twice* it means a purely acoustic impeding variable. This code reflects how often K_{mech} must be multiplied by A (reed area):
$K_a = K_{mech} \times A$,
$K_{aa} = K_{mech} \times A \times A$.

Note that explicit mention of the acoustic system is not always needed. For example the damping factor "*g*" ($=R_a/M_a$) is always the same whether *mech*, *a* or *aa*. The same applies to quality factor and resonance frequency.

In the models used here there is an ideal transformer that links the acoustical and the mechanical domains. Unlike the conventional transformer whose turns ratio *1:N* is dimensionless, in this one *N* is numerically equal to the area acting as interface. The side where 1 occurs is the acoustic part, N occurs on the mechanical side. This technique leads to a clear distinction of acoustics and mechanics. Another difference is that, whereas a conventional transformer can only transform AC signals, an ideal transformer can transform DC just as well.

Remark: There are four different area parameters:

(1) The mechanical area is that part of the reed that is free to oscillate and in the lumped model constitutes the so-called effective area, which is only meaningful when compared with a distributed reed model with approximately the same properties.

(2) The inner acoustic area lies inside the mouthpiece and is constant.

(3) The outer acoustic area is usually smaller than the inner one, as the lower lip of the player hinders the air pressure to act onto the rear part of the reed.

(4) The fourth area is not a solid surface. It is the cross-sectional area of the slit aperture perpendicular to air flow. This slit between mouthpiece tip and reed tip plays a role in introducing gaseous viscosity and inertial effects (inertance of the air mass). In our models this slit is always placed on the acoustical side of the circuit, but was omitted here for simplicity.

6. REFERENCES

[1] Micro-Cap, Electronic Circuit Analysis Program, Spectrum Software 1021 South Wolfe Road, Sunnyvale, CA 94086

[2] Schueller, F., Poldy, C.: Improving a G-high Clarinet using Measurement Data and an Electronic Circuit Analysis Program, Proceedings of the 3 rd Conference, Viennatalk, Sept. 2015

[3] Schueller, F., Poldy, C.: Using software simulation of the tone-hole lattice in clarinet-like systems, Proceedings of the 3 rd Conference, Viennatalk, Sept. 2015

[4] Avanzini, F., Walstijn, M.v.: Modelling the Mechanical Response of the Reed-Mouthpiece-Lip System of a Clarinet. Part I. A One-Dimensional Distributed Model, Acta Acustica united with Acustica, Vol. 90 (2004) 537 –547

[5] Walstijn, M.v., Avanzini, F.: Modelling the Mechanical Response of the Reed-Mouthpiece-Lip System of a Clarinet. Part II. A Lumped Model Approximation, Acta Acustica united with Acustica, Vol. 93 (2007) 435-446

[6] Philippow, Eugen, Taschenbuch Elektrotechnik, Band 3, Nachrichtentechnik, VEB Verlag Technik Berlin, 1969

[7] Fletcher, N. H.: Excitation mechanisms in woodwind and brass instruments, Acustica 43, 63-72 (1979).

SPATIAL MANIPULATION OF MUSICAL SOUND: INFORMED SOURCE SEPARATION AND RESPATIALIZATION

Sylvain Marchand
University of Brest, France
sylvain.marchand@univ-brest.fr

ABSTRACT

"Active listening" enables the listener to interact with the sound while it is played, like composers of electroacoustic music. The main manipulation of the musical scene is (re)spatialization: moving sound sources in space. This is equivalent to source separation. Indeed, moving all the sources of the scene but one away from the listener separates that source. And moving separate sources then rendering from them the corresponding scene (spatial image) is easy. Allowing this spatial interaction / source separation from fixed musical pieces with a sufficient quality is a (too) challenging task for classic approaches, since it requires an analysis of the scene with inevitable (and often unacceptable) estimation errors. Thus we introduced the informed approach, which consists in inaudibly embedding some additional information. This information, which is coded with a minimal rate, aims at increasing the precision of the analysis / separation. Thus, the informed approach relies on both estimation and information theories. Since the initial presentation at VITA 2010, several informed source separation (ISS) methods were proposed. Among the best methods is the one based on spatial filtering (beamforming), with the spectral envelopes of the sources (perceptively coded) as additional information. More precisely, the proposed method is realized in an encoder-decoder framework. At the encoder, the spectral envelopes of the (known) original sources are extracted, their frequency resolution is adapted to the critical bands, and their magnitude is logarithmically quantized. These envelopes are then passed on to the decoder with the stereo mixture. At the decoder, the mixture signal is decomposed by time-frequency selective spatial filtering guided by a source activity index, derived from the spectral envelope values. The real-time manipulation of the source sources is then possible, from musical pieces initially fixed (possibly on some support like CDs), and with an unequaled (controllable) quality.

MODELING THE SPECTRUM STRUCTURE WITHIN THE NMF FRAMEWORK. APPLICATION TO INHARMONIC SOUNDS

Bertrand David[1]*, Francois Rigaud*[2]*, Laurent Daudet*[3]
[1] Institut Mines-Télécom; Télécom ParisTech; CNRS LTCI , France
[2] Audionamix, France
[3] Institut Langevin; Paris Diderot Univ.; ESPCI ParisTech; CNRS, France
bertrand.david@telecom-paristech.fr
francois.rigaud@audionamix.com
laurent.daudet@espci.fr

ABSTRACT

The Non negative Matrix Factorization has received much attention during the last decade, with some remarkably successful applications in the field of audio source separation or automatic music transcription. To that aim, prior information and modeling have often been included in the general framework to account for our knowledge on the spectral structure of sounds, such as the harmonicity, characteristic of a number of musical sounds, or the smoothness of their spectrum envelope. These help the algorithm to approach a relevant solution. The NMF indeed decomposes a non negative time-frequency representation of a musical scene into the product of low rank non negative matrices: the matrix of spectral atoms or templates and the matrix of their time activation. But this decomposition is not unique and moreover it is not rare that the convergence reaches a local minimum of the cost function where the spectral atoms are not easily identifiable, or at least, have to be post-processed either to separate the contributions of different audio events or to aggregate them to recover a single, coherent, musical note. This presentation will review techniques we developed in the past few years to model the spectrum structure within the NMF framework and their application to analyze inharmonic sounds, such as those of the piano. This allows us to examine some of large scale properties that characterize the state of the instrument, like the design of its tuning, or the inharmonicity curve along the whole compass.

TOWARDS REALISTIC AND NATURAL SYNTHESIS OF MUSICAL PERFORMANCES: PERFORMER, INSTRUMENT AND SOUND MODELING

Alfonso Perez, Rafael Ramirez

Music Technology Group
Universitat Pompeu Fabra, Barcelona, Spain
alfonso.perez@upf.edu

ABSTRACT

Imitation of musical performances by a machine is an ambitious challenge involving several disciplines such as signal processing, musical acoustics or machine learning. The most important techniques are focused on modeling either the instrument (physical models) or the perceived sound (signal models) and advances in the last decades in the field of sound synthesis allow for the recreation of highly realistic sounds. However, these models generally lack an explicit representation of the performer and the consequence is that despite the realistic sounds, synthetic reproductions do not sound natural as a human performance. The role of the performer is usually captured with expressivity models and more recently, on the analysis of instrumental controls acquired during real performances.

In this work we present a framework that combines the modeling of the characteristics of the sound, the instrument as well as the performer in order to render natural performances with realistic sounds automatically from a musical score. The framework is based on a source-filter model, which is driven by performer controls. Performer modeling is based on automatic rendering of perceptual features (i.e. fundamental frequency, energy, timbre and tempo contours); sound source is modeled through functions that map those perceptual features into spectral envelopes, which are translated into the temporal domain through additive synthesis; and the instrument is represented as a multi-directional filter that encodes the sound radiation properties of the instrument body. The case study is the violin, but the framework is general and could be applied to any kind of musical instrument.

1. INTRODUCTION

A musical performance can be regarded as a process in which symbolic information in the form of a musical score is transformed into sound. The main components in this process are the performer and the music instrument. The performer interprets the score and generates a sequence of actions that control the instrument, which in turn produces the sound. It is therefore of paramount importance in order to produce realistic and natural synthetic sounds, to model both the instrument sound as well as the performer. In this work, we mean by realistic, how the synthetic sound resembles that of the instrument, and natural, it is related to the sound evolution in time and the resemblance to a human performance.

Sound synthesis techniques for musical instruments [1, 2] can be divided into two main categories, physical models [3] that are focused on the sound production mechanism of the instrument, and signal models [4, 5, 6, 7] that are focused on the perceived sound. These techniques are used with great success with impulsively excited instruments such as hammered strings [8] or plucked strings [9], however, in the case of continuously excited instruments such as bowed strings or wind instruments, for which the degree of control is much higher, obtaining a natural sounding synthesis is still an open issue and it is a consequence of the lack of an explicit representation of the performer in the models.

The role of the musician in a musical performance is usually approached through computational techniques for modeling expressive performances. So called expressivity models, aim to describe and characterize deviations in a real performance from the musical score. Deviations come in the form of continuous numerical aspects of expressivity, mainly timing, dynamics and pitch. The inclusion of the performer in synthesis models has been the main subject in the recent work by Perez-Carrillo [10] and Maestre [11] with the violin, based on a representation of the performer as continuous bowing controls. Although this technique is able to render much more natural and realistic sounds than previous techniques, the performer representation is specific to bowed strings. Grounded on this previous work [12, 13, 10], we aim to provide a more general framework that can be extended to other types of instruments by representing the performer as features typical in expressivity models, instead of instrumental controls.

A musical instrument can be seen as the association of an exciter and a resonator. The exciter produces the excitation vibration (glottal chords, lips, reed or bow-string interaction) but does not produce sound and the resonator is the sounding structure (body and air cavity) that acts as a sound radiator. The excitation is typically non-linear and resonating bodies are mostly linear, passive (dissipate energy) and harmonically resonating structures. Based on this assumption, we approach the rendering of the sound of the instrument as a source-filter (exciter-resonator) model.

This works proposes a framework for realistic and natural synthesis of musical instruments by combining the modeling of the characteristics of the sound, the instrument as well as the performer. The procedure, represented in Figure 1, is based on a source-filter model, which is driven by performer controls. The first module is responsible for the representation of performer. It involves the automatic rendering of the most important perceptual features that are related to expressivity, namely, energy envelope, fundamental frequency ($f0$), tempo and timbre. These features conform the controls that drive the second module, the sound source synthesis engine. This module is responsible for mapping the timbre feature to harmonic and residual spectral envelopes. These envelopes are then filled with harmonic content corresponding to the pitch and filtered white noise for the residual part and translated to the time domain through additive synthesis. The third module is related to the acoustics of the instrument and consists of a model of sound radiation represented as filters that filter the source signal.

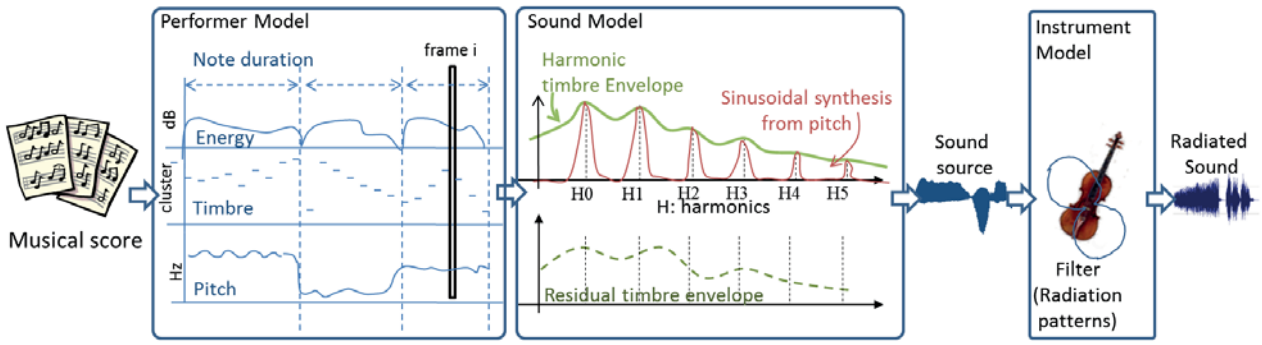

Figure 1: The synthesis framework procedure is based on a source-filter model driven by performer controls. The first module involves the automatic rendering of the most important perceptual features that are related to the performer, namely, energy, fundamental frequency ($f0$), tempo and timbre. These features conform the controls that drive the second module, the sound source synthesis engine, which is responsible for mapping the timbre feature to harmonic and residual spectral envelopes. These envelopes are then filled with harmonic content corresponding to the pitch and filtered white noise for the residual part and translated to the time domain through additive synthesis. The third module is related to the acoustics of the instrument and consists of a model of sound radiation represented as filters that filter the source signal.

2. PERFORMER MODEL

The role of the performer is represented by expressive contours of $f0$, energy, timbre and tempo. Given a symbolic representation of a musical score, the performer model generates contours for these four parameters. This process of transformation between a symbolic domain to a continuous control signal domain is represented in Figure 2. It starts by enhancing (manually or automatically) a musical score with explicit indications about the way of playing (i.e. articulations, slurs, fingering and dynamics) followed by a codification into intra-note segments for which a local envelope is generated. Finally, envelopes are stretched in time and amplitude to match the estimated segment duration 2.5. Two approaches are proposed for the generation of the segment envelopes. The first one consists of a concatenation of intra-note median contours, which is used for the generation of $f0$ (Section 2.2) and the second one is a concatenation of note envelopes retrieved from the database, used for the energy (Section 2.3). Alternative more sophisticated techniques for the rendering of such control contours are found in [11, 14].

2.1. Score codification as intra-note segments

Codification of the musical score as intra-note segments (Figure 2) is of crucial importance as the evolution of performer parameters (specially pitch and energy) largely depend on the type of segment and they show common patterns inside each of the categories. The definition of categories is based on a previous analysis of intra-note segments and bowing parameters in violin playing [15].

2.1.1. Attacks

There are two main types of attacks, *isolated attacks* and *connected attacks*. *Isolated attacks* are found after a silence and *connected attacks* are contiguous to the preceding note and therefore codified as part of a note transition. *Isolated attacks* are, in the case of the violin, divided into *on-string* and *off-string*. A *on-string attack* starts with the bow in contact with the string and it is typically found in *staccato* (and similar strokes such as *martelé*) and can also be found at the first note of a series of *legato* or *detaché*. During *off-string* attacks the bow has an air-borne phase before it gets in contact with the string. Typical bowing strokes with *off-string* attacks are bouncing bow-strokes (e.g. *spiccato*, *saltato*) and can also be found at the first note of a legato or detaché sequence.

2.1.2. Transitions

Note-transitions are segments where a change of note occurs. They are unstable parts where the first note is finishing (release) and the second is beginning (attack). The main bow strokes involved are *detaché* and *legato*. Note transitions in violin playing can be mainly caused through four types of changes in control actions (and their combinations, making a total of 15 types of transitions), a change in the of the pressing finger, a left hand position change, a change of string and a change of bowing direction.

2.1.3. Releases

We only label as releases the ones that are followed by a silence. Releases in contiguous notes are treated as part of a transition. We can identify two types, the first one is the freely-vibrating *release* that lasts until the string stops vibrating by itself, and the second type is the broken *release*, which is caused by stopping the string with the bow.

2.2. Pitch Contour Rendering

Pitch is rendered as a piecewise function of intra-note pitch segments corresponding to the note's attack, sustain, transition and release (Figure 2). A database of violin performances was automatically segmented and labeled according to those categories [15]. For each category, all the matching segments in the database are normalized in length and amplitude and the median pitch contour is used as representative. During the pitch rendering process, representatives of each segment are retrieved, time-stretched to match the note duration and amplitude-stretched to match the difference in the nominal note pitches and finally, the contours are concatenated.

Sustains are treated differently as they are highly variable in duration and may include vibrato. In this case (sustains), the pitch is rendered flat and vibrato is added in sustains longer than the vibrato offset (Figure 3). Vibrato curve is rendered by spectral synthesis of a sinusoid with associated frequency and amplitude envelopes that include fade-ins and fade-outs (Figure 3).

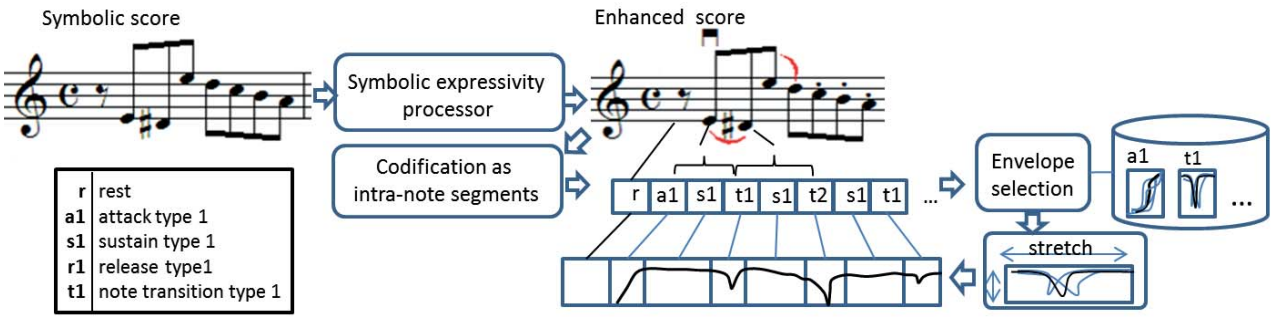

Figure 2: Process of transformation from a symbolic musical score to continuous control signals. It starts by enhancing a musical score with explicit indications about the way of playing (i.e. articulations, slurs, fingering and dynamics) followed by a codification into intra-note segments for which a local envelope is generated. Finally, envelopes are stretched in time and amplitude to match the estimated segment duration.

All parameters of the vibrato can be customized and randomly altered.

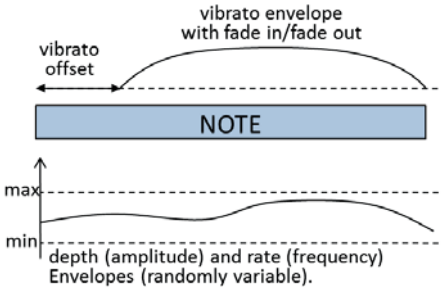

Figure 3: Vibrato is rendered by spectral synthesis of a sinusoid with associated frequency and amplitude envelopes that include fade-ins and fade-outs.

2.3. Energy Contour Rendering

The same procedure applied to the pitch based on concatenation of medians of intra-note segment categories was applied with little success. Instead of that method, sampling was used. For each note in the score, the most similar note in the database is selected according to the note context (duration, dynamics and articulation) and the context of the surrounding notes (previous and next). Finally the selected energy envelope is time-stretch to match the note duration.

2.4. Timbre Trajectory

Timbre in the database is encoded as a number corresponding to a cluster in the timbre space of the database. Details about the timbre space are given in Section 3. The timbre trajectory of a note is then represented as a series of consecutive cluster numbers for each frame in the note. The synthesis of a timbre trajectory is carried out in the same manner as the energy, that is, by retrieving from the database the timbre trajectory of the closest note. Then, for each frame of the timbre trajectory the spectral envelope of the center of the cluster is used. Finally, smoothing between consecutive frames belonging to different clusters is applied.

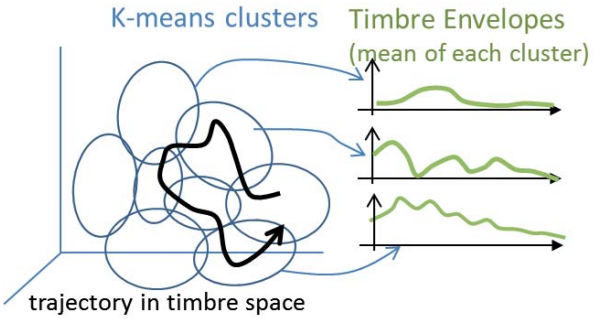

Figure 4: The timbre space is divided into clusters. A timbre trajectory is represented as a series of consecutive cluster numbers. Each sound frame in the database has an associated timbre cluster. To recreate its spectral content, it is mapped into the spectral envelopes corresponding to the enter of the cluster.

2.5. Tempo

Tempo is represented as the note duration rate respect to the nominal note duration in the score. It is computed by training feed-forward neural networks with the following inputs at the current, previous and next note: score tempo, dynamics [pp,p,mf,f,ff], note duration in beats, metrical strength [0..1] and melodic boundary [0..1]. The melodic boundary is computed following the local boundary detection model by Cambouropoulos [16]. The output of the neural network is the rate between the notes' duration in the score and in a performance of the score. Alternative methods are reported in [17, 18].

3. SOUND-SOURCE MODEL

The sound-source in bowed strings corresponds to the vibration of th string. The model is based on spectral analysis of the recordings in the database [10] based on the harmonic plus residual model [19]. Harmonic and residual components are both represented as the energy in 40 overlapping frequency bands with centers following a logarithmic scale. The band's overlapping factor is 50% and the energy of each band is estimated as the average of the corresponding frequency bins, weighted by a triangular function. The selection of the bands is inspired by perceptual models such as the Mel scale. In the case of the harmonics, the amplitude at each bin is determined by a *harmonic envelope*. This envelope is obtained at each frame by interpo-

lating harmonic peaks using a 3rd order spline (see Figure 5).

Harmonic and residual timbre space (40-dimensional) are built with all the computed envelopes in the database (normalized to the energy) and a K-means algorithm is run to automatically partition the space into 32 timbre clusters. Each cluster represents a specific envelope shape. Timbre characteristics of any audio fragment can then be represented as a succession of cluster and each cluster is represented by the 40 spectral envelope coefficients of its center as explained in Subsection 2.4 and Figure 4.

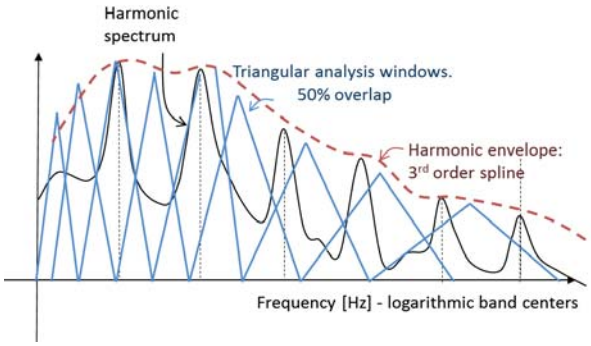

Figure 5: Harmonic and residual components are both represented as the energy in 40 overlapping frequency bands with centers following a logarithmic scale. The energy of each band is estimated as the average of the corresponding frequency bins, weighted by a triangular function. In the case of the harmonics, the amplitude at each bin is determined by a *harmonic envelope*, which is obtained at by interpolating harmonic peaks using a 3rd order spline.

4. INSTRUMENT SOUND RADIATION

The third and last module of the framework is the model of the resonator, the sound radiator structure of the instrument, which determines the characteristic color of the sound of the specific instrument. One of the advantages of modeling this part separately is the possibility of simulating different instruments of the same family as well as the simulation of directional sound effects. In a simplified model of sound production and perception, we can consider this part to be linear. It is usually modeled as a linear filter [20, 21] by measuring its response to a known excitation and computing its body transfer function (BTF) or body impulse response (BIR). There exist many different methods to obtain BTF's depending on the specific instrument.

The presented method here is based on previous work[13] where violin BIR are measured based on non-impulsive deconvolution of signals. Excitation signal was applied by bowing glissandi (sweeping the lowest octave) and the response was measured simultaneously with a bridge-pickup and a microphone in an anechoic chamber. An impulse response is obtained by performing a deconvolution between these non-impulsive bridge-pickup and microphone recordings.

The deconvolution process (Figure 6) starts with the alignment of excitation and response signals. Then, both signals are windowed and expressed in the spectral domain, obtaining two frame streams that are aligned in time. At this point, we apply a frame-by-frame deconvolution. The magnitude is weighted and averaged by the energy content of each spectral bin. Regarding the phase, due to its cyclic behavior, carrying out a classical weighted average would not provide good estimations. As a first attempt, we explored a method based on constructing a histogram of the phase values estimated for each spectral bin, weighted by their corresponding energy. However, the resulting BIR's were not causal, so finally we computed the minimum phase BIR's from the estimated BTF magnitudes by using the cepstrum and converting anti-causal exponentials to causal exponentials [22].

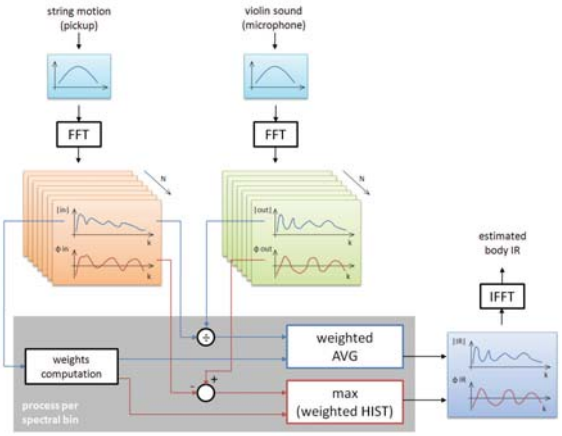

Figure 6: Schematic block diagram of the body impulse response estimation process.

Using multiple microphones, it is possible to simultaneously measure a set of impulse responses in various directions around the violin. The impulse responses can be convolved with a source signal, which improves the sound quality of the synthesizer and allows the simulation of sound directivity effects. Figure 7 shows an example of directivity patterns in the violin.

Although the method is used here for the violin, this is a general procedure that can be applied to other musical instruments as well. The requirement is that there must be a way to measure an excitation signal together with the response signals.

4.1. Directional sound effects

By computing several BTF's around the instrument, we can recreate the sound perceived by a listener at different directions and provide a better listening experience by simulating effects such as stereo or the movement of the player. Stereo can be simulated by using two different BIR's, one for each ear. The movement of the performer is another important effect. Ancillary gestures are constantly changing the position and orientation of the instrument, so the listener is perceiving the sound radiated at continuously changing directions. To simulate this motion we need to estimate the situation of the listener with respect to the sound source and apply a dynamic convolution with the corresponding BIR at each instant. Typical durations of a BIRs restrict the rate at which the listener position can be updated that may result in significant changes between consecutive convolutions. In order to avoid this artifact, an algorithm for dynamic convolution is proposed based on the fragmentation of BIR's into smaller sub-BIR's and a convolution algorithm that processes sub-BIRs concurrently and a sum of all the running convolutions is delivered.

5. CONCLUSIONS

We have presented a framework that combines the modeling of the characteristics of the sound, the instrument as well as the

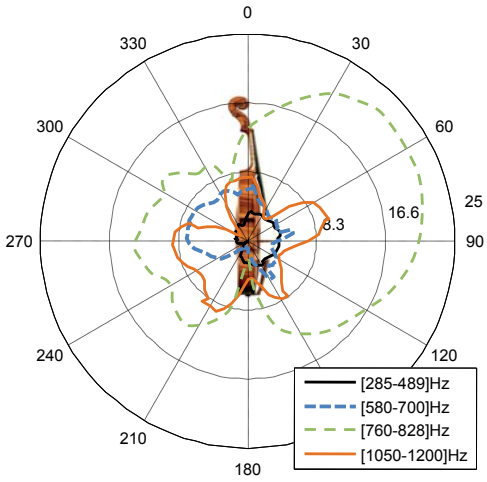

Figure 7: Directivity patterns in the x-z plane. Violin directivity at different frequencies. The patterns show the difference [dB] of sound levels depending on frequency and direction. The patterns were obtained with the performer holding the violin.

performer in order to render natural performances with realistic sounds automatically from a musical score. The framework is based on a source-filter model, which is driven by performer controls. Performer modeling is based on automatic rendering of perceptual features (i.e. fundamental frequency, energy, timbre and tempo contours); sound source is modeled through functions that map those perceptual features into spectral envelopes, which are translated into the temporal domain through additive synthesis; and the instrument is represented as a multidirectional filter that encodes the sound radiation properties of the instrument body. The case study is the violin, but the framework is general and could be applied to any kind of musical instrument.

Acknwoledgements

This work has been partly sponsored by the Spanish TIN project TIMUL (TIN2013-48152-C2-2-R).

6. REFERENCES

[1] Julius Orion Smith, "Viewpoints on the history of digital synthesis," in *Proc. Int. Computer Music Conf.*, Montreal, October 1991, pp. 1–10.

[2] Tero Tolonen, Vesa Vlimki, and Matti Karjalainen, "Evaluation of modern sound synthesis methods," Tech. Rep., 1998.

[3] Julius Orion Smith, "Physical modeling synthesis update," Tech. Rep., 2000.

[4] Jordi Bonada and Xavier Serra, "Synthesis of the singing voice by performance sampling and spectral models," *IEEE signal processing magazine*, vol. 24, pp. 67–80, 2007.

[5] Jordi Bonada, *Voice Processing and Synthesis by Performance Sampling and Spectral Models*, Ph.D. thesis, Universitat Pompeu Fabra, Barcelona, Spain, 2008.

[6] Eric Lindemann, "Musical synthesizer capable of expresive phrasing," *J. Acoust. Soc. Am.*, vol. 117, pp. 2700–2730, 2005.

[7] Bernd Schoner, *Probabilistic Characterization and Synthesis of Complex Driven Systems*, Ph.D. thesis, MIT Media Lab, Cambridge, Massachusetts, USA, 2000.

[8] Vesa Välimäki, Henri Penttinen, Jonte Knif, Mikael Laurson, and Cumhur Erkut, "Sound synthesis of the harpsichord using a computationally efficient physical model," *EURASIP J. on Appl. Signal Processing*, vol. 2004, pp. 934–948, 2004.

[9] Vesa Välimäki and Tero Tolonen, "Development and calibration of a guitar synthesizer," *J. Audio Engineering Soc.*, vol. 46, no. 9, pp. 766–778, September 1998.

[10] A. Pérez-Carrillo, J. Bonada, E. Maestre, E. Guaus, and M. Blaauw, "Performance control driven violin timbre model based on neural networks," *IEEE Transactions on Audio, Speech, and Language Processing*, vol. 20, no. 3, pp. 1007 –1021, March 2012.

[11] Esteban Maestre, Merlijn Blaauw, Jordi Bonada, Enric Guaus, and Alfonso Pérez, "Statistical modeling of bowing control applied to sound synthesis," *IEEE Transactions on Audio, Speech and Language Processing. Special Issue on Virtual Analog Audio Effects and Musical Instruments*, vol. 18, no. 4, pp. 855–872, 2010.

[12] Alfonso Perez, *Enhancing Spectral Synthesis Techniques with Performance Gestures using the Violin as a Case Study*, Ph.D. thesis, Universitat Pompeu Fabra, Barcelona, Spain, 2009.

[13] Alfonso Pérez-Carrillo, Jordi Bonada, Jukka Ptynen, and Vesa Välimäki, "Method for measuring violin sound radiation based on bowed glissandi and its application to sound synthesis," *J. Acoust. Soc. Am.*, vol. 130, pp. 1020–1029, 2011.

[14] Akshaya Thippur, Anders Askenfelt, and Hedvig Kjellström, "Probabilistic modeling of bowing gestures for gesture-based violin sound synthesis," in *proceedings of SMAC*, 2013.

[15] Alfonso Pérez-Carrillo, "Characterization of bowing strokes in violin playing in terms of controls and sound: Differences between bouncing and on-string bow strokes.," in *Proceedings of International Conference on Acoustics*, 2013.

[16] Emilios Cambouropoulos, "The local boundary detection model (lbdm) and its application in the study of expressive timing," in *In: Proc. of the International Computer Music Conference, Havana*, 2001.

[17] Rafael Ramirez, Esteban Maestre, and Alfonso Perez, *Guide to Computing for Expressive Music Performance*, chapter Chapter 5: Modeling, Analyzing, Identifying, and Synthesizing Expressive Popular Music Performances, pp. 123–144, Springer-Verlag, London, 2013.

[18] Rafael Ramirez, Alfonso Perez, Stefan Kersten, David Rizo, Placido Roman, and Jose M Inesta, "Modeling violin performances using inductive logic programming," *Intelligent Data Analysis*, vol. 14, pp. 573–585, 2010.

[19] Xavier Serra, *A System for Sound Analysis/Transformation/Synthesis based on a Deterministic plus Stochastic Decomposition*, Ph.D. thesis, Stanford University, 1989.

[20] Angelo Farina, Andreas Langhoff, and Lamberto Tronchin, "Subjective comparisons of 'virtual' violins obtained by convolution," in *Proc. 2nd Int. Conf. on Acoustics and Musical Research*, Ferrara, Italy, May 1995, pp. 36–41.

[21] Lothar Cremer, *Physics of the Violin*, pp. 201–382, The MIT Press, Cambridge, MA, November 1984.

[22] A. V. Oppenheim and R. W. Schafer, *Digital Signal Processing*, chapter 10, pp. 480–531, Prentice Hall Press, Upper Saddle River, NJ, 1975.

A COMPARISON OF SINGLE-REED AND BOWED-STRING EXCITATIONS OF A HYBRID WIND INSTRUMENT

Kurijn Buys, David Sharp, and Robin Laney

Faculty of Mathematics Computing and Technology,
The Open University, Milton Keynes, UK
Kurijn.Buys@open.ac.uk

ABSTRACT

A hybrid wind instrument is constructed by connecting a theoretical excitation model (such as a real-time computed physical model of a single-reed mouthpiece) to a loudspeaker and a microphone which are placed at the entrance of a wind instrument resonator (a clarinet-like tube in our case). The successful construction of a hybrid wind instrument, and the evaluation with a single-reed physical model, has been demonstrated in previous work [1, 2]. In the present paper, inspired by the analogy between the principal oscillation mechanisms of wind instruments and bowed string instruments, we introduce the stick-slip mechanism of a bow-string interaction model (the hyperbolic model with absorbed torsional waves) to the hybrid wind instrument set-up. Firstly, a dimensionless and reduced parameter form of this model is proposed, which reveals the (dis-)similarities with the single-reed model. Just as with the single-reed model, the hybrid sounds generated with the bow-string interaction model are close to the sounds predicted by a complete simulation of the instrument. However, the hybrid instrument is more easily destabilised for high bowing forces. The bow-string interaction model leads to the production of some raucous sounds (characteristic to bowed-string instruments, for low bowing speeds) which represents the main perceived timbral difference between it and the single-reed model. Another apparent timbral difference is the odd/even harmonics ratio, which spans a larger range for the single-reed model. Nevertheless, for both models most sound descriptors are found within the same range for a (stable) variety of input parameters so that the differences in timbre remain relatively low. This is supported by the similarity of both excitation models and by empirical tests with other, more dynamic excitation models.

1. INTRODUCTION

The development and early evaluation of a hybrid wind instrument using a loudspeaker has been described in earlier work [1, 2]. Figure 1 explains the concept: a physical "excitation model" (for instance a single-reed embouchure) is simulated on a computer and interacts with a real acoustical resonator so that the whole is able to generate hybrid self-sustained sounds.

Such a device supports two main research interests. First, placing it in the context of acoustic wind instrument research, it would be of substantial value to have a repeatable and precisely quantified control over an exciter that is linked to a resonator of interest. This matches with the objectives of the now well-established "artificial mouths" for wind instruments (e.g. [3]). A second interest, is the exploration of the device's potential as a musical instrument, mostly from the timbre perspective, which is an active musical focus of today. Here, the same control precision can play a role in the accessibility of certain (variations of) sounds. While, the computed environment allows

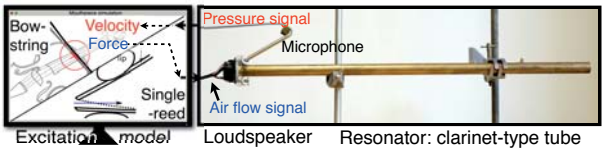

Figure 1: The hybrid wind instrument set-up: a computed excitation model (a single-reed embouchure model or a bow-string interaction model) in interaction with a physical resonator by means of a loudspeaker and a microphone.

modeling any conceivable excitation and handles electronic parameter variations, the physical control over the resonator (the fingering) remains, which opens up an alternative range of musical expression with the advantage of relatively low computational power needs.

Only minor contributions on the hybrid wind instrument concept have been made to date. Maganza first briefly explored a set-up [4] and since then a small number of works on closely related subjects have been carried out, for example [5, 6, 7]. More recently, an identical approach has been implemented, but using an electrovalve as flow actuator [8]. For our hybrid instrument, a loudspeaker is used to perform the actuation and it has been shown that, by introducing some correcting filters, a very good accuracy can be achieved, so that realistic clarinet tones can be produced [1, 2]. The hybrid instrument set-up is briefly reviewed in section 2.

Given the similar fundamental oscillation principle of wind and bowed string instruments [9], the pressure and air-flow at the resonator entrance can be interpreted by the computer as respectively a string velocity and force, so that the stick-slip mechanism of a bow-string interaction model (hereafter referred to as a BS model) can be introduced to the hybrid wind instrument set-up. This idea is of particular musical interest, since such a physically impossible combination can potentially lead to uncommon timbres.

In the present paper, we compare the quasi-static single-reed embouchure model (hereafter referred to as the SR model) and a BS model and their evaluation with the hybrid wind instrument. While an earlier study by Ollivier et al. [10] has discussed the analogy between woodwinds and the bowed string, their BS model was based on a mathematical simplification of the hyperbolic model [9] whose parameters have a poor connection to the physical reality. This model was initially introduced by Weinreich and used later by Müller for their hybrid string instruments [11, 12]. In our study, we propose a dimensionless and reduced parameter form of the original hyperbolic BS model.

After the presentation of the SR and BS models in section 3, in section 4 a theory for the estimation of sound features is

proposed and applied for those excitation models. In section 5 both excitation models are evaluated with the hybrid instrument and with an entire simulation.

We note that, for simplicity, the t argument for time domain signals is not repeated after the introduction of a variable.

2. PRESENTATION OF THE HYBRID WIND INSTRUMENT

Preliminary work has been carried out to investigate the behaviour of a loudspeaker mounted on a tube [1, 2, 13] (see those papers for a detailed explanation).
As the loudspeaker doesn't provide an ideal rigid termination to the tube, coupled physical models of the loudspeaker and tube are considered. Also, measurements are performed to find the parameter values that are used both to predict a calibrated "flow rate response" for the loudspeaker and to account for the coupling. For coherent functioning of the hybrid instrument, the calculated flow rate signal by the excitation model should be acoustically reproduced by the loudspeaker as a physical air flow. Therefore, two filters are considered: a feedforward filter, to flatten the loudspeaker response and a feedback filter, to account for the coupling with the tube. These filters are executed by the real-time computing system[1] that is also used to execute the excitation models. The resonator is a clarinet-like tube with an inner diameter of 14.2 mm, a length of 58 cm and entrance impedance $Z_t = \frac{P}{Q}$ (where P and Q are the Fourier transform of respectively the pressure $p(t)$ and air flow rate $q(t)$ at the resonator entrance). Its first resonance frequency is found at 139.8 Hz while, for example, the fifth resonance lies at 1275.3 Hz. This is 17.2 Hz higher than the integer multiple of the first resonance, which attests for a positive inharmonicity.

2.1. Accounting for the loudspeaker

Figure 2 depicts a schematic diagram of the implemented feedforward- and feedback filters to account for the presence of the loudspeaker (we used a 1 " Tang Band loudspeaker of type W1-1070SE with an additional mass on the membrane).

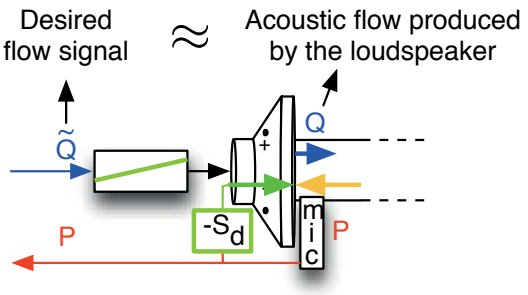

Figure 2: A feedback- and a feedforward filter account for the loudspeaker

Assuming the loudspeaker to be a simple mass-spring-damper system, the feedforward filter that would undo its response would simply be the inverse of the loudspeaker transfer function. The loudspeaker's resonant frequency lies far enough below the playing frequencies so that mainly the inertia is of importance, which can be compensated by a derivative filter. Further, a "lead-lag filter" is also added to compensate for phase deviations near the loudspeaker resonant frequency (for a detailed description, see [13]). The total filter is found to effectively flatten the gain response of the filter-loudspeaker system, while the phase response remains at 0 just after the loudspeaker resonance and then slowly decreases by about $18°\text{kHz}^{-1}$ (which cannot be compensated for).

When the loudspeaker is placed at the entrance of the tube, the strong pressure variations in front of it will impose an important force on the membrane so that those components will be in a coupled interaction. A simple resolution for this issue is based on Newton's third law: in order to undo the force on the loudspeaker diaphragm (with area S_d) due to the pressure p in front of it (measured with a microphone), it is necessary to add an opposite force ($-S_d\ p$) to the electric force generated by the voice coil. This can be done with a feedback filter, by taking into account the voltage-to-force transfer function of the electrical loudspeaker part.

Altogether, the impedance $\widetilde{Z}_{ts} = \frac{\widetilde{Q}}{P}$, measured with a sine-swept signal on the filters-loudspeaker-tube-system (that will be put in interaction with the excitation model), turns out to be fairly close to the original measured tube impedance $Z_t = \frac{Q}{P}$. The zero-crossings of their phase responses, which are an important indicator for potential self-sustained playing frequencies, match reasonably well. Finally it is noted that the increasing phase lag (and another nonlinear side-effect which we will not discuss in the present paper), causes the initially positive inharmonicity in Z_t to become negative in the impedance that is visible to the programmed excitation model.

3. SINGLE-REED AND BOW-STRING EXCITATION MODELS

This section provides a physical description of the excitation models. For the numerical implementation it is important to consider that the physical situation, which is bi-directional in nature, needs to be converted into a looped sequential procedure. This involves converting the presented "implicit equations" into "explicit equations" which exceeds the scope of this paper (however, for the numerical evaluation the explicit equations are used).

3.1. Single-reed embouchure model

For the SR model, we adopted the classical theory from Wilson and Beavers [3] (and further developed in [15]).

3.1.1. Physical model

The reed (including the player's lower lip) is considered to behave as a mass-spring-damper system, driven by the pressure difference across the reed $\Delta p(t) = p_m - p$ (with p_m the mouth pressure and $p(t)$ the pressure inside the mouthpiece), acting on part of the reed surface S_r. Hence, the reed's dynamics are described by:

$$\frac{1}{\omega_r^2}\frac{d^2\,y}{dt^2} + \frac{1}{Q_r\,\omega_r}\frac{d\,y}{dt} + y = \frac{-S_r \Delta p}{k}, \qquad (1)$$

with $y(t)$, the displacement of the reed with stiffness k, resonance frequency ω_r and quality factor Q_r.

The air flow that enters the instrument can be expressed as the product of the flow velocity $v_f(t)$ and the effective reed opening cross-section S_f. The former can be found by the Bernoulli theorem applied between the mouth and the reed flow

[1] In order to fulfill the real-time requirements, we made use of the *Xenomai* framework [14], applied on a standard PC equipped with an acquisition card (with analogue in and outs). A sampling rate of $f_s = 40$ kHz could be obtained, which is high enough for our purpose.

channel (thus between the mentioned pressure difference) and the latter is assumed to be linearly related to the reed displacement. The resulting flow rate can be expressed as:

$$q = \underbrace{sgn(\Delta p)\sqrt{\frac{2|\Delta p|}{\rho}}}_{v_f}\underbrace{\mathcal{H}(y+H)(y+H)w}_{S_f},$$

where ρ is the air density and w is the effective reed width. The sgn operator is introduced to make the calculation of negative flows possible and the Heaviside function $\mathcal{H}$ to hold a zero flow rate when the reed hits against the lay at position $y = -H$, which occurs above the "beating pressure" P_M .

These equations can be simplified and made dimensionless by defining $\bar{y} = \frac{y}{H}$, $\bar{p} = \frac{p}{P_M}$, $\bar{q} = \frac{q\,Z_c}{P_M}$, $\bar{\Delta p} = \frac{\Delta p}{P_M}$:

$$\begin{cases} \dfrac{1}{\omega_r^2}\dfrac{d^2\,\bar{y}}{dt^2} + \dfrac{1}{Q_r\,\omega_r}\dfrac{d\,\bar{y}}{dt} + \bar{y} = -\Delta p \\ \bar{q} = sgn(\bar{\Delta p})\sqrt{|\bar{\Delta p}|}\zeta\mathcal{H}(\bar{y}+1)(\bar{y}+1), \end{cases} \tag{2}$$

where ζ lumps all remaining embouchure parameters together and its time variation is related to the lip-pressure variation on the reed. We note the dimensionless mouth pressure $\gamma = \frac{p_m}{P_M}$, so that $\bar{\Delta p}(t) = \gamma - \bar{p}$, with $\bar{p}(t)$, the dimensionless mouthpiece pressure.

There are three main remaining independent parameters: P_M, which determines the signal amplitude (without timbre variation within the linear dynamic range of a resonator), the mouth pressure γ and the "embouchure parameter" ζ, which both have an effect on the signal shape and transients, and thus the timbre of the sound. It is further assumed that the mouth pressure remains constant.

Typical parameter ranges for the clarinet are $P_M < 10$kPa, $\zeta \approx [0.1, 0.8]$ and $\gamma \approx [1/3, 2.5]$. The dynamic parameters are of importance to the brightness and to choosing the desired register. The quality factor range is $Q_r = [5, 125]$ and ω_r should be above the frequency of the first harmonic [3].

By separating the dimensionless mouthpiece pressure as pointed out earlier: $\bar{p} = \bar{p}_h + \bar{q}$, eqs. (2) become an implicit relation which can be solved analytically by following a recently proposed solution by Guillemain et al. [16]. We don't develop the discretisation steps here, but the detailed development can be found in [16, 13].

3.2. Bow-string interaction model

3.2.1. Analogy

As McIntyre et al. [9] have pointed out, there are significant common features in the fundamental physical functioning of instruments that produce self-sustained tones. They all consist of a resonator that is coupled to an excitation mechanism, with the resonator and excitation mechanism each imposing a relation between two physical quantities so that the combined set of relations can result in a self-sustained oscillation. As such, the sound production of a single-reed instrument can be compared to that of a bowed-string instrument, the resonator being respectively the vibrating air column and the string (when symmetrical and bowed exactly at its midpoint), the excitation mechanism being the embouchure and the bow-string interaction, and the physical quantities being the pressure-air flow-rate coupling and the bow/string velocity-force coupling.

This analogy inspired the idea of combining the BS mechanism with an acoustic resonator. The computer allows a pressure and flow rate signal to be interpreted as if it were respectively a velocity and force between a bow and a string, so that the concept can be realised on a hybrid instrument. Knowing that the more detailed functioning of both instruments differs and is responsible for their characteristic sounds, it can be anticipated that such a combination will produce a sound that contains a mixture of characteristics of the wind and bowed-string instrument.

3.2.2. Physical model

In contrast to the SR case, several BS models are currently in common usage, which is probably due to the empirical persistence of elementary models that allow mathematical simplicity [2]. For this reason of simplicity, it was initially decided to employ the "hyperbolic model", which draws from the stick-slip mechanism. In this model, during the "sticking phase", the velocity difference between bow and string surface $\Delta v'(t)$ remains zero until the force $f(t)$ between those parts reaches a break-away sticktion force $f_b\mu_s$. During the "slipping phase", Coulomb (viscous-less) friction with the Stribeck effect occurs as long as the bow and string differ in velocity. This is modeled by the following set of equations:

$$\begin{cases} & \text{as long as:} \\ f = sgn(\Delta v')f_b(\mu_d + \frac{(\mu_s-\mu_d)v_0}{|\Delta v'|+v_0}) & \Delta v' \neq 0 \\ \Delta v' = 0 & f < f_b\mu_s \end{cases} \tag{3}$$

It has been reported that the quality of simulations significantly improves by including the string rotations in this model[9]. By defining $\Delta v(t) = v_b - v(t)$ as the difference between the bow and the string axis, the previous velocity difference can be expressed as :

$$\Delta v' = \Delta v - \frac{f}{2Z_R}, \tag{4}$$

where Z_R is the characteristic impedance for torsional waves. Note that these waves are assumed to be completely absorbed so that no reflections are considered.

3.2.3. A dimensionless and reduced parameter form

Just as for the SR model, it is possible to rewrite the equations of this BS model in terms of dimensionless quantities and with a reduced set of independent input parameters. By introducing the dimensionless force $\bar{f} = \frac{f}{2Z_c v_0}$ and velocity $\bar{\Delta v} = \frac{\Delta v}{v_0}$ and using eq.(4), eqs. (3) can be rewritten as:

$$\bar{f} = \begin{cases} & \text{as long as:} \\ sgn(\bar{\Delta v})\zeta_b(\delta + \frac{1-\delta}{|\Delta v - \alpha\bar{f}|+1}) & |\bar{\Delta v}| > \alpha\zeta_b \\ \frac{\bar{\Delta v}}{\alpha} & |\bar{\Delta v}| \leq \alpha\zeta_b, \end{cases} \tag{5}$$

where $\zeta_b = \bar{f}_b\mu_s = \frac{f_b\mu_s}{2Z_c v_0}$, $\delta = \frac{\mu_d}{\mu_s}$ and $\alpha = \frac{Z_c}{Z_R}$. This form shows that the parameter v_0 is solely controlling the amplitude of the oscillations (for a bowing force proportionally varying with v_0, i.e. for a constant $\bar{f}_b$). Due to the fact that μ_s and $\bar{f}_b$ play the same role (for constant δ), these parameters are merged into a global bow-force related parameter ζ_b (chosen in analogy to the embouchure parameter ζ). While there is still an $\alpha\bar{f}$ term in the equation of the slipping branch, it is small enough compared with $\bar{\Delta v}$ for typical BS parameters that ζ_b is almost directly proportionally controlling the excitation amplitude of that curve. Also in analogy with the SR model, we introduce the dimensionless bowing velocity $\gamma_b = \frac{v_b}{v_0}$, so that $\bar{\Delta v}$=$\gamma_b - \bar{v}$,

[2] e.g. a recent more advanced model takes into account the thermal effects of rosin [17]

where $\bar{v} = \frac{v}{v_0}$ is the dimensionless velocity of the string axis. Typical parameter values are $v_0 \approx 0.2$ m/s, $\delta \approx [3/8, 2/4]$, $\alpha \approx [0.26, 1]$, $\zeta_b \approx \frac{[10,50]}{\mathrm{N}} f_b$, with $f_b \approx [0.15, 3]$N and $\gamma_b \approx (5\,\mathrm{s/m})\, v_b$ with $v_b \approx [0.04, 3]$m/s [18, 19, 9]. However, these bow force and velocity ranges are based on low bow-bridge distances; much lighter forces (or higher bow velocities) are required when the middle of the string is bowed [9].
For the numerical simulation, an explicit analytical expression is obtained in a similar manner as for the SR model (a detailed description will be published later).

4. EXCITATION MODELS VS. SOUND FEATURES

In this section, the issue of how the interaction of the excitation models and the resonator determine the sounds produced is discussed. Understanding this relationship allows us to pre-estimate the sound features, providing a tool to select excitation models and/or parameters as a function of a desired sound output.

We consider the excitation models to be non-dynamic in nature here. The SR model's reed resonance frequency and Q factor are considered (and programmed) high enough so that the model may assumed to be quasi-static and only the non-hysteretic case of the BS model is considered (the hysteretic case requires high ζ_b values which result in the appearance of parasitic noises with the hybrid instrument.)

In this section we mainly refer to the SR case, but the theory also applies to the BS case (by replacing q by f and p by v). Also, from here onwards, $\gamma_{(b)}$ and $\zeta_{(b)}$ refer to each of the relevant SR and BS parameters. That is, $\gamma_{(b)}$ refers to both γ and γ_b, while $\zeta_{(b)}$ refers to both ζ and ζ_b.

4.1. Oscillation conditions and amplitude

In order for an oscillation to occur, the excitation should provide a positive energy contribution that sufficiently compensates for the acoustic losses. Hence, for given excitation parameters, the nonlinear function should have a minimal rise (also known as a "negative resistance") at $p = 0$, i.e. $\bar{q}'(\bar{p} = 0) > 1 - \lambda \gtrsim 0$, where $\lambda(< 1)$ is a real constant that represents the frequency independent losses of the acoustic resonator. [3].

First we consider how a new nonlinear function can be obtained, which includes the resonator's frequency independent losses λ [20]. This theory states that an equivalent system can be obtained, consisting of a resonator without the frequency independent losses and a new nonlinear curve $\tilde{\bar{q}}(\tilde{\bar{p}})$ corresponding to $\bar{q}(\bar{p})$ stretched away by a factor $\frac{1}{\lambda}$ from a line that crosses the $\{\bar{p}, \bar{q}\}$ origin at 45°. Both of these curves, and the mirrored $\tilde{\bar{q}}$ and $\tilde{\bar{f}}$ curves, are depicted (for $\{\zeta = 0.2, \gamma = 0.8\}$, $\{\zeta_b = 0.6, \gamma_b = 1\}$ and $\lambda = 0.94$) in figure 3 for the SR model and figure 4 for the BS model.

It can be shown (e.g. using an iterative approach as in [20]) that a (stable) oscillation requires three intersections between the new nonlinear curve and its mirrored counterpart. The amplitude will settle at the outer intersections, which increases for increasing $\gamma_{(b)}$ (becoming linear, until near the oscillation's extinction when the intersection jumps to one point again).

4.2. Brightness

To explain the spectral development as a function of the excitation model's parameters, we need to consider how the remaining, frequency dependent, acoustic losses intervene. These losses introduce a dispersion that will enforce high frequencies to decrease in amplitude. On the other hand, the nonlinear characteristic excitation curve has the potential to re-introduce high frequencies so that finally the oscillation will settle on a balanced amount of high frequencies. Given that the resonator accentuates odd harmonics, and given that it is the anti-symmetrical component of the excitation curve (which is an "odd function") that is responsible for the introduction of odd harmonics, one can understand that the amount of asymmetry will be an indicator of the "spectral compensation". [4]. This function can be obtained by $\tilde{\bar{q}}_o = \frac{\tilde{\bar{q}}(\tilde{\bar{p}}) - \tilde{\bar{q}}(-\tilde{\bar{p}})}{2}$, which is also depicted in figure 3 and $\tilde{\bar{f}}_o$ in figure 4.
Given that this "spectral compensation rule" applies over the entire evaluated pressure domain of the nonlinear function, and that a precise study of the spectral turnout would be complicated, we make the empirical assumption that the mean absolute amplitude of this curve $< |\tilde{\bar{q}}_o| >$ (later referred to as the "odd amplitude") is positively compensating and thus acts as a global indicator of the relative spectral richness or "brightness" [5]. Therefore it is interesting to study the evolution of this odd amplitude for various excitation parameter ranges. The $\gamma_{(b)}$ values used in figures 3 and 4 result in maximal odd amplitudes (indicated by the blue shaded area). Above and below these mouth pressures and bow velocities these amplitudes decrease, as can

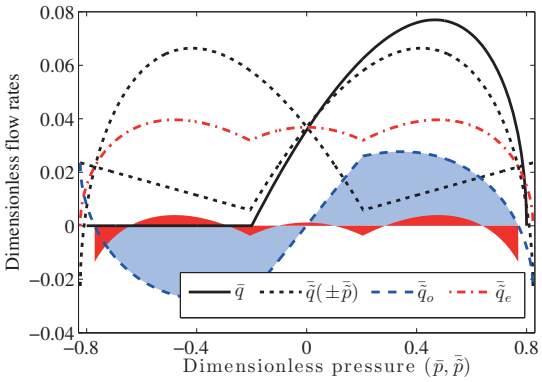

Figure 3: Characteristic nonlinear curves for the SR model

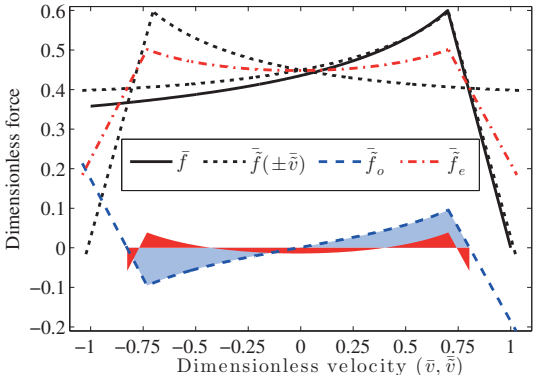

Figure 4: Characteristic nonlinear curves for the BS model.

[3] For a cylindrical open tube with no radiation at the open end, so that losses only occur inside the tube, $\lambda = \exp(-2\alpha_a l)$, where α_a is the absorption coefficient. For our particular resonator we have $\lambda \approx 0.94$.

[4] It has been shown that the odd function part is responsible for the generation of odd harmonics and thus for maintaining the oscillation of cylindrical half-open resonators (e.g.[21])

[5] This could be explained with more clearness by using a representation based on the iterative approach as in [20], but that would exceed the scope of this paper

be seen in figure 5 where the amplitude evolutions are shown for $\zeta = \{0.1, 0.2, 0.3\}$ and $\zeta_b = \{0.2, 0.6, 1\}$ and for $\gamma_{(b)}$ values between the oscillation threshold and extinction. We will refer to these curves to discuss the evaluation in the next section.

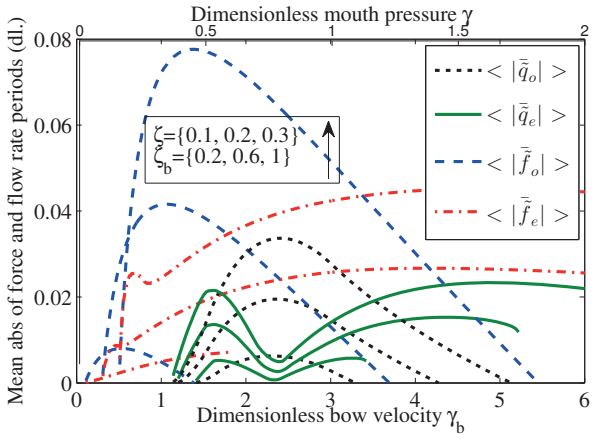

Figure 5: Mean amplitude progressions of the odd and even parts of the SR and BS characteristic nonlinear curves.

4.3. Pitch

While constant excitation parameters result in a sound with a fixed pitch, the resonator's inharmonic modal distribution together with the variation of the mouthpiece pressure spectrum will result in a varying oscillation frequency. Since the inharmonicity of our resonator is found to be positive, we may expect that an increasing brightness imposes an increasing fundamental frequency (see e.g. [21]).

4.4. Odd-even harmonics amplitude ratio

Based on the odd harmonics in the mouth pressure, the remaining even part of the excitation model's function $\tilde{\bar{q}}_e = \frac{\tilde{\bar{q}}(\tilde{p}) + \tilde{\bar{q}}(-\tilde{p})}{2}$ (also shown in figure 3 and 4 for the BS model) will generate even harmonics in the radiated sound, albeit not so loud. After removing the offset (accounting for the mean air flow) from this curve (by subtracting its mean value), just like for the odd function, the "(mean absolute) even amplitude" is calculated $< |\tilde{\bar{q}}_e| >$, whose evolution for the excitation parameter ranges is also shown in figure 5. It is interesting to note that, particularly for the SR case, the even amplitude reaches a minimum where its odd counterpart is maximal. By studying the mean amplitudes of both functions this provides a crude preestimation of what the odd/even harmonics amplitude ratio of the produced sound will be.

5. EVALUATION

Both the SR and BS models were executed with the hybrid instrument as well as with a modal simulation of the resonator with 14 modes[6]. As the resonator simulation is fairly accurate [1, 13] (and the amplifier and microphone responses are reasonably flat), it may be supposed that the shortcomings of the loudspeaker (such as nonlinearities) are the main reason for the difference between hybrid and simulated results. In order to obtain a pressure signal that corresponds to the sound radiated by the instrument, the approximated external pressure can be calculated by $p_{ext} \propto \frac{d(p+q)}{dt}$ (supposing a monopole radiation). To cope with the amplification of high frequency noise, prior to the derivative a steep low-pass filter is applied, with $f_{cutoff} = 4\,\text{kHz}$, at the resonance frequency of the upper simulated mode.

To allow for a quantitative and relevant comparison of hybrid and simulated sounds, we use so-called "sound descriptors". These represent a standardized set of features that describe relational values derived from the spectral, temporal and harmonic representations of the sound. We chose to consider two physically and perceptively relevant descriptors: the "harmonic spectral centroid" (HSC), which can be seen as the spectral gravity centre of the harmonic content and is known to be highly correlated to the brightness of that part of the sound (the normal spectral centroid turned out to be influenced by the raucous sound for the BS case, which we want to ignore for that comparison); and the "odd/even harmonics ratio" (OER), which is the ratio of odd and even harmonic amplitude components[7]. We also studied the mean (RMS) amplitude evolution of the mouthpiece pressure and the progression of the fundamental frequency.

Only the steady state regime is evaluated and the applied parameter values are $\zeta = \{0.1, 0.2, 0.3\}$ and $\zeta_b = \{0.2, 0.6, 1\}$ with $\gamma_{(b)}$ increasing from the oscillation threshold until extinction and $\delta = 0.375$, $\alpha = 0.5$. The relatively low $\zeta_{(b)}$ values are due to parasitic noises with the hybrid instrument. However, for the SR case, ζ still spans about half of the aforementioned typical range, and for the BS case it can be argued that the ζ_b range is reasonable as it is implied that "the string is bowed in the middle". The dynamic parameters for the SR model are held fixed to the values used in [16]: $\omega_r = 2\pi \times 2500\,\text{rad}\,\text{s}^{-1}$ and $Q_r = 5$. This is a relatively high resonance frequency for a fundamental frequency of $f_0 \approx 140\,\text{Hz}$, but that makes the model similar to the more elementary static reed model (we note that an evaluation with $\omega_r = 2\pi \times 10\,\text{krad}\,\text{s}^{-1}$ had virtually the same results). Since the SR case has already been discussed in earlier papers [2, 1], we will mainly consider the BS results and the comparison with the SR results. We note that a higher $\zeta_{(b)}$ implies a wider oscillatory $\gamma_{(b)}$ domain, so that this can be used to identify the $\zeta_{(b)}$ values of the curves in figures 6 to 9.

Figure 6 shows the progressions of the mean (RMS) mouthpiece pressure signals.

The theoretical results are obtained from the intersection of the nonlinear curves that include the frequency independent losses. They are close to the simulated results for low $\gamma_{(b)}$ values, but it should be noted that the theoretical curves represent the peak-to-peak amplitude, so that the decreasing RMS amplitudes may be explained by the reduction of high frequencies. The extinctions (where the RMS amplitudes drop to zero with increasing $\gamma_{(b)}$) coincide fairly well, except for $\zeta_b = 0.6$. Considering the BS's odd amplitude in figure 5, it becomes clear that this is most likely due to the lack of odd harmonics delivered by the BS excitation.

The simulated and hybrid curves for both BS and SR models match closely, apart from the fact that the hybrid extinction occurs slightly earlier, which may be due to the influence of the uncompensated loudspeaker losses. Another important difference occurs for the BS model near to the oscillation threshold: a raucous sound (characteristic to bowed strings) appears, but for the hybrid instrument that state is more prominent and is sustained for much longer, particularly for high bow forces. For

[6] The sounds can be found online on: http://users.mct.open.ac.uk/kb22747/

[7] For the precise mathematical definition of the sound descriptors see [22, 23].

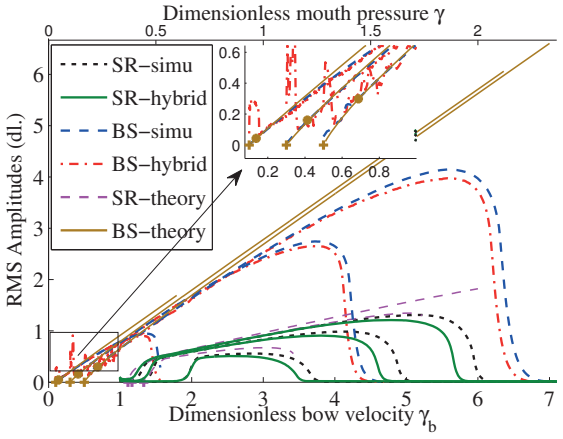

Figure 6: Mean (RMS) amplitude progressions of the pressure at the resonator entrance for the hybrid and simulated results with the SR and BS models, and theoretical SR and BS peak-to-peak amplitudes.

very low bowing velocities, the hybrid instrument produced unstable squeaks (visible as overshooting peaks). We assume that this occurrence, and the generally unstable hybrid behaviour when the nonlinear function contains steep variations (e.g. for $\zeta_{(b)}$ values above the here applied range), is due to the phase lag introduced by the loudspeaker. At high frequencies it can rotate the phase by $180°$ so that the downwards going static friction curve will be converted into a (high) negative resistance which makes the system unstable.

Figure 7 represents the harmonic spectral centroid ("HSC") curves. Comparing these curves with the odd amplitudes in figure 5 we find a surprisingly good overall resemblance of the relative progressions where even the interrelation between SR and BS curves is respected to a good extent. It appears that the relationship between the odd amplitude and the HSC is reasonably linear. The simulated and hybrid BS cases correlate with a similarly good precision as for the SR case.

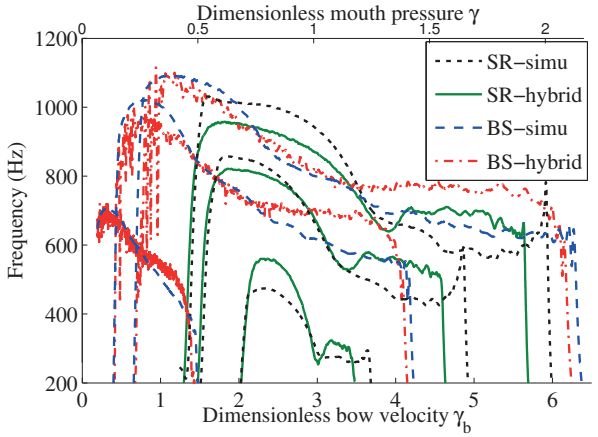

Figure 7: Harmonic spectral centroids for the hybrid and simulated results with the SR and BS model.

We note that for the case of the SR model, it has been shown that both the spectral centroid and the attack time of a note onset are highly correlated features, which are mainly controlled by the excitation amplitude ζ [22, 2]. This feature is not studied in this paper, but we assume that similar results can be expected for the BS model.

Figure 8 represents the fundamental frequency (f_0) progressions for all cases. As predicted, this feature is well correlated with the spectral centroid due to the positive inharmonicity of the resonator. However, as pointed out earlier, the loudspeaker introduces a phase lag that makes the inharmonicity negative, resulting in an inverse correlation for the hybrid cases. It can further be seen that these hypotheses are supported by the outcome with the BS model.

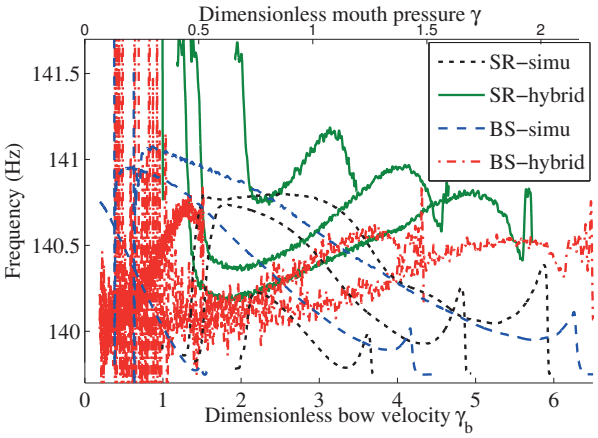

Figure 8: Fundamental frequency progressions for the hybrid and simulated results with the SR and BS model.

Finally, figure 9 depicts the odd/even harmonics amplitude ratio ("OER").

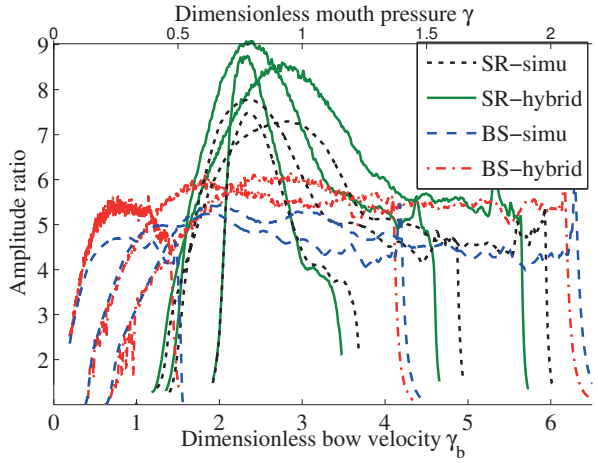

Figure 9: Odd/even harmonics ratio progressions for the hybrid and simulated results with the SR and BS model.

Considering the even amplitudes in figure 5, it can be seen that the OER has important correlations with the ratio of the odd and even amplitudes. For the SR case, the coinciding peak/dip situations in the latter explains the peaks for the OER, while for the BS this is far less the case, resulting in a more moderate OER progression.

6. DISCUSSION AND CONCLUSIONS

After a brief review of the hybrid wind instrument set-up, we presented the classical single-reed (SR) mouthpiece model and

the hyperbolic bow-string (BS) interaction model with absorption of torsional waves. Via analogy with the SR model, a dimensionless and reduced parameter form is proposed for the BS model, which reveals that the SR model's dimensionless mouth pressure γ has an analogous function as the dimensionless bowing speed γ_b. The SR model's "embouchure parameter" ζ is a direct factor to the whole nonlinear function whereas for the BS model, the bow force ζ_b has a similar role but it does not affect the slope of the static friction curve. This shifts the γ_b "oscillation threshold" and "raucous threshold" (as indicated by Schelleng's maximum bowing force [24]) upwards for increasing ζ_b. Solely considering (quasi-)static excitation models (which is sufficient for our study), we derived a graphical method to draw an intuitive link between the characteristic nonlinear curve and a few features of the produced sound: the amplitude of oscillation, the spectral richness and the amount of odd and even harmonics.

Next, the SR and BS excitation models were implemented with both the hybrid wind instrument and a modal simulation of the resonator. The resulting differences can be mainly attributed to uncompensated characteristics of the loudspeaker. For both models, typical parameter values were applied, although the $\zeta_{(b)}$ range had to be constrained to prevent parasitic noises with the hybrid instrument. These are assumed to occur as a result of phase shifts which can exceed 180° at high frequencies, thereby transforming the (higher) positive resistance slope in the nonlinear functions into a negative one, which can cause an instability at those frequencies.

Three $\zeta_{(b)}$ values were applied with an increasing $\gamma_{(b)}$ from oscillation threshold until extinction. The resulting sound features (RMS pressure, harmonic spectral centroid, fundamental frequency and odd/even harmonics amplitude ratio) were found to be well predicted by the graphical method. The hybrid results are in overall good accordance with the simulations and hypotheses related to the loudspeaker are made to explain the differences.

The difference in sound between the SR and BS models is not substantial, except for the (typical) raucous sound appearing with the BS model when γ_b/ζ_b is low. This similarity is potentially a result of the simplifications (static) in both models. An empirical evaluation with more dynamic models (e.g. the "lip-reed" as in brass instruments) resulted in a stronger timbral variation.

7. REFERENCES

[1] K. Buys, D. Sharp, and R. Laney, "Developing a hybrid wind instrument : using a loudspeaker to couple a theoretical exciter to a real resonator," in *Proc. Int. Symp. Music. Acoust.*, 2014.

[2] K. Buys, D. Sharp, and R. Laney, "Developing and evaluating a hybrid wind instrument excited by a loudspeaker," in *Proc. Inst. Acoust.*, 2014, vol. 36.

[3] T. A. Wilson and G. S. Beavers, "Operating modes of the clarinet," *J. Acoust. Soc. Am.*, vol. 56, pp. 653–658, 1974.

[4] C. Maganza, *Excitations non linéaire d'un conduit acoustique cylindrique. Observations de doublements de période précédant un comportant chaotique. Application à la Clarinette*, Ph.D. thesis, Université du Maine, 1985.

[5] J. Guérard, *Modélisation numérique et simulation expérimentale de systèmes acoustiques - Application aux instruments de musique*, Ph.D. thesis, Université Paris 6, 1998.

[6] N. Grand, *Etude du seuil d'oscillation des systèmes acoustiques non-linéaires de type instrument à vent*, Ph.D. thesis, Université Paris 7, 1994.

[7] T. Meurisse, A. Mamou-Mani, R. Caussé, B. Chomette, and D. B. Sharp, "Simulations of Modal Active Control Applied to the Self-Sustained Oscillations of the Clarinet," *Acta Acust. united with Acust.*, vol. 100, no. 6, pp. 1149–1161, 2014.

[8] K. Buys and C. Vergez, "A hybrid reed instrument: an acoustical resonator with a numerically simulated mouthpiece," in *Proc. Acoust. 2012*, Nantes, 2012.

[9] M. E. McIntyre, R. T. Schumacher, and J. Woodhouse, "On the oscillations of musical instruments," *J. Acoust. Soc. Amer.*, vol. 74, no. 5, pp. 1325–1345, 1983.

[10] S. Ollivier, J. P. Dalmont, and J. Kergomard, "Idealized models of reed Woodwinds. Part I: Analogy with the bowed string," *Acta Acust. united with Acust.*, vol. 90, no. 6, pp. 1192–1203, 2004.

[11] G. Weinreich and R. Caussé, "Elementary stability considerations for bowed-string motion," *J. Acoust. Soc. Amer.*, vol. 89, no. 2, pp. 887–895, 1991.

[12] G. Muller and W. Lauterborn, "The Bowed String as a Nonlinear Dynamical System," *Acustica*, vol. 82, no. t 996, pp. 657–664, 1996.

[13] K. Buys, D. B. Sharp, and R. Laney, "Developing and evaluating a hybrid wind instrument," *Acta Acust. united with Acust.*, p. to appear.

[14] "Xenomai: Real-Time Framework for Linux," .

[15] A. Hirschberg, "Aero-acoustics of wind instruments," in *Mech. Music. Instruments*, A. Hirschberg J. Kergomard and G. Weinreich, Eds. Springer, Wien, 1995.

[16] P. Guillemain, J. Kergomard, and T. Voinier, "Real-time synthesis of clarinet-like instruments using digital impedance models," *J. Acoust. Soc. Am.*, vol. 118, no. 1, pp. 483, 2005.

[17] J. H. Smith and J. Woodhouse, "The tribology of rosin," *J. Mech. Phys. Solids*, vol. 48, pp. 1633–1681, 2000.

[18] R. Pitteroff and J. Woodhouse, "Mechanics of the contact area between a violin bow and a string. Part I: Reflection and transmission behaviour," *Acta Acust. united with Acust.*, vol. 84, no. 3, pp. 543–562, 1998.

[19] A. Askenfelt, "Measurement of the bowing parameters in violin playing. II: Bow-bridge distance, dynamic range, and limits of bow force," *J. Acoust. Soc. Amer.*, vol. 86, no. 2, pp. 503–516, 1989.

[20] P.-A. Taillard, J. Kergomard, and F. Laloë, "Iterated maps for clarinet-like systems," *Nonlinear Dyn.*, vol. 62, no. 1-2, pp. 253–271, Dec. 2010.

[21] J. Kergomard, S. Ollivier, and J. Gilbert, "Calculation of the Spectrum of Self-Sustained Oscillators Using a Variable Truncation Method : Application to Cylindrical Reed Instruments," vol. 86, no. June 1999, pp. 685–703, 2000.

[22] M. Barthet, *De l'interprète à l'auditeur : une analyse acoustique et perceptive du timbre musical*, Ph.D. thesis, Université de la Méditerranée Aix-Marseille II, 2009.

[23] G. Peeters, B. L. Giordano, P. Susini, N. Misdariis, and S. McAdams, "The Timbre Toolbox: Extracting audio descriptors from musical signals," *J. Acoust. Soc. Amer.*, vol. 130, no. 5, pp. 2902–2916, Nov. 2011.

[24] J. C. Schelleng, "The bowed string and the player," *J. Acoust. Soc. Am.*, vol. 53, no. 1, pp. 26, 1973.

AUTOMATIC MUSIC TRANSCRIPTION USING SPECTROGRAM FACTORIZATION METHODS

Emmanouil Benetos
Centre for Digital Music, Queen Mary University of London, UK
emmanouil.benetos@qmul.ac.uk

ABSTRACT

Automatic music transcription (AMT) is defined as the process of converting an acoustic music signal into some form of human- or machine-readable musical notation. It can be divided into several subtasks, which include multi-pitch detection, note onset/offset detection, instrument recognition, pitch/timing quantisation, extraction of rhythmic information, and extraction of dynamics and expressive information. AMT is considered a key enabling technology in music signal processing but despite recent advances it still remains an open problem, especially when considering multiple-instrument music. A large part of current AMT research focuses on spectrogram factorization methods, which decompose a time-frequency representation of a music signal into a series of note templates and note activations. This has led to music transcription systems that are computationally efficient, robust, and interpretable. In this talk, I will present recent advances in AMT focusing on proposed systems that are able to detect multiple pitches and instruments, and are able to support tuning changes and frequency modulations. Recent work on creating a transcription system that models the temporal evolution of each note as a succession of sound states (such as attack, sustain, and decay) will also be presented. The final part of this talk will be on the applicability of AMT methods to fields beyond music signal processing, namely musicology, performance science, and music education. Specific examples on the use of AMT technology will be given in problems related to the analysis of temperament, the analysis of non-Western music, and the creation of systems for automated piano tutoring.

ACKNOWLEDGEMENT

EB is supported by a Royal Academy of Engineering Research Fellowship (grant no. RF/128).

STEADY STATE SOUND PRODUCTION AND INVESTIGATIONS ON CLASICAL GUITARS

Hellmut Schmücker, Starnberg, Germany
hellmut.schmuecker@me.com

1. ABSTRACT

The discussion about the quality of a guitar goes back to the early days of this instrument. Due to its growing popularity in the last decades numerous experiments and theoretical investigations have been published in order to better understand the instrument and to improve the quality of the tone production.
The possibilities and tools to investigate the functionality and properties of a guitar have developed dramatically in recent years due to the application of fast and cheap computers. Mathematical procedures and modelling with finite element methods allow to simulating any instrument.
Here, a more practical approach is presented. The guitar is slightly modified to produce the sound in the very same way the string tension acts on the bridge. The guitar under test is agitated with steady state signals or, for range measurements, as sweep-sine or MLS (Maximum Length Sequence) signals.
With such defined steady state signals, analysis is by far more easier to accomplish.
Shown are frequency response measurements on famous old guitars and new models, the influence of string tension and weight distribution, temperature and humidity. All results are verified by conventional measuring methods.

2. INTRODUCTION

The discussion about the quality of a guitar has a long history. Recently, however, the instrument has gained much popularity, presumably because many think it is not difficult to learn. By no means, it is! My teacher tends to claim that it is by far the most difficult instrument! Neither is it an instrument easy to investigate: it has a complex structure, non steady state tone production, and large design variations. Due to its growing popularity in the last decades numerous experiments and theoretical investigations have been published in order to better understand its physics and improve the quality of tone production.
Vibration analysis and modal investigations are common to most engineers in design and development today. They look into vibration behaviour of washing machines, jumbo jets, and skyscrapers. These procedures are used to optimising properties and minimising potential dangers and failures.
These tools can easily be applied to musical instruments. For such investigations, analytical procedures and numerical calculations are cast into easy to handle programs.

Here, we describe a new procedure applied to guitars of various origins and age. Extensive and comparative measurements allow showing differences throughout the whole audio spectrum. The interpretations of these results are presented for discussion.

3. RECENT LITERATURE

Many publications are available on single aspects of the guitar. A concise presentation of the properties was published in 1985 [1]. Systematic measurements and conclusive analysis show the influence of many parameters of the guitar and may be used as guidance for luthiers. A simple correlation between physical parameters and the sound quality is, however, difficult, maybe impossible. Therefore, an audio evaluation of different guitars by experts is added for orientation. A collection of methods and measurements was presented 2010 on several string instruments. Quality criteria are suggested, bases on statistical methods [38].
Modal analysis using laser vibrometers and other optical methods show the various oscillating modes of the guitar body [2]–[16], [40]. The analysis requires defined excitation parameters. If the agitation forces are unknown, operational modal analysis (OMA) is also possible, but it requires many measuring points to isolate modes from noisy signals. Nevertheless, modal behaviour does not necessarily relate to the quality of a guitar.

Finite element methods were applied to the guitar models to simulate vibration modes or isolate critical parts and to investigate their influence on the sound performance [25], [26], [37]. Two severe problems are encountered, however:
1st, wood is an un-isotropic matter in terms of physical and mechanical properties. They vary with time and space.
2nd, tone production on the guitar is a non-steady state process and therefore requires small increments in time and space. This asks for extensive computer power and speed.

Numerous investigations present measurements on the input admittance, impedance or transfer function using piezoelectric transducers [7], [10], [18], [27]. These measurements provide a good insight of the ability of the instrument body or parts of it to oscillate, when the string is released. The visualisation of the soundboard movements [40] is also a proper tool to reveal to the luthier “lazy” parts of the soundboard. The artist, however, wants to hear the sound of a guitar. He wants to find out, if the tone production suits his imagination and taste and if the tone can be formed at his will.
Therefore, the straightforward analysis is to investigate the transfer function between agitation and sound radiation by using a professional microphone.

4. SEADY STATE TONE PRODUCTION

To apply home computer based tools, a steady state signal from the guitar is desirable. Studying and understanding the mechanism of tone production with a guitar shows, that the oscillating sting rocks the bridge not only by transversal forces, but also by longitudinal forces. This longitudinal force results from the string displacement causing a variation in longitudinal tension. The longitudinal forces are smaller than the transvers forces according to calculations by Fletcher [40]. Nevertheless, they rock the bridge resulting in tilting movements. We replace the bridge inlay (fishbone/ivory) by a brass inlay having a lever arm on the bass string side. The lever arm extends vertical to the soundboard and is connected to an electromagnetic shaker. The

shaker is fed with an electric signal. This agitation gives a steady state tone at any desired frequency and sound level by changing the frequency and output level of the driving generator.

5. THE TEST FACILITIES

The experimental set-up is designed in such a way, that the sound production is reproducible under all circumstances. The apparatus itself shall not vibrate in the audio frequency range and shall not hinder the guitar to vibrate and respond to agitating forces applied. The guitar under test is ready to be played. All strings are mounted and tuned, so the soundboard of the guitar is under operational tension. The strings, however, are damped with a noun strip. The string vibrations do not contribute to the sound measured by a calibrated microphone.
The guitar body is mounted vertically on a very rigid aluminium structure of one pillar and two arms. Four wooden brackets fix the guitar body at the back and front.
Little force is applied to the guitar at the very edge of the soundboard and back plate. At the lower end of the guitar body the shaker (Brüel & Kjaer 4810) is placed on an aluminium table extending from the main pillar structure. The piston of the shaker is connected to the lever arm made from a carbon fibre tube. This tube is very rigid and has a low mass. The shaker can be moved horizontally, so no momentum is applied to the lever arm when the shaker is unpowered. An extra mass of 900 grams is added to the bottom of the shaker to lower resonant frequencies.

6. AGITATION OF THE GUITAR AND MEASURING DEVICES

The shaker is fed with a sine wave signal, a white or pink noise signal from a signal generator (Brüel & Kjaer 1049), or by audio signals produced by the computer. A linear amplifier (Brüel & Kjaer 2706) gives enough power to drive the shaker. The sound radiated from the guitar is received by a condenser microphone (Brüel & Kjaer 4165, calibrated) and amplified by a microphone amplifier (Brüel & Kjaer 2807). The microphone is placed in front of the guitar at a distance of 0,5 or 1 m from the plane formed by the strings, directly opposite the sound hole. The sound level is measured by a calibrated amplifier (Brüel & Kjaer 2636) or processed via the A/D converter. This dual channel A/D - D/A processor converts at a clock frequency up to 96 kHz at a depth of 24 bits (MOTU microbook I)

7. COMPUTER AIDED ANALYSIS

Today, A/D converters and home computers are well capable of running fast data acquisition systems, performing complex data conversion and analysis programs. Loudspeaker designers in particular have developed measuring procedures using MLS signals (Maximum Length Sequence) and sweep sine signals. The impulse response functions are recorded. By mathematical transformation the frequency response and many other functions can be obtained. The experiments can even be performed without using anechoic chambers.
Maximum Length Sequence (MLS) measuring procedures have a limited dynamic range and are sensitive to non-linearity in time and space. Therefore, sweep-sine signals are preferred. These signals are widely used in modern acoustic measurement analysis [19] – [21], [28] -[29]. The received impulse response function is processed by mathematical procedures called de-convolution. A higher level of excitation is possible, background noise is suppressed, and the immunity against harmonic distortion and time variance is excellent.
A number of software solutions were tested for this purpose, running either on a PC or on a MacBook Pro. The main objectives were to achieve consistent measurements, easy operation, and reliable and reproducible results. The systems under consideration were ARTA, SYSTune, FuzzMeasure, Baudline, Signal Scope Pro, WinMLS, Sample Champion PRO 3.8, Audio Tester V3.0, Data Physics SignalCalc, and a few others. For data presentation the systems ARTA (on a PC) and FuzzMeasure (on a MacBook) were used due to easy handling.

Fig. 1 Agitation of the guitar

8. ANECHOIC CHAMBER AND FEE FIELD MEASUREMENTS

A few measurements were performed in an anechoic chamber. This laboratory was available just a few days before it was demolished. Comparing these results with the measurements performed in the conventional laboratory room of 30 square meters, wall reflections and other acoustic characters did not deteriorate the measurements using sweep – sine signals. However, to be on the save side, acoustic panels where used to shield the test stand. Free-field measurements in the open air were only possible during late evening hours. The showed no significant deviation from laboratory results.

Fig. 2: Analogue measuring instruments

9 GENERAL CONSIDERATIONS ON THE FREQUENCY RESPONSE

The purpose of this test installation is the presentation of the guitar in the state as if played by the artist. The damping of the guitar due to the armrest and leg support is not simulated. The strings are tuned, so the soundboard is under normal tension. The strings are damped by a piece of felt. For all measurements the electric power to the shaker is kept constant within plus minus 1.5 dB, independent of frequency and time.

In order to familiarize with the test installation, simple resonance measurements were performed with the audio generator, amplifier, and shaker. More than 10 outstanding resonance peaks can be detected easily in the frequency range between 65 Hz (C) and 1000 Hz (b"). The resonance peaks are reproducible with an accuracy of less than 0,2% in amplitude and frequency.

Fig. 3 shows the typical frequency response of a sample guitar. It was obtained with a sweep sine signal from 40 Hz to 15.000 Hz in 10 seconds. The exciter was powered with 0,5 VA, resulting a maximum sound level pressure of 90 db.

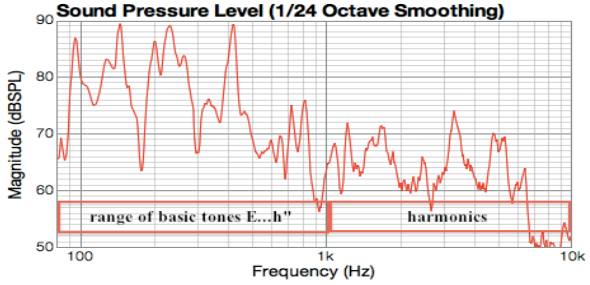

Fig.3: Frequency response of a guitar.

The microphone (Brüel & Kjaer ½ " type 4165) was places in front of the soundboard hole at a distance of 0,5 meters. Prominent resonance peaks are detected. At around 100 Hz we find the so-called Helmholtz resonance, depending on the volume of the guitar body and the size of the sound hole. The basic tones start at 82,4 Hz (E-string) and go up to 987 Hz (b", 19th fret). In this range we see deep drops followed by outstanding resonance peaks produced by modal oscillations of the soundboard and the bottom plate. From 1 kHz upwards the resonance peaks are still prominent, but do not reach the power of the lower range peaks. Deep valleys represent week energy radiation because of low efficiency at these frequencies. This frequency plot represents a "footprint" of the guitar under test.

10. THE FREQUENCY RANGES

Violins have been tested extensively in the attempt to classify their quality in terms of frequency response and acoustic performance [22]-[24], [33]-[36]. If we follow their analysis, the frequency range versus sound pressure level (SPL) is responsible for the performance of the instrument. The frequency ranges and their contribution to the sound are shown in Fig. 4.

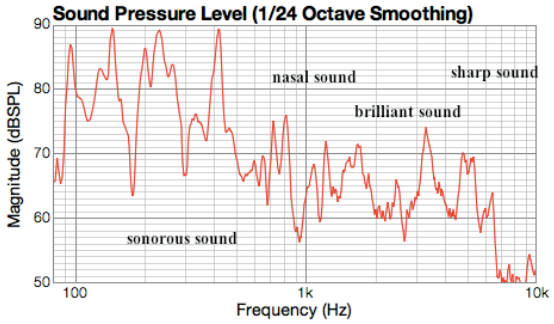

Fig. 4: Frequency ranges and their contribution to the sound character

At the lower end we have the Helmholtz resonance. Standard sized guitars resonate between E and G#. Up to 1000 Hz we find the basic tones of the guitar. The scale starts at E and ends at h" at the 18th fret of the fingerboard. The corresponding frequencies start at 82,4 Hz and reach to 988 Hz. We call this range the basic tones. High sound pressure levels in this range with not too deep valleys stand for a powerful, sonorous instrument.

Above 1kHz we see all the harmonics. They are responsible for the character of the instrument, its timbre, sweetness, modulation ability, clarity, even sustain.

Between 1,1 and 1,5 kHz the levels should not be too high, as the instruments tends to sound nasal and potty. With high sound pressure levels above 1,5 kHz the instrument sounds brilliant and penetrating. Around 1 kHz we find the formant "a", at 2 kHz the formant "e" and around 3 kHz the formant "i". The formats characterize a singer´s ability to fill the concert hall, even at high orchestra levels. If the guitar is strong in this frequency range, its tone is carried to the listener in the very last row of the hall.

11. DIRECTIONAL RADIATION OF SOUND

The guitar has no symmetry axis or plane. Therefore, it is obvious, that the sound perception of the listener depends very much on his position in reference to the guitar, at least at small distances. Different microphone position were chosen to show

this effect: the reference position is in front of the sound hole at a distance of 0,5 m. This position is compared to a 90-degree position in the virtual plane of the soundboard. This is approximately the position of the player's ear**.**

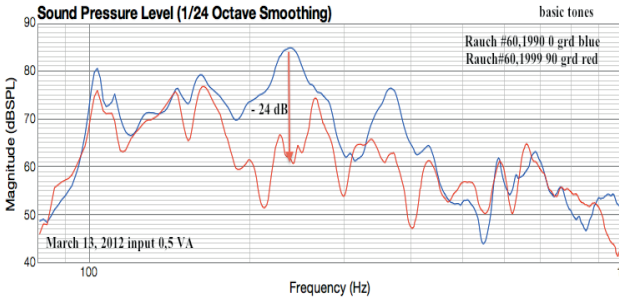

Fig.5: Sound pressure level near the artist´s hears (red) compared to the sound radiated perpendicular to the soundboard (blue)

12. THE INFLUENCE OF THE STRING TENSION ON THE SOUND PRODUCTION

A number of investigations on guitar frequency response report measurements without strings. The strings, when tuned to their nominal tension, impose a force of about 500 N to the soundboard. The soundboard acts as a membrane, agitated to different modal oscillations. These modes are influenced by the applied tension as shown in Fig. 6. Though the character remains, variations in frequency and volume are detected. The difference in the frequency response depends very much on the construction of the soundboard, e. g. stiffness and board thickness. All guitars are tested with strings under tension.

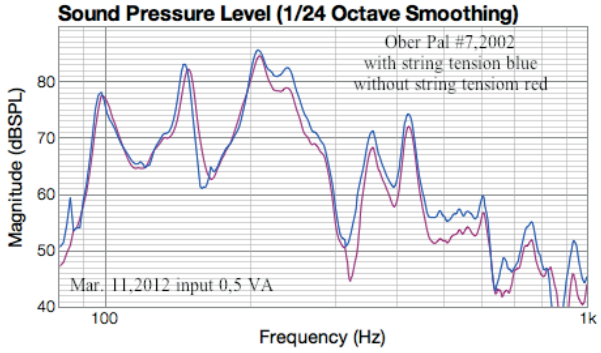

Fig. 6: Frequency response of the sample guitar with (red) and without (blue) sting tension.

13. HOW TO COMPARE GUITARS

All tests are performed using identical procedures. The shaker is driven with a constant power level of 0,5 VA plus minus 1,5 dB. For efficiency measurements, white noise signals and a single frequency of 1000 Hz are applied. As reference, a precision sound level meter (Brüel & Kjaer 2223) measures the emitted sound pressure level. A sweep sine signal is applied for the impulse transfer function response. The sweep time is 10 s for a frequency range from 40 Hz to15 kHz. A calibrated microphone (Brüel & Kjaer 4165) picks up the emitted signal. To verify the sound pressure levels calculated by the computer program, resonance peaks are verified by steady state measurements using a tone generator (Brüel & Kjaer 1049) and a measuring amplifier (Brüel & Kjaer 2436). These measurements do correspond with a deviation less than 0,5% in frequency and sound pressure level. The guitars under test are listed in the appendix.

14. PARAMETERS INFLUENCING THE SOUND

Above, we have discussed how direction determines the perception of the sound as well as the influence of sting tension on the sound production. There are, off course, many more parameters like temperature, humidity, positioning of the instrument (back plate damping) geometric parameters, mass distribution (machine head), age, and frequent usage of the instrument.
A few parameters have been examined within accessible limits. The impact of temperature is less prominent than expected. A 10 K difference causes less than 2 dB variations in SPL and less than 1% in frequency shift of resonance peaks. Off course, detuning of the strings by temperature is not considered, as their oscillations are excluded. Humidity variations up to 10 % rel. humidity are detectable by shift of peak frequency. Back plate damping was realized by sliding a foam panel between the structure pillar and the guitar back plate. No significant change was detected on the forward radiated sound.

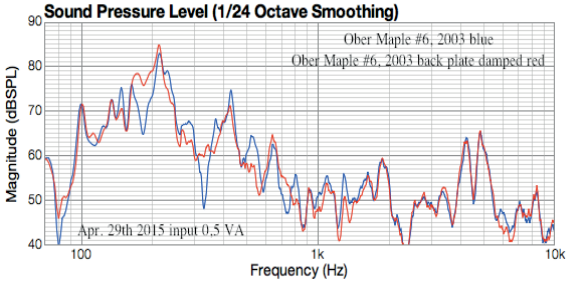

Fig. 7: Change of frequency response cause by back plate damping (red)

A chance in mass distribution was realized by fastening a mass of nearly 0,6 kg to the machine head of the guitar. Only very small changes in frequency response were detected at very high harmonics.

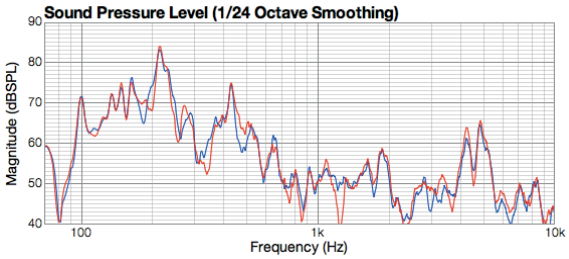

Fig. 8: Adding a mass of 0,6 kg to the machine head (red) has very little impact on the frequency response

Serious guitar artist is aware of the fact that his new guitar has to mature. The soundboard in particular will develop it´s full potential in colour and brightness with time and usage. This is demonstrated in Fig. 9. Not only the volume changes by more than 10 db in the basic tone range (below 1000 Hz), but also the

harmonics change significantly, presenting a different tone colour.

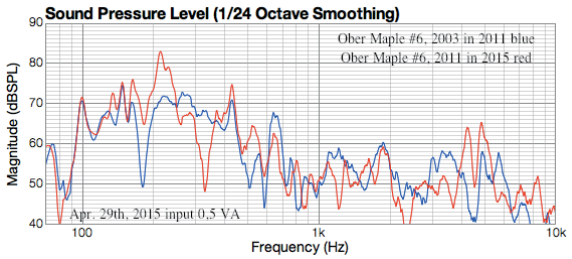

Fig 9: The guitar matures with time, blue: test in 2011, red: test in 2015

Historic instruments are sought after because of this maturing effect. Obviously, spruce rebuilds its cellular structure in such a way, that it is able to transform string oscillations into soundboard vibrations with a higher efficiency. This effect may well be achieved by a controlled heat treatment of the soundboard. The thermal modification process is similar to the aging process and is applied by a number of luthiers.

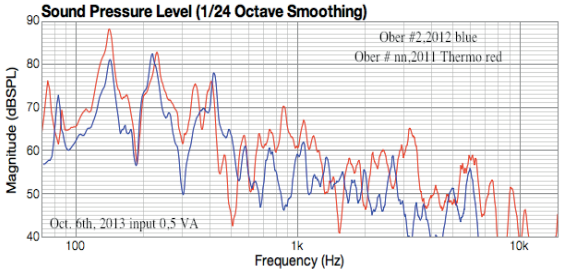

Fig. 10: Effect of thermal treatment of a spruce soundboard

New soundboard designs incorporate technologies developed in the aviation industries. The idea is to reduce the mass without decreasing stiffness and the ability to vibrate. Fig. 11 shows an example of a sandwich design. Although the character of the instrument does not change significantly, the sound pressure increases by a few db´s. Another welcoming effect is the quick response of the guitar, due to the low mass of the soundboard.

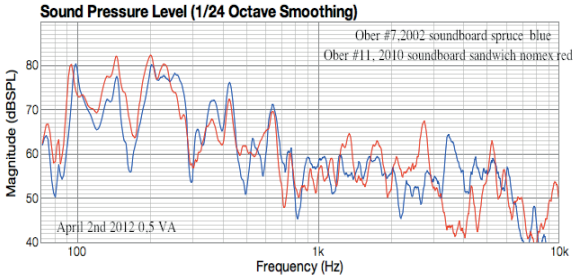

Fig. 11: Sandwich soundboard

On the other hand, many luthiers use historic instruments as an inspiring example to follow. So did Hermann Hauser I when he first saw, heard and measured a Torres guitar in the 30ies of last century. So do many followers today and offer "Hauser" models.
Ambitious artist even duplicate famous models to see if they can meet expectations and produce an instrument of equal sound pattern. Fig. 12 shows the frequency pattern of a H. Hauser II and the replica of the well known "La Leona" FE04 by Antonio Torres. This guitar is equipped with the tornavoz, a brass funnel, placed between the sound hole and the back plate. The effect can easily be recognized at 133 Hz, near C.

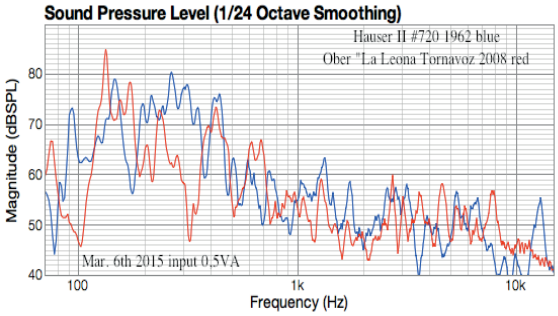

Fig. 12: Replica "La Leona" versus a H. Hauser II of 1962

15. CONLUSIONS

The frequency analysis is an excellent and easy to use tool to investigate and document the "footprint" of a guitar. Even small changes in size, weight, wood, and technology are detected. The method is simple and requires little investment. A lab-top computer is available everywhere, the software mentioned above is easy to handle and requires no programming skills. It should become a standard method to any luthier.

APPENDIX

Fritz Ober # 6, 2003, spruce, maple
Fritz Ober #7, 2002, spruce, rosewood
H. Hauser II #720, 1962, spruce, rosewood
H. Hauser I # ??, 1938, spruce, rosewood
H. Hauser I #??, 1935, spruce, rosewood
Guitarra Espaniola K04 MZ. #2004, spruce, side unknown
Fritz Ober # ??, 2010, spruce sandwich, rosewood
Armin Hanika Mod. 56 PF, 2009, spruce, Indian rosewood
Armin Hanika Mod 60PF, 2008, spruce, Indian rosewood
Otto Rauch #60, 1999, spruce, maple
Fritz Ober # 2010, spruce nomex, rosewood
Fritz Ober #?? 2011, thermo spruce, rosewood
Jose Garcia #??, 1912, spruce, rosewood
Santos Hernandez #??, 1925, spruce, rosewood
Manuel Ramierez #??, 1912, spruce, rosewood
Ulrike Meinel #2168, 1983 spruce, rosewood
Fritz Ober #5, 2012 sandwich thermo spruce/nomex, rosewood
Fritz Ober #nn 2012 sandwich thermo spruce/laser rosewood
Klaus Härtel #2013 spruce, rosewood
Fritz Ober #2, 2015 Copy "La Leona", spruce, cypress
Fritz Ober #1, 2015 (Kasein) thermospruce, Rosewood

ACKNOWLEDGEMENTS

Fritz Ober, München, an innovative luthier, for his contributions of excellent ideas during many discussions and for providing new and experimental designs.
Johannes Tonio Kreusch, München, a gifted artist on the guitar, for many inspiring discussions.

16. REFERENCES

[1] Meyer Jürgen: Akustik der Gitarre in Einzeldarstellungen, Verlag E. Bochinsky Frankfurt 1985

[2] Fleischer, H., Admittanzmessungen an akustischen Gitarren. Forschungs- und Seminarberichte aus dem Gebiet Technische Mechanik und Flächentragwerke 01/97. Herausgeber F.A. Emmerling und A.H. Heinen, Universität der Bundeswehr München, Neubiberg 1997.

[3] Fleischer, H., In-situ-Messung der Schwingungen von E-Gitarren. In: Fortschritte der Akustik (DAGA '98), DEGA, Oldenburg 1998, 630 - 631.

[4] Fleischer, H., Schwingungen akustischer Gitarren. Beiträge zur Vibro- und Psychoakustik 1/98. Herausgeber H. Fleischer und H. Fastl. Universität der Bundeswehr München, Neubiberg 1998.

[5] Fleischer, H., Diagnosing dead spots of electric guitars and basses by measuring the mechanical conductance. Poster auf dem ASA/EAA/DAGA ï99 Meeting, Berlin 1999.

[6] Fleischer, H., Zwicker, T., Dead Spots. Zum Schwingungsverhalten elektrischer Gitarren und Baßgitarren. Beiträge zur Vibro- und Psychoakustik 1/96. Herausgeber H. Fleischer und H. Fastl. Universität der Bundeswehr München, Neubiberg 1996.

[7] Fleischer, H., Zwicker, T., Admittanzmessungen an Elektrobässen. In: Fortschritte der Akustik (DAGA '97), DEGA, Oldenburg 1997, 301 - 302.

[8] Fleischer, H., Zwicker, T., Mechanical vibrations of electric guitars. Acustica - acta acustica 84 (1998), 758 - 765.

[9] Fleischer, H., Zwicker, T., Investigating dead spots of electric guitars. Acustica - acta acustica 85 (1999), 128 - 135.

[10] Fleischer H.: Betriebsschwingungsformen und Admittanzen von Gitarren, Mitteilung des Instituts für Mechanik, UniBW München 2003(?)

[11] Heise, U., Untersuchungen zur Ursache von Dead Spots an Baßgitarren. Das Musikinstrument 42 (1993), Heft 6/7, 112 - 115.

[12] Jansson, E.V., Acoustics for the guitar player. In: Function, construction and quality of the guitar. Royal Swedish Academy of Music, Publication No. 38 (1983), 7 - 26.

[13] Jansson, E.V., Acoustics for the guitar maker. In: Function, construction and quality of the guitar. Royal Swedish Academy of Music, Publication No. 38 (1983), 27 - 50.

[14] Lemme, H., Elektrogitarren, 4. Aufl. Frech-Verlag, Stuttgart 1982.

[15] May, U., Elektrische Saiteninstrumente in der populären Musik. Dissertation, Universität Münster, Münster 1984.

[16] Meinel, E., Elektrogitarren. E. Bochinsky, Frankfurt a. M. 1987.

[17] Valenzuela, Miriam Noemi, Zur Rolle des Gehörs bei akustischen Untersuchungen an Musikinstrumenten. Beiträge zur Vibro- und Psychoakustik 1/99. Herausgeber H. Fleischer und H. Fastl. Universität der Bundeswehr München, Neubiberg 1999.

[18] Wogram, K., Schwingungsuntersuchungen an Musikinstrumenten. In: Fortschritte der Akustik (DAGA '94), DPG-GmbH, Bad Honnef 1994, 53 - 64.

[19] Gloth G., Sinapius M.: Swept-Sine Excitation during Modal Identification of large Aerospace Structures, DLR, Göttingen 2002

[20] Müller Swen, Massarani P.: Transfer Function measurement with Sweeps, Inst. für technische Akustik, RWTH Aachen 2000

[21] Farina Angelo: Simultaniouse measurement of impulse response and distortion with a swept- sine technique, Dipartimento di Ingegneria, Universita di Parma, 108th AES Convention, Paris 18-22 February 2000

[22] Heike Georg, Dünnwald Heinrich: Neuere Klanguntersuchungen an Geigen und ihre Beziehung zum Gesang, Köln 2003

[23] Heike Georg: Das gemeinsame Klangideal von Belcanto und altitalienischen Geigen, Hallesche Schriften zur Sprachwissenschaft und Phonetik Bd. 3, 1997

[24] Woodhouse Jim: The Bridge Hill of the Violin, Cambidge University Engineering Department, Acta Acustica united with Acustica, Vol 91, p 155 – 165, 2005

[25] Woodhouse Jim: On the Synthesis of Guitar Plucks, Cambidge University, Engineering Department, Acta Acustica united with Acustica, Vol 90, p 928 – 944,

[26] Woodhouse Jim: Plucked Guitar Transients: Comparison of Measurements and Synthesis, Cambidge University Engineering Department, Acta Acustica united with Acustica, Vol 90, p 945 - 965, 2004

[27] Berdahl E. J., Smith III J. O.: Transfer Function Measurement Tool Box, CCRMA, Dep. Elect. Eng., Stanford University, Stanford USA

[28] Sali Samo, Kopac Janez: Modelling of frequency response function of a guitar in Annals of DAAAM for 2000 & Proceedings of the 11th International DAAAM symposium "Intelligent Manufacturing & Automation: Man - Machine - Nature", University of Rijeka, 19-21st October 2000, Opatija, Croatia.

[29] Sali Samo, Kopac Janez: Measuring a frequency response of a guitar. Proceedings of IMAC-XVIII: A Conference on Structural Dynamics, San Antonio, Texas, February 7-10, 2000

[30] Sali Samo, Kopac Janez: Optimisation of guitar quality. 7th International Scientific Conference on Production Engineering, Lumbarda, KorCula, Croatia, June 14-15, 2001.

[31] Sali Samo, Kopac Janez: Brace trimming for tone improvement of a guitar, Proceedings of IMAC-XIX: a Conference on Structural Dynamics, Kissimmee, Florida, February 5-8, 2001

[32] Sali Samo, Kopac Janez. Positioning of braces on a guitar soundboard. Proceedings of IMAC-XX: a Conference on Structural Dynamics, Los Angeles, California, February 4-7, 2002

[33] Westerkamp Ariadne: Die Geige gestrichen und verglichen, Ein akustisches, optisches und statistisches Verfahren zur Überprüfung der Klangqualität von Violinen, Diss. FB Kommunikation und Geschichtswissenschaften, TU Berlin 1990

[34] Dünnwald Heinrich: Akustische Messung an zahlreichen Violinen zur Ableitung objektiver Kriterien für deren klangliche Eigenschaften, Diss. Fakt. Elektrotechnik RWTH Aachen 1984

[35] Carleen m. Hutchins: Musical acoustics Vol. 1 and Vol. 2
Stroudsburg, Penn. Dowden, Hutchinson & Ross 1975-1976

[36] Carleen M. Hutchins: Research papers in violin acoustics 1975- 1993 Vol.1 and Vol.2
Woodbury, Acoustical Society of America 1997

[37] Rolf Bader: Computational Mechanics on the Classical Guitar, Springer Verlag Berlin Heidelberg 2005

[38] Gunter Ziegenhals: Subjektive und objektive Beurteilung von Musikinstrumenten, TUDpress, Verlag der Wissenschaften GmbH, Dresden 2010

[39] Martin Schleske: Empirical Tools in Contemporary Violin Making: Part II. Psychoacoustic Analysis and Use of Acoustical Tools, CASJ Vol. 4, No. 6 (Series II), Nov. 2002

[40] Neville H. Fletcher, Thomas D. Rossing: The Physics of Musical Instruments, p 207 – 226, Springer-Verlag New-York 1991

The author received his education in mechanical engineering at the Technical University of München and holds a PhD in thermodynamics and heat transfer. He retired from services at CERN, Geneva in 2006.

List of Authors